

Dynamic operation, efficient calibration, and advanced data analysis of gas sensors: from modelling to real-world operation

Dissertation
zur Erlangung des Grades
des Doktors der Ingenieurwissenschaften der
Naturwissenschaftlich-Technischen Fakultät
der Universität des Saarlandes

von
Tobias Baur

Saarbrücken
2022

Tag des Kolloquiums: 20.03.2023

Dekan: Prof. Dr. Ludger Santen

Berichterstatter: Prof. Dr. Andreas Schütze

Prof. Dr. Maximilian Fleischer

PD Dr. Tilman Sauerwald

Prof. Dr. Kathrin Flaßkamp

Vorsitz: Prof. Dr. Uwe Hartmann

Akad. Mitarbeiter: Dr.-Ing. Sarah Fischer

“All models are wrong, but some are useful.”¹

George Box, 1979

¹ “Now it would be very remarkable if any system existing in the real world could be exactly represented by any simple model. However, cunningly chosen parsimonious models often do provide remarkably useful approximations. For example, the law $PV = RT$ relating pressure P , volume V and temperature T of an “ideal” gas via a constant R is not exactly true for any real gas, but it frequently provides a useful approximation and furthermore its structure is informative since it springs from a physical view of the behavior of gas molecules. For such a model there is no need to ask the question “Is the model true?”. If “truth” is to be the “whole truth” the answer must be “No”. The only question of interest is “Is the model illuminating and useful?”. [327]

Abstract

This thesis demonstrates the use of dynamic operation, efficient calibration and advanced data analysis using metal oxide semiconductor (MOS) gas sensors as an example – from modeling to real-world operation. The necessary steps for an application-specific, selective indoor volatile organic compound (VOC) measurement system are addressed, analyzed and improved. Factors such as sensors, operation, electronics and calibration are considered. The developed methods and tools are universally transferable to other gas sensors and applications. The basis for selective measurement is temperature cyclic operation (TCO). The model-based understanding of a semiconductor gas sensor in TCO for the optimized development of operating modes and data evaluation is addressed and, for example, the tailored and stable detection of short gas pulses is developed. Two successful interlaboratory tests for the measurement of VOCs in independent laboratories are described. Selective measurements of VOCs in the laboratory and in the field are successfully demonstrated. Calibrations using the proposed techniques of randomized design of experiment (DoE), model-based data evaluation and calibration with machine learning methods are employed. The calibrated models are compared with analytical measurements using release tests. The high agreement of the results is unique in current research.

Kurzfassung

Diese Thesis zeigt den Einsatz von dynamischem Betrieb, effizienter Kalibrierung, und fortschrittlicher Datenanalyse am Beispiel von Metalloxid Halbleiter (MOS) Gassensoren – von der Modellierung bis zum realen Betrieb. Die notwendigen Schritte für ein anwendungsspezifisches, selektives Messsystem für flüchtige organische Verbindungen (VOC) im Innenraum werden adressiert, analysiert und verbessert. Faktoren wie z.B. Sensoren, Funktionsweise, Elektronik und Kalibrierung werden berücksichtigt. Die entwickelten Methoden und Tools sind universell auf andere Gassensoren und Anwendungen übertragbar. Grundlage für die selektive Messung ist der temperaturzyklische Betrieb (TCO). Auf das modellbasierte Verständnis eines Halbleitergassensors im TCO für die optimierte Entwicklung von Betriebsmodi und Datenauswertung wird eingegangen und z.B. die maßgeschneiderte und stabile Detektion von kurzen Gaspulsen entwickelt. Zwei erfolgreiche Ringversuche zur Messung von VOCs in unabhängigen Laboren werden beschrieben. Selektive Messungen verschiedener VOCs im Labor und im Feld werden erfolgreich demonstriert. Dabei kommen Kalibrierungen mit den vorgeschlagenen Techniken des randomisierten Design of Experiment (DoE), der modellbasierten Datenauswertung und Kalibrierung mit Methoden des maschinellen Lernens zum Einsatz. Die kalibrierten Modelle werden anhand von Freisetzungstests mit analytischen Messungen verglichen. Die hohe Übereinstimmung der Ergebnisse ist einzigartig in der aktuellen Forschung.

Table of Contents

Abstract.....	iii
Kurzfassung.....	v
Table of Contents	vii
1 Introduction and Motivation.....	1
2 Publications.....	5
2.1 Appended Papers and Author's Contribution as part of the Thesis	5
2.2 Other Appended Papers.....	6
2.3 Other Related Publications.....	7
3 State of the Art and Fundamentals.....	9
3.1 Metal Oxide Semiconductor Gas Sensor.....	9
3.1.1 <i>Introduction.....</i>	9
3.1.2 <i>Conductivity of SnO_2</i>	9
3.1.3 <i>Gas Sensing Mechanism.....</i>	10
3.1.4 <i>Temperature Cycled Operation.....</i>	14
3.2 Calibration.....	15
3.2.1 <i>What does Calibration mean?.....</i>	15
3.2.2 <i>Generation of an Artificial Gas Environment for Calibration</i>	16
3.2.3 <i>Design of Experiment</i>	20
3.2.4 <i>Multivariate Data Evaluation</i>	20
3.3 Indoor Air Quality	26
3.3.1 <i>Fundamentals</i>	26
3.3.2 <i>Volatile Organic Compounds</i>	31
3.3.3 <i>VOC Measurement</i>	34
4 Results	37
4.1 Metal Oxide Semiconductor Gas Sensors in Temperature Cycled Operation	37
4.1.1 <i>Synopsis.....</i>	37
4.1.2 <i>Paper A – Optimierung des temperaturzyklischen Betriebs von Halbleitergassensoren.....</i>	41
4.1.3 <i>Paper B – A novel Approach towards calibrated Measurement of trace Gases using Metal Oxide Semiconductor</i>	51
4.1.4 <i>Paper I – Novel Method for the Detection of short trace Gas Pulses with Metal Oxide Semiconductor Gas Sensors</i>	65
4.1.5 <i>Paper C – Facile Quantification and Identification Techniques for Reducing Gases over a Wide Concentration Range Using a MOS Sensor in Temperature-Cycled Operation</i>	75
4.2 Methods and Tools for the Development of Gas Sensor Systems	90
4.2.1 <i>Synopsis.....</i>	90
4.2.2 <i>Paper 2 – Device for the Detection of short trace Gas Pulses (Messsystem zur Detektion von kurzen Spurengaspulsen)</i>	92

4.2.3	<i>Paper 3 – Random Gas Mixtures for efficient Gas Sensor Calibration</i>	101
4.2.4	<i>Paper 4 – DAV³E – a MATLAB toolbox for multivariate sensor data evaluation</i>	116
4.3	VOC Sensor Systems based on MOS Gas Sensors	138
4.3.1	<i>Synopsis</i>	138
4.3.2	<i>Paper D – Highly Sensitive and Selective VOC Sensor Systems Based on Semiconductor Gas Sensors</i>	142
4.3.3	<i>Paper 5 – Highly Sensitive Benzene Detection with Metal Oxide Semiconductor Gas Sensors - an Inter-laboratory Comparison</i>	156
4.3.4	<i>Paper E – Comparison of ppb-level Gas Measurements with a Metal-oxide Semiconductor Gas Sensor in two independent Laboratories</i>	168
4.3.5	<i>Paper 6 – Field Study of Metal Oxide Semiconductor Gas Sensors in Temperature Cycled Operation for Selective VOC Monitoring in Indoor Air</i>	182
4.3.6	<i>Paper F – Measuring Hydrogen in Indoor Air with a Selective Metal Oxide Semiconductor Sensor</i>	205
5	Discussion	219
5.1	Model for MOS Gas Sensor in TCO	219
5.2	Model-based Data Evaluation	220
5.3	Calibration and Field Testing	222
5.3.1	<i>Design of Experiment</i>	222
5.3.2	<i>Data Evaluation</i>	224
5.4	Measurement of VOCs	225
5.5	Interfering Gases.....	228
5.6	Gas Mixing Apparatus.....	229
5.7	Electronics	230
5.8	Interlaboratory Tests.....	231
6	Conclusion and Outlook.....	233
7	References	235

1 Introduction and Motivation

Recently, more and more low-cost gas sensor systems were introduced into the market. They use different sensor principles. Many of them are based on metal-oxide semiconductor (MOS) gas sensors. Various applications demand selective and quantitative measurements. Industrial fire detection in power stations [1–3], breath analysis [4; 5] or air quality monitoring [6–9] are just a few examples. However, the performance and resilience against interferents of the available sensors and systems are often not sufficient [10; 11].

The central application of this thesis is the high-grade indoor air quality (IAQ) monitoring, with a focus on volatile organic compounds (VOCs). IAQ has received increasing awareness recently and is a multifaceted parameter. It is influenced by air temperature and humidity [12–14], carbon monoxide (CO), ozone (O₃), the group of VOCs and particulate matter [13; 15–18]. Besides temperature and humidity, the best-known IAQ criterion is the CO₂ concentration. However, CO₂ concentration is only an indicator for humanly emitted VOCs and other gases. Pettenkofer proposed this already in 1858 for better air quality through ventilation [19]. It is still used as an indicative IAQ parameter today [20]. The health effect and the influence of CO₂ on human productivity is unclear [20]. The concentrations of CO₂ that clearly show adverse health effect on humans are generally not reached indoors [20].

VOCs, along with particulate matter, play an important role in assessing the links between IAQ and disease as well as health effects [17]. More than 350 different VOCs can be typically detected indoors using standardized analytical methods [21; 22]. But the health effects of most single or combinations of individual VOCs on humans are unclear [23]. Health effects are clear for only a few substances, e.g. benzene and formaldehyde. They are classified as carcinogenic [24; 25]. In most studies, humans are exposed to only a few VOCs and the effects are examined [26]. Assessing the human exposure to organic pollutants is complex due to the variety of substances, the general difficulty of research concerning the human body and missing feasible measurement methodology [27]. A more detailed investigation of the health effects can be done by large-scale cohort studies with continuous measurements of VOCs in real-life. However, these studies are not feasible with current analytics alone due to the cost and complexity of analytical measurements.

Low-cost gas sensor systems could support cohort studies. Systems based on MOS gas sensors were able to provide continuous measurement data of the total VOC concentration, as well as quantification of specific groups or even individual VOCs [28]. Comparability and traceability would have to be ensured for these low-cost sensor systems to be appropriate for this usage.

The development of such gas sensor systems involves many interdisciplinary steps. This applies to systems with all gas sensor principles. Knowledge on the application, including all target and interferent gases, selection of possible sensor types, development of the electronics, optimization of the sensor's operation mode, design of experiment, data evaluation and algorithm design are required along the development process. The key factor for a successful sensor system is not only the most sophisticated sensor or most elaborate data evaluation model. The combination and understanding of all

interdisciplinary steps are necessary for a successful sensor system. This interaction of all factors is a prerequisite for sensor technology to reach its full potential.

In this thesis, especially the development of gas sensor systems based on MOS gas sensors is addressed. MOS gas sensors are characterized by their high sensitivity, quick response time, small dimensions, low-power consumption (at least for MEMS sensors) and low-cost production [6–9; 29–32]. These properties make them particularly well-suited for the local online measurement of VOCs in every room or as a personal monitor. Their disadvantages, such as poor selectivity, drift or aging, must be overcome for this task. This is one reason why there are currently very few successful sensor systems with MOS gas sensors on the market. Several methods are presented in the literature to compensate these disadvantages.

Selectivity can be improved by tailored material compositions or properties of the sensitive layer like thickness or topology and different operating temperatures [33–35]. Different sensitive layers can be combined into a sensor with one heating element each [2; 36] or integrated on a single heater [6; 37]. The temperature of the sensitive layer can also be cyclically modulated to generate a virtual sensor array, which is called temperature cycled operation (TCO) [38–41]. A (virtual) sensor array needs to be calibrated by using machine learning algorithms to tune the naturally poor selectivity of these sensors [2; 6; 36–41]. Characterization and calibration requires reproducible gas exposures in the laboratory and systems that can generate complex gas mixtures [42; 43]. Characterization using single gases in the laboratory is in many publications a vehicle to show the performance of a new material [44–54]. In some publications, the calibration was performed with gas mixtures based on combinatorial design of experiments (DoE), i.e. combinations of very few fixed concentration levels for each gas [39; 48; 51; 52; 55–59], which can easily lead to overfitting [55; 60].

Drift or aging can have different causes. One reason can be the surface modification by certain gases (H_2S , SO_2 , siloxanes) [61]. Another reason can be diffusion effects inside the bulk of the sensor [62; 63]. One idea for prevention of poisoning (e.g. for siloxanes) is protection by a size selective membrane filter [64]. Continuous aging effects due to the mode of operation can be compensated by extended calibration [65].

In this thesis, these methods (i.e. integrated sensor array, TCO, machine learning algorithm, extended calibration for drift compensation) as well as new ideas (i.e. model-based data evaluation, efficient DoE with random gas mixtures, extended field tests) were combined and systematically driven forward for the measurement of VOCs. The potential and limitations of MOS gas sensors in TCO for IAQ are demonstrated using realistic calibration and testing methods. Many of these methods are not exclusive to MOS gas sensors but can be applied to other gas sensor principles.

Chapter 2 provides an overview of the author's publications and contributions that formally contribute to this dissertation. Furthermore, a list of other attached papers and related publications by the author relating to this thesis is shown.

Chapter 3 will introduce the state of the art and fundamentals of MOS gas sensors in TCO, calibration, applications and challenges of IAQ.

Subsequently, the results of the present thesis are presented in Chapter 4 in form of several publications. Those results can be categorized into three sections.

Section 4.1 presents a simplified model describing the behavior of MOS gas sensors during the dynamic phases after a fast temperature change in TCO from an engineering

perspective. The focus is on using the model-based description for the optimization of the TCO and model-based data evaluation. For this purpose, one parameter, the rate constant, is described. The added value by using this model is shown in two examples: A mobile recalibration method based on the model-based rate constant and its superposition property is demonstrated. The model is also used to develop a specially designed operation and data evaluation method for detecting short trace gas pulses. Furthermore, the limits of determining the rate constant for high concentrations and a simple extension of the model by introducing a time constant of the relaxation are shown in the following.

Section 4.2 introduces tools and methods for the development of gas sensor systems. An electronics platform for the control of dynamic operation modes and data acquisition were developed. For analog MOS gas sensors, the electronic is designed to control a heater and cyclically vary its temperature and to measure the sensor resistance with logarithmic amplification of the very low currents over several orders of magnitude. For digital MOS gas sensors that recently came onto the market, electronics and firmware that enable dynamic operation modes in addition to the manufacturer's default were implemented. Calibration with combinatorial DoE obviously cannot be successful due to the large number of target and interfering gases in most applications. To enable more efficient and realistic calibration in the laboratory, a new DoE method based on randomized gas exposures is introduced. For data evaluation an open-source MATLAB Toolbox DAV³E is presented. DAV³E enables the user to easily apply complex methods of the complete evaluation chain via a GUI.

Section 4.3 specifically addresses the VOC measurement for IAQ using the same model-based TCO described before. Two interlaboratory tests are discussed that demonstrate the capabilities and challenges of such systems as well as their testing and characterization. DoE based on randomized gas exposures presented in Section 4.2 is validated by further laboratory measurements, but also in an extensive field test campaign. Field tests over several weeks with release tests of different substances and comparison with reference analytics prove the effectiveness of the introduced methods from model-based TCO to DoE with random gas exposures for calibration.

Chapter 5 discusses the results in the overall context and compares them with previous and current studies. The results are interpreted and possible improvements are explained. The thesis ends with a summary and outlook in Chapter 6.

2 Publications

2.1 Appended Papers and Author's Contribution as part of the Thesis

In this section, six papers of the author are listed, which are formally included in the thesis. The papers highlight key points of the understanding and the development of gas sensor systems. Papers 1 and 2 also include results from the author's master's thesis. These papers are supplemented by other papers, described in the next section, that are not an official part of the thesis but offer deeper understanding.

Paper 1 T. Baur, C. Schultealbert, A. Schütze and T. Sauerwald: Novel Method for the Detection of short trace Gas Pulses with Metal Oxide Semiconductor Gas Sensors, *Journal of Sensors and Sensor Systems* (2018)

I developed the model, designed and performed all measurements, evaluated and interpreted the measurement data and wrote the main part of the manuscript.

Paper 2 T. Baur, C. Schultealbert, A. Schütze and T. Sauerwald: Device for the Detection of short trace Gas Pulses (Messsystem zur Detektion von kurzen Spurengaspulsen), *tm - Technisches Messen* (2018)

I developed the electronics, firmware and sensor chamber, designed and performed the measurements, evaluated and interpreted all measurement data and wrote the main part of the manuscript.

Paper 3 T. Baur, M. Bastuck, C. Schultealbert, T. Sauerwald and A. Schütze: Random Gas Mixtures for efficient Gas Sensor Calibration, *Journal of Sensors and Sensor Systems* (2020)

I developed the concept of randomized calibration scheme, designed and performed the measurements together with the second and third author. I performed most of the evaluation and interpretation and wrote the main part of the manuscript.

Paper 4 M. Bastuck, T. Baur and A. Schütze: DAV³E – a MATLAB toolbox for multivariate sensor data evaluation, *Journal of Sensors and Sensor Systems* (2018)

The first author developed and implemented the prototype DAV³E is based on. I improved upon this prototype with new ideas, concepts and implementations together with the first author and contributed with substantial revisions of the manuscript.

Paper 5 T. Sauerwald, T. Baur, M. Leidinger, W. Reimringer, L. Spinelle, M. Gerboles, G. Kok and A. Schütze: Highly Sensitive Benzene Detection with Metal Oxide Semiconductor Gas Sensors - an inter-laboratory Comparison, *Journal of Sensors and Sensor Systems* (2018)

I designed the test measurement at Saarland University together with T. Sauerwald and M. Leidinger. I performed most of the evaluation and interpretation of the data. I generated most of the figures and wrote part of the manuscript.

Paper 6 T. Baur, J. Amann, C. Schultealbert and A. Schütze: Field Study of Metal Oxide Semiconductor Gas Sensors in Temperature Cycled Operation for Selective VOC Monitoring in Indoor Air, *Atmosphere* (2021)

I conceptualized and developed the methodology of the project together with the second author and supervised the realization of the measurement and formal analysis. I wrote the software for randomized calibration. I supervised and performed the data evaluation and visualization together with the second author and wrote the main part of the manuscript.

2.2 Other Appended Papers

In this section, papers of the author are listed, which are included in the thesis but not as an official contribution. The papers are within the direct scope of this work and provide a deeper insight concerning the big picture of the thesis. Paper A is a preliminary work and a result of the author's bachelor thesis. This paper is the basis of the thesis and all other papers, as it provides the fundamentals for the optimization and understanding of the sensor in the temperature cycled operation, which has been deepened in Paper B.

Paper A T. Baur, A. Schütze and T. Sauerwald: Optimierung des temperaturzyklischen Betriebs von Halbleitergassensoren, *tm - Technisches Messen* (2015)

Paper B C. Schultealbert, T. Baur, A. Schütze, S. Böttcher and T. Sauerwald: A novel Approach towards calibrated Measurement of trace Gases using Metal Oxide Semiconductor, *Sensors and Actuators B: Chemical* (2017)

Paper C C. Schultealbert, T. Baur, A. Schütze and T. Sauerwald: Facile Quantification and Identification Techniques for Reducing Gases over a Wide Concentration Range Using a MOS Sensor in Temperature-Cycled Operation, *Sensors* (2018)

Paper D A. Schütze, T. Baur, M. Leidinger, W. Reimringer, R. Jung, T. Conrad and T. Sauerwald: Highly Sensitive and Selective VOC Sensor Systems Based on Semiconductor Gas Sensors, *Environments* (2017)

Paper E M. Bastuck, T. Baur, M. Richter, B. Mull, A. Schütze and T. Sauerwald: Comparison of ppb-level Gas Measurements with a Metal-oxide Semiconductor Gas Sensor in two independent Laboratories, *Sensors and Actuators B: Chemical* (2018)

Paper F C. Schultealbert, J. Amann, T. Baur and A. Schütze: Measuring Hydrogen in Indoor Air with a Selective Metal Oxide Semiconductor Sensor, *Atmosphere* (2021)

2.3 Other Related Publications

This section lists all papers and patents of the author that go beyond the scope of this thesis but are built on the results presented in this thesis.

Paper i H. Lensch, M. Bastuck, T. Baur, A. Schütze and T. Sauerwald: Impedance model for a high-temperature ceramic humidity sensor, *Journal of Sensors and Sensor Systems* (2019)

Paper ii C. Schultealbert, R. Diener, J. Amann, T. Baur, A. Schütze and T. Sauerwald: Differential scanning calorimetry on micro hotplates for temperature calibration and mass quantification (Dynamische Differenzkalorimetrie auf Mikroheizern zur Temperaturkalibrierung und Massenquantifizierung), *tm - Technisches Messen* (2019)

Paper iii C. Schultealbert, I. Uzun, T. Baur, A. Schütze and T. Sauerwald: Siloxane treatment of metal oxide semiconductor gas sensors in temperature-cycled operation – sensitivity and selectivity, *Journal of Sensors and Sensor Systems* (2020)

Paper iv C. Schultealbert, I. Uzun, T. Baur, T. Sauerwald and A. Schütze: Erkennung und Kompensation von Vergiftung durch Siloxane auf Halbleitergassensoren im temperaturzyklischen Betrieb (Identification and compensation of siloxane poisoning in metal oxide semiconductor gas sensors in temperature cycled operation), *tm - Technisches Messen* (2020)

Paper v Y. Robin, J. Amann, T. Baur, P. Goodarzi, C. Schultealbert, T. Schneider and A. Schütze: High-Performance VOC Quantification for IAQ Monitoring Using Advanced Sensor Systems and Deep Learning, *Atmosphere* (2021)

Paper vi A. Schütze, J. Amann, T. Baur and C. Schultealbert: Messung von VOCs in Innenräumen mit low-cost Sensorik und Vergleich mit analytischen Messungen, *UMWELT UND GESUNDHEIT 01/2022, Sonderheft WaBoLu-Innenraumtag* (2021)

Paper vii C. Fuchs, H. Lensch, O. Brieger, T. Baur, C. Bur, A. Schütze: Concept and Realization of a Modular and Versatile Platform for Metal Oxide Semiconductor Gas Sensors, *Technisches Messen* (2022, submitted)

Patent i S. Beck, T. Conrad, J. Peter, T. Baur, T. Sauerwald, A. Schütze and C. Schultealbert: Method and device for determining indication of a leak of a test object filled with test fluid, *EP3527966A1*, Application granted (2021)

Patent ii T. Sauerwald, A. Schütze, C. Schultealbert, T. Baur and I. Uzun: Method and device for determining a degradation of a semiconductor gas sensor, *DE102019130990A1*, Publication (2021)

3 State of the Art and Fundamentals

3.1 Metal Oxide Semiconductor Gas Sensor

3.1.1 *Introduction*

Metal oxide semiconductor (MOS) gas sensors change their electrical conductivity based on chemical reactions on the surface. In 1953, Brattain and Bardeen already reported gas-sensitive effects for germanium [66]. One year later Heiland [67] announced it for zinc dioxide. Seiyama published “*A new detector for gaseous components using semiconductive thin films*” [68] based on zinc dioxide in 1962. The first commercial MOS gas sensor was patented and introduced by Taguchi [69] in Japan. The gas leak detection sensor based on tin dioxide (SnO_2) for homes and industrial usage was designed to prevent gas explosions. In 1969, Taguchi founded Figaro Engineering Inc. which sells those as well as other gas sensors named Taguchi gas sensor (TGS) [70]. The construction of the sensor was a simple ceramic tube with integrated heater coil coated with sintered SnO_2 with two electrodes on the surface [71]. The sensor was operated at constant temperature. In the following years, research was done on materials, design and operation mode. The most common and widely studied material for commercial sensors is still polycrystalline tin dioxide (SnO_2) [72; 73]. However, sensitivity, selectivity and stability have been improved with catalyst doping and decorating. This means that pure SnO_2 sensors are generally not available today. The greatest innovations in design were the miniaturization [71] as well as the integration of application-specific integrated circuits (ASIC) into the sensors [6–9]. MOS gas sensors are still often operated at constant temperature. Already in 1974, temperature modulation of MOS gas sensors was reported and patented to increase the selectivity and sensitivity [74; 75]. Nowadays, temperature modulation is also integrated in commercial sensors [8; 76]. More companies entered the market, and the MOS gas sensors have a wide range of applications today. Relevant usages are for example the automatic ventilation flap control in automobile industry [77–79], industrial fire detection in power stations [1–3] or indoor air quality (IAQ) monitoring [6–9].

The following subsections discuss the conductivity of polycrystalline SnO_2 , the theory of operation, the operation modes of MOS gas sensors and especially the temperature cycling.

3.1.2 *Conductivity of SnO_2*

SnO_2 is a wide band gap n-type semiconductor. The conductivity can be explained using the electronic band model. It describes the range of energy levels in solids, which may (bands) or must not (band gaps) be filled with electrons. The valence band (E_V) is the highest energy band with filled electronic states. The conduction band (E_C) is the lowest energy band of vacant electronic states. Both bands are separated by a bandgap ($E_C - E_V$) of 3.6 eV for SnO_2 [80]. Therefore, no intrinsic conductivity can be expected due to the low thermal energy in the normal operation temperatures between 100 and 500 °C (32 – 67 meV). The conductivity is dominated by ionized oxygen vacancies [81]. Tin interstitials can also contribute to the conductivity, even as the dominant effect [82]. Porte et al. [83] show how to control intrinsic defect formation in SnO_2 thin films during

deposition by the oxygen partial pressure and temperature. This implies that the dominant effect also depends on the production process. As described in most publications and for a simplified description, ionized oxygen vacancies are assumed to be the dominant effect [72; 81; 84; 85].

The crystal structure of SnO_2 is not ideal and has an excess of tin atoms because of oxygen vacancies. Oxygen vacancies can occur in single or double ionized form. The energy required for the first ionization is approx. 30 meV and for the second ionization approx. 150 meV [86]. As a consequence, the ionized vacancies act as donors with energy levels approx. 30 meV and 150 meV under the conduction band. For operating temperatures between 100 and 500 °C, the average thermal energy of an electron is between 32 and 67 meV. Therefore, only the first ionized vacancies are probably completely depleted. On that basis, the donor density N_D can be assumed to be constant in this temperature range. That means that N_D dominates the electron density.

Some publications show drift processes due to mobile donors with temperature [62; 63; 87]. N_d can also be a function of time and position. The kinetics of drift processes are rate controlled by the surface exchange reaction of oxygen on SnO_2 , with time constants ranging from a few minutes for high temperatures to days for low temperatures [62]. The electrical conductivity of the bulk of semiconductors is determined by electrons, holes and ions. As an n-type semiconductor due to the oxygen vacancies, electrons play the major and holes a minor role for the conductivity of SnO_2 . The density of ions and electrons are of the same order of magnitude and due to the lower mobility (factor 100-1000) of the ionic charge carriers (oxygen vacancies). A pure electrical conductivity can be assumed [84, p. 39]. The electrical conductivity σ_b due to electrons depends on the elementary charge (q), electron density (n_e) and mobility of the electrons (μ_e). The electron density corresponds to the donor density (N_d) due to the oxygen vacancies.

$$\sigma_b = q \cdot n_e \cdot \mu_e = q \cdot N_d \cdot \mu_e \quad (3.1)$$

The electron mobility μ_e is dependent on the temperature. For typical operating temperatures of a MOS gas sensor, phonon interactions dominate and the electron mobility is proportional $T^{-3/2}$ [84, pp. 19–20].

3.1.3 Gas Sensing Mechanism

Chemo-resistive gas sensing describes the effect of resistance change of a MOS material in oxidizing or reducing atmosphere. The MOS resistance increases in oxidizing atmosphere (e.g. clean air) and decreases in reducing atmosphere (e.g. clean air with carbon monoxide). After nearly 70 years of research, the chemo-resistive gas sensing mechanism still cannot be completely described and there are only different theories without spectroscopic evidence [88].

The rule-of-thumb explanation for the gas sensing mechanism is the oxygen ionosorption model [88; 89], which was developed in the 1950s [90]. In this theory, charged oxygen ions and their reactions with reducing gases play the major role for the gas sensing effect. Its basic concept is that atmospheric oxygen adsorbs as molecular ($\text{O}_2^{-\text{ads}}$) or atomic ($\text{O}^{-\text{ads}}$, $\text{O}^{2-\text{ads}}$) ions on the SnO_2 surface, trapping electrons from the conduction band. The surface itself becomes negatively charged and a band bending at the surface is induced [81; 84; 91; 92]. The electron is taken from the conduction band

and the conductivity decreases. A reducing gas molecule, for example carbon monoxide (CO), can react (Eley-Rideal or Langmuir-Hinshelwood mechanism) with such an oxygen ion to carbon dioxide (CO₂). The formerly trapped electron is released to the conductance band, i.e. there is reduced band bending and the conductivity increases [93]. This shows that the effect is very broadband. It is not possible to simply identify the gas type from the change in conductance. A reaction with the charged oxygen on the surface leads to a free electron, regardless of which gas molecule has reacted.

To describe the mechanism of the gas sensing effect of MOS gas sensors, for example SnO₂, it is important to understand the interaction of the surrounding atmosphere with the SnO₂ surface.

Generally, two adsorption mechanisms are distinguished, the physisorption and chemisorption. Chemisorption changes the adsorbate and/or the adsorbent chemically. Physisorption does this not. Far away from the surface molecules, van-der-Waals forces occur and the molecule (adsorbate) is physisorbed to the surface (adsorbent). The binding energy is small, in the order of 0.2 eV per molecule [91, p. 229]. This is usually not enough to initiate processes such as dissociation or reaction. Chemisorption can establish a stronger bond to the surface. In that case, the chemical bond between the molecules and the surface atoms is either ionic or covalent. The binding energy is in the order of 0.65 eV per molecule [84, p. 72].

The interaction with the gas takes place on the surface of the sensitive SnO₂ layer. At the surface, additional states occur in the band gap that are not present in the volume. These are called surface states. According to Madou, Morrison [84] and Kohl [81] extrinsic surface states contribute crucially to the detection of gases. *“Extrinsic surface states are localized energy levels created by adsorbed gas molecules at the surface. For semiconductor gas sensors, adsorbed oxygen ions have a decisive influence on the surface conductivity”* [94]. Electrons from the conduction band can occupy these free surface sites due to the energetically more favorable state. If an electron occupies a surface state, it is localized and can no longer contribute to the conductivity of the semiconductor. The more electrons fill free surface states, the greater the negative surface charge. This causes a displacement of the electrons inside the volume by electrostatic repulsion to compensate for the negative surface charge. This space charge zone qV_s is also called surface barrier or band bending.

At this stage, the sensing layer morphology makes an important difference. In a compact layer, the interaction of the gas is limited to the space charge region at the geometric surface. Depending on the thickness of the layer, only a thin part of it is depleted and forms the described surface barrier. The conduction process takes place in the not depleted part of the layer. Due to the small influence of the interaction with the gas on the surface, the sensitivity is severely limited.

Generally, porous polycrystalline SnO₂ with a high surface area is used for MOS gas sensors. In a porous layer, each grain has a depleted surface zone. Local electrical states in the band gap occur at each grain-boundary of the crystallites and not only at the geometric surface. However, the situation can become more complex if grains sinter and there are necks, which create a conduction channel. With non-sintered grains we distinguish in the following between large ($x_g > \lambda_D$) and small grains ($x_g < \lambda_D$), depending on the ratio between grain size x_g and Debye length λ_D . [72]

For a porous layer with large grains, band bending at the grain-boundaries dominate the conductivity, due to the missing conduction channel through the sensor. This means that an electron has to overcome the band bending to contribute to the conductivity. The sensor conductivity σ_s can be described by equation (3.2) as an exponential function of the surface barrier and the inverse temperature multiplied with the bulk conductivity σ_b [84; 91, p. 42]. k_b is the Boltzmann constant.

$$\sigma_s = \sigma_b \cdot \exp\left(-\frac{qV_s}{k_b T}\right) \quad (3.2)$$

The potential barrier V_s can be calculated using the Schottky model² with the one-dimensional Poisson equation [91, pp. 29–31]. V_s is thereby a function of the occupied surface states N_s and the donor density N_d [91, p. 31] and can be described with equation (3.3).

$$V_s = \frac{qN_s^2}{2\epsilon_r\epsilon_0 N_d} \quad (3.3)$$

ϵ_r is the relative and ϵ_0 the vacuum permittivity. The conductance G of the sensor can be described with equation (3.4) [94]. The factor g is depending on the semiconductor geometry and can be used to define the prefactor G_0 in equation (3.4). G_0 is often assumed to be constant. The bulk conductivity is temperature-dependent with $T^{-3/2}$ [84, pp. 19–20], but the change of G_0 is less sensitive compared to the exponential factor [94].

$$G = g \cdot \sigma_s = g \cdot q \cdot \mu_e \cdot N_d \cdot \exp\left(\frac{-qV_s}{k_b T}\right) = G_0 \cdot \exp\left(\frac{-qV_s}{k_b T}\right) \quad (3.4)$$

However, publications also show mobile donors [62; 63; 87]. Therefore, the donor density N_d can be a function of time and position. Investigations show a reduced surface barrier as a result and also a change in the prefactor G_0 [62; 63; 87].

In literature, also other mechanisms are suggested [93; 95]. Besides the ionosorption model, the oxygen-vacancy model (reduction–reoxidation mechanism) [93] exists. There is an indication for both. The dominating mechanism depends more on the material and the operating conditions, e.g. temperature, composition of gaseous phase or hydroxylation of the surface [93].

The oxygen-vacancy model describes the sensor response of SnO_2 through the Mars–van-Krevelen mechanism. It is based on the alternating reduction and reoxidation of the surface by oxygen [93; 96]. Thus, no ionosorbed oxygen, but rather oxygen vacancies near the surface play the major role. In this case, surrounding oxygen or oxidizing gases in the atmosphere adsorb at the surface and the oxygen atom can fill the vacancy and restore a lattice oxygen anion ($\text{O}^{2-}_{\text{lat}}$). The electron is taken from the conduction band and the conductivity decreases. If a reducing gaseous molecule, e.g. CO, is adsorbed to the surface, the CO reacts with a lattice oxygen anion and the oxidation product, CO_2 ,

² “This simply assumes that the space charge in the solid near the surface is immobile and is independent of distance in the entire space charge region.” [91, p. 29]

desorbs. The resulting oxygen vacancy ionizes. The electron contributes to the conductivity and the conductivity increases.

However, both mechanisms have critical points. The problem of the ionosorbed model is that there is no spectroscopic evidence of this mechanism yet. Pulkkinen et al. [97] did a kinetic Monte-Carlo simulation of the oxygen exchange on the surface and calculated that the dominant species changes from O_2^- to O^- at a temperature of 700 K. Gurlo remarked in a review in 2016 that “*neither superoxide ions O_2^- , nor charged atomic oxygen O^- , nor peroxide ions O_2^{2-} have been observed on SnO_2 under the real working conditions of sensors*” [88]. In 2021, Kostiantyn et al. [89] analyzed all charged O-related species on three naturally occurring surfaces of SnO_2 . They observed that two types of surface acceptors can form spontaneously upon the adsorption of atmospheric oxygen O_2^- and O^{2-} , depending on the surface. In contrast, the oxygen-vacancy mechanism near the surface dominates the spectroscopic studies and there is some spectroscopic evidence for this mechanism [98–101]. But Gurlo [93] mentioned three problems of the oxygen-vacancy mechanism:

- First, most of the studies under unrealistic experimental conditions (e.g. gas composition) cannot simply be transferred into a real-world application.
- Second, the slow kinetics of oxygen exchange at the surface.
- Third, the diffusion process in the oxide lattice.

For SnO_2 the oxygen would have to migrate a small distance to become ionized in the bulk [81; 93]. This diffusion process is relatively slow and depends on the temperature [62; 63]. The diffusion coefficient is, however, measured for bulk material and can be much faster for porous polycrystalline material (grain boundaries) [93]. Degler [33] summarizes in a review the sensing mechanism for doped and loaded semiconductor material. He also shows the influence of oxygen vacancies near the surface. The oxygen-vacancy mechanism could also be the origin of the typical drift behavior of MOS gas sensors [62; 63]. In 2019, Elger et al. [102] studied the mechanism of ethanol detection on SnO_2 with operando Raman-FTIR (Fourier-transform infrared spectroscopy) and UV/Vis (ultra-violet/visible) spectroscopy. They show that the surface reoxidation correlates with the number of surface oxygen vacancies. However, this cannot explain the major sensor response and the “*results show that ionosorption is of more general importance in (ethanol) gas sensing.*” [102].

Overall, there is no clear evidence for or against either mechanism. The two mechanisms probably overlap depending on the material, doping, loading, temperature, design, operation mode and so on. Still nowadays authors propose new theories for the gas sensing mechanism, for example Blackman (2021) in a perspective article with the title: *Do We Need “Ionosorbed” Oxygen Species? (Or, “A Surface Conductivity Model of Gas Sensitivity in Metal Oxides Based on Variable Surface Oxygen Vacancy Concentration”)* [95]. This shows that even 70 years after the description of the chemoresistive effect, further research will be needed to even prove the basic principle. Therefore, comprehensive physical and chemical modeling of complex material compositions (material composition, catalysts, morphologies and so on) is not yet feasible today.

Since in this thesis the sensors are operated with fast temperature changes, the ionosorption mechanism is considered as dominant. The oxygen-vacancy mechanism would only cause secondary sensor changes with longer time constants.

3.1.4 Temperature Cycled Operation

The aim of the measurement with a MOS gas sensor is the selective quantification or discrimination of one or more gases. Due to the broadband reactivity of MOS gas sensors, the sensor resistance correlates with a sum signal of almost all reducing and oxidizing gases in the atmosphere. Typically, a MOS gas sensor contains a single sensitive layer. Further, it is operated at constant temperature and the ohmic resistance is measured. With an optimized temperature and additional catalysts in the sensitive layer, an enhanced selectivity and sensitivity can be achieved, but a certain cross-sensitivity remains.

More information is necessary for a selective measurement. This is often realized using a so-called multi-sensor [103]. There are different possibilities to create a multi-sensor. One method is to create a physical multi-sensor with different single sensors containing different sensitive layers and reaction properties, e.g. due to different doped or decorated materials [2; 36]. Another solution is to create a sensor with different sensitive layers on one heater [6; 37]. Combining multiple sensors or layers is usually more expensive and sensor-specific aging over time makes automated compensation more complex. These drawbacks can be overcome by creating a virtual multi-sensor with only one physical sensor.

The most common method is the temperature cycled operation (TCO) [40; 41]. In this case, the temperature of the sensitive layer is changed periodically to exploit the different temperature-dependent reaction properties. Moreover, several sensors with different sensitive layers combined with TCO can be used – creating a hybrid virtual and physical multi-sensor [40]. The approach of cyclic temperature modulation to increase the selectivity and sensitivity was already reported in 1974 [74; 75]. The information gain results from different effects:

- I. On the one hand, the information results from the static sensor response at different temperatures for multiple static sensors or slow temperature cycles. The sensor response depends on the temperature-dependent reactivity of each gas.
- II. On the other hand, the information results from the dynamic sensor response due to fast temperature changes. Fast temperature changes force the sensor from an equilibrium state to a non-equilibrium state, and the temperature-dependent relaxation generates more information [94]. The relaxation of these non-equilibrium states to equilibrium states is caused by different coupled physical and chemical processes, with time constants between microseconds and hours [104, p. 12]. These processes go along with a change of the surface states, but it can also imply changes in the intrinsic state density. As also described in Subsection 3.1.3, we assume that due to the rapid temperature changes, the ionosorption mechanism dominates.

In Figure 1 a temperature cycle with a step from a high (e.g. 400 °C) to a low (e.g. 150 °C) temperature is illustrated. On the left side grain boundaries at the high and low temperature for four states (isothermal and transient for both temperatures) are shown. The figure illustrates the Arrhenius plot in the middle and the logarithmic conductance for the same states on the right. At high temperature there is more ionosorbed oxygen on the surface compared to low temperature.

At point (1) the temperature is low, and the surface has a small concentration of ionosorbed oxygen on the surface. A fast temperature change from (1) to (2) occurs. For micromachined membrane MOS gas sensors, with thermal time constants of a few milliseconds, the surface states cannot change that fast and remain (nearly) constant due to the slower chemical processes. The conductance increases during this state transition only due to the temperature change. Therefore, to reach the equilibrium at high temperature more oxygen has to be ionosorbed. In point (3) this equilibrium is reached. A high density of surface states is observed and the conductance decreases. When the temperature changes again rapidly to the low temperature from point (3) to (4), the surface density does not change. A high number of ionosorbed oxygen remains on the surface and the conductance drops strongly, due to the exponential correlation. To reach the new equilibrium state the oxygen coverage has to be reduced. This relaxation to the new equilibrium highly depends on the gaseous composition of the atmosphere. Higher concentrations of reducing gases like carbon monoxide or hydrogen speed up the relaxation. This allows a large increase in sensor response compared to operation at constant temperature. A more detailed description of the TCO, the model conception and the possibilities are part of this work and are described in Section 4.1 Paper A and B.

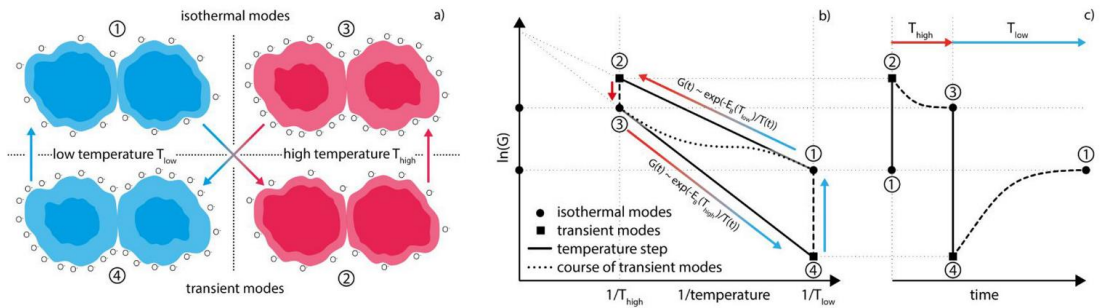


Figure 1: a) Schematic illustration of the stationary and transient states of a grain-grain boundary in temperature cycled operation. The lighter areas of the grains symbolize the depletion layer near the surface due to ionosorbed oxygen (shown schematically as O^-). b) Illustration of the Arrhenius plot of the sensor signal with two temperatures. Solid line: States with rapid change in temperature. Dashed line: Relaxation at a constant temperature. Dotted line: steady states. c) Illustration of the logarithmic sensor conductance during the TCO. Solid line: States with rapid change in temperature. Dashed line: Relaxation at a constant temperature. [Paper A]

3.2 Calibration

3.2.1 What does Calibration mean?

At the beginning of the development of MOS gas sensors, the aim was to create a sensor in static operation with a linear correlation to the measurand. Therefore, sophisticated data analysis was not required. Due to the limited selectivity, the physical or virtual multi-sensors were introduced, as described in Subsection 3.1.4. Especially with virtual multi-sensors, not only one, but practically infinite sensor signals are available for data evaluation. After 50 years of research, the gas sensing mechanism is still unclear as described in Subsection 3.1.3. Hence, no physical and chemical models are available to describe the complex interaction of gas sensors with the atmosphere. A further increase in complexity comes from variability of the sensitive layers with different material compositions and morphology. Due to the high complexity and lack of physical

and chemical models, multivariate methods are necessary to create empirical models to calculate different target values from the signals [41; 105].

This calibration means model building using annotated data on the observed relationship between a dependent and one or more independent variables. The aim is to make estimates for the dependent variable based on new observations of the independent variables [106–108]. The term (statistical) calibration is not to be confused with the term calibration in measurement technology and metrology. The second case means the comparison of the measured value between a measurement system under test and a calibration standard [109].

Calibration is one of the crucial steps during the development of gas sensor systems and involves many fields of expertise. As described above, MOS gas sensors are usually not selective. Therefore, the evaluation algorithm has to be calibrated to classify between target and interfering gases or to quantify the target gases independent of the interfering gases or other background conditions. Obviously, this means that for the calibration of a sensor or sensor system, full knowledge about the application and the background conditions is a prerequisite. Any evaluation or model can only be as good as the data it is trained on. This is well summarized in the well-known saying “garbage in, garbage out”. This means that a fully or sufficiently representative dataset is needed to create an empirical model for a defined application. Various methods have been established for the creation of such datasets. A distinction can be made between calibration in a real environment or in an artificial environment.

In a real environment, calibration takes place directly in the application. Reference measurement systems measure on-site the concentrations of the target gases, which has for example been done for outdoor air pollution [110–113].

In an artificial environment, calibration is usually performed in the laboratory with a gas mixing apparatus (GMA) or individual gases in a controlled environment. For an artificial environment, the design of experiment to create a statistically comprehensive training dataset for the data evaluation is one of the crucial steps. In the following, the generation of an artificial gas environment, the design of experiment and the data evaluation are discussed in more detail.

3.2.2 Generation of an Artificial Gas Environment for Calibration

3.2.2.1 Fundamentals of the Dynamic Generation of Gas Mixtures

Gas sensors are typically characterized and calibrated using standard gas mixtures. The generation of standard gas mixtures can be divided into two groups: static or dynamic methods [114]. Table 1 gives an overview of different static and dynamic methods to produce standard gas mixtures. A description of the methods can be found in Namieśnik [114] and EN ISO-1:2019 [115].

Constant single gas mixtures, such as pressurized test gas cylinders, are normally produced with static methods. Static gas mixture generation can only be done with stable substances, whose storage is possible in the gaseous phase [114]. The measurements in this work were performed using dynamic methods, which are described in more detail below. Dynamic methods allow the continuous production of gas quantities [114] and also quick changes of the gas composition, which is necessary for a complex calibration.

ISO 6145 series describes the preparation of calibration gas mixtures using dynamic methods [115].

Table 1: Production of standard gas mixtures according to [114; 116].

Static		Dynamic	
Pressurized	Atmospheric pressure		
Gravimetric	Single rigid chamber	Gas stream mixing	
Partial pressure	Multiple rigid chambers		
Volumetric	Flexible chambers		

Gas stream mixing or flow dilution is a fundamental dynamic process for generating a standard gas mixture [116]. To achieve a desired concentration, flows of several single gases or gas mixtures at known rates are mixed. The gas flows can be produced by pressurized test gas cylinders, pressure controllers and flow restricting orifices or controlled leaks as well as electronically controlled by a mass flow controller (MFC). These techniques can also be combined with other methods like permeation or injection [116].

Lower concentrations or higher dynamic ranges can be achieved by multiple dilution stages [116]. A versatile method to bring a gas or liquid into a base gas stream is the injection with injection devices like pumps or mechanically driven syringes [116]. The continuous mechanically driven syringe injection is the most commonly used method, in which the gas or liquid is injected with constant rate into the base gas stream followed by a mixing chamber [117]. Substance mixtures can also be injected.

Test gases of organic components in the concentration range from a few $\mu\text{g}/\text{m}^3$ to several mg/m^3 can be generated with the permeation method [117]. A base gas stream is flowing through a temperature controlled permeation oven. In the permeation oven the organic substance is in an inert plastic tube, like PTFE, and is permeating through the walls of the tube at a constant and reproducible rate [116]. Each permeation tube can be gravimetrically calibrated for a specific temperature [116]. The loss of mass in the tube represents the mass of the permeating gas [116].

A very similar method is the gas generation by diffusion. For this, the permeation tube is replaced by a diffusion vessel with a capillary tube of accurately known dimensions containing the volatile liquid [117]. The diffusion vessel is placed in a temperature controlled chamber and the liquid evaporates. The vapor diffuses slowly through the capillary tube into the base gas stream. With the diffusion rate and the flowrate of the base gas stream, the vapor concentration can be calculated [116].

Some substances in gaseous phase tend to adsorb at surfaces and are difficult to prepare with the static or presented dynamic methods [117]. Therefore, the saturation method should be used. The simplest setup is the bubbling method. A base gas stream flows through a bubbler filled with the liquid target substance. A vessel is connected downstream to separate any aerosols that may be carried by the gas flow [117]. The

saturated vapor concentration can only be achieved with a sufficiently long contact time. To achieve a complete saturation, the bubbler can be controlled at a temperature T_1 and the saturated gas can be led into a condenser with a temperature T_2 , where T_2 is smaller than T_1 . With a high enough temperature difference a complete saturation can be ensured [117]. Evaporation can also be actively done in an evaporator with integrated heater. The liquid is added with a pump or syringe into the evaporator, which is flushed with a defined flow of carrier gas controlled with a mass flow controller. The heat evaporates the liquid, which is diluted by the carrier gas flow [118]. The concentration can be controlled by the ratio of carrier gas and added liquid.

Gas generation through chemical reaction is another method. Examples are the generation of ozone or nitrogen oxide [119; 120] and also the generation of hydrogen [121; 122].

3.2.2.2 Gas Mixing Apparatus

Gas mixing apparatuses (GMA) are systems for dynamic generation of gaseous mixtures. At the Lab for Measurement Technology (LMT), there exist different GMAs which combine dynamic methods for gas generation, presented in Subsection 3.2.2.1. The GMAs are described in other publications [42; 43; 123]. They are operated with an automated sequence control software, called GRUpy [124]. GMAs at LMT use gas stream mixing. Different gas line modules are connected to a mixing chamber to generate a gas mixture. The carrier gas stream can be mixed from three gas lines which provide dry and humid zero air as well as nitrogen. The gas sensors can be characterized at reduced oxygen atmosphere by increasing the nitrogen concentration. Into the carrier gas stream different gases can be injected with further gas lines. These gases can be provided by different dynamic gas generation methods like flow dilution, permeation or saturation.

For generating trace gas mixtures in the range below 100 ppb, a clean carrier gas, i.e. zero air, is necessary. Zero air is generated from pressurized air by a zero air generator (GC Plus 15000 Zero Air Generator, VICI Inc.). It contains a multistage filtration to transform the incoming compressed air into zero air. A pressure swing adsorption dryer removes water vapor. A scrubber removes carbon dioxide, nitrogen oxide and ozone. In a final step, a high-temperature catalyzer removes carbon monoxide, hydrogen and hydrocarbons.

MFCs control the flows, which are based on a pressure difference between input and output. A mass flow sensor measures the flow, and a proportional valve with a closed-loop feedback controller controls it. Dry zero air and nitrogen are controlled with one MFC each to generate a carrier gas stream. Humid zero air is generated by the bubbling method. For this, again controlled by an MFC, dry zero air is brought in a wash bottle filled with HPLC (high performance liquid chromatography) grade water. The gas distribution in the water is optimized by a fritted glass filter to reach a high saturation state. The humid gas stream is flushed into a second wash bottle filled with glass wool to filter water drops. The two wash bottles are in a temperature controlled water bath at 20 °C. The temperature is cooler compared to the room temperature of 22 °C and this avoids condensation. This means that the maximum relative humidity at 22 °C is limited to 89 %, which corresponds to the full saturation at 20 °C.

Gases or gas mixtures from pressurized gas cylinders can be injected by single or two-stage dilution. For the single-stage dilution, the pressurized gas cylinder is connected with

a pressure regulator to the injection MFC, which controls the gas injection flow. For faster gas changeover, a 3/2-valve is placed between the MFC and the gas mixing chamber. The gas flow can be redirected to the exhaust to flush the gas line. For two-stage dilution, a predilution stage is placed between the pressurized gas cylinder and the injection MFC. The predilution stage contains one MFC for the target gas or gas mixture and a second MFC for carrier gas, normally dry zero air. The target gas is mixed with dry air in a mixing chamber, e.g. a long 1/16" stainless-steel tube for diffusion mixing. The gas mixture after the predilution stage is kept at an overpressure to achieve a pressure difference between input and output of the injection MFC. The pressure is controlled with an overpressure valve which vents to the exhaust. A single dilution gas line has a dynamic concentration range of 1:50 which can be increased with a predilution step to up to 1:125000³.

Substances with low vapor pressure that cannot be provided in pressurized gas cylinders are generated with the permeation method in the GMAs at LMT. A MFC with dry zero air or nitrogen flushes a permeation oven with one or more permeation tubes. The carrier gas with the permeated substance is kept at overpressure with an overpressure valve, like the predilution stage. The gas mixture is injected with another MFC into the main gas stream.

A different concept of gas mixing apparatus was developed at the Joint Research Centre (JRC) in Ispra, Italy. The concept and setup are described in detail in [125; 126]. This GMA is also based on different dynamic methods for gas generation. The special feature is an "O"-shaped ring-tube system as exposure chamber with reference measurement systems and a feedback loop for the concentration adjustment of numerous gaseous components. The GMA allows controlling numerous gaseous mixtures including benzene, toluene, m/p-xylene, ethane, propane, n-butane, n-pentane and ozone. All gases except ozone are generated based on the dynamic dilution principle, as described before, with MFCs and higher concentrated gas from pressurized gas cylinders injected into zero air. The concentrations of the gaseous components inside the ring-chamber are measured using a PTR-MS (proton-transfer-reaction mass spectrometer). The measured concentrations are processed in a specific LabVIEW software with multiple proportional-integral-derivative (PID) feedback loops to ensure the stability of the concentration.

Two MicroCal 5000 Umwelttechnik MCZ GmbH generators generates Ozone, which dissociate O₂ molecules with UV light. The resulting reactive O^{*} atoms combine with O₂ molecules and form O₃. The TEI 49C UV-photometer from Thermo Environmental Inc. controls the generated ozone. The software also controls the temperature, relative humidity and wind speed are. Humidified air is also generated with the bubbling method and an MFC. Temperature is controlled with a cryostat and wind speed by internal fans. Additionally, reference values are measured by a gas chromatograph with a photo ionization detector (GC-PID 955 from Syntech).

Richter et al. [117] developed a GMA at BAM (Bundesanstalt für Materialforschung und -prüfung) fully based on evaporation. Pure liquid substances of the individual component are filled into stainless-steel bottles, so that a sufficiently large gas space is retained above the surface of the liquid. Each stainless-steel bottle is placed in a thermally

³ Calculated for a carrier gas flow of 1000 ml/min. The injection and the pressurized gas cylinder MFCs have a maximum flow of 10 ml/min, the predilution MFC of 500 ml/min. The minimal opening for all MFCs is 2 %.

insulated alumina chamber, which can be temperature controlled with a Peltier element. The inert carrier gas nitrogen is brought via a capillary in the top of the substance bottle. The resulting gas mixture due to the evaporation flows out through a second capillary. The resulting gas mixtures of each bottle are mixed into a mixing chamber (desiccator) with purified and humidified air. The carrier gas is air filtered through activated charcoal, but no catalytic removal. Therefore, not all inorganic gases, like hydrogen or carbon monoxide, are removed. For a homogeneous gas distribution, the desiccator has an integrated ventilator. The flow through several bottles is controlled with one single MFC, which is split into sub-flows by the flow resistances of the capillaries to the bottles. The gas concentration of each substance can be controlled via the length of each capillary. For a faster change of the concentration, more than one MFC and mixing chamber needs to be used. This is described in Paper E (Section 4.3).

3.2.3 Design of Experiment

Design of experiment (DoE) is critical for calibration and a prerequisite for the success of a system in its final application. The calibration model in an artificial environment can be almost perfect, but it still fails in the field tests. Therefore, field tests are a crucial validation of successful calibration [127; 128]. One main issue hindering successful field tests is the lack of appropriate realistic DoEs for gas sensor systems in complex environments. DoE is in many works a vehicle to show the performance of new materials or data processing methods [44–54]. Such DoEs often consist of a few fixed concentration levels per gas. In this case, the sensor is exposed only to a single target gas at a time. The resulting data are easy to evaluate and understand in terms of sensitivity, selectivity and speed of response. But they usually do not represent complex real-world scenarios and are of little use for this purpose. Nearly every application requires selective, quantitative measurements in an ever-changing background of interfering gases, for example industrial fire detection [1; 2; 36], automatic ventilation flap control in automobile industry [77–79], air quality monitoring [10; 128], breath analysis [4; 5], detection of explosives [129] or nerve gases [130]. DoEs with single gases do not reveal any masking effects or other gas interactions altering the sensor response for these applications. In some publications, this is considered by performing calibration with gas mixtures [39; 48; 51; 52; 55–59]. These studies use for DoE between three and five fixed concentration levels for each gas. The usage of too few levels for the quantization of a continuous quantity or classification of different substances easily leads to overfitting. This is shown for regression models with artificial neural networks (ANN) and partial least squares (PLS) in [55] or for classification in [60]. Therefore, for successful field tests, a more sophisticated DoE is necessary. In Paper 3 (Section 4.2) the DoE based on random gas mixtures is presented.

3.2.4 Multivariate Data Evaluation

3.2.4.1 Data Evaluation Chain

The data evaluation chain contains several steps. Before starting the data evaluation, the data integrity needs to be checked. All signals in one cycle have to be annotated to the related observation. The dataset must be split into different subsets for model training, optimization of hyperparameters in a validation step and testing the final model

(Subsection 3.2.4.2). Known outliers have to be removed and missing data needs to be interpolated. In a preprocessing step, cycles can be smoothed, filtered or standardized. In the next step a dimensionality reduction takes place (Subsection 3.2.4.3). The aim is to reduce the number of signals per cycle through feature extraction and selection. Depending on the target regression or discriminant analysis (Subsection 3.2.4.4) can be done for quantification or classification in a training step. Performance metrics have to be selected, and the hyperparameters of the model can be optimized by using the validation dataset. The optimized model could be tested with the remaining test subset. For the data evaluation different software tools and frameworks like MATLAB (Statistics and Machine Learning Toolbox or Deep learning Toolbox) or Python (scikit-learn, Keras or TensorFlow) are available. At LMT, a MATLAB toolbox named DAV³E was designed [124; 131]. The aim was to optimize the workflow for the data evaluation of cyclic data. Further information about DAV³E can be obtained in Paper 4 (Section 4.2). A complete overview about statistical data evaluation and machine learning can be found in [132–134].

3.2.4.2 Resampling: Training, Validation and Testing

For creating a model with good generalization performance [135] the resampling of data, i.e., data splitting for training, validation and testing, is of underestimated importance.

Parameters of a classifier or regressor are fitted with the training subset. Hyperparameters for controlling the machine learning process are optimized with the validation subset. Using different subsets avoids overfitting⁴. Performance of the final model is assessed based on the test subset. Sometimes only a training and validation or training and testing subset is used for building a model. To simplify the explanations below, only one training and validation subset will be used.

There are different methods for data splitting. The *validation set approach* or *hold-out* method is the easiest way to split the data [132]. A randomly selected ratio of the dataset, for example 80 %, is selected for training and the rest, in this case 20 %, for validation. The problem of this method is that the resulting performance depends strongly on the selected observations for training and validation. That makes it difficult to tell whether the model generalizes well [132]. The reason is that the randomly selected subsets are not necessarily representative of the whole dataset. It is generally difficult to decide whether an observation is representative or not [134]. Especially for datasets with uneven class⁵ sizes or only a few observations, this random *hold-out* can lead to unclear and varying results.

One possibility to improve the method is *stratification*. In the case of classification, each class of the dataset is represented in the same ratio in the training and validation subsets [134]. For regression, it is not that simple, because with continuous data there are no clear classes. The continuous data has to be split into representative classes, e.g. sorted stratification [136]. For sorted stratification, the observations are sorted based on the target variables. Then, the sorted observations are split in k equal classes, or the target value range can be split in k ranges. The splitting can be for example equidistant or

⁴ “Models that contain more unknown parameters than can be justified by the data.“ [328]

⁵ Classes describe observations with the same target value.

another distribution. The observations are sorted into these classes. An alternative selection is based on the DUPLEX algorithm. Here, the two observations with the farthest target values are included alternating into the calibration and validation subset [137; 138]. When the desired number of observations for the validation subset is achieved, the remaining observations are put into the training subset [138].

A statistical method to mitigate the impact of the resampling selection is to repeat the process of *hold-out* with different randomized data splits, called *repeated hold-out* [134, p. 153]. However, this does not ensure that every observation is selected at least once for both the training and the validation.

A more sophisticated method is *cross-validation* [132, pp. 176–186; 134, pp. 152–154]. There are different *cross-validation* methods, like *leave-one-out cross-validation* or *k-fold cross-validation* [132, pp. 178–183]. *Leave-one-out cross-validation* has for N observations N repetitions. In each repetition one of the observations is iteratively used for validation and the other $N-1$ observations for training. After N repetitions each single observation was predicted for the validation and an average performance value can be calculated. A disadvantage is the high computing expense for large datasets. For *k-fold cross-validation* the dataset is split into k randomized or stratified subsets. In each of the k repetitions, one of the k subsets is iteratively selected for validation.

Another resampling method is *bootstrapping*, which is based on resampling with replacement. The resampled training subset have the same number of observations as the original dataset. Observations selected for validation are replaced in the training subset with other observations in the dataset that are not selected for validation. The resulting training or validation subsets have multiple instances of an observation. A more in-depth description of *bootstrapping* can be found in [139].

10-fold stratified cross-validation is often performed based on some publications [134; 140; 141] which tested bootstrapping against cross-validation methods. However, also 5- to 20-folds is typically used [134, p. 153]. In [140] bootstrapping shows low variance, but huge bias on some problems. However, there is often not much of difference between *k-fold cross-validation* and *bootstrapping* [142].

An extension of all described methods is *group-based* resampling. For example, a calibration of a gas sensor with a GMA, could include four consecutive observations for the same gas mixture. These four observations are not statistical independent and must be considered as one group. Therefore, if only two of these four dependent observations are left out from the training, it is nearly the same as if the same observation is used for training and validation. This would result in an overoptimistic estimation of the model performance [60]. Therefore, in a *group-based hold-out validation* or *k-fold cross-validation* not only one observation is assigned to the validation or training subset, but the whole group.

Moreover, a cascade of *cross validation* for validation and testing is possible and is called *nested cross validation* [143–145]. *Nested cross validation* is used for hyperparameter optimization and to avoid overfitting [146; 147]. For k, j -*fold nested cross validation*, the dataset is split into k outer folds. Each training subset of the outer fold is split into j inner folds as well for inner training and validation. Then, the inner model with the best performance (e.g. the lowest minimal error or variance) is applied to the outer test fold. A final model is created with the best outer fold model.

3.2.4.3 Dimensionality Reduction

The number of independent variables (i.e. raw sensor data) can be reduced by dimensionality reduction. The relevant information is extracted, and overfitting is avoided. There are different types of dimensionality reduction methods. They can also be applied in parallel or in series. They can be divided into feature extraction and feature selection methods.

Feature extraction can be performed manually or automated [148–151]. Manual feature extraction is also called feature engineering because knowledge about the field of interest is beneficial. Statistical features can be, for example, the mean, variance, skewness or kurtosis of the whole raw data of one observation (cycle) or only a part of the cycle [40; 152; 153]. By understanding the raw data, features based on physical models ("model-based features") can be extracted in addition to statistical features. Model-based features can be based on physical or chemical models of the sensors [41; 154]. Model-based feature extraction methods for MOS gas sensors are part of this thesis and described in the papers in Section 4.1.

Automated feature extraction is performed with methods like adaptive linear approximation (ALA), principal component analysis (PCA), best Fourier coefficients (BFC), linear discriminant analysis (LDA), best Daubechies wavelet (BDW) or autoencoders. A deeper view into automated feature extraction and its methods can be found in [124; 131; 148–151]. For MOS gas sensors in TCO the methods ALA, PCA and LDA are the most widely used automated feature extraction methods. ALA splits a cycle into linear segments with variable length. The algorithm presented in [151] extracts the mean and slope of each segment of the cycle, which is also implemented in the software DAV³E [124; 131]. The number of segments and the segment length is calculated automatically depending on the approximation error and/or the desired number of features. PCA is an unsupervised algorithm, which means that the algorithm needs no information about the targets. PCA helps to reduce highly correlated data to a smaller number of variables. These are called principal components, that collectively explain most of the variance in the original data [132, p. 374]. The orthogonal linear transformation transforms the data to a new coordinate system so that the first principal component direction is along the direction of the largest variance of the dataset. LDA is a supervised algorithm, which means that the algorithm requires the information about the observations, i.e. target values. LDA is used to create a linear classifier, but also for dimensionality reduction, which is considered here. The term LDA is often used as a synonym with Fisher's linear discriminant. Fisher's linear discriminant function optimizes the data projection so that the within-scatter (variance of the observations in a class) is minimized, while the between-scatter (distance between the group mean values) is maximized [155; 156, p. 215 ff.].

Feature selection is an approach to use only a subset of all available features. This is necessary if the number of features exceeds the number of observations. On the one hand to reduce overfitting and on the other hand to use all available features if it is technically not possible. There are different approaches for feature selection. They can be divided into three types: filter, wrapper and embedded methods [157]. *Filter-type feature selection* algorithms select features based on the feature importance. The feature importance is only based on a characteristic of the feature, like the feature correlation to

the target value or the feature variance. The model is trained only with the subset with the best performing features.

One drawback is that there is no feedback-loop back to the feature selection. *Wrapper-type feature selection* algorithms are methods which combine feature selection with model training. A model is trained with a feature subset and the performance is measured. In a next step, features are added or removed with a selection criterion. A feedback-loop enables the optimization of a selection criterion. The algorithm is repeated until a desired stopping criterion is fulfilled. In an *embedded-type feature selection* algorithm the feature selection is part of the model training. The model algorithm selects features based on its learning progress, e.g. the least absolute shrinkage and selection operator (LASSO) [158], regularized trees [159] or decision trees [160]. In the following, filter and wrapper methods will be discussed in more detail.

A filter-type feature selection requires a kind of ranking algorithm according to some criterion. *Pearson correlation* determines the linear relationship between a specific feature and the target values. The higher the correlation coefficient, the more important the feature. Another method for feature scoring is based on the *Relief* algorithm from Kira and Randell for two-class problems [161]. The idea behind the Relief algorithm is to estimate the importance of features based on the goodness of discrimination between two observations which are close to each other. For multi-class problems the Relief algorithm is extended to *ReliefF* [162; 163] and for regression to the *RReliefF* [163; 164] algorithm. Another feature selection is based on *Neighborhood Component Analysis* (NCA) which is a non-parametric function. NCA performs a linear transformation of the features with the aim of a new distance metric in the transformed space maximizing the prediction accuracy of a regression and classification algorithm [165–167]. For the partial least squares algorithm for regression (PLS regression or PLSR), there are different weighting criterions to select the important features. Wold et al. introduced the well-known variable importance on projection (VIP) parameter for PLS projections [168]. It is the weighted sum of squares of the PLS weights for each feature, considering the amount of explained variance by each PLS component [169, Ch. 4.6.3]. A detailed description can be found in Eriksson et al. [169, Ch. Appendix II]. An overview over different approaches can also be found in [170].

Wrapper-type feature selection combines iterative search algorithms and model performance evaluation [171]. The optimal way to find the model with the best performance is to calculate it with all possible combinations of features. Wrapper type selection methods tend towards overfitting because they involve training with different combinations of features. Therefore, a good validation procedure is necessary [160]. The space of feature subsets grows exponentially with the number of features [157]. The number of models to be computed can be reduced by heuristic search methods. The simplest case is the sequential feature selection. It can be distinguished between *sequential forward feature selection* and *sequential backward feature elimination* [172, p. 234 ff].

For the *sequential forward feature selection*, the performance criterion for each feature is calculated, and the best feature is selected. In the next step, the criterion for all possible two-dimensional vectors that contain the best feature from the first step and a second feature is calculated. The best two-dimensional feature vector is selected. In each further iteration, the feature which improves the model most will be added to the

selection. The algorithm ends when a stopping criterion is satisfied. The *sequential backward feature elimination* works backwards and therefore starts with training a model with all features. In each iteration, the feature with the lowest influence on the model performance is eliminated from the selection. Both methods have a similar limitation. The forward selection can not remove features after adding another feature [173]. Moreover, the backward selection has no possibility to reevaluate the usefulness of a feature after it has been removed [173]. To eliminate these limitations, there are algorithms that allow the addition and removal of features. Two of these algorithms are *sequential forward* and *sequential backward floating feature selection* methods [173].

A less computationally intensive method for *sequential backward feature elimination* is called *recursive feature elimination* (RFE), which is described by Guyon [174]. The RFE algorithm is based on the selection of a feature subset according to the top-down principle like the *sequential backward feature elimination*. In the first step, the classification or regression method is trained with the full feature set. According to the weighting factor of the used machine learning algorithm, one or more features with the lowest weighting are eliminated. The model training is performed again without these features. This is repeated iteratively until a predefined number of features or a certain accuracy is reached. This means that not so many feature combinations have to be tried out in comparison to sequential forward or backward feature elimination. Further, more than one feature at a time can be removed from the subset. Different combinations with machine learning algorithm exist. For classifications, combinations with support vector machines (RFE-SVM) [174] or with linear discriminant analysis (RFE-LDA) [175] are possible. Regression algorithms like support vector regression (RFE-SVR) [176] or partial least squares regression (RFE-PLSR) [177] can be combined with RFE. Other search methods can also be used such as best-first search, hill-climbing or beam search [160].

3.2.4.4 Regression

Machine learning algorithms can be divided into two different groups, classification and quantification. Both can be further divided into supervised and unsupervised methods, which means training with known or unknown targets. Since this work only aims to quantify gas concentrations with sensors calibrated in a gas mixing apparatus with known gas concentrations, supervised regression methods are used. An overview about different supervised and unsupervised methods for classification and quantification can be found in [132–134].

The linear regression aims to find a scalar expression between a response (or dependent variable) and one (simple linear regression, LR) or more (multiple linear regression, MLR) predictors (or independent variables). The most common estimator for linear regression is the (ordinary) least squares (OLS or LS) method. The idea behind the method is to reduce the sum of the squared errors between the target variable and the model prediction.

MLR requires statistically independent predictor variables, i.e. there is no correlation between any pair of them [178]. For numerous regression problems, however, this requirement is not satisfied. But there are extended regression methods which address this issue. A regression method based on PCA is the principal component regression (PCR), which is not to be confused with the SARS-CoV-2 polymerase chain reaction (PCR) test.

In a first step, a PCA is performed, and the non-correlated principal components (PCs) are used as the new independent variables. A regression with OLS is performed between the PCs and response values. The resulting regression coefficients are then transformed back into the original space. PCA is an unsupervised method, thus, if the target variable correlates with a direction of low variance in the dataset the performance of this method drops.

Wold et al. introduced a supervised method for transformation and regression which is called partial least squares regression (PLS regression or PLSR) [168]. PLSR is the most used regression in chemistry and technology [179]. PLSR transforms both the predictor variables and target variable(s) into new spaces before regression. Different algorithms exist for PLSR calculations, like SIMPLS [180] or NIPALS [181]. The algorithms allow the simultaneous modelling of several target variables and also to analyze data with numerous strongly correlated and noisy predictor variables [179].

There are further regression methods available. Examples are support vector regression (SVR) [182, Ch. 5], logistic [183] or Gaussian process [184] regression, which can also be fitted to non-linear problems. Linear and non-linear problems can also be fitted with neural networks [185] or regression trees [183] but these methods tend to overfitting.

The assessment of a regression requires a quality measure. There are different quality measures reported in literature [186]. The most common one for regression is the coefficient of determination or R^2 . It is a pure statistical measure which describes the proportion of variance for a dependent variable which is explained by the regression model. Also, the mean squared error (MSE) or the root mean squared error (RMSE) can be used as quality measure. The use of different quality measures is discussed in Paper 3 (Section 4.2.).

3.3 Indoor Air Quality

3.3.1 Fundamentals

A study of 44 U.S. cities in the 1960s [15] and the “National Human Activity Pattern Survey” (NHAPS) from 2001 [187] conclude that people in North America and Europe spend 90 % of a day indoors. This includes 60 % of the time in their homes [188]. In a 2018 YouGov survey, 16,000 homeowners in Northern Europe and North America were asked how much time they spend indoors. On average, it was only 66 % of the time during the day [189; 190]. Obviously, there is a mismatch between the reality and the assessment of people. Most people in the industrialized world spend almost all of their lifetime in an indoor location. Therefore, a good indoor air quality (IAQ) is necessary for a healthy and comfortable life.

“Research directed at indoor air pollution and its adverse health effects began in the late 1960s and early 1970s. Investigation in this area was subsequently stimulated by concerns that reduced ventilation of buildings for the purpose of energy conservation would increase pollutant concentrations and lead to adverse effects on health.” [15]. The relationship between indoor and outdoor air pollution was investigated [191; 192] and it is evident that the major factor of human exposure to many pollutants is the inhalation of indoor air [15; 193]. A bad IAQ with high pollutant load or outside the well-being zone of persons can have adverse health effects like fatigue, headaches, irritation of the mucosa

and eyes, skin rash – in sum known as the sick building syndrome (SBS) [12; 17; 194] – as well as long-term effects of genotoxic or carcinogenic pollutants. A better insulation of buildings for energy and climate reasons can have a negative impact on IAQ as air exchange rates are reduced to save costs [195]. *“Over 2 million disability adjusted life years⁶ (DALY) are annually lost in the European Union due to compromised indoor air quality, but this burden of disease can be reduced by adjusting ventilation, filtration of intake air and by controlling indoor sources”* [196]. Therefore, the determination and assessment of chemical contaminants in the air of indoor rooms is an important field for people’s health and well-being. Indoors means, according to DIN EN ISO 16000-1:2006-06 [197], all private living rooms, rooms in public buildings (e.g. hospitals, sports halls, libraries and restaurants), workrooms and workplaces in buildings that are not subject to regulations on hazardous substances and also interiors of motor vehicles and public transports. The IAQ is not only determined through the measurement of pollutants and hazardous substances in the air, but also of variables that are essential for human comfort. Therefore, IAQ contains several factors like temperature, humidity and air movement [12–14], carbon monoxide (CO), ozone (O₃), the radioactive radon, volatile organic compounds (VOC), like formaldehyde or benzene [13; 15–18]. Also, particles (PM_{2,5}, PM₁₀), mold and fungal spores, asbestos or synthetic mineral fibers are significant factors [13; 15; 17; 18] for IAQ. Since the variables for IAQ are diverse and a toxicological or health assessment is not always feasible, there are different assessment concepts in the World. In Germany, there are legally binding limit values, health-/hygiene-/toxicology-based guide and guideline values as well as statistical reference values which are shown in Table 2 [196].

For various substances, the German environmental agency (UBA, Umweltbundesamt) and the World Health Organization (WHO) published different assessment values (reference, guideline, guide and limit values). In Table 3 there is a list with a selection of different substances and their assessment values. Limit values only exist for a few substances like benzene, carbon monoxide or particles. Most values are guideline or guide values which are not legally binding and therefore are less monitored or there is no mandatory monitoring. There are also hygienic-based guideline values with indicative meaning. Indicator values like carbon dioxide (CO₂) or total VOC (TVOC) are also used for IAQ.

CO₂ concentration is an indicator for humanly emitted VOCs and other gases, and it is still used as an indicative IAQ parameter today [20]. Usually, the CO₂ concentration reached indoor itself does not have health effects or influence on human productivity [20]. The concept of CO₂ as indicator for humanly emitted VOCs is comparatively old and is based on a publication from Pettenkofer in the year 1858 [19]. He investigated the need for ventilation and assumed that the greatest influence are the different VOCs in air, which are responsible for observable odors. Often the Pettenkofer number of 1000 ppm CO₂ is mentioned as the limit for bad air. *“Although the Pettenkofer number is widely used, the significance of this indicator is not sufficiently clear from today’s point of view, as the situation indoors no longer corresponds to the conditions of housings at that time.”* [20].

⁶ “An attempt to measure the suffering caused by an illness that takes into account both the years of potential life lost due to premature mortality as well as the years lost due to a disease or health condition. One DALY represents the equivalent of the loss of one year of full health. Useful in comparisons across diseases and in setting national and international health priorities.” [328]

Therefore, UBA calls a 3-stage evaluation system for CO₂ (Table 3). Therefore, direct measurement of VOCs is desirable. VOCs are a group of over thousands of substances and more than 350 from them could be typically measured in indoor environments [21; 198]. In 1858 it was impossible and also today it is difficult to achieve. A second aspect is that indicative CO₂ measurement assumes, that the main source for odors and VOCs indoors are humans. However, not everyone emits the same amount of VOCs at every time and this does not cover other VOC sources. The variety of sources today is high, for example furniture, plastics or activities such as cooking or cleaning. Assuming that VOCs are a cause of poor IAQ, VOC must be measured directly, which is hardly possible given the available analytical methods and comes with well-known drawbacks like long sampling intervals and time needed for the analyses as well as high costs. However, health effects of individual VOCs on humans are also not clear and there are only guideline values for a few substances [199]. Therefore, the UBA defined a five level evaluation system for total VOC (TVOC) in Table 3 [199], based on the concept of Seifert [200]. It should be noted that the definition of TVOCs does not refer to all VOCs. It only refers to those VOCs which are measured with the analytical method defined in ISO16000:6 [201], by which, for example, formaldehyde or ethanol cannot be measured. The definition, distribution and measurement methods of VOCs are discussed in more detail in the next sections.

Table 2: Assessment concept for indoor air quality in Germany according to VDI 6022-3:2011-07 [202].

Assessment Concept	Definition	Comment
Reference value (Referenzwert)	Statistical state description; mapping of the indoor situation only at a specific time period for a defined indoor space under defined measurement conditions. [203]	Not based on health; not legally binding.
Guideline value (Leitwert)	<i>“Health-/hygiene-based assessment value for a substance knowledge about which does not suffice to derive a toxicology-based guide value.”</i> [202]	Not legally binding.
Guide value (Richtwert)	<i>“Toxicology-based value derived from suitable findings about the toxic effects and the dose-effect relationship of the substance in question.”</i> [202] Guide value I: <i>“The guide value I is the concentration of a substance in indoor air at which, within the framework of an individual substance consideration, no adverse health effects are to be expected according to the current state of knowledge, even in the case of lifelong exposure of sensitive persons.”</i> [199] Guide value II: <i>“The guide value II represents the concentration of a substance in the indoor air, which, if reached or exceeded, requires immediate action, as this concentration is likely to endanger the health of sensitive persons, including children, especially if they stay in the rooms for a long time.”</i> [199]	Not legally binding but may acquire legal significance.
Limit value (Grenzwert)	<i>“Legally specified assessment value to be observed; any value must be sufficiently less than the limit value.”</i> [202]	Legally binding; legislative or administrative limit values.

The awareness of clean air and low emission of hazardous substances from, for example furniture, building materials or toys is rising. For low emission materials or furniture several labels with governmental assistance were introduced, like *Blauer Engel* [204] in Germany, *Indoor Climate Label* [205] in Denmark and Norway, *M 1-Emission Classification of Building Materials* [206] in Finland or the *Émissions dans l'air intérieur* [207] in France. Also, some labels from the private sector, like the *Eco Institut-Label* [208] or *natureplus* [209] in Germany have been established.

Outdoor air monitoring of particulate matter, nitrogen oxides and ozone have also become common practice, especially in Europe, as there are clear limit values for these pollutants [210].

In contrast, continuous monitoring in indoor air is not widely established. In the past, measurements were usually taken only based upon reasonable suspicion to verify guide and guideline values, due to the expensive and slow analytical measurements. As the awareness of clean indoor air is increasing and the well-being and health also affects the productivity of people, clean air and monitoring IAQ in buildings is gaining importance. The *WELL Building Standard* of the International WELL Building Institute [211] was established, which, among other things, provides requirements and recommendations for continuous IAQ monitoring [212].

One method for improving indoor air quality is optimized ventilation. Nowadays, there are two established concepts for controlling mechanical ventilation. One concept is that the systems deliver a continuous flow of fresh air to generate a constant air exchange in the room, the constant air ventilation (CAV). The other concept is the controlled mechanical ventilation, either with a manual control, i.e. user-controlled or demand-controlled ventilation (DCV). DCV can be a cost- and energy-efficient alternative to CAV [213; 214] and can also be profitable [214]. A special case is the sensor-based DCV (SBDCV). The SBDCV is not standard yet but rather a niche market. In 1998, for Fisk et al., key constraints are the high price of CO₂ sensors, the fact that CO₂ sensors do not respond to indoor pollution and inadequate performance of many VOC sensors [213]. For offices and meeting rooms with several people some newer studies showed an improved air quality with SBDCV in schools or office spaces in parallel with energy savings [215; 216]. In both studies the ventilation was controlled based on CO₂ measurement and Mysen et al. [216] compared CO₂-DCV with infrared (IR) occupancy DCV. The results show that IR-DCV is cheaper, but CO₂-DCV saved more energy.

Table 3: Example of assessment values of substances/sum values in indoor air.

Substance or Sum Values	Assessment Values
Carbon dioxide (CO ₂)	<u>(Hygienic) guideline⁷ values (UBA)</u> [20]: <ul style="list-style-type: none"> (1) < 1000 ppm: harmless (2) 1000–2000 ppm: elevated (3) > 2000 ppm: unacceptable
Carbon monoxide (CO)	<u>Guideline values (WHO/UBA)</u> [217]: <ul style="list-style-type: none"> • 80 ppm for 15 min • 28 ppm for 1 h • 8 ppm for 8 h • 5.6 ppm for 24 h <u>Limit Value (39. BImSchV and 2008/50/EG)</u> [210; 218]: <ul style="list-style-type: none"> • 10 µg/m³ (8 ppm) for 8 h
Particles (PM _{2,5})	<u>Guideline values (UBA)</u> [219]: <ul style="list-style-type: none"> • 25 µg/m³ 24-hour mean without any absence of indoor specific dust sources. <u>Guideline values (WHO)</u> [220]: <ul style="list-style-type: none"> • 10 µg/m³ annual mean. • 25 µg/m³ 24-hour mean. <u>Limit Value (39. BImSchV and 2008/50/EG)</u> [210; 218]: <ul style="list-style-type: none"> • 25 µg/m³ annual mean.
Particles (PM ₁₀)	<u>Guideline values (WHO)</u> [220]: <ul style="list-style-type: none"> • 20 µg/m³ annual mean. • 50 µg/m³ 24-hour mean. <u>Limit Value (39. BImSchV and 2008/50/EG)</u> [210; 218]: <ul style="list-style-type: none"> • 40 µg/m³ annual mean. • 50 µg/m³ 24-hour mean.
Total VOC ⁸ (TVOC)	<u>Reference</u> [199] and/or <u>(hygienic) guideline⁷</u> [221] <u>values (UBA)</u> : <ul style="list-style-type: none"> (1) ≤ 0.3 mg/m³: No hygienic objections, target value. (2) 0.3-1.0 mg/m³: No relevant objections, but increased ventilation recommended. (3) 1.0-3.0 mg/m³: Concerning hygienic aspects, some objections due to elevated concentration level. Upper range for a maximum of 12 months. Search for sources, increased ventilation recommended. (4) 3.0-10 mg/m³: Major objections. Should not be tolerated for > 1 month. Restricted use only. Search for sources, intensified ventilation necessary (5) ≥10 mg/m³: Situation not acceptable. Use only if unavoidable and then for short periods (hours) only with intensified ventilation.

⁷ „Hygienic guide values are determined when practical experience has demonstrated simultaneous increase of the likelihood of complaints and adverse health effects with the concentrations of an indoor air pollutant, but for which the state of knowledge is lacking to derive a toxicologically based indoor air guide value only.“ [329]

⁸ „The toxicologically derived indoor air guide values take precedence over the TVOC scheme.“ [329]

Substance or Sum Values	Assessment Values
Toluene (C ₇ H ₈)	<u>Guide Value I (UBA)</u> [222]: <ul style="list-style-type: none"> • 0.3 mg/m³ (73 ppb) <u>Guide Value II (UBA)</u> [222]: <ul style="list-style-type: none"> • 3 mg/m³ (730 ppb)
Xylene (C ₈ H ₁₀)	<u>Guide Value I (UBA)</u> [222]: <ul style="list-style-type: none"> • 0.1 mg/m³ (21 ppb) <u>Guide Value II (UBA)</u> [222]: <ul style="list-style-type: none"> • 0.8 mg/m³ (170 ppb)
Benzene (C ₆ H ₆)	<u>Preliminary guideline value (UBA)</u> [223]: <ul style="list-style-type: none"> • 4.5 µg/m³ (1.4 ppb) <u>Limit Value (39. BImSchV and 2008/50/EG)</u> [210; 218]: <ul style="list-style-type: none"> • 5 µg/m³ (1.5 ppb) mean over one year
Formaldehyde (CH ₂ O)	<u>Guide Value I (UBA)</u> [224]: <ul style="list-style-type: none"> • 0.1 mg/m³ (80 ppb) <u>Guideline value (WHO)</u> [217]: <ul style="list-style-type: none"> • 0.1 mg/m³ (80 ppb)
Limonene (C ₁₀ H ₁₆)	<u>Guide Value I (UBA)</u> [225]: <ul style="list-style-type: none"> • 0.2 mg/m³ (32 ppb) <u>Guide Value II (UBA)</u> [225]: <ul style="list-style-type: none"> • 2 mg/m³ (320 ppb)
Ozone (O ₃)	<u>Guideline value (WHO)</u> [220]: <ul style="list-style-type: none"> • 0.1 mg/m³ (47 ppb) mean value over 8 h

3.3.2 Volatile Organic Compounds

Volatile organic compounds (VOCs) are a group of chemical substances which do not have a distinct definition. In general, VOCs are organic substances with a high vapor pressure or low boiling point. The general definition is often narrowed down by excluding certain species or classes according to other criteria than volatility, like the source of emission or measurement method. In Table 4, there are different definitions of VOCs.

The German directive defines VOCs by their vapor pressure or volatility and the creosote fraction [218]. ISO16000:6 defines VOCs by the measurement method [201]. This implies that all substances separated by gas chromatography using a 5 % phenyl 95 % methyl polysiloxane capillary column and all organic substances eluting between and including n-hexane and n-hexadecane are VOC. All substances eluted before n-hexane are classified as very volatile organic compounds (VVOCs). All after n-hexadecane are classed as semi-volatile organic compounds (SVOCs).

The EU directive defines VOCs as all organic compounds and, among other things, according to their source, e.g. human activities [226] or from anthropogenic and biogenic sources [210]. There is a high number of other definitions in literature or directives. In

most cases, CH_4 is excluded from the group of VOCs which is therefore sometimes called non-methane volatile organic compound (NMVOC).

Table 4: Different VOC definitions in standards or EU directives. This shows that the definition of VOCs is not clear and unique.

Substance or Sum Values	Definition
31. BImSchV [227]	An organic compound having a vapor pressure of 0.01 kilopascal or more at 293.15 Kelvin or having a corresponding volatility under the respective conditions of use. The creosote fraction that exceeds this vapor pressure at 293.15 Kelvin or has a corresponding volatility under the respective conditions of use is considered a volatile organic compound.
ISO16000:6 2020-08 [201]	<u>VVOC</u> : Organic compound eluting before n-hexane on a gas chromatographic column specified as 5 % phenyl 95 % methyl polysiloxane capillary column <u>VOC</u> : Organic compound eluting between and including n-hexane and n-hexadecane on a gas chromatographic column specified as a 5 % phenyl 95 % methyl polysiloxane capillary column. <u>SVOC</u> : Organic compound eluting after n-hexadecane and up to and including n-C30 on a gas chromatographic column specified as a 5 % phenyl 95 % methyl polysiloxane capillary column.
EU directive 2001/81/EC [226]	Volatile organic compounds and VOC mean all organic compounds arising from human activities, other than methane, which are capable of producing photochemical oxidants by reactions with nitrogen oxides in the presence of sunlight.
EU directive 2008/50/EC [210]	Volatile organic compounds (VOC) shall mean organic compounds from anthropogenic and biogenic sources, other than methane, that are capable of producing photochemical oxidants by reactions with nitrogen oxides in the presence of sunlight;

The group of VOCs contains more than ten thousand different substances which can be found in low concentrations, i.e. in the range of parts per billion or below, as trace gases in the atmosphere. Contrary to other gases in the clean atmosphere (Table 5), VOCs occur only as trace gases. They are, despite their concentration being very low, the “fuel” for the oxidative atmospheric photochemistry [228]. Most VOCs are emitted into the atmosphere from biogenic sources, often from flora with high emission of isoprene, terpenes or pinene [229]. Large quantities of VOCs are also emitted into the atmosphere from anthropogenic sources (generated by humans) every day [230]. The typical emitters are the use of fossil fuels for transport, the production of consumer goods and various industrial processes [230].

Almost everything the humanity do in their daily lives results in emission of VOCs into the atmosphere. There are emissions of VOCs from consumer products (e.g. cleaners or solvents) [231; 232], personal care products (cosmetic and hygiene products) like shampoo, shower gel, soaps or conditioner [233; 234], building materials like floor and wall coverings, paint, insulation or carpet [231; 235] or processes like smoking, cooking or fireplace combustion [15; 236–238] and so on. Therefore, more than 350 different VOCs can be typically found in indoor rooms in measurable concentrations [21; 198]. A

major problem is that most studies are based on measurements according to ISO16000:6 [201]. This standard has a very strict definition of VOCs based on the analytical method described before. This means, the sum of VVOCs, VOCs and SVOCs according to this standard does not correspond to the sum of all known VOCs. Salthammer notes and criticizes that VVOC is “*an understudied class of indoor air pollutants*” [239] and that there is no clear definition for it [239]. This lack of knowledge is not caused by the absence of interest for broader VOC measurements. It is rather the lack of fully comprehensive analytical methods.

Table 5: Concentration of gases in clean atmospheric.

Substance	in %	Substance	in ppm _v	Substance	in ppb _v
Nitrogen (N ₂)	78.08 [240, p. 8]	Carbon Dioxide (CO ₂)	407.8 [241]	Hydrogen (H ₂)	500 [242]
Oxygen (O ₂)	20.95 [240, p. 8]	Neon (Ne)	18.2 [243, p. 13]	Nitrous oxide (N ₂ O)	331 [241]
Water vapor (H ₂ O)	0 – 5 [240, p. 8]	Helium (He)	5.2 [243, p. 13]	Carbon monoxide (CO)	100 – 300 [244]
Argon (Ar)	0.93 [240, p. 8]	Methane (CH ₄)	1.9 [241]	Xenon (Xe)	87 [243, p. 13]
		Krypton (Kr)	1.1 [243, p. 13]	Ozon (O ₃)	10-60 [245]

VOCs in a general definition can be subdivided into different chemical classes: Alcohols, aldehydes, alkanes, aromatics, esters, ketones, terpenes, organic acid and others. The previously mentioned chemical classes are those found in studies [21; 198] with the highest P90 and P95 concentration. In Table 6 the 90th (P90) and 95th (P95) percentile sum concentration in $\mu\text{g}/\text{m}^3$ and ppb and the representative substance with the highest concentration for this chemical class are shown. Ethanol, the substance with the highest concentration found in the class of alcohols. It is emitted during fermentation of sugary and starchy foods (e.g. from dough or alcoholic drinks), during cooking [246; 247], household and consumer products (e.g. perfume, deodorant or detergent) [248; 249] but also increasingly from disinfectants during the COVID-19 pandemic [250]. Formaldehyde is emitted from wood-based materials (e.g. plywood or chipboard), flooring, furniture, textiles or smoking [251]. It can also be a product from terpene/ozone reactions in summer [252]. n-hexane, n-heptane and toluene are often found as solvents for coatings, printing inks and adhesives [239; 252; 253]. n-hexane and toluene can also be associated with outside sources such as fossil fuel combustion or power plants [252]. Ethyl acetate and acetone are mainly found as solvents in various products like nail polish remover or oil paint [248; 249]. Acetone can also be emitted through exhaled breath [239]. α -pinene emits mainly from wood-based materials, especially pine wood. Limonene and other terpenes are typically used for a “fresh” smell in cleaning products and detergents, cosmetics, shower gel and shampoo [248]. Acetic acid is emitted from decomposition of wooden buildings [247; 254] and during cooking or from foods like vinegar [246].

Table 6: 90th (P90) and 95th (P95) percentile sum concentration in $\mu\text{g}/\text{m}^3$ and ppb (calculated from the individual substances dominating for each chemical class) for the eight chemical classes with the highest sum concentrations as determined from analytical studies [21; 22; 198]. The substance in parentheses is the representative with the highest concentration for this chemical class. [Paper 6]

Chemical class (Representative)	P90 in $\mu\text{g}/\text{m}^3$ (ppb)	P95 in $\mu\text{g}/\text{m}^3$ (ppb)
Alcohols (Ethanol)	320 (~170)	520 (~790)
Aldehydes (Formaldehyde)	340 (~270)	480 (~390)
Alkanes (n-Hexane, n-Heptane)	180 (~50)	350 (~90)
Aromatics (Toluene)	190 (~50)	370 (~90)
Esters (Ethyl acetate)	140 (~30)	280 (~70)
Ketones (Acetone)	250 (~100)	420 (~170)
Terpenes (Limonene, α -Pinene)	170 (~30)	330 (~60)
Organic acid (Acetic acid)	150 (~60)	240 (~100)

Wallace investigated the personal exposure to 25 different VOCs in Los Angeles (California, USA) [255]. He showed that the personal exposure is higher than the indoor air concentrations, which were in turn greater than the outdoor concentrations. He concludes that personal activities account for a large part of the total exposure. But it also depends strongly on the investigated substances. As the examples of the most common substances mentioned before show, many of them are emitted during human activities. The studies measured according to ISO16000:6 the average pollution of indoor rooms without this human factor. Therefore, short time events and human influence are not considered, which, however, would be necessary for a comprehensive analysis of indoor air quality. Larger studies on the real-time VOC pollution measurements with human presence and activities are a blind spot in the literature. Only real-time measurements for short periods of time in single houses are possible due to the high instrumentation effort. One example is a study in a single home which monitored 200 VOCs during eight weeks in summer and five in winter with a proton-transfer-reaction mass spectrometer (PTR-MS) [247]. It is found that in the investigated “*80-year-old, wood-framed single-family residence in California, the building materials and furnishings dominate for most measured VOCs, with a surprisingly large contribution from what appears to be wood decomposition*” which leads to a high VOC baseline [247]. The most important source of emissions indoors is cooking which appears as a short-term spike and “*outdoor air is relatively unimportant as a contributor to indoor air VOC levels at this site*” [247].

3.3.3 VOC Measurement

Measurements for the determination of VOC pollution normally imply analytical sampling methods, which are described in the ISO16000 series. This means that the indoor air is sampled with sorption tubes in-situ and later analyzed in a laboratory. The most common material for sorption tubes is Tenax TA®, a porous polymer based on 2,6-diphenyleneoxide. The sorption tube is desorbed thermally in the laboratory, VOCs are separated by gas chromatography (GC) and measured with mass spectrometry (MS) with or without an additional flame ionization detector (FID).

The measurement procedure is defined in ISO 16000-6:2021. Tenax TA® is used to measure VOCs as it can sample “*all organic compounds eluting between and including n-hexane and n-hexadecane on a gas chromatographic column specified as a 5 % phenyl 95 % methyl polysiloxane capillary column*” [201]. Compounds eluting after n-hexadecane (SVOC) can also be measured with the same methods.

For the compounds eluting before n-hexane (VVOC) carbon black sorbents, like Carbopack X® or Carbograph 5 TD® are recommended in ISO 16000-6:2021. The carbon black sorbents can also be thermally desorbed and analyzed with GC-MS or GC-MS-FID. Not all VVOC can be measured with this method. Not all carbonyl-compounds in the group of VVOCs like ketones or aldehydes are adsorbed sufficiently on standard porous polymer-based sampling materials like Tenax TA® or carbon black and therefore are not found in the analysis with these methods. This is the reason why VVOCs are an understudied class in the field of indoor air [239]. The best known and studied substance among aldehydes is formaldehyde. Formaldehyde can be sampled with DNPH (2,4-dinitrophenylhydrazine) tubes and analyzed with high-performance liquid chromatography (HPLC) and an ultraviolet (UV) absorption detector. The method is described in ISO 16000-3:2021 for formaldehyde and recognized for at least 12 other aldehydes.

Some special substances also need other sorbents or analytical methods. For the detection of very low benzene concentrations, Tenax TA® suffers from high blind values because of benzene artifacts formed by the material over time. Therefore, a second measurement with a carbon black sorbent is necessary. Depending on the method and goal of measurement passive or active sampling is used. Passive sampling is based on diffusion and is often used for long-term sampling and to control long-term limit values like for benzene or formaldehyde, as described in ISO 16000-4:2012 or measured in [256]. For active sampling in ISO 16000-6:2021 a defined volume of indoor air is pumped through the sorbent tube, depending on the expected concentrations and sorbent material.

In research, other sorbent materials like metal-organic frameworks (MOF) [257] or gas chromatograph with other detectors like electron ionization time of flight mass spectrometer (EI-TOF-MS) [258] are also sometimes used for a higher resolution and lower detection limits. Most analytical methods have in common that they are based on sampling that needs several minutes on site for a measurement, have to be analyzed afterwards in the laboratory and are therefore cost-intensive.

Analytical in-situ real-time measurements nowadays are possible with new technology and methods. In 1995, Hansel et al. introduced the proton-transfer-reaction mass spectrometry (PTR-MS) for online trace gas analysis at ppb level [259]. This enables real-time studies in-situ. But only molecules with a proton affinity higher than water can be detected. To improve this, the use of other ions can extend the substance spectrum [260]. Also, the combination with time-of-flight mass spectrometry (TOF-MS) can improve the performance [261]. However, PTR-MS requires a high equipment effort, is expensive and has various other disadvantages. One is the challenging calibration because the reaction rate constants for many relevant compounds are still unknown [262]. Hence, only a few studies are done with PTR-TOF-MS [247] or with GC-TOF-MS [258]. An overview about the possibilities and limitations of the PTR technique in this field of research is presented in [262].

There are other non- or less analytical systems for in-situ measurement of VOCs. One option are mobile GCs with a PID (photoionization detector), e.g. the Dräger X-pid® 9000/9500 (Dräger Safety AG & Co. KGaA) or the meta GC-PID III (meta Messtechnische Systeme GmbH). Selective measurement of a range of gases in-situ is possible with these systems, but not as complete as a VOC screening with TD-GC-MS systems. Those systems are cheaper than laboratory equipment, but still cost more than 10,000 €.

The sum of VOCs is often measured with single PID systems without GC in industrial safety. These systems are cheaper than analytical and mobile GC systems, but still not suitable for the mass market. As described in Subsection 3.3.1, indoor air quality, of which VOC is an important aspect, is gaining importance and awareness for it is rising. Therefore, cheaper sensors, suitable for every single room, are needed. MOS gas sensors are suitable in terms of sensitivity for VOC measurements in indoor air and, therefore, several companies designed small sensors with application-specific integrated circuits (ASIC) [6–9] for VOC measurement and IAQ assessment. This thesis discusses especially VOC measurements with MOS gas sensors in the lab and the field based on temperature cycled operation to extend and overcome the drawbacks of the available MOS gas sensors.

4 Results

4.1 Metal Oxide Semiconductor Gas Sensors in Temperature Cycled Operation

4.1.1 Synopsis

The benefits of temperature cycled operation (TCO) have been known for a long time and were first reported in 1974. More information from a single MOS gas sensor can be obtained by TCO. Despite this, TCO has almost only been used in research so far. Only a few manufacturers are currently starting to introduce gas sensors with TCO to the market. The possibilities to design a TCO with different shapes, durations or temperatures, are infinite. The choice of the right TCO for an application is not easily made. Understanding and knowledge of the sensor in TCO is necessary to decide for an appropriate cycle. In the literature, as summarized in Subsections 3.1.2 – 3.1.4, the gas sensing mechanism of a MOS gas sensor is described completely from a chemical or physical perspective. Experimental MOS gas sensors, which are manufactured for research only, e.g., to test a new material or dopant, are predominantly studied in static operation. The sensitive layers are usually not deposited on membrane micro-hotplates, but on heaters with larger thermal masses. This macro structured design is necessary, for example, to analyze the surface processes or the reaction products using chemical or physical methods. The results cannot be easily applied to commercial (micro-)sensors. Many application-specific questions about the appropriate combination of sensor and TCO remain unanswered from an engineering perspective. Applications typically require measurement rates between seconds and a few minutes so that only short temperature cycles are possible. The papers in this section provide a model for the AS-MLV (ScioSense B.V.), a commercial SnO_2 -based MOS gas sensor, in TCO.

All TCOs in the following papers are based on quick steps from one high ($400 - 450^\circ\text{C}$) to several low temperatures ($75 - 350^\circ\text{C}$) with different durations of the constant temperature phases, which is described in Paper A and B. At the end of the high temperature plateau, the sensor is near equilibrium and the surface is covered with a high concentration of ionosorbed oxygen (or another dominant species, c.f. Subsection 3.1.3). For micromachined membrane MOS gas sensors, like the AS-MLV, with a thermal time constant of a few microseconds, the surface states remain (nearly) constant during such a temperature change. If a fast temperature change to a low temperature occurs, the conductance decreases mainly due to the temperature change. The sensor is in a non-equilibrium state with a considerably higher surface coverage compared to the equilibrium state at low temperature. The relaxation of these non-equilibrium states to equilibrium states goes along with different coupled physical and chemical processes. Due to the dominant relaxation caused by the reaction of ionosorbed oxygen with reducing gases, the state at low temperature is very sensitive to these gases.

Paper A is the result of the author's bachelor thesis and is the basis for all subsequent papers. It contains a brief description of the model for the AS-MLV in TCO for low concentration of VOCs including the study of two gases, ethanol and benzene, in a concentration range from 10 to 1000 ppb. The sensor in TCO has an 800 times higher signal towards 1000 ppb ethanol in that very sensitive state during relaxation compared

to the signal in equilibrium at 140 °C. This very high signal difference results from the dominant reaction with the high amount of chemisorbed oxygen with ethanol. It is physically derived and experimentally shown that during a short time interval after the temperature change, the relaxation of the logarithmic conductance can be described using a linear approximation. The slope of the linear approximation is proportional to the reaction rate of ethanol with ionosorbed oxygen. The reaction rate depends on the substance, its concentration and the reaction temperature. For single-step reaction, a linear relation between the concentration and the rate constant can be seen. Due to the reaction rate depending on these factors, substances can be distinguished by measuring at several temperatures. The different signal curves for one cycle are shown for concentrations between 10 and 1000 ppb ethanol and benzene. The different shape of temperature and reaction rate curves of ethanol and benzene is illustrated. Benzene has a maximum in its reaction rate at approximately 275 °C, with a sharp decrease above and below this temperature. Ethanol has no clear maximum and a nearly constant reaction rate at all temperatures. The simple model for the AS-MLV in TCO has been successfully validated.

In Paper B the simple model is described more deeply and applied to a novel approach towards calibrated measurement of trace gases using MOS gas sensors. Quantification based on the reaction rate of the model is explicitly described in the form of superposition of more than one substance in the atmosphere. An estimation of the conditions when desorption dominates over adsorption is done, which is the assumption for the model. For field calibration, a reproducible, adjustable calibration method based on the equilibrium vapor headspace over a liquid solution of toluene and squalane in the range from 10 ppb to 600 ppm is described and tested in a range from 10 ppb to 10 ppm. The toluene concentration dependence does not follow a linear curve but a power law. This may be due to the more complex reaction of toluene (compared to the single-step reaction of ethanol) and the much larger concentration range. Squalane also acts as a filter and binds a large fraction of other VOCs in the atmosphere, thereby generating a reproducible almost VOC-free background. The headspace concentration of the calibration sample is calculated by an estimation with the UNIFAC (Universal Quasichemical Functional Group Activity Coefficients) model and Henry's law. The concentration inside the calibration samples is verified via GC-MS and the sensor reaction is compared to measurements in the GMA. A differential measurement is necessary to calculate the reaction rate of toluene against the background atmosphere for the calibration method. This is implemented with a squalane sample without toluene to generate a virtual null signal. Another result of the paper is that the quantification with the rate constant shows a constant value directly after a gas change. In contrast, the raw signal (conductance) has a run-in behavior after the concentration change.

A further amendment of the model and a model-based description of the influence of siloxane poisoning is shown in Paper ii. Siloxane causes an irreversible change of the sensor surface. Reason for that is the slowing down oxygen adsorption and reaction with reducing gas. The behavior of the sensor at high temperature and the readsorption of oxygen as a measure of surface reactivity are described. Paper iii describes the possibility to compensate the poisoning effects due to siloxane exposure on the sensor. Schultealbert investigates and describes this effect and compensation more deeply [263], which resulted in Patent ii.

Paper 1 describes a novel method for the detection of short trace gases pulses with MOS gas sensors based on the model-based TCO and the reaction rate. For this purpose, the time-dependent slope of the logarithmic conductance when the sensor is exposed to a gas pulse during the low temperature step is evaluated. For comparison, in the previous paper with constant gas supply within a cycle, the constant slope of the logarithmic conductance during relaxation at low temperature was evaluated.

Here the logarithmic conductance is an integrating signal, so the integrated rate constant over time is evaluated. Therefore, the dose (concentration times duration) is proportional to the logarithmic conductance change from the start and end point of the gas pulse. Gas pulses with concentrations from 1 to 1000 ppb and durations of 1 to 10 s are supplied to an AS-MLV, with doses between 1 and 5000 ppb s. The integral signal is independent of concentration between 1 and 1000 ppb and depends solely on the dose. For doses from 1 to 500 ppb s the integrated rate constant is nearly directly proportional to the dose. At higher doses, the integral deviates slightly from the linear characteristic. This is because the assumption of a linear approximation during the low temperature phase no longer applies and other effects, e.g., readsorption of oxygen, play a measurable role. It is estimated using FEM simulations that the sensor consumes or reacts at most 1.6 % of the injected gas quantity. Therefore, the detection limit would be approximately 47 fg. This shows the strengths, but also limitations of the model.

An implementation of the method in the application of leakage detection is shown in patent i. Thereby, a test object filled with tracer gas (e.g. reducing gases) is placed in a chamber and flushed with clean air. If there is a leak, the test fluid emits into the chamber during the subsequent accumulation time. The air from the chamber is extracted and is passed over a sensor. The sensor is previously operated in clean air at high temperature and when the air from the chamber is approaching, it is switched to low temperature. The air from the chamber is passed over the sensor as a gas pulse. This allows small leakages to be measured.

Paper C shows quantification and identification techniques of reducing gases over a wide concentration range using a MOS gas sensor in TCO. The substitute for the AS-MLV, the AS-MLV-P2, is used as sensor. The structure and material composition of both sensors are very similar; therefore, the method can be applied to the new sensor. As described before, the linear approximation only applies to a certain dose and cannot be applied to an unlimited range of concentration. Instead, the calculated time constant of the relaxation process at low temperature is used. This is an advanced method for higher concentration. The time constant of relaxation is calculated as the point of time to reach 63.2 % of the difference between the minimum and maximum during the low temperature step. Hence, no approximation function is needed. Both methods (linear fitting and time constant) are tested with four different substances (carbon monoxide, hydrogen, ammonia and benzene) over a wide concentration range from 10 ppb to 100 ppm. The time constant also follows the concentration in the form of a linear function except for benzene. For benzene, the time constant follows the concentration in the form of a power law, probably due to the multistage reaction process.

A simple model for a commercial sensor, the AS-MLV, in TCO has been successfully validated and exploited in different aspects within the presented papers. All papers show

the advantages of model-based evaluation. In summary, the following key results are achieved:

- With the special shape of the cycle, sensor sensitivity increases for ethanol by factor 800 compared to static operation.
- The rate constant of the reaction of the reducing gas with the sensor can be estimated via a linear approximation of the logarithmic sensor conductance after the temperature change.
- The rate constant is dependent on temperature, substance and concentration. Therefore, it is a good parameter for discrimination of gases.
- The rate constant is related to the concentration in the form of a linear or power function, depending on the substance and the concentration ranges.
- The logarithmic conductance of the sensor, at the low temperature phase, shows a dosing effect. Thus, this enables the quantification of gas pulses.
- The linear approximation assumption is limited and applies only to a specific maximum concentration or dose.
- For a wide concentration range, a second parameter, the time constant of relaxation, can be used. It also correlates with the concentration.

4.1.2 Paper A – Optimierung des temperaturzyklischen Betriebs von Halbleitergassensoren

Tobias Baur, Andreas Schütze and Tilman Sauerwald
Saarland University, Lab for Measurement Technology, Saarbrücken, Germany

tm - Technisches Messen (2015), 82 (4), 187-195

The original paper can be found, in the online version, at <https://doi.org/10.1515/teme-2014-0007>.

© Used with permission of Walter de Gruyter and Company, from Optimierung des temperaturzyklischen Betriebs von Halbleitergassensoren, Baur, Tobias; Schütze, Andreas; Sauerwald, Tilman, 82, 4, 2022; permission conveyed through Copyright Clearance Center, Inc.

Beiträge

Tobias Baur*, Andreas Schütze und Tilman Sauerwald

Optimierung des temperaturzyklischen Betriebs von Halbleitergassensoren

Optimization of temperature cycled operation of semiconductor gas sensors

Zusammenfassung: Wir stellen ein Verfahren zur Optimierung des temperaturzyklischen Betriebs (TCO, *temperature cycled operation*) im Hinblick auf Sensorsignal, Sensitivität und Selektivität vor. Dieses basiert auf der Grundlage eines Sensormodells unter der Annahme, dass die Leitwertänderung durch die Besetzungsänderung mit ionosorbierten Sauerstoff auf dem Sensor hervorgerufen wird. Das Verfahren wurde mit einem SnO_2 -Sensor (AS-MLV, ams Sensor Solutions Germany GmbH, Reutlingen) auf einem Membransubstrat getestet, welches aufgrund der geringen thermischen Masse eine schnelle Temperaturänderung zulässt. Das Optimierungsverfahren kann sehr hohe Sensorsignale ($G_{\text{Gas}}/G_{\text{Luft}} - 1$) erzielen, beispielsweise ein Sensorsignal von ca. 8000 bei 1 ppm ethanolhaltiger synthetischer Luft, die das isotherme Sensorsignal um den Faktor 800 übertrifft. Der Zusammenhang zwischen dem Sensorsignal und der Gaskonzentration kann für die meisten Zeitpunkte im TCO durch eine Potenzfunktion mit Exponenten von 0,5 bis 4 beschrieben werden. Es zeigt sich, dass direkt nach einem Temperaturabfall das Modell so stark vereinfacht werden kann, dass nur noch ein freier Modellparameter bleibt. Die Geschwindigkeit der Relaxation bei reduzierendem Gasangebot kann durch Ratenkonstanten beschrieben werden, die in guter Näherung proportional zur Gaskonzentration sind. Die Temperaturcharakteristik der Ratenkonstanten variiert für verschiedene Gase unabhängig von der Konzentration. Daher kann auch die Selektivität optimiert werden, wie am Beispiel von ethanol- und benzolhaltiger synthetischer Luft gezeigt wird.

Schlüsselwörter: Halbleitergassensoren, MOS, temperaturzyklischer Betrieb, TCO.

Abstract: A method for optimization of temperature cycled operation (TCO) with respect to sensor response, sensitivity and selectivity is introduced based on a simplified sensor model regarding the change of occupancy of ionosorbed oxygen on the sensor. The method was tested using a SnO_2 sensor (AS-MLV, ams Sensor Solutions Germany GmbH, Reutlingen) on a membrane which allows a fast temperature change due to its low thermal mass. This method can achieve very high sensor responses, e. g. a sensor response ($G_{\text{gas}}/G_{\text{air}} - 1$) of approx. 8000 to 1 ppm ethanol in synthetic air, which exceeds the isothermal sensor response by the factor 800. The relation between sensor response and gas concentration can be for most of the points within the TCO approximated by a power function with an exponent of about 0.5 to 4. It is shown that directly after a temperature drop only one model parameter is relevant. The speed of relaxation in reducing gas can be described by rate constants which are proportional to the gas concentration. The temperature characteristic of the rate constants varies for different gases independent of concentration. Therefore, also the selectivity can be optimised shown for the example with benzene and ethanol in synthetic air.

Keywords: Semiconductor gas sensor, MOS, temperature cycled operation, TCO.

DOI 10.1515/teme-2014-0007

Eingang 7. Januar 2015; angenommen 22. Februar 2015

1 Einleitung

Halbleitergassensoren auf Basis von Zinndioxid (SnO_2) reagieren auf eine Vielzahl verschiedener reduzierender und oxidierender Gase bereits in Konzentrationen von wenigen ppm (*parts per million*). Deswegen wird diese Art von Sensoren bei einer Vielzahl von Anwendungen eingesetzt, wie beispielsweise zum Detektieren von flüchtigen organischen Verbindungen (*volatile organic compounds*, VOCs)

*Korrespondenzautor: Tobias Baur, Universität des Saarlandes, Lehrstuhl für Messtechnik, Saarbrücken, E-Mail: s9tobaur@stud.uni-saarland.de

Andreas Schütze, Tilman Sauerwald: Universität des Saarlandes, Lehrstuhl für Messtechnik, Saarbrücken

in der Raumluft [2]. Bereits auf dem Markt erhältliche Sensorsysteme können breitbandig und unspezifisch VOCs im ppm-Bereich, die sog. TVOCs (*total volatile organic compounds*), messen. Für den spezifischen Nachweis von toxischen VOCs (z. B. Benzol) in der Raumluft ist es notwendig Spuren von krebserregenden Substanzen wie z. B. Benzol mit hoher Empfindlichkeit und Selektivität im ppb- (*parts per billion*) und ppt- (*parts per trillion*) Bereich zu erfassen [2, 3]. Für Benzol gilt europaweit ein Grenzwert von 5 µg/m³ (ca. 1,5 ppm) [21].

Um Gase identifizieren zu können, wird der Sensor mit einer zyklischen Variation der Betriebstemperatur betrieben. Dieses Verfahren, vielfach zur Verbesserung der Selektivität sowie zur Multigaserkennung eingesetzt [4–6], wird im Folgenden als TCO (*temperature cycled operation*) bezeichnet. Parameter des TCO wie Zykluslänge, Temperaturbereich und Form des Temperaturverlaufs werden in vielen Untersuchungen heuristisch gewählt. Ein effizientes und praktikables Verfahren zur Optimierung des Temperaturverlaufs im Zyklus mit dem Ziel hoher Sensitivität und Selektivität existiert derzeit nicht. Eine Optimierung des Temperaturzyklus über das temperaturabhängige Sensorsignal aus einem beliebigen Temperaturzyklus ist aufgrund der vielen dynamischen Prozesse während eines Temperaturzyklus nicht möglich. Dabei treten viele gekoppelte Effekte auf, wodurch das Sensorsignal in Abhängigkeit zur Temperatur stark mit der Zyklusform und den Umgebungsbedingungen variiert. Rein iterative Optimierungsverfahren für verschiedene Zyklus-Formen wie sie z. B. von Polese et al. beschrieben werden [8] sowie spektrale Verfahren von Vergana et al. [9] können nur eine kleine Auswahl an möglichen Zyklenformen testen. Ein Verfahren, welches sehr aussichtsreich ist, ist die modellhafte Beschreibung der Nichtgleichgewichtsprozesse von Oberflächenzuständen bei Temperaturänderung. Es existieren verschiedene Untersuchungen [10–12] in denen das Sensorsignal eines SnO₂-Sensors über Ratengleichungen beschrieben wird. Der praktische Nutzen zur Optimierung eines Temperaturzyklus ist eingeschränkt und stößt durch die vielen möglichen Oberflächenprozesse, der zeitlichen Änderung der Donatordichte und weiteren zeitlichen Effekte schnell an die Grenzen. In unserer Arbeit wollen wir versuchen, einen praktikablen Ansatz zur Optimierung der Temperaturzyklen zu finden, der auf einer Vereinfachung der Betrachtung der Ratengleichungen basiert und mit welchem sich Temperaturzyklen mit optimaler Sensitivität und Selektivität erzielen lassen.

2 Modellvorstellung

Das am weitesten verbreitete Modell zur Beschreibung der Leitfähigkeit des SnO₂-Sensors reduziert die Betrachtung auf die Korn-Kornübergänge unter der Annahme [12], dass diese die Leitfähigkeit überwiegend bestimmen. Die Annahme ist für die meisten granularen SnO₂-Filme gerechtfertigt, da (in Luft) SnO₂ nahe der Oberfläche durch adsorbierten Sauerstoff stark an Elektronen verarmt ist und zum Transport über die Korngrenze eine Energiebarriere E_b überwunden werden muss.

Die Leitfähigkeit σ der Korngrenze kann dadurch als Funktion der Temperatur T durch

$$\sigma = \sigma_0 \cdot e^{-\frac{E_b}{k_b T}} \quad (1)$$

beschrieben werden [12, 13]. Dabei ist k_b die Boltzmann-Konstante und σ_0 der Leitwert des nicht verarmten SnO₂ (bulk). Die Energiebarriere kann aus der Oberflächenladungsdichte N_s und der Donatordichte N_d berechnet werden. Für die eindimensionalen Poisson-Gleichung mit Schottky-Näherung ergibt sich [12]:

$$E_b = qV_s = \frac{q^2 N_s^2}{2\epsilon_r \epsilon_0 N_d}, \quad (2)$$

mit der Elementarladung q , der Permittivität des Vakuums ϵ_0 und des Zinndioxides ϵ_r . Wir gehen davon aus, dass sich die Betrachtung des einzelnen Korn-Kornüberganges (Gleichung (1)) analog auf den gesamten Film übertragen lässt. Der exponentielle Vorfaktor G_0 ist dann definiert durch

$$G_0 = A_{geom} \sigma_0 = A_{geom} q \mu_s N_d. \quad (3)$$

A_{geom} ist eine Konstante in Abhängigkeit zur Geometrie des Sensors und μ_s die Elektronenbeweglichkeit. Dabei ist zu beachten, dass

$$\mu_s \propto T^{-3/2} \quad (4)$$

aufgrund der Zusammenstöße der Elektronen mit Phononen und anderen Gitterdefekten temperaturabhängig ist [11]. Die Donatordichte N_d im SnO₂ wird durch einfache und zweifach ionisierte Sauerstofffehlstellen hervorgerufen. Die nötige Energie für die erste Ionisierung von SnO₂ liegt bei ca. 30 meV; die Energie der zweiten Ionisierung bei ca. 150 meV [16]. Da die Bandlücke von Zinndioxid bei ca. 3,7 eV [17] liegt, kann bei typischen Betriebstemperaturen keine Eigenleitung erwartet werden. Die Leitfähigkeit kommt somit vollständig aufgrund der ionisierten Donatoren zustande, wobei Untersuchungen bewege

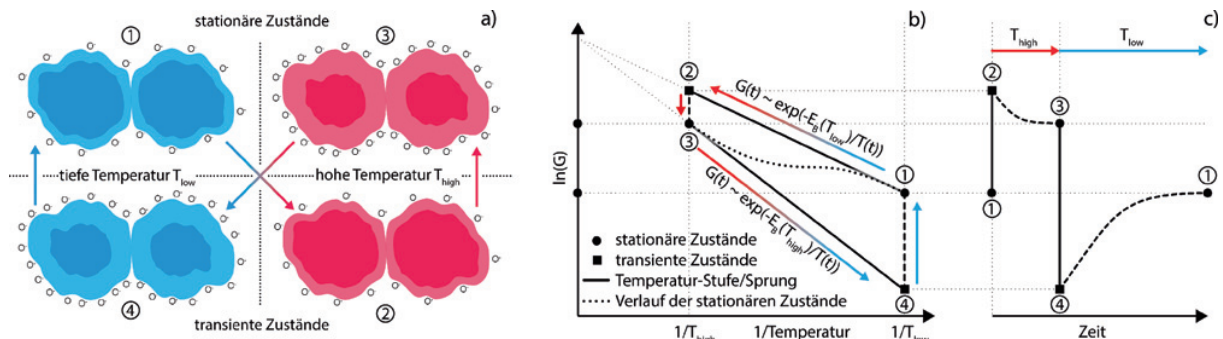


Abbildung 1: (a) Schematische Darstellung der stationären und transienten Zustände eines Korn-Kornüberganges im temperaturzyklischen Betrieb. Die hellen Bereiche der Körner symbolisieren die Verarmungszone nahe der Oberfläche bedingt durch ionosorbierten Sauerstoff (schematisch als O- bezeichnet). (b) Arrhenius-Darstellung des Sensorsignals eines Temperaturzyklus mit zwei Temperaturen. Durchgezogene Linie: Zustände bei beliebig schnellen Temperaturwechseln. Gestrichelte Linie: Relaxation bei einer konstanten Temperatur. Gepunktete Linie: stationäre Zustände. (c) Zeitlicher Verlauf des Sensorsignals eines Temperaturzyklus mit zwei Temperaturen. In Anlehnung an [22].

Donatoren zeigen [18–20]. Die Ergebnisse zeigen von der Temperatur und der Korngröße abhängige Zeitkonstanten im Bereich von wenigen Minuten für hohe Temperaturen bis hin zu Tagen für niedrige Temperaturen. Die Donatordichte kann dabei eine zeitliche und örtliche Funktion darstellen, d. h. die Donatordichte selbst stellt eine Funktion der Temperatur da.

Bei einem mikrostrukturierten Sensor (Zeitkonstante bei Temperaturwechsel < 10 ms) erhöht sich nach einem Temperaturanstieg der Leitwert (vgl. Gleichung (1)) instantan. Danach wird ein langsamer Abfall des Leitwertes beobachtet, d. h. nach einer Temperaturänderung wird erst langsam ein stationärer Zustand ausgebildet. Im Allgemeinen gilt, dass die Zeitkonstante einer Temperaturänderung viel kleiner ist als die Relaxation zu dem stationären Zustand. Diese Relaxation dauert von einigen Sekunden bis hin zu Minuten, wodurch die Sensoren in einem typischen Temperaturzyklus immer im Nichtgleichgewicht sind. Dieser Abfall im Leitwert resultiert aus einer Änderung der Energiebarriere, d. h. aus einer Änderung der Oberflächenladung N_s . Die negative Oberflächenladung bei SnO_2 wird im Wesentlichen durch ionosorbierteren Sauerstoff bestimmt, wodurch die Relaxation auf die Änderung der Sauerstoffbedeckung der sensiblen Schicht zurückgeführt werden kann (vgl. Gleichung (3)). Die Änderung der Sauerstoffbedeckung N_s kann mit Rategleichungen beschrieben werden [10–12].

Abbildung 1a zeigt eine schematische Darstellung eines Korn-Kornüberganges bei einem Temperaturzyklus mit zwei Temperaturen. Bei einer abrupten Temperaturhöhung steigt der Leitwert an, nimmt jedoch bei gleichbleibender Temperatur zeitlich wieder ab. Dies liegt daran, dass die Sauerstoffbedeckung bei einer hohen Tempe-

ratur viel höher ist. In Abbildung 1b wird die Arrhenius-Darstellung des Sensorsignals aufgezeigt. In dieser Grafik ist der Verlauf des Sensorsignals in stationären (gepunktete Linie) und transienten Zuständen (gestrichelte Linie) bei einem Temperaturzyklus mit abrupter Temperaturänderung (durchgezogene Linie) zu erkennen. Wenn ein Sensor einen Temperatursprung von der Temperatur T_{low} nach T_{high} erfährt, wird auch dessen Leitwert (Zustand 1 nach 2) sprunghaft vergrößert. Der Temperatursprung ist so schnell, dass die Relaxation der Sauerstoffbedeckung nicht weit fortgeschritten ist. Die Änderung des Leitwertes von Zustand 1 nach 2 ist eine Funktion der Temperatur bei einer konstanten Aktivierungsenergie. Die Änderung von Zustand 2 nach 3 ist hingegen eine Funktion der Aktivierungsenergie bei konstanter Temperatur. In dieser Zeit bestimmt die Relaxation des Sensors die Änderung des Leitwertes, d. h. je nach zeitlicher Länge eines Temperaturplateaus besteht die Möglichkeit jeden Zustand zwischen den Zuständen 2 und 3 anzunehmen. Die Leitwerte der stationären Zustände bilden zusammen mit den Leitwerten bei einem Temperatursprung ein Trapez (vgl. Abbildung 1b). Bei dieser Darstellung wird deutlich, dass im statischen Betrieb viel weniger Zustände angenommen werden können als im dynamischen Betrieb. Bei entsprechendem Verlauf des Temperaturzyklus können alle Zustände innerhalb des Trapezes angenommen werden. Zur Optimierung muss das Trapez vollständig durchlaufen werden um eine optimale Kombination aus den Eigenschaften (Sensitivität, Sensorsignal und Selektivität) zu finden. Im Zyklus werden vollständig relaxierte Oberflächenzustände angenommen, wodurch auch ein grobes Raster sehr lange dauert. Jedoch sind die einzelnen Bereiche bei konstanter Temperatur aufgrund der angenomme-

nen stationären Zustände unabhängig voneinander, d. h. einzelne Bereiche können für einen optimierten Zyklus zusammengesetzt werden. Dabei wird ein Temperaturbereich reproduzierbar durchlaufen, wenn der Leitwert im Bereich davor in einen stationären Zustand gelaufen ist. Damit ist mit diesem Ansatz eine Optimierung des Temperaturzyklus in Hinsicht auf Sensitivität E (dS/dc – dabei bezeichnet c die Konzentration des Gases), Sensorsignal S (Änderung des Leitwerts bei Gasangebot $G_{Gas} - G_0$ geteilt durch den Leitwert in Luft G_0) und Selektivität (Quotient S_{Gas1}/S_{Gas2}) möglich.

3 Experimentelles

Die Effekte werden an einem SnO_2 -basierten mikrostrukturierten AS-MLV-Sensor (ams Sensor Solutions Germany GmbH, Reutlingen) untersucht. Die Messung der Spannung sowie die Temperaturregelung und -messung wird mit einem SniffChecker (Firma 3S GmbH, Saarbrücken) durchgeführt. Die Leitwertänderung wird bei einer konstanten Spannung von 250 mV über die sensitive Schicht gemessen. Um einen größeren Dynamikbereich messen zu können, wird der Sensorstrom mit einem analogen Logarithmierer (Messbereich von 100 pA–3,5 mA) in eine messbare Spannung umgewandelt.

Durch den mikrostrukturierten Sensor mit seiner geringen thermischen Masse liegen die Zeitkonstanten bei einem Temperatursprung unter 10 ms (z. B. bei $T = 450^\circ\text{C} \rightarrow T = 150^\circ\text{C}$: $\tau = 6,6$ ms). D. h. bei einem Temperatursprung kann angenommen werden, dass die Zeit der Relaxation sehr viel größer ist als die des Temperatursprunges. Für das Rastern des Trapezes wird aufgrund der relativ langen Relaxationsdauer der Oberflächenzustände ein grobes Raster von 50 °C verwendet. Die Starttemperatur liegt bei 150 °C und die Endtemperatur bei 450 °C. Je die Temperaturstufe wird ausgehend von dem vollständig relaxierten Zustand bei der höchsten Temperatur angefahren.

Alle Messungen werden an einer automatisierten Gasmischanlage (GMA) durchgeführt. Für das Hintergrundgas wird synthetische Luft 5.0 (Reinheit von 99,999%) mit einer Restkonzentration von < 1 ppm an sensorrelevanten Gasen (CO , H_2) verwendet. Die Untersuchung der Effekte wird mit den Prüfgasen Ethanol (als Bestandteil der Raumluft) sowie Benzol (als ein typisches toxisches VOC) untersucht. Die Herstellung dieser niedrigkonzentrierten Prüfgase wird durch eine zweistufige Vorverdünnung aus einer Prüfgasflasche mit 200 ppm (Ethanol) und 50 ppm (Benzol) realisiert [1]. Alle Messungen wurden bei einem

Fluss von 200 ml/min bei einer relativen Feuchte von 50% durchgeführt.

4 Ergebnisse

Für eine Untersuchung des Modelles wird die mittlere Energiebarriere E_b der Korn-Kornübergänge und des exponentiellen Vorfaktors G_0 bei den stationären Zuständen bestimmt. Der beschriebene Temperaturbereich von 150 °C bis 450 °C wird in 25 °C-Schritten vermessen. Für die Bestimmung der Energiebarriere im stationären Zustand wird der Sensor auf eine konstante Temperatur geheizt, bis ein stationärer Zustand eingestellt ist. Das kann, je nach Temperatur, von einer Stunde (450 °C) bis zu einem Tag (150 °C) dauern. Die lange Relaxationszeit wird nicht alleine durch die Relaxation der Energiebarriere, sondern auch durch einen zweiten Prozess, möglicherweise die Änderung der Donatordichte, bestimmt. Nach dem Erreichen des stationären Zustandes wird ein Temperaturzyklus mit einem 30 s langen Temperaturplateau, bei dem die Energiebarriere gemessen werden soll, mit danach folgendem kurzen 50 ms Peaks mit $\pm 25^\circ\text{C}$ durchlaufen. Da der Relaxationsprozess der Sauerstoffbedeckung sowie die Gleichgewichtseinstellung der Donatordichte sehr viel langsamer als die Temperaturänderung ist, kann bei den kurzen Peaks die Energiebarriere näherungsweise als konstant angenommen werden. Die Energiebarriere kann mit diesen Annahmen, durch

$$E_b = k_b \cdot \ln \left(\frac{G_h}{G_l} \right) \cdot \left(\frac{T_h T_l}{T_h - T_l} \right) \quad (5)$$

bestimmt werden. Der Vorfaktor G_0 kann mit der Energiebarriere E_b über

$$G_0 = G_i \cdot \exp \left(\frac{E_b}{k_b T_i} \right) \quad (6)$$

berechnet werden.

Die Ergebnisse von der Bestimmung der Energiebarriere E_b und des exponentiellen Faktors G_0 ist in Abbildung 2 dargestellt. Die Energiebarriere nimmt mit höheren Temperaturen stark zu und liegt im Bereich zwischen 200 meV und 900 meV, wobei die relative Änderung für hohe und niedrige Temperaturen kleiner wird. Die Tatsache, dass die Energiebarriere zwischen 400 °C und 450 °C wieder leicht sinkt ist vermutlich auf einen Messfehler zurückzuführen, da die Annahme einer langsamen Relaxation der Oberflächenzustände bei 450 °C nicht mehr erfüllt ist.

Vorherige Untersuchungen zeigen eine starke Ausprägung der Relaxation von einem stationären Zustand

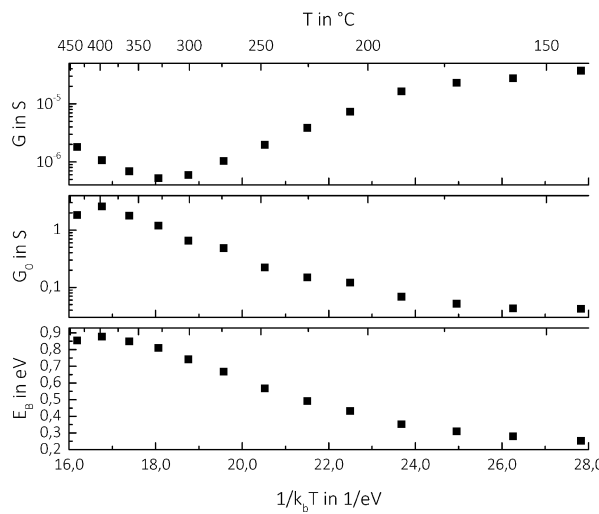


Abbildung 2: Übersicht des gemessenen stationären Leitwertes G , des Vorfaktors G_0 und der Energiebarriere E_{in} . Oben: gemittelter Leitwert im stationären Zustand in Abhängigkeit zur Temperatur. Mitte: berechnete exponentielle Vorfaktoren in Abhängigkeit zur Temperatur. Unten: berechnete Energiebarriere in Abhängigkeit zur Temperatur.

bei hohen Temperaturen zu Zuständen bei niedrigen Temperaturen. Daher werden für den Temperaturzyklus zur Charakterisierung des Sensors mit ethanolhaltiger (10 ppb–1 ppm) bzw. benzolhaltiger (10 ppb–1 ppm) Luft nur Leitwertsprünge von einem relaxierten Zustand bei 450 °C auf Zustände mit niedrigen Temperaturen betrachtet. Aufgrund des mikrostrukturierten AS-MLV-Sensors mit seiner geringen thermischen Masse liegt die Zeitkon-

stante für die Abkühlvorgänge bei < 10 ms. D. h. im Vergleich zu der Zeitkonstante der Relaxation folgt ein Temperatursprung nahezu instantan.

In Abbildung 3 ist der Leitwert- und das Sensorsignal des gewählten Temperaturzyklus bei ethanolhaltiger Luft dargestellt. Dabei ist erkennbar, dass der Verlauf dem in Abbildung 1 dargestellten Schema entspricht. Die Änderung des Leitwertes innerhalb eines Temperaturplateaus bei reiner und ethanolhaltiger Luft ist besonders ausgeprägt (Abbildung 1b gestrichelte Linie), was auf eine sehr starke Änderung der Bandverbiegung im Temperaturverlauf (vgl. Abbildung 2) hindeutet. Dabei ist zu beobachten, dass die Relaxation bei ethanolhaltiger Luft sehr viel schneller fortschreitet als bei reiner Luft. Im dynamischen Fall wird dadurch eine deutliche Empfindlichkeitssteigerung im Vergleich zum stationären Fall hervorgerufen.

In dem Verlauf des Sensorsignals kann dadurch bei einem Temperatursprung von 420 °C auf 140 °C bei 1 ppm ethanolhaltiger Luft ein maximales Sensorsignal von 8000 beobachtet werden, wohingegen im stationären Zustand nur ein Sensorsignal von 10 erwartet wird. Dabei ist bei ethanolhaltiger Luft sehr auffällig, dass das Maximum des Sensorsignals mit höherer Temperatur abnimmt.

In Abbildung 4 ist das Sensorsignal in Abhängigkeit zur Konzentration der ethanolhaltigen Luft für verschiedene Temperaturen und Zeiten in einem doppellogarithmischen Plot dargestellt. Erkennbar ist dabei, dass das Sensorsignal bei den transienten Zuständen deutlich größer ist als im stationären Zustand. Die Maxima der Sensorsignale treten mit steigender Konzentration zeitlich gesehen früher auf. Dieser Effekt kann mit der schnelleren Relaxa-

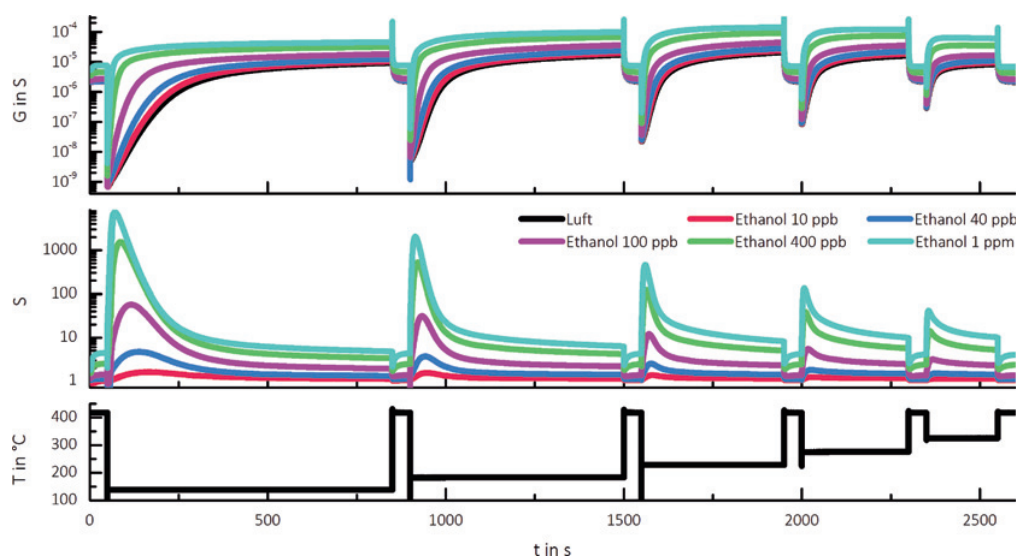


Abbildung 3: Leitwert- und Sensorsignalverlauf bei verschiedenen Konzentrationen ethanolhaltiger Luft.

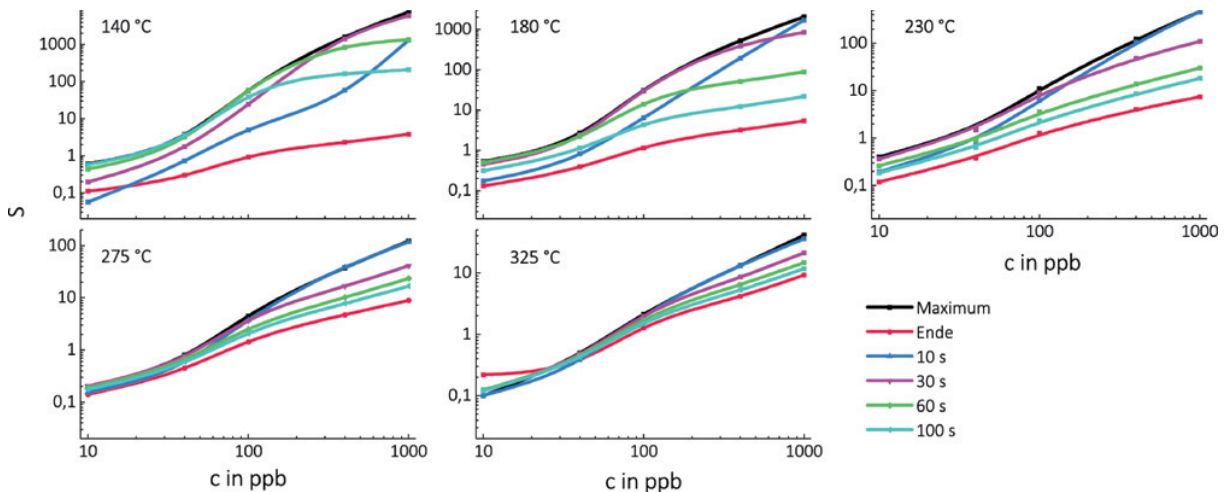


Abbildung 4: Konzentrationsabhängige Sensorsignale an unterschiedlichen Zeitpunkten nach einem Temperatursprung von $420\text{ }^\circ\text{C}$ auf die angegebene Temperatur bei ethanolhaltiger Luft. Maximum: maximale Sensorsignale bei dem jeweiligen Temperaturplateau. Ende: Sensorsignale am Ende des jeweiligen Temperaturplateaus.

tion bei steigender Konzentration erklärt werden. Dies bedeutet, dass bei geeigneter Wahl des Abtastzeitpunktes ein Signal mit konstanter Sensitivität, d. h. lineares Sensorverhalten, gefunden werden kann.

Ein interessanter Grenzfall des Sensorsignals kann direkt nach dem Sprung von einer hohen zu einer niedrigen Temperatur betrachtet werden. In diesem Fall liegt ein hoher Überschuss an Oberflächenladung vor, der abgebaut werden muss. Im Wesentlichen spielt daher die Rate für den Abbau der Oberflächenzustände eine Rolle. Im Fall ei-

ner kleinen Änderung der Oberflächenladung kann die Änderung der Energiebarriere linear genähert werden, daher folgt im Grenzfall für kleine Zeiten nach einem Temperatursprung ($t = 0\text{ s}$) näherungsweise

$$\ln\left(\frac{G(t)}{G(t=0)}\right) = K \cdot t, \quad (7)$$

mit einer von der Gasart und der Konzentration abhängigen Konstanten K .

In Abbildung 5 ist die Näherung bei einem Temperatursprung von $420\text{ }^\circ\text{C}$ auf $180\text{ }^\circ\text{C}$ (bei $t = 0\text{ s}$) dargestellt. Dabei kann das Sensorsignal sehr gut mit der Relation (7) in einem Bereich von $\Delta t = 3\text{ s}$ beschrieben werden. Die Änderung des Leitwertes beträgt ca. e^3 , was einer Bandverbiegung von $3k_bT$ entspricht.

Die Messungen zeigen, dass die Konstante $K = k_1 c + k_2$ linear von der Gaskonzentration abhängig ist. Der Term $k_1 c$ kann bei Angeboten von reduzierenden Gasen in synthetische Luft auf die der Reaktion des reduzierenden Gases mit dem Oberflächensauerstoff zurückgeführt werden.

Die Steigung des Sensorsignals im logarithmischen Plot ist daher ein Maß für die Konzentration des reduzierenden Gases. Selbst bei relativ kleinen Konzentrationen von z. B. 100 ppb ist die Relaxation des Oberflächenzustands im Wesentlichen durch das reduzierende Gas bestimmt. In der betrachteten Näherung nehmen das Sensorsignal sowie die Sensitivität exponentiell mit der Konzentration zu.

In Abbildung 6 werden die kompensierten Steigungen $k_1 c$ der ethanolhaltigen synthetischen Luft im Vergleich zu der benzolhaltigen in Abhängigkeit zur Tem-

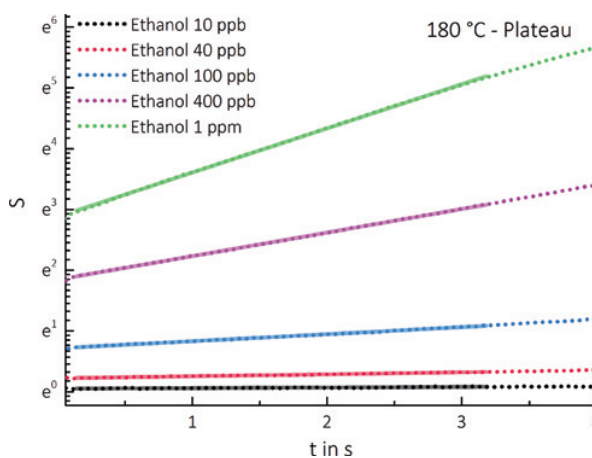


Abbildung 5: Gemessene Sensorsignale (gepunktete Linie) eines AS-MLV-Sensors nach einem Temperatursprung von $420\text{ }^\circ\text{C}$ auf $180\text{ }^\circ\text{C}$ bei verschiedenen Ethanolkonzentrationen in halblogarithmischer Auftragung. Die Messwerte folgen in guter Näherung einer Exponentialkurve (durchgezogene Linie), die in der halblogarithmischen Auftragung auf einer Geraden liegen.

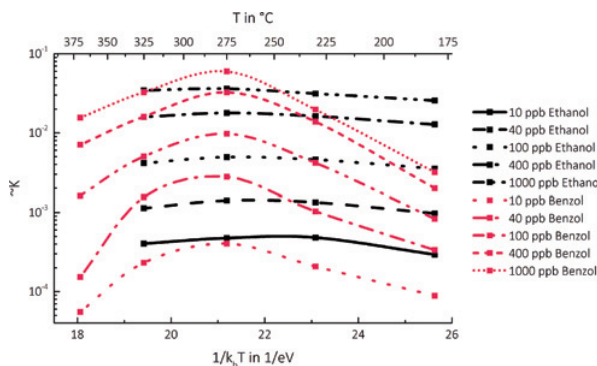


Abbildung 6: Temperaturabhängige Darstellung der Steigung zu Beginn eines Temperatursprungs für verschiedene Konzentrationen ethanol- und benzolhaltiger Luft.

peratur gezeigt. Dabei sind die charakteristischen Unterschiede bei dem temperaturabhängigen Verlauf der Ratenkonstanten für die Optimierung der Selektivität sehr interessant. Der Verlauf der Ratenkonstanten von Ethanol zeigt eine schwache temperaturabhängige Änderung. Im Vergleich dazu zeigt Benzol eine starke Temperaturabhängigkeit mit einem Maximum bei 275 °C. Das charakteristische Verhalten der Ratenkonstanten ist, wie bei Benzol und Ethanol erkennbar, gastypisch und nicht konzentrationsabhängig.

Ein weiterer Aspekt in der Optimierung der Selektivität von Gasen ist der Vergleich der Sensorsignal-Kurven. Abbildung 7 zeigt die Sensorsignale für verschiedene Konzentrationen ethanol- und benzolhaltiger Luft. Dabei sind die charakteristischen Unterschiede beider Gase interessant. Bei Benzol ist das Maximum des Sensorsignals bei

275 °C zu erkennen, bei Ethanol dagegen bei 140 °C. Aufgrund der unterschiedlichen chemischen Reaktivität von Benzol und Ethanol ist bei höheren Temperaturen ein höheres Sensorsignal bei Benzol zu erwarten. Die Höhe der temperaturabhängigen Maxima ist nicht nur von der Steigung (Ratenkonstante) abhängig, sondern auch von der Differenz der Energiebarrieren der stationären Zustände unterschiedlicher Temperatursprünge, die bei der Relaxation überwunden werden müssen.

D. h. für die Optimierung der Selektivität können die charakteristischen Temperatur-Verläufe der Ratenkonstanten sowie die Sensorsignale für verschiedene Gase verglichen werden.

5 Fazit

Das beschriebene Modell und Verfahren zur Entwicklung eines temperaturzyklischen Betriebes mit optimalen Eigenschaften (Sensitivität, Sensorsignal und Selektivität) hat sein Potential mit unterschiedlichen Beispielen gezeigt. Aufgrund des voll relaxierten Zustandes als Ausgangspunkt der Relaxation können beliebige Bereiche jeder Relaxation ausgewählt und zu einem neuen Zyklus zusammengefügt werden, der die gewünschten Eigenschaften zeigt. Dieses Optimierungsverfahren für einen Temperaturzyklus ist über einen geschlossenen Algorithmus beschrieben. Demnach kann es auch automatisiert werden, um z. B. das höchste Sensorsignal zu ermitteln.

Des Weiteren kann die Grenzbetrachtung der Relaxation über das vereinfachte Modell dabei helfen, bestimmte Eigenschaften des Sensors vorherzusagen. Das zeigt, dass

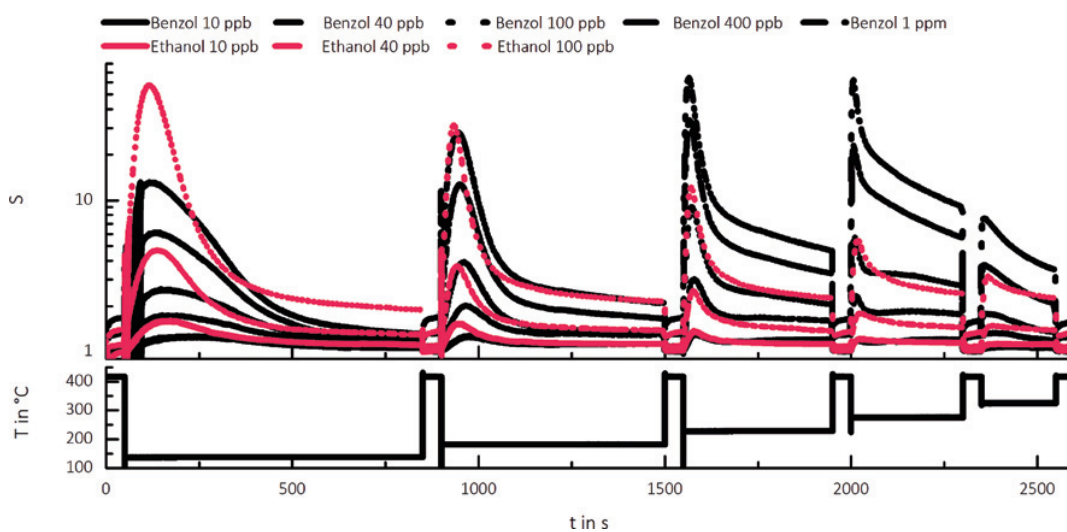


Abbildung 7: Sensorsignale für verschiedene Konzentrationen von ethanol- und benzolhaltiger Luft.

dieses Modell den interessanten Bereich des TCO gut beschreiben kann und dadurch auch für die Optimierung des Temperaturzyklus geeignet ist. Dies kann durch Bestimmung der Steigung zu Beginn der Relaxation nach einem Temperatursprung ermöglicht werden, der mit der Höhe des logarithmischen Sensorsignals korreliert. Die Beschreibung der Relaxation ermöglicht auch die Bestimmung von Parametern für das Modellieren und Simulieren des Sensorverhaltens im Temperaturzyklischen Betrieb.

Die Automatisierung des Verfahrens sowie die modellhafte Beschreibung des Sensorsignals ist Gegenstand weitergehender Untersuchungen und wird in folgenden Arbeiten beschrieben.

Danksagung: Die Arbeiten wurden durch das Bundesministerium für Bildung und Forschung (MNT-ERA.net-Projekts VOC-IDS Förderkennzeichen 16SV5480K) sowie durch die Europäische Union (FP7 Projekt SENSIIndoor) gefördert.

Literatur

1. Helwig, N.; Schüler, M.; Bur, C.; Schütze, A.; Sauerwald, T.: „Gas mixing apparatus for automated gas sensor characterization“, *Meas. Sci. Technol.*, 25, 055903, 9 pp; doi:10.1088/0957-0233/25/5/055903, 2014.
2. Leidinger, M.; Sauerwald, T.; Reimringer, W.; Ventura, G.; Schütze, A.: „Selective detection of hazardous VOCs for indoor air quality applications using a virtual gas sensor array“, *J. Sens. Sens. Syst.*, 3, 253–263, 2014.
3. Leidinger, M., Sauerwald, T., Conrad, T., Reimringer, W., Ventura, G., Schütze, A.: „Selective Detection of Hazardous Indoor VOCs Using Metal Oxide Gas Sensors“, *Procedia Engineering, Eurosensors XXVIII*, Sep. 08.–10. 2014, Brescia, Italy; Volume 87, pp. 1449–1452, 2014.
4. Heilig, A.; Bârsan, N.; Weimar, U.; Schweizer-Berberich, M.; Gardner, J. W.; and Göpel, W.: „Gas identification by modulating temperatures of SnO₂-based thick film sensors“, *Sensors and Actuators B*, 43, 45–51, 1997.
5. Lee, A. P.; Reedy, B. J.: „Temperature modulation in semiconductor gas sensing“, *Sensors and Actuators B*, 60, 35–42, 1999.
6. Gramm, A.; Schütze, A.: „High performance solvent vapor identification with a two sensor array using temperature cycling and pattern classification“, *Sensors & Actuators B*, 95, 58–65, 2003.
7. Vergara, A.; Benkstein, K. D.; Montgomery, C. B.; Semancik, S.: „Demonstration of Fast and Accurate Discrimination and Quantification of Chemically Similar Species Utilizing a Single Cross-Selective Chemiresistor“, *Analytical Chemistry*, 86(14), 6753–6757, 2014.
8. Polese, D.; Martinelli, E.; Catini, A.; D'Amico, A.; Di Natale, C.: „Self-adaptive thermal modulation of gas sensors“, *Procedia Engineering*, 5, 156–159, 2010.
9. Vergara, A.; Llobet, E.; Brezmes, J.; Vilanova, X.; Ivanov, P.; Gracia, I.; Cané, C.; Correig, X.: „Optimized Temperature Modulation of Micro-Hotplate Gas Sensors Through Pseudorandom Binary Sequences“, *IEEE Sensors Journal*, 5(6), 2005.
10. Pulkkinen, U.; Rantala, T. T.; Rantala, Tu. S.; Lantto, V.: „Kinetic Monte Carlo simulation of oxygen exchange of SnO₂ surface“, *Journal of Molecular Catalysis A: Chemical*, 166, 15–21, 2001.
11. Ding, J.; McAvoy, T. J.; Cavicchi, R. E.; Semancik, S.: „Surface state trapping models for SnO₂-based microhotplate sensors“, *Sensors and Actuators B*, 77, 597–613, 2001.
12. Morrison, S. R.: „Semiconductor Gas Sensors“, *Sensors and Actuators*, 2, 329–341, 1982.
13. Kohl, D.: „Surface processes in the detection of reducing gases with SnO₂-based devices“, *Sensors and Actuators*, 18, 71–113, 1989.
14. Gurlo, A.: Interplay between O₂ and SnO₂: „Oxygen Ionosorption and Spectroscopic Evidence for Adsorbed Oxygen“, *ChemPhysChem*, 7, 2041–2052.
15. Helwig, N.; Schüler, M.; Bur, C.; Schütze, A.; Sauerwald, T.: „Gas mixing apparatus for automated gas sensor characterization“, *Meas. Sci. Technol.*, 25, 055903, 9 pp, 2014.
16. Kappler, J.: Charakterisation of high-performance SnO₂ gas sensors for CO- detection by in situ techniques., Dissertation Universität Tübingen, Skaker Verlag, ISBN: 3826590406, 2001.
17. Jae-Ho, C.; Yong-Sahn, C.; Dae-Seung, K.: „Effect of low energy oxygen ion beam on optical and electrical characteristics of dual ion beam sputtered SnO₂ thin films“, *Thin Solid Films*, 349(1–2), 126–129, 1999.
18. Rantala, T. S.; Lantto, V.; Rantala, T. T.: „Effects of mobile donors on potential distribution in grain contacts of sintered ceramic semiconductors“, *Journal of Applied Physics*, 79(12), 9206, 1996.
19. Kamp, B.; Merkle, R.; Maier, J.: „Chemical diffusion of oxygen in tin dioxide“, *Sensors and Actuators B: Chemical*, 77(1–2), 534–542, 2001.
20. Kamp, B.; Merkle, R.; Lauck, R.; Maier, J.: „Chemical diffusion of oxygen in tin dioxide: Effects of dopants and oxygen partial pressure“, *Journal of Solid State Chemistry*, 178(10), 3027–3039, 2005.
21. Geiss, O.; Giannopoulos, G.; Tirendi, S.; Barrero-Moreno, J.; Larsen, Bo R.; Kotzias, D.: „The AIRMEX study – VOC measurements in public buildings and schools/kindergartens in eleven European cities: Statistical analysis of the data“, *Atmospheric Environment*, 45(22), 3676–3684, 2011.
22. Sauerwald, T.; Baur, T.; Schütze, A.: Strategien zur Optimierung des temperaturzyklischen Betriebs von Halbleitergassensoren: in: Andreas Schütze, Bastian Schmitt (Hrsg.): XXVIII. Messtechnisches Symposium des Arbeitskreises der Hochschullehrer für Messtechnik, Tagungsband, Shaker Verlag, Aachen, 2014.

Autoreninformationen



B. Sc. Tobias Baur

Universität des Saarlandes, Lehrstuhl für Messtechnik, 66123 Saarbrücken
 s9tobaur@stud.uni-saarland.de

Tobias Baur absolviert derzeit sein Masterstudium der Mikrotechnologie und Nanostrukturen an der Universität des Saarlandes. Bereits seit seinem Bachelorstudium arbeitet er als wissenschaftliche Hilfskraft an dem Lehrstuhl für Messtechnik der Universität des Saarlandes bei Prof. Dr. Andreas Schütze. Schwerpunktmaßig untersucht er dabei chemische Messsysteme, insbesondere Halbleitergassensoren. Im Rahmen seiner Bachelorarbeit erforschte er ein Modell eines Halbleitergassensors im temperaturzyklischen Betrieb, welches Gegenstand des vorliegenden Artikels ist. Durch ein Stipendium der European Cooperation in Science and Technology (COST) bekam er die Möglichkeit einer Short Term Scientific Mission (STSM) an der Universität Oulu (Finnland). Vor Ort untersuchte er die Herstellung von sensitiven Schichten für Halbleitergassensoren mit Hilfe des Pulsed Laser Deposition (PLD; Laserstrahlverdampfen).



Prof. Dr. rer. nat. Andreas Schütze

Universität des Saarlandes, Lehrstuhl für Messtechnik, 66123 Saarbrücken
 schuetze@lmt.uni-saarland.de

Andreas Schütze studierte Physik an der RWTH Aachen und promovierte in Angewandter Physik an der Justus-Liebig-Universität Gießen. Nach einer mehrjährigen Tätigkeit in der Wirtschaft wurde er 1998 als Professor für Sensorik und Mikrosystemtechnik an die FH Niederrhein berufen. Seit 2000 leitet er den Lehrstuhl für Messtechnik in der Fachrichtung Mechatronik der Universität des Saarlandes. Seine Forschungsschwerpunkte sind chemische Messsysteme für die Gasphase und für Flüssigkeiten sowie Condition Monitoring. Er ist u. a. Koordinator mehrere internationaler Verbundprojekte, Vorsitzender des Wissenschaftsrates der AMA,

Verband für Sensorik und Messtechnik, (seit 2009) sowie Vorstandsmitglied der f. m. s., Forschungsgesellschaft für Messtechnik, Sensorik und Medizintechnik e. V. Dresden, und Vorsitzender des fms/ProcessNet-Gemeinschaftsausschusses Sensoren und Sensorsysteme (seit 2010) sowie Mitglied von IEEE und VDE. An der Universität des Saarlandes ist er einer der Gründer des Mikrotechnologie-Transferzentrum Mitranz und des Zentrums für Mechatronik und Automatisierungstechnik (ZeMA) GmbH. Er ist aktiv als Mitglied des Editorial Boards und Gutachter für verschiedene wissenschaftliche Zeitschriften (u. a. J Sensors and Sensor Systems, J of Sensors, Sensors & Actuators B, IEEE Sensors Journal) und Mitglied des Programmkomitees verschiedener Tagungen und Konferenzen. Er betreibt seit 2006 das Schülerlabor SinnTec und engagiert sich in der Nachwuchsförderung, insbesondere mit Themen aus dem Bereich Sensorik und Messtechnik.



Dr. rer. nat. Tilman Sauerwald

Universität des Saarlandes, Lehrstuhl für Messtechnik, 66123 Saarbrücken
 t.sauerwald@lmt.uni-saarland.de

Tilman Sauerwald promovierte im Institut für Angewandte Physik an der Universität Gießen. Während seiner Promotion beschäftigte er sich mit Oberflächenreaktionen auf Halbleitergassensoren, besonders im temperaturzyklischen Betrieb sowie mit der Entwicklung neuer Gassensormaterialien. Seit 2011 arbeitet er am Lehrstuhl für Messtechnik an der Universität des Saarlandes. Seine derzeitigen Forschungsaktivitäten beziehen sich auf die selektive In-situ-Messung von Spurengasen mit Sensorsystemen. Die Untersuchungen umfassen ein breites Themenfeld: von Methodenentwicklung für die Herstellung von Prüfgasen und anderen Kalibrierstandards im ppb Bereich, über die Modellierung und Optimierung der Multisignalgewinnung im temperaturzyklischen Betrieb, bis zur Fortentwicklung mathematischer Methoden für die Sensorsignalauswertungen. Ein weiteres Forschungsfeld ist die Entwicklung von Kalibrationsverfahren für Sensorsysteme im Feld und zur Sensorselbstüberwachung. Tilman Sauerwald leitet zwei Arbeitsspäkete in einem europäischen Verbundprojekt zur Messung von toxischen Spurengasen in Innenraumluft und hält einen Researcher Excellence Grant für die Herstellung von Referenzmaterialien zur Emissionsmessung sowie zur Modellierung von Sensoren.

4.1.3 Paper B – A novel Approach towards calibrated Measurement of trace Gases using Metal Oxide Semiconductor

C. Schultealbert, T. Baur, A. Schütze, S. Böttcher and T. Sauerwald
Saarland University, Lab for Measurement Technology, Saarbrücken, Germany

Sensors and Actuators B: Chemical (2017), 239, 390-396

The original paper and supplementary data can be found, in the online version, at
<http://dx.doi.org/10.1016/j.snb.2016.08.002>.

© Used with permission of Elsevier Science & Technology Journals, from *A novel approach towards calibrated measurement of trace gases using metal oxide semiconductor sensors*, Schultealbert, Caroline; Baur, Tobias; Schütze, Andreas; Böttcher, Stefan; Sauerwald, Tilman, 239, 2022; permission conveyed through Copyright Clearance Center, Inc.



A novel approach towards calibrated measurement of trace gases using metal oxide semiconductor sensors



Caroline Schultealbert^{a,*}, Tobias Baur^a, Andreas Schütze^a, Stefan Böttcher^b,
Tilman Sauerwald^a

^a Lab for Measurement Technology, Saarland University, Saarbrücken, Germany

^b Pharmaceutical and Medicinal Chemistry, Saarland University, Saarbrücken, Germany

ARTICLE INFO

Article history:

Received 13 January 2016

Received in revised form 24 June 2016

Accepted 1 August 2016

Available online 2 August 2016

Keywords:

Metal oxide semiconductor gas sensor

In field calibration

Indoor air quality

TVOC quantification

Model based temperature cycled operation

Trace level detection

ABSTRACT

We present a method for quantitative measurements of metal oxide semiconductor gas sensors (MOS) which is based on relaxation of surface states using temperature cycled operation (TCO). The method provides sensor response to toluene in form of a power law and a reliable quantification in the concentration range of about 10 ppb to 10 ppm. For the calibration of the sensor, a method is developed based on the equilibrium vapour headspace over a liquid solution of toluene and squalane yielding reliable concentrations in the range of 10 ppb to 600 ppm. The calibration method was shown to be stable under ambient conditions and thus to be applicable for field calibration of gas sensors.

© 2016 Elsevier B.V. All rights reserved.

1. Introduction

MOS sensors are highly sensitive, robust and inexpensive devices which have been reported to detect volatile organic compounds (VOC) in the low ppm or even ppb range [1] and utilised in devices for the specific detection of toxic VOC indoors [2]. For this application, like for many other, a stable quantification based on a traceable calibration is a prerequisite. The response of MOS sensors in respect to the concentration of reducing gas in stationary conditions is typically given by a power law which can be derived from the surface reaction of reducing specimen with adsorbed oxygen [3,4] considering an equilibrium condition on the sensor surface. However, many applications require sensors in non-equilibrium conditions e.g. using temperature cycled operation (TCO) in order to increase selectivity [2], stability [5] and sensitivity [6,7]. Recently some of us showed experimentally that the power law approach is suited in some cases for sensor responses obtained by temperature

cycles [8], however not for all [6]. In the specific case described by Baur [6] the sensor surface is covered with an excess of oxygen obtained by a rapid temperature change. Here the response in respect to the concentration was found to be exponential. Baur proposed a concept for quantitative measurement based on the relaxation of the oxygen equilibrium, which will be utilised in this work. The calibration of gas sensors is typically performed using test gases e.g. from gas cylinders. For comprehensive tests gas mixing systems have been reported [9]; some of them are specifically dedicated to trace gases [10]. This approach is convenient for an initial calibration in the laboratory but under application conditions, comprehensive tests using gas mixing systems require extensive effort. Regular calibration, however, has been shown to improve the long term stability of sensor systems [11]. Therefore, we present an easy to use calibration method based on the equilibrium vapour pressure of diluted VOC samples. To this end mixtures of VOC with non-volatile liquids can be used as vapour pressure standard. Similar methods have been reported as calibration standards for electroantennography measurements [12]. Toluene is selected as test substance as it is often used as reference substance for total VOC quantification. The international standard ISO16000-6 for example describes that volatile organic compounds, sampled on Tenax TA, which elute between *n*-hexane and *n*-hexadecane on a non-polar capillary column, detected with mass spectrometric detector

* Corresponding author.

E-mail addresses: c.schultealbert@lmt.uni-saarland.de (C. Schultealbert), t.baur@lmt.uni-saarland.de (T. Baur), schuetze@lmt.uni-saarland.de (A. Schütze), s.boettcher@mx.uni-saarland.de (S. Böttcher), t.sauerwald@lmt.uni-saarland.de (T. Sauerwald).

(TVOC-MS), should be quantified by converting the total area of the chromatogram in that analytical window to a nominal mass using the chromatographic response factor for toluene [13].

2. Concept of quantitative measurement

The most common model to describe the conductivity of SnO_2 -based sensors reduces the viewing on the grain-grain boundaries [3]. In many cases these boundaries determine the conductivity. The assumption has been confirmed for various granular SnO_2 -films in air [14], [6] in view of the fact that these films are strongly depleted near the surface by binding electrons from ionosorbed oxygen. For electron transport across the grain-grain boundaries the electrons have to overcome the energy barrier E_b . The functionality of metal oxide semiconductor gas sensors is based on the interaction between ionosorbed oxygen and gas molecules. If a reducing gas is applied, the gas reacts with the ionosorbed oxygen on the surface. In this process the oxygen atom emits its electron to the conduction band, so that the energy barrier will be reduced [6].

The conductance of the entire sensor based on the conductivity of grain boundaries is given by [3]

$$G = G_0 \cdot e^{-\frac{E_b}{k_b T}}. \quad (1)$$

where k_b is the Boltzmann constant and G_0 an exponential prefactor. The energy barrier is defined by

$$E_b = \frac{q^2 N_s^2}{2 \varepsilon_r \varepsilon_0 N_d} = N_s^{*2}, \quad (2)$$

with the donator density N_d , the occupied surface states N_s , the elemental charge q , the permittivity of SnO_2 ε_r and vacuum ε_0 .

In TCO semiconductor gas sensor changes the operating temperature cyclic and is placed in different non-equilibrium states. Fig. 1a) shows a schematic illustration of a grain-grain boundary in a temperature cycle with two temperatures. In an abrupt rise in temperature $T_{low} \rightarrow T_{high}$, the conductance increases instantaneously, but decreases at the constant temperature T_{high} during a relaxation. [14] and [6] report that after a temperature change a new equilibrium between ad- and desorption of oxygen has to be established before a constant surface occupation is reached. The relaxation of a non-equilibrium to an equilibrium state takes place by different coupled processes and depends on the type of gas and the temperature. The duration of this will be between milliseconds and hours. It can be seen that the surface occupation is much higher at a high temperature. Fig. 1b) illustrates the Arrhenius plot of the sensor signal. In this graph, the course of the sensor signal can be recognized (solid line) at a temperature cycle with abrupt temperature change, in steady states (dashed line) and in transient states. Looking at an abrupt rise in temperature from $T_{low} \rightarrow T_{high}$ (state 1–2), the conductance increases rapidly. The temperature change is much faster than the relaxation of the surface occupation with oxygen. Therefore, the conductance change from state 1 → 2 is a temperature dependent function with a constant energy barrier. For the change from state 2 → 3, the function is dependent on the relaxation of the surface occupation. This means, it depends on the energy barrier with a constant temperature. State 3 → 4 and 4 → 1 can be described analogously.

If we look at the change from state 3 → 4, from a high to low temperature ($T_{high} \rightarrow T_{low}$), the temperature jumps so fast, that the surface occupancy will not be changed and Eq. (1) depends only on the temperature with a constant energy barrier (analogous 1 → 2). In this case, it is possible to calculate the energy barrier:

$$E_b = k_B \ln \left(\frac{G_{high}}{G_{low}} \right) \frac{T_{high} T_{low}}{T_{high} - T_{low}} \quad (3)$$

The conductance function Eq. (1) during the relaxation at a constant temperature T_{low} depends on the energy barrier. During this time, the relaxation of the sensor determines the change in the conductance. The concept of quantitative measurement in our work is based on a mathematical description of the occupied surface states relaxation due to the reaction of ionosorbed oxygen with reducing gases. The important surface reaction is according to [14] for temperatures below approximately 150 °C



and for temperatures above approximately 150 °C



The reaction with a reducing gas R is



Assuming that one oxygen species O_x^- is dominant dependent on the temperature, the following rate equation describes the surface reaction [14]

$$\frac{d [O_x^-]}{dt} = k_a n_s [O_{2,ads}]^{x/2} - k_d [O_x^-] \quad (7)$$

where $[O_x^-]$ is the density of the dominant species with $x = 2$ for O_2^- or $x = 1$ for O^- , k_a is the forward, k_d the reverse reaction rate and the density of electrons at the surface [14]

$$n_s = N_d \exp \left(-\frac{N_s^{*2}}{k_b T} \right). \quad (8)$$

Assuming that the chemisorption of oxygen on the surface is a fast thermodynamic process and as a result always in equilibrium, the density of chemisorbed oxygen can be described according to the Lennard-Jones model [15] by

$$[O_2] = A \exp \left(\frac{\Delta H}{kT} \right). \quad (9)$$

where A is a pre-exponential factor and ΔH the heat of oxygen chemisorption. According to the assumption that only one oxygen species on the surface is dominant, the ionosorbed density of oxygen $[O_x^-]$ is equal to the occupied surface states N_s . So the exchange of electrons between the surface states and the conduction band can be described with Eq. (7) by

$$\frac{dN_s}{dt} = k_a N_D \exp \left(-\frac{N_s^{*2}}{k_b T} \right) \cdot A \exp \left(\frac{x \Delta H}{2 k_b T} \right) - k_d N_s. \quad (10)$$

Eq. (10) can be rewritten with the substitution $N_s^* = \frac{q N_s}{\sqrt{2 \varepsilon_r \varepsilon_0 N_d}}$, $k_a^* = \frac{q}{\sqrt{2 \varepsilon_r \varepsilon_0 N_D}} k_a N_D C$ and $k_d^* = k_d$ as

$$\frac{dN_s^*}{dt} = k_a^* \exp \left(-\frac{N_s^{*2}}{k_b T} \right) \exp \left(\frac{x \Delta H}{2 k_b T} \right) - k_d^* N_s^*. \quad (11)$$

After a temperature step $T_0 \rightarrow T_1$ ($T_0 > T_1$) for a short time $t \ll \tau_{relaxation}$, the density of new ionosorbed oxygen on the surface is smaller than the density of desorbed oxygen. The density's decrease is based on the reaction with reduced gas in air as a result of the higher occupation of surface states by higher temperature (T_0) (see Supplementary material B). Therefore, Eq. (11) is by approximation

$$\frac{dN_s^*}{dt} \approx -k_d^* N_s^*. \quad (12)$$

The solution of the approximated differential equation is

$$N_s^*(t) \approx N_s^*(0) \cdot \exp(-k_d^* \cdot t), \quad (13)$$

Please note that this can only be assumed if the contribution of the adsorption term $\exp \left(-\frac{N_s^{*2}}{k_b T} \right) \exp \left(\frac{x \Delta H}{2 k_b T} \right)$ is negligible. For

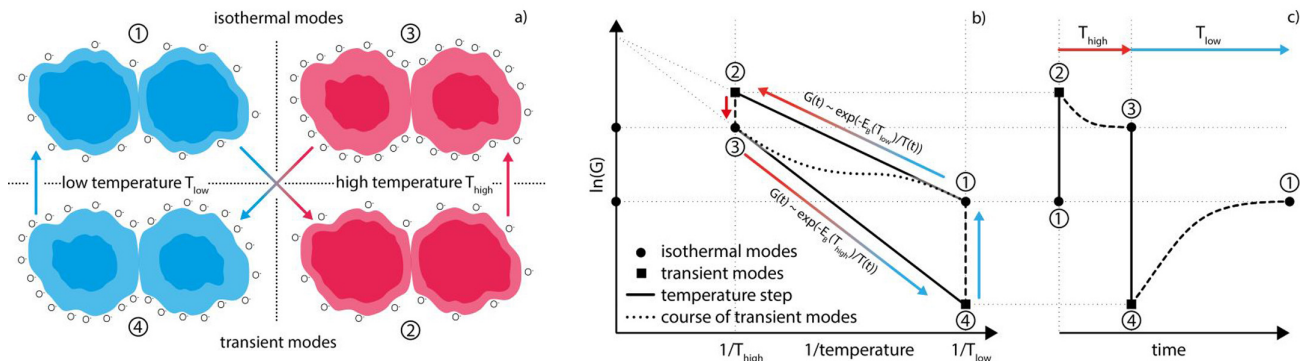


Fig. 1. a) Schematic illustration of the stationary and transient states of a grain-grain boundary in temperature cycled operation. The bright areas of the grains symbolize the depletion layer near the surface due to ionosorbed oxygen (shown schematically as O^-). b) Illustration of the Arrhenius plot of the sensor signal with two temperatures. Solid line: States with any rapid change in temperature. Dashed line: Relaxation at a constant temperature. Dotted line: steady states. Based on [6,7].

a temperature variation over a larger range e.g. from 420 °C to 200 °C this estimation is reliable. Baur reports a change of $E_b(T)$ of about 550 meV, therefore the adsorption term at 200 °C is factor 10⁻⁶ below the stationary case (see Supplementary material B for detailed calculation).

For small times after a temperature step Eq. (2) can be rewritten by

$$E_b(t) \approx N_s^*(t)^2 = E_b(0) \cdot \exp(-2k_d^* \cdot t). \quad (14)$$

Inserting in Eq. (1) and expanding by kT gives the conductance expressed by

$$kT \cdot \ln(G) \approx c_1(T) - E_b(0) \cdot \exp(-2k_d^* \cdot t) \quad (15)$$

or for very short times with a linear Taylor approximation by

$$\frac{1}{2}kT \cdot \ln(G) \approx \frac{1}{2}c_1(T) + E_b(0) \cdot k_d^* \cdot t \quad (16)$$

with temperature dependent constant $c_1 = kT \cdot \ln G_0$. The reverse reaction rate k_d^* can be split into two parts for gas concentration in ppb and low ppm range

$$k_d^* = k_{d,air}^* + \sum_i k_{d,gas,i}^* \quad (17)$$

where $k_{d,air}^*$ is the combined reaction rate for the reaction with residual compounds in air and for desorption by intrinsic processes and $k_{d,gas,i}^*$ for the reaction with the i th supplied gas molecules. This means that the logarithmic conductance can be described by an exponential function for short times respectively for very short times by a linear function. For low gas concentrations it is possible to describe the logarithmic conductance by a superposition of reaction rates.

3. Calibration strategy

For in field calibration one or more defined gas concentrations in a transportable way are needed. The calibration relies on the equilibrium headspace of the VOC (in our case toluene) soluted in a non-volatile liquid (squalane). A chemical model of the solution can estimate the gas concentration. To ensure traceable calibration GC-MS analytics was used to quantify the prepared samples.

The headspace concentration of a liquid solution in a closed volume in thermodynamic equilibrium is specified by the substance's vapour pressure p_{vap} and hence through Dalton's law the concentration can be calculated [16]. For highly diluted solutions the

vapour pressure p_i is proportional to the mole fraction x_i inside the solution according to Henry's law [16].

$$p_i = k_H \cdot x_i \quad (18)$$

The so called Henry's constant k_H is unique for every set of components and thus experimental values are not always obtainable, but the constant can be estimated for example by means of the UNIFAC (Universal Quasichemical Functional Group Activity Coefficients) model [17]. It estimates activity coefficients, which stand for the deviation from ideal behaviour inside chemical mixtures, for almost any combination of components, using their molecular structure and the interaction between functional groups. By assuming an ideal gas inside the calibration system (which is valid for normal ambient conditions), partial pressure and therefore the Henry's constant can be calculated from the activity coefficient γ_i [18]:

$$p_i = \gamma_i \cdot x_i \cdot p_{vap} \quad (19)$$

The UNIFAC model's gives an approximation of the equilibrium vapour pressure. Based on this the target concentration in the sample is estimated for preparation, which can later be compared with experimental results. The advantage of the model in consideration of a more complex approach like Monte-Carlo simulation on atomic scale is that values for new mixtures can be obtained very easily. In the end, this allows us, to produce different concentrations of a test gas by just modifying the substance's mole fraction inside the solution.

Henry's constant is highly temperature dependent but according to [19] the behaviour can be approximated by the temperature variation of the component's saturation vapour pressure and, what is normally negligible, activity coefficient inside the mixture. The insignificance has been verified by UNIFAC calculations, which state that deviation is below 1% for normal room temperatures. Toluene's vapour pressure for temperatures between 286 K and 409 K is given through the Antoine equation [20]:

$$\log(p_{vap}(\text{bar})) = 4.05043 - \frac{1327.62}{T(K) + 217.625 - 273.15} \quad (20)$$

A change in ambient temperature of about 10 K can change vapour pressure and thereby the headspace concentration by a factor of two. Under normal conditions, this means the theoretical concentration has to be adapted in dependence of the actual sample temperature, by using Eq. (20) and:

$$\frac{p_{T1}}{p_{T0}} = \frac{c_{T1}}{c_{T0}} \quad (21)$$

After bringing the sensor inside the calibration chamber, equilibrium has to be established before starting the measurement. The

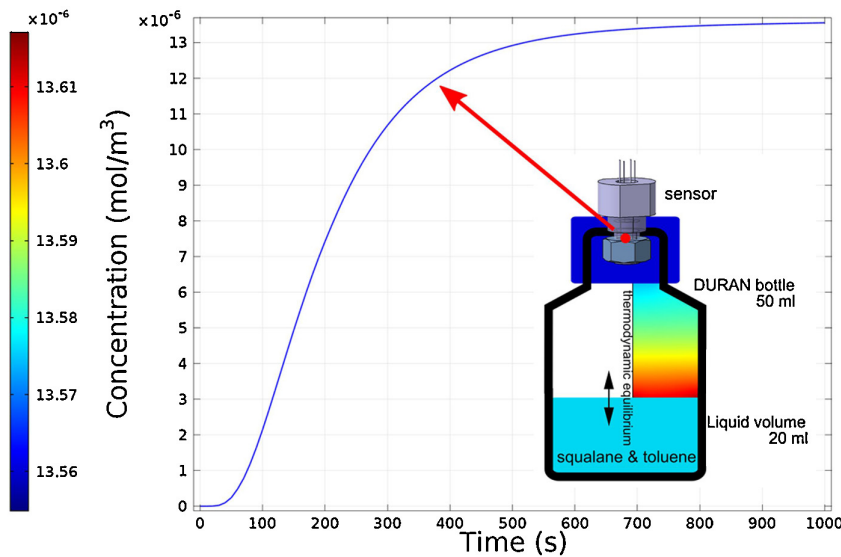


Fig. 2. Comsol Multiphysics simulation on the equilibrium establishment inside the calibration bottle, after 1000 s the concentration's variation inside the full volume is only 0.4% (colourbar). The line shows the concentration over time at the sensor's position, after about 600 s the concentration is nearly constant and equilibrium is reached.

required time can be estimated using FEM simulations (finite element method, software: COMSOL Multiphysics, model: Transport of Diluted Species). To this end we used a 2D geometrical model with rotational symmetry, details can be found in Supplementary material D. Assuming the diffusion coefficient of toluene in air from [21] and the self-diffusion coefficient from squalane [22] at 20 °C, toluene's partition coefficient obtained from the UNIFAC calculations, a stiff-spring velocity of 10000 m/s (as proposed from the software's documentation) and starting from a concentration of zero inside the bottle's headspace, the concentration at the sensor reaches an almost constant value after about 10 min (see Fig. 2).

Besides the generation of a defined headspace concentration for calibration, this thermodynamic equilibrium can also be used to generate the lowest possible concentration by using an empty squalene sample. The partition coefficient between liquid and gaseous phase is high enough to reduce the VOC concentration inside the headspace by a factor of at least 10^{-3} . This allows generating zero air and therefore a background signal under the same ambient conditions (humidity, permanent gases, temperature). By assuming additivity between the reaction rates caused by different gases from Eq. (17) a background independent sensor signal can be obtained.

This concept enables us to perform a field calibration using a small transportable bottle, containing a known concentration of gas, which sometimes has to be corrected, depending on ambient temperature and quantify background independent because of squalane's cleaning function.

4. Experimental setup and sample preparation

Gas sensor measurements were performed with an AS-MLV sensor from ams Sensor Solutions Germany GmbH. This SnO_2 sensor is specified for measuring VOCs and among these aromatic compounds like toluene. The sensor is built up on a silicon nitride membrane, which makes heating less power consuming and, what is more important for us, fast (time constant $t_1 = 7\text{ms}$, see Supplementary material C). The originally mounted protection membrane was removed for our experiments. For sensor heating and conductance measurement a SniffChecker module from 3S GmbH – Sensors, Signal Processing, Systems was used. It provides pro-

grammable temperature cycles and a measurement frequency of 100 Hz. The working range of the conductance measurement was enhanced by attaching a log amplifier LOG112 from Texas Instruments Inc. so that the combined system is capable of measuring conductance in the range of 100 nS to mS on a logarithmic scale (details can be found in [6]). The relaxation process described above therefore yields a linear sensor signal as shown in Eq. (16). The high measurement range is needed because of the high temperature jumps in our temperature cycle: it principally consists of two parts, 300 ms at 450 °C for surface oxidation and 200 ms at a lower temperature for measuring the oxygen relaxation after the cooling. Ten different lower temperatures between 200 °C and 380 °C with a step width of 20 °C were chosen, which gives a total temperature cycle of 5 s.

The isolated volume was realised by a 50 ml DURAN laboratory bottle (see Fig. 2). The amount of liquid was set to 20 ml. Assuming that the whole headspace is replaced by ambient air with every opening, the sample can be used more than 30 times before exceeding 5% deviation. The sensor itself is mounted inside a GL 32 DURAN cap, which can be mounted on the bottle and ensures proper tightness.

The calibration liquids were produced using the precision balance KB 240-3N (KERN & Sohn GmbH) and a magnetic stirrer to ensure proper mixing. The test substance toluene was diluted in squalane (CAS: 111-01-3), which is a long-chained isoalkane (Hexamethyltetrasicosane) and has a negligible vapour pressure below 0.02 μPa [23] at room temperature. The substance was cleaned from all volatile substances before at 80 °C and a 500 ml/min flow of zero air (see Supplementary material A, blue highlighted samples) or to achieve even higher purity and avoid oxidation, which is needed for sub-ppm standards, nitrogen (other samples). To achieve small headspace concentrations down to 10 ppb subsequent dilution steps are needed, for proper mixing the liquid is stirred for a minimum of 15 min. Two logarithmic serial dilutions were produced yielding liquids with mole fractions from 180 ppm to 35%.

All samples and their UNIFAC predicted headspace concentrations ($k_H = 1.9\text{kPa}$ at 20 °C) can be received from the Supplementary material A. On the first, zero air cleaned dilution series analytical reference measurements using a Thermo Scientific GC-MS system (TRACE Ultra Gas Chromatograph, DSQ II mass

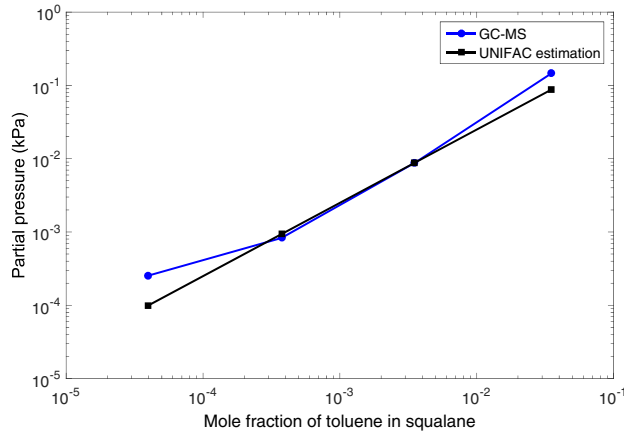


Fig. 3. Comparison of the UNIFAC predicted vapour pressures (black, squares) and the quantification done by the Thermo Scientific GC-MS system. Agreement is quite good, the deviation of the lowest sample probably is due to adsorption on the injection needle's surface.

spectrometer) were done to ensure the calibration's reproducibility and verify the UNIFAC prediction. 5 ml of calibration headspace were injected by hand with a gas tight syringe into a split/splitless injector. Additionally 5 μ l liquid toluene was injected later during each run and used as an internal standard. 5 ml of a pure toluene headspace was used to quantify the calibration samples. Since no separation was needed an isothermal temperature profile at 120 °C was used and only mass to charge ratios $m/Z = 91$ (toluene main peak) were recorded (SIM, selected ion monitoring). Hence, partial pressures p_i can be calculated by the quotient of the peak areas from sample A_{sample} and pure toluene headspace A_{toluene} . All measurements were normalised by the internal standards $A_{\text{int_sample}}$ and $A_{\text{int_toluene}}$. Calculated pressures $p_i = \frac{A_{\text{sample}}}{A_{\text{toluene}}} \cdot \frac{A_{\text{int_toluene}}}{A_{\text{int_sample}}} \cdot p_{0,\text{toluene}}$ can be seen in Fig. 3. UNIFAC prediction seems to work out very well for this set of compounds. Only for the smallest observed concentration deviation is a bit higher, which is probably due to some adsorption on the injection needle's surface.

For quantification and comparison additional measurements with our gas mixing apparatus (GMA), which is described in [10],

were done. Zero air at 0% humidity containing 10, 30, 100, 300 ppb, and 1, 2.6, 3, 5, 11 ppm toluene was produced using a permeation device emitting 38 ng/min and an accuracy of $\pm 50\%$.

5. Results

5.1. Feature calculation

From the conductance of one cycle (see Fig. 4), ten rate constants (one for each low temperature plateau) can be calculated. As seen in the inset of Fig. 4 especially for low temperatures in pure air and at low concentration the conductance exceeds the measurement range. As shown above, compare Eq. (16), for a short time after the temperature change, conductance follows an exponential curve. The sensor system (logarithmic amplifier) therefore yields a linear output over time. The valid time interval for this assumption mainly depends on two things: the gas concentration and the height of the temperature step. The lower the change in temperature and the higher the gas concentration the faster the relaxation and the smaller is the valid time interval. The energy barrier is calculated, according to Eq. (3), from the conductance value before and right after the step, ideally before any relaxation took place. Some error arises on the one hand from the fact that the conductance is not perfectly constant at the end of the 450 °C plateau, on the other hand the cooling does not occur immediately ($t_1 = 7\text{ms}$, see Suppl. material C). Moreover, it is possible, that the lowest conductance value appears between two data points because the interval between two measurements is 10 ms. Since this energy barrier is a property of the high temperature state, it should be equal for every temperature step. Energy barrier values typically are around 550–600 meV (depending on gas concentration) and, looking at the ten values obtained from one cycle, show a standard deviation of about 20 meV.

5.2. Feature properties

Quantification and feature extraction were tested by GMA measurements. Measurement process was as follows: after 15 min of pure zero air, the sensor was exposed to the gas for another 15 min, following again 15 min of zero air. The rate constants for every temperature and every cycle were computed. Compared to the quasistatic conductance (the conductance at the end of the first 450 °C

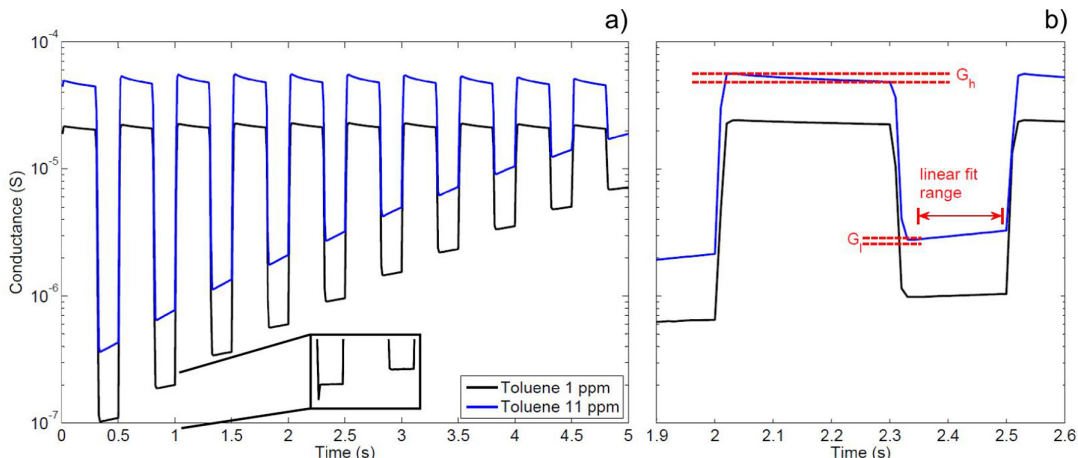


Fig. 4. a) Conductance of one full cycle for 1 and 11 ppm toluene, at low temperatures sometimes the end of measurement range is reached (see inset), this applies mainly to measurements with low toluene concentrations or in pure background, where the conductance is below 100 nS (GMA). The features needed for the quantification are shown in b) the energy barrier is calculated from the logarithmic conductance difference $\ln(G_h) - \ln(G_l)$ and the height of the temperature jump, for the rate constant a linear fit is performed on the logarithmic data (corresponding to an exponential fit on normal data).

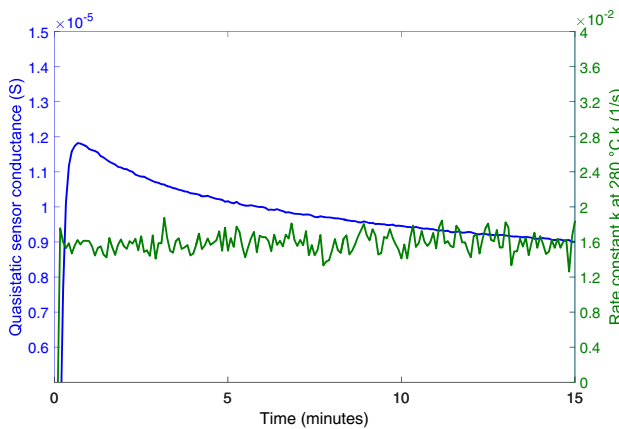


Fig. 5. Behaviour of quasistatic conductance (at 450 °C) with notable overshoot at the beginning of each toluene exposure (starting at $t = 0$) versus calculated rate constant (for 280 °C, similar time dependence for other temperatures) with almost constant value over observed time.

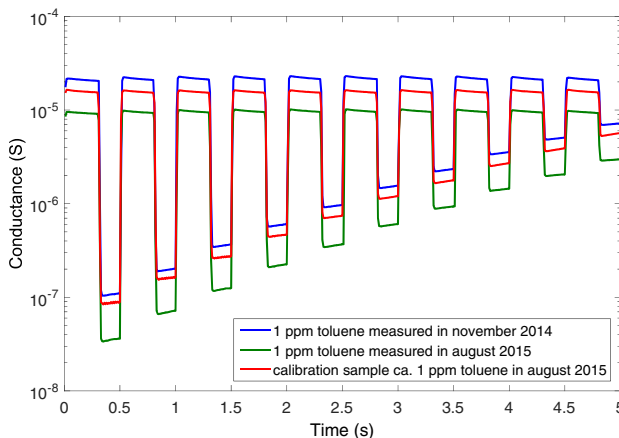


Fig. 6. a) Sensor conductance changes significantly (factor 2) for the same concentration within a time interval of six months. b) During the same time rate constant nevertheless still offers a nearly correct quantification, especially for high temperatures.

plateau over time) the rate constant shows a much more suitable response to the gas exposure for quantification. Fig. 5 shows the signal for both, quasistatic conductance and rate constant at 280 °C, for an exposure of 1 ppm toluene beginning at $t = 0$. Rate constant reaches its final value almost immediately after toluene reaches the sensor surface whereas the conductance shows some overshooting and still no stable value after 15 min, which makes quantification slow and difficult. This overshooting can be observed for concentrations above 100 ppb and increases with higher concentrations.

Besides this short-term effect rate constant is a more stable feature compared to sensor conductance also for long-term examinations. 1 ppm of toluene gas inside the GMA was measured two times within a time interval of six months. During storage the sensor conductance reduced significantly, as can be seen in Fig. 6a). Evaluating the reaction rate constant it is still possible to perform a correct quantification, which is shown in Fig. 6b). The shape of a gas sensor signal often is more stable than the conductance itself, which is explainable with the described sensor model above. By only evaluating the signal's shape the exponential prefactor G_0 in Eq. (1) does not affect the quantification, which mainly depends on

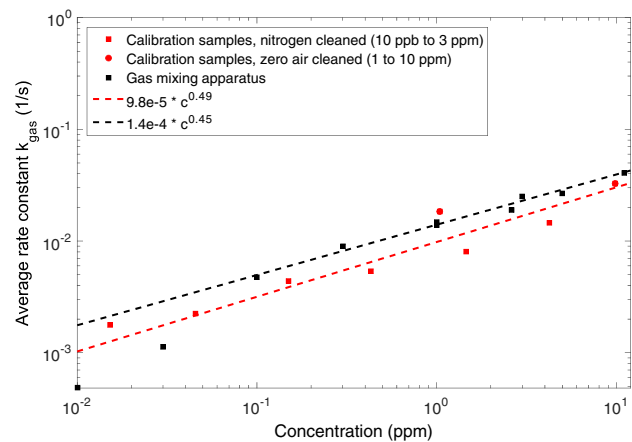


Fig. 7. Average rate constants (50 cycles) obtained from measurements inside our gas mixing system in zero air and with the produced calibration standards under normal room conditions. Accordance is quite good, although the scattering still is quite high, a quantification with an error of one half magnitude is possible. Dotted lines show the best representing power law for both types of measurements.

the changing energy barrier E_b , which is dominated by the surface oxygen occupation, compare Eq. (2).

5.3. Calibration and quantification

For comparison between room air and zero air measurements and the generation of a calibration curve, the mean value of all gas's reaction rates is used. Toluene shows only slightly temperature dependent reaction rate and therefore its response is used, as it is in gas chromatographic analysis [13], to quantify the total VOC concentration of ambient air. Looking at each single temperature is especially needed to achieve selectivity, which needs further investigations. Here we are aiming for quantification.

Concentrations between 10 ppb and 11 ppm have been measured inside our GMA with zero air background. The background signal is orders of magnitude smaller than the gas signals and furthermore often cannot be calculated because within the 200 ms plateau at T_f no relaxation occurs and no slope can be extracted. For this reason no background rate constant was subtracted for the GMA measurements. The mean values of all ten rate constants over 50 cycles are shown in Fig. 7 as black squares on a double logarithmic scale. Since all points are in one line, the best representation for the sensor signal is a power law of the form $a \cdot c^b$ with gas concentration c , and constants $a = 1.4 \cdot 10^{-4}$ and $b = 0.45$. For the two lowest concentrations, the calculated rate constants might be a bit too low, because there is still too little gas to cause a significant relaxation in such a short time.

Calibration standards were each measured for a time of 30 min to ensure proper equilibrium. Between each calibration sample an zero sample is measured and by this a background signal is recorded. The subtracted mean value of every temperature and 50 cycles for the low concentrated calibration probes are also shown in Fig. 7, but as red squares. In principle, all measured points, GMA and calibration standards show similar behaviour. Both follow an exponential curve, despite the constants $a = 9.8 \cdot 10^{-5}$ and $b = 0.49$ deviate slightly. Especially at low concentration deviation increases, which is probably due to the mentioned missing relaxation in almost clean air at low concentrations, which makes the calculated rate constant appear too low. The deviation allows a quantification with an error of about a half order of magnitude although measurements were done under very different ambient conditions.

6. Conclusion

A method for quantitative measurement using TCO was implemented based on a sensor model. To this end, we derived rate constants for the surface reaction between target gas and adsorbed oxygen temperature dependent. The results indicate that rate constants are less subjected to short and long-term sensor drift compared to the sensors conductance. We could show that rate constants are depending on the concentration by a power law and that this method is feasible for measuring toluene in a wide concentration range (at least 10 ppb to 10 ppm). For calibration, particularly in the field calibration, standards were prepared based on equilibrium vapour pressure. The vapour pressure can be predicted by a simple model (UNIFAC) allowing an easy transfer of the obtained results to arbitrary mixture of VOCs in non-volatile liquids. The obtained samples have been characterised using GC–MS and sensor quantification was performed under field conditions. The quantification was possible in various backgrounds (in pure air at the gas mixing system as well as in ambient air for the calibration standards). This emphasises that the model predicted compensation of the gas background is likely. Based on the concept presented in this work comprehensive field calibration systems using various VOC standards especially to achieve statistical relevant data and selectivity can be foreseen.

Acknowledgements

Part of this work was funded from the European Union's Seventh Framework Programme for research, technological development and demonstration under grant agreement No 604311, Project SENSIIndoor. We also thank the partners inside the Key-VOCs project, ENV56 from the European Metrology Research Programme (EMRP), for inspiring discussions especially Birte Mull, Matthias Richter and Wolfgang Horn from the Bundesanstalt für Materialforschung und –prüfung.

Appendix A. Supplementary data

Supplementary data associated with this article can be found, in the online version, at <http://dx.doi.org/10.1016/j.snb.2016.08.002>.

References

- [1] I. Elmi, S. Zampolli, E. Cozzani, F. Mancarella, G.C. Cardinali, Development of ultra-low-power consumption MOX sensors with ppb-level VOC detection capabilities for emerging applications, *Sens. Actuators B Chem.* 135 (2008) 342–351, <http://dx.doi.org/10.1016/j.snb.2008.09.002>.
- [2] M. Leidinger, T. Sauerwald, W. Reimlinger, G. Ventura, A. Schütze, Selective detection of hazardous VOCs for indoor air quality applications using a virtual gas sensor array, *J. Sens. Sens. Syst.* 3 (2014) 253–263, <http://dx.doi.org/10.5194/jsss-3-253-2014>.
- [3] M.J. Madou, S.R. Morrison, *Chemical Sensing with Solid State Devices*, Academic Press, San Diego, 1989.
- [4] N. Barsan, U. Weimar, Conduction model of metal oxide gas sensors, *J. Electroceram.* 7 (2001) 143–167, <http://dx.doi.org/10.1023/A:1014405811371>.
- [5] P. Reimann, A. Schütze, Fire detection in coal mines based on semiconductor gas sensors, *Sens. Rev.* 32 (2012) 47–58, <http://dx.doi.org/10.1108/02602281211197143>.
- [6] T. Baur, A. Schütze, T. Sauerwald, Optimierung des temperaturzyklischen Betriebs von Halbleitergassensoren, *Tech. Mess.* 82 (2015) 187–195.
- [7] T. Sauerwald, T. Baur, A. Schütze, Strategien zur Optimierung des temperaturzyklischen Betriebs von Halbleitergassensoren, in: XXVIII. Messtechnisches Symp. Des Arbeitskreises Der Hochschullehrer Für Messtechnik, Shaker Verlag, Aachen, 2014, pp. 65–74, <http://dx.doi.org/10.5162/AHMT2014/3.1>.
- [8] M. Bastuck, M. Leidinger, T. Sauerwald, A. Schütze, Improved quantification of naphthalene using non-linear partial least squares regression, in: 16th Int. Symp. Olfaction Electron., Nose, Dijon, Fr., 2015 <http://arxiv.org/abs/1507.05834>.
- [9] H.-E. Endres, H.D. Jander, W. Göttler, A test system for gas sensors, *Sens. Actuators B Chem.* 23 (1995) 163–172, [http://dx.doi.org/10.1016/0925-4005\(94\)01272-J](http://dx.doi.org/10.1016/0925-4005(94)01272-J).
- [10] N. Helwig, M. Schüller, C. Bur, A. Schütze, T. Sauerwald, Gas mixing apparatus for automated gas sensor characterization, *Meas. Sci. Technol.* 25 (2014), <http://dx.doi.org/10.1088/0957-0233/25/5/055903>.
- [11] A.C. Romain, J. Nicolas, Long term stability of metal oxide-based gas sensors for e-nose environmental applications: an overview, *Sens. Actuators B Chem.* 146 (2010) 502–506, <http://dx.doi.org/10.1016/j.snb.2009.12.027>.
- [12] S. Paczkowski, M. Paczkowska, S. Dippel, N. Schulze, S. Schütz, T. Sauerwald, et al., The olfaction of a fire beetle leads to new concepts for early fire warning systems, *Sens. Actuators B Chem.* 183 (2013) 273–282, <http://dx.doi.org/10.1016/j.snb.2013.03.123>.
- [13] M. Schüller, N. Helwig, A. Schütze, T. Sauerwald, G. Ventura, Detecting trace-level concentrations of volatile organic compounds with metal oxide gas sensors, in: IEEE Sensors, Baltimore, 2013, pp. 1–4.
- [14] J. Ding, T.J. Mcavoy, R.E. Cavicchi, S. Semancik, Surface state trapping models for SnO₂–based microhotplate sensors, *Sens. Actuators B Chem.* 77 (2001) 597–613.
- [15] S.R. Morrison, *The Chemical Physics of Surfaces*, Springer, US, Boston, MA, 1977, <http://dx.doi.org/10.1007/978-1-4615-8007-2>.
- [16] P.W. Atkins, *Physikalische Chemie*, WILEY-VCH, Verlag GmbH, Weinheim, 2001.
- [17] A. Fredenslund, R.L. Jones, J.M. Prausnitz, Group-contribution estimation of activity coefficients in nonideal liquid mixtures, *AIChE J.* 21 (1975) 1086–1099, <http://dx.doi.org/10.1002/aic.690210607>.
- [18] J.H. Hildebrand, J.M. Prausnitz, R.L. Scott, *Regular and Related Solutions*, Litton Educational Publishing Inc., New York, 1970.
- [19] F.L. Smith, A.H. Harvey, Avoid common pitfalls when using Henry's law, *Chem. Eng. Prog. (September)* (2007) 33–39.
- [20] B.E. Poling, J.M. Prausnitz, J.P. O'Connell, *The Properties of Gases & Liquids*, 5th ed., McGraw-Hill Inc., New York, 2001, <http://dx.doi.org/10.1036/0070116822>.
- [21] H.Y. Erbil, Y. Avci, Simultaneous determination of toluene diffusion coefficient in air from thin tube evaporation and sessile drop evaporation on a solid surface, *Langmuir* 18 (2002) 5113–5119, <http://dx.doi.org/10.1021/la011557a>.
- [22] B. a. Kowert, M.B. Watson, N.C. Dang, Diffusion of squalane in *n*-alkanes and squalane, *J. Phys. Chem. B* 118 (2014) 2157–2163, <http://dx.doi.org/10.1021/jp411471r>.
- [23] V. Piacente, D. Fontana, P. Scardala, Enthalpies of vaporization of a homologous series of *n*-alkanes determined from vapor pressure measurements, *J. Chem. Eng. Data* 39 (1994) 231–237, <http://dx.doi.org/10.1021/je00014a009>.

Biographies

Caroline Schultealbert studied microtechnology and nanostructures at Saarland University and received her master's degree in 2015. She is currently a Ph.D. student at the Lab for Measurement Technology at Saarland University and focusses on the model based temperature cycled operation of gas sensors, their calibration and emission materials.

Tobias Baur studies microtechnology and nanostructures at Saarland University and received his bachelor's degree in 2014. He developed a mos gas sensor model for the temperature cycled operation during his bachelor thesis at the Lab for Measurement Technology at Saarland University and is there currently working on the development of a micro GC system during his master thesis.

Andreas Schütze studied Physics and received his doctorate in Applied Physics from Justus-Liebig-Universität in Gießen in 1994 with a thesis on micro gas sensor systems. After some years in industry, he joined the University of Applied Sciences in Krefeld, Germany, as professor for Microsystems Technology from 1998 to 2000. Since 2000 he is a full professor for measurement science and technology in the Department of Mechatronics at Saarland University, Saarbrücken, Germany. His research interests include microsensors and microsystems, especially advanced chemical sensor systems, both for gas and liquid phase, for security and control applications.

Dr. Stefan Boettcher, born March 31, 1972 in Frankenthal (Germany), studied chemistry in Kaiserslautern. His PhD thesis "Reaktivität von Enyl- und Dienylkomplexen gegenüber Alkinen und Vinylcyclopropan" had a strong focus on structure elucidation, using preparative HPLC and NMR techniques. After a first job in industries in the field of GC/MS and LS/MS he joined the department of pharmaceutical and medicinal chemistry of Saarland University. Since that he is working on method development for ADME in drug discovery in different projects, like estrogen dependent diseases, HCV, congestive heart failure, novel type antibiotics. Furthermore he supported other groups inside Saarland University (Drug Delivery, Pharmaceutical Biology, Physics, Helmholtz Institute HIPS) and international groups (Drug Safety, University of Damascus, Syria) in analytic method development.

Tilman Sauerwald received his PhD in 2007 at the University of Giessen working on the influence of surface reactions to the multi-signal generation of metal oxide sensors. Since 2011 he is working at the Lab of Measurement Technology at the Saarland University. His current focus is the detection of trace gases by developing of model based techniques for multi-signal generation.

Supplementary material A

sample nr.	toluene's mole fraction	UNIFAC predicted concentration at 20 °C
1.1	35 ‰	660 ppm
1.2	3.5 ‰	65 ppm
1.3	0.38 ‰	7.1 ppm
1.4	0.040 ‰	740 ppb
2.1	180 ppm	3.3 ppm
2.2	64 ppm	1.2 ppm
2.3	18 ppm	330 ppb
2.4	6.6 ppm	120 ppb
2.5	1.9 ppm	35 ppb
2.6	0.67 ppm	12 ppb

Table A1: Prepared calibration standards, their toluene content and the UNIFAC predicted headspace concentration. Blue samples were produced using zero air cleaned squalane and analysed with a Thermo Scientific GC-MS system. Not highlighted samples are based on nitrogen cleaned squalane (the higher purity is needed for sub-ppm standards).

Supplementary material B

The rate equation Eq. (11) describes the change of the surface occupation

$$\frac{dN_s^*}{dt} = p_{ads}(T) \cdot \exp\left(-\frac{N_s^{*2}}{k_b T}\right) - p_{des}(T) \cdot N_s^* \quad (B1)$$

where $p_{ads}(T) = k_a^*(T) \cdot \exp\left(\frac{x\Delta H}{2k_b T}\right)$ is the adsorption factor and $p_{des}(T) = k_d^*(T)$ is the desorption factor. Both factors are only temperature dependent parameters and their values change instantly with a temperature variation [12]. Thus, the parameters do not change their values during the relaxation of the surface occupation. In steady state, the variation of the surface occupation is near to zero.

$$\frac{dN_s^*}{dt} \Big|_{t \rightarrow \infty} = p_{ads}(T) \cdot \exp\left(-\frac{N_s^{*(t \rightarrow \infty)^2}}{k_b T}\right) - p_{des}(T) \cdot N_s^*(t \rightarrow \infty) \stackrel{!}{=} 0 \quad (B2)$$

The ratio of adsorption and desorption parameter is in the steady state ($N_s^*(t \rightarrow \infty) = N_{s,\infty}^*$)

$$\frac{p_{ads}(T)}{p_{des}(T)} = \frac{N_{s,\infty}^*(t \rightarrow \infty)}{\exp\left(-\frac{N_{s,\infty}^{*2}}{k_b T}\right)}. \quad (B3)$$

Baur ([6]) measured the temperature dependent energy barrier (proportional to the surface occupation) in the steady state for the used sensor (AS-MLV). Thereby, it is possible to calculate the adsorption-desorption-factor ratio with Eq. (24) and the measured values. For a temperature change from a high to low temperature ($T_{high} \rightarrow T_{low}$) the relaxation of the surface occupation starts with the value of the temperature T_{high} in steady state and the adsorption and desorption parameters instantly change their value to $p_{ads/des}(T_{low})$. Thus, Eq. (22) results for small times $t \rightarrow 0$ after a temperature change in

$$\frac{dN_s^*}{dt} \Big|_{t \rightarrow 0} = p_{ads}(T_{low}) \cdot \exp\left(-\frac{N_{s,\infty}^{*(T_{high})^2}}{k_b T_{low}}\right) - p_{des}(T_{low}) \cdot N_{s,\infty}^*(T_{high}) \quad (B4)$$

The adsorption-desorption ratio is equal to

$$ratio = \frac{p_{ads}(T_{low})}{p_{des}(T_{low})} \frac{\exp\left(-\frac{N_{s,\infty}^{*(T_{high})^2}}{k_b T_{low}}\right)}{N_{s,\infty}^*(T_{high})} = \frac{N_{s,\infty}^*(T_{low})}{N_{s,\infty}^*(T_{high})} \exp\left(\frac{N_{s,\infty}^{*(T_{high})^2} - N_{s,\infty}^{*(T_{low})^2}}{k_b T_{low}}\right) \quad (B5)$$

Figure B1 shows a temperature dependent adsorption-desorption ratio for temperature steps from $T_{high} = 420$ °C to $T_{low} = 145 \dots 395$ °C. Thereby, the adsorption term is negligible for a

ratio equal to 10^{-1} . So we see, it is possible to neglect the adsorption term for temperature changes with $\Delta T = 50$ °C.

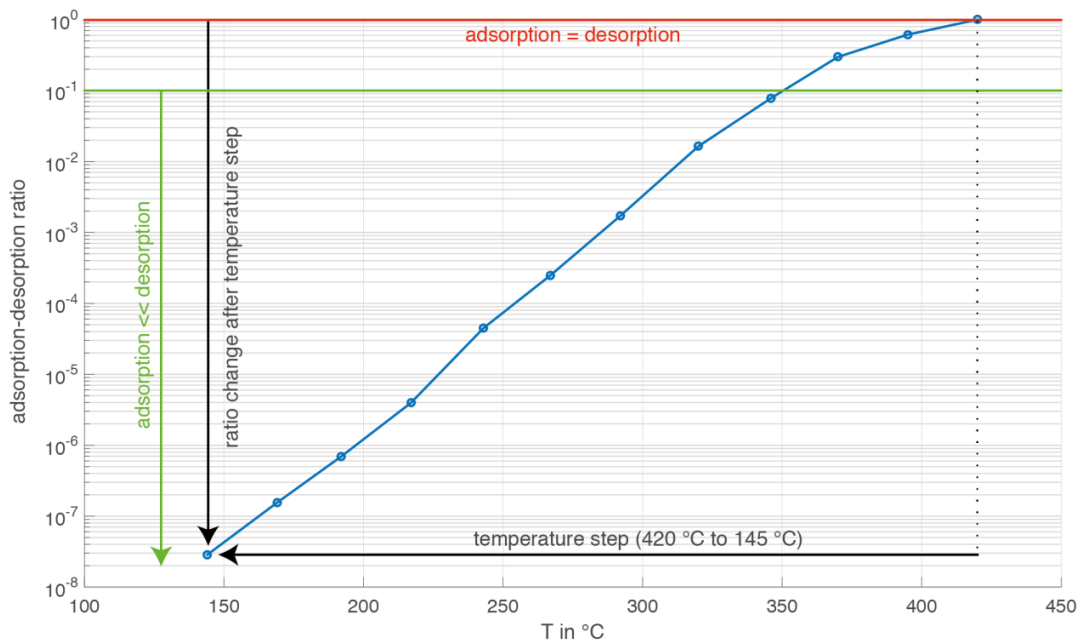


Figure B1. Adsorption-desorption ratio of temperature changes from 420 °C to 145...395 °C.

Supplementary material C

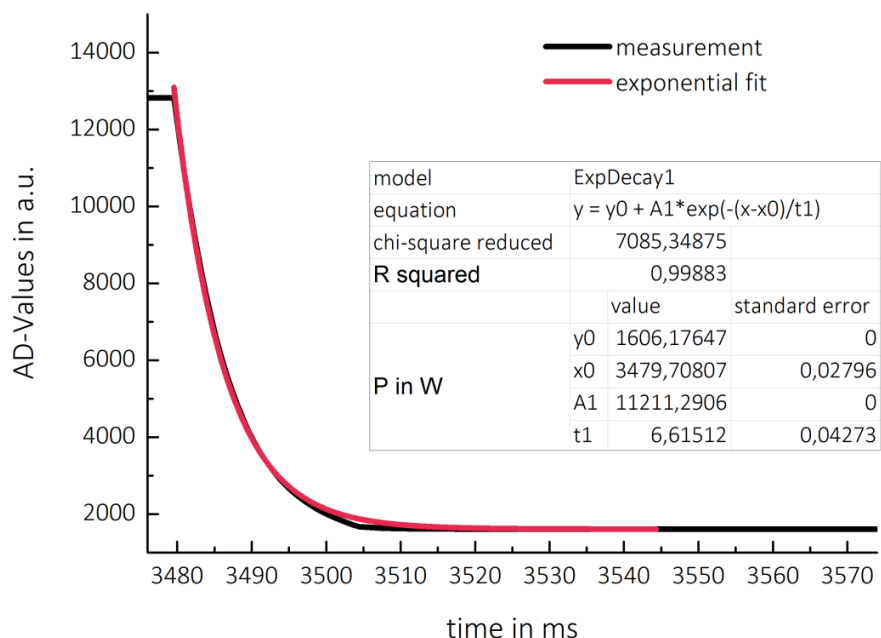


Figure C1. Measured time constant (by thermal imaging, camera: Flir i7) of the used AS-MLV sensors.

Supplementary material D

FEM simulations were done using COMSOL Multiphysics 4.2a. The bottle's geometry is represented by a 2D structure with rotational symmetry that can be seen in Fig. D1. The inner radius of the bottle (area 1 and 2) is 2 cm. The bottle necks radius (area 3) is 0.9 cm. Since the $r = 0.25$ cm wide sensor mount (area 4) extends 0.5 cm into the bottle a ridge is drawn by a difference between the bottle neck and a 0.2×0.5 cm rectangle. The height of area 1 (fluid level) is 1.8 cm, which is 22.6 ml. The overall volume of the bottle is approximately 80 ml.

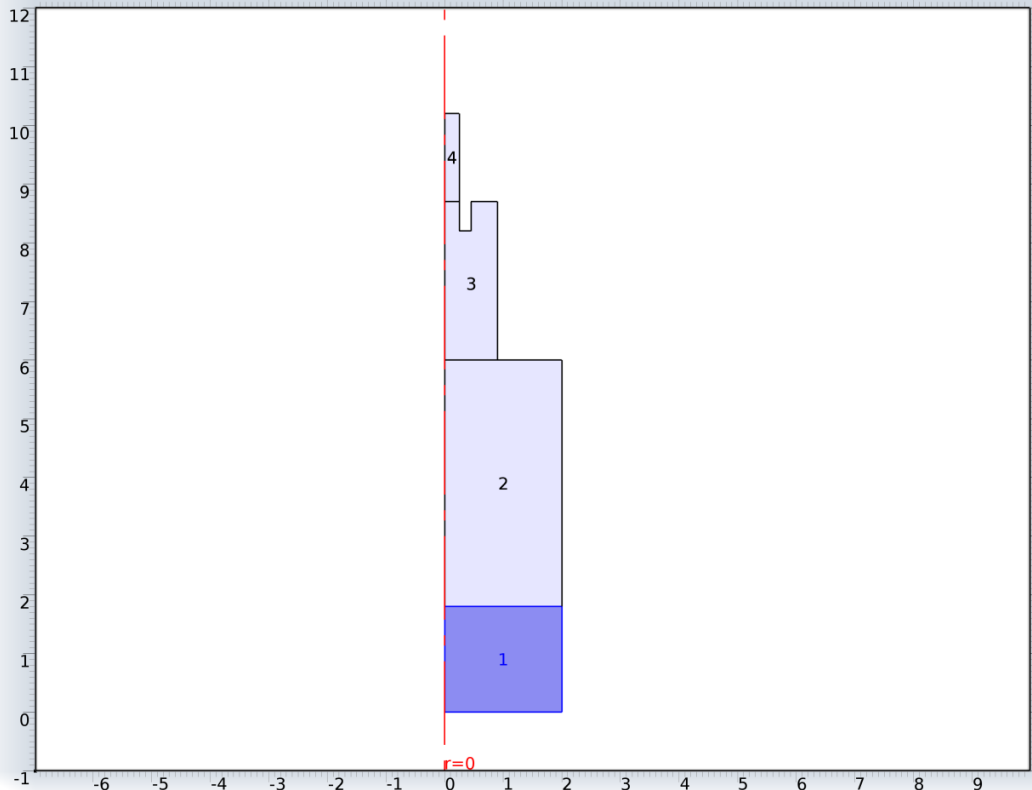


Figure D1. Rotationally symmetric geometry used for FEM simulations. Area 1 (blue) is defined as squalane with toluene and areas 2, 3 and 4 as air. 1 and 2 represent the bottle's body, 3 the bottle neck and 4 the sensor's mount.

Both phases (area 1 and areas 2, 3 and 4) are modelled separately but with the same implemented model "Transport of diluted species". This model mainly depends on convection and diffusion (Fick's laws of diffusion), flow velocity is set to zero and temperature is homogenous, so only diffusion occurs. To enable a transition of the diluted species between both phases, an in and outflow is defined between area 1 and 2. The transition velocity

depends on the concentration at the boundary weighted with the partition coefficient K (formula: $M^*(K*c_2 - c_1)$ respectively $M^*(c_1 - K*c_2)$, where c_1 is the headspace concentration and c_2 the fluid concentration). Additionally a stiff-spring velocity M is used and set to the recommended value of 10000 m/s to ensure continuity and solvable differential equations. The needed parameters to perform the simulation are given in Table D1

parameter	description	value
K	Partition coefficient obtained from UNIFAC calculations	0.0004063
M	Stiff-spring velocity (as recommended)	10000 m/s
Dc1	Toluene's diffusion coefficient inside air	8e-6 m ² /s [21]
Dc2	Self-diffusion coefficient from squalane	3.3e-7 cm ² /s [22]
C1_initial	Initial headspace concentration	0 mol/m ³
C2_initial	Initial fluid concentration	0.03561 mol/m ³

Table D1: Parameters used for the FEM simulation of the thermodynamic equilibrium.

4.1.4 Paper 1 – Novel Method for the Detection of short trace Gas Pulses with Metal Oxide Semiconductor Gas Sensors

T. Baur, C. Schultealbert, A. Schütze and T. Sauerwald
Saarland University, Lab for Measurement Technology, Saarbrücken, Germany

J. Sens. Sens. Syst. (2018), 7, 411–419

The original paper can be found, in the online version, at <https://doi.org/10.5194/jsss-7-411-2018>.

© 2018 by the authors. This article is an open access article distributed under the terms and conditions of the Creative Commons Attribution (CC BY) license (<http://creativecommons.org/licenses/by/4.0/>).



Novel method for the detection of short trace gas pulses with metal oxide semiconductor gas sensors

Tobias Baur, Caroline Schultealbert, Andreas Schütze, and Tilman Sauerwald

Laboratory for Measurement Technology, Saarland University, 66123 Saarbrücken, Germany

Correspondence: Tobias Baur (t.baur@lmt.uni-saarland.de)

Received: 19 January 2018 – Accepted: 22 April 2018 – Published: 28 May 2018

Abstract. A novel method for the detection of short pulses of gas at very low concentrations, the differential surface reduction (DSR), is presented. DSR is related to the temperature pulsed reduction (TPR) method. In a high temperature phase, e.g., at 400 °C, the surface of a metal oxide semiconductor gas sensor (MOS) is oxidized in air and then cooled abruptly down to, e.g., 100 °C, conserving the large excess of negative surface charge. In this state reactions of reducing gases with surface oxygen are strongly favored, which increases the sensitivity. Due to the large energy barrier between metal oxide grains caused by the excess surface charge, a highly precise electrical measurement at very low conductance (down to 10^{-11} S) is a prerequisite for this method. Moreover, the electrical measurement must be very fast to allow a good resolution of retention times. Applying the method to a doped SnO_2 detector, gas pulses down to a dosage of 1 ppb times seconds can be detected. The gas transport inside the detector is simulated using the finite element method (FEM) to optimize the gas transport and to keep response and recovery time as short as possible. With this approach, we have demonstrated a detection limit for ethanol of below 47 fg.

1 Introduction

Gas chromatography (GC) is a very versatile method for the analysis of gases as it allows the separation of different gases over time. For gas analysis, GC combined with mass spectrometry (MS) is the gold standard, but it is restricted to large and relatively high-cost systems mainly for laboratory use. However, the demand for mobile gas analysis systems has steadily increased over the past few years, especially for selective detection of trace gases, e.g., for outdoor (Mead et al., 2013; Spinelle et al., 2015, 2017) or indoor air quality measurement (Geiss et al., 2011; Koistinen et al., 2008) or medical diagnostics (Bajtarevic et al., 2009). For some applications sensors and adaptable sensor arrays have been investigated (Leidinger et al., 2015; Roberts et al., 2014; Sasahara et al., 2007). The classification of various hazardous VOCs at ppb concentration level has been demonstrated by some of us in earlier works using metal oxide sensors combined with temperature cycled operation (TCO) and pattern recognition as well as with novel MOF-based micro-preconcentrators (Leidinger et al., 2014; Wilhelm et al., 2016). Under ideal conditions this facile ap-

proach allows low-cost, online measurements with sub-ppb accuracy (Leidinger et al., 2017). However, the training effort for a sensor array approach – independent if a virtual multi-sensor or a physical array approach is used – increases strongly with the number of gases because combinations of gases at various concentrations need to be tested to identify potential interactions between gases. For complex gas mixtures a chromatographic system, therefore, seems to be more adequate. The miniaturization of the chromatographic system is a prerequisite for many applications to ensure mobility and reduce system costs. The miniaturization of GC columns (μ GC) (Sanchez et al., 2010; Zampolli et al., 2005) and additional building blocks like injectors and sampling units (Trzciński et al., 2017; Zampolli et al., 2007) has been investigated intensively and proven to be feasible. However, these systems are restricted in the choice of detectors compared to lab equipment. The most common GC detector principles, the flame ionization detector (FID) and the mass spectrometer (MS), cannot be scaled to miniature size without loss of performance, i.e., time of operation due to gas consumption for FIDs or loss of resolution for MS. Detectors

for μ GC are therefore an important research topic. In addition to the miniaturization of common detector principles like, e.g., TCD (thermal conductivity detector) (Mahdavifar et al., 2015) and PID (photoionization detector) (Narayanan et al., 2014), the combinations with other detector principles, e.g., nanocantilevers (Chapman et al., 2007) or ion mobility spectrometers (Eiceman et al., 2002), have been demonstrated. The combination with metal oxide semiconductor (MOS) gas sensors also goes back many decades (Bârsan and Ionescu, 1994). MOS sensors are very sensitive (Zampolli et al., 2005), inexpensive and able to detect a broad range of gases. Recently, we have demonstrated that the sensitivity of MOS sensors can be increased significantly by a certain temperature cycled operation (TCO) mode (Baur et al., 2015) and that the quantity of gas can be derived directly from the sensor signal using a simple model for the surface reduction process (Schultealbert et al., 2017). From this starting point, this article demonstrates a new method of using a MOS sensor to detect short trace gas pulses called differential surface reduction (DSR) which shows an unprecedented detection limit and stable detection properties. This method of course is not limited to the use as GC detector, but can also improve the capabilities of sensor-micro-preconcentrator systems.

2 Concept of differential surface reduction (DSR)

A GC detector detects the amount of substance during peaks generated by the separation of gas mixtures in the GC column. In the time interval $[t_0, t]$ at a constant volume flow \dot{V} , the amount of substance n of one peak passes the sensor. In gas measurements, the concentration c is generally the mole fraction x of the analyte. The relationship between the amount of substance n and the time-dependent concentration $c(t)$ can be written with the molar volume V_m as Eq. (1).

$$n = \int_{t_0}^t \frac{\dot{V}}{V_m} \cdot c(t) dt \quad (1)$$

In the case of a constant carrier gas flow, the amount of substance is proportional to the integral of the gas concentration c . In most measurement setups, the volume flow and molar volume are well-known constants. To determine the amount of substance in a peak with a MOS sensor therefore requires a signal proportional to the concentration. A suitable signal is the reverse rate constant of the surface coverage, i.e., the desorption of surface oxygen, due to supplied reducing gas. In a previous work we introduce this process as DSR (Baur et al., 2017). The concept of DSR is based on a model for MOS sensors with temperature-modulated operation (Baur et al., 2015; Schultealbert et al., 2017). In this model, the conductance of MOS sensors is limited by grain–grain boundaries which depend on surface charges that can be modeled by surface trapping.

A widely accepted model for the conductance of the grain–grain boundaries dates back to Morrison and Madou (1989).

A depletion zone near the surface is formed by electrons of the n -type semiconductor being bound to ionosorbed oxygen. Conduction electrons must overcome the resulting energy barrier E_b for a current flow across the grain–grain boundaries. Barsan and Weimar (2001) showed that a similar model can also be used for nanocrystalline sensors in which the whole grain is part of the depletion zone. Therefore, the conductance of the sensor can be described by (Madou and Morrison, 1989)

$$G = G_0 \cdot e^{-\frac{E_b}{k_b T}}, \quad (2)$$

with the Boltzmann constant k_b , the temperature T of the sensor film and a prefactor G_0 . The energy barrier is defined by (Madou and Morrison, 1989; Schultealbert et al., 2017)

$$E_b = \frac{q^2 N_s^2}{2 \varepsilon_r \varepsilon_0 N_d} = N_s^{*2}, \quad (3)$$

with the donor density N_d , the occupied surface states N_s , the elemental charge q , the permittivity of SnO_2 ε_r and vacuum ε_0 . N_s^* is the normalized surface state according to Schultealbert et al. (2017).

We assume that the sensor can be modeled with good accuracy by reducing the complexity of the model to a minimum. The following idealizations can be made.

- ii. The sensor is described by a single grain–grain boundary.
- i. The surface charge is caused by a single species of adsorbed oxygen.
- iii. The adsorbed oxygen reacts in a single step reaction with the reducing gas and the reaction rate is linear to the gas concentration.

A real sensor is normally a granular layer with a multitude of grain boundaries and other transport mechanisms, e.g., necks from strongly sintered grains. However, the conductance of the sintered grain is very high compared to the grain boundaries. Hence, the resistance will be dominated by the serial grain–grain boundaries. According to Eq. (3) all grain boundaries have the same barrier height, and nanocrystalline material with fully depleted grains shows an equivalent behavior. The surface charge can be measured by the thermal activation of the sensor layer. Although assumption (i) seems a strong idealization of the sensor, earlier work on the investigated sensor type AS-MLV (ams AG) did prove that the sensor properties can be modeled quite accurately by this approach measuring the thermal activation of the conductance (Baur et al., 2015).

The types of oxygen species at the sensor surface are discussed controversially in the literature. There is no spectroscopic evidence for the oxygen interaction with metal oxides

(Gurlo, 2006). Madou describes two different forms of adsorbed oxygen at the sensor surface (Madou and Morrison, 1989): atomic (O^-) and molecular (O_2^-) ions. The formation of O^- by dissociation is modeled by him in the form of a mass action law. Some authors attribute a change in sensor behavior over temperature around 350 °C to a change in the predominating oxygen species from O_2^- to O^- (Pulkkinen et al., 2001). Other authors expect the double charged atomic ion O^{2-} to be the predominant species in dry air between 350 and 450 °C, and a competitive adsorption of O^- and O^{2-} around 300 °C (Suematsu et al., 2014). In humid air, water vapor is believed to block the O^{2-} adsorption sites, changing the predominant species to O^- (Yamazoe et al., 2012). For our model, however, precise knowledge of the dominant species is not necessary. We assume that for a certain temperature, the surface charge is dominated by one species of adsorbed oxygen ion at the surface (ii).

The chemical reaction of the gas with the surface can be either a direct reaction of the gas with the adsorbed oxygen (Eley–Rideal) or a reaction of the pre-adsorbed gas (Langmuir–Hinshelwood). In the second case, the number of adsorbed species may depend on not only the concentration, but also on the number of surface sites. For our experiment, the reducing gases are prevalent at very low concentrations. We assume that the reaction rate is, therefore, linear to the gas concentration. In the case of ethanol at low temperatures of 150 °C, a single step oxidation, (iii) namely the dehydration and formation of water, has been reported for SnO_2 with various dopants (Cheong and Lee, 2006).

The functional principle of gas sensing with MOS sensors is based on oxidation and reduction on the surface (Ding et al., 2001). It affects an exchange of electrons between the conduction band of the semiconductor and adsorbed oxygen ions. The surface will be oxidized in clean air atmosphere. Reducing gas molecules interact and react with adsorbed oxygen ions. Thus, oxygen ions emit their electrons to the conduction band and the energy barrier will decrease (Ding et al., 2001; Madou and Morrison, 1989). Relating to Eq. (3), this means that the occupied surface states (oxygen ions) N_s will be increased with oxidation and decreased with reduction. Besides the energy barrier in Eq. (2), the temperature of the sensor film is an important factor concerning the conductance. In TCO, the MOS sensor temperature is changed periodically. With fast temperature changes the sensor is in non-equilibrium states with respect to the oxygen coverage on the surface during TCO (Schultealbert et al., 2017). Furthermore, the equilibrium oxygen surface coverage decreases with decreasing temperature. The relaxation of a non-equilibrium state to an equilibrium state takes places by different coupled oxidation and reduction processes. These processes depend on the type of gas and the temperature and can take from milliseconds at high temperatures to hours at low temperatures (Baur et al., 2015). Figure 1 shows a schematic Arrhenius plot of the logarithmic sensor conductance in TCO consisting of two temperature plateaus. Figure 1 also illus-

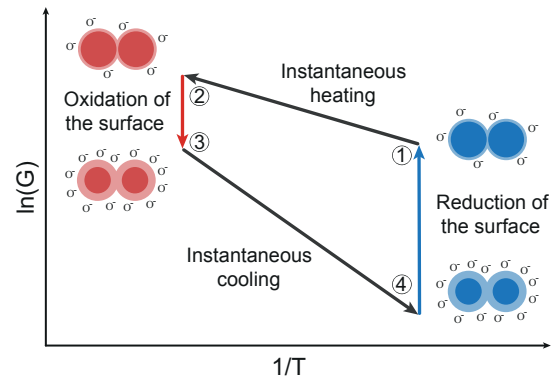


Figure 1. Schematic Arrhenius plot of a MOS sensor and a schematic grain–grain boundary during TCO (Baur et al., 2017).

trates schematically the single grain to grain boundary in different states during the temperature cycle.

State 1 represents the low temperature equilibrium of the sensor with a low surface coverage. An instantaneous temperature increase from state 1 to 2 results in a non-equilibrium state of the sensor at high temperature. The temperature rise does not affect the surface coverage because of the comparatively slow oxidation and reduction processes (Baur et al., 2015). Regarding Eq. (2), a temperature increase with a constant surface coverage, i.e., a constant energy barrier, leads to a strong increase in the conductance. Then, the surface is slowly oxidized to reach the high temperature equilibrium with a highly covered surface (state 3). This increases the energy barrier and thus reduces the conductance, as shown by Eq. (2) for a constant temperature. An instantaneous temperature decrease from state 3 to 4 results in an abrupt decrease in the conductance in analogy to the change between state 1 and 2. Thus, the surface coverage in state 4 corresponds to the coverage of the high temperature equilibrium (state 3), which results in a high energy barrier and a very low conductance of the sensor. The surface coverage is reduced either by slow desorption of the ionosorbed oxygen or by reactions with reducing gases until the low temperature equilibrium surface coverage is reached. During this process, the conductance rises again until equilibrium is reached (state 4 to 1).

The beginning of the change from state 4 to 1 is the most important time section for the DSR. We have previously shown (Schultealbert et al., 2017) that for a short time ($t \ll \tau_{\text{relaxation}}$) after a temperature step from state 3 to 4 the oxidation, i.e., additional ionosorption of oxygen, is negligible. The low equilibrium surface coverage at T_{low} means that the high surface coverage must be reduced after the temperature step. Especially at low temperatures, this process is very slow in purified air, with time constants of several minutes. The time-resolved variation of the normalized surface states N_s^* therefore depends mainly on the surface reduction caused

by reducing gases. The time differential can be approximated by (Schultealbert et al., 2017)

$$\frac{dN_s^*}{dt} = -k_d N_s^*. \quad (4)$$

Here, k_d is the reverse reaction rate. For gas concentrations of ppb to low ppm levels, the reverse reaction rate can be split (Schultealbert et al., 2017):

$$k_d = k_{d,air} + \sum k_{d,gas,i}(t), \quad (5)$$

with the combined reaction rate k_d resulting from desorption by intrinsic processes, $k_{d,air}$, and $k_{d,gas,i}$ for the reaction with the i th reducing gas being present. If we look at a GC or pre-concentrator application the concentration of the supplied gas is time-dependent. The reaction rate $k_{d,air}$ is time-independent due to a constant background of purified air during a measurement. The solution of the time differential Eq. (4) with Eq. (5) is

$$N_s^*(t) = N_s^*(t_0) \cdot \exp \left(- \left(k_{d,air}(t - t_0) + \int_{t_0}^t \sum k_{d,gas,i}(\tau) d\tau \right) \right). \quad (6)$$

The energy barrier is given by Eq. (3) and for short times after a temperature step the exponential function can be approximated with $\exp(x) = 1 - 2x$. The energy barrier is approximately

$$E_b(t) \approx E_b(t_0) \cdot \left(1 - 2 \cdot \left(k_{d,air}(t - t_0) + \int_{t_0}^t \sum k_{d,gas,i}(\tau) d\tau \right) \right). \quad (7)$$

The time derivative of Eq. (7) is

$$\frac{dE_b(t)}{dt} = -2E_b(t_0) \cdot \left(k_{d,air} + \sum k_{d,gas,i}(t) \right). \quad (8)$$

The combination of the time derivative of Eq. (2) $\frac{dE_b}{dt} = -k_b T \frac{d\ln(G)}{dt}$ with Eq. (8) leads to Eq. (9).

$$\sum k_{d,gas,i}(t) = \frac{k_b T}{2E_b(t_0)} \frac{d\ln(G)}{dt} - k_{d,air} \quad (9)$$

Thus, the reaction rate $k_{d,air}$ is a constant offset during the measurement and can be removed with an offset correction. The energy barrier $E_b(t_0)$ at time t_0 can be calculated from the conductance change during the temperature decrease, state 3 to 4 in Fig. 1 (Schultealbert et al., 2017). If

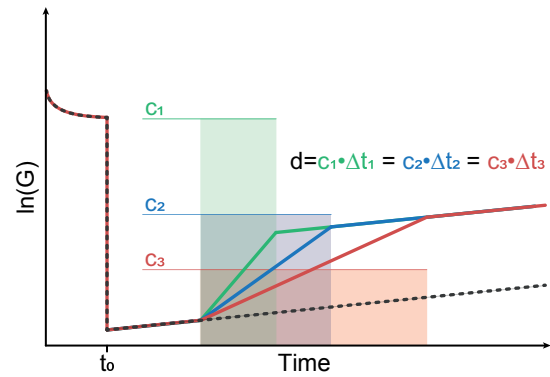


Figure 2. Schematic conductance curve with a temperature jump from high to low temperature; during the relaxation at the low temperature stage, three peaks with different peak width and the same gas dosage are assumed.

we look at only one peak from a GC separation caused by a single gas, Eq. (9) can be rewritten as

$$k_{d,gas} = \frac{k_b T}{2E_b(t_0)} \frac{d\ln(G)}{dt} - k_{d,air}. \quad (10)$$

We can assume that $k_{d,gas}(c)$ is proportional to c for small concentrations (Baur et al., 2015; Schultealbert et al., 2017). The amount of substance in the time interval $[t_0, t]$ with Eq. (1) is proportional to

$$n \sim \frac{\dot{V}}{V_m} \cdot \int_{t_0}^t k_{d,gas}(c(\tau)) d\tau. \quad (11)$$

Figure 2 shows a schematic sensor reaction to concentration peaks with different peak widths but the same dosage, i.e., the same concentration–time integral. The sensor jumps from high to low temperature at t_0 . During the relaxation at the low temperature stage, three different gas “peaks” with different width $w = \Delta t$ but the same dosage d , i.e., constant concentration c with $d = c \cdot \Delta t = \text{const.}$, are assumed. The slope of the sensor reaction changes due to the concentration change. However, according to Eq. (11) all three different peaks will result in the same shift of the sensor signal; i.e., the operating mode will result in a measured signal directly proportional to the dosage, i.e., the total amount of substance, in the GC peak.

3 Measurement setup

Measurements were performed with a commercially available SnO_2 sensor (AS-MLV, ams Sensor Solutions Germany GmbH) in TCO. The sensor is highly sensitive to VOCs (volatile organic compounds), e.g., for monitoring indoor air quality. The AS-MLV has a large dynamic range in TCO

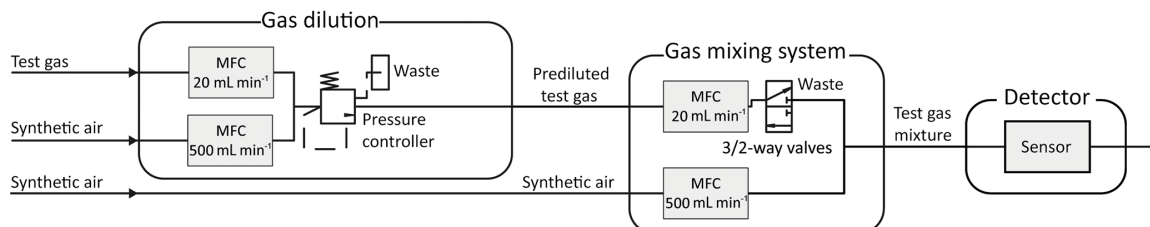


Figure 3. Schematic structure of the gas mixing system.

from 0.1 nS (10 GΩ) due to the non-equilibrium states up to 0.1 mS (10 kΩ) due to the high sensitivity. For exact temperature control and fast, high-precision measurement of the sensor conductance we use an electronic board developed in our group (Baur et al., 2018). The sensor temperature is controlled via the heater resistance with a digital PID (proportional–integral–derivative) controller. The time constant of the controller is much smaller than that of the sensor, allowing fast temperature changes from 400 to 100 °C within 50 ms. A resolution of 0.1 °C is feasible with this closed-loop control (Baur et al., 2018). The sensor signal read-out is based on the conversion of the sensor conductance into a voltage with a logarithmic amplifier. The core of the board is the LOG114 logarithmic amplifier from Texas Instruments (Texas Instruments Inc., 2007), which can measure currents from 100 pA to 10 mA, i.e., over 8 orders of magnitude. This read-out method is well adapted to the sensor model and the measured voltage scales with the change in the energy barrier and the rate constant (Eq. 10). An error in the voltage measurement of the logarithmic amplifier contributes linearly to the error for the rate constant. Over the entire measurement range, the error is dominated by the error of the voltage measurement (Baur et al., 2018).

$$\log G \pm \Delta \log G = k_d \pm \Delta k_d \quad (12)$$

With this version of the sensor electronic, it is possible to measure conductance in a range from 0.25 mS (4 kΩ) down to 0.25 nS (40 GΩ) with a data acquisition rate of 2 kHz. We achieve a relative resolution of better than 1 % per decade (Baur et al., 2018).

For the characterization of the sensors with trace gases, we use a gas mixing apparatus (GMA) with pre-dilution lines (Helwig et al., 2014). Figure 3 shows the schematic setup of the GMA. The sensitivity and response of various sensors can be tested by passing trace amounts of gas over the sensor in specific test chambers. For this purpose, the GMA uses gas dilution lines consisting of two mass flow controllers (MFC), one (e.g., 20 mL min⁻¹) for the test gas and one (500 mL min⁻¹) for the carrier gas. The outputs of the two pre-dilution MFCs are connected to each other and are kept at a constant pressure by a pressure regulator. According to Helwig et al. (2014), a dynamic concentration range

$c_{\text{bottle}}/c_{\text{sensor}}$ from 5 to 312 750 is reached, where c_{sensor} is the concentration over the sensor and c_{bottle} is the concentration in the test gas bottle. Diluted gas is dosed via another MFC (20 mL min⁻¹) and regulated by a 3/2-way valve. The dilution line and a MFC (500 mL min⁻¹) for dry synthetic air are combined in a mixing block. The carrier gas stream, in this case dry zero air, is automatically readjusted when a gas supply is switched on, so that the total flow across the sensor remains constant. Finally, a mass flow meter (MFM) measures the flow at the outlet. This makes it possible to simulate gas peaks with the same total amount of substance with different shapes. A two-stage cleaning process generates the zero air (Baur et al., 2017). Hydrocarbons (larger than C₃) are removed efficiently in the first step with a carbon filter system, while CO₂ and humidity are removed with a pressure swing. To remove smaller hydrocarbons as well as hydrogen and carbon monoxide, a catalytic conversion is used in the second step.

The detector (MOS sensor plus sensor chamber) must achieve two important properties for gas chromatography. It must show a high separation performance (low peak broadening and low tailing) and a good reproducibility (the same amount of substance must produce the same signals). As described above, the change in the sensor signal during a low temperature plateau is caused by the temporal concentration gradient at the sensor location. In addition to the concentration in the flow, it also depends on the flow velocity and the diffusion of the gas to the sensitive MOS layer of the sensor. Therefore, it is important to provide a sensor chamber that transports the carrier gas and with it the separated gas sample close to the sensor surface and that does not have any dead volumes or long diffusion paths. The fluidic design of the sensor chamber and the housing or cap of the sensor have a great influence on this. Since we used a commercially available AS-MLV sensor the geometry is limited at this point, but that standard TO5 lid was removed to allow better gas access and shorter diffusion distance. A specific sensor chamber as shown in Fig. 4 was developed, simulated and tested.

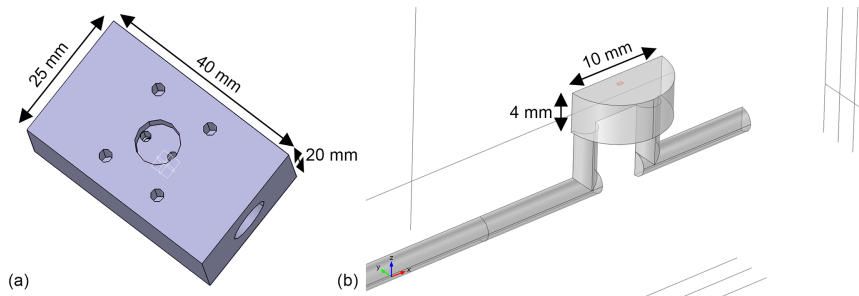


Figure 4. Sensor chamber with low dead volumes and short diffusion paths from the carrier gas flow to the sensor surface for fast and sensitive peak detection. (a) CAD model showing the side where the sensor is mounted and fixed with screws. (b) 3-D model (cut in half due to symmetry) of the gas path used for simulations; the position and size of the gas-sensitive layer ($500 \times 500 \mu\text{m}^2$) are marked in red.

4 Results and discussion

4.1 FEM simulations

To characterize the detector housing a FEM model using COMSOL Multiphysics was set up. The geometry was already shown in Fig. 4. Using the module *Laminar flow* and a stationary study the flow conditions inside the chamber are simulated. Applying this flow field to the *Transport of diluted species* model offers the possibility of investigating the shape evolution of incoming Gaussian peaks and estimating the maximum number of molecules that can reach and therefore react on the sensor surface. The parameters used for the simulation are a total flow rate of 100 mL min^{-1} , a gas pulse with a Gaussian concentration profile with a standard deviation of 0.2 s at the inlet, a channel radius of 1.2 mm and the diffusion constant of the considered molecules (in this case toluene in air) of $8 \times 10^{-6} \text{ m}^2 \text{ s}^{-1}$. The cavity for the sensor itself has the footprint of a TO5 housing (radius 5 mm) and a height of 4 mm, resulting in a total volume of 0.31 mL. The sensor itself is represented by a rectangle with the estimated size of the sensitive layer ($500 \mu\text{m} \times 500 \mu\text{m}$).

In a first step we investigated whether incoming Gaussian concentration peaks can be correctly detected at the sensor's position. For this purpose, the concentration over time at the entrance and at the sensor are shown in Fig. 5. Obviously, there is a time offset between both curves due to the transport through the channel and chamber. In addition, the maximum concentration is slightly lower (8.6 %) due to the peak broadening at the sensor. The FWHM is increased by the same ratio and thus the integral under the curve, i.e., the amount of substance in Eq. (11), which is measured, remains unchanged. This means that time resolution for GC systems is only slightly reduced with this design. Furthermore, the detector presented here can be improved to some extent by using a sensor without a TO5 footprint and an optimized detector housing and sensor chamber.

In the current setup with a much wider channel (10 mm) compared to the sensor surface (500 μm), a large percentage of the incoming molecules just pass the detector without re-

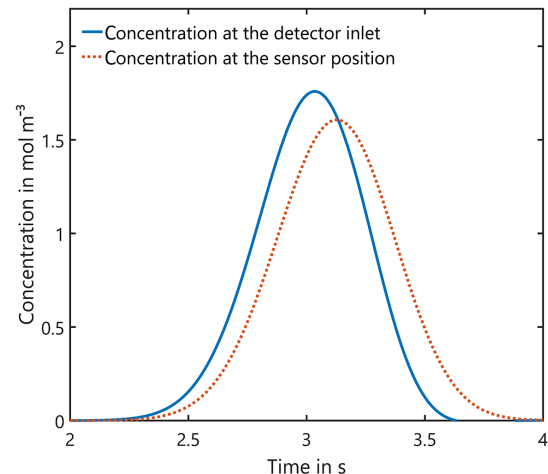


Figure 5. Influence of the detector housing on the shape of incoming Gaussian peaks: the peak width of 0.2 s at the entrance is increased by 8.6 % and the maximum concentration is reduced correspondingly, but the integral, i.e., the amount of substance, remains unchanged.

acting on the sensor surface, which means they do not contribute to the sensor signal. To estimate the amount of substance actually required for the measured sensor signal, i.e., the real limit of detection for a system with optimized detector geometry, another simulation is performed. Here, the sensor is assumed to be an ideal gas sink, which means that the concentration is always zero at the position of the sensitive layer, with all molecules reaching the surface being consumed by the sensor reaction, i.e., disappearing in the simulation. By comparing the incoming and outgoing peak areas, the amount of substance that can reach the sensor surface and thus the maximum amount that can contribute to the sensor signal can be estimated. This ratio is mainly dependent on geometry. For our chamber, only 1.6 % of the incoming peak is consumed, which means that up to $60 \times$ lower amounts of substance than presented in this paper can be detected, if all

Table 1. Concentration and duration combinations for ethanol peaks.

concentration in ppb	duration in s	Dosage (concentration \times duration) in ppb s
1	1, 2, 5, 10	1, 2, 5, 10
2	1, 5, 10	2, 10, 20
5	1, 2, 4, 10	5, 10, 20, 50
10	1, 2, 5, 10	10, 20, 50, 100
20	1, 5, 10	20, 100, 200
50	1, 2, 4, 10	50, 100, 200, 500
100	1, 2, 5, 10	100, 200, 500, 1000
200	1, 5, 10	200, 1000, 2000
500	1, 2, 4, 10	500, 1000, 2000, 5000
1000	1, 2, 5	1000, 2000, 5000

molecules in a gas peak are brought to the sensor surface by a more suitable geometry and a lower flow rate.

4.2 Proof of concept

Measurements were performed to evaluate the concept of differential surface reduction regarding high separation efficiency and reproducibility of the total amount of substance in a pulse. The original lid and the protective membrane of the standard AS-MLV sensor were removed for our experiments to obtain an improved flow across the sensor. The programmable temperature cycle was set to a 60 s surface oxidation at 400 °C and a 600 s surface reduction phase at 100 °C. All measurements with the sensor setup were performed with the gas mixing apparatus described above with a carrier gas flow of dry zero air with a flow rate of 100 mL min⁻¹; 240 s after the start of the reduction phase we tested different dosages (concentration times duration) of ethanol with variation in concentration, duration and dosage to test the reproducibility of the signal for the amount of substance (see Table 1). The gas pulses were generated with valves in the gas mixing unit.

Figure 6 shows an exemplary evaluation of the sensor signal in the time range from 200 to 500 s of the cycle with a 20 ppb s (5 ppb for 4 s) ethanol pulse. The black dashed line is the conductance signal of the previous sensor cycle in dry zero air without gas exposure (background). The logarithmic sensor signal is linear over time, as described by our model. The black solid line shows the sensor conductance with ethanol pulse offered at 300 s, when an ethanol concentration of 5 ppm was introduced for 4 s. Immediately, the signal shows a fast increase in the sensor conductance. After the ethanol exposure, the conductance increase continues with an offset parallel to the background. This offset of the conductance curve is proportional to the amount of substance. The grey line is the rate constant calculated according to Eq. (10) for ethanol, which correctly represents the peak

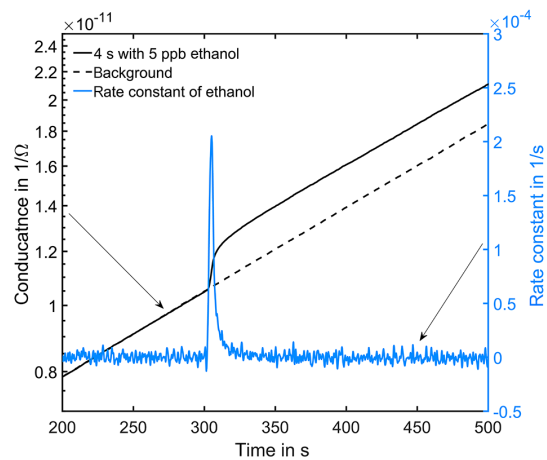


Figure 6. Conductance curve in the low temperature plateau in clean air (black dashed line). At 300 s in the cycle a 4 s peak with 5 ppb ethanol was offered (black solid line). The grey line is the calculated rate constant of ethanol.

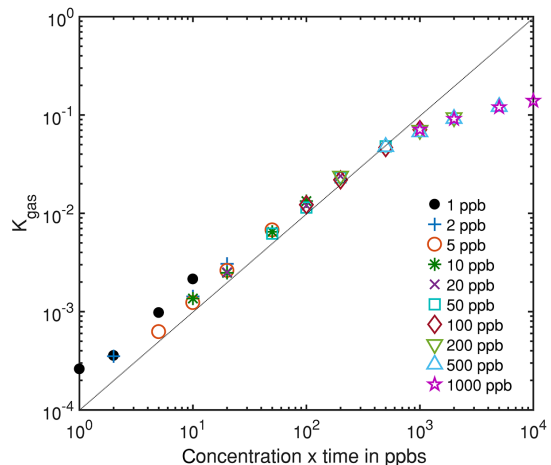


Figure 7. Integrated rate constant dependent on the gas dosage, i.e., the product of pulse concentration and duration, which is proportional to the amount of substance for different gas pulses.

shape, with a small tailing effect. To improve the numerical differentiation of the signal a cubic smooth spline and a Savitzky–Golay filter with 1000 points (500 ms) to reduce the noise of the conductance measurement were used before numerical differentiation of the signal. The integrated rate constant K_{gas} representing the peak area is plotted in Fig. 7 for all 36 ethanol pulses from Table 1. Figure 7 shows the integrated rate constant in dependence on the dosage, i.e., the product of concentration and duration. Different shapes of the marker represent different pulse concentrations. For most concentrations evaluated rate constants with the same dosage are very close to each other, proving the novel detector concept. The integrated rate constant is linear up to

approximately 200 ppb s. For higher dosages the curve flattens somewhat, presumably because the assumed linearity of the logarithmic conductance is no longer valid due to the far advanced surface reduction. Nevertheless, reproducible quantification is still possible based on the integrated rate constant. Pulses generated with an ethanol concentration of 1 ppb (black points) show a clear deviation from the trend line. The MFC set point for this concentration is only 2.5 %, which is beyond the recommended range of use according to the manufacturer. Thus, the concentration is probably higher than wanted, which would explain the constant offset from the trend line.

5 Conclusions

We have demonstrated that a metal oxide semiconductor gas sensor is able to detect and quantify short pulses of reducing gas at very low concentrations using the differential surface reduction mode. A simple model describing the change in the surface charge during temperature changes that was previously developed to improve the sensor performance during temperature cycled operation is used here to evaluate the sensor signal and achieve an output signal proportional to the gas dose. Experimental results over a wide range of gas dosages correspond well to this model and demonstrate a linear behavior of the integrated rate constant over 3 orders of magnitude. For ethanol, the gas pulses are well represented even at 100 °C; for other, less reactive reducing gases a higher measurement temperature might be required to achieve sufficient sensitivity. FEM simulations have shown that the sensor consumes at most 1.6 % of the injected gas quantity. This corresponds to a detection limit of below 47 fg for ethanol. This method can be used to realize small and inexpensive micro-detectors for GC systems able to detect and quantify trace gases as well as integrated sensor pre-concentrator systems, e.g., for air quality applications.

Data availability. The underlying measurement data are not publicly available and can be requested from the authors if required.

Competing interests. The authors declare that they have no conflict of interest.

Special issue statement. This article is part of the special issue “Sensor/IRS2 2017”. It is a result of the AMA Conferences, Nuremberg, Germany, 30 May–1 June 2017.

Edited by: Jürgen Wöllenstei

Reviewed by: two anonymous referees

References

Bajtarevic, A., Ager, C., Pienz, M., Klieber, M., Schwarz, K., Ligor, M., Ligor, T., Filipiak, W., Denz, H., Fiegl, M., Hilbe, W., Weiss, W., Lukas, P., Jammig, H., Hackl, M., Haidenberger, A., Buszewski, B., Miekisch, W., Schubert, J., and Amann, A.: Non-invasive detection of lung cancer by analysis of exhaled breath, *BMC Cancer*, 9, 348, <https://doi.org/10.1186/1471-2407-9-348>, 2009.

Bârsan, N. and Ionescu, R.: SnO₂-based gas sensors as chromatographic detectors, *Sensor. Actuat. B-Chem.*, 19, 470–473, [https://doi.org/10.1016/0925-4005\(93\)01042-3](https://doi.org/10.1016/0925-4005(93)01042-3), 1994.

Bârsan, N. and Weimar, U.: Conduction Model of Metal Oxide Gas Sensors, *J. Electroceram.*, 7, 143–167, <https://doi.org/10.1023/A:1014405811371>, 2001.

Baur, T., Schütze, A. and Sauerwald, T.: Optimierung des temperaturzyklischen Betriebs von Halbleitergasensoren, *Tech. Mess.*, 82, 187–195, <https://doi.org/10.1515/teme-2014-0007>, 2015.

Baur, T., Schütze, A., and Sauerwald, T.: Detection of short trace gas pulses, in: *Proceedings Sensor 2017*, Nürnberg, Germany, 30 May–1 June 2017, 87–91, <https://doi.org/10.5162/sensor2017/A4.2>, 2017.

Baur, T., Schulzealbert, C., Schütze, A., and Sauerwald, T.: Device for the detection of short trace gas pulses, *Tech. Mess.*, 0, 0, <https://doi.org/10.1515/teme-2017-0137>, 2018.

Chapman, P. J., Vogt, F., Dutta, P., Datskos, P. G., Devault, G. L., and Sepaniak, M. J.: Facile hyphenation of gas chromatography and a microcantilever array sensor for enhanced selectivity, *Anal. Chem.*, 79, 364–370, <https://doi.org/10.1021/ac061389x>, 2007.

Cheong, H.-W. and Lee, M.-J.: Sensing characteristics and surface reaction mechanism of alcohol sensors based on doped SnO₂, *J. Ceram. Process. Res.*, 7, 183–191, 2006.

Ding, J., McAvoy, T. J., Cavicchi, R. E., and Semancik, S.: Surface state trapping models for SnO₂-based micro-hotplate sensors, *Sensor. Actuat. B-Chem.*, 77, 597–613, [https://doi.org/10.1016/S0925-4005\(01\)00765-1](https://doi.org/10.1016/S0925-4005(01)00765-1), 2001.

Eiceman, G. A., Nazarov, E. G., Miller, R. A., Krylov, E. V., and Zapata, A. M.: Micro-machined planar field asymmetric ion mobility spectrometer as a gas chromatographic detector, *Analyst*, 127, 466–471, <https://doi.org/10.1039/b111547m>, 2002.

Geiss, O., Giannopoulos, G., Tirendi, S., Barrero-Moreno, J., Larsen, B. R., and Kotzias, D.: The AIRMEX study – VOC measurements in public buildings and schools/kindergartens in eleven European cities: Statistical analysis of the data, *Atmos. Environ.*, 45, 3676–3684, <https://doi.org/10.1016/j.atmosenv.2011.04.037>, 2011.

Gurlo, A.: Interplay between O₂ and SnO₂: oxygen ionosorption and spectroscopic evidence for adsorbed oxygen, *Chem. Phys. Chem.*, 7, 2041–2052, <https://doi.org/10.1002/cphc.200600292>, 2006.

Helwig, N., Schüler, M., Bur, C., Schütze, A., and Sauerwald, T.: Gas mixing apparatus for automated gas sensor characterization, *Meas. Sci. Technol.*, 25, 55903, <https://doi.org/10.1088/0957-0233/25/5/055903>, 2014.

Koistinen, K., Kotzias, D., Kephalaopoulos, S., Schlitt, C., Carrer, P., Jantunen, M., Kirchner, S., McLaughlin, J., Mølhav, L., Fernandes, E. O., and Seifert, B.: The INDEX project: Executive summary of a European Union project on indoor air

pollutants, *Allergy*, 63, 810–819, <https://doi.org/10.1111/j.1398-9995.2008.01740.x>, 2008.

Leidinger, M., Sauerwald, T., Reimringer, W., Ventura, G., and Schütze, A.: Selective detection of hazardous VOCs for indoor air quality applications using a virtual gas sensor array, *J. Sens. Sens. Syst.*, 3, 253–263, <https://doi.org/10.5194/jsss-3-253-2014>, 2014.

Leidinger, M., Huotari, J., Sauerwald, T., Lappalainen, J., and Schütze, A.: Nanostructured WO₃ Semiconductor Gas Sensor for Selective Detection of Naphthalene, in: *Proceedings Sensor 2015*, Nürnberg, Germany, 19–21 May 2015, 723–728, <https://doi.org/10.5162/sensor2015/E8.2>, 2015.

Leidinger, M., Baur, T., Sauerwald, T., Schütze, A., Reimringer, W., Spinelle, L., and Gerboles, M.: Highly sensitive benzene detection with MOS gas sensors, in: *Proceedings Sensor 2017*, Nürnberg, Germany, 30 May–1 June 2017, 92–97, <https://doi.org/10.5162/sensor2017/A4.3>, 2017.

Madou, M. J. and Morrison, S. R.: *Chemical Sensing with Solid State Devices*, Academic Press, Inc., 1989.

Mahdavifar, A., Navaei, M., Hesketh, P. J., Findlay, M., Stetter, J. R., and Hunter, G. W.: Transient thermal response of micro-thermal conductivity detector (µTCD) for the identification of gas mixtures: An ultra-fast and low power method, *Microsystems Nanoeng.*, 1, 15025, <https://doi.org/10.1038/micronano.2015.25>, 2015.

Mead, M. I., Popoola, O. A. M., Stewart, G. B., Landshoff, P., Calleja, M., Hayes, M., Baldovi, J. J., McLeod, M. W., Hodgson, T. F., Dicks, J., Lewis, A., Cohen, J., Baron, R., Saffell, J. R., and Jones, R. L.: The use of electrochemical sensors for monitoring urban air quality in low-cost, high-density networks, *Atmos. Environ.*, 70, 186–203, <https://doi.org/10.1016/j.atmosenv.2012.11.060>, 2013.

Narayanan, S., Rice, G., and Agah, M.: A micro-discharge photoionization detector for micro-gas chromatography, *Microchim. Acta*, 181, 493–499, <https://doi.org/10.1007/s00604-013-1146-9>, 2014.

Pulkkinen, U., Rantala, T. T., Rantala, T. S., and Lantto, V.: Kinetic Monte Carlo simulation of oxygen exchange of SnO₂ surface, *J. Mol. Catal. A-Chem.*, 166, 15–21, [https://doi.org/10.1016/S1381-1169\(00\)00466-0](https://doi.org/10.1016/S1381-1169(00)00466-0), 2001.

Roberts, T. J., Saffell, J. R., Oppenheimer, C., and Lurton, T.: Electrochemical sensors applied to pollution monitoring: Measurement error and gas ratio bias – A volcano plume case study, *J. Volcanol. Geoth. Res.*, 281, 85–96, <https://doi.org/10.1016/j.jvolgeores.2014.02.023>, 2014.

Sanchez, J. B., Schmitt, A., Berger, F., and Mavon, C.: Silicon-micromachined gas chromatographic columns for the development of portable detection device, *J. Sensors*, 2010, 409687, <https://doi.org/10.1155/2010/409687>, 2010.

Sasahara, T., Kato, H., Saito, A., Nishimura, M., and Egashira, M.: Development of a ppb-level sensor based on catalytic combustion for total volatile organic compounds in indoor air, *Sensor. Actuat. B-Chem.*, 126, 536–543, <https://doi.org/10.1016/j.snb.2007.04.001>, 2007.

Schultealbert, C., Baur, T., Schütze, A., Böttcher, S., and Sauerwald, T.: A novel approach towards calibrated measurement of trace gases using metal oxide semiconductor sensors, *Sensor. Actuat. B-Chem.*, 239, 390–396, <https://doi.org/10.1016/j.snb.2016.08.002>, 2017.

Spinelle, L., Gerboles, M., Villani, M. G., Aleixandre, M., and Bonavitacola, F.: Field calibration of a cluster of low-cost available sensors for air quality monitoring. Part A: Ozone and nitrogen dioxide, *Sensor. Actuat. B-Chem.*, 215, 249–257, <https://doi.org/10.1016/j.snb.2015.03.031>, 2015.

Spinelle, L., Gerboles, M., Kok, G., Persijn, S., and Sauerwald, T.: Review of Portable and Low-Cost Sensors for the Ambient Air Monitoring of Benzene and Other Volatile Organic Compounds, *Sensors*, 17, 1520, <https://doi.org/10.3390/s17071520>, 2017.

Suematsu, K., Yuasa, M., Kida, T., Yamazoe, N., and Shimano, K.: Determination of Oxygen Adsorption Species on SnO₂: Exact Analysis of Gas Sensing Properties Using a Sample Gas Pretreatment System, *J. Electrochem. Soc.*, 161, B123–B128, <https://doi.org/10.1149/2.004406jes>, 2014.

Texas Instrumens Inc.: LOG114 – Logarithmic Amplifier Features, Datasheet (May 2004), 2007.

Trzciński, J. W., Pinalli, R., Riboni, N., Pedrini, A., Bianchi, F., Zampolli, S., Elmi, I., Massera, C., Ugozzoli, F., and Dalcanale, E.: In Search of the Ultimate Benzene Sensor: The EtQxBox Solution, *ACS Sensors*, 2, 590–598, <https://doi.org/10.1021/acssensors.7b00110>, 2017.

Wilhelm, I., Rieger, M., Hürtlen, J., Wittek, M., Alépée, C., Leidinger, M., and Sauerwald, T.: Novel Low-Cost Selective Pre-Concentrators Based on Metal Organic Frameworks, in: *Procedia Engineering*, 168, 151–154, <https://doi.org/10.1016/j.proeng.2016.11.186>, 2016.

Yamazoe, N., Suematsu, K., and Shimano, K.: Extension of receptor function theory to include two types of adsorbed oxygen for oxide semiconductor gas sensors, *Sensor. Actuat. B-Chem.*, 163, 128–135, <https://doi.org/10.1016/j.snb.2012.01.020>, 2012.

Zampolli, S., Elmi, I., Stürmann, J., Nicoletti, S., Dori, L., and Cardinali, G. C.: Selectivity enhancement of metal oxide gas sensors using a micromachined gas chromatographic column, *Sensor. Actuat. B-Chem.*, 105, 400–406, <https://doi.org/10.1016/j.snb.2004.06.036>, 2005.

Zampolli, S., Betti, P., Elmi, I., and Dalcanale, E.: A supramolecular approach to sub-ppb aromatic VOC detection in air, *Chem. Commun.*, 2007, 2790–2792, <https://doi.org/10.1039/b703747c>, 2007.

4.1.5 Paper C – Facile Quantification and Identification Techniques for Reducing Gases over a Wide Concentration Range Using a MOS Sensor in Temperature-Cycled Operation

C. Schultealbert, T. Baur, A. Schütze and T. Sauerwald
Saarland University, Lab for Measurement Technology, Saarbrücken, Germany

Sensors (2018), 18(3), 744

The original paper and supplementary data can be found, in the online version, at
<https://doi.org/10.3390/s18030744>.

© 2018 by the authors. This article is an open access article distributed under the terms and conditions of the Creative Commons Attribution (CC BY) license (<http://creativecommons.org/licenses/by/4.0/>).

Article

Facile Quantification and Identification Techniques for Reducing Gases over a Wide Concentration Range Using a MOS Sensor in Temperature-Cycled Operation

Caroline Schultealbert ^{*}, Tobias Baur, Andreas Schütze and Tilman Sauerwald

Lab for Measurement Technology, Saarland University, 66123 Saarbrücken, Germany;
t.baur@lmt.uni-saarland.de (T.B.); schuetze@lmt.uni-saarland.de (A.S.); t.sauerwald@lmt.uni-saarland.de (T.S.)

^{*} Correspondence: c.schultealbert@lmt.uni-saarland.de; Tel.: +49-681-302-5017

Received: 11 January 2018; Accepted: 26 February 2018; Published: 1 March 2018

Abstract: Dedicated methods for quantification and identification of reducing gases based on model-based temperature-cycled operation (TCO) using a single commercial MOS gas sensor are presented. During high temperature phases the sensor surface is highly oxidized, yielding a significant sensitivity increase after switching to lower temperatures (differential surface reduction, DSR). For low concentrations, the slope of the logarithmic conductance during this low-temperature phase is evaluated and can directly be used for quantification. For higher concentrations, the time constant for reaching a stable conductance during the same low-temperature phase is evaluated. Both signals represent the reaction rate of the reducing gas on the strongly oxidized surface at this low temperature and provide a linear calibration curve, which is exceptional for MOS sensors. By determining these reaction rates on different low-temperature plateaus and applying pattern recognition, the resulting footprint can be used for identification of different gases. All methods are tested over a wide concentration range from 10 ppb to 100 ppm (4 orders of magnitude) for four different reducing gases (CO, H₂, ammonia and benzene) using randomized gas exposures.

Keywords: MOS gas sensor; temperature-cycled operation; differential surface reduction; quantification; sensitivity; selectivity; linear calibration

1. Introduction

Metal oxide semiconductor (MOS) gas sensors are widely used for the detection of reducing and oxidizing gases. Applications are reported in many fields, e.g., the detection of explosive gases [1,2], fire detection [3,4], odour monitoring [5] and air quality control [6,7]. Accordingly, a sensor should be capable of measuring a large variety of gases over a broad range of concentrations.

For the identification of different gases either a multisensor array [8] or a virtual multisensor, e.g., using temperature-cycled operation (TCO) [3,9,10], is set up and pattern recognition methods are applied [11]. TCO dates back more than 40 years, utilized for the discrimination of carbon monoxide and hydrocarbons [12]. It used, as most of the early attempts, a heuristically defined temperature cycle and only very few virtual multi-sensors, e.g., on temperature plateaus, instead of using an optimized cycle and virtual multi-sensor generation. This is probably due to the fact that modelling the sensor response throughout a cycle is quite challenging. The relaxation of surface-state occupancy can be relatively slow (cf. [13]) compared to practical temperature cycle and, therefore, a model of the sensor response needs to address the transient effects of one or more surface species throughout the full temperature range. While the observation of the temperature-dependant rate constants is limited for the classical Taguchi-type sensors due to their high thermal time constants, micro-machined sensor

allowed a more comprehensive study of the transient sensor response, including determination of rate constants for several extrinsic and intrinsic surface states [14]. Despite the limited ability to determine the rate constant for Taguchi-type sensors, a rate constant-based model had been used to describe a method for the generation of virtual sensor from TCO data [15]. Following the line of the rate equation approach by Ding et al. [14], we described a concept for the optimization of TCO and feature generation in earlier work [16,17], which gives the basis for the quantification technique presented in this paper.

Especially for isothermal sensors [18,19] but as well for some sensor with TCO [20] calibration curves for quantification are in the form of a power law even if multivariate methods are sometimes needed [21]. A facile and preferably linear method for the quantification of gases independent from environmental impacts like humidity can contribute to practical applications of MOS gas sensors. The method should be free of complex algorithms to keep computational effort as low as possible.

In the past, we developed a model for the conductance of a SnO_2 -based MOS sensor during specific transient states of a temperature cycle [17], where the sensor shows improved sensitivity [22]. In this paper, we demonstrate two facile methods allowing linear calibration of gas sensors that are derived from this model and demonstrate their suitability by measuring four gases (CO , H_2 , ammonia and benzene) over four decades of concentration (10 ppb to 100 ppm). The identification of these gases using supervised pattern recognition (LDA, linear discriminant analysis) based on the parameters extracted for quantification and calculated on different temperature levels is also shown.

The mentioned model is based on the conductance of grain–grain boundaries, which is the dominating effect for a SnO_2 layer. The conductance of these boundaries (Equation (1)) is dominated by a negatively charged surface state, causing an energy barrier E_B between grains where the height of the barrier is a quadratic function of the density of these surface states N_S :

$$G = G_0 \cdot e^{-\frac{E_B}{k_B T}} \wedge E_B \propto N_S^2 \quad (1)$$

Please note that Equation (1) does not specify the surface state and indeed several types of intrinsic [14] and extrinsic [23], mainly oxygen-related surface states, have been reported and discussed in literature. The interplay of the extrinsic oxygen-related surface states is still discussed in literature [24–26] especially with respect to changing sensor temperature and surrounding conditions. At lower temperatures, O_2^- is often found to be the dominating species being replaced by O^- for higher temperatures (e.g., above 700 K in [26]). Some models also include O^{2-} in this higher-temperature region [27] and an interplay with humidity, as in humid air the adsorption of O^{2-} is reported to be blocked and O^- becomes dominant [28]. Despite the high variety in possible surface states, we could show in earlier work that for the specific operation mode used in this paper it is found to be sufficient to assume one single dominating ionosorbed species on the surface and single-step reaction with reducing gas [17]. This operation mode will shortly be described in the following section.

The reaction of a reducing gas with this reactive species reduces the energy barrier and increases the conductance strongly. We have reported that the energy barrier, and thereby the surface coverage of the semiconductor with negative surface charge, are temperature-dependent [22]. In the temperature range from 130 °C to 420 °C a strong increase can be observed, which in turn results in a gas-specific temperature profile allowing identification of different gases by temperature-cycled operation [9,10]. However, temperature cycling must not be understood as a sequence of equilibrium measurements of the sensor conductance at different temperature as the time constant for equilibration of ionosorbed surface species is typically higher than the duration of the temperature cycle. Ding et al. have demonstrated that a set of rate equations for adsorption and desorption of surface states can be used to describe the profile of the conductance throughout the temperature cycle [14]. Following this observation, we have shown that an excess of negative surface charge coverage can be obtained with a fast temperature decrease, which can be utilized for a strong enhancement of the sensor response and sensitivity [22]. After the fast temperature reduction, the sensor surface is far from equilibrium with a large excess of negative surface

charge and the rate constant for equilibration is very small due to the low temperature [17]. The sensor surface is then predominantly reduced by desorption of excess surface states. We have shown that a simple model with only one rate equation for this desorption is sufficient to describe the surface coverage and, with Equation (1), the conductance shortly after the temperature reduction is described by

$$\frac{dN_S}{dt} = -k(c_{gas})N_S \quad (2)$$

In this equation the rate constant k is a linear function of the gas concentration c_{gas} . Using Equation (1) the change of the logarithmic sensor conductance at the beginning of a low temperature becomes

$$\frac{d\ln(G(t))}{dt} \sim k(c) = k_{gas}c_{gas} + k_0 \quad (3)$$

The constant term k_0 subsumes the desorption of negative surface charge without gas reaction and the desorption caused by traces of reducing gases in the clean air background. Please note that Equation (2) is only valid if the surface charge is still well above equilibrium, otherwise the inverse reaction, that is, adsorption of new surface charge, is not negligible anymore. While we could demonstrate that for small gas concentrations a calculation of the rate constant by a linear fit of $\ln(G)$ shortly after the temperature reduction is a suitable method for estimating the rate constant, it is obvious that this method fails when applied over a wide range of concentrations. In the following we will present a facile method for estimation of the rate constant and therefore quantification of gases over a wide range of concentrations.

2. Materials and Methods

Data treatment is kept as simple as possible and was performed with the toolbox DAV³E, which is a software developed at our institute [29]. To cover the high dynamic concentration range, two methods (i–ii) for quantification are used:

- (i). For the quantification of low concentrations when the sensor does not approach equilibrium of surface coverage during the low-temperature phase, the rate constant is estimated by the calculation of \tilde{k} which denotes the slope of $\ln(G(t))$. Following the line of [17], \tilde{k} is calculated by a linear fit of $\ln(G(t))$ at the beginning of the low-temperature range. According to Equation (3), \tilde{k} is proportional to the reaction rate constant k and, furthermore, linear to the concentration c [17]. The proportionality factor f between k and \tilde{k} can be calculated using the initial surface coverage at low temperature [17]:

$$f = E_B(0) \cdot 2k_B T_{high} \wedge E_B(0) = k_B \ln\left(\frac{G_{high}}{G_{low}}\right) \cdot \frac{T_{high} T_{low}}{T_{high} - T_{low}} \quad (4)$$

However, as the calculated feature \tilde{k} is calibrated with the measurement results and the calculation is much more complex than one single linear fit, the explicit calculation of k will be omitted for most of the measurements except for one explicit comparison in Section 4. To compensate the background, the slope of zero air $\tilde{k}_0 = fk_0$ is subtracted from all calculated values [17].

- (ii). For the quantification of high concentrations when the sensor almost reaches equilibrium surface coverage during the low-temperature phase, the time constant of the relaxation process is evaluated by taking the highest and lowest values of $\ln(G)$ and evaluating the time-constant τ for reaching $63.2\% = 1 - 1/e$ of the difference using the MATLAB function *interp1*:

$$\tau = t(0.632 \cdot (\ln(G_{max}) - \ln(G_{min}))) - t_{start} \quad (5)$$

According to the solution of the simple differential Equation (3), the inverse value $1/\tau$ equals $2k$ and is therefore linear to c . For practical reasons, the constant k_0 can be omitted as it is negligible in the

high concentration range compared to $k_{gas}c_{gas}$. Therefore, the signal $1/\tau$ will be proportional to the gas concentration.

For the investigations a commercially available SnO_2 -based MOS gas sensor (AS-MLV-P2, ams Sensor Solutions Germany GmbH) is used. During the TCO, the sensor is periodically oxidized at a high temperature so that the reduction of the oxygen excess at a lower temperature can be analyzed as proposed. The full cycle consists of three of these temperature steps, each starting with 3 s at 450 °C followed by 27 s at a lower temperature (150 °C, 200 °C and 250 °C), resulting in a total duration of 90 s.

The concentration at which the method needs to be switched depends on the sensitivity of the sensor to the given gas at the considered temperature. We decided to switch the methods when the sensor reaches a stable value during the 27 s long low-temperature phase (concentration values for the method switching can be found in Table 1), which can also be implemented as an automatic evaluation algorithm. For the quantification, one single temperature step is sufficient, we chose the lowest one (150 °C) which, according to the presented model, should provide the highest sensitivity. For the identification of reducing gases, all three temperature steps are evaluated (cf. Section 3.3). The linear fit for the calculation of \tilde{k} according to (i) is always performed between 10 and 20 s. For the τ -evaluation (ii), the whole plateau from 3 to 30 s is considered. The identification using several temperature steps is demonstrated by \tilde{k} -evaluation, the additional ranges for the calculation of \tilde{k} are 34–36 s and 64–65 s, they are much closer to the temperature change because of the much faster relaxation at the higher temperatures (200 °C and 250 °C, respectively).

The electronic system basically consists of two parts: temperature control and sensitive layer read-out (specific information can be found in [30]). The heater was calibrated according to a power-to-temperature curve provided by the manufacturer. We transform this power-temperature curve to a resistance-temperature curve by a calibration measurement. The heater is then controlled via a closed-loop control. A stable temperature is reached after approximately 140 ms (see Supplementary Material Figure S1). The read-out is based on a logarithmic amplifier, which is placed directly at the sensor to allow low noise amplification of the low currents induced by a constant voltage over the sensing layer. Data acquisition is performed by a Teensy, a microcontroller system similar to Arduino, with a sample rate of 1 kHz. Before applying any data treatment, the signal quality is enhanced by averaging with $n = 20$. No further data treatment is needed, as both presented methods are based on the logarithmic conductance $\ln(G)$, which means that the recorded ADC-values can be directly used for all evaluations. However, the value of G can be calculated according to Equation (6), the measured values during the measurements are in the range of 300 kΩ and 6 GΩ

$$G = 249 \cdot 10^{2 \cdot 10^{\frac{-6.3574 \cdot \text{ADC}}{2^{16}} + 4.65367}} \quad (6)$$

The gas profile is generated by our gas mixing system (GMA) operating with dynamic dilution. The system consisting of several mass flow controllers (MFCs) and valves has been described in detail in [31]. The carrier gas is mixed by two MFCs with a maximum flow of 500 mL/min each, one with dry zero air (provided by a ULTRA zero air generator with catalytic conversion and a dew point of –70 °C) and one humidified by leading the zero air through an isothermal water bubbler at 20 °C. The relative humidity (RH) can be set through the mixing ratio of these two flows and the flows of the dry test gases. The temperature of the laboratory, thus the temperature in the sensor chamber, is approximately 22.5 °C, which means that the relative humidity at the sensor is slightly lower than set. The system provides four pre-dilution lines for gases from pressure cylinders, which means that the gas from the cylinder is diluted in two steps: first via two MFCs (500 mL/min and 10 or 20 mL/min respectively) and then in a second step by adding it to the carrier gas flow via a valve with a 10 or 20 mL/min MFC. There are two lines with 10 mL/min and two with 20 mL/min MFCs, giving possible dilution factors of 500,000 and 125,000, respectively, for this investigation, which used a total carrier gas flow of 250 mL/min for all experiments. Using three-way valves, the dilution line can be set to the desired

concentration to reach equilibrium before the gas mixture is actually offered to the sensor. The sensor is connected to the GMA via a stainless-steel block with one drill hole for the flow (diameter ca. 8 mm) and an orthogonal drill hole with the diameter of the TO cap of the sensor. The distance between the top of the sensor housing and the gas flow is approximately 4 mm.

Four gases (carbon monoxide CO, $c_{cylinder} = 1995$ ppm, 10 mL/min dilution line; hydrogen H₂, $c_{cylinder} = 104$ ppm, 20 mL/min dilution line; ammonia NH₃, $c_{cylinder} = 2903$ ppm, 10 mL/min dilution line; benzene C₆H₆, $c_{cylinder} = 99.2$ ppm, 20 mL/min dilution line) are used to verify the model. Three concentrations per decade (10, 25, 50, 100, 250, 500 ppb, etc.) have been offered starting at 10 ppb and ending at the highest possible concentration (see Table 1). Each concentration is offered for 30 min to the sensor followed by pure zero air for 10 min. The dilution line configuration for the next planned gas and concentration is already set at the beginning of the preceding one, which means 40 min for reaching equilibrium inside each dilution line. Gases are always offered in the same order: NH₃, H₂, CO, C₆H₆. The concentration order is randomized using the MATLAB function *randperm* to prevent time-dependent effects from affecting the quantification method. The full profile is performed at two humidities (40% RH and 50% RH) to investigate the influence of humidities.

Table 1. Overview of the measured gases, their concentrations and the used quantification method.

Gas	Concentrations Measured	\tilde{k} -Evaluation	τ -Evaluation
CO	0.01–79.8 ppm	0.01–0.1 ppm	0.1–5 ppm
H ₂	0.01–25 ppm	0.01–0.5 ppm	0.5–25 ppm
NH ₃	0.01–116 ppm	0.01–1 ppm	1–50 ppm
C ₆ H ₆	0.01–7.9 ppm	0.01–0.1 ppm	0.1–7.9 ppm

3. Results

3.1. Overview

In Figure 1, full cycles for 1 ppm of each gas are shown at different humidities. It can be observed that humidity influences the absolute value of $\ln(G)$ but the shape of the $\ln(G)$ curves are almost parallel for the two tested humidities. Only on the 250 °C plateau a significant deviation of the shape can be observed for background air. The suggested quantification methods evaluating the shape of the signal should, therefore, not be affected by humidity. Figure 1 also shows that different gases show different sensitivities: while the ammonia signal (yellow) has not reached equilibrium during the first low-temperature phase and the slope-method can be applied, the other gases all show a linear response initially but quickly run in during this phase. While H₂ and CO show nearly constant values after the first linear response, that is, have reached equilibrium, Benzene shows a second relaxation process with a higher time constant, so no constant value is reached during that temperature plateau.

Figure 2 gives an overview of the low-temperature phase at 150 °C starting at 3 s relevant for the quantification at 50% RH for all gases and all measured concentrations. For the data analysis, we always used the last cycle of each gas exposure to ensure that the concentration has reached a stable value inside the sensor chamber. For low concentrations, all gases can be quantified using the \tilde{k} -evaluation. Curves ascending with the concentration can be clearly observed for CO, H₂ and benzene. For ammonia, the absolute values at low concentrations show a wrong order: the curve for 10 ppb is above that for 25 ppb and 50 ppb is above 100 ppb. This wrong order is also observed for the \tilde{k} -evaluation. The GMA is completely set up with stainless steel and ammonia is known to adsorb on such surfaces [32], which could explain this inconsistency, because the two displaced concentrations 10 ppb and 50 ppb followed after 50 ppm and 116 ppm ammonia. Looking at the higher concentrations, the faster relaxation and reaching of equilibrium can be observed very well for all gases. Similar to the benzene cycle in Figure 1, the highest concentrations of CO and ammonia as well as H₂ (although the effect is very small here) show a second time constant with a further slight increase of $\ln(G)$ after the linear range has ended and equilibrium should be reached.

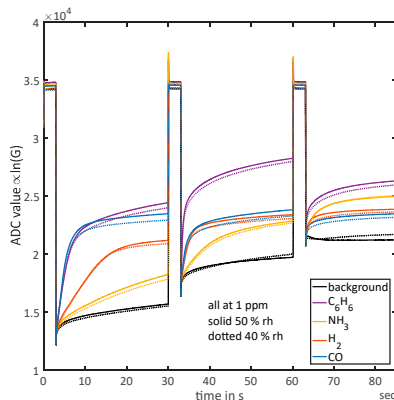


Figure 1. Sensor signal for all gases at 1 ppm and background gas (zero air) at both humidities measured (40% RH and 50% RH), the measured ADC-values are proportional to the logarithmic conductance due to the logarithmic amplifier. Temperatures: 0–3 s 450 °C, 3–30 s 150 °C, 30–33 s 450 °C, 33–60 s 200 °C, 60–63 s 450 °C and 63–90 s 250 °C.

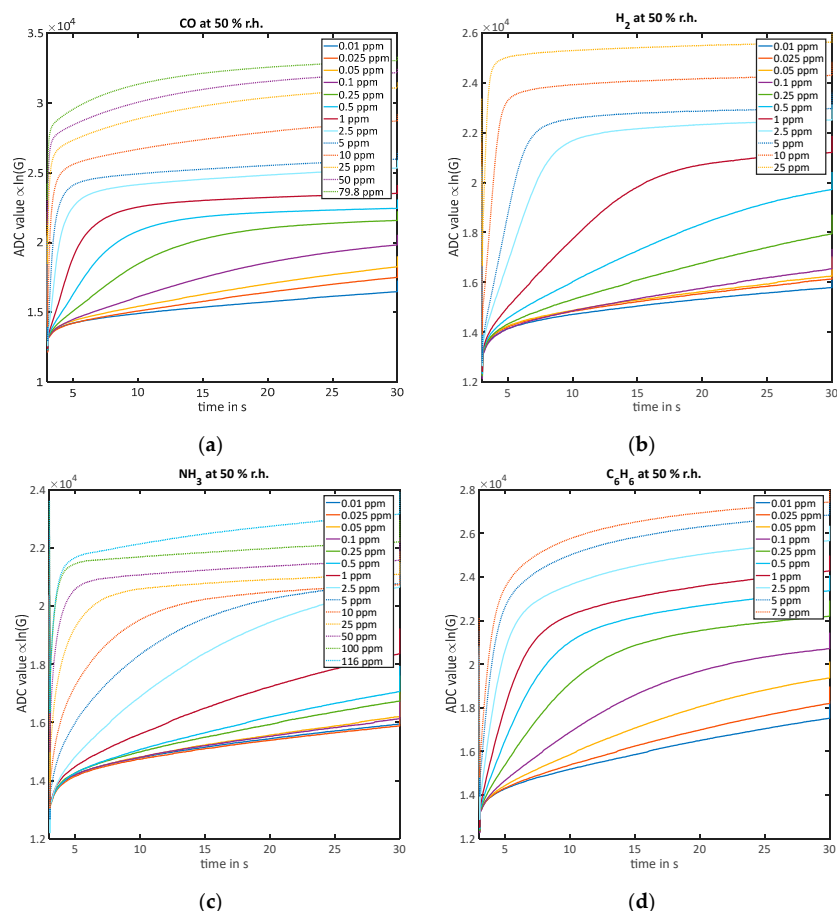


Figure 2. Measured ADC signal which is proportional to the logarithmic conductance $\ln(G)$ during the 150 °C temperature phase (3–30 s during the cycle) at 50% RH for all measured concentrations: (a) CO; (b) H₂; (c) NH₃; (d) C₆H₆.

3.2. Quantification

3.2.1. Quantification of Low Concentrations without Reaching Equilibrium during the Low-Temperature Phase (\tilde{k})

For low concentrations, the \tilde{k} -evaluation was tested for quantification. The goal of this treatment is to achieve a linear calibration curve. Since the zero air \tilde{k}_0 has been subtracted from all computed \tilde{k} , the expected function is a line through the origin, so fitting was performed using the very simple function $f(x) = a \cdot x$. The results for all gases and both humidities can be seen in Figure 3; all obtained fit parameters are summarized in Table 2. Figure 3a shows the results for CO: for 40% RH, a_{40} is 1939; for 50% RH, $a_{50} = 1995$. Both values lie within the 95% confidence bounds of each other. The coefficients of determination R^2_{40} are 0.9851 and 0.9252, respectively. The low value of R^2_{50} is mainly caused by the point at 25 ppb, which was the very first CO concentration in this measurement. The results for hydrogen, shown in Figure 3b, are $a_{40} = 393.1$ and $a_{50} = 351.9$, $R^2_{40} = 0.9986$ and $R^2_{50} = 0.9983$. In this case, the values for a are not within the confidence interval of each other, but the quality of both fits is very high. For ammonia (Figure 3c), fitting quality is lower than for the other gases, which could be already expected from the raw data in Figure 2c. We get $a_{40} = 108.5$, $a_{50} = 108.9$, $R^2_{40} = 0.9381$ and $R^2_{50} = 0.9606$. Only for benzene (Figure 3d) a linear fit was not possible. In this case a power law $f(x) = a \cdot x^b$ represents the data much better, resulting in $a_{40} = 569.9$ and $b_{40} = 0.4065$, $a_{50} = 691.1$ and $b_{50} = 0.4935$. The fit quality is $R^2_{40} = 0.9835$ and $R^2_{50} = 0.9938$.

Table 2. Fitting parameters for all gases using the \tilde{k} -evaluation.

Gas	Humidity	Fit Function	a	b	R^2
CO	40%RH	$f(x) = a \cdot x$	1939	-	0.9851
	50%RH	-	1995	-	0.9252
H_2	40%RH	$f(x) = a \cdot x$	393.1	-	0.9986
	50%RH	-	351.9	-	0.9983
NH_3	40%RH	$f(x) = a \cdot x$	108.5	-	0.9381
	50%RH	-	108.9	-	0.9606
C_6H_6	40%RH	$f(x) = a \cdot x^b$	569.9	0.4065	0.9835
	50%RH	-	691.1	0.4935	0.9938

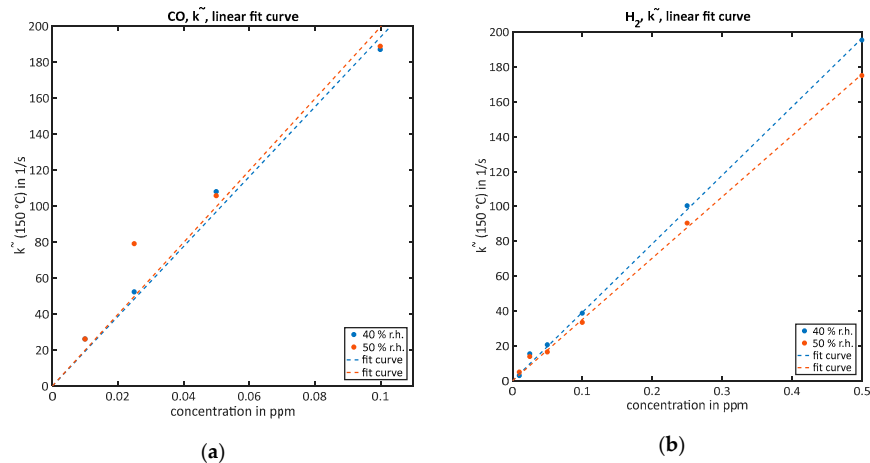


Figure 3. Cont.

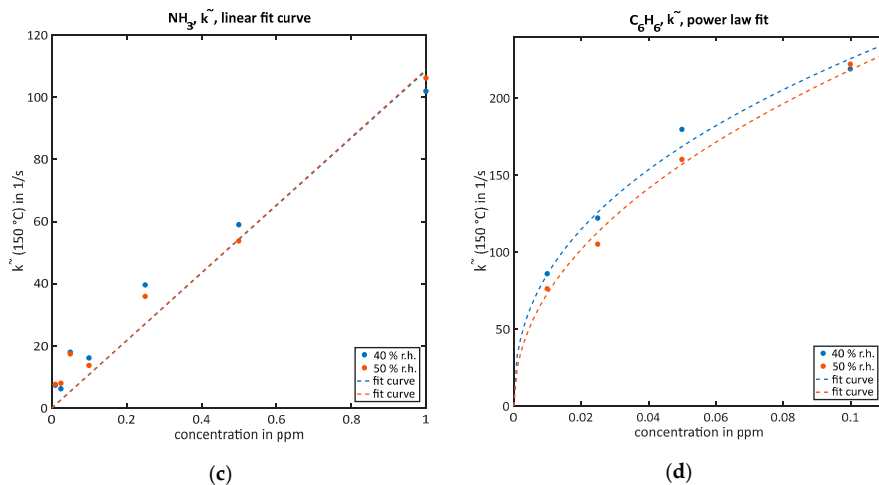


Figure 3. Quantification of the correspondent gases via the \tilde{k} -evaluation and their fit curves for both humidities: (a) CO, linear fit curve; (b) H_2 , linear fit curve; (c) NH_3 , linear fit curve; (d) C_6H_6 , power law fit.

3.2.2. Quantification of High Concentrations While Reaching Equilibrium during the Low-Temperature Phase (τ)

For higher concentrations starting with the highest one used in the last Section (3.2.1), the τ -evaluation is used for quantification. Again, the calculated values $1/\tau$ over corresponding concentrations are shown in Figure 4 for all gases together with the corresponding fit curves, which are again straight lines through the origin for CO, H_2 and ammonia and a power law for benzene. The fit parameters can be found in Table 3. For CO, in Figure 4a the obtained results are: $a_{40} = 0.3827$ and $a_{50} = 0.365$, both results are again inside the respective confidence intervals, and $R_{40}^2 = 0.9874$ and $R_{50}^2 = 0.9883$. For H_2 , in Figure 4b the obtained results are: $a_{40} = 0.1317$ and $a_{50} = 0.1167$, as before for H_2 the results for different humidities are outside the confidence intervals, but the fit quality again is very high with $R_{40}^2 = 0.9972$ and $R_{50}^2 = 0.9955$. The higher ammonia concentrations evaluated here follow the expected model much better than the lower ones shown above. We get (Figure 4c) $a_{40} = 0.03078$ and $a_{50} = 0.03224$, both results are inside the confidence intervals, and the corresponding coefficients of determination $R_{40}^2 = 0.9888$ and $R_{50}^2 = 0.996$. Also, for this method and the higher benzene concentrations it is not possible to perform a linear approximation as shown in Figure 4d. Again, a power law is used instead, yielding: $a_{40} = 0.3358$ and $a_{50} = 0.3114$, $b_{40} = 0.3977$ and $b_{50} = 0.3987$, almost all values are inside the confidence intervals of each other, except a_{40} . The fit quality again is high, $R_{40}^2 = 0.9963$ and $R_{50}^2 = 0.9942$.

The highest concentrations of CO (10 ppm) and ammonia (100 ppm) in Figure 4 show significant deviations from the fit curves and were not used for the approximation. This is caused by the strong effect of the observed second time constant after the relaxation considered in the model is finished. The very simple quantification rule used here is not able to compensate this effect. Therefore, higher concentrations above 10 ppm CO and 100 ppm ammonia cannot be evaluated with the presented method.

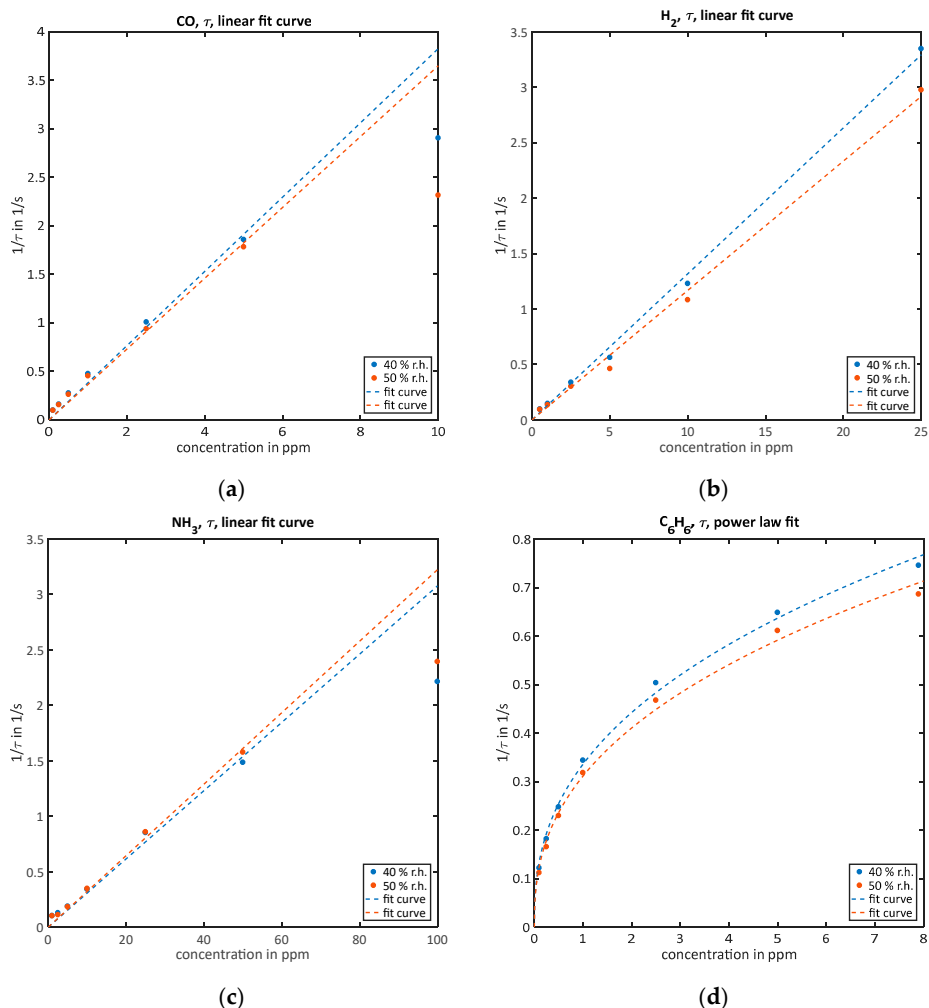


Figure 4. Quantification of the correspondent gases via the τ -evaluation and their fit curves for both humidities: (a) CO, linear fit curve; (b) H_2 , linear fit curve; (c) NH_3 , linear fit curve; (d) C_6H_6 , power law fit.

Table 3. Fitting parameters for all gases using the τ -evaluation.

Gas	Humidity	Fit Function	a	b	R^2
CO	40%RH	$f(x) = a \cdot x$	0.3827	-	0.9874
	-	-	0.365	-	0.9883
H_2	40%RH	$f(x) = a \cdot x$	0.1317	-	0.9972
	-	-	0.1167	-	0.9955
NH_3	40%RH	$f(x) = a \cdot x$	0.03078	-	0.9888
	-	-	0.03224	-	0.9960
C_6H_6	40%RH	$f(x) = a \cdot x^b$	0.3358	0.3977	0.9963
	-	-	0.3114	0.3987	0.9942

3.3. Identification

Looking back to Figure 1, it becomes clear that the four gases can be distinguished based on their different reaction rates at the three temperatures. At 150 °C, CO and benzene show similar reaction rates, but for both higher temperatures benzene exceeds CO clearly with CO even showing the lowest rate at 250 °C. Ammonia always shows the lowest reaction rate except at the highest temperature of 300 °C, where it shows the second strongest response after benzene. For all temperatures the reaction to H₂ is between the other gases.

Pattern recognition is needed for this type of analysis. We chose to show the possibility of identification with model-based TCO and model-based data evaluation with Linear Discriminant Analysis (LDA). This method projects the data into a new often lower dimensional feature space while maintaining as much relevant information as possible [33]. For this, the coefficients for the linear feature combinations are chosen in order to minimize the within-class scatter while maximizing the between-class scatter in the new discriminant space. As features we use the three \tilde{k} calculated for the three low temperatures. For training we use all measured temperature cycles at the highest concentrations of each gas (12 per humidity), which can be correctly quantified using the \tilde{k} -evaluation (CO 0.1 ppm, H₂ 1 ppm, NH₃ 1 ppm, C₆H₆ 0.1 ppm) and background gas, all at both humidities. To compensate for unequal class sizes, selections are removed randomly from larger classes before LDA, resulting in a total of 120 observations (temperature cycles) for the training dataset (24 per class). We use three discriminant functions and a 10-fold cross-validation [33], the error from this validation for the training dataset is 0%. After the training, all lower concentrations are predicted using the obtained model, as shown in Figure 5a for the first two discriminant functions and Figure 5b for the second and third discriminant functions. Filled circles are trained observations, empty ones predicted observations. It can be seen that all lower concentrations start near the trained background observations (black) and then scatter in the direction (arrows) of the corresponding highest concentration which has been trained. Especially ammonia and benzene can be distinguished clearly in Figure 5a. For CO and H₂, the third discriminant function needs to be considered, which still contains 8.45% of the relevant information. In Figure 5a, few of the red empty circles (H₂) scatter in the direction of ammonia. Tracing back those points, it becomes clear that these are low H₂ concentrations which directly follow high ammonia concentrations, for example, the confusion is presumably caused by carry-over in the GMA due to adsorption of ammonia on the internal surfaces.

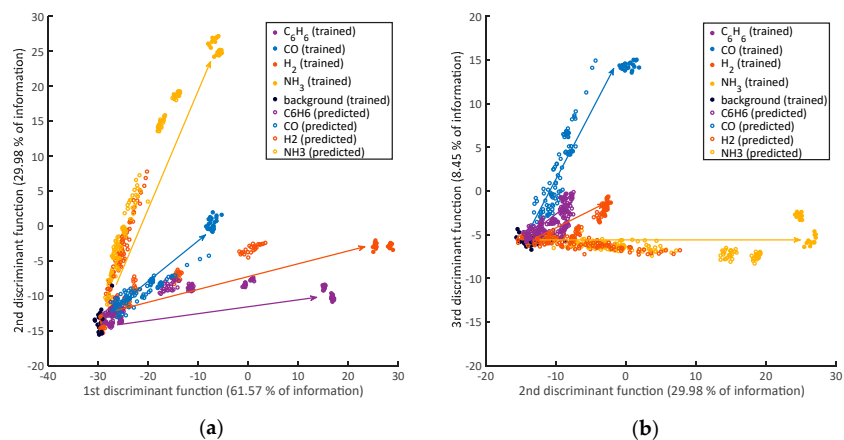


Figure 5. A 3D-LDA (Linear Discriminant Analysis) scatterplot trained (filled circles) by background air and the highest concentration from the \tilde{k} -evaluation of each gas, all other lower concentrations are predicted (empty circles), each gas has its own direction to step out of the background air data. The \tilde{k} for the three different low temperatures have been used as features; (a) shows the first two discriminant functions; (b) the second and third.

4. Discussion

A comparison of all four investigated gases is given in Figure 6a for the \tilde{k} -evaluation and Figure 6b for the τ -evaluation. Both graphs are on a double logarithmic scale to give a better overview. A linear calibration curve is exceptional for MOS gas sensors, although we see that the relative error for both evaluations increases in the lower concentration range. This can be avoided by applying a logarithm to x- and y-data before performing the fit (function: $f(x) = \log(a) + x$), because then points from every order of magnitude have the same influence on the fitting quality. With this approach, of course the absolute error for the higher concentrations increases. The poorest agreement between fit and data points is observed for low ammonia concentrations in Figure 6a. Applying a linear fit with an offset (function: $f(x) = a \cdot x + b$) improves the fit notably. The reason for this could be a systematic error in the generation of small ammonia concentrations, giving an additional background compared to the zero air. Ammonia is known to adsorb easily on stainless steel surfaces, an additional error can therefore be expected, caused by ad- and desorption of ammonia inside the dilution line [32].

Using the presented quantification methods on several temperatures, an identification of the gas can be achieved rather easily directly upon the observed differences in reaction kinetics.

In Figure 6, benzene immediately sticks out because of its very different behavior. Despite the expectations from the model and in contrast to the other gases, the benzene data is not represented by a linear calibration curve but by a power law with an exponent of approx. 0.4. In previous works, we also found similar results for gases with aromatic structures, especially toluene [17]. The simple model assumes that there is no competition for adsorption sites on the surface (Henry adsorption), no interaction between molecules and only one surface species for the reaction. For aromatic substances, it is likely that a precursor is needed to crack the ring structure resulting in a Freundlich isotherm, which would suit the power law. The chemical products resulting from the precursor reaction tend to have very low vapor pressures and thus stay on the surface for a long time, as we have already observed when measuring short trace gas pulses [16], which explains the very high sensitivity at low concentrations compared to the other gases, because of possible multi-stage reaction processes.

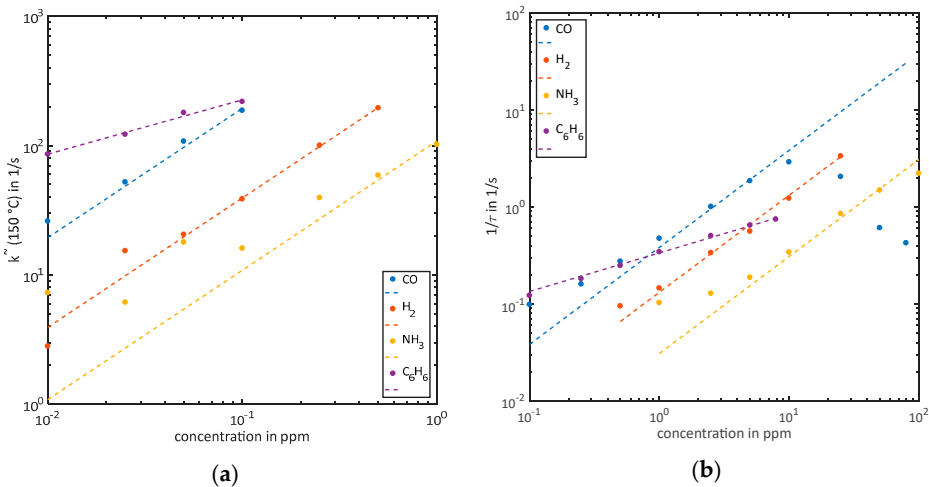


Figure 6. The results from Section 3.2 on a double logarithmic scale and for all gases in one graph: (a) \tilde{k} -evaluation for low concentrations showing the very high response of benzene compared to the other gases; (b) τ -evaluation for the higher concentrations, here the response of benzene is below the others because of the different correlation between concentration and sensor signal.

For the other gases, a linear quantification using the two simple methods presented here is clearly possible. There are distinct concentration ranges where each method is valid with the boundaries

depending on the sensitivity of the respective gas at the given temperature. From Figure 6a, the upper limit for the slope-evaluation can be estimated at slope value of about 110–120 1/s. Similarly, the validity of the τ -method ends at approx. 1.2 1/s for all gases; at higher values the effect of the second time constant observed in Figure 2 limits the performance of the simple algorithm. A more complex algorithm for the linear approximation and calculation of τ would overcome this limitation. We also tested evaluating the time required to reach a certain threshold level starting from $\ln(G_{min})$, which all concentrations reach inside the 27 s; this is also suitable for quantification over the full range of concentrations but does not yield a linear calibration curve. The slow increase in conductance with a second time constant observed mainly in the ammonia and CO measurements is not covered by the presented model. For the description of the effect, a multitude of possible additions to the model could be discussed, ranging from the impact of adsorbed reducing species [34] to a gradual reduction of the sensing materials due to a change in oxygen vacancies (bulk donors) equilibrium density N_D [35]. However, the effect is small compared to the total relaxation and the two time constants differ strongly so they can clearly be discriminated by the naked eye. Therefore, an optimization of the feature extraction method is likely to be the best solution.

To apply one single calibration curve, the values for \tilde{k} and $1/\tau$ must be converted to k , which is possible using Equation (4) and $2k = 1/\tau$. We tested this conversion for H_2 at 2.5 ppm, where the linear fit needs to be reduced to the first 3 s after the temperature change and τ -evaluation works properly. We obtained $k(\tilde{k}_{40}) = 0.0282 \frac{1}{s}$, $k(\tilde{k}_{50}) = 0.0256 \frac{1}{s}$ and $k(\tau_{40}) = 0.1682 \frac{1}{s}$, $k(\tau_{50}) = 0.1501 \frac{1}{s}$; thus, a factor of approximately 6 between both methods. The model used here is probably not considering additional processes which occur during relaxation at the low temperature and therefore needs to be extended.

Another advantage of the presented method is the suppression of humidity effects: almost all fit parameters lie within the confidence bounds of each other for both tested RH values. This is a common result for the use of TCO [17]. H_2 is the only gas where humidity causes significant deviations. We have already started further work to better understand the reaction mechanisms in dry and humid air. The measurement results clearly show that the deliberately simplified model we apply to the sensor does cover most, but not all, observed effects. For CO, H_2 and NH_3 , the response follows the predicted model with a correlation coefficient close to 1, as well for the \tilde{k} as for the $1/\tau$ parameter. The deviation at low NH_3 concentration is likely to be caused by errors in gas generation. For benzene, the simplified physical model cannot be applied directly, but requires an empirical extension as described above.

Optimizing the temperature cycle (the last 10 s of all three low-temperature phases are not used in any of the evaluations), one measurement per minute can be conducted. The presented results define a facile technique for the calibration of gas sensor elements for various gases in a high concentration range at minimal cost, that is, with minimal number of calibration points.

5. Conclusions

We have shown that the previously presented simple model for MOS sensors based on a single grain–grain boundary offers two new methods for gas quantification with a model-based TCO to obtain linear calibration curves over the full investigated range of concentrations covering 3 to 4 orders of magnitude, which is exceptional for MOS gas sensors. Both methods can be implemented with completely independent algorithms, using a simple rule for switching between both methods. In addition, pattern recognition methods can be applied using the same features to allow identification of the gases. Since the method can be traced back to physical quantities via the model, it is more comprehensible, and therefore credible, compared to highly complex black-box data-based models. Especially for traceable calibration linear, physically motivated models are highly preferable to make use of standard metrology methods, e.g., for determining the limit of detection (LOD) and limit of quantification (LOQ). IUPAC recommendations, for example, have high requirements [36] for being applied to measurement data; future developments here could help to use the full information coming from TCO by also considering more complex data structures. Furthermore, a prerequisite for the calibration of every single gas sensor for a dedicated application, which might be needed for proper

results, is the availability of a simple and general correlation between the target concentration and the sensor signal.

We have also shown that our model is able to predict key features of the TCO, but there are still some effects missing, e.g., the appearance of a second relaxation process especially for high concentrations. This might be caused by a changing donor density, but further experiments are required to elucidate the relevant processes and expand the model.

Supplementary Materials: The following are available online at <http://www.mdpi.com/1424-8220/18/3/744/s1>, Figure S1: Heater temperature calculated from the heater resistance around the temperature step from 450 °C to 150 °C.

Author Contributions: C.S. and T.S. conceived and designed the experiments; C.S. performed the experiments; C.S. and T.B. analyzed the data; T.B. contributed the electronic system; C.S. wrote the paper. A.S. and T.S. contributed with substantial revisions.

Conflicts of Interest: The authors declare no conflict of interest.

References

1. Kohl, D. Function and applications of gas sensors. *J. Phys. D Appl. Phys.* **2001**, *34*, R125. [\[CrossRef\]](#)
2. De Angelis, L.; Riva, R. Selectivity and stability of a tin dioxide sensor for methane. *Sens. Actuators B Chem.* **1995**, *28*, 25–29. [\[CrossRef\]](#)
3. Kohl, D.; Kelleter, J.; Petig, H. Detection of Fires by Gas Sensors. *Sens. Update* **2001**, *9*, 161–223. [\[CrossRef\]](#)
4. Reimann, P.; Schütze, A. Fire detection in coal mines based on semiconductor gas sensors. *Sens. Rev.* **2012**, *32*, 47–58. [\[CrossRef\]](#)
5. Maekawa, T.; Suzuki, K.; Takada, T. Odor identification using a SnO₂-based sensor array. *Sens. Actuators B* **2001**, *80*, 3–6. [\[CrossRef\]](#)
6. Peterson, P.; Aujla, A.; Grant, K.; Brundle, A.; Thompson, M.; Vande Hey, J.; Leigh, R. Practical Use of Metal Oxide Semiconductor Gas Sensors for Measuring Nitrogen Dioxide and Ozone in Urban Environments. *Sensors* **2017**, *17*, 1653. [\[CrossRef\]](#) [\[PubMed\]](#)
7. Leidinger, M.; Sauerwald, T.; Reimringer, W.; Ventura, G.; Schütze, A. Selective detection of hazardous VOCs for indoor air quality applications using a virtual gas sensor array. *J. Sens. Sens. Syst.* **2014**, *3*, 253–263. [\[CrossRef\]](#)
8. Llobet, E.; Brezmes, J.; Vilanova, X.; Sueiras, J.E.; Correig, X. Qualitative and quantitative analysis of volatile organic compounds using transient and steady-state responses of a thick-film tin oxide gas sensor array. *Sens. Actuators B Chem.* **1997**, *41*, 13–21. [\[CrossRef\]](#)
9. Lee, A.P.; Reedy, B.J. Temperature modulation in semiconductor gas sensing. *Sens. Actuators B Chem.* **1999**, *60*, 35–42. [\[CrossRef\]](#)
10. Gramm, A.; Schütze, A. High performance solvent vapor identification with a two sensor array using temperature cycling and pattern classification. *Sens. Actuators B Chem.* **2003**, *95*, 58–65. [\[CrossRef\]](#)
11. Jurs, P.C.; Bakken, G.A.; McClelland, H.E. Computational methods for the analysis of chemical sensor array data from volatile analytes. *Chem. Rev.* **2000**, *100*, 2649–2678. [\[CrossRef\]](#) [\[PubMed\]](#)
12. Eicker, H. Method and Apparatus for Determining the Concentration of One Gaseous Component in a Mixture of Gases. U.S. Patent 4012692A, 15 March 1977.
13. Clifford, P.K.; Tuma, D.T. Characteristics of semiconductor gas sensors II. transient response to temperature change. *Sens. Actuators* **1982**, *3*, 255–281. [\[CrossRef\]](#)
14. Ding, J.; Mcavoy, T.J.; Cavicchi, R.E.; Semancik, S. Surface state trapping models for SnO₂-based microhotplate sensors. *Sens. Actuators B Chem.* **2001**, *77*, 597–613. [\[CrossRef\]](#)
15. Nakata, S.; Ozaki, E.; Ojima, N. Gas sensing based on the dynamic nonlinear responses of a semiconductor gas sensor: Dependence on the range and frequency of a cyclic temperature change. *Anal. Chim. Acta* **1998**, *361*, 93–100. [\[CrossRef\]](#)
16. Baur, T.; Schütze, A.; Sauerwald, T. Detektion von kurzen Gaspulsen für die Spurengasanalytik. *TM—Tech. Mess.* **2017**, *84*, 88–92. [\[CrossRef\]](#)

17. Schultealbert, C.; Baur, T.; Schütze, A.; Böttcher, S.; Sauerwald, T. A novel approach towards calibrated measurement of trace gases using metal oxide semiconductor sensors. *Sens. Actuators B. Chem.* **2017**, *239*, 390–396. [[CrossRef](#)]
18. Barsan, N.; Weimar, U. Conduction Model of Metal Oxide Gas Sensors. *J. Electroceram.* **2001**, *7*, 143–167. [[CrossRef](#)]
19. Yamazoe, N.; Shimanoe, K. Theory of power laws for semiconductor gas sensors. *Sens. Actuators B Chem.* **2008**, *128*, 566–573. [[CrossRef](#)]
20. Bastuck, M.; Leidinger, M.; Sauerwald, T.; Schütze, A. Improved quantification of naphthalene using non-linear Partial Least Squares Regression. In Proceedings of the 16th International Symposium on Olfaction and Electronic Nose, Dijon, France, 28 June–1 July 2015; pp. 1–2.
21. Wolfrum, E.J.; Meglen, R.M.; Peterson, D.; Sluiter, J. Metal oxide sensor arrays for the detection, differentiation, and quantification of volatile organic compounds at sub-parts-per-million concentration levels. *Sens. Actuators B Chem.* **2006**, *115*, 322–329. [[CrossRef](#)]
22. Baur, T.; Schütze, A.; Sauerwald, T. Optimierung des temperaturzyklischen Betriebs von Halbleitergassensoren. *Tech. Mess.* **2015**, *82*, 187–195. [[CrossRef](#)]
23. Madou, M.J.; Morrison, S.R. *Chemical Sensing with Solid State Devices*; Academic Press: San Diego, CA, USA, 1989; ISBN 0-12-464965-3.
24. Barsan, N.; Schweizer-Berberich, M.; Göpel, W. Fundamental and practical aspects in the design of nanoscaled SnO_2 gas sensors: A status report. *Fresenius J. Anal. Chem.* **1999**, *365*, 287–304. [[CrossRef](#)]
25. Gurlo, A. Interplay between O_2 and SnO_2 : Oxygen Ionomerization and Spectroscopic Evidence for Adsorbed Oxygen. *ChemPhysChem* **2006**, *7*, 2041–2052. [[CrossRef](#)] [[PubMed](#)]
26. Pulkkinen, U.; Rantala, T.T.; Rantala, T.S.; Lantto, V. Kinetic Monte Carlo simulation of oxygen exchange of SnO_2 surface. *J. Mol. Catal. A Chem.* **2001**, *166*, 15–21. [[CrossRef](#)]
27. Suematsu, K.; Yuasa, M.; Kida, T.; Yamazoe, N.; Shimanoe, K. Determination of Oxygen Adsorption Species on SnO_2 : Exact Analysis of Gas Sensing Properties Using a Sample Gas Pretreatment System. *J. Electrochem. Soc.* **2014**, *161*, B123–B128. [[CrossRef](#)]
28. Yamazoe, N.; Suematsu, K.; Shimanoe, K. Extension of receptor function theory to include two types of adsorbed oxygen for oxide semiconductor gas sensors. *Sens. Actuators B Chem.* **2012**, *163*, 128–135. [[CrossRef](#)]
29. Bastuck, M.; Baur, T.; Schütze, A. P7 Messunsicherheit und Funktionssicherheit von Messsystemen. In *DAV³E: Data Analysis and Verification/Visualization/Validation Environment für die Multisensor-Datenfusion*; 2016; pp. 729–734. Available online: <http://www.ama-science.org/proceedings/details/2435> (accessed on 26 February 2018).
30. Baur, T.; Schütze, A.; Sauerwald, T. Detection of short trace gas pulses. In Proceedings of the Sensor 2017, Nürnberg, Germany, 30 May–1 June 2017; pp. 87–91.
31. Leidinger, M.; Schultealbert, C.; Neu, J.; Schütze, A.; Sauerwald, T. Characterization and calibration of gas sensor systems at ppb level—A versatile test gas generation system. *Meas. Sci. Technol.* **2018**, *29*. [[CrossRef](#)]
32. Vaittinen, O.; Metsälä, M.; Persijn, S.; Vainio, M.; Halonen, L. Adsorption of ammonia on treated stainless steel and polymer surfaces. *Appl. Phys. B* **2014**, *115*, 185–196. [[CrossRef](#)]
33. Gutierrez-Osuna, R. Pattern analysis for machine olfaction: A review. *IEEE Sens. J.* **2002**, *2*, 189–202. [[CrossRef](#)]
34. Bårsan, N.; Hübner, M.; Weimar, U. Conduction mechanisms in SnO_2 based polycrystalline thick film gas sensors exposed to CO and H_2 in different oxygen backgrounds. *Sens. Actuators B Chem.* **2011**, *157*, 510–517. [[CrossRef](#)]
35. Kamp, B.; Merkle, R. Å.; Lauck, R.; Maier, J. Chemical diffusion of oxygen in tin dioxide: Effects of dopants and oxygen partial pressure. *2005*, *178*, 3027–3039. [[CrossRef](#)]
36. Danzer, K.; Currie, L.A. Guidelines for calibration in analytical chemistry. Part I. Fundamentals and single component calibration (IUPAC Recommendations 1998). *Pure Appl. Chem.* **1998**, *70*, 993–1014. [[CrossRef](#)]



© 2018 by the authors. Licensee MDPI, Basel, Switzerland. This article is an open access article distributed under the terms and conditions of the Creative Commons Attribution (CC BY) license (<http://creativecommons.org/licenses/by/4.0/>).

4.2 Methods and Tools for the Development of Gas Sensor Systems

4.2.1 Synopsis

The development of gas sensor systems can be supported by different tools and methods. Three main points are considered in this section: Electronics and fluidics, design of experiments (DoE) and the data evaluation with machine learning algorithms.

The electronics and the sensor chamber for the detection of trace gas pulses are presented in Paper 2. The fluidic design of the sensor chamber is one of the main parts for the detection of such short gas pulses. The sensor chamber was designed for fast gas exchange with low dead volume so that short gas pulses can be measured. On the other hand, the gas needs to be brought very close to the sensor surface so that reactions can take place. Furthermore, special electronics had to be developed for measuring the highly dynamic conductance values over eight orders of magnitude, including currents in the range of 100 pA. The exponential relationship between resistance and energy barrier implies that even a small change in the energy barrier can cause a large change in the resistance. Through the logarithmic measurement, the change in the energy barrier can be measured with the same relative resolution over several decades. When measuring such low currents, a good PCB design and shielding are necessary. In addition, the temperature control must be very accurate. This is implemented by a voltage-controlled proportional–integral–derivative (PID) feedback-loop controller, which regulates to a constant heater resistance.

A complete electronics framework, Sensor Control (SC), was designed based on these electronics. In addition to analog electronics for various analog sensors, the framework has been expanded by a system for digital sensors. This allows to operate gas sensors with digital interface in TCO. In addition to MOS gas sensors, other sensors (temperature-, humidity-, NDIR-CO₂-sensors, EC-cells) are supported. The current state and further development of electronics is shown in [264] and Paper vii. Different versions of these electronics were used within Paper E, 6 and F in the next Section 4.3. Besides the classical gas measurements, a modified version was designed for differential scanning calorimetry on micro hotplates for temperature calibration and mass quantification [265]. The accurate temperature calibration of micro hotplate gas sensors as important parameter for the gas reaction on the sensor is a remarkable challenge.

DoE is an essential and critical step for the calibration of gas sensor systems. As described in Subsection 3.2.3, classical designs with single gases do not reveal any masking effects or other gas interactions altering the sensor response for these applications. DoE with several substances and three or five fixed concentration levels for each gas do not lead to success. Gas mixtures are created using combinatorial permutations of the individual fixed concentrations. The usage of too few levels for the quantization of a continuous quantity or classification of different substances easily leads to overfitting. However, with many substances and concentration levels, this results in an extremely long calibration duration due to the numerous combinations. Therefore, in Paper 3 the calibration with randomized DoE is introduced and tested. The DoE reduces the effort and at the same time gives better results than sequential calibration. This randomized approach is also more realistic due to the variable composition. The

calibration method is tested with four VOCs (acetone, benzene, toluene, formaldehyde), two interferents (hydrogen, carbon monoxide) and relative humidity. Two sensors, the AS-MLV and the AS-MLV-P2, are compared. An optimized data evaluation with PLSR and feature extraction are shown. The model calibrated with the randomized DoE predicts both the randomized and the sequential test data well, whereas the sequential model fails to predict the randomized data. The statistical nature of the introduced approach of randomized mixtures makes it robust to overfitting and therefore well-suited for machine learning algorithms. To perform the DoE in the laboratory, an important point is the generation of artificial gas environments with a GMA. At LMT different GMAs are available, as described in Subsection 3.2.2. Randomized DoE allows complex calibration sequences to be performed efficiently with even more gases. For that purpose, a new modularized GMA has been developed for this purpose to mix and expose up to 18 gases at the same time [123].

Data evaluation with machine learning algorithms, including the complete evaluation chain requires a large programming effort. To reduce the effort for complex data evaluation and make it accessible for a broad range of scientists, an open-source MATLAB toolbox called DAV³E (Data Analysis and Verification/Visualization/Validation Environment) was developed and described in Paper 4. It combines the complete evaluation chain with import, preprocessing, labeling, feature extraction and selection, regression and classification with validation and testing. Files of the data acquisition software of the electronics (Sensor Control Center [264]) and the control software for the GMA (GRUpy [124]) can directly be imported and synchronized with DAV³E. This enables a very fast workflow from identification of an application to application-specific detection algorithm. The further developed version 2.0 is described in [131] and available on GitHub⁹.

Methods and tools for the development of gas sensor systems are presented. In summary, the following key results are achieved:

- A fast electronics framework, especially for temperature cycled operation with high resolution sensor resistance measurement over several order of magnitudes.
- A more realistic DoE with randomized gas mixtures. This approach reduces the effort and gives better results compared to sequential calibration. The randomized calibration is also more realistic due to the variable composition. Its statistical nature makes it robust to overfitting and therefore well-suited for machine learning algorithms.
- The data evaluation tool DAV³E, which enables complex data evaluation with import, preprocessing, labeling, feature extraction and selection, regression and classification with validation and testing. DAV³E has a simple user interface and enables the direct import of files from the Sensor Control Center (sensor electronics framework) and GRUpy (GMA).
- Because all these methods and tools can be connected and interfaces were developed, a very fast workflow from identification of an application to detection and quantification algorithm is established.

⁹ <https://github.com/lmtUds/dav3e-beta>

4.2.2 *Paper 2 – Device for the Detection of short trace Gas Pulses (Messsystem zur Detektion von kurzen Spurengaspulsen)*

T. Baur, C. Schultealbert, A. Schütze and T. Sauerwald
Saarland University, Lab for Measurement Technology, Saarbrücken, Germany

tm - Technisches Messen (2018), 85(7-8), 496-503

The original paper can be found, in the online version, at <https://doi.org/10.1515/teme-2017-0137>.

© Used with permission of Walter de Gruyter and Company, from *Device for the detection of short trace gas pulses*, Baur, Tobias; Schultealbert, Caroline; Schütze, Andreas; Sauerwald, Tilman, 85, 7-8, 2022; permission conveyed through Copyright Clearance Center, Inc.

Tobias Baur*, Caroline Schultealbert, Andreas Schütze, and Tilman Sauerwald

Device for the detection of short trace gas pulses

Messsystem zur Detektion von kurzen Spurengaspulsen

<https://doi.org/10.1515/teme-2017-0137>

Received December 8, 2017; accepted March 29, 2018

Abstract: A device for detection of short gas pulses at very low concentrations is presented. The approach is based on a special temperature modulation technique enabling a differential surface reduction (DSR) measurement of a metal oxide semiconductor (MOS) gas sensor. With this method, the sensor surface is highly covered with oxidized surface states at high temperature (e. g. 400 °C) initially. The temperature is then reduced abruptly to, e. g., 100 °C resulting in a state with strong excess of negative surface charge. Reactions of these surface charges with reducing gases are prevailing and lead to very high sensitivity. For the measurement a dedicated detector (electronics and fluidic system) is presented. The electronics allows a high-resolution conductance measurement of the sensitive layer and accurate temperature control. The fluidic system is examined in terms of peak shape and optimal sensor response via FEM simulations.

Keywords: MOS gas sensor, differential surface reduction (DSR), short gas pulses.

Zusammenfassung: Ein Messsystem zur Detektion von kurzen Gaspulsen bei sehr niedrigen Konzentrationen wird vorgestellt. Der Ansatz basiert auf einem speziellen Temperaturmodulationsverfahren, das eine differentielle Messung der Oberflächenreduktion (DSR) eines Metalloxid-Halbleiter-Gassensors (MOS) ermöglicht. Bei diesem Verfahren wird die Sensoroberfläche bei hoher Temperatur (z. B. 400 °C) oxidiert. Ein abrupter Temperatursprung auf z. B. 100 °C führt zu einem Zustand mit starkem Überschuss an negativer Oberflächenladungen. Reaktionen dieser Oberflächenladungen mit reduzierendem Gas sind vorherrschend und führen zu einer sehr hohen Empfindlichkeit. Für die Messung wird ein eigen entwickelter Detektor (elektronisches und fluidisches System) vorgestellt. Die Elektronik ermöglicht eine hochauflösende Leitwertmessung der sensiven Schicht und eine ge-

näue Temperaturregelung. Das fluidische System wird mittels FEM-Simulationen auf Peakform und optimale Sensorsresponse untersucht.

Schlagwörter: MOS-Gassensor, differentielle Oberflächenreduktion (DSR), kurze Gaspulse.

1 Motivation

The measurement of short gas pulses is essential in analytical gas sensing microsystems, e. g. integrated sensor-pre-concentrator systems [1] and micro gas chromatographs (μ GC) [2]. While some progress has been reported in the miniaturization of GC columns [2, 3] there is still a lack of miniature detectors with low detection limit. MOS sensors are ideal due to their small size [2] and high sensitivity [4]. Combinations of μ GC and semiconductor gas sensors in static mode have also been reported [5]. Moreover, recent results show that the sensitivity of MOS sensors can be enhanced significantly by a special operation mode [6, 7, 8]. For the detection of short trace gas pulses, it is necessary to pay attention to some measuring aspects, especially electric measurement and fluidics.

2 Differential surface reduction

The principle of gas sensing with metal oxide semiconductor gas sensors is based on oxidation and reduction reactions at the surface. Reducing gas molecules react with ionosorbed oxygen and the oxygen molecules release their electron into the conduction band. To measure short gas pulses, we use a particularly sensitive method, called differential surface reduction (DSR). DSR is derived from a model for semiconductor gas sensors under temperature modulation presented in our earlier work [7, 8]. This model is based on a simplified single grain to grain contact [9, 10]. The surface of each grain is covered with negatively charged surface species forming a repulsive potential and a respective energy barrier E_b for the grain-to-grain conduction. In clean dry air, the main species present in this surface coverage, formally an oxidation, is ionosorbed oxygen [9, 10]. The conductance of the sensor

*Corresponding author: Tobias Baur, Saarland University, Laboratory for Measurement Technology, Saarbrücken, Germany, e-mail: t.baur@lmt.uni-saarland.de

Caroline Schultealbert, Andreas Schütze, Tilman Sauerwald, Saarland University, Laboratory for Measurement Technology, Saarbrücken, Germany

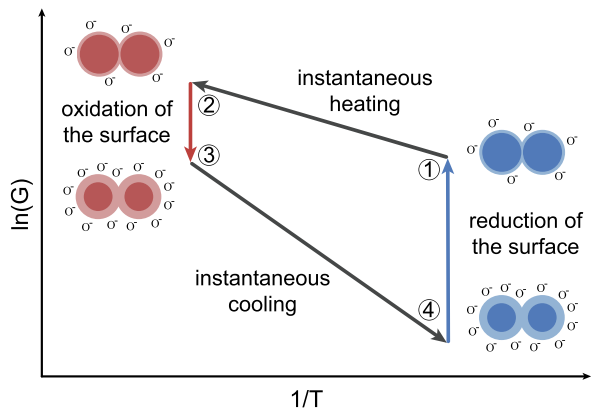


Figure 1: Schematic Arrhenius plot of a MOS-sensor during TCO with sketches depicting the grain-grain boundary in different states [12].

can be described by Eq. (1) showing the exponential dependence of the conductance from E_b with the Boltzmann constant k_b , the temperature T of the sensor film and a prefactor G_0 .

$$G = G_0 \cdot e^{-\frac{E_b}{k_b \cdot T}} \quad (1)$$

The equilibrium surface coverage and hence the energy barrier in air is strongly dependent on temperature. The energy barrier increases with temperature over a wide range [7]. In air the relaxation of the surface state after a temperature variation is a fairly slow process. The time constant can be in the order of several minutes especially for lower temperatures (e. g. 100 °C) [11]. Fig. 1 shows the schematic Arrhenius plot for instantaneous sensor heating and cooling and the relaxation of the conductance on long hot and cold temperature plateaus, respectively. It includes a sketch of the grain-to-grain boundary for different points of the temperature cycle.

In equilibrium state 1 at low temperature, the sensor has a small negative surface charge. A fast rise from low to high temperature (1 to 2) causes a rise in sensor conductance. Due to the fast temperature change the surface occupation remains nearly constant. During relaxation at high temperature a decrease in conduction is observed, caused by oxidation of the surface (2 to 3). This means that most of the surface states are covered with ionosorbed oxygen.

Abruptly cooling down to a low temperature (3 to 4) causes a strong excess of negative surface charge, because of the unchanged high surface occupation stemming from the high temperature equilibrium. In this low temperature phase reactions with reducing gases are strongly favoured over additional oxidation of the surface. For a short duration, the derivative of the logarithmic conductance $\ln G$ is

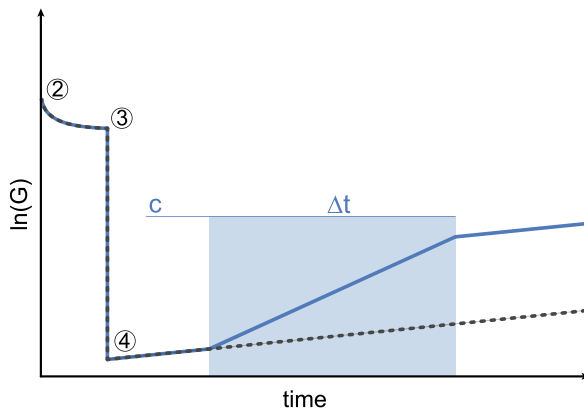


Figure 2: Schematic conductance curve for DSR with a temperature step from high to low temperature; during the relaxation at the low temperature stage, one concentration peak is assumed [12].

proportional to the time-dependent rate constant k of the surface reduction by a reducing gas (Eq. (2)) [8].

$$\frac{d \ln G}{dt} \sim k(t) \sim c(t) \quad (2)$$

For low concentrations, the rate constant is proportional to the concentration [7, 8]. Therefore, the measurement of the differential reduction of the surface in this phase especially at a very low temperature (e. g. 100 °C) allows a very sensitive detection of short gas pulses as well as quantification of the dosage.

$$\ln G(t_2) - \ln G(t_1) \sim \int_{t_2}^{t_1} c(t) \quad (3)$$

Fig. 2 shows the schematic conductance curve with a temperature jump from low to high temperature at $t = 0$ followed by relaxation at high temperature and a subsequent step to a lower temperature. During the low temperature stage, a concentration peak (with dosage $c \cdot \Delta t$) is present.

3 Detector electronics

The DSR method aims to measure the rate constant of the change in surface charge at a constant temperature. The change in surface charge is proportional to the logarithmic conductance. Thus, a low relative error especially at low conductances, a high sample rate, and an accurate temperature control are prerequisites to achieve a low detection limit. To this end, we developed a new detector electronics board. The concept of the detector is shown in

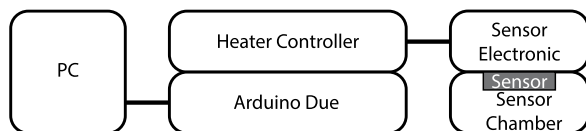


Figure 3: Concept of the detector.

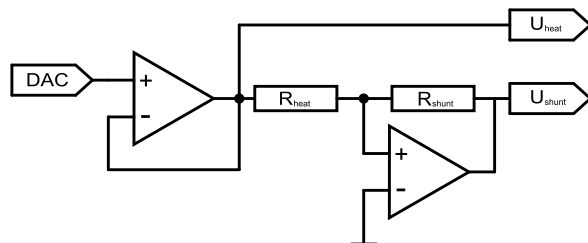


Figure 4: Basic circuit for the heater controller.

Fig. 3. The detector electronics consists of three parts: the open-source board Arduino Due, with its Atmel SAM3X8E ARM Cortex-M3 as the basis for the detector electronics, the heater controller and the sensor electronics.

The heater controller is based on an inverting amplifier (cf. Fig. 3). A voltage is applied to the heater from a digital to analog converter (DAC) and the current through the sensor is measured via a shunt resistor. The temperature of the sensor is controlled via the heater resistance with a closed-loop digital PID (proportional–integral–derivative) controller with an effective resolution of 0.1 °C. The time constant τ_{63} for cooling down of the sensor (450 °C to 150 °C) is below 7 ms, which is close to the minimum value achievable with the sensor device [5].

With the temperature modulations used in this investigation the conductance of the AS-MLV sensor (ams Sensor Solutions Germany GmbH) has a large dynamic range from 100 μ S down to 2.5 pS. The resulting current through the sensor is usually measured using a reference resistor. At low sensor conductance, however, the voltage drop over the reference resistor is very small. The resolution and noise of the voltage measurement is, therefore, limiting the measurement range at low conductance. In our approach, we measure the resulting current with a logarithmic amplifier (LogAmp). Errors in the conductance measurement are then contributing linearly to the rate constant's error (Eq. (4)).

$$\log G \pm \Delta \log G = k_d \pm \Delta k_d \quad (4)$$

To achieve reliable measurements at very low conductance values, the voltage across the sensor is increased to 4 V, compared to 0.25 V in an earlier set-up [7]. To limit the

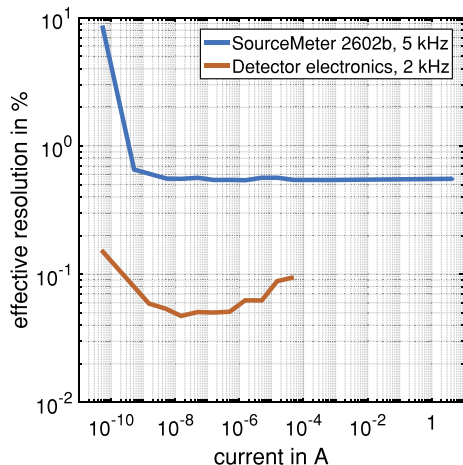


Figure 5: Effective resolution of the LogAmp tested with reference resistors; measurement conditions: 0.5 V across the reference resistor, log out voltage measured with a SourceMeter (Keithley, 2602b) at 5 kHz sample rate (blue line) [12]; 0.5 V across the reference resistor, log out voltage measured with the detector electronics at 2 kHz sample rate.

influence of Joule heating across the sensor and to protect it at low sensor resistance, a 100 k Ω resistor is connected in series with the sensor. The sensor read-out circuit covers a resistance range over 8 orders of magnitude, e. g. from 250 μ S down to 2.5 pS, with a fast sample rate of 2 kHz. We tested the effective resolution of the LogAmp system with a test setup, i. e. the smallest variation in sensor current that can reliably be detected by the sensor electronics. A voltage of 0.5 V is applied from a filtered linear voltage regulator across the reference resistors (100 Ω to 10 G Ω). The output voltage of the LogAmp is measured with a reference (Keithley, SourceMeter 2602b) at 5 kS/s (50,000 points) and with our newly developed electronics at 2 kS/s (restricted to the measurement range). The reference resistors had wire leads and an accuracy of 1%. The whole test setup was placed in a shielded housing. Fig. 5 shows the effective resolution of the sensor electronics dependent on the current. In the measurement range between 500 pA and 10 mA the error of the measurement with the SourceMeter is almost constant at 0.6 %. This indicates that the error is dominated by noise in the voltage measurement setup at the LogAmp output. For current values below 500 pA the error is strongly depending on the current and is, presumably, dominated by noise in the input current. One reason for this electromagnetic noise can be the wire leads of our reference resistors. With a restricted measurement range and a better shielding, we achieve with our detector electronics an effective resolu-

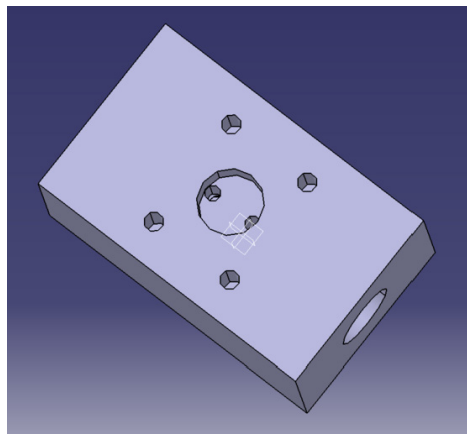


Figure 6: CAD model of the sensor chamber [12].

tion below 0.1%. The gas sensor has much shorter leads, therefore we expect to achieve lower noise (compare Fig. 5) compared to the reference resistor.

4 Detector fluidics

Of high importance for the performance is the fluidic system that brings the short trace gas pulses fast and without any deformations onto the sensor's surface. To build such a system and investigate further possible improvements, a FEM (finite element method) model was set up using the software COMSOL Multiphysics (4.2a).

The footprint of the housing for measurements is limited to TO-39 dimensions, which means a diameter of ca. 10 mm, due to the sensor used. The developed sensor chamber with low dead volumes and optimized gas transport to the sensor is shown in Fig. 6 as a CAD drawing whereas Fig. 7 shows one half of the inner hidden geometry (symmetry is used for lower computational effort). The sensor is represented by a flat cylinder (height 100 μm , radius 500 μm) with one active surface, i. e. an open boundary for the gas pulse species with a constant concentration of zero. Therefore, in this assumption every molecule that reaches the sensor surface is consumed in a reaction with (surface) oxygen in a one-stage reaction process.

Simulation is performed in two steps: First a stationary solution for the laminar flow is found and, based on this flow, a time dependent study with a gaussian concentration peak (maximum at 2 s, $\sigma = 0.2$ s) at the inflow using COMSOL's convection and diffusion module is performed. Parameters for air like viscosity, density etc. are taken from the COMSOL database, the diffusion coefficient

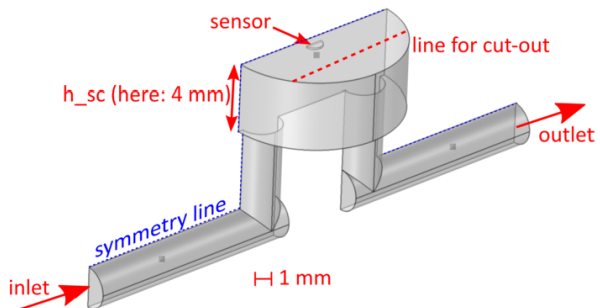


Figure 7: Inner parts of the geometry and model for COMSOL simulations.

$D = 8 \cdot 10^{-6} \text{ m}^2/\text{s}$ [13] of toluene in air is used. Since the model for the diffusion rate is not concentration dependent, arbitrary units can be used in this section. The parameters that are investigated are: the height h_{sc} (4 mm in the used chamber) and the width of the sensor chamber (represented by a cut out which is indicated in Fig. 7), the total flow rate \dot{V} (75 ml/min if not mentioned otherwise) and the size of the sensing layer.

The best possible sensor signal would be achieved if every incoming molecule reacts with oxygen on the sensor surface and, thus, contributes to the surface reduction. We define a gas consumption factor χ_c as the number of gas molecules that react with the sensor divided by the total number of molecules. With the aforementioned open surface at the sensor's position and by comparing the incoming gas pulse with the outgoing one, an estimate for the proportion of reacted to incoming molecules can be achieved and used as an indicator for the strength of the sensor signal inside the given geometry. It is determined by the speed of passing molecules and their respective exposure time, by the diffusion constant, and by the length of the diffusion path. This length is at least the boundary layer between flow channel and sensor surface, but can also be artificially extended.

Furthermore, the shape of incoming peaks should be represented correctly at the sensor's position, especially for GC applications. Fig. 8 shows the concentration over time 100 μm below the sensor surface for $h_{sc} = 1 - 11$ mm, which means a dead volume around the sensor of 0.079–0.86 ml. The FWHM (full width at half maximum) of the incoming peak is 0.5 s, which corresponds to a volume of about 0.625 ml. For ascending h_{sc} the flow rate inside the chamber is reduced, which means broader peaks and tailing. For very high h_{sc} (> 7 mm) a second time constant for diffusion out of the chamber appears and the tailing becomes worse. Additionally, the maximum concentration decreases with increasing h_{sc} .

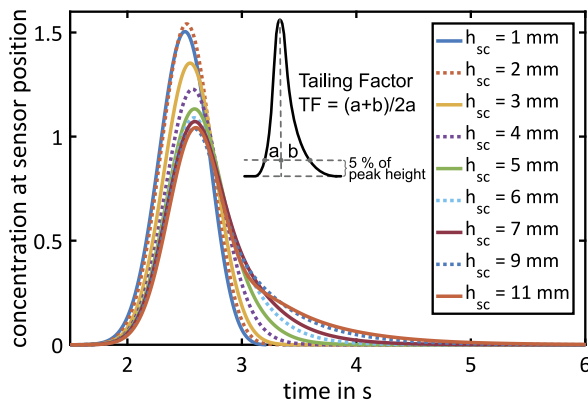


Figure 8: The concentration over time at the sensor position and the illustrated calculation rule for the tailing factor TF.

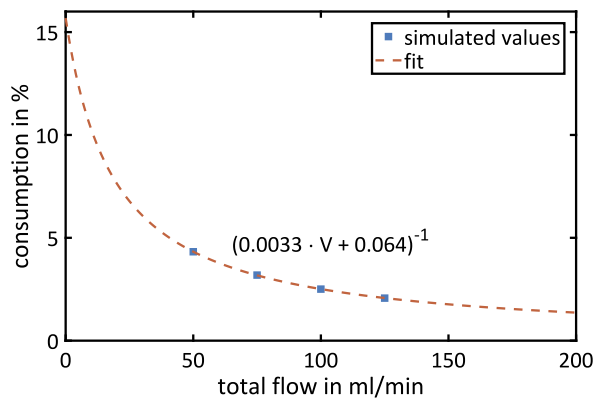


Figure 10: The gas consumption factor over the total flow through the system follows a function of the form $\frac{1}{ax+b}$.

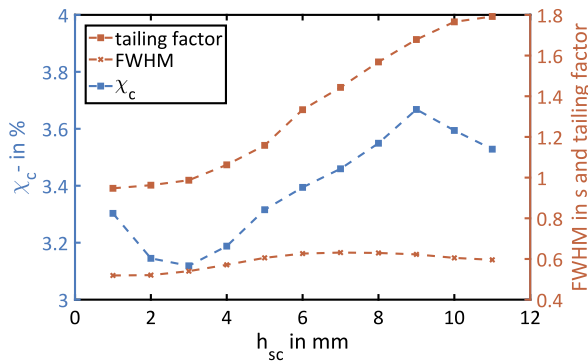


Figure 9: The gas consumption factor χ_c , the tailing factor and the FWHM of incoming peaks over the height of the sensor chamber h_{sc} .

In Fig. 9 all relevant parameters, i. e. FWHM and tailing factor (calculated according to Fig. 8) for peak shape and the gas consumption through reactions at the sensor surface over h_{sc} , are shown. The tailing factor increases almost linearly for $h_{sc} > 3$ mm with a slope of $0.1/\text{mm}$. As expected, FWHM is weakly affected by the transit through the detector, it increases up to $h_{sc} = 7$ mm by 21.7%, then again decreases slightly by 5.7%. χ_c shows a minimum at 3 mm as well as a maximum at 9 mm. For very low values of $h_{sc} < 3$ mm the flow velocity above the sensor surface increases so that the boundary layer width decreases. For values above 9 mm the diffusion path starts to become that long that it overweighs the advantage of longer exposure time due to lower flow velocities.

The flow velocity has a very high influence on the sensor signal (see Fig. 10). In accordance with Fick's law the sensor consumption is in inverse proportion with the flow rate, because the width of the boundary layer, which has to be overcome through diffusion, is proportional to the

fluid's velocity. The fit function for the simulated values is of the form $1/(ax + b)$ because there is a natural limit given by the geometry.

Doubling the radius of the sensor surface, i. e. a four times larger sensing layer, gives a 2.15 times higher gas consumption on the sensor. To test whether a smaller sensor footprint than the currently used TO-39 can have a positive impact, we examined a sensor chamber with smaller volume in the simulation by removing the part of the chamber beyond the dashed line (Fig. 7). This change results in a 20% higher sensor consumption. The lower width of the boundary layer gives only a small advantage due to the shorter exposure time. Nevertheless, in contrast to higher sensor chambers for a higher sensor signal, this does not affect the peak shape in a negative way but reduces the FWHM and the tailing factor by nearly 10%.

The actual setup used for the measurements in the next section does not yield the optimal sensor consumption (only 2.5% of the incoming peak at a flow rate of 100 ml/min) but is appropriate for detecting well-shaped peaks (TF = 1.06).

5 Measurement

To validate the DSR approach we use a temperature cycle with two temperature plateaus: an oxidation phase at 400 °C with a duration of 60 s and a reduction phase at 100 °C with a duration of 600 s. The gas measurements were realized with our gas mixing apparatus (GMA) based on gas pre-dilution to achieve very low concentrations and a large concentration range [14]. The current setup comprises four pre-dilution lines for the generation of trace gases with a dynamic concentration range c_{bottle}/c_{set} from

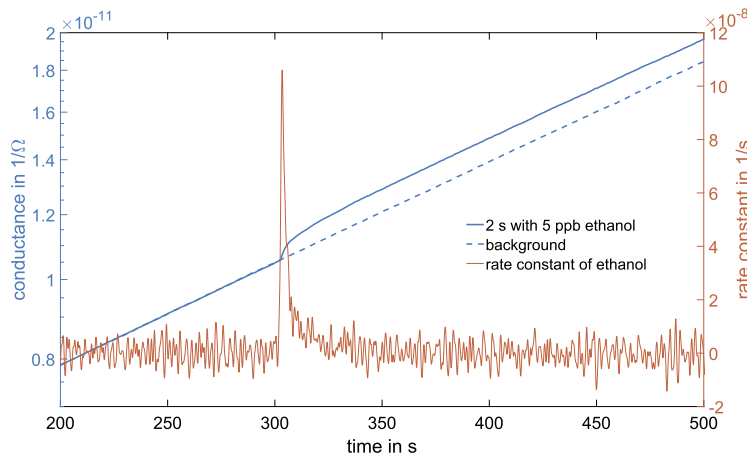


Figure 11: Blue: time-dependent conductance during 100 °C phase without (dotted) and with (solid) 10 ppb·s ethanol pulse. Orange: time-dependent rate constant of ethanol [12].

5 to 312,750. Here, c_{set} is the set concentration and c_{bottle} is the concentration in the test gas bottle. Dry zero air with a flow of 100 ml/min is used as carrier gas. The zero air is generated by a two-step purification process. The first step is a charcoal filter system which removes hydrocarbons (larger than C_3) very efficiently as well as humidity and CO_2 with a pressure swing. The second step is based on catalytic conversion to remove smaller hydrocarbons as well as hydrogen and carbon monoxide. Ethanol as test gas was supplied by a gas cylinder with 200 ppm in synthetic air 4.6 and subsequent dilution in zero air. The mixing ratio of the pre-dilution was allowed to stabilize for several minutes before measurements. Gas pulses were created by switching a solenoid valve.

Fig. 11 shows the result proving the DSR functional principle with an ethanol pulse with a dosage of 10 ppb·s (5 ppb for 2 s). For two DSR measurements (at 100 °C) the time-dependent conductance is shown with (blue solid line) and without ethanol (blue dotted line) peak. Obviously, the reproducibility of the measurements is very high as the solid and the dotted line are matching almost perfectly up to the injection of ethanol. The measurement without ethanol is used as background and the constant slope of this background $k_{d,air}$ was subtracted from the measurement curve. The time-dependent rate constant $k_{d,gas}$ (orange line) is derived from the derivative of the measurement curve (Eq. (5)) [5].

$$k_{d,gas} = \frac{k_b T}{2 \cdot E_b(t_0)} \frac{d \ln G}{dt} - k_{d,air} \quad (5)$$

Here, $E_b(t_0)$ is the energy barrier at time t_0 when the temperature changes. $E_b(t_0)$ can be calculated from the conductance difference from high to low temperature [8].

Table 1: Peak areas for different duration and concentration combinations with the same dosage [12].

dosage (ppb·s)	duration (s)	concentration (ppb)	integrated rate constant (a.u.)
10	1	10	0.00136
10	5	2	0.00142
100	1	100	0.0122
100	5	20	0.0120

We use a cubic smooth spline and a Savitzky–Golay filter with 1000 points (500 ms) to reduce the noise in the conductance measurement and to improve the numerical differentiation of the signal. The prediction of the sensor model (Eq. (2)) is very good. Furthermore, the reproducible detection of the same amount of substance by different combinations of pulse duration and concentration was tested. Tab. 1 shows the results of the integrated rate constants for pulses with dosages of 100 and 1000 ppb·s of ethanol. Good agreement of gas pulses with the same total dose is observed as predicted by Eq. (3).

6 Conclusion

We designed a detector electronics with a closed-loop heater controller and an adjustable measurement range over eight decades for the sensitive layer. The detector electronics achieved an effective temperature resolution of 0.1 °C for the AS-MLV sensor and an effective conductance resolution of 0.1% when measuring the sensitive layer in the relevant range. Despite the high requirements of the

DSR method, the detector system can be implemented at relatively low cost. In addition to the electronics system, the fluidic coupling of the sensor contributes to the quality of short gas pulse measurements. The performed simulations indicate in which directions the system can be optimized. To achieve well-shaped peaks and high sensor signals further miniaturization of the sensor chamber is necessary. Much lower flow rates can be expected in GC applications making optimized fluidics even more important. At the same time, such low flow rates could be exploited by building a system which generates its signal from the overall shape of an incoming gas peak, thereby improving its detection limit. We have successfully demonstrated that the detector can detect short pulses of reducing gas at very low concentrations. This paves the way for small and inexpensive microsystems for the detection of trace gases using sensor pre-concentrator or μ GC systems. Depending on the application the system has to be optimized in accordance to the given boundary conditions.

References

1. M. Leidinger, M. Rieger, T. Sauerwald, C. Alépée, A. Schütze. Integrated pre-concentrator gas sensor microsystem for ppb level benzene detection, *Sensors and Actuators B: Chemical*, 236:988–996, 2016.
2. S. Zampolli, I. Elmi, F. Mancarella, P. Betti, E. Dalcanale, G.C. Cardinali, et al. Real-time monitoring of sub-ppb concentrations of aromatic volatiles with a MEMS-enabled miniaturized gas-chromatograph, *Sensors and Actuators, B: Chemical*, 141(1):322–328, 2009.
3. M. Akbar, H. Shakeel, M. Agah. GC-on-chip: integrated column and photoionization detector, *Lab Chip*, 15(7):1748–1758, 2015.
4. M. Leidinger, T. Sauerwald, W. Reimringer, G. Ventura, A. Schütze. Selective detection of hazardous VOCs for indoor air quality applications using a virtual gas sensor array, *Journal of Sensors and Sensor Systems*, 3(2):253–263, 2014.
5. A. Sklorz, S. Janßen, W. Lang. Application of a miniaturised packed gas chromatography column and a SnO₂ gas detector for analysis of low molecular weight hydrocarbons with focus on ethylene detection, *Sensors and Actuators B: Chemical*, 180:43–49, 2013.
6. P.K. Clifford, D.T. Tuma. Characteristics of semiconductor gas sensors II. transient response to temperature change, *Sensors and Actuators*, 3:255–281, 1982.
7. T. Baur, A. Schütze, T. Sauerwald. Optimierung des temperaturzyklischen Betriebs von Halbleitergassensoren, *tm – Technisches Messen*, 82(4):187–195, 2015.
8. C. Schultealbert, T. Baur, A. Schütze, S. Böttcher, T. Sauerwald. A novel approach towards calibrated measurement of trace gases using metal oxide semiconductor sensors, *Sensors & Actuators: B. Chemical*, 239:390–396, 2017.
9. J. Ding, T.J. McAvoy, R.E. Cavicchi, S. Semancik. Surface state trapping models for SnO₂-based microhotplate sensors, *Sensors and Actuators B: Chemical*, 77(3):597–613, 2001.
10. M.J. Madou, S.R. Morrison. Chemical Sensing with Solid State Devices, Academic Press, Inc., 1989.
11. T. Baur, A. Schütze, T. Sauerwald. Detection of short gas pulses for trace gas analysis, *Technisches Messen*, 84(s1), 2017.
12. T. Baur, A. Schütze, T. Sauerwald. Detection of short trace gas pulses, In: Proceedings Sensor 2017. 2017. p. 87–91.
13. H.Y. Erbil, Y. Avci. Simultaneous Determination of Toluene Diffusion Coefficient in Air from Thin Tube Evaporation and Sessile Drop Evaporation on a Solid Surface, *Langmuir*, 18(13):5113–5119, 2002.
14. N. Helwig, M. Schüler, C. Bur, A. Schütze, T. Sauerwald. Gas mixing apparatus for automated gas sensor characterization, *Measurement Science and Technology*, 25(5):55903, 2014.

Bionotes



Tobias Baur

Saarland University, Laboratory for Measurement Technology, Saarbrücken, Germany
 t.baur@lmt.uni-saarland.de

Tobias Baur studied microtechnology and nanostructures at Saarland University and received his master's degree in 2016. He is currently a Ph.D. student at the Lab for Measurement Technology at Saarland University and focuses on the model-based temperature cycled operation of gas sensors, the development of gas sensor electronics and the measurement of short trace gas pulses.



Caroline Schultealbert

Saarland University, Laboratory for Measurement Technology, Saarbrücken, Germany
 c.schultealbert@lmt.uni-saarland.de

Caroline Schultealbert studied microtechnology and nanostructures at Saarland University and received her master's degree in 2015. She is currently a Ph.D. student at the Lab for Measurement Technology at Saarland University and focuses on the model-based temperature cycled operation of gas sensors, their calibration and emission materials and the optimization of the corresponding systems via FEM simulations.



Andreas Schütze
Saarland University, Laboratory for
Measurement Technology, Saarbrücken,
Germany
schuetze@lmt.uni-saarland.de

Andreas Schütze studied Physics and received his doctorate in Applied Physics from Justus-Liebig-Universität in Gießen in 1994 with a thesis on micro gas sensor systems. After some years in industry, he joined the University of Applied Sciences in Krefeld, Germany, as professor for Microsystems Technology from 1998 to 2000. Since 2000 he is a full professor for measurement science and technology in the Department Systems Engineering at Saarland University, Saarbrücken, Germany. His research interests include microsensors and Microsystems, especially advanced chemical sensor systems, both for gas and liquid phase, for security and control applications.



Tilman Sauerwald
Saarland University, Laboratory for
Measurement Technology, Saarbrücken,
Germany
t.sauerwald@LMT.uni-saarland.de

Tilman Sauerwald received his PhD in 2007 at the University of Giessen working on the influence of surface reactions to the multi-signal generation of metal oxide sensors. Since 2011 he is working at the Lab of Measurement Technology at the Saarland University. His current focus is the detection of trace gases by developing of model-based techniques for multi-signal generation.

4.2.3 Paper 3 – Random Gas Mixtures for efficient Gas Sensor Calibration

T. Baur, M. Bastuck, C. Schultealbert, T. Sauerwald, A. Schütze
Saarland University, Lab for Measurement Technology, Saarbrücken, Germany

J. Sens. Sens. Syst. (2020), 9, 411-424

The original article can be found, in the online version, at <https://doi.org/10.5194/jsss-9-411-2020>.

© 2020 by the authors. This article is an open access article distributed under the terms and conditions of the Creative Commons Attribution (CC BY) license (<http://creativecommons.org/licenses/by/4.0/>).



Random gas mixtures for efficient gas sensor calibration

Tobias Baur¹, Manuel Bastuck¹, Caroline Schultealbert¹, Tilman Sauerwald^{1,a}, and Andreas Schütze¹

¹Lab for Measurement Technology, Saarland University, 66123 Saarbrücken, Germany

^acurrently at: Fraunhofer Institute for Process Engineering and Packaging IVV, 85354 Freising, Germany

Correspondence: Tobias Baur (t.baur@lmt.uni-saarland.de)

Received: 30 May 2020 – Revised: 27 August 2020 – Accepted: 18 September 2020 – Published: 27 November 2020

Abstract. Applications like air quality, fire detection and detection of explosives require selective and quantitative measurements in an ever-changing background of interfering gases. One main issue hindering the successful implementation of gas sensors in real-world applications is the lack of appropriate calibration procedures for advanced gas sensor systems. This article presents a calibration scheme for gas sensors based on statistically distributed gas profiles with unique randomized gas mixtures. This enables a more realistic gas sensor calibration including masking effects and other gas interactions which are not considered in classical sequential calibration. The calibration scheme is tested with two different metal oxide semiconductor sensors in temperature-cycled operation using indoor air quality as an example use case. The results are compared to a classical calibration strategy with sequentially increasing gas concentrations. While a model trained with data from the sequential calibration performs poorly on the more realistic mixtures, our randomized calibration achieves significantly better results for the prediction of both sequential and randomized measurements for, for example, acetone, benzene and hydrogen. Its statistical nature makes it robust against overfitting and well suited for machine learning algorithms. Our novel method is a promising approach for the successful transfer of gas sensor systems from the laboratory into the field. Due to the generic approach using concentration distributions the resulting performance tests are versatile for various applications.

1 Motivation

Despite impressive advances in sensitivity, selectivity and response time of gas sensor systems over the last decades (Marco and Gutierrez-Galvez, 2012; Sharma et al., 2018), there is a striking lack of publications on successful field tests or real-world applications. A search on Google Scholar (from 31 March 2020) returns more than 3.4 million results for “gas sensor + material” and 553 000 results for “gas sensor + “data processing””, but only around 28 000 results for “gas sensor + “field test””. At the same time, field tests are a crucial link to the successful implementation of gas sensors in large-volume consumer applications (Borrego et al., 2016; Castell et al., 2017). Also, from our own experience field test data very often are hard to interpret due to deviations from the ideal conditions during the original lab calibration, for example in terms of baseline and dynamics. We believe that one main issue hindering successful field tests is the lack of appropriate realistic calibration procedures for

modern gas sensor systems. Calibration is only a side note in many works, as a vehicle to show the performance of a new material or data processing method. The experimental design often consists of a few fixed concentration levels per gas, and, in many cases, the sensor is exposed to one and only one target gas at a time. The resulting data are relatively easy to evaluate in terms of sensitivity, selectivity and speed of response, but of little use for complex real-world scenarios.

Virtually all applications – for example, air quality (Castell et al., 2017; Spinelle et al., 2017), fire detection (Kohl et al., 2001; Fonollosa et al., 2016), detection of explosives (Tomchenko et al., 2005; Yu et al., 2005) and breath analysis (Bajtarevic et al., 2009; Lourenço and Turner, 2014) – require selective, quantitative measurements in an ever-changing background of interfering gases. A sensor calibration with single substances (as, for example, in the datasets of Fonollosa et al., 2015a, b; Fonollosa, 2016; Bastuck and Fricke, 2018) does not reveal any masking effects or other gas interactions altering the sensor response. Some publications take this into

account by performing calibration with gas mixtures (Sundgren et al., 1991; Wolfrum et al., 2006; Zhang et al., 2013; Fonollosa, 2015; Sauerwald et al., 2018). Most of these except two (Zhang et al., 2013; Fonollosa, 2015) use between three and five fixed concentration levels for each gas. This quantization of a continuous quantity can, with too few levels, easily lead to overfitting due to systematic errors in the experimental equipment, contamination¹ of validation data through repetitions or misleading model performance measures.

In the past we could show good results in interlaboratory tests, as a first step towards a transferable calibration, with sequential calibration (Spinelle et al., 2017; Bastuck et al., 2018a; Sauerwald et al., 2018). However, there is still a gap between calibrating a sensor for interlaboratory tests and real-word scenarios (Sauerwald et al., 2018; Karagulian et al., 2019).

In this paper, we present and test a calibration scheme based on the method of random effects (Oehlert, 2000). It tackles the mentioned issues by drawing random concentrations from predefined distributions of a, theoretically, arbitrary number of gases. The result is a large number of gas exposures for calibration, each a unique mixture of all available gases. The approach is easy to configure and use, can be applied to a wide range of target applications, and is shown to be superior to sequential calibration.

2 Experimental

2.1 Study design

The calibration method with randomized gas mixtures is shown using the example of indoor air quality (IAQ) but can be applied to any application and target variable. The gases used for this study were chosen to represent different approaches in IAQ assessment. Volatile organic compounds (VOCs) are an important indicator of IAQ, as many of the substances show irritating or even toxic behavior. Generally, a VOC is any organic compound that can be found in the gas phase at room temperature. The European Union defines VOC as any organic compound with an initial boiling point less than or equal to 250 °C measured at standard pressure of 101.3 kPa (Anon, 2004). In analytical chemistry these VOCs are normally divided into three subgroups: very volatile organic compounds, volatile organic compounds and semi-volatile organic compounds. Specific sampling and measurement protocols are associated with each group. However, from a health perspective, there is no need to treat these groups separately since both toxic and harmless compounds can be found in each. We will, therefore, subsume all three groups under the term VOC for direct-measuring gas sensor

¹The term “contamination” here refers to observations used in the training of a model “spilling” or “leaking” into datasets used for validation or testing. Predicting observations used in the training usually results in deceptively better model performance.

systems. The total sum of VOCs, TVOC (total VOCs), is one target value that can be used for calibration and is, for example, defined by the German Environment Agency (UBA) for IAQ classification (Seifert, 1999; Anon, 2007). A study on behalf of the UBA (Hofmann and Plieninger, 2008) lists the statistical distribution of more than 300 different VOCs in indoor environments. The VOCs can be divided into interfering VOCs and target VOCs with regard to human health: while the former are harmless in usual concentrations, the latter are mostly toxic or carcinogenic. Measuring all of these hundreds of VOCs in varying concentrations is not feasible, so a preselection must be made based on the expected concentrations. Since our equipment (Helwig et al., 2014; Leidinger et al., 2018) is limited to six gases plus humidity, two representatives each were selected for inorganic background gases, interfering VOCs and target VOCs.

The carrier gas stream consists of zero air with varying humidity plus the background gases carbon monoxide and hydrogen. Carbon monoxide is a ubiquitous gas with highly variable concentrations ranging from the atmospheric background at 150 ppb (Schleyer et al., 2013) up to several ppm (WHO Regional Office for Europe, 2010). The atmospheric background concentration of hydrogen is 500 ppb (Schleyer et al., 2013). We could not find any studies on H₂ concentration in indoor air. We assume large fluctuations up to the ppm range (Schultealbert et al., 2018b) since hydrogen is emitted by humans (Levitt, 1969; Tomlin et al., 1991) and can, like CO₂, be another indicator for human presence. For interfering VOCs we selected acetone and toluene, two common representatives with high average concentrations (Hofmann and Plieninger, 2008) but negligible health effects. The interfering gases were added to achieve a realistic TVOC concentration in indoor air (Hofmann and Plieninger, 2008). To represent the TVOC concentration with only two gases, they are supplied at 10 to 20 times the typical indoor concentrations. The target VOCs are two carcinogenic gases, formaldehyde and benzene. The concentration range of these target gases is based on the observed statistical distribution in indoor air (Hofmann and Plieninger, 2008) and WHO guidelines (WHO Regional Office for Europe, 2010; Anon, 2016). Since only a limited number of VOCs are present in this configuration, the sum of all measured VOCs is defined as VOC_{sum} to clearly distinguish it from the common TVOC term.

The random mixtures were generated using a Python script (Bastuck, 2019) which iteratively determines the ratios of all components as shown schematically in Fig. 1. To generate a randomized gas mixture, the concentrations of the background components (carbon monoxide, hydrogen and humidity) and VOC_{sum} were varied independently of each other. The concentrations of humidity, carbon monoxide, hydrogen and VOC_{sum} are uniformly distributed over a realistic range (see Table 1). For the generation of the single VOC concentrations, the randomly selected VOC_{sum} concentration is divided into several steps. First, the ratio of interfering

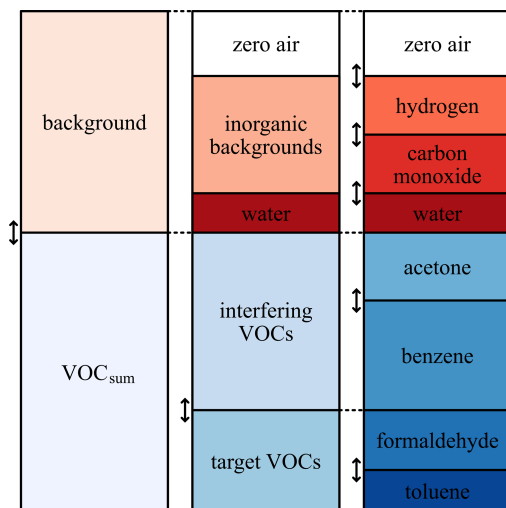


Figure 1. Schematic overview of the random gas mixture generation. The scheme can be adapted to reflect different applications. Please note that this figure represents the measurement as it was actually performed, taking into account the accidental swapping of benzene (which should have been a target) and toluene (which should have been an interferent).

($\text{VOC}_{\text{interfering}}$) and target ($\text{VOC}_{\text{target}}$) VOCs in VOC_{sum} is randomly selected to be between 0 and 20 % target VOC. Second, $\text{VOC}_{\text{interfering}}$ and $\text{VOC}_{\text{target}}$ are again divided randomly into the individual VOCs, both with a ratio between 0 and 100 %. The parameters for the generation are shown in Table 1, and the resulting concentration ranges for the single gases and VOC_{sum} in Table 2.

Due to an error in the measurement setup, the concentrations of toluene and benzene were swapped, and the concentrations planned for benzene were offered as toluene and vice versa. Therefore, the concentration levels of the carcinogenic benzene are rather high in this study compared to their true occurrence, while the concentrations of toluene are unusually low (ppb range). This does not have any impact on the general conclusions drawn from this experiment, but the results for selective quantification of these two VOCs should be interpreted with caution. The concentration distributions of the individual gases can be found in Fig. A1. Each randomized gas mixture was supplied to the sensors for 20 min each. Twelve measurements with 99 randomized gas mixtures each were conducted over a period of 5 weeks, resulting in a total of 1188 randomized gas mixtures.

To compare the performance of our novel approach with a conventional sequential calibration strategy (one gas at a time, ascending concentration levels), a gas profile of this kind was measured for comparison. Each gas was supplied at four different concentrations (see Table 3), which were kept constant for 20 min. The background gases (hydrogen and carbon monoxide) were always kept at their atmospheric concentrations (500 and 150 ppb) except during their expo-

Table 1. Parameters for the generation of randomized gas mixtures.

	Range
hydrogen	300–2500 ppb
carbon monoxide	100–2000 ppb
humidity	25–75 %RH
VOC_{sum} in $\mu\text{g}/\text{m}^3$	100–5000 $\mu\text{g}/\text{m}^3$
$\text{VOC}_{\text{target}}/\text{VOC}_{\text{sum}}$	0 %–20 %
$\text{VOC}_{\text{interfering}}/\text{VOC}_{\text{sum}}$	100 %– $\text{VOC}_{\text{target}}/\text{VOC}_{\text{sum}}$
acetone/ $\text{VOC}_{\text{interfering}}$	0 %–100 %
benzene/ $\text{VOC}_{\text{interfering}}$	0 %–100 %
formaldehyde/ $\text{VOC}_{\text{target}}$	0 %–100 %
toluene/ $\text{VOC}_{\text{target}}$	0 %–100 %

Table 2. Resulting concentration ranges by the generation of randomized gas mixtures.

	Concentration range
hydrogen	301–2499 ppb
carbon monoxide	101–1995 ppb
humidity	25–75 %RH
VOC_{sum} in $\mu\text{g}/\text{m}^3$	21–4902 $\mu\text{g}/\text{m}^3$
VOC_{sum} in ppb	6–2312 ppb
acetone	0–1846 ppb
benzene	0–1180 ppb
formaldehyde	0–723 ppb
toluene	0–245 ppb

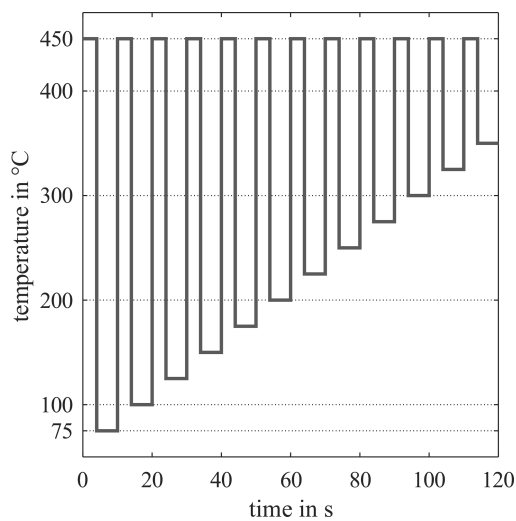
sures as target gas. The profile was repeated three times at different relative humidities – 25, 50 and 75 %RH – resulting in a total of 72 different gas exposures. The comparison was made only for the gas concentration ranges which were common to both calibration profiles.

2.2 Setup

In the overall measurement setup, a total of 11 different sensors were tested, seven of them metal oxide semiconductor gas sensors (MOS) and four gas-sensitive field effect transistors (GasFET). An overview of the results of all systems for a reduced dataset with the last five measurements and a slightly different evaluation method can be found in Bastuck (2019). The results and findings in this paper are shown for two analog sensors from ams, namely AS-MLV and AS-MLV-P2. They were chosen due to our long experience with these two types of sensors (Baur et al., 2015, 2018b; Schütze et al., 2017; Schultealbert et al., 2018a). In recent interlaboratory tests we have also found that transferring a sensor calibration from one laboratory to another works with these types of sensor. However, we have also seen that missing gas concentrations can lead to misinterpretation in our models. In Sauerwald et al. (2018) we trained interfering gases with only a few gas concentrations, since each additional concentration would have meant a doubling of time. Therefore, we

Table 3. Gas concentrations used for the sequential calibration.

Gas	Concentration (ppb)			
acetone	250	500	750	1000
benzene	250	500	750	1000
carbon monoxide	150	300	450	600
formaldehyde	40	80	120	160
hydrogen	500	750	1000	1250
toluene	5	25	45	65

**Figure 2.** Temperature cycle of the AS-MLV and AS-MLV-P2.

had problems with an extended humidity range, which was not covered by our calibration. In Bastuck et al. (2018a) we had a similar problem with hydrogen. Those previous issues make them good candidates for this study on a more efficient calibration strategy. The sensors were not operated in the operating modes recommended by the respective manufacturers, but with a self-designed temperature-cycled operation (TCO) (Gramm and Schütze, 2003; Baur et al., 2015; Schütze and Sauerwald, 2019). The temperature cycle is chosen to benefit from the highly sensitive differential surface reduction (DSR) method (Baur et al., 2018b). The total cycle for the presented sensors with a duration of 120 s is shown in Fig. 2. The MOS sensors were operated with electronics with logarithmic conductance measurement and resistance-based temperature control developed in our lab (Baur et al., 2018a).

The gas mixtures were supplied by our gas mixing apparatus (GMA), which is described in detail in Helwig et al. (2014) and Leidinger et al. (2018). It consists of several mass flow controllers (MFCs) to supply carrier gas (zero air) and add the desired gas concentrations from gas cylinders. A two-stage cleaning process generates the zero air (Leidinger et al., 2018). Hydrocarbons (larger than C3) are removed efficiently in the first step with a carbon filter system. In the second step,

humidity is removed with a pressure swing, and smaller hydrocarbons as well as hydrogen and carbon monoxide are removed by catalytic conversion. The test gases from the cylinders are diluted twice to achieve very low and highly variable concentrations while avoiding the impact of different impurities contained in the synthetic air (Helwig et al., 2014). Humidity is supplied from a washing bottle with HPLC-grade water at room temperature (22 °C), which is flushed with zero air at the desired flow rate.

Since several sensors ran in the same experiment and should not affect each other, the total flow of 400 mL/min supplied by the GMA was split into four independent lines. To ensure proper split ratios, flow restrictions (10 cm of 1/16") were installed in each line, dominating the total flow resistance of each line, given that the rest of the setup is built with 1/8" tubing (<25 cm per line, PTFE and stainless steel). The sensor chambers are made of PTFE and aluminum.

2.3 Evaluation methods

The evaluation is performed with the open-source software DAV³E (Bastuck et al., 2018b) and can be divided into five steps: feature extraction, dimensionality reduction, regression, hyperparameter optimization and testing. For feature extraction, the 120 s sensor cycle is divided into 120 equidistant ranges. In each of these ranges, the mean value and slope, in total 240 features per sensor cycle, are computed. To prevent overfitting during modelling, a dimensionality reduction with principal component analysis (PCA) is carried out. For the next steps of modelling, the first 20 principle components are used as features. The quantification of the desired target value (concentration of a single gas or a partial gas mixture, e.g., VOC_{sum}) is performed with partial least squares regression (PLSR). For hyperparameter optimization and testing we use two different procedures. For evaluations with reduced datasets of the measurement we use the hold-out method for testing; for instance, 10 % of the dataset is excluded from training. For hyperparameter optimization – i.e., the determination of the number of PLSR components – a 10-fold cross-validation is applied. For evaluations with the complete dataset, a nested cross-validation, also known as double cross-validation (Stone, 1974), is performed for testing and hyperparameter optimization. We perform an outer 10-fold cross-validation for testing, by randomly dividing the data in 10 parts once. One part in turn is set aside as the test dataset, while all other parts comprise the training dataset and are used to optimize the hyperparameters of the model. For this optimization, we also perform a 10-fold cross-validation on the training dataset for different numbers of PLSR components. In the inner loop, the training dataset of the outer loop is also randomly divided into 10 parts; nine parts are used for training and one for the hyperparameter validation. For nested cross-validation we treat all sensor cycles within the same gas exposure as one unit (group-based). Otherwise, very similar cycles could end up in both the training and

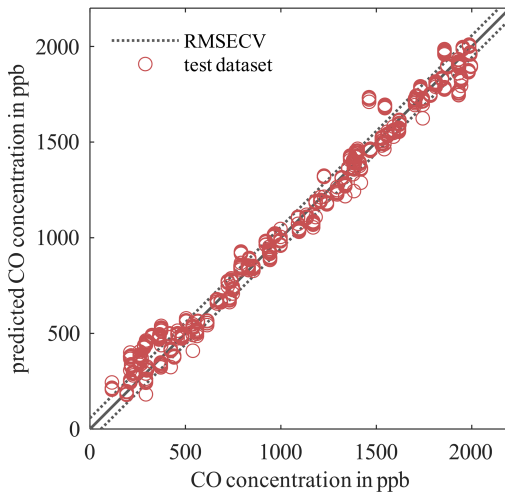


Figure 3. PLSR model for the AS-MLV-P2 for quantification of carbon monoxide (CO). The model was calculated and 10-fold cross-validated from a reduced dataset with 198 randomized gas mixtures (measurements 8 and 9). The model was tested with 99 randomized gas exposures containing seven cycles each (measurement 10, open circles).

test dataset of an iteration, effectively “contaminating” the training data and leading to over-optimistic performance estimates. The mean predictive performance for these validation sets is calculated for each number of PLSR components over the inner and outer loop. The best number of PLSR components is decided as the minimal number of PLSR components still giving a good² predictive performance.

Generally, different metrics are used to describe the performance of a regression model. Arguably the most prevalent is the coefficient of determination R^2 , which describes the ratio of the explained to the total variance. Its range from 0 to 100 % is, however, hard to interpret in terms of, for example, accuracy and precision of a model. This interpretation becomes much easier for the root-mean-square error (RMSE) since it has the same unit as the model output. A distinction is made between the RMSE of calibration (RMSEC) for the training, the RMSE of cross-validation (RMSECV) for hyperparameter optimization and the RMSE of prediction (RMSEP) for testing. However, expecting the same precision between two models covering different concentration ranges is unrealistic. An RMSE of 50 ppb would be considered quite poor for formaldehyde (having an exposure limit of 80 ppb) but excellent for hydrogen. Since we choose the concentration ranges for all gases based on realistic data, it seems natural to define a metric “dynamic range” (DNR) as

$$DNR = \frac{c_{\max, t}}{RMSE_t}, \quad (1)$$

²The definition of “good” in this context is arbitrary. We defined it as a model with an average error less than the minimum achieved error at any number of components plus 1 standard deviation.

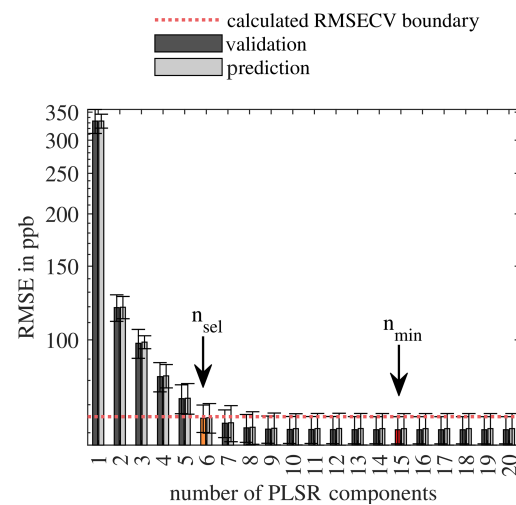


Figure 4. Calculated RMSECV (hyperparameter optimization) and RMSEP (testing) with error bars depending on the number of PLSR components for the AS-MLV-P2 for the carbon monoxide model. The dotted red line indicates the boundary for the calculation of the minimum number of PLSR components, and the orange marked bar shows the RMSECV at the resulting number of components according to Eq. (2).

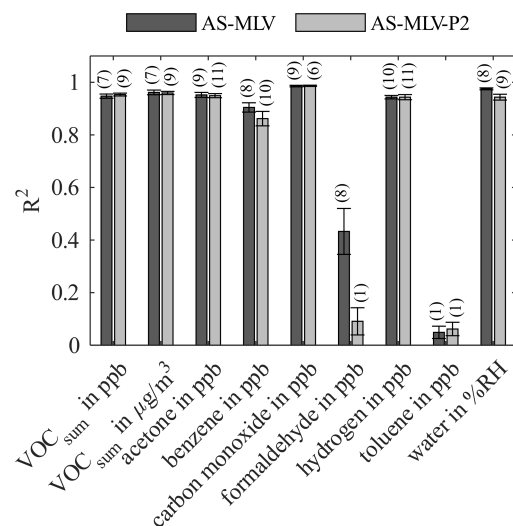


Figure 5. Coefficient of determination (R^2) for AS-MLV and AS-MLV-P2 for different models. Calculation of the regression model with the complete dataset with 10-fold nested cross-validation for hyperparameter optimization (PLSR components) and testing. The number of PLSR components of the model, determined with Eq. (2), is given in parentheses.

with the maximum concentration $c_{\max, t}$ and the root-mean-square error RMSE_t for the target t . While not transferrable to arbitrary applications, the DNR allows comparison of sensor and model performances for different gases and concentration ranges in this case.

To find the optimal number of PLSR components, we calculate the $\text{RMSECV}_{n, i, j}$ for each number of PLSR components $n \in N$, $N = \{x \in Z | 1 \leq x \leq 20\}$ for all 10 cross-validation folds $i \in I$, $I = \{x \in Z | 1 \leq x \leq 10\}$ in all 10 testing folds $j \in J$, $J = \{x \in Z | 1 \leq x \leq 10\}$. Thereby, the maximum number of PLSR components is limited to the number of predictor variables, in this case, the 20 first principle components. The RMSECV_n is the mean value over all folds at the same n . We selected the number of PLSR components n_{sel} with Eq. (2). This means we take the minimum number of PLSR components for which the RMSECV_n is less than the $\text{RMSECV}_{n_{\min}}$ plus the standard deviation of $\text{RMSECV}_{n_{\min}}$ at the point of the minimum. A visualization of the data evaluation procedure can be found in Appendix B as pseudocode. Figure 4 shows the selection of the best number of PLSR components according to Eq. (2).

$$n_{\text{sel}} = \min \left\{ n \mid \text{RMSECV}_n < \text{RMSECV}_{n_{\min}} + \text{SD}_{i \in I, j \in J} \text{RMSECV}_{n_{\min}, i, j} \right\}$$

with $n_{\min} = \arg \min_{n \in N} \text{RMSECV}_n$. (2)

3 Results and discussion

Twelve measurements were performed. Each of the 1188 gas exposures contains 10 sensor cycles. Due to the time constant of the gas exchange, we omitted two sensor cycles at the beginning and one cycle at the end of the gas exposure in the evaluation. Therefore, we have a total of seven useful cycles per gas exposure, amounting to 8316 from the complete measurement campaign. Two and a half measurements (numbers 5, 6 and 7), in sum 245 random gas exposures, had formaldehyde completely missing because the bottle had run empty. Additionally, 74 random gas exposures are missing for the AS-MLV-P2 and 115 for the AS-MLV due to issues with the sensor system. Therefore, we can use 828 (AS-MLV) or 869 (AS-MLV-P2) random gas exposures for formaldehyde models and 1073 (AS-MLV) or 1114 (AS-MLV-P2) for all other models.

Figure 3 shows an example of a PLSR model for the AS-MLV-P2 for quantification of carbon monoxide. For better visualization we reduced the dataset: this model was trained with 198 randomized gas exposures (measurements 8 and 9); the hyperparameter optimization was done by 10-fold cross-validation. The dotted lines show the RMSECV of the hyperparameter optimization; the red circles show the predicted carbon monoxide concentration from 99 additional randomized gas exposures (measurement 10). A good agreement of

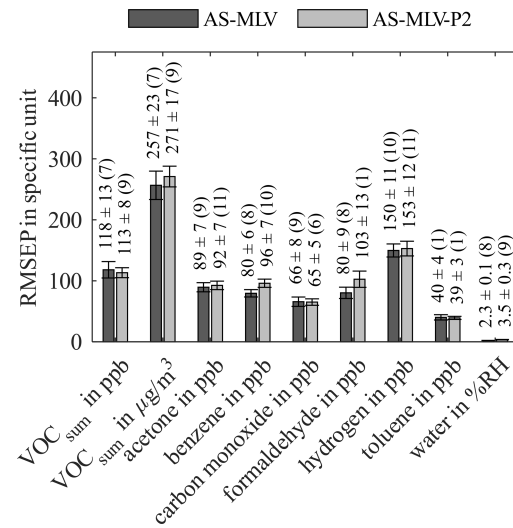


Figure 6. Root-mean-square error of prediction (RMSEP) for AS-MLV and AS-MLV-P2 for different models. Calculation of the regression model with the complete dataset with 10-fold nested cross-validation for hyperparameter optimization (PLSR components) and testing. The number of PLSR components, determined with Eq. (2), is given in parentheses.

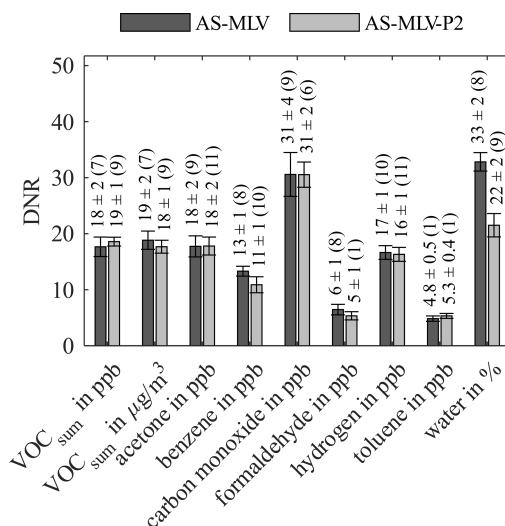


Figure 7. Dynamic range (DNR) for AS-MLV and AS-MLV-P2 for different models. Calculation of the regression model with the complete dataset with 10-fold nested cross-validation for hyperparameter optimization (PLSR components) and testing. The number of PLSR components, determined with Eq. (2), is given in parentheses.

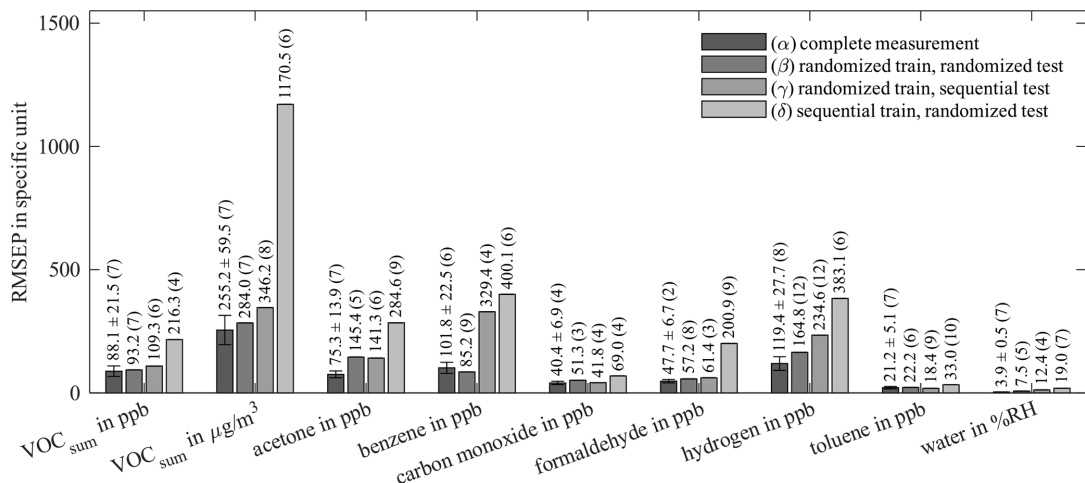


Figure 8. Root-mean-square error of prediction (RMSEP) of AS-MLV-P2 for different training and testing models. All models use 10-fold cross-validation for hyperparameter optimization; the resulting number of PLSR components, determined with Eq. (2), is given in parentheses. A detailed description of (α)–(δ) is given in Table 4.

the reduced dataset with an RMSECV of 57.3 ppb and a RMSEP of 73.9 ppb is found. This means the unknown measurement can be predicted with a DNR of 27 in the range of 100 to 2000 ppb carbon monoxide.

For the evaluation of the complete measurement campaign, 10-fold nested cross-validation is used. Figure 4 shows the hyperparameter optimization for the selection of the number of PLSR components according to Eq. (2) as an example for the quantification of carbon monoxide with the AS-MLV-P2. The dark and light grey bars show the RMSECV and the RMSEP, respectively; the error bars indicate the standard deviation of the cross-validation folds. The red bar indicates the absolute minimum of the RMSECV at $n_{\min} = 15$. The dotted red line represents the $\text{RMSECV}_{n_{\min} + \text{SD}_{i \in I, j \in J} \text{ RMSECV}_{n_{\min}, i, j}}$ as a boundary for selecting the number of PLSR components. The orange bar indicates the RMSECV for the number of PLSR components n_{sel} selected according to Eq. (2), i.e., the minimum number with an RMSECV below the defined boundary, in this case $n_{\text{sel}} = 6$. It shows that we can achieve a similarly good result – i.e., low RMSECV – with a small number of PLSR components compared to the minimum of the RMSECV.

Figure 5 shows the R^2 value for both AS-MLV and AS-MLV-P2 for different models. All models except the model for formaldehyde and toluene achieve an R^2 over 0.86, and even over 0.94 with the exclusion of benzene. This indicates that a satisfying quantification of VOC_{sum} and all gases except formaldehyde and toluene is possible with both sensors. The performance of the models is assessed with the RMSEP in Fig. 6 and the DNR in Fig. 7. Similar RMSEP values are achieved with both sensors for the different models. The regression models of AS-MLV and AS-MLV-P2 show the best performance for carbon monoxide with a DNR of 31. The re-

gression models for acetone and hydrogen also achieve satisfactory results with a DNR between 16 and 18. The DNR for benzene with a value of 13 is relatively low considering the (unrealistically) high concentrations. The two gases with very low concentrations, toluene and formaldehyde, cannot be selectively quantified in this complex background, indicated by a DNR below 6. VOC_{sum} can be quantified with a DNR of 18–19 independent of the unit ($\mu\text{g}/\text{m}^3$ or ppb). This is interesting because the two dominating VOCs, acetone and benzene, represent different chemical classes and have a 30 % difference in molecular weight.

For a comparison between randomized and sequential calibration methods, we compare different combinations of training/validation and testing (Table 4). For compatibility, the randomized dataset with a higher concentration dynamic is reduced to a dataset in which all concentrations are in the range of 0–120 % of the sequential measurement, resulting in 153 gas exposures. The distribution of all gases and VOC_{sum} is shown in Fig. A2. Since the last six gas exposures (75 %RH, 750 and 100 ppb benzene, all formaldehyde concentrations) are missing from the sequential dataset due to a technical error, there are 66 sequential gas mixtures in total. Combination (α) shows the evaluation of the reduced randomized dataset with 153 gas exposures. For the evaluation we used 10-fold nested cross-validation for hyperparameter optimization and testing like the evaluation in Figs. 6 and 7. We split the reduced dataset from the randomized measurement for combinations (β) to (δ) into two datasets. The first dataset contains the first 72 randomized gas exposures for training and hyperparameter optimization, and the second dataset the remaining 81 for testing. This allows us to compare randomized calibration with sequential testing and vice versa. The hyperparameter optimization during the training

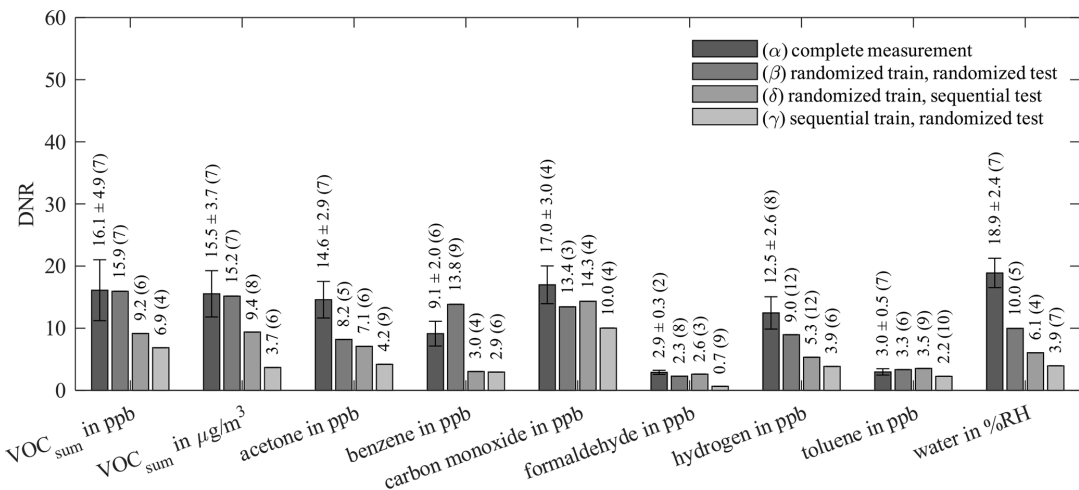


Figure 9. Dynamic range (DNR) of AS-MLV-P2 for different training and testing models. All models use 10-fold cross-validation for hyperparameter optimization; the resulting number of PLSR components, determined with Eq. (2), is given in parentheses. A detailed description of (α)–(δ) is given in Table 4.

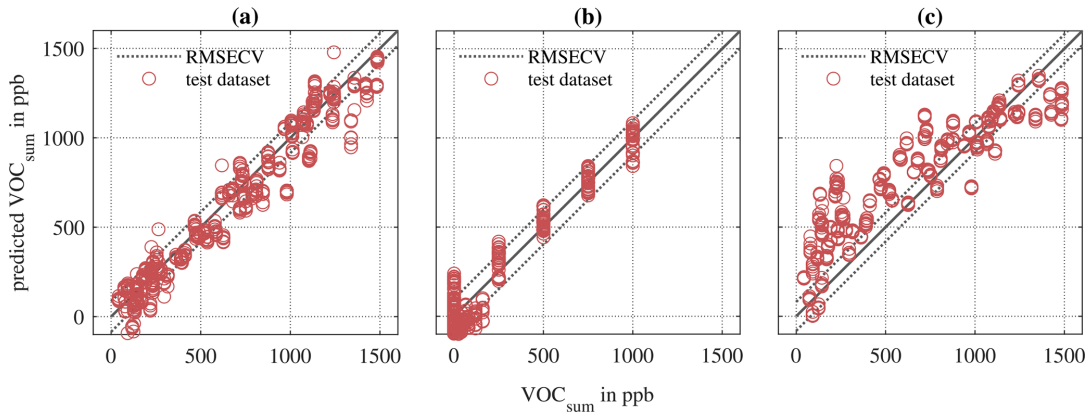


Figure 10. PLSR models for AS-MLV-P2 for quantification of VOC_{sum} in ppb for different training and testing models. (a) Randomized training and testing (Table 4, α). (b) Randomized training and sequential testing (Table 4, β). (c) Sequential training and randomized testing (Table 4, δ).

was always based on 10-fold cross-validation for randomized and sequential training.

Comparing the results of (α) and the previous evaluation in Figs. 6 and 7 shows the influence of reducing the randomized dataset for better compatibility with the sequential test scenario. The results of (α) and (β) show the influence of the two different evaluations. (γ) explores the prediction ability of a model trained with randomized data for sequential data, and (δ) vice versa. The performances of these four models are compared in Fig. 8 (RMSEP) and Fig. 9 (DNR) for the AS-MLV-P2. The AS-MLV shows similar results and can be found in Figs. C1 and C2. The RMSEPs of the models with randomized training (α) to (γ) are close together. The only exception is sequential testing – i.e., model (γ) – for benzene, producing a significantly larger RMSEP. The reverse

case – i.e., model (δ) predicting randomized data after a sequential training – results in considerably larger RMSEPs in practically all cases. Despite the RMSEPs being similar for (α) to (γ) and Fig. 6, the DNR (Fig. 9) reveals the superiority of the results shown in Fig. 7 trained with a larger concentration range. The comparison between the randomized (β , γ) and sequential (δ) training of the reduced dataset only shows similar performance for carbon monoxide. The randomized data are obviously more challenging to predict and, at the same time, provide a better model with a higher DNR for prediction, which is to be expected due to the much larger variability of the background. At the same time, this allows for more efficient training closer to reality, since one data point is obtained for each gas from each gas mixture.

Table 4. Combinations of training including hyperparameter optimization and testing datasets for a comparison between randomized and sequential calibration methods for the reduced dataset.

	Training	Testing
(α)	randomized (all)	randomized (all)
(β)	randomized (first 72)	randomized (remaining 81)
(γ)	randomized (first 72)	sequential (all)
(δ)	sequential (all)	randomized (remaining 81)

Comparing the PLSR models for VOC_{sum} (in ppb) for combinations (β), (γ) and (δ) from Table 4 indicates that classical sequential calibration (see Fig. 10b) is a subset of the randomized calibration presented here (see Fig. 10a). The models trained with randomized mixtures in Fig. 10a and b show a slightly larger RMSECV compared to the sequential training shown in Fig. 10c. However, only these random models can accurately and precisely predict both the randomized and sequential dataset. The sequentially trained (and validated) model in Fig. 10c achieves a slightly lower RMSECV but fails to predict the more complex randomized dataset. Note that the measurement duration for both datasets is identical.

4 Conclusion and outlook

In this paper an efficient and effective gas sensor calibration based on randomized gas mixtures is presented. The results are compared with a classical calibration strategy based on individual gas exposures with sequentially increasing concentrations and fixed steps. While a model trained with data from the sequential calibration performs poorly in the more realistic case of complex gas mixtures, the novel randomized calibration achieves very promising results for all tested datasets, making it more effective. Since generating the required data with randomized gas mixtures does not take more time (and could, potentially, take considerably less for more targets) than the classical sequential calibration strategy, it is also more efficient. Our method was developed and tested with the real-world application of indoor air quality monitoring in mind and thus presents an important tool for the successful transfer of chemical sensors from the laboratory to the field. Its statistical nature makes it robust against overfitting and well suited for machine learning algorithms.

Since only single gases were measured sequentially in the study presented here, an investigation of the performance and stability of sequential calibrations with fully sampled combinations should follow for a more complete comparison to the randomized strategy. The aim of these investigations should be to determine the ideal number of randomized mixtures for obtaining a reliable model for predicting the concentration of an individual gas or a gas mixture. To check for generalizability, tests with different mixture compositions, for example by replacing one or two gases, will also be considered.

The six gases investigated in this work are probably not enough to fully characterize the performance of sensors for indoor air quality assessment, especially for a quantification of a single VOC. Therefore, the complexity, for example the number of backgrounds and interfering and target gases, should be rigorously increased in order to get closer to reality. A next step is the development of new gas mixing apparatus allowing a higher number of gases to be measured. By testing different distributions, efficiency and performance could be further improved. In addition, extensive field tests with reference analysis are necessary to demonstrate the advantage of the calibration strategy for real-world applications.

Appendix A: Appendix A: Histogram of the complete and reduced dataset

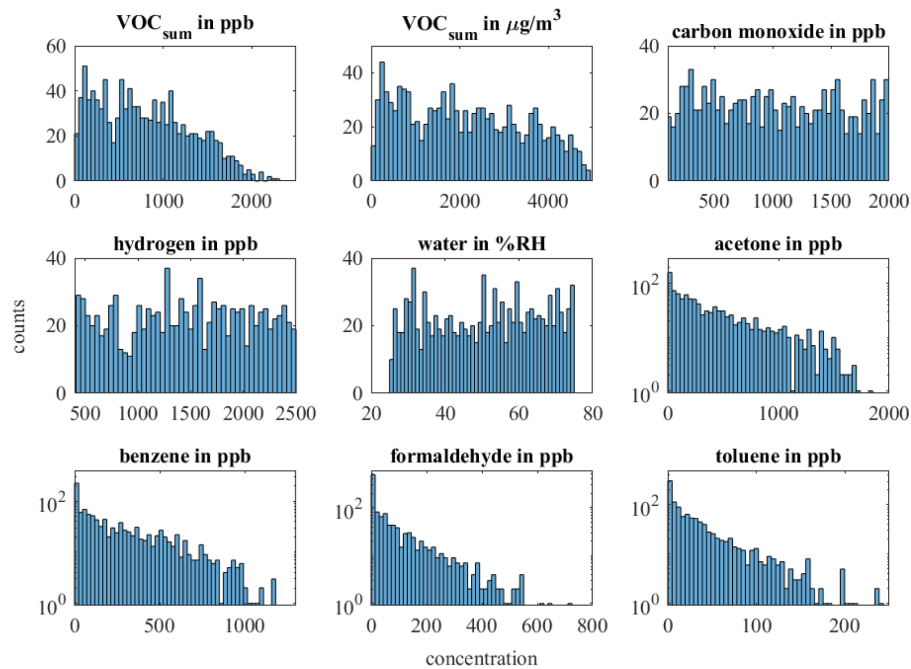


Figure A1. Concentration histogram of the observations in the complete measurement campaign for all gases and VOC_{sum} .

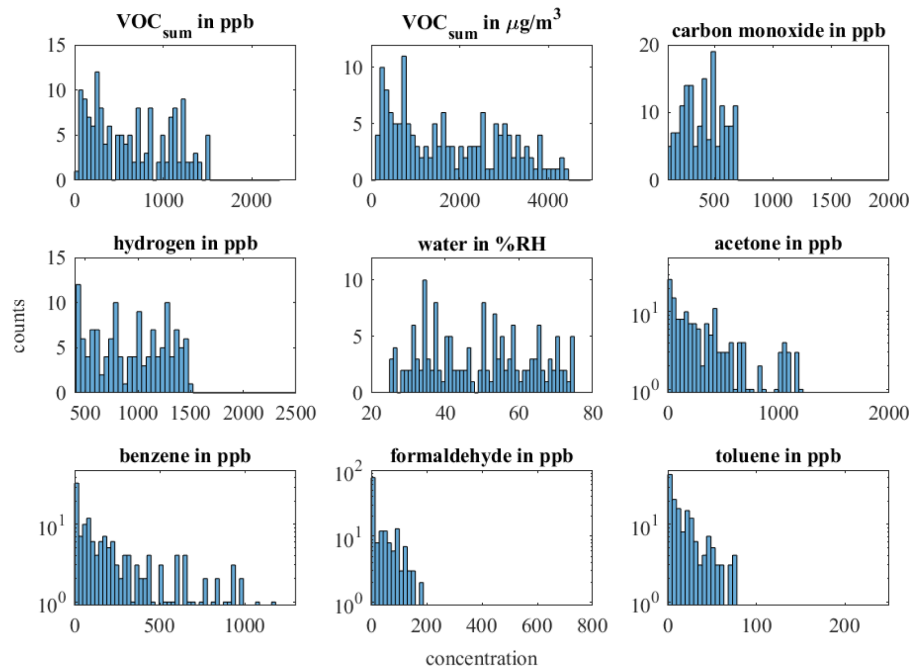


Figure A2. Concentration histogram of the observations for the reduced dataset (comparison between the randomized and sequential measurement) for all gases and VOC_{sum} .

Appendix B: Pseudocode for data evaluation

```
# feature extraction
for each cycle:
    for each one-second segment in cycle:
        compute mean
        compute slope
        compute PCA for [mean,slope]
        features = first 20 PCA components

# hold-out-based hyperparameter optimization
testset = e.g. 10 % of observations
rest_features = features without testset
cvparts = divide rest_features into 10 parts
for each hyperparameter_set:
    for each cvpart:
        train model with (rest_features without cvpart)
        predict cvpart with model
        compute RMSECV
best_model = choose hyperparameter_set according to Eq. (2).
predict testset with best_model
compute RMSEP

# nested cross-validation hyperparameter optimization
testparts = divide features into 10 parts
for each hyperparameter_set:
    for each testpart:
        rest_features = features without testpart
        cvparts = divide rest_features into 10 parts
        for each cvpart:
            train model with (rest_features without cvpart)
            predict cvpart with model
            compute RMSECV
        predict testset with model
        compute RMSEP
best_model = choose hyperparameter_set according to Eq. (2).
```

Appendix C: Results of the AS-MLV for comparison between randomized and sequential calibration

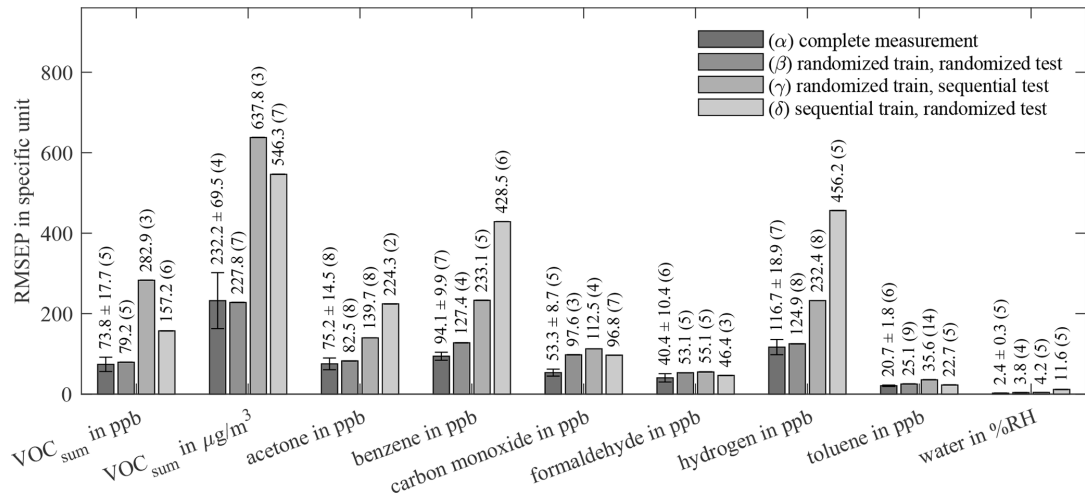


Figure C1. Root-mean-square error of prediction (RMSEP) of AS-MLV for different training and testing models and targets. All models use 10-fold cross-validation for hyperparameter optimization; the resulting number of PLSR components, determined with Eq. (2), is given in parentheses. A detailed description of (α)–(δ) is given in Table 4.

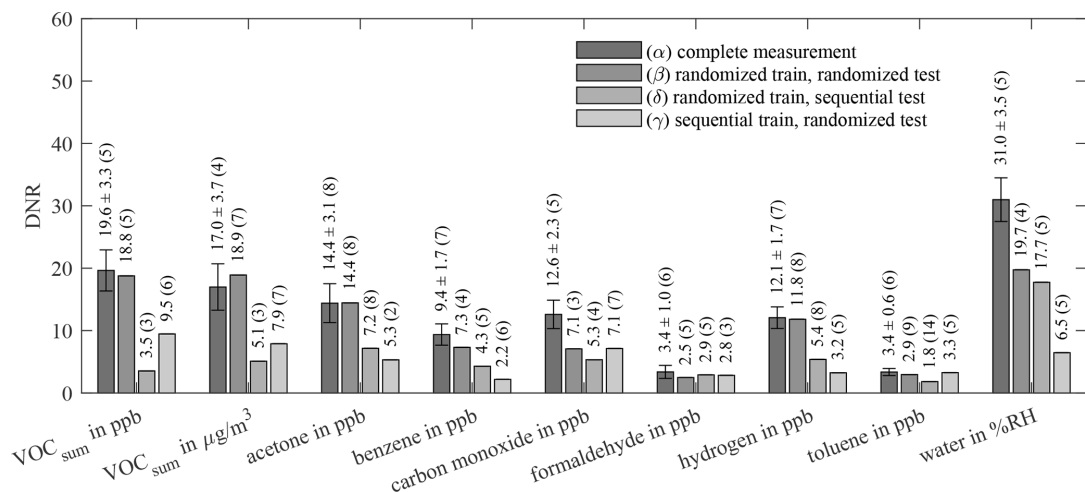


Figure C2. Dynamic range (DNR) of AS-MLV for different training and testing models and targets. All models use 10-fold cross-validation for hyperparameter optimization; the resulting number of PLSR components, determined with Eq. (2), is given in parentheses. A detailed description of (α)–(δ) is given in Table 4.

Data availability. The data presented in this article are stored in an internal system according to the guidelines of the German Research Foundation (DFG). The data for the evaluation can also be found at <https://doi.org/10.5281/zenodo.4264224> (Baur et al., 2020).

Author contributions. TB, MB and CS conceptualized the project. TB and CS built the setup for the MOS sensors. MB wrote the software for the randomized calibration. TB and MB performed the measurements and evaluation. TB visualized the results and wrote with MB and CS the original draft of the paper. TS and AS reviewed and edited the paper.

Competing interests. The authors declare that they have no conflict of interest.

Special issue statement. This article is part of the special issue “Dresden Sensor Symposium DSS 2019”. It is a result of the “14. Dresden Sensor-Symposium”, Dresden, Germany, 2–4 December 2019.

Acknowledgements. We acknowledge support by the Deutsche Forschungsgemeinschaft (DFG, German Research Foundation) and Saarland University within the funding program Open Access Publishing.

Review statement. This paper was edited by Winfried Vonau and reviewed by two anonymous referees.

References

Anon: Directive 2004/42/EC of the European Parliament and of the Council of 21 April 2004 on the limitation of emissions of volatile organic compounds due to the use of organic solvents in certain paints and varnishes and vehicle refinishing products and amend, available at: <https://eur-lex.europa.eu/eli/dir/2004/42/2019-07-26> (last access: 27 May 2020), 2004.

Anon: Beurteilung von Innenraumluftkontaminationen Mittels Referenz- und Richtwerten?: Handreichung der Ad-hoc-Arbeitsgruppe der Innenraumlufthygiene- Kommission des Umweltbundesamtes und der Obersten Landesgesundheitsbehörden, Bundesgesundheitsblatt – Gesundheitsforschung – Gesundheitsschutz, 50, 990–1005, <https://doi.org/10.1007/s00103-007-0290-y>, 2007.

Anon: Richtwert für Formaldehyd in der Innenraumluft, Bundesgesundheitsblatt – Gesundheitsforschung – Gesundheitsschutz, 59, 1040–1044, <https://doi.org/10.1007/s00103-016-2389-5>, 2016.

Bajtarevic, A., Ager, C., Pienz, M., Klieber, M., Schwarz, K., Ligor, M., Ligor, T., Filipiak, W., Denz, H., Fiegl, M., Hilbe, W., Weiss, W., Lukas, P., Jamnig, H., Hackl, M., Haidenberger, A., Buszewski, B., Miekisch, W., Schubert, J., and Amann, A.: Non-invasive detection of lung cancer by analysis of exhaled breath, BMC Cancer, 9, 348, <https://doi.org/10.1186/1471-2407-9-348>, 2009.

Bastuck, M.: Improving the Performance of Gas Sensor Systems with Advanced Data Evaluation, Operation, and Calibration Methods, Linköping University Electronic Press, Linköping, 2019.

Bastuck, M. and Fricke, T.: Temperature-modulated gas sensor signal, Zenodo, <https://doi.org/10.5281/ZENODO.1411209>, 2018.

Bastuck, M., Baur, T., Richter, M., Mull, B., Schütze, A., and Sauerwald, T.: Comparison of ppb-level gas measurements with a metal-oxide semiconductor gas sensor in two independent laboratories, Sens. Actuators, B, 273, 1037–1046, <https://doi.org/10.1016/j.snb.2018.06.097>, 2018a.

Bastuck, M., Baur, T., and Schütze, A.: DAV³E – a MATLAB toolbox for multivariate sensor data evaluation, J. Sens. Sens. Syst., 7, 489–506, <https://doi.org/10.5194/jsss-7-489-2018>, 2018b.

Baur, T., Schütze, A., and Sauerwald, T.: Optimierung des temperaturzyklischen Betriebs von Halbleitergassensoren, Tech. Mess., 82, 187–195, <https://doi.org/10.1515/teme-2014-0007>, 2015.

Baur, T., Schultealbert, C., Schütze, A., and Sauerwald, T.: Device for the detection of short trace gas pulses, Tech. Mess., 85, 496–503, <https://doi.org/10.1515/teme-2017-0137>, 2018a.

Baur, T., Schultealbert, C., Schütze, A., and Sauerwald, T.: Novel method for the detection of short trace gas pulses with metal oxide semiconductor gas sensors, J. Sens. Sens. Syst., 7, 411–419, <https://doi.org/10.5194/jsss-7-411-2018>, 2018b.

Baur, T., Bastuck, M., and Schultealbert, C.: Random gas mixtures for efficient gas sensor calibration: Dataset, Zenodo, <https://doi.org/10.5281/zenodo.4264224>, 2020.

Borrego, C., Costa, A. M., Ginja, J., Amorim, M., Coutinho, M., Karatzas, K., Sioumis, T., Katsifarakis, N., Konstantinidis, K., De Vito, S., Esposito, E., Smith, P., André, N., Gérard, P., Francis, L. A., Castell, N., Schneider, P., Viana, M., Minguillón, M. C., Reimringer, W., Otjes, R. P., von Sicard, O., Pohle, R., Elen, B., Suriano, D., Pfister, V., Prato, M., Dipinto, S., and Penza, M.: Assessment of air quality microsensors versus reference methods: The EuNetAir joint exercise, Atmos. Environ., 147, 246–263, <https://doi.org/10.1016/j.atmosenv.2016.09.050>, 2016.

Castell, N., Dauge, F. R., Schneider, P., Vogt, M., Lerner, U., Fishbain, B., Broday, D., and Bartonova, A.: Can commercial low-cost sensor platforms contribute to air quality monitoring and exposure estimates?, Environ. Int., 99, 293–302, <https://doi.org/10.1016/j.envint.2016.12.007>, 2017.

Fonollosa, J.: Gas sensor array under dynamic gas mixtures Data Set, UCI Machine Learning Repository, available at: <https://archive.ics.uci.edu/ml/datasets/Gas+sensor+array+under+dynamic+gas+mixtures> (last access: 31 March 2020), 2015.

Fonollosa, J.: Twin gas sensor arrays Data Set, UCI Machine Learning Repository, available at: <https://archive.ics.uci.edu/ml/datasets/Twin+gas+sensor+arrays> (last access: 31 March 2020), 2016.

Fonollosa, J., Rodríguez-Luján, I., and Huerta, R.: Chemical gas sensor array dataset, Data in Brief, 3, 85–89, <https://doi.org/10.1016/j.dib.2015.01.003>, 2015a.

Fonollosa, J., Rodríguez-Luján, I., Trincavelli, M., and Huerta, R.: Dataset from chemical gas sensor array in turbulent wind tunnel, Data in Brief, 3, 169–174, <https://doi.org/10.1016/j.dib.2015.02.014>, 2015b.

Fonollosa, J., Solórzano, A., Jiménez-Soto, J. M., Oller-
Moreno, S., and Marco, S.: Gas sensor array for reliable fire detection, *Procedia Engineer.*, 168, 444–447, <https://doi.org/10.1016/j.proeng.2016.11.540>, 2016.

Gramm, A. and Schütze, A.: High performance solvent vapor identification with a two sensor array using temperature cycling and pattern classification, *Sens. Actuators, B*, 95, 58–65, [https://doi.org/10.1016/S0925-4005\(03\)00404-0](https://doi.org/10.1016/S0925-4005(03)00404-0), 2003.

Helwig, N., Schüler, M., Bur, C., Schütze, A., and Sauerwald, T.: Gas mixing apparatus for automated gas sensor characterization, *Meas. Sci. Technol.*, 25, 055903, <https://doi.org/10.1088/0957-0233/25/5/055903>, 2014.

Hofmann, H. and Plieninger, P.: Bereitstellung einer Datenbank zum Vorkommen von flüchtigen organischen Verbindungen in der Raumluft, *WaBoLu-Hefte*, 5, 161, 2008.

Karagulian, F., Barbiere, M., Kotsev, A., Spinelle, L., Gerboles, M., Lagler, F., Redon, N., Crunaire, S., and Borowiak, A.: Review of the Performance of Low-Cost Sensors for Air Quality Monitoring, *Atmosphere*, 10, 506, <https://doi.org/10.3390/atmos10090506>, 2019.

Kohl, D., Kelleter, J., and Petig, H.: Detection of Fires by Gas Sensors, *Sensors Updat.*, 9, 161–223, [https://doi.org/10.1002/1616-8984\(200105\)9:1<161::AID-SEUP161>3.0.CO;2-A](https://doi.org/10.1002/1616-8984(200105)9:1<161::AID-SEUP161>3.0.CO;2-A), 2001.

Leidinger, M., Schulthealbert, C., Neu, J., Schütze, A., and Sauerwald, T.: Characterization and calibration of gas sensor systems at ppb level – a versatile test gas generation system, *Meas. Sci. Technol.*, 29, 015901, <https://doi.org/10.1088/1361-6501/AA91DA>, 2018.

Levitt, M. D.: Production and excretion of hydrogen gas in man, *The New England journal of medicine*, 281, 122–127, <https://doi.org/10.1056/NEJM196907172810303>, 1969.

Lourenço, C. and Turner, C.: Breath Analysis in Disease Diagnosis: Methodological Considerations and Applications, *Metabolites*, 4, 465–498, <https://doi.org/10.3390/metabo4020465>, 2014.

Marco, S. and Gutierrez-Galvez, A.: Signal and data processing for machine olfaction and chemical sensing: A review, *IEEE Sens. J.*, 12, 3189–3214, <https://doi.org/10.1109/JSEN.2012.2192920>, 2012.

Oehlert, G. W.: *A First Course in Design and Analysis of Experiments*, University of Minnesota Digital Conservancy, W. H. Freeman & Company, ISBN-10: 0-7167-3510-5, 2000.

Sauerwald, T., Baur, T., Leidinger, M., Reimringer, W., Spinelle, L., Gerboles, M., Kok, G., and Schütze, A.: Highly sensitive benzene detection with metal oxide semiconductor gas sensors – an inter-laboratory comparison, *J. Sens. Sens. Syst.*, 7, 235–243, <https://doi.org/10.5194/jsss-7-235-2018>, 2018.

Schleyer, R., Bieber, E., and Wallasch, M.: Das Luftnetz des Umweltbundesamt, available at: https://www.umweltbundesamt.de/sites/default/files/medien/378/publikationen/das_luftmessnetz_des_umweltbundesamtes_bf_0.pdf (last access: 19 November 2020), 2013.

Schulthealbert, C., Baur, T., Schütze, A., and Sauerwald, T.: Facile quantification and identification techniques for reducing gases over a wide concentration range using a MOS sensor in temperature-cycled operation, *Sensors*, 18, 744, <https://doi.org/10.3390/s18030744>, 2018a.

Schulthealbert, C., Baur, T., Schütze, A., and Sauerwald, T.: Investigating the role of hydrogen in the calibration of MOS gas sensors for indoor air quality monitoring, *Conference Proceedings Indoor Air, 15th Conference of the International Society of Indoor Air Quality & Climate, oral presentation, 22–27 July 2018, Philadelphia, PA, USA*, 2018b.

Schütze, A. and Sauerwald, T.: Dynamic operation of semiconductor sensors, in: *Semiconductor Gas Sensors*, edited by: Jaaniso, R. and Tan, O. K., 385–412, Woodhead Publishing Series in Electronic and Optical Materials, 385–412, 2019.

Schütze, A., Baur, T., Leidinger, M., Reimringer, W., Jung, R., Conrad, T., and Sauerwald, T.: Highly Sensitive and Selective VOC Sensor Systems Based on Semiconductor Gas Sensors: How to?, *Environments*, 4, 20, <https://doi.org/10.3390/environments4010020>, 2017.

Seifert, B.: Richtwerte für die Innenraumluft Die Beurteilung der Innenraumluftqualität mit Hilfe der Summe der flüchtigen organischen Verbindungen (TVOC-Wert), *Bundesgesundheitsblatt – Gesundheitsforschung – Gesundheitsschutz*, 42, 270–278, <https://doi.org/10.1007/s001030050091>, 1999.

Sharma, B., Sharma, A., and Kim, J. S.: Recent advances on H₂ sensor technologies based on MOX and FET devices: A review, *Sens. Actuators, B*, 262, 758–770, <https://doi.org/10.1016/j.snb.2018.01.212>, 2018.

Spinelle, L., Gerboles, M., Kok, G., Persijn, S., and Sauerwald, T.: Review of Portable and Low-Cost Sensors for the Ambient Air Monitoring of Benzene and Other Volatile Organic Compounds, *Sens.*, 17, 1520, <https://doi.org/10.3390/s17071520>, 2017.

Stone, M.: Cross-Validatory Choice and Assessment of Statistical Predictions, *J. Roy. Stat. Soc. B Met.*, 36, 111–133, <https://doi.org/10.1111/j.2517-6161.1974.tb00994.x>, 1974.

Sundgren, H., Winquist, F., Lukkari, I., and Lundstrom, I.: Artificial neural networks and gas sensor arrays: quantification of individual components in a gas mixture, *Meas. Sci. Technol.*, 2, 464, <https://doi.org/10.1088/0957-0233/2/5/008>, 1991.

Tomchenko, A. A., Harmer, G. P., and Marquis, B. T.: Detection of chemical warfare agents using nanostructured metal oxide sensors, *Sensor. Actuat. B-Chem.*, 108, 41–55., 2005.

Tomlin, J., Lowis, C., and Read, N. W.: Investigation of normal flatus production in healthy volunteers, *Gut*, 32, 665–669, <https://doi.org/10.1136/gut.32.6.665>, 1991.

WHO Regional Office for Europe: WHO guidelines for indoor air quality: selected pollutants, Copenhagen, available at: <https://www.ncbi.nlm.nih.gov/books/NBK138705/> (last access: 19 November 2020), 2010.

Wolfrum, E. J., Meglen, R. M., Peterson, D., and Sluiter, J.: Calibration transfer among sensor arrays designed for monitoring volatile organic compounds in indoor air quality, *IEEE Sens. J.*, 6, 1638–1643, <https://doi.org/10.1109/JSEN.2006.884558>, 2006.

Yu, C., Hao, Q., Saha, S., Shi, L., Kong, X., and Wang, Z. L.: Integration of metal oxide nanobelts with microsystems for nerve agent detection, *Appl. Phys. Lett.*, 86, 1–3, <https://doi.org/10.1063/1.1861133>, 2005.

Zhang, L., Tian, F., Liu, S., Guo, J., Hu, B., Ye, Q., Dang, L., Peng, X., Kadri, C., and Feng, J.: Chaos based neural network optimization for concentration estimation of indoor air contaminants by an electronic nose, *Sensor. Actuat. A-Phys.*, 189, 161–167, <https://doi.org/10.1016/j.sna.2012.10.023>, 2013.

4.2.4 Paper 4 – DAV³E – a MATLAB toolbox for multivariate sensor data evaluation

M. Bastuck^{1,2}, T. Baur¹ and A. Schütze¹

¹Saarland University, Lab for Measurement Technology, Saarbrücken, Germany

²Linköping University, Applied Sensor Science, SAS, IFM, Linköping, Sweden

J. Sens. Sens. Syst. (2018), 7, 489–506

The original paper and supplementary data can be found, in the online version, at
<https://doi.org/10.5194/jsss-7-489-2018>.

© 2018 by the authors. This article is an open access article distributed under the terms and conditions of the Creative Commons Attribution (CC BY) license (<http://creativecommons.org/licenses/by/4.0/>).



DAV³E – a MATLAB toolbox for multivariate sensor data evaluation

Manuel Bastuck^{1,2}, Tobias Baur¹, and Andreas Schütze¹

¹Lab for Measurement Technology, Saarland University, 66123 Saarbrücken, Germany

²Applied Sensor Science, SAS, IFM, Linköping University, 58183 Linköping, Sweden

Correspondence: Manuel Bastuck (m.bastuck@lmt.uni-saarland.de)

Received: 15 April 2018 – Revised: 10 August 2018 – Accepted: 14 August 2018 – Published: 20 September 2018

Abstract. We present DAV³E, a MATLAB toolbox for feature extraction from, and evaluation of, cyclic sensor data. These kind of data arise from many real-world applications like gas sensors in temperature cycled operation or condition monitoring of hydraulic machines. DAV³E enables interactive shape-describing feature extraction from such datasets, which is lacking in current machine learning tools, with subsequent methods to build validated statistical models for the prediction of unknown data. It also provides more sophisticated methods like model hierarchies, exhaustive parameter search, and automatic data fusion, which can all be accessed in the same graphical user interface for a streamlined and efficient workflow, or via command line for more advanced users. New features and visualization methods can be added with minimal MATLAB knowledge through the plug-in system. We describe ideas and concepts implemented in the software, as well as the currently existing modules, and demonstrate its capabilities for one synthetic and two real datasets. An executable version of DAV³E can be found at <http://www.lmt.uni-saarland.de/dave> (last access: 14 September 2018). The source code is available on request.

1 Introduction

In recent years, a new paradigm has been developing in science, introducing a whole new field of both research and tools: big data (Chang et al., 2014; Kitchin, 2014). With enough data and computing power, a wide variety of systems, previously inaccessible to physical models due to their complexity, have become available to scientific description and treatment with the use of statistical models. New challenges arise for data processing because (semi-)automatic approaches and smart assistant systems are essential to handle and evaluate the huge amounts of data.

Many software packages exist for statistical data evaluation or machine learning. A non-exhaustive list includes commercial and closed-source packages like SPSS Statistics (IBM), Minitab (Minitab Inc.), Statistica (StatSoft), and RapidMiner (RapidMiner, Inc.), as well as open-source alternatives like Weka (University of Waikato), R (The R Foundation), and orange (University of Ljubljana). The PLS_Toolbox (Eigenvector Research, Inc.) is a noteworthy

member of this list by being commercial, but partly open-source, and the only of the tools known to the authors that is MATLAB-based. Many of these programs can be extended by the user with modules written in Python or Java, so, in general, it is often possible to add missing features and functions oneself. However, mechanical or electronic engineers, who most often work with sensors and sensor systems, often do not have any, or little, training in programming and data science in general. The existing software packages usually try to be as flexible as possible, which can seem overwhelming to new users. From personal experience, we know that many engineers in this field prefer MATLAB over Java or Python due to its out-of-the-box numerical abilities while providing a simple and easy-to-learn script language.

However, this observation was not the only reason for the development of DAV³E (Data Analysis and Verification/Visualization/Validation Environment). A problem common in many statistical software packages, including, to the best of the authors' knowledge, the PLS_Toolbox, is the assumption that the data are already available in the form of a

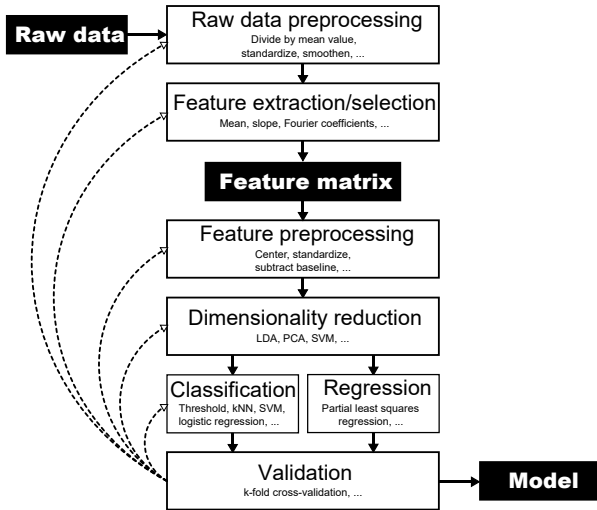


Figure 1. Flowchart of the steps involved in building a statistical model from raw data. The validation step is crucial to check the model's performance. Any step and its parameters in the process influence the model performance. However, the exact way is usually hard to predict, which results in a time-consuming trial-and-error process to find a model that performs well. Most available software packages for machine learning or statistical model building usually start at the feature matrix, thus ignoring the need for feature extraction from the raw data, which is a crucial step, especially, but not only, for cyclic sensor signals.

feature matrix (Fig. 1). This assumption does not take into account that features must often first be generated, or extracted, from raw data, which is a highly relevant and all too often neglected part of the evaluation process.

A prime example of this issue is the cyclic operation of sensors. An operation mode called temperature cycled operation (TCO) has long been known (Eicker, 1977; Lee and Reedy, 1999) to improve sensitivity and selectivity for chemical sensors and gas sensors in particular (Bur, 2015; Reimann and Schütze, 2014). TCO works by collecting data from the sensor at different operating temperatures. The operating temperature influences the physical and chemical reactions on the sensor surface and, thus, the sensor behavior. The result is an array of sensor responses very similar to an actual sensor array, which is why this approach is also known as a virtual multisensor system (Reimann and Schütze, 2014; Schütze et al., 2004). In this example, one temperature cycle can take several minutes, which is the effective sampling period of the sensor. However, the sensor must actually be sampled much faster, usually in the range from Hz to kHz, during the cycle. The information about the present gas is not contained so much in one of the resulting several thousand points in one cycle, but rather in the overall signal shape during one cycle. To avoid the curse of dimensionality (Böhm et al., 2001; Gutierrez-Osuna, 2002; James et al., 2013), it is

therefore necessary to extract information-rich features from the cyclic sensor signal.

Several other approaches following the same principle exist, e.g., voltammetry in electronic tongues (Apetrei et al., 2004), gate bias cycled operation (GBCO) (Bur, 2015) for gas-sensitive field-effect transistors (GasFETs) (Andersson et al., 2013), or exploitation of the working cycle of hydraulic machines for online condition monitoring of those machines (Helwig et al., 2015).

Several methods have been established for feature extraction from cyclic signals. TCO-MOX sensor signals are often processed by a fast Fourier transform (FFT) (Heilig et al., 1997) or a discrete wavelet transform (DWT) (Cetó et al., 2014; Ding et al., 2005; Huang et al., 2006; Moreno-Barón et al., 2006), usually in combination with a suitable, i.e., sine wave, temperature cycle. Other approaches include windowed time slicing (Apetrei et al., 2007; Gutierrez-Osuna and Nagle, 1999) or principal component analysis (PCA) (Winquist et al., 1997). A comprehensive review of these and more methods is given in Sect. II A1 in Marco and Gutierrez-Galvez (2012). In contrast to these projection methods, DAV³E specializes in extracting shape-describing features from a cyclic signal. It has been shown that such features can outperform FFT and DWT features (Gramm and Schütze, 2003). They are also very easy to compute, unlike DWT or other complex decompositions, so they can easily be implemented in cheap hardware, i.e., microprocessors. Finally, the feature extraction implementation in DAV³E is a superset of the above-mentioned methods: if desired, DWT can still be applied to the whole cycle, but if a physical model suggests that, e.g., the slope in one specific part of the cycle is a suitable feature (Baur et al., 2015), this slope can additionally be extracted to improve the model. To the best of the authors' knowledge, there is no software which provides both aspects of statistical data evaluation, i.e., shape-describing feature extraction and statistical model building. In particular, a tool for manual, graphical feature extraction from cycles was not available before. But implementing only this functionality could easily lead to inefficient workflows since the user would constantly have to switch between at least two different software tools.

As a solution to this problem, we have developed DAV³E, a MATLAB-based, object-oriented framework. It covers the cycle-based data preprocessing and feature extraction missing in contemporary data-mining software packages and sensor-aware functions like correction of time offset and sample rate without resampling, as well as simple or hierarchical statistical models, both for classification and regression. The graphical user interface (GUI) leads the user through the process and, thus, is suitable for beginners and advanced users, which is especially important in fields in which new people are constantly starting their work on statistical data evaluation, like universities. For advanced users who prefer a textual interface or want to perform batch processing or other kinds of automation, the functionality is also

available via the command line. To further aid the user, the evaluation is supported by static, animated, or interactive visualizations in every step.

2 Basic concepts and structures

2.1 Workflow

The model-building workflow implemented in DAV³E is depicted in Fig. 1 and follows the process outlined by Gutierrez-Osuna for machine olfaction in (Gutierrez-Osuna, 2002). Raw data are the data collected from sensors or lab equipment. The data are assumed to be of a cyclic nature; i.e., there is at least one setpoint parameter which repeats a cyclic pattern over time. Hence, each data stream can also be seen as a matrix with as many rows as there are cycles in the whole measurement, and as many columns as there are data points in one cycle. The typical length of a cycle is in the order of seconds or minutes, with sampling rates in the order of Hz or kHz. However, the exact values can vary greatly between use cases. Note that this approach also covers simple time series data, if not only a single value but a certain time window is used for evaluation.

The cyclic approach offers some unique preprocessing methods for the raw data, e.g., dividing each cycle by its mean value to mitigate sensor drift (Gramm and Schütze, 2003). At the same time, the information contained in the cycles mean value is then eliminated. Whether drift compensation or more information is more important for the model performance is often not immediately clear and must be determined by validating the final model. This is just one of many parameters influencing the model, and often model validation and subsequent adjustments to the parameters, i.e., trial and error, is the only way to improve model performance as there is no guarantee that a certain data evaluation algorithm will yield optimum results.

Another special feature of cyclic sensor operation is the way features are extracted from the raw data. One cycle can have many thousands of highly correlated data points or features. Both the high number (Hastie et al., 2009; James et al., 2013) as well as the collinearity (Næs and Mevik, 2001) can cause problems like instabilities in many machine learning methods, so the dimensionality of the feature space must be reduced. This reduction is achieved by describing the shape of the signal with as few parameters as possible while maintaining most of the information. For example, an area in the cycle where the signal is nearly flat over thousands of points is described equally well with just one parameter: the mean of all of these points. This step typically reduces the number of features by 90 % or more and results in less correlation between the features. Which parts in the cycle and which fit functions are used is often determined manually, so the result can depend on the experience of the user. In rare cases, a rough physical model allows for a more targeted extraction of features from the raw data. In all cases, the result of

this step is a feature matrix with the same number of rows (observations) as the raw data, but fewer columns (features). Most machine learning tools assume the data to have this or an equivalent shape.

Hence, the following steps are the steps involved in every multivariate statistical analysis (Gutierrez-Osuna, 2002). The feature columns can be preprocessed, e.g., standardized, to remove scaling and achieve more stable numerical results (van den Berg et al., 2006). The same can be done to the target vectors, if they are numeric, e.g., to linearize a logarithmic sensor response. Further dimensionality reduction is often done using unsupervised principal component analysis (PCA) (Gutierrez-Osuna, 2002; Risvik, 2007) or supervised linear discriminant analysis (LDA) (Gutierrez-Osuna, 2002). Both steps are optional, and dimensionality reduction is often a part of classification or regression (“prediction” in general), as in the case of support vector machines (SVMs) (Smola and Schölkopf, 2004) or partial least squares regression (PLSR) (Abdi, 2010; Geladi and Kowalski, 1986). Other classifiers available in DAV³E are k nearest neighbors (kNN) (Hastie et al., 2009), discriminant analysis (DA) (Hastie et al., 2009), logistic regression (LR) (Hastie et al., 2009), and more. It is necessary to validate the whole evaluation chain to prevent overfitting, an effect whereby a model fits the training data very well, but is not able to predict new data correctly (Hawkins, 2004). Validation can be done with new data when the correct outcomes are known for each observation. If such a validation dataset is not available, validation is still possible, e.g., with k -fold cross-validation (Browne, 2000; Kohavi, 1995), which uses one part of the dataset for training and the other for testing. The eventual performance of the model is then determined with a test dataset which contains only data that were never used in training or validating the model.

2.2 Data structure and fusion

DAV³E saves imported data in a hierarchical structure consisting of measurement, cluster, and sensor objects. A sensor is the smallest unit and contains the data associated with the sensor. This can be data from an actual physical sensor, e.g., an acceleration or gas sensor, one of many channels of a scientific instrument, e.g., the measured voltage of channel 1 of a multichannel data acquisition system, or a virtual sensor which is computed from other physical sensors, e.g., the resistance which is computed as the quotient of voltage and current. Each sensor can be assigned a unique data evaluation chain with different raw data preprocessing and feature extraction algorithms, which accounts for the fact that data from different sensors can be very dissimilar.

Sensors are organized in clusters, which contain information about time offset (to a reference time) of the data acquisition, sampling rate, and number of data points per cycle. While this information could well also be saved directly with each sensor, there are often natural “groups” of sensors in

real measurements, e.g., three channels from a device that measures (1) voltage and (2) current over (3) time. Two virtual sensors, “virtual data points” and “virtual time”, are derived from each cluster’s sampling rate and offset information. They serve as default abscissa for sensors in this cluster for plots or during feature extraction. Default values are useful because, quite often, information about time and/or data points is not provided as a sensor. As virtual sensors are computed dynamically, later changes to time offset or sampling rate are as easy as changing the specific value, and the time information is automatically adapted accordingly.

Clusters are contained in measurements. A measurement always has a defined starting time and date and can thus provide a time reference for its clusters. It also stores time ranges during which the environmental conditions influencing the sensors, i.e., gas concentrations or system failure states, were constant. This is only useful if not all points in time of the measurement are of interest for the evaluation, which is, however, often the case. Experimental systems are often proprietary and not integrated with each other. This means that, for example, the gas sensor data acquisition and the test environment, e.g., a gas mixing apparatus (Helwig et al., 2014) providing defined gas mixtures for the characterization, run in parallel, but are not necessarily exactly synchronized. It is thus easier to start both systems and combine their data afterwards, which will result in undefined states when the gas mixing apparatus is changing states while the sensor proceeds with its current cycle. This and potentially a few following cycles are obtained under unknown conditions and must therefore be excluded from the evaluation. In a measurement, relevant time segments with known environmental conditions can be selected (or imported) so that only cycles recorded during these times are considered for further evaluation.

All sensors in the same measurement will add to the number of features available in the observations in this measurement; i.e., the sensors are fused in parallel. Consequently, the environmental conditions defined in the measurement are automatically assumed by newly added sensors without any action from the user. Sensors in different measurements, however, are added in series; i.e., they add to the total number of observations. Sensors from different measurements are associated by their name, so data from identical sensors are automatically combined (Fig. 2).

2.3 Programming concepts and plug-ins

One focus during the development was easy extendibility of all important aspects of the software. The object-oriented design helps to keep a clear structure and maintainable code. Additionally, a plug-in concept was implemented that allows all users with basic MATLAB knowledge to add new functions. Contrary to other programming languages, MATLAB knowledge is widespread amongst engineers, who are the main target users of DAV³E. If necessary, scripts in other

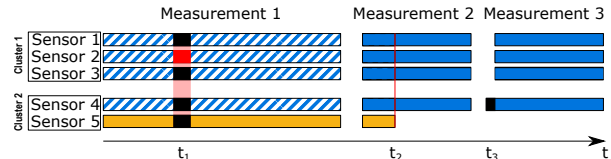


Figure 2. Illustration of data fusion with five sensors from two different sources (cluster 1/2). If one sensor sends faulty or noisy data over some time (sensor 2 at t_1), DAV³E will automatically ignore all data during that time in the fused dataset. If a sensor fails (sensor 5 at t_2), the user can choose to have more observations, but without that sensor (blue data), or to include all sensors, but with fewer observations (orange data). If a sensor starts too early (sensor 4 at t_3), its data will be ignored until data from all sensors are available. Such events can either be annotated by the user or imported directly from the test setup if the data are available.

languages like R or Python can easily be accessed from within MATLAB. Currently, the plug-in system covers the following algorithm types: dimensionality reduction, feature extraction, feature and response preprocessing, data import sources, virtual sensor computation, raw data preprocessing, postprocessing, classifiers, regressors, and validation. A subset of those, i.e., dimensionality reduction, classifiers, and regressors, provides the addition of custom plots as plug-ins.

For each type of plug-in, a template file defines available functions with a fixed interface, so all available data can easily be accessed and the user can concentrate on the correct implementation of their function instead of programmatic technicalities.

Depending on the sample rate and duration of the measurement, the sensor dataset can become rather large. Several gigabytes are easily reached, and certain applications in condition monitoring have already produced data with several tens of terabytes. Currently, DAV³E’s ability to handle such data are still limited by the size of system memory (RAM, random access memory). However, measures have been taken not to use up more space than necessary.

One important aspect is to omit resampling of the data. Downsampling can lead to loss of information, while upsampling can lead to significantly increased size in memory, especially if the dataset contains one or more sensors with very high sample rates. In the evaluation process, selections must be made in the data which, ultimately, must refer to the same point in time for all sensors in a measurement to ensure consistent results for sensors with different offsets, sample rates, or cycle lengths. Any selection is thus stored as a timestamp. Given an arbitrary sensor, this timestamp can be used to calculate which point or part of its data should be selected.

2.4 Dependencies

The toolbox is designed to have as few dependencies on other MATLAB toolboxes as possible. Most dimensionality reduction, classification, and regression methods rely on their im-

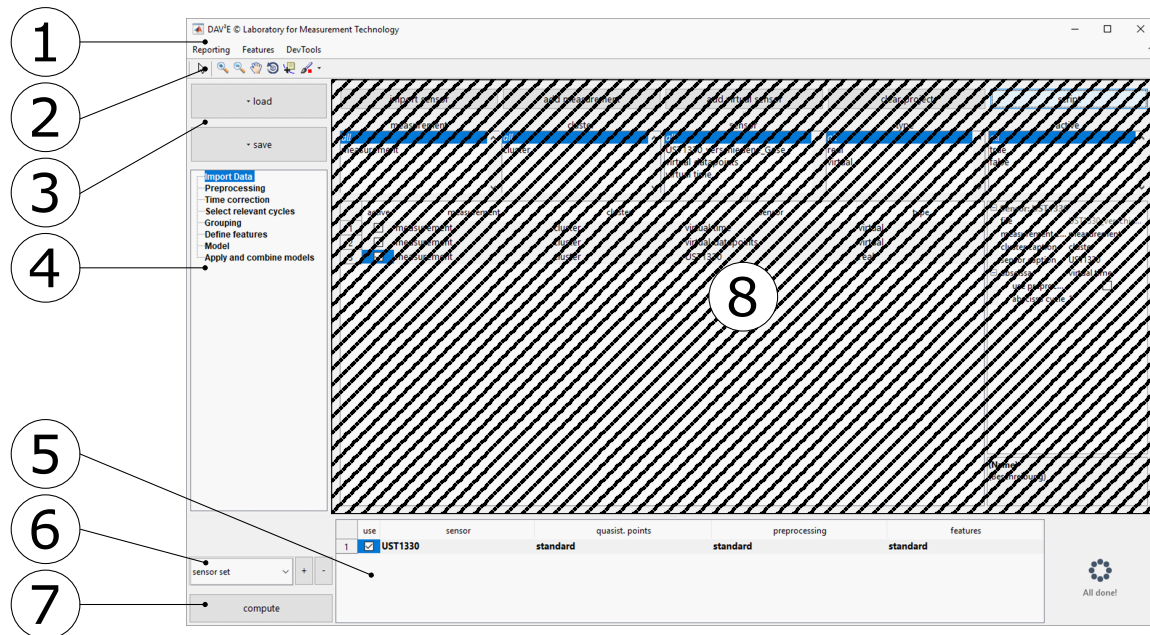


Figure 3. Main GUI with menu bar (1), toolbar (2), load and save buttons (3), the list of modules (4), the list of selected sensors (5), the current sensor set (6), the compute button for features (7), and the currently selected module (8, shaded).

lementation in the Statistics and Machine Learning Toolbox. The LDA projection can be computed by `manova1` from this toolbox. In a newer version of DAV³E currently in development, however, we replace most of these functions by our own implementations. These are based on the MATLAB implementation, but drop many type checks, etc., resulting in quicker execution. Checking the input to these low-level functions is not necessary in this context as errors are already caught by higher level functions.

The report functionality additionally needs the Report Generator, and special, but nonessential functions rely on the Curve Fitting Toolbox (fitting Gauss peaks) and the Econometrics Toolbox (feature correlation plot, `corrplot`). Especially the latter could easily be rewritten, if necessary. The same applies to the function that is used to determine well-distinguishable colors for new elements which, coming from FileExchange, makes uses of the Image Processing Toolbox. This functionality can easily be bypassed if the toolbox is not available.

DAV³E is compatible with MATLAB R2016b or later.

2.5 Graphical user interface

A graphical user interface (GUI) is the main way the average user actively interacts with a computer program. It gives a graphical representation of all options the user currently has which can lead to a more efficient workflow. Without a GUI, the user can call functions of the program directly in the command line, which can be of benefit to more advanced users

when performing complex tasks or some degree of automation. Both interfaces are available in DAV³E; however, as statistical methods tend to have many different options to tune their behavior, it is often easier to see a list of available options in a GUI instead of memorizing or researching different parameters. Additionally, research often needs to explore its datasets looking for distinct features, a task for which static, animated, or interactive plots, an essential part of the GUI, are very helpful. For an example of the command line interface, refer to the supplement.

The GUI is based on the GUI Layout Toolbox (Tordoff and Sampson, 2014), which enables layout-based GUI programming in MATLAB. MATLAB GUIs are based on Java and the JIDE framework (jidesoft). Not all the framework's elements and functionality are currently implemented, but can relatively easily be added directly or retrofitted with the `findobj` function (Altman, 2012). For DAV³E, the standard MATLAB GUI components have been extended with `PropertyTables`, `JTrees`, and `JTables`.

The main GUI (Fig. 3) consists of a frame providing a menu bar (1), toolbar (2), load and save buttons (3), a list of all loaded modules (4), a table showing the currently active sensors (5), a drop-down menu to select the current sensor set (6), and a button to compute features from the current configuration (7). GUI modules (8) can communicate with the main GUI via defined interfaces and are otherwise decoupled from the main GUI and each other. A module can be added with a plug-in system similar to the one described before, and performs one or more specific functions by read-

ing or manipulating the data in the underlying structure of measurements, clusters, and sensors.

3 Example datasets

In Sects. 4 and 5, various modules and features of DAV³E are shown for three example datasets to facilitate easier understanding of the descriptions. The datasets were chosen from different areas to demonstrate why a high versatility of the toolbox is required.

3.1 Hill-Valley dataset

This dataset is publicly available (Graham and Oppacher, 2018) from the UCI machine learning repository (Lichman, 2013). It consists of a training set with 606 observations, i.e., cycles, with 100 data points each, and a test set with the same dimensions. The data in each cycle show either a hill or a valley when plotted, and the classification task is to discriminate hill cycles from valley cycles. The dataset is provided both with and without noise. For this demonstration, only the noisy variant is used. Before the data are imported into DAV³E it is first sorted by the class information, which allows easier handling afterwards.

3.2 Gas sensor dataset

In the gas sensor dataset (Bastuck and Fricke, 2018), the commercial gas sensor GGS1330 by UST (UmweltSensorTechnik GmbH, Germany) was exposed to different concentrations of different gases in synthetic air at constant relative humidity: carbon monoxide, CO (100, 200, 300 ppm), ammonia, NH₃ (75, 150, 225 ppm), nitrogen dioxide, NO₂ (10, 20, 30 ppm), and methane, CH₄ (500, 1000, 1500 ppm). It was operated with a triangle-shaped TCO cycle, rising linearly from 200 to 400 °C in 20 s, and decreasing back to 200 °C in another 20 s. Each gas exposure lasted for 15 min and contained at least 20 complete sensor temperature cycles, with a total of 190 observations.

3.3 Condition monitoring dataset

The condition monitoring dataset (Helwig et al., 2018) is taken from Helwig et al. (2015), where more detailed information can be found. Several sensors for monitoring pressure, vibration, electrical power, and other variables have been recorded from a hydraulic machine with a 1 min working cycle. Some sensors were sampled with 1 Hz, some with 10 Hz, and some with 100 Hz, resulting in approx. 50 000 sensor values per cycle. Faults with different grades of severity like leaks, valve malfunction, and others in all possible permutations were then simulated in the system. The aim is to classify the type of fault and quantify its severity. The total number of observations is 1260.

4 Modules, features, and plots

4.1 Data import

The first step in the evaluation process is to import experimental data. The button “import sensor” opens a Choose File dialog in which all data types that DAV³E can handle can be selected. Import routines are currently implemented for files with simple structures like CSV or MAT, as well as for more complex, proprietary formats stored as HDF5 (HDF5 Group, 2016), for instance. The expected format is always a data matrix in which each row corresponds to one cycle, i.e., observation. The columns consequently represent the sampling points, i.e., features. The import plug-in system provides an easy means of adding data types or even import from databases.

Importing the first sensor automatically creates a new measurement. When a second sensor is to be imported, it can either be added in parallel to an already existing sensor, i.e., in the same measurement, or to a new measurement, i.e., in series. Parallel sensors add features, and serial sensors add observations to the dataset. To keep a good overview, especially with many sensors, the table can be filtered by measurement, cluster, sensor, type, and selection, with the list boxes above the table.

In the import module, virtual sensors can be computed from real sensors, currently only with predefined (plug-in-enabled) functions which are determined upon import by the data type. Each sensor can serve as another sensor’s abscissa. While the default, virtual time, is often useful, there are cases, i.e., impedance spectroscopy, where another abscissa, i.e., the logarithmic frequency, is commonly used instead of the time.

For the Hill-Valley dataset (Fig. 4), the most sensible abscissa is the sensor “virtual datapoints”. This information is only implicitly provided in the raw dataset by its matrix structure, so it makes sense to provide it as an explicit, virtual sensor for further evaluation. Two measurements are created, “training” and “testing”, so that the number of observations in the dataset is increased. Clusters and sensors must then have identical names in both measurements because DAV³E will automatically combine data of sensors with the same name only.

4.2 Preprocessing

First and foremost, the preprocessing module provides a first look on the data from two different perspectives. The upper plot shows “quasistatic” signals generated from points selected in the bottom plot. Quasistatic refers here to the fact that by always taking the sensor signal from the same point in the cycle, the resulting signal behaves like a statically operated sensor with a sampling period of one cycle length. The bottom plot, in turn, shows distinct cycles (observations) which are selected in the upper plot. Selectors in both plots

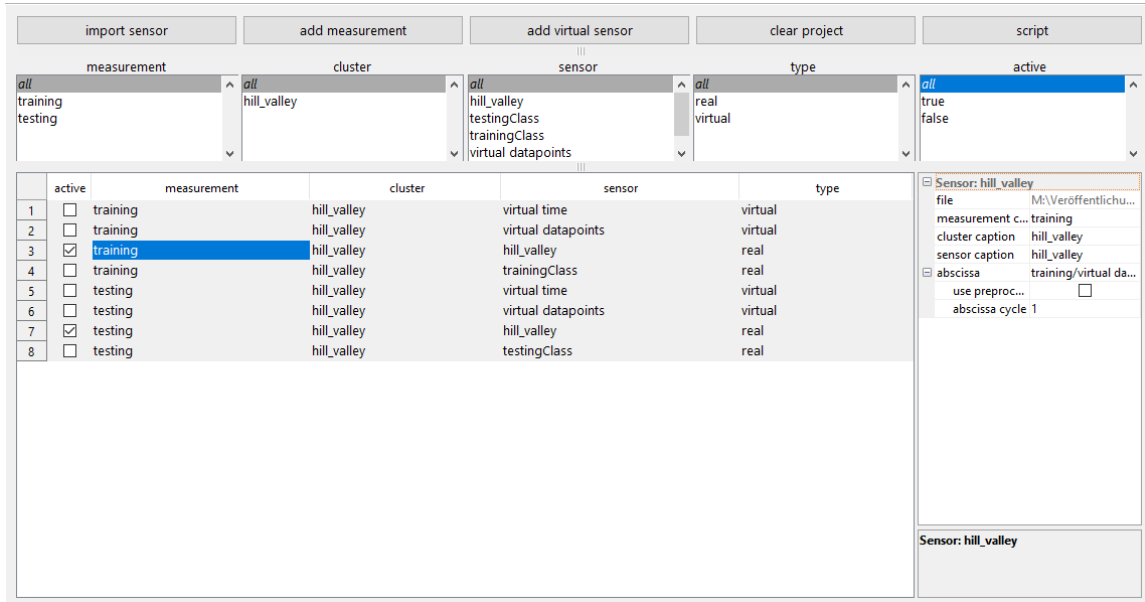


Figure 4. Data import module with two measurements. All available sensors are listed in the table which can be filtered with the list boxes above. Properties of the currently selected measurement, cluster, and sensor can be edited in the PropertyTable on the right.

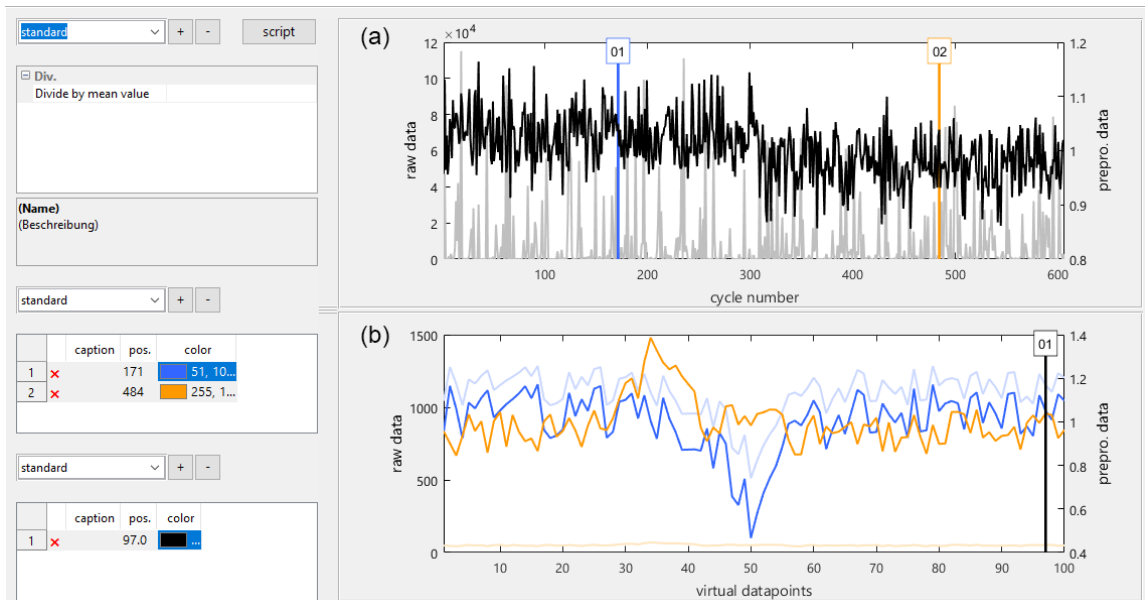


Figure 5. Preprocessing module showing the quasistatic (a) and cyclic (b) view of the preprocessed data, with pale raw data in the background for comparison.

can be added or deleted and moved either with the mouse or the keyboard, or by typing the desired position. They are color-coded so that a clear, visual link between the selector and the graph is established. An arbitrary number of sets can be created for the selectors in the cycle plot which generate the quasistatic signal. These sets can later be chosen for each

sensor separately, which is very useful if sensors with different cycle shapes are evaluated in one dataset.

Additionally, an arbitrary number of preprocessing functions can be applied to the raw data in this module. A preprocessing function is always applied to the output data of the previous preprocessing function, which can be useful in

many cases, e.g., adding an offset to data to make it nonnegative before applying the logarithm. In the example in Fig. 5, only one preprocessing function is applied. It divides each cycle by its mean value. The original data are always shown pale in the background for the user to see the impact of the current preprocessing chain. As before, several preprocessing sets can be created and assigned to sensors separately. This feature not only allows an optimal treatment of many different sensors, but also enables the user to quickly change between preprocessing methods to assess their impact on the final result.

For the Hill-Valley dataset, it is obvious that the chosen preprocessing highlights differences between the classes. Valley data (from 1 to 307 in the upper plot, blue in the lower plot) tend to higher values at the end of the cycle (selected in the lower plot) than hill data (from 308 to 606 in the upper plot, orange in the lower plot). Similar differences can be seen for the beginning of the cycles, but not for the middle (not shown). In comparison to the raw data (pale in the background), this preprocessing step already provides clear differences between both classes.

4.3 Time correction

Depending on data source and hardware, a sensor signal can have a wrong offset compared to the start of the measurement, or an incorrect sampling rate. A simple example is data loaded from a CSV file with nothing but sensor data: in this case neither offset nor sample rate can be automatically determined and both are set to their defaults (0 s and 1 Hz). Failing to adjust these values can lead to erroneous results especially in combination with other sensors. The time correction module plots the quasistatic representation of one sensor of each cluster in a common graph, so that the user can immediately check whether the adjusted offset and sampling rate are correct.

4.4 Select relevant cycles

Especially in characterization measurements, often only few cycles are of interest, e.g., the cycles during which the sensor was exposed to gas or during which a certain fault was observed in a machine. While it would of course be possible to record data only during these times, it is often more convenient from an automation point of view to acquire data during the whole period of measurement. This can also be helpful to identify unexpected events in the data or drift over time, for instance. Nevertheless, usually only parts of the data are interesting for the evaluation.

This module enables easy and efficient selection and annotation of cycles of interest. The graph shows the previously determined quasistatic view for the chosen sensor. Ranges can be created, deleted, and moved by mouse or keyboard directly in the plot. Annotation means that independent states can be assigned to each range, e.g., the concentration of all

test gases during each range, or, for the Hill-Valley data, whether hills or valleys are represented in this range. These annotations can later be used to create various target vectors for the model training.

The position of the ranges is internally stored as a timestamp. This allows for the correct cycle numbers to be dynamically determined for each sensor independent of its offset, sample rate, and cycle length. Thus, no resampling is necessary, which can be very resource-intensive, especially for large datasets. If two sensors with different cycle lengths are combined, resampling on a feature basis is necessary to equalize the number of observations gained from each sensor. Preliminary work to find the best resampling approach for this case has been described in Bastuck et al. (2016b).

The selection is very easy for the Hill-Valley data (Fig. 6) because the data were sorted before the import and there are no faulty or irrelevant cycles in this dataset.

4.5 Groupings

The grouping module is closely related to the select relevant cycles module as it uses the previously determined cycle ranges. A grouping is a vector which assigns one and only one class to each cycle range. This vector can then be expanded to a target vector that assigns a class to each cycle. The elements of the vector must be numeric if regression analysis is to be performed, but can be arbitrary strings or numbers for classification problems. Colors can be assigned to each group which are displayed in the quasistatic plot at the top, which can be helpful to discover errors in the grouping vector.

Like the range selection before, the grouping vector is trivial for the Hill-Valley dataset (Fig. 7) as for most binary classification tasks. There are usually many more options for multi-class problems, e.g., different gases with different concentrations, so that one grouping could discriminate between gases independent of concentration, while another could quantify the concentration of one gas independent of all other gases. This is discussed in detail in Sect. 5.

4.6 Feature extraction

The last step before model training is feature extraction from the cyclic data. This is a type of dimensionality reduction, considering that the number of features is reduced from, potentially, several thousand data points per cycle (depending on the sample rate) to a few features, e.g., describing the general shape. Adjacent points in a cycle are typically highly correlated, which can be problematic for many methods employed in machine learning (Næs and Mevik, 2001).

A feature is computed from the cycle with a mathematical function; features that are implemented are, for example, mean, slope, minimum and maximum values, and standard deviation. For every function, an individual set of ranges can be defined directly in the cyclic sensor signal. Thus, mean-

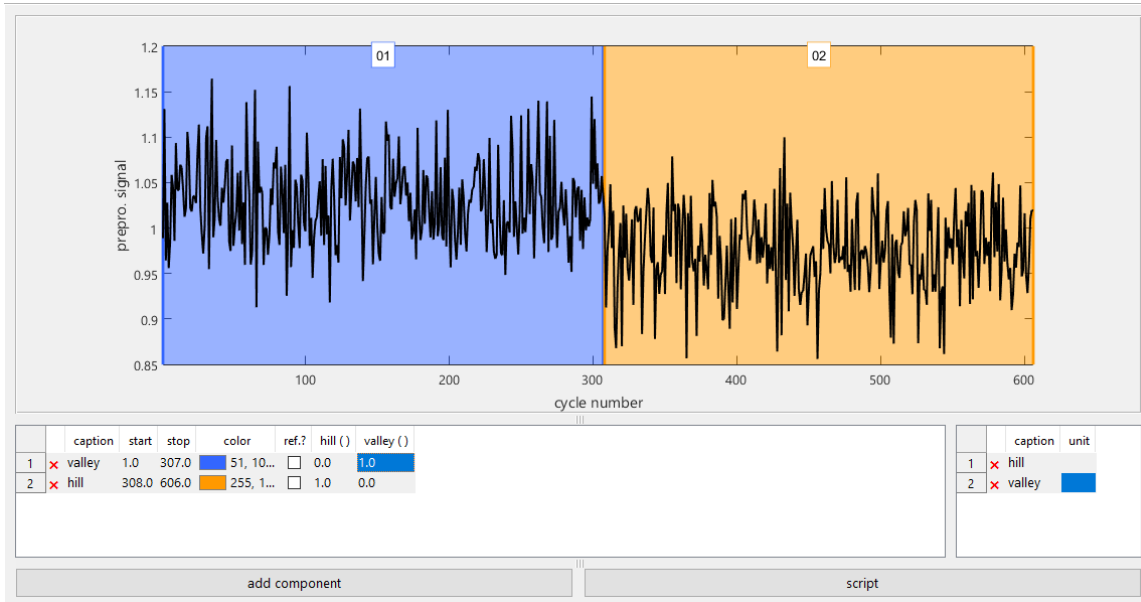


Figure 6. Module to select cycle ranges which pool cycles with the same underlying conditions.

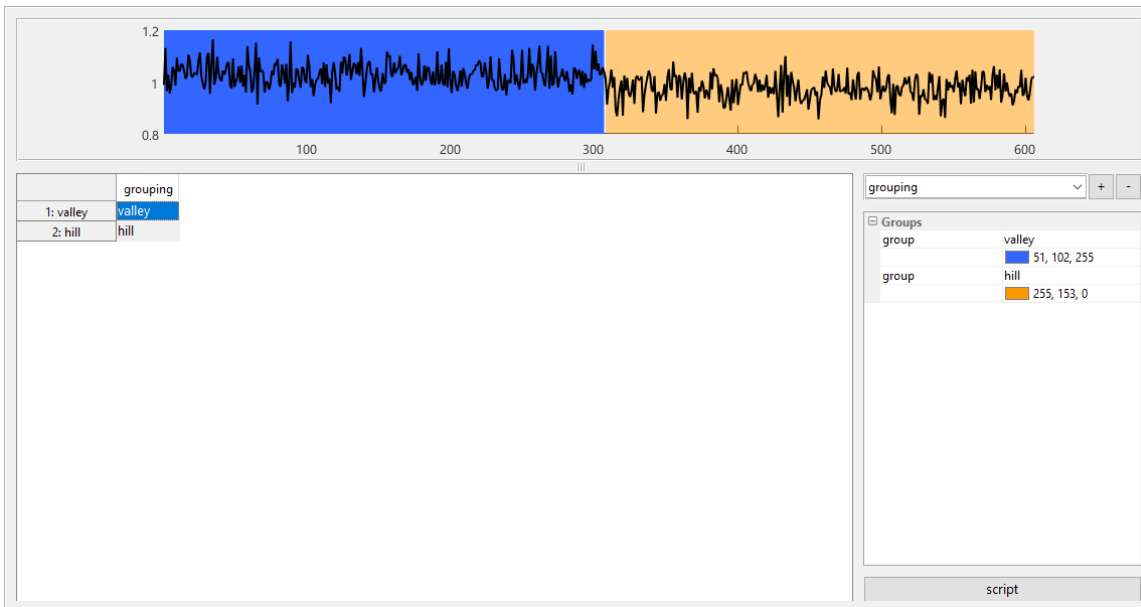


Figure 7. Grouping module which is used to assign classes to the previously selected ranges. An arbitrary number of grouping vectors can be created which can later be selected as target vectors during model training. The plot shows a graphical representation of the currently selected grouping to highlight errors and to show the structure of the data at one glance.

ingful ranges can be selected for the respective function, e.g., long plateaus for the mean and slopes for the slope function. The ranges are defined in the bottom plot, which shows a representation of several cycles computed as the mean value of all cycles in a group of the current grouping vector. The top plot shows a preview of the current feature function applied

to these mean cycles with the same colors as the examples shown in the lower plot. This kind of plot gives a first impression of the discriminating power of the selected features by visually comparing the spread between ranges, i.e., colors, that should be similar or dissimilar, respectively.

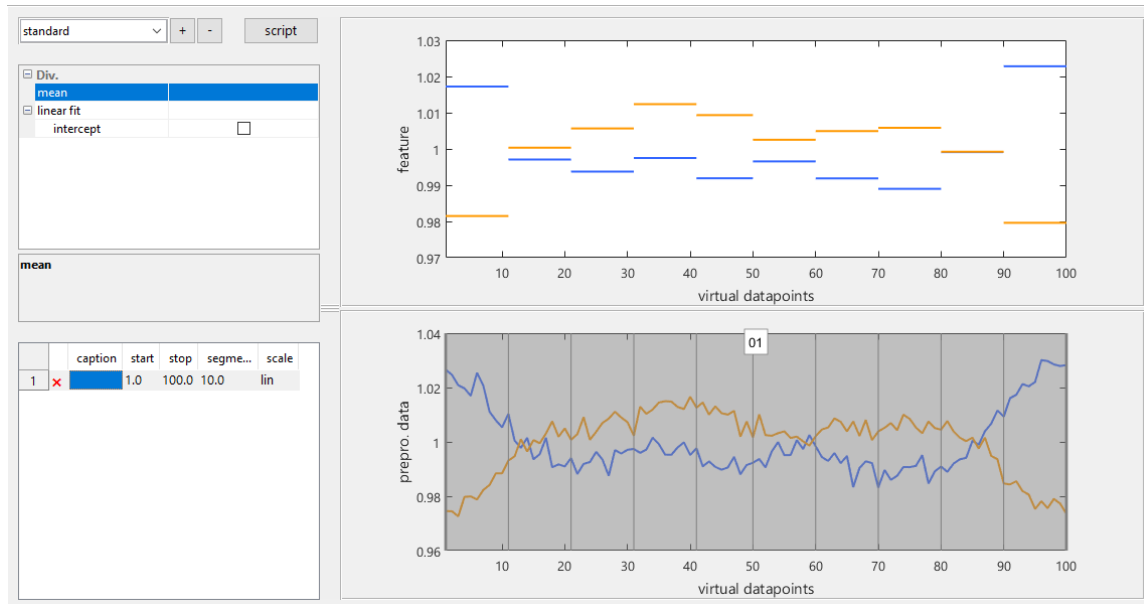


Figure 8. The feature extraction module displays a representation of the average cycle shape for each group in the grouping vector. Different mathematical functions are available to summarize the points in a selected range in the cycle as one or a few values. A feature preview, here for the mean in 10 parts of the cycle, computed from the averaged cycles for speed, is shown in the top plot.

For the Hill-Valley dataset (Fig. 8), the cycle is divided into 10 equal parts for which both the mean and slope are computed; i.e., the number of features is reduced from 100 to 20. The cyclic plot (bottom) shows a significant difference between the average cycles for both classes, and the feature preview (top) confirms that the shape differences are captured by the mean feature, especially in the outermost parts as already indicated from the preprocessing; cf. Fig. 6. Distinct differences between both classes are also observed for the slope feature (not shown).

4.7 Model

The model module brings all previously defined parts of the evaluation together. Features can be selected or deselected from a list of all computed features, e.g., to observe the influence of one specific feature or feature group on the final result. The target vector for the training is defined by choosing one of the previously defined groupings. Each group's role can be determined separately, so it is possible to use a few groups for training and predict the others for model validation, or ignore groups entirely. Alternatively or additionally, a certain percentage of randomly chosen observations out of each group can be held back for testing the validated model. The model can also equalize the number of observations in each group by randomly deleting observations from larger groups. This step can significantly increase the model performance especially for small groups which would otherwise

have only a small or even negligible weight in the optimization compared to large groups.

After the training data have been defined, the model-building process follows a “chain” approach very similar to the preprocessing sequence described before. One or several preprocessing steps for both features and target vectors can be applied. Note that these preprocessing functions act on the individual features and are to be distinguished from the raw data preprocessing. A typical example of feature preprocessing is rescaling the data for variance-based algorithms like PCA (van den Berg et al., 2006; Risvik, 2007), or taking the logarithm of both features and target values to model a power law, e.g., between gas sensor response and concentration (Yamazoe and Shimano, 2008), with the linear PLSR. Afterwards, dimensionality reduction algorithms like LDA or PCA can be applied, followed by a classifier like kNN, DA, or LR. The whole model can be validated using k -fold cross-validation or leave-one-out cross-validation. All parameters of these algorithms can be adjusted directly in the GUI, and a click on “train” performs the training and validation as defined.

The results of the validation are given as classification error in percent or, for regression analysis, RMSE (root mean squared error). Additionally, many algorithms provide plots like histograms, scatter plots, or territorial plots to visualize the classification performance or areas, respectively, of the classifier in a 2-D plane. An arbitrary number of independent models can be created.

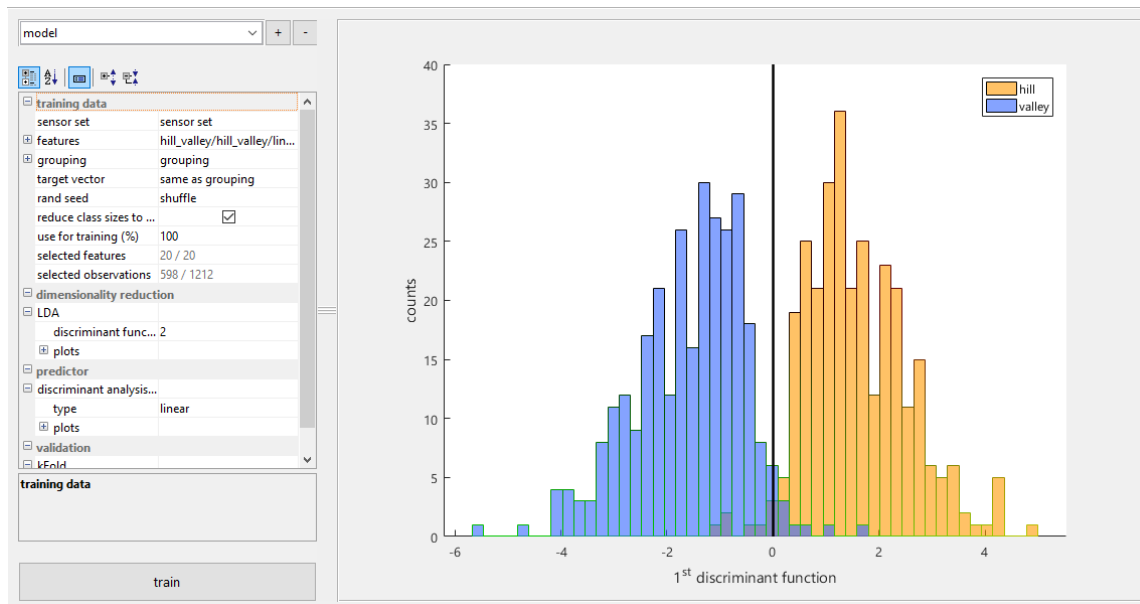


Figure 9. The model module provides the possibility to exclude features or observations from the training data to see their influence on the model. In this image, the model consists of a 2-D LDA with a linear DA classifier which is validated with 10-fold cross-validation. The data distribution resulting from the dimensionality reduction is shown, with class information, as a histogram.

For the demonstration with the Hill-Valley dataset, a 1-D LDA is used as model (Fig. 9). The training data and classification threshold is shown in Fig. 9. Validation is done using 10-fold cross-validation (CV) and achieves a classification error of 2.5 % with all 20 features. The error increases to 5.4 % when only the 10 mean value features are used. Further inspection shows that features at the beginning and end of the cycle are the most important, so an error of 2.7 % is achieved with only eight features, i.e., means and slopes from the two outermost parts.

4.8 Model hierarchies

Classification results can often be improved with more than one model for a certain classification or quantification task (Darmastuti et al., 2015; Schütze et al., 2004). Each model can specialize or focus on a certain aspect of the task, e.g., classifying the prevalent gas with a first model and then selecting a second, specialized quantification model for this gas.

This module provides an easy interface to build such hierarchies from the previously defined models. The sensor set from which input data are taken can be defined; the data is subsequently treated according to the options for the training data given in each model separately. The previous training of the models can be used directly to predict the new data. Alternatively, the models can first be trained within the hierarchical context, in which every model splits the data accord-

ing to the known classes and forwards the respective parts to the next model.

The hierarchy in Fig. 10 is an example of a gas classification and quantification task as hierarchical classification is not applicable to the Hill-Valley dataset. The behavior is often influenced by humidity, which is why the first model tries to estimate the level of humidity from the sensor data. It then forwards the data to a model specialized in gas classification in either low humidity or high humidity conditions. If benzene (C_6H_6) is detected, a third model is invoked, specialized in benzene quantification under either low or high humidity conditions.

4.9 Hyperparameter optimization

Finding optimal parameters for the selected model algorithms can be a complex and time-consuming task. These parameters are also called “hyperparameters” to distinguish them from the parameters that are computed by, e.g., LDA for the dimensionality reduction.

The grid search module (Fig. 11) provides an interface in which a list of values can be given as valid MATLAB expressions for all available parameters in a model. DAV³E will then automatically perform an exhaustive search with all possible combinations of all parameter values, recording the validated model error for all combinations. After the search, the best parameter value combination is determined, and the influence of each parameter visualized.

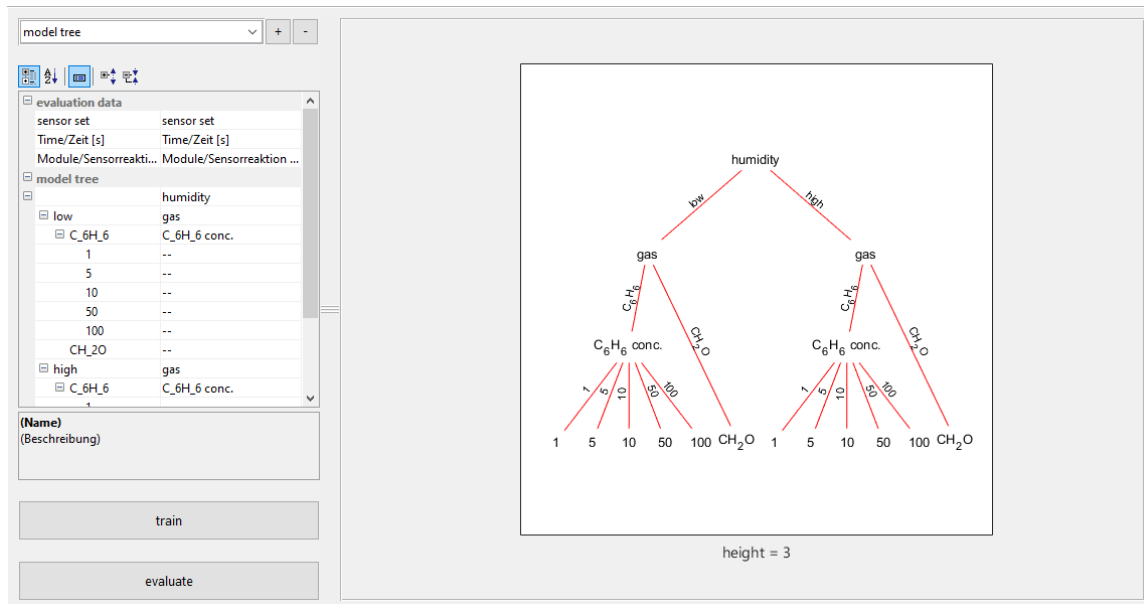


Figure 10. The hierarchical model module allows for the combination of previously defined models. They can be trained with the whole dataset or only with data relevant to the model, which can lead to specialization and better results. The hierarchy is shown as a directed graph with data flow along the edges and models as nodes.

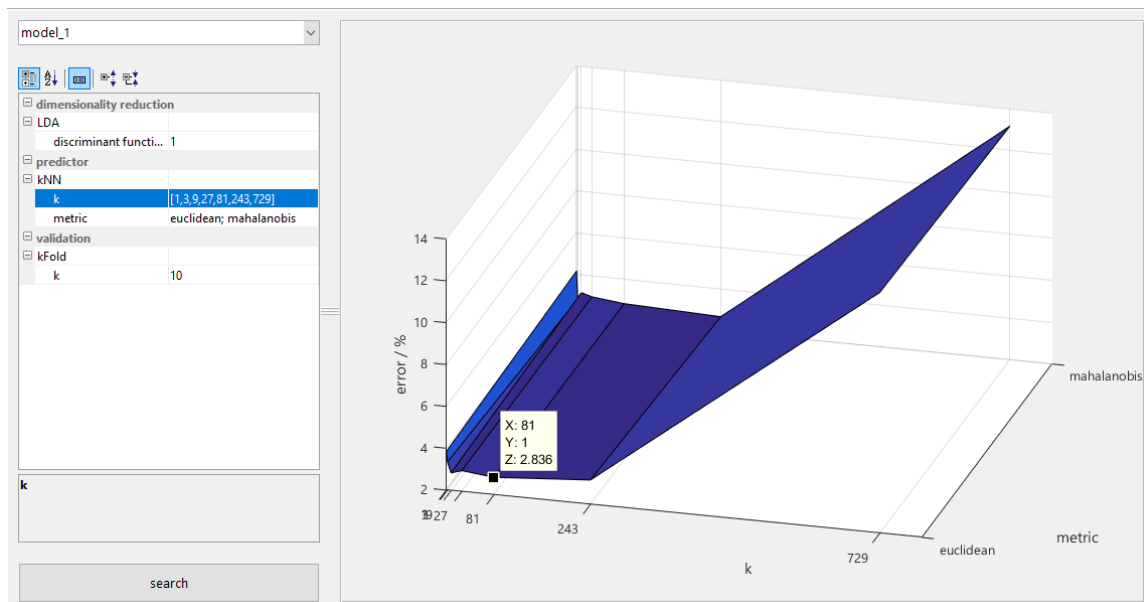


Figure 11. The grid search module lists all parameters of a particular model and accepts valid MATLAB expressions as their values, so lists of values can be given for each parameter. The automated grid search evaluates the model for all permutations of parameter values and plots the model error dependent on parameter values, highlighting the optimum solution.

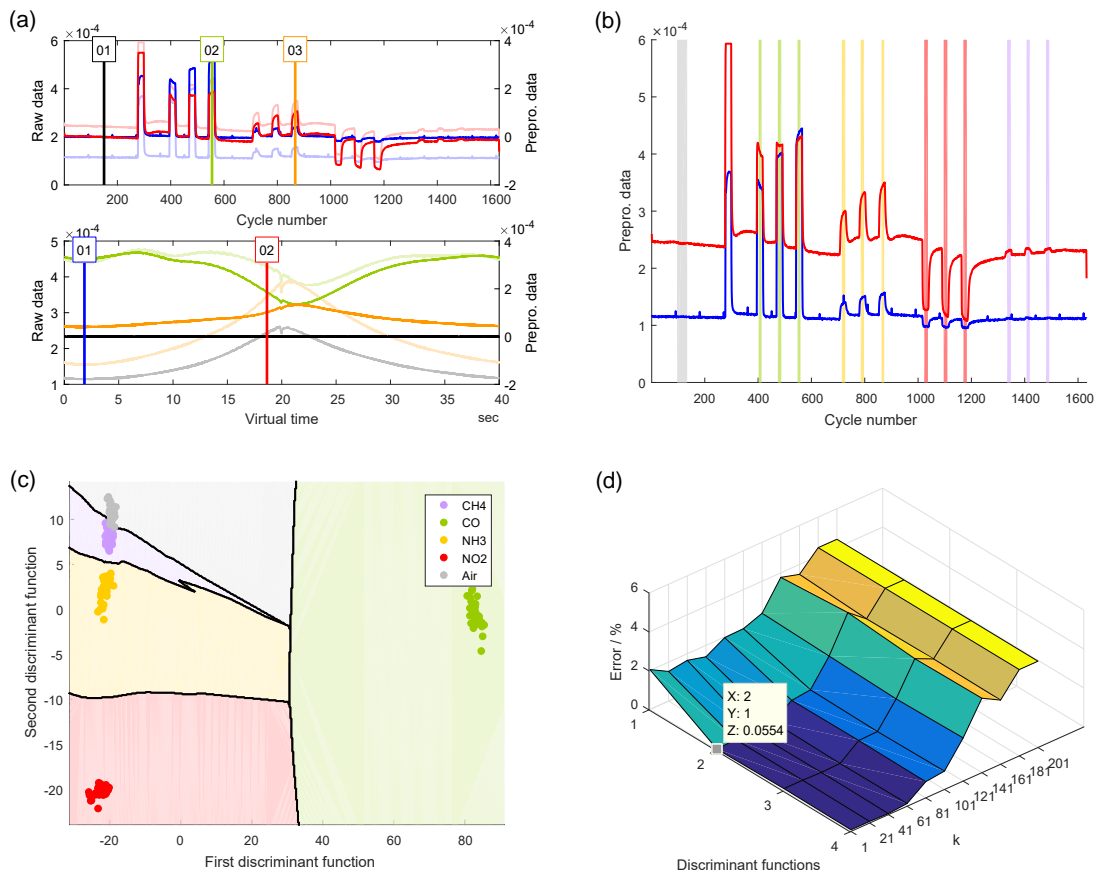


Figure 12. (a) Quasistatic and cyclic signal from the UST GGS1330 gas sensor. The cycles shown are in pure air (black), CO (green), and NH₃ (orange), while the quasistatic signals show the sensor reaction at low (blue) and high (red) temperature. (b) Graphical representation of a grouping for the discrimination of five classes, i.e., four gases and air. (c) Territorial plot of the resulting discrimination with the kNN classifier. (d) A grid search evaluating the model for different numbers of discriminant functions and k values of the kNN classifier.

For the Hill-Valley dataset, an exhaustive search has been performed for the parameters of a kNN classifier, i.e., the number of neighbors k (tested values: 1, 3, 9, 27, 81, 243, 729) and the metric (Euclidean or Mahalanobis distance). The search shows that $k = 1$ and $k = 729$ (which is actually reduced to 605, the maximum possible number of neighbors in this dataset) lead to increased error rates. This is understandable, as the result is easily negatively influenced by outliers for $k = 1$, and each class has approximately 300 points; therefore, for $k = 605$ the larger class will always win, which leads to many misclassifications. The distance metric's influence is almost negligible, with the Euclidean giving the optimal result of 2.8 % at $k = 81$ for all tested parameter combinations.

5 Example projects

In this section, different features and aspects of DAV³E are presented for two real datasets from our research activities. All graphs shown are exported, without post-processing, directly from DAV³E. The same graphs, with all parameters, can also be automatically exported to a report document in Microsoft Word or PDF format.

5.1 Gas sensor dataset

The project described in this section is based on the dataset from Sect. 3.2. A cyclically driven gas sensor was exposed to four different gases in each of three different concentrations. Figure 12a shows the plots from the preprocessing module, i.e., quasistatic and cyclic plot. The black cycle was subtracted from all cycles, which highlights the differences in the signal shape arising from exposure to different gases. Figure 12b is a graphical representation of a grouping that

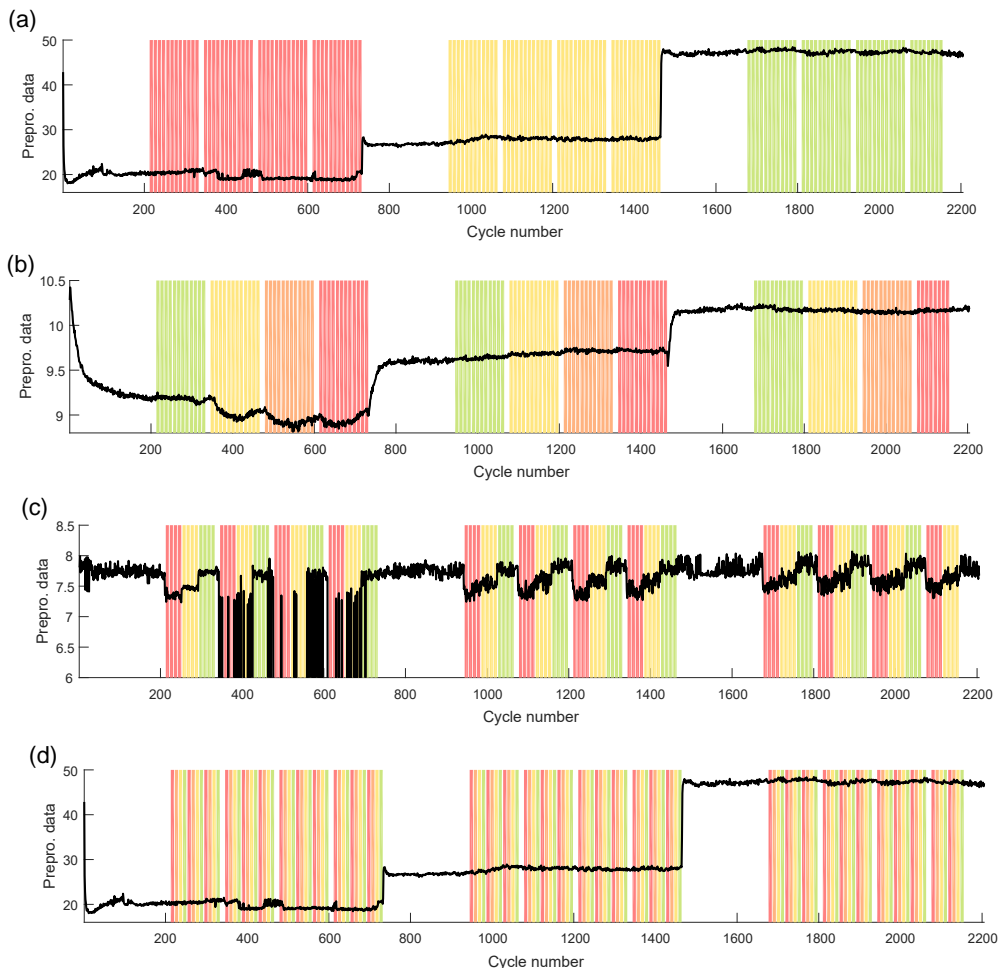


Figure 13. Graphical representation of four different grouping vectors to discriminate between the severity of four different faults. Panel (a) shows three different cooler faults and the resulting cooling efficiency as a signal, and in panel (b), the pressure of the hydraulic accumulator is changed, which can be observed, e.g., in a flow sensor signal. Panel (c) shows several grades of pump leakage, evident in a different flow sensor. In (d), different grades of valve faults were experimentally simulated, which cannot be observed directly in any one individual sensor signal.

discriminates between gas types, including air selected at the beginning, independent of their concentration. Other possible groupings are concentrations of one of the gases for a quantification task. These groupings can either ignore other gases, or include them explicitly as zero concentration to achieve selective quantification of a certain gas. In this dataset, the ranges can be loaded directly from the configuration file for the measurement. However, they were then shortened (using a batch script for range manipulation implemented in DAV³E) to account for fluidic time constants in the gas mixing system, resulting in approximately 10 cycles per gas exposure.

A total of 11 features are defined: the mean value of the whole cycle, and the slopes of 10 sections of equal length in the cycle.

Figure 12c is the territorial plot resulting from a 2-D LDA and a kNN classifier with Euclidean distance and $k = 5$. Using 10-fold CV reveals a classification error of about 2.0 %, and the resulting confusion matrix identifies three points that are confused between air (gray) and methane (violet), which can already be anticipated from the plot. All other gases are identified perfectly, with distances from the air group that roughly correlate with the sensor response observed for the gas in the quasistatic plot. In contrast to all other gases, CO is a strong reduction agent and exerts more influence on the surface oxygen coverage during the cycle (Baur et al., 2015; Schultealbert et al., 2017), which leads to significant changes in the cycle shape and, thus, a shift in two dimensions instead of only one. Note that this effect is actually dominant as the CO shift is along the first discriminant axis.

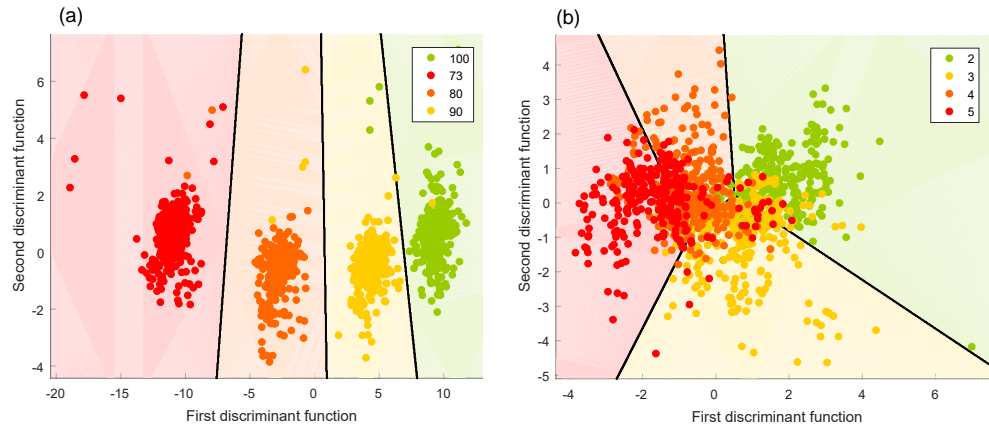


Figure 14. Territorial plots of the discrimination of fault severity for (a) a valve and (b) a hydraulic accumulator.

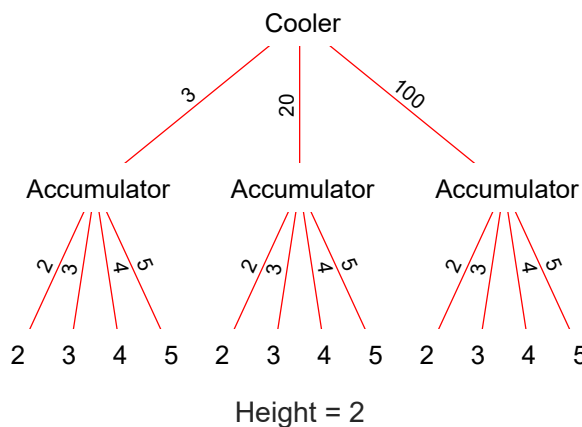


Figure 15. Graph of a hierarchical model which achieves better accuracy when predicting the hydraulic accumulator fault by training specialized models for different cooling efficiencies.

In Fig. 12d, the model was evaluated for different numbers of discriminant functions and different k 's for the kNN classifier. It shows that a model with only one discriminant function (DF) has a large error, which can also be understood from the territorial plot due to the significantly different effect of CO. The optimum is at two DFs and $k = 1$. For increasing k , the error increases only slightly up to 81, which is the first time that k is greater than the sum of points in two groups. For higher k , the error increases rapidly. This is because, for equally sized classes, the correct class cannot win the decision since it is missing one point (the one under consideration) and, thus, the nearest wrong class will win.

5.2 Condition monitoring dataset

The project described in this section is based on the dataset from Sect. 3.3. A hydraulic system with a constant work-

ing cycle is monitored by 17 sensors with different sampling rates. Simulated faults and their severity are to be classified and quantified.

Figure 13 is a graphical representation of four different groupings, which are the grades of severity of four different faults, where red denotes severe, and green denotes a good condition. Panel (a) shows three grades of a cooler fault with the cooling efficiency signal which is obviously strongly influenced. As a matter of fact, the cooler efficiency has a strong influence on all 17 sensor signals and is thus a strong interfering signal that the model must ignore when other faults are to be detected. In panel (b), the pressure in the hydraulic accumulator is changed, which is observed, for example, in the signal of a flow sensor. A pump leakage is simulated in panel (c) and can be detected, amongst others, by a different flow sensor. A faulty valve is not immediately observable from any individual sensor (panel d).

For this demonstration, one feature, the mean value of the cycle, is defined per sensor, which results in a total of 17 features. The power of statistical models is shown by the fact that the valve fault, which cannot be seen in any individual sensor, can be detected almost perfectly when all features are combined (Fig. 14a; 2-D LDA, DA classifier, 0.9 % error with 10-fold CV). On the other hand, faults of the hydraulic accumulator are superimposed by cooler faults, resulting in a classification error of 35 % (Fig. 14b).

This effect can be mitigated using a hierarchical approach (Fig. 15), whereby a model first determines the severity of the cooler fault, and then forwards the data to specially trained models for detection of the accumulator fault severity at the determined cooler fault. This reduces the error from 35 % to 4 %, which improves the best result from the original paper (Helwig et al., 2015) by 6 percent points with three fewer features.

The severity of a fault and the concentration of a gas, as well as many other variables, are continuous instead of categorical. Classification methods were used here to be able

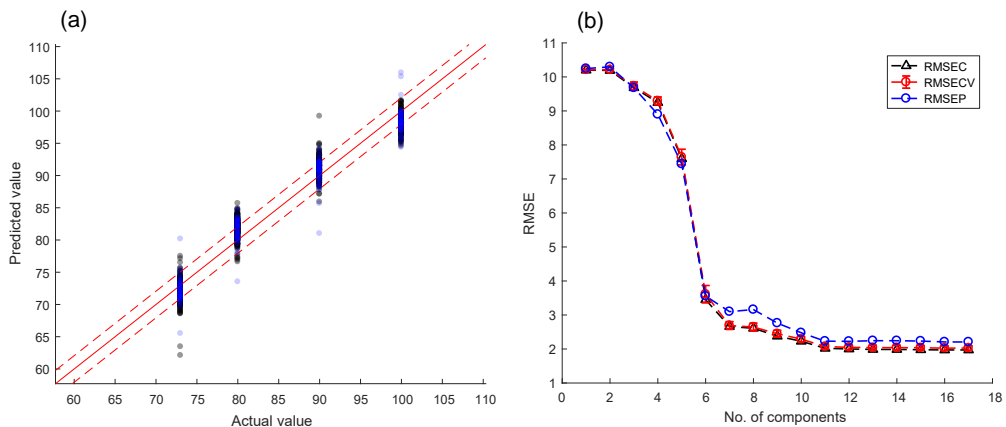


Figure 16. (a) PLSR model of the valve fault with an RMSE of 2 (dashed lines), where the optimal number of components was determined with the error/component graph in (b).

to compare the results to the original paper (Helwig et al., 2015), but in general, regression methods should be used for quantification of continuous variables instead. PLSR, one of the implemented regression methods, is demonstrated in Fig. 16a for quantification of the valve fault severity. The model was built with 11 components and 80 % of the dataset. The optimal number of components can be determined with the plot in Fig. 16b, which shows the RMSEC (RMSE of calibration, black) for the training data, the RMSECV (RMSE of cross-validation, red) of a 10-fold cross-validation, and the RMSEP (RMSE of prediction, blue) for data which have not been used in training or validation. RMSEC and RMSECV are both close to 2.0 %, and the RMSEP is slightly higher with 2.2 %, which indicates that the model is able to predict previously unknown data reliably. Note that the RMSEs are given in percent because the target values are given in percent of the original valve functionality; 100 % means perfect function, whereas 73 % is close to complete failure. Hence, an RMSE of 2 % still allows an early detection of a decline of the valve's performance.

6 Conclusions

We have presented DAV³E, our MATLAB-based toolbox with GUI for building and evaluating statistical models from cyclic sensor data. Especially the feature extraction from cyclic or, more generally, time series sensor data, which can be time-consuming and hard to formalize, is lacking in current machine learning software. For a seamless workflow, DAV³E is not limited to feature extraction, but also implements many algorithms for dimensionality reduction, classification, regression, and validation, which can be extended through a simple plug-in system. Feature extraction and many other steps feature interactive plots since data visualization is becoming more and more important with the ever-increasing size of datasets. We have demonstrated sev-

eral aspects of the software for three example datasets and how DAV³E was used to arrive from the raw data of many sensors to a set of statistical models for, e.g., gas classification or fault severity prediction. Many more examples can be found in our recent publications (Bastuck et al., 2016a, 2017; Leidinger et al., 2016; Sauerwald et al., 2017).

Several new functions are planned for the future, including the fusion of sensors with different cycle lengths, online prediction, and an improved grid search to test different algorithms instead of only different parameters for one algorithm.

An executable version of DAV³E can be found at <http://www.lmt.uni-saarland.de/dave>. The source code is available on request.

Data availability. The “Hill-Valley Data Set” (Graham and Opipacher, 2008) and the dataset “Condition monitoring of hydraulic systems” (Helwig et al., 2018) are available on the UCI machine learning repository (Lichman, 2013). The dataset “Temperature-modulated gas sensor signal” is available in Bastuck and Fricke, 2018.

Supplement. The supplement related to this article is available online at: <https://doi.org/10.5194/jsss-7-489-2018-supplement>.

Author contributions. MB developed and implemented the prototype DAV³E is based on. MB and TB improved upon this prototype with new ideas, concepts, and implementations. MB wrote the manuscript, and TB and AS contributed with substantial revisions.

Competing interests. Andreas Schütze is a member of the editorial board of the journal.

Acknowledgements. The authors would like to thank Nikolai Helwig and Thomas Fricke for kindly providing the condition monitoring data and the gas sensor data, respectively, Tizian Schneider for recommending the Hill-Valley dataset, and the UCI machine learning repository for providing a platform for the publication of machine learning datasets.

Edited by: Michele Penza

Reviewed by: two anonymous referees

References

Abdi, H.: Partial least squares regression and projection on latent structure regression, *WIREs Comput. Stat.*, 2, 97–106, <https://doi.org/10.1002/wics.051>, 2010.

Altman, Y. M.: *Undocumented Secrets of MATLAB-Java Programming*, CRC Press, 2012.

Andersson, M., Pearce, R., and Spetz, A. L.: New generation SiC based field effect transistor gas sensors, *Sensor. Actuat.-B Chem.*, 179, 95–106, <https://doi.org/10.1016/j.snb.2012.12.059>, 2013.

Apetrei, C., Rodríguez-Méndez, M. L., Parra, V., Gutierrez, F., and De Saja, J. A.: Array of voltammetric sensors for the discrimination of bitter solutions, *Sensor. Actuat.-B Chem.*, 103, 145–152, <https://doi.org/10.1016/j.snb.2004.04.047>, 2004.

Apetrei, C., Apetrei, I. M., Nevares, I., del Alamo, M., Parra, V., Rodríguez-Méndez, M. L., and De Saja, J. A.: Using an e-tongue based on voltammetric electrodes to discriminate among red wines aged in oak barrels or aged using alternative methods. Correlation between electrochemical signals and analytical parameters, *Electrochim. Acta*, 52, 2588–2594, <https://doi.org/10.1016/j.electacta.2006.09.014>, 2007.

Bastuck, M. and Fricke, T.: Temperature-modulated gas sensor signal (Version 1.0.0), Data set, Zenodo, <https://doi.org/10.5281/zenodo.1411209>, 2018.

Bastuck, M., Puglisi, D., Huotari, J., Sauerwald, T., Lappalainen, J., Spetz, A. L., Andersson, M., Schütze, A., Lloyd Spetz, A., Andersson, M., and Schütze, A.: Exploring the selectivity of WO₃ with iridium catalyst in an ethanol/naphthalene mixture using multivariate statistics, *Thin Solid Films*, 618, 263–270, <https://doi.org/10.1016/j.tsf.2016.08.002>, 2016a.

Bastuck, M., Baur, T., and Schütze, A.: Fusing cyclic sensor data with different cycle length, 2016 IEEE International Conference on Multisensor Fusion and Integration for Intelligent Systems (MFI), IEEE, Baden-Baden, Germany, 19–21 September 2016, 72–77, 2016b.

Bastuck, M., Daut, C., and Schütze, A.: Signalkompensation mittels Gate-Potential bei gassensitiven Feldeffekttransistoren, in 13. Dresden Sensor-Symposium, 277–282, 2017.

Baur, T., Schütze, A., and Sauerwald, T.: Optimierung des temperaturzyklischen Betriebs von Halbleitergassensoren, *tm – Tech. Mess.*, 82, 187–195, <https://doi.org/10.1515/teme-2014-0007>, 2015.

Böhm, C., Berchtold, S., and Keim, D.: Searching in high-dimensional spaces: Index structures for improving the performance of multimedia databases, *ACM Comput. Surv.*, 33, 322–373, <https://doi.org/10.1145/502807.502809>, 2001.

Browne, M.: Cross-Validation Methods, *J. Math. Psychol.*, 44, 108–132, <https://doi.org/10.1006/jmps.1999.1279>, 2000.

Bur, C.: *Selectivity Enhancement of Gas Sensitive Field Effect Transistors by Dynamic Operation*, Linköping University Electronic Press/Shaker Verlag, 2015.

Cetó, X., Apetrei, C., Del Valle, M., and Rodríguez-Méndez, M. L.: Evaluation of red wines antioxidant capacity by means of a voltammetric e-tongue with an optimized sensor array, *Electrochim. Acta*, 120, 180–186, <https://doi.org/10.1016/j.electacta.2013.12.079>, 2014.

Chang, R. M., Kauffman, R. J., and Kwon, Y.: Understanding the paradigm shift to computational social science in the presence of big data, *Decis. Support Syst.*, 63, 67–80, <https://doi.org/10.1016/j.dss.2013.08.008>, 2014.

Darmastuti, Z., Bur, C., Lindqvist, N., Andersson, M., Schütze, A., and Lloyd Spetz, A.: Chemical Hierarchical methods to improve the performance of the SiC-FET as SO₂ sensors in flue gas desulphurization systems, *Sensor. Actuat.-B Chem.*, 206, 609–616, <https://doi.org/10.1016/j.snb.2014.09.113>, 2015.

Ding, H., Ge, H., and Liu, J.: High performance of gas identification by wavelet transform-based fast feature extraction from temperature modulated semiconductor gas sensors, *Sensor. Actuat.-B Chem.*, 107, 749–755, <https://doi.org/10.1016/j.snb.2004.12.009>, 2005.

Eicker, H.: Method and apparatus for determining the concentration of one gaseous component in a mixture of gases, US Pat. 4012692, 1977.

Geladi, P. and Kowalski, B. R.: Partial least-squares regression: a tutorial, *Anal. Chim. Acta*, 185, 1–17, [https://doi.org/10.1016/0003-2670\(86\)80028-9](https://doi.org/10.1016/0003-2670(86)80028-9), 1986.

Graham, L. and Oppacher, F.: Hill-Valley Data Set, UCI Machine Learning Repository, 2008, available at: <http://archive.ics.uci.edu/ml/datasets/hill-valley>, last access: 14 September 2018.

Gramm, A. and Schütze, A.: High performance solvent vapor identification with a two sensor array using temperature cycling and pattern classification, *Sensor. Actuat.-B Chem.*, 95, 58–65, [https://doi.org/10.1016/S0925-4005\(03\)00404-0](https://doi.org/10.1016/S0925-4005(03)00404-0), 2003.

Gutierrez-Osuna, R.: Pattern analysis for machine olfaction: A review, *IEEE Sens. J.*, 2, 189–202, <https://doi.org/10.1109/JSEN.2002.800688>, 2002.

Gutierrez-Osuna, R. and Nagle, H. T.: A method for evaluating data-preprocessing techniques for odor classification with an array of gas sensors, *IEEE T. Syst. Man Cy. B*, 29, 626–632, <https://doi.org/10.1109/3477.790446>, 1999.

Hastie, T., Tibshirani, R., and Friedman, J.: *The Elements of Statistical Learning*, Springer, 2009.

Hawkins, D. M.: The Problem of Overfitting, *J. Chem. Inf. Comput. Sci.*, 44, 1–12, <https://doi.org/10.1021/ci0342472>, 2004.

HDF5 Group: HDF5, available at: <https://www.hdfgroup.org/HDF5/>, last access: 13 February 2016.

Heilig, A., Bârsan, N., Weimar, U., Schweizer-Berberich, M., Gardner, J. W., and Göpel, W.: Gas identification by modulating temperatures of SnO₂-based thick film sensors, *Sensor. Actuat.-B Chem.*, 43, 45–51, [https://doi.org/10.1016/S0925-4005\(97\)00096-8](https://doi.org/10.1016/S0925-4005(97)00096-8), 1997.

Helwig, N., Schüler, M., Bur, C., Schütze, A., and Sauerwald, T.: Gas mixing apparatus for automated gas sensor characterization, *Meas. Sci. Technol.*, 25, 055903, <https://doi.org/10.1088/0957-0233/25/5/055903>, 2014.

Helwig, N., Pignanelli, E., and Schütze, A.: Condition monitoring of a complex hydraulic system using multivariate statisti-

tics, 2015 IEEE International Instrumentation and Measurement Technology Conference (I2MTC) Proceedings, 210–215, <https://doi.org/10.1109/I2MTC.2015.7151267>, 2015.

Helwig, N., Pignanelli, E., and Schütze, A.: Condition monitoring of hydraulic systems Data Set, UCI Machine Learning Repository, 2018, available at: <https://archive.ics.uci.edu/ml/datasets/Condition+monitoring+of+hydraulic+systems>, last access: 14 September 2018.

Huang, X. J., Choi, Y. K., Yun, K. S., and Yoon, E.: Oscillating behaviour of hazardous gas on tin oxide gas sensor: Fourier and wavelet transform analysis, *Sensor. Actuat.-B Chem.*, 115, 357–364, <https://doi.org/10.1016/j.snb.2005.09.022>, 2006.

James, G., Witten, D., Hastie, T., and Tibshirani, R.: An introduction to statistical learning: with applications in R, Springer, 2013.

Kitchin, R.: Big Data, new epistemologies and paradigm shifts, *Big Data Soc.*, 1, 1–12, <https://doi.org/10.1177/2053951714528481>, 2014.

Kohavi, R.: A Study of Cross-Validation and Bootstrap for Accuracy Estimation and Model Selection, *IJCAI'95 Proceedings of the 14th international joint conference on Artificial intelligence*, 14, 1137–1143, 1995.

Lee, A. P. and Reedy, B. J.: Temperature modulation in semiconductor gas sensing, *Sensor. Actuat.-B Chem.*, 60, 35–42, [https://doi.org/10.1016/S0925-4005\(99\)00241-5](https://doi.org/10.1016/S0925-4005(99)00241-5), 1999.

Leidinger, M., Huotari, J., Sauerwald, T., Lappalainen, J., and Schütze, A.: Selective detection of naphthalene with nanostructured WO₃ gas sensors prepared by pulsed laser deposition, *J. Sens. Sens. Syst.*, 5, 147–156, <https://doi.org/10.5194/jsss-5-147-2016>, 2016.

Lichman, M.: UCI Machine Learning Repository, Univ. California, Irvine, Sch. Inf. Comput. Sci., available at: <http://archive.ics.uci.edu/ml> (last access: 14 September 2018), 2013.

Marco, S. and Gutierrez-Galvez, A.: Signal and data processing for machine olfaction and chemical sensing: A review, *IEEE Sens. J.*, 12, 3189–3214, <https://doi.org/10.1109/JSEN.2012.2192920>, 2012.

Moreno-Barón, L., Cartas, R., Merkoçi, A., Alegret, S., Del Valle, M., Leija, L., Hernandez, P. R., and Muñoz, R.: Application of the wavelet transform coupled with artificial neural networks for quantification purposes in a voltammetric electronic tongue, *Sensor. Actuat.-B Chem.*, 113, 487–499, <https://doi.org/10.1016/j.snb.2005.03.063>, 2006.

Næs, T. and Mevik, B. H.: Understanding the collinearity problem in regression and discriminant analysis, *J. Chemom.*, 15, 413–426, <https://doi.org/10.1002/cem.676>, 2001.

Reimann, P. and Schütze, A.: Sensor Arrays, Virtual Multisensors, Data Fusion, and Gas Sensor Data Evaluation, in *Gas Sensing Fundamentals*, vol. 15, edited by: Kohl, C.-D. and Wagner, T., Springer Berlin Heidelberg, Berlin, Heidelberg, 67–107, 2014.

Risvik, H.: Principal component analysis (PCA) & NIPALS algorithm, 2007.

Sampson, D. and Tordoff, B.: GUI Layout Toolbox, available at: <https://de.mathworks.com/matlabcentral/fileexchange/47982-gui-layout-toolbox>, last access: 28 January 2017.

Sauerwald, T., Baur, T., Leidinger, M., Spinelle, L., Gerboles, M., and Schütze, A.: Laborübertragbare Kalibrierung von Sensoren für die Messung von Benzol, 13. Dresdner Sensor-Symposium, Dresden, Germany, 4–6 Dezember, 2017, 105–110, 2017.

Schultealbert, C., Baur, T., Schütze, A., Böttcher, S., and Sauerwald, T.: A novel approach towards calibrated measurement of trace gases using metal oxide semiconductor sensors, *Sensor. Actuat.-B Chem.*, 239, 390–396, <https://doi.org/10.1016/j.snb.2016.08.002>, 2017.

Schütze, A., Gramm, A., and Rühl, T.: Identification of organic solvents by a virtual multisensor system with hierarchical classification, *IEEE Sens. J.*, 4, 857–863, <https://doi.org/10.1109/JSEN.2004.833514>, 2004.

Smola, A. J. and Schölkopf, B.: A tutorial on support vector regression, *Stat. Comput.*, 14, 199–222, <https://doi.org/10.1023/B:STCO.0000035301.49549.88>, 2004.

van den Berg, R. a, Hoefsloot, H. C. J., Westerhuis, J. a, Smilde, A. K., and van der Werf, M. J.: Centering, scaling, and transformations: improving the biological information content of metabolomics data, *BMC Genomics*, 7, 142, <https://doi.org/10.1186/1471-2164-7-142>, 2006.

Winquist, F., Wide, P., and Lundström, I.: An electronic tongue based on voltammetry, *Anal. Chim. Acta*, 357, 21–31, [https://doi.org/10.1016/S0003-2670\(97\)00498-4](https://doi.org/10.1016/S0003-2670(97)00498-4), 1997.

Yamazoe, N. and Shimano, K.: Theory of power laws for semiconductor gas sensors, *Sensor. Actuat.-B Chem.*, 128, 566–573, <https://doi.org/10.1016/j.snb.2007.07.036>, 2008.

Supplement of J. Sens. Sens. Syst., 7, 489–506, 2018
<https://doi.org/10.5194/jsss-7-489-2018-supplement>
© Author(s) 2018. This work is distributed under
the Creative Commons Attribution 4.0 License.



Supplement of

DAV³E – a MATLAB toolbox for multivariate sensor data evaluation

Manuel Bastuck et al.

Correspondence to: Manuel Bastuck (m.bastuck@lmt.uni-saarland.de)

The copyright of individual parts of the supplement might differ from the CC BY 4.0 License.

Here we demonstrate the command line interface and use the steps involved to arrive from raw data to Fig. 16b. The presented syntax is based on a DAV³E version currently in development with improved command line interface.

The first step is to create a project as a container for everything else:

```
prj = Project();
```

The clusters are created directly from plain text files (tab-separated). In this case, the sampling rate must be supplied as it is not available from this file type.

```
cluster100Hz = Cluster.fromFile(...  
    {'PS1','PS2','PS3','PS4','PS5','PS6','EPS1'},'tsv',...  
    'samplingPeriod',0.01);  
cluster10Hz = Cluster.fromFile(...  
    {'FS1','FS2'},'tsv','samplingPeriod',0.1);  
cluster1Hz = Cluster.fromFile(...  
    {'TS1','TS2','TS3','TS4','VS1','CE','CP','SE'},'tsv',...  
    'samplingPeriod',1);
```

We then create a feature definition set (fds) which holds one or more feature definitions (fd). A feature definition holds, in turn, a range, defining what part of the cycle to operate on, and the function to compute on this part. Note that the range is created from the cluster. This allows to give its begin and end in actual sample points, which are then internally converted to a timestamp, which is important to make the ranges independent of the sampling rate. The range that is created here will span the whole cycle independent of its sampling rate. Having only one range and one feature definition here is a very naïve approach and can, and should, be replaced by a more sophisticated selection for a real evaluation. The feature definition set is finally set as default in the project, so that it is automatically applied to every newly added sensor.

```
fds = FeatureDefinitionSet();  
fd = FeatureDefinition(@FeatureExtraction.meanFeature,...  
    cluster1Hz.makeIndexRange([1,60]));  
fds.addFeatureDefinition(fd);  
prj.poolFeatureDefinitionSets = fds;
```

The project setup is then finished by adding the clusters and defining a range to select which cycles shall be included in the evaluation. Similar to above, we create only one range spanning the whole measurement. This is because the target values are already available for each cycle. If this were not the case, and the data had to be annotated manually, several ranges like shown in Fig. 13 would significantly facilitate this process because groups of ranges can be annotated at once.

```
prj.addCluster([cluster100Hz,cluster10Hz,cluster1Hz]);  
prj.ranges = cluster1Hz.makeCycleRange([1,2205]);
```

In the following, the 17 defined features (the mean value from each sensor) are computed with one simple command and can be fused in parallel employing a data processing block. Data processing blocks are the common interface for almost all functions in DAV³E, so that the user can extend many different areas of functionality after learning this basic, simple interface. They can have parameters and plot functions attached and, thus, provide improved functionality over a simple function while requiring less special knowledge from the user compared to writing class definitions. The output is a data object, which contains the concatenated features, but also meta data like target values, feature captions, etc. Features and cycles can be (de-)selected in the dataset and it ensures an always consistent state. Here, we load the target values from an external file.

```
features = prj.computeFeatures();  
parallelFusion = DataProcessingBlock(@FeatureFusion.parallel);  
data = parallelFusion.apply(features);  
targets = dlmread('profile.txt','\t');  
data.setTarget(targets(:,2),'numeric');
```

The data object will also contain predictions after a model has been applied to it, so that it can always traced back which data lead to which prediction. Hence, it makes sense to also define splits of the dataset here. DAV³E supports

nested cross-validation, which is automatically applied when both validation and testing are set to cross-validation. In this case, we only validate the model with cross-validation, but test it with a hold-out set. Defining this within in the data object again ensures traceability and prevents data leakage from training into testing sets.

```
data.setValidation('kFold','folds',10);
data.setTesting('holdout','percent',10);
```

Now we can set up the model. In this case, a simple PLS regression is enough, but additional blocks, e.g. feature preprocessing, could be added as the data processing blocks are elements of a double-linked list. The head of this list is given to the model which then takes care of training, validating, and testing the whole processing chain with the supplied data. Note that the options struct enables to give parameters for each element of the processing chain, and also supports lists of hyperparameters. If a list is given for more than one hyperparameter, the model automatically does a grid search and computes training, validation, and testing error for all parameter combinations.

```
plsr = DataProcessingBlock(Regression.plsr);
mdl = Model(plsr);
options = struct('plsr',struct('nComp',1:17));
mdl.train(data,options);
```

The next line then creates the graph in Fig. 16b. Eventually, the project is saved in its current state, so that it can be loaded again with all data and results in a new session.

```
mdl.plotErrors('plsr.nComp');
save('savedProject.mat','prj');
```

As an example for the data processing block interface, we show the definition of the PLS regression used in the code above:

```
function info = plsr()
    info.type = DataProcessingBlockTypes.Regression;
    info.caption = 'PLS regression';
    info.shortCaption = mfilename;
    info.description = '';
    info.parameters = [
        Parameter('shortCaption','trained', 'value',false,...)
        'hidden',true)...
        Parameter('shortCaption','beta0', 'hidden',true)...
        Parameter('shortCaption','offset', 'hidden',true)...
        Parameter('shortCaption','nComp', 'value',1)...
    ];
    info.apply = @apply;
    info.train = @train;
end

function [data,params] = apply(data,params)
    if ~params.trained
        error('Regressor must first be trained.');
    end
    b = params.beta0(:,params.nComp);
    o = params.offset(params.nComp);
    pred = data.getSelectedData() * b + o;
    data.setSelectedPrediction(pred);
end

function params = train(data,params)
    params.trained = true;
    [b,o] = quickPLSR(data.data,data.target); % external function
    params.beta0 = b;
    params.offset = o;
end
```

4.3 VOC Sensor Systems based on MOS Gas Sensors

4.3.1 Synopsis

This section focuses on the development of (selective) VOC sensor systems. VOC measurements usually take place in a complex atmosphere. Paper D gives an overview on the measurement of VOCs in different applications, for example indoor air quality, environmental or odor monitoring. In all these applications, it is required to measure target substances in a complex background of other organic or inorganic gases. The target substances may occur in a wide range of concentrations. These concentrations may be orders of magnitude smaller compared to other substances in the background atmosphere. Paper D shows the requirements, pitfalls and possible solutions for the usage of low-cost gas sensors in such applications. The use and benefits of different low-cost sensors in optimized dynamic operation is presented. The focus is on sensitive MOS gas sensors, which are operated in TCO as presented in Subsection 3.1.4. The use and need of sensitive and fast electronics for the operation of MOS gas sensors based on logarithmic conductance measurement is demonstrated. For a selective measurement also at very low concentrations, the combination of a MOS gas sensor with an integrated preconcentrator is shown.

One of the most important applications in the field of gas sensor technology is the monitoring of indoor air quality. Indoor air quality is a multifaceted parameter that is composed of various measurands, as described in Section 3.3. For several measurands, such as carbon dioxide, temperature or humidity, there are established low-cost sensor systems for monitoring. For VOCs, on the other hand, there is no established solution. MOS gas sensors have been proposed for this purpose in recent years and their performance capabilities were demonstrated, especially in lab studies. Currently, there is no standard definition of what VOC monitors based on low-cost sensors should measure and how to assess their performance. MOS gas sensors are very broadband and therefore react to a wide range of reducing and oxidizing substances. MOS gas sensors have for example a high cross-sensitivity to hydrogen or carbon monoxide, which can vary over a wide concentration range. Calibration and test are an often underestimated challenge but are necessary to achieve and understand the full potential of these systems. The more complex the measurement task, i.e. several target substances and complex and variable background atmosphere, the more complex the calibration has to be. Thus, the data analysis is not based on a physical model of the sensor but instead on pattern recognition techniques. The model and evaluation methods presented in Subsection 3.2.4 can be used for the evaluation of single gases or gas mixtures with very few components. For complex applications like IAQ, the model-based features carry a lot of information for pattern recognition techniques. Pattern recognition requires comprehensive, reproducible, all-encompassing but still affordable calibration for such applications. A reproducible calibration has to work not only in the own laboratory but also in external laboratories and in the field. Interlaboratory tests are described in Paper 5 and E, field tests in Paper 6 and F.

In Paper 5 the benzene detection with a MOS gas sensor system is tested in the laboratory at LMT and in the laboratory at the European Commission Joint Research Center (JRC) in Ispra, Italy. Both GMAs are described in the paper and Subsection 3.2.2.2. The calibration in LMT's laboratory was done with six gas

concentrations from 0.5 to 10 ppb and three relative humidities (10, 25, 40 %RH). The influence of toluene and carbon monoxide as background interferences is also investigated. The calibration at JRC was done with various benzene concentrations at 60 %RH without any variation of inorganic background. The benzene concentration was measured with a GC-MS reference system. The evaluation of the rate constant of the sensor system has a linear relation to the measured benzene concentration of the GC-MS system. The linear relationship is valid for the three low temperatures of the used TCO. A PLSR model calibrated with the JRC data results in an offset between JRC and LMT data. The offset can be explained by the different humidities (10, 25, 40 %RH at LMT and 60 %RH at JRC). A calibration with the LMT data has an offset in the same order. The study presented the measurement of benzene in two independent laboratories with good correlation. However, the study also shows that the calibration must necessarily include all variables, in this case humidity.

In Paper 5 an inter-laboratory comparison with the Bundesanstalt für Materialforschung und -prüfung (BAM) is presented. Aim is the comparison of ppb-level gas measurements with MOS gas sensors in two independent laboratories. Both GMAs are described in Paper 5 and subsection 3.2.2.2. A more complex calibration at the LMT was done with three single VOCs (formaldehyde, benzene, naphthalene), two VOC mixtures and humidity variations. At BAM eight measurements were done with the three single VOC and an additional VOC mixture. The background mixture was measured at BAM with different analytical methods. The sensor system is using a complex PLSR model for prediction. For formaldehyde, the sensor system does not achieve good agreement between the two laboratories. The TVOC signal calibrated with BAM data predicted the LMT data with a good agreement. The model prediction vice versa has a strong offset on the BAM data. A significant difference between the two laboratories is the background air generation. LMT uses a zero air generator as described in Subsection 3.2.2.2. BAM uses only an activated carbon filter to clean the compressed air, which does not remove carbon monoxide or hydrogen. Therefore, it can be assumed that especially the variation of hydrogen and carbon monoxide in the carrier gas makes a relevant difference in the prediction. This illustrates that not only the target gases, but also the correct background gases, must be included in a calibration.

The interlaboratory tests emphasize that the main challenge is incomplete calibration. When more and more gases are included in the training, calibration effort becomes much more costly. In the previous papers, sequential calibration with few fixed concentrations are used. Gas mixtures are created using combinatorial permutations of the individual fixed concentrations. However, with many substances, this results in an extremely long calibration duration due to the numerous combinations. Therefore, in Paper 3 (Section 4.2) the calibration with randomized DoE was introduced and tested, which reduces the effort and at the same time gives better results than sequential calibration.

The next step is to test the randomized DoE scheme in the field. Paper 6 and F are based on a measurement campaign with different lab and field measurements. For this purpose, new digital multi-sensors with integrated logarithmic conductance measurement and temperature control are included. The results in the manuscripts are mainly based on the Sensirion SGP30. The SGP30 contains four different sensitive sensor layers on a single μ -hotplate with an integrated ASIC for temperature control and conductance measurement. Calibration measurements are done at the LMT GMA with predilution.

Four VOCs (acetone, toluene, formaldehyde and ethanol), two background gases (hydrogen and carbon monoxide) and relative humidity are varied. Additional measurements in the laboratory are done after four weeks and again after additional three weeks in the field. Feature selection with RFE-PLS with PLSR is used as machine learning model. Training with the calibration measurement at the beginning of the measurement campaign has a small offset after four weeks in the field. An extended calibration after four weeks can remove this drift. This results in a drift-resilient model during the complete measurement campaign over eight weeks. For each substance (VOCs and background gases) a prediction with an RMSE between 20 and 40 ppb is achieved with the randomized calibration, with the exceptions of carbon monoxide (80 ppb). Release tests with several gases, for example ethanol, hydrogen, toluene and m/p-xylene, are done on the field test site, a standard office at the Lab for Measurement Technology (LMT) at Saarland University. The release tests are accompanied by reference analytics (TDS-GC-MS, mobile GC-MS and GC-RCP, a hydrogen reference measurement system). The sensor signals during release tests with toluene and acetone achieve good agreement with the reference analytics. This demonstrates that the sensor with a calibration based on the randomized DoE described before can selectively predict the calibrated gases in the field. Releases of gas mixtures also result in selective responses in the individual signals. At the same time, the calibrated VOC_{sum} signal correctly predicts the sum of the individual VOC concentrations.

Additional gases that were not included in the calibration are tested in the field or lab, for example benzene, m/p-xylene, isopropanol or limonene, to check whether a representative of a substance class is sufficient for calibration and how the quantification models react to completely unknown substances. For example, m/p-xylene results in a rise of the toluene signal, but all other signals show no response. This indicates that the model for toluene is more like an aromatic sum signal. Isopropanol, on the other hand, does not generate any response in any of the calibrated signals while a response is observed in the raw signal.

A reference measurement system for hydrogen, a GC-RCP (reducing compound photometer), accompanied the field study over several days. In Paper F an additional pre-conditioned SGP30 is evaluated. This SGP30 is pre-treated with siloxane to produce a selective hydrogen sensor [263]. The untreated and pre-treated SGP30 – both additionally calibrated with the same randomized DoE and data treatment as in Paper 6 – achieve a good correlation to the reference system. Both sensors also have good agreement during the hydrogen release tests. However, major differences between both sensors are observed upon an (unplanned) event, during construction work in the building and a limonene release test. The release of unknown substances during the construction work creates a large response in the untreated sensor. In contrast, the pre-treated sensor reacts only to the limonene release. This could be an effect of the removed selective membrane for siloxane protection [64]. Since the molecular size of limonene is of a similar order of magnitude to most siloxanes, it can be assumed that limonene is also hindered to reach the sensor surface and the untreated sensor cannot react. Only hydrogen should react on the surface of the conditioned sensor. A possible explanation is that hydrogen is produced during the decomposition of limonene or its reaction with other gases. This needs to be investigated in more detail.

Both studies – Paper 6 and F – illustrate that calibration in the laboratory based on randomized DoE is the today most promising approach to yield selective, stable and robust sensor signals from MOS gas sensors in TCO and achieve good agreement with reference analytics in the field. The assumption that one substance per substance group is sufficient for calibration is not proven for all tested substance groups. Further research on a complete calibration scheme for VOC measurement in IAQ is needed.

An overview of different applications for VOC measurements and the complexity of calibration, especially indoor air quality, is given. Two interlaboratory tests with two independent reference laboratories were performed. A new calibration method using randomized DoE was demonstrated in the laboratory and field. In summary, the following key results were achieved:

- Calibration is an often underestimated challenge but is necessary to achieve the full potential of gas sensor systems.
- For complex applications like IAQ, model-based evaluation methods produce useful features for machine learning techniques.
- A reproducible calibration has to work out not only in the own laboratory but also in other laboratories. This is the first step towards successful field tests and helps to identify unaddressed interfering factors.
- The randomized DoE was successfully tested in several field tests over a longer period. The studies show that calibration in the laboratory with randomized gas mixtures achieves good agreement with reference analytics in the field.
- Further research is needed on the composition of a full calibration scheme including all relevant substances. The hypothesis that one substance of each class might be sufficient could not be confirmed for all classes but seems valid for BTX

4.3.2 *Paper D – Highly Sensitive and Selective VOC Sensor Systems Based on Semiconductor Gas Sensors*

A. Schütze¹, T. Baur¹, M. Leidinger¹, W. Reimringer², R. Jung¹, T. Conrad², T. Sauerwald¹

¹Saarland University, Lab for Measurement Technology, Saarbrücken, Germany

²3S GmbH—Sensors, Signal Processing, Systems, Saarbrücken, Germany

Environments 2017, 4(1), 20

The original paper can be found, in the online version, at

<https://doi.org/10.3390/environments4010020>.

© 2017 by the authors. This article is an open access article distributed under the terms and conditions of the Creative Commons Attribution (CC BY) license (<http://creativecommons.org/licenses/by/4.0/>).

Article

Highly Sensitive and Selective VOC Sensor Systems Based on Semiconductor Gas Sensors: How to?

Andreas Schütze ^{1,*}, Tobias Baur ¹, Martin Leidinger ¹, Wolfhard Reimringer ², Ralf Jung ¹, Thorsten Conrad ² and Tilman Sauerwald ¹

¹ Lab for Measurement Technology, Department of Systems Engineering, Saarland University, Saarbrücken 66041, Germany; t.baur@lmt.uni-saarland.de (T.B.); m.leidinger@lmt.uni-saarland.de (M.L.); ralfjung@gmx.net (R.J.); t.sauerwald@lmt.uni-saarland.de (T.S.)

² 3S GmbH—Sensors, Signal Processing, Systems, Saarbrücken 66121, Germany; reimringer@3s-ing.de (W.R.); conrad@3s-ing.de (T.C.)

* Correspondence: schuetze@lmt.uni-saarland.de; Tel.: +49-681-302-4664

Academic Editors: Ki-Hyun Kim and Abderrahim Lakhout

Received: 31 December 2016; Accepted: 24 February 2017; Published: 1 March 2017

Abstract: Monitoring of volatile organic compounds (VOCs) is of increasing importance in many application fields such as environmental monitoring, indoor air quality, industrial safety, fire detection, and health applications. The challenges in all of these applications are the wide variety and low concentrations of target molecules combined with the complex matrix containing many inorganic and organic interferents. This paper will give an overview over the application fields and address the requirements, pitfalls, and possible solutions for using low-cost sensor systems for VOC monitoring. The focus lies on highly sensitive metal oxide semiconductor gas sensors, which show very high sensitivity, but normally lack selectivity required for targeting relevant VOC monitoring applications. In addition to providing an overview of methods to increase the selectivity, especially virtual multisensors achieved with dynamic operation, and boost the sensitivity further via novel pro-concentrator concepts, we will also address the requirement for high-performance gas test systems, advanced solutions for operating and read-out electronic, and, finally, a cost-efficient factory and on-site calibration. The various methods will be primarily discussed in the context of requirements for monitoring of indoor air quality, but can equally be applied for environmental monitoring and other fields.

Keywords: low-cost sensors; VOC sensor systems; sensitivity; selectivity; virtual multisensor; calibration

1. Introduction

Measurements of volatile organic compounds (VOCs) are becoming ever more important due to stringent environmental regulations and increasing health concerns. Typical compounds with high relevance are benzene, naphthalene, formaldehyde, and tetrachloroethylene, but there are many more depending on the specific environment and the target application. Exposure to VOCs for a long time can have negative effects on human health, including damage to the respiratory system and skin irritations [1]. Moreover, VOCs are the main cause of the sick building syndrome [2,3]. Besides these unspecific adverse health effects, some VOCs are proven to be carcinogenic (e.g., benzene [4]) or are suspected to be carcinogenic (e.g., formaldehyde [5]). The specific challenge for VOC measurements are the low target concentrations: the respective guideline threshold values for some critical substances (in indoor air) are 0.1 mg/m³ (81 ppb) for formaldehyde and 0.01 mg/m³ (1.9 ppb) for naphthalene according to the World Health Organization (WHO) [4], and 5 µg/m³ (1.6 ppb) for benzene according to EU guidelines [6]. In other fields such as industrial monitoring and workplace safety, higher values apply, but these are currently trending down sharply, e.g., in Germany [7].

Furthermore, very high selectivity is required to discriminate highly toxic or carcinogenic VOCs from inorganic gases such as carbon monoxide (CO), nitrous oxides (NO_x), ozone (O_3), or hydrogen (H_2), all of which occur naturally or are generated by (other) pollution sources less toxic or from benign VOCs such as ethanol. For the total VOC concentration (TVOC), WHO suggests a limit value of 1 ppm, i.e., three orders of magnitude above the lowest threshold limit values for hazardous VOCs. In other applications, the ratio between target VOC and interferent can even reach five orders of magnitude, e.g., for smoldering fire detection on coal mines, where 100 ppb ethane (C_2H_4) should be detected against a background of up to 1% methane (CH_4) [8]. A field that has gained increasing interest in recent years in monitoring of odor compounds, which, while often not having a direct health effect, nevertheless considerably impact our quality of life. Typical compounds in this context are isovaleric acid ("sweat odor"), organosulfur compounds (thiols or mercaptan, e.g., (di-)methyl sulfide) as well as many esters, terpenes, amines, ketones, and, of course, aromatic compounds as well as hydrogen sulfide as an important inorganic odorant. Odor monitoring plays an increasing role in indoor air quality, but also in outdoor environmental monitoring, both at the source (emission measurements at the stack or the fence line) and at the impact side (odor nuisance monitoring) for various industries, e.g., waste treatment. Figure 1 gives an overview over VOC monitoring applications, also indicating relevant target gases and interferents. A more comprehensive overview is given in [9].

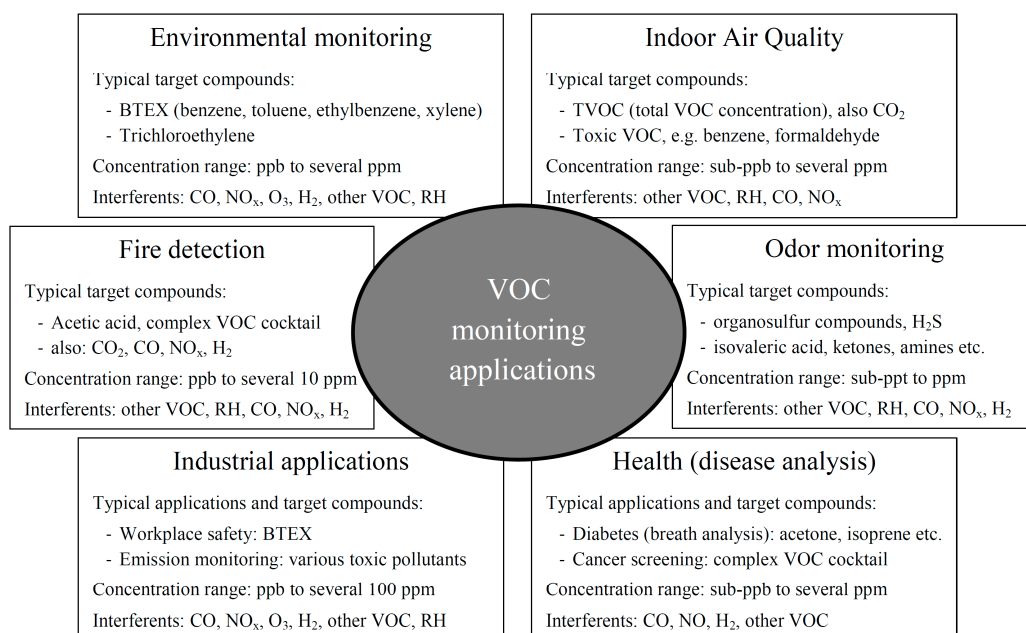


Figure 1. Overview over various applications requiring monitoring of VOCs plus typical target gases and relevant concentration ranges. Due to the wide variety of gases and applications in the specific fields, this is indicative only. Common challenges for most applications are the low target concentrations and the complex matrix. Note that in some cases the same compounds can be seen as target and interfering gases due to different sources.

Very few monitoring techniques actually achieve ppb (or even sub-ppb) level sensitivity so that sampling techniques are generally used for VOC monitoring. The standard method for VOC monitoring is sampling, e.g., with Tenax® as absorbent material, and then releasing the sampled gas into a gas chromatograph followed by identification of the VOCs by mass spectrometry (GC-MS). This method, while widely accepted, does however pose serious problems for comprehensive VOC monitoring as both very volatile organic compounds (VVOCs) and semivolatile organic compounds

(SVOCs) will not be sampled with the standard technique [10]. VVOCs will simply pass through the sampling material, while SVCOCs are not released due to their very high boiling point. One prominent example for this shortcoming is formaldehyde for which a specific separate sampling and quantification protocol is required [11]. On the other hand, weak sorbents are required for trapping SVOCs. This means that standard measurement techniques are actually blind to a fairly wide range of compounds and that our understanding of environmental pollution and health effects is somewhat limited due to missing data on these compounds. Research is ongoing in finding suitable sorbent materials, e.g., multibed focusing traps, to allow the acquisition of more complete information on VOCs [12]. In addition, sampling only allows determining time-weighted average (TWA) values either for the long term (1 h to 24 h) or the short term (5 min to 60 min), thus possibly missing relevant short concentration peaks. Sensor-based monitoring, on the other hand, would allow both an improved temporal resolution and a wider detection spectrum, as sensors will respond to practically all VOCs including VVOCs and SVOCs.

2. Highly Sensitive Semiconductor Gas Sensor Principles

One candidate sensor principle for direct monitoring of even sub-ppb level VOC concentrations are metal oxide semiconductor (MOS) gas sensors [13,14], but gas-sensitive field effect transistors (GasFETs), e.g., based on silicon carbide (SiC-FET), have also proven their suitability for this task [15]. For simplification, we will concentrate on MOS sensors in the following discussion, but many aspects also apply to SiC-FET sensors, so the approach is presented for semiconductor gas sensors. Note that both sensor principles allow low-cost sensor solutions, at least for markets with high volumes. Even taking into account the advanced electronics and data processing that are necessary to achieve high sensitivity, selectivity, and stability, high performance sensor systems can be realized for well below 1.000€, as has been demonstrated for fire detection [16]. In mass applications, the system cost can drop to below 10€. Commercial screen-printed ceramic MOS sensors achieve detection limits down to sub-ppb levels due to the well-known grain boundary effect [17]. A small grain size down to nanocrystals [18] also improves the sensitivity as the bulk conductance of the material is not affected by gas adsorbed on the grain surface. Recently, nanostructured sensors based on nanowires [19] have been proposed and sometimes postulated as being necessary for achieving very low detection limits due to the high surface area achieved. Especially carbon nanotube-based sensors have been extensively studied with the expectation that these provide the key for very high sensitivity [20–22]. However, so far no rigorous study has proven that MOS nanowires or carbon nanotubes in fact achieve superior sensitivity compared to standard granular materials. Novel manufacturing methods for metal oxide layers, especially Pulsed Laser Deposition [23], achieve highly porous sensor layers with well-controlled morphology that can even reach high selectivity for some relevant target VOCs such as naphthalene [24].

On the other hand, we have recently developed a model that shows that the sensitivity of MOS sensors can be improved significantly by temperature cycling. The first benefit of varying the sensor temperature over a broad range is immediately obvious as the sensor will at some time in the cycle reach the optimal temperature, i.e., with the highest sensitivity, for the target gas(es). In addition, temperature cycling with fast temperature changes will lead to non-equilibrium surface conditions and thus reaches states that cannot be achieved in static operation at constant temperature. By carefully choosing the operating parameters, the sensitivity can actually be boosted considerably, e.g., by first operating the sensor at high temperature which leads to a high surface coverage with ionosorbed oxygen. If the sensor is then cooled down rapidly, this leads to a surface at low temperature but with an abundance of reactive oxygen ions—a condition that cannot be achieved in static mode. Without gas, the ionosorbed oxygen will slowly desorb to reach the equilibrium state with only few oxygen ions at low temperature. A gas interacting with the adsorbed oxygen will strongly influence this relaxation process leading to faster equilibration. The sensitivity and the respective sensor response $G_{\text{gas}}/G_{\text{zero}}$ during dynamic operation have been shown to be orders of magnitude higher than in static operating

mode [25]. Figure 2 describes this effect schematically. The non-equilibrium states during dynamic operation can also improve the selectivity, so optimized cycling can be used to address the three “S’s”—sensitivity, selectivity, and stability—the key aspects for chemical sensor systems [26].

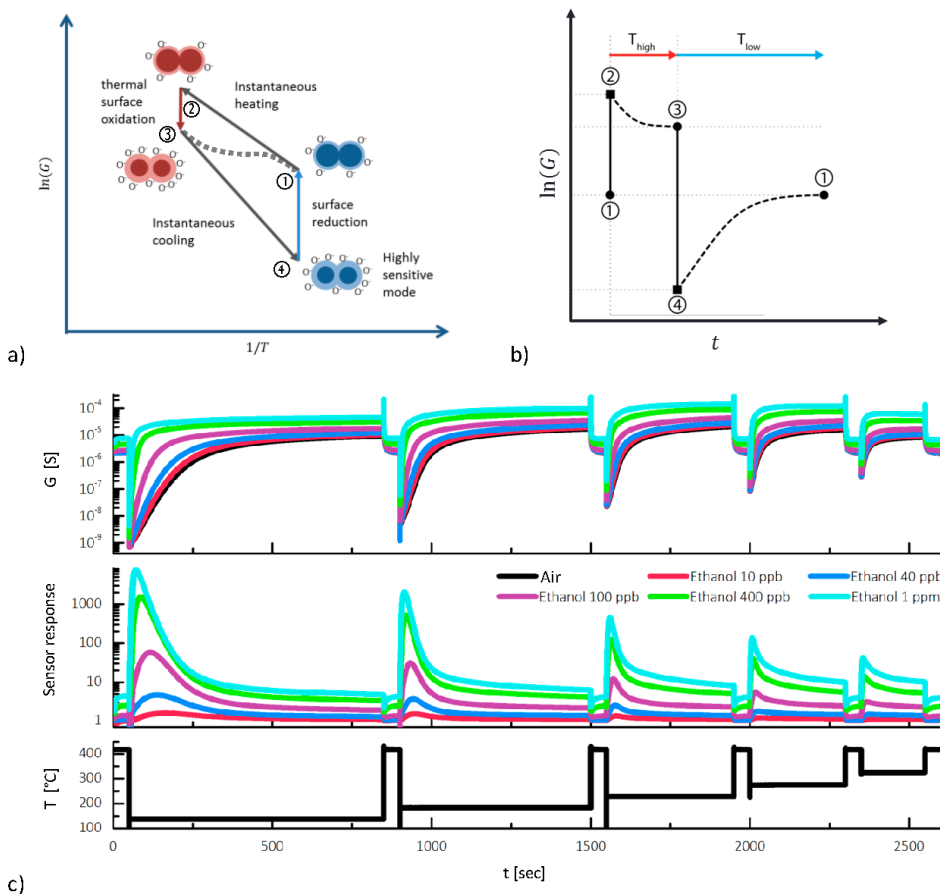


Figure 2. Boosting sensitivity of MOS sensors with temperature cycled operation (TCO): (a) MOS sensors show low oxygen coverage at low temperatures ① and high coverage at high temperatures ③ in steady state conditions (dashed line indicates equilibrium conditions between min and max temperature). Non-equilibrium surface states (②, ④) are achieved by fast temperature changes. Especially high oxygen coverage at low temperature will lead to a highly sensitive mode as target gases will react with the adsorbed oxygen. (b) Dynamic relaxation of the conductance after fast temperature changes boosts the sensitivity. (c) Admixture of VOCs leads to faster relaxation compared to pure air. Plotting the sensor response shows that a huge increase in sensitivity of several orders of magnitude can be achieved compared to the steady state response reached at the end of the relaxation process. The relaxation behavior at various temperatures is typical for the specific target gas and can thus be used to increase the selectivity of MOS-based sensor systems.

There are also other possibilities to enhance the response and increase the sensitivity of semiconductor gas sensors, especially optical excitation, which has been addressed by various groups [27,28]. Especially excitation with quantum energy above the bandgap energy of the semiconductor allows low-temperature operation and/or achieves higher sensitivity. In addition, light modulation can be used to extract signal patterns similar to TCO which can also increase the selectivity and stability of the overall sensor system.

3. Highly Selective Sensor Systems

The drawback of MOS (and SiC-FET) sensors is their inherent low selectivity, which is due to the sensor function principle. The high sensitivity of MOS sensors is due to the grain-boundary effect that is caused by ionosorbed oxygen leading to band bending at the surface of the grains and, thus, an energy barrier between grains with the conductance of the sensor being exponentially dependent on the height of this energy barrier. Any gas that either chemisorbs on the surface or interacts with the ionosorbed oxygen will change the energy barrier. Therefore, MOS sensors show a response to practically all relevant target and interfering gases except carbon dioxide (CO_2). To achieve the required high selectivity for gas discrimination and/or quantification of target gases in a background of interfering gases, several approaches are possible: (a) enhancing gas measurement systems with analytical tools, i.e., a GC tube to separate the various gas components (which will, however, suffer from similar drawbacks as sampling techniques for VVOC and SVOC); (b) making use of multisensor arrays and pattern recognition (often referred to as electronic nose) [9]; and (c) using dynamic operation, e.g., temperature cycling, to realize a virtual multisensor, which is also evaluated using typical pattern recognition methods [29]. The different methods employed for increasing the selectivity can also be combined, for example, by integrating several dynamically operated sensors in a hybrid sensor array or combining gas pre-concentration (see below) with temperature cycling to boost sensitivity and selectivity. Especially temperature cycled operation (TCO) has proven a very powerful and versatile tool for various sensor principles (MOS sensors [14,30–32], SiC-FETs [33], pellistors [34]), which is easily understandable as the chemical interaction between sensor and gas atmosphere is strongly influenced by the surface temperature. For example, some gases such as CO or H_2 will react at relatively low temperatures, while others such as CH_4 are more stable and thus require higher activation energies to cause a sensor reaction. Due to its simple implication and low cost (only some additional electronics are required), TCO is now widely accepted as a method to boost selectivity, especially as it also improves the stability of the sensor system due to self-cleaning of the sensor surface at higher temperatures [35] and the possibility to use features which are stable over time [32]. Furthermore, in addition to identifying and quantifying target gases, this approach allows sensor self-monitoring [36], which is a crucial aspect especially for applications in safety and security. For VOC monitoring, selective identification of hazardous VOCs down to concentrations of 1 ppb could be demonstrated even in a background of other VOCs of several ppm and against changing humidity using a commercial ceramic MOX sensor at least under lab conditions [14]; similarly, quantification of VOCs at low ppb levels was demonstrated with this approach both for MOS [26] and SiC-FET [15,37] sensors. Further approaches to improve the performance of semiconductor gas sensor systems with dynamic operation are optical excitation [27,28] and impedance spectroscopy [38] often applied to MOX sensors or gate bias cycled operation for GasFETs [39]. These approaches can also be combined to boost the selectivity further [40,41].

One often underestimated aspect for highly sensitive and selective sensor systems is the electronics for sensor operation and signal read-out. To make use of the full potential of dynamic operation, dedicated electronics that allow exact control of the sensor operating parameters and synchronized data acquisition are required. For temperature cycling, exact temperature control is key. Here, the heater integrated in each MOS (and SiC-FET) sensor is preferably also used as a temperature sensor to allow exact closed-loop control. This allows exact control even for highly dynamic cycles, especially for microstructured gas-sensors based on micro-hotplates, which exhibit thermal time constants of typically a few ms. This type of sensor is now manufactured at high volumes by various companies, e.g., ams Sensor Solutions, CCMOSS, Figaro, and SGX Sensortech, achieving very low-cost sensor elements. Appropriate electronics have been developed over several generations [42–44] and are today commercially available from 3S GmbH (3S Toolbox, [45]), which has been successfully employed also for outdoor odor nuisance monitoring [46]. To make full use of the TCO mode for MOS sensors, the sensor resistance has to be acquired with high temporal resolution ($\geq 1 \text{ kHz}$) over a wide dynamic range of several orders of magnitude from $\text{k}\Omega$ (high gas concentrations at high operating

temperatures) to $G\Omega$ or even $T\Omega$ (low gas concentration, non-equilibrium state after fast cool down, cf. Figure 2), ideally with constant relative resolution. The voltage across the sensor layer is limited, typically to ≤ 1 V, to prevent unwanted effects such as electromigration in the layer leading to sensor drift. However, this voltage limit (or more exactly the maximum field strength) also depends on the operating temperature, allowing higher voltages and thus more sensitive measurement at low temperature. Thus, electronics are required that allow fast and accurate measurement of very low currents in the pA range. One suitable approach is the use of logarithmic amplifiers, which achieve a measurement range of up to 8 orders of magnitude (Figure 3), and another is dynamic signal amplification to adapt the output voltage to the current signal level [47]. Both approaches can and need to be closely integrated with the sensor element to achieve a high signal quality also under field conditions. Similarly, electronics suitable for field use were developed for Electrical Impedance Spectroscopy (EIS), allowing novel sensor self-monitoring strategies for MOX sensors [48,49] as well as for Gate Bias Cycling (GBC) of SiC-FETs [41] in both cases combined with TCO.

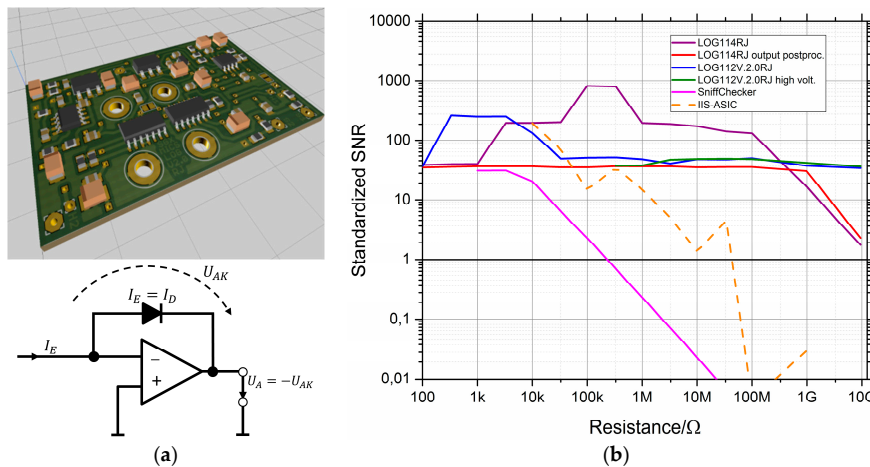


Figure 3. (a) Operating principle of a logarithmic amplifier based on the exponential current-voltage characteristic of a diode or transistor and PCB implementation. (b) Signal-to-Noise-Ratio (SNR) standardized to the same bandwidth of different logarithmic amplifiers compared to conventional electronics based on a linear AD converter (“SniffChecker” by 3S) and an integrated ASIC solution based on dynamic variation of measurement voltage and gain factor (IIS-ASIC, [47]).

4. Novel Integrated Pre-Concentrator Gas Sensor Microsystem

Despite the impressive sensitivities and very low detection limits that are achieved with MOS and SiC-FET sensors, some application targets are still difficult to achieve either due to very low target gas concentrations well below 1 ppb, e.g., trimethylamine with an odor threshold of 0.21 ppb; ethyl acrylate (and hydrogen sulfide) with an odor threshold of 0.47 ppb [50], or due to strong interference by other gases. Especially for measurements at very low gas concentrations, adsorbent materials are often used to achieve the required detection limits. Typical methods for detection of low VOC concentrations are based on sampling a defined gas volume using, e.g., Tenax® tubes. From these, the adsorbed gas is thermally desorbed during subsequent lab analysis based on gas chromatography (GC), often coupled with mass spectrometry (MS), to allow sensitive and selective gas detection. This approach has been miniaturized with the goal to achieve sensor systems for nearly continuous monitoring operating in adsorption/desorption cycles. However, these systems today are typically based on closed pre-concentrators combined with micro-pumps leading to systems that are not low-cost [51,52]. We have developed a new approach based on open pre-concentrators, i.e., absorbing material based on metal organic frameworks (MOF) deposited on a micro-hotplate similar to the gas sensor substrates.

These μ -pre-concentrators are integrated with the sensors in a common package with a small gas access. VOCs present in the ambient enter the package through the gas access and accumulate in the MOF material which has a large inner surface reaching partition coefficients orders of magnitude better than standard Tenax® [53]. Heating the μ -pre-concentrator will release the adsorbed gas molecules resulting in a considerably increased gas concentration within the sensor package, which is detected by the sensors [54]. Figure 4 illustrates the function principle of this novel approach which is based on gas transport by diffusion only thus requiring a miniaturized packaging solution. The function principle is also illustrated in a video to allow better understanding of the complex interaction within the microsystem [55]. Note that after release of the target gases from the pre-concentrator and subsequent cool-down, the pre-concentrator actually achieves a zero-air atmosphere within the package, at least for all gases adsorbing on the pre-concentrator [54]. This will actually allow an internal reference, as the sensors are briefly exposed only to permanent gases such as CO and H₂, thus improving the performance for target VOC detection and quantification by taking this into account in the signal evaluation. Furthermore, discrimination of different VOCs can be improved by taking into account the desorption temperature, i.e., for slow heating of the pre-concentrator. To make full use of this potential to boost sensitivity and selectivity, an application specific operating mode has to be designed as slow heating will decrease the peak concentration, while fast heating will release all VOCs simultaneously, thus limiting the selectivity. This novel integration approach is compatible with existing mass fabrication technologies and achieves sensor systems with greatly improved sensitivity at very low cost—at large volumes, the cost for the integrated system with, e.g., two sensors and one pre-concentrator could be less than one euro.

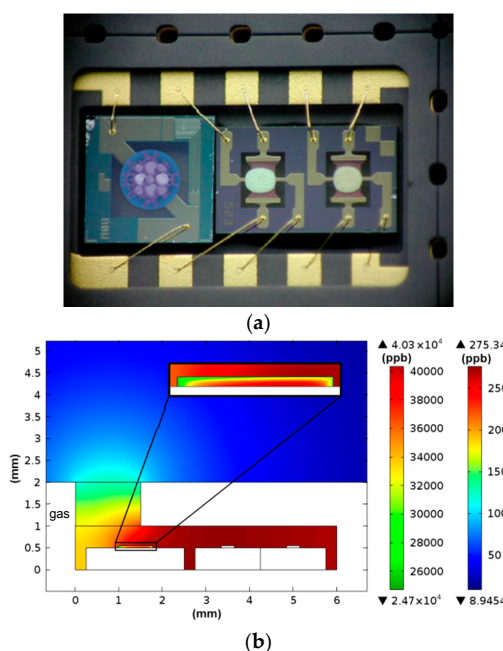


Figure 4. (a) Novel integrated pre-concentrator gas sensor microsystem combining a micro-pre-concentrator realized by deposition of MOF material on a micro-hotplate (left) with one or two gas sensors (right) in a single SMD package. Gas access is through a small opening above the pre-concentrator only. (b) Simulated gas concentrations inside the pre-concentrator material (left scale) and in the air (right scale), simulated for benzene and HKUST-1 as pre-concentrator material 1.5 s after start of desorption at 200 °C. The highest gas concentration is obtained inside the microsystem, i.e., at the locations of the two gas sensor chips S1 and S2. Adapted from [54].

5. Sensor System Testing and Evaluation

The impressive sensitivities and very low detection limits reported above can be achieved under well-defined laboratory conditions, which are, however, not easily achieved—in fact, very few test systems actually allow reliable testing of sensors at ppb and sub-ppb levels in a complex matrix. A pre-requisite for testing ultra-low concentrations is a suitable test setup, i.e., a gas mixing apparatus allowing exact control of gas admixtures under realistic and controlled ambient conditions. Some publications present very low detection limits, but these are sometimes just extrapolations from measurements at (much) higher concentrations or achieved in pure nitrogen as carrier gas, i.e., without oxygen or humidity, which has a huge influence on many sensors. Furthermore, standard zero air, which is also used for mixing of test gases, typically contains contaminations of approx. 10 ppm (zero air 5.0) and even the best zero air standards still contain approx. 1 ppm of unwanted and uncontrolled contaminations. While many of these do not influence the measurement (i.e., noble gases or CO₂), relevant trace contaminations can occur at concentrations orders of magnitude higher than the target gases to be tested. As the zero air used for the test gas is different from that used in the rest of the test setup, the observed sensor response can be caused by the contamination and not by the intended target gas when standard test gases with very low concentrations are used for direct measurement at ppb-level. Suitable approaches are the use of permeation tubes to introduce the target gas directly into the (zero air) carrier gas stream or two-stage gas dilution, allowing the use of test gases with concentrations much higher than any contaminations [56]. In both cases, the gas to be tested is injected into a carrier gas stream, which still contains contaminations, but the setup, which uses the same zero air throughout the system, ensures that the concentration of all contaminants stays constant, allowing the measurement of the sensor response to a change of only the target gas concentration. Further sources of error can be due to either VOC sources inside the system, e.g., from lubricants in valves or mass flow controllers, or due to adsorption of VOCs on inner surfaces preventing the target gas from reaching the sensor. The latter is especially problematic for SVOC which will then slowly diffuse out of the system, which can lead to large carry-over or “memory” effects. These effects can only be monitored by regular reference measurements of the overall system with analytical methods. Note that a gas test bench for broadband sensors such as MOS and SiC-FET should be based on a flow-through approach instead of gas re-circulation as reaction products from the interaction of the test gas with the sensor might otherwise lead to false results.

Finally, to accurately reflect measurements in ambient air, the typical mixture of natural air, which contains, in addition to nitrogen, oxygen, CO₂, and RH, approx. 1.8 ppm methane (CH₄), 550 ppb H₂, 325 ppb nitrous oxide (N₂O), and 150 ppb CO [57,58], has to be taken into account. CO shows the strongest variations with an annual cycle between 100 and 250 ppb [58]. While the effect of CH₄ is negligible, even the low-level exposure to H₂ and CO can easily change the baseline resistance of MOS sensors by one order of magnitude. At the same time, this will also reduce the sensitivity to other gases and distort the response pattern of sensor arrays and virtual multisensors. To achieve realistic test results, relevant background gases therefore have to be added to the zero air in gas test systems, and the natural variations have to be taken into account when determining detection limits and quantification resolution.

6. Factory and On-Site Calibration

To make full use of the potential of low-cost sensors for ultra-low VOC concentrations, calibration is an often underestimated challenge. The more complex the expectations, i.e., several target gases, mixtures of target gases, complex and variable background, the more complex the calibration procedure. This is due to the fact that data analysis is not based on a physical model of the sensor(s) but instead only on calibration data combined with pattern recognition techniques [29]—the calibration therefore has to span the full range of gases and concentrations expected in the later application. Due to slight variations in the individual sensors, at least part of this calibration has to be performed for each sensor individually, which can considerably contribute to the overall cost of the final gas

sensor system. Furthermore, as the background can vary considerably for individual application environments, an extended calibration on-site might be necessary—this basically depends on the expected data quality to be achieved. While a scale-up of standard test benches (see above) can allow efficient factory calibration even for large production volumes, a test with various test gas cylinders would be impossible for on-site calibration. To address this issue, we have developed a novel approach for on-site calibration [59] based on VOCs dissolved in squalane, a long-chain alkane with low vapor pressure. This approach also allows producing a “zero air” atmosphere on-site within a confined volume in which the sensor and a vessel with squalane are kept: due to the large Henry constant, practically all VOCs present in the ambient will dissolve in the squalane resulting in a practically VOC free reference atmosphere (which will, however, still contain most inorganic gases such as CO, H₂, and NO_x). Note that this is similar to the pre-concentrator briefly achieving a VOC free atmosphere after cool-down, cf. Section 4. Similarly, using squalane loaded with a defined target VOC concentration will provide a source desorbing with a defined amount of the VOC, which can be used to calibrate sensors on-site. Note that this approach not only allows cost-efficient testing of the correct function of the sensor system, but also quantitative re-calibration to counteract sensor drift.

7. Conclusions and Outlook

Bringing together the different aspects outlined above—highly sensitive sensor elements; optimized dynamic operation (TCO, EIS, GBC) of the sensors; high-performance electronics for dynamic operation combined with advanced signal processing to achieve high sensitivity, selectivity and stability; low-cost pre-concentration to boost sensitivity and selectivity further; gas test bench for ppb and sub-ppb VOC concentrations, efficient factory, and on-site calibration—is a pre-requisite for the systematic development of low-cost sensor systems for VOC detection in various applications and for their validation in field tests. This integrated approach is at the core of the EU project SENSIIndoor [60] addressing indoor air quality and demand controlled ventilation based on sensor systems placed in each room, i.e., offices, living and sleeping rooms, public buildings, transport, etc. On the one hand, the approach is used for optimization of the sensor elements themselves, i.e., based on novel nanotechnology approaches such as Pulsed Laser Deposition (PLD) and novel sensor materials [23,24,61–64]. On the other hand, extensive field tests are required which include reference tests based on existing standards. These developments will also lead to the development of new standards for VOC testing because existing standards do not cover the high spatial and temporal resolution that can be achieved with networks based on low-cost sensor systems. This aspect is currently addressed in the KEY-VOCs project under the European Metrology Research Program (EMRP) [65,66].

Note that in this contribution we have addressed sensor systems as a somewhat abstract concept, i.e., a device able to detect and quantify specific VOCs against a background of interfering gases. Not addressed here, but equally relevant to providing solutions for real world problems is a somewhat wider view that includes a structural model similar to the ISO-OSI model used in the field of communications. Systems based on low-cost semiconductor gas sensor principles will never achieve a universal performance independent of their application field, i.e., specific interferents and ambient conditions. Instead, application specific sensor systems are required—systems that would function well in the context for which they are designed, i.e., workplace safety monitoring or indoor air quality control, but that cannot be used to cover the full range of applications outlined in Figure 1. The structural model would cover the full range from expected benefits and application parameters at the top end down to the VOC atmosphere and the sampling method at the lower end [67] for realization of application specific sensor systems. By following this approach, it will be possible to address many different applications in environmental monitoring, indoor air quality, and industrial safety and health applications based on VOC monitoring, thus attaining a better understanding of VOC sources and effects to achieve a safer and healthier environment for all.

Acknowledgments: This work was in part performed within the SENSIIndoor project. The SENSIIndoor project is funded by the European Union’s Seventh Framework Programme for research, technological development and demonstration under grant agreement No. 604311. Some foundations were laid within the MNT-ERA.net project VOC-IDS for which funding by the German Ministry for Education and Research (BMBF, funding codes 16SV5480K and 16SV5482) is gratefully acknowledged. The authors also acknowledge many useful discussions and suggestions from members of the COST action TD1105 EuNetAir and the EMRP project KEY-VOCS.

Author Contributions: Andreas Schütze and Tilman Sauerwald coordinated the research on trace VOC measurements at LMT together, Tilman Sauerwald designed most of the experiments and developed the model for MOS sensors in TCO mode together with Tobias Baur. Tobias Baur performed and evaluated the measurements for optimization of TCO (Figure 2). Martin Leidinger performed the simulations and corresponding experiments for the novel integrated sensor system (Figure 4). Wolfhard Reimringer designed the electronics that were used in most experiments. Ralf Jung designed the log-amp electronics supported by Tobias Baur and performed the SNR measurements within his Bachelor thesis (Figure 3). Thorsten Conrad contributed to the concept of the paper and especially to the chapter on sensor system calibration. Andreas Schütze wrote the paper.

Conflicts of Interest: The authors declare no conflicts of interest.

References

1. Jones, A.P. Indoor air quality and health. *Atmos. Environ.* **1999**, *33*, 4535–4564. [[CrossRef](#)]
2. Brinke, J.T.; Selvin, S.; Hodgson, A.T.; Fisk, W.J.; Mendell, M.J.; Koshland, C.P.; Daisey, J.M. Development of new volatile organic compound (VOC) exposure metrics and their relationship to sick building syndrome symptoms. *Indoor Air* **1998**, *8*, 140–152. [[CrossRef](#)]
3. Burge, P.S. Sick building syndrome. *Occup. Environ. Med.* **2004**, *61*, 185–190. [[CrossRef](#)] [[PubMed](#)]
4. World Health Organization. WHO Guidelines for Indoor Air Quality: Selected Pollutants, Geneva (2010). Available online: http://www.euro.who.int/__data/assets/pdf_file/0009/128169/e94535.pdf (accessed on 31 December 2016).
5. Guo, H.; Lee, S.C.; Chan, L.Y.; Li, W.M. Risk assessment of exposure to volatile organic compounds in different indoor environments. *Environ. Res.* **2004**, *94*, 57–66. [[CrossRef](#)]
6. European Parliament, Council of the European Union: Directive 2008/50/EC of the European Parliament and of the Council of 21 May 2008 on Ambient Air Quality and Cleaner Air for Europe. Available online: <http://eur-lex.europa.eu/legal-content/EN/TXT/?uri=celex%3A32008L0050> (accessed on 31 December 2016).
7. TRGS 910: Technische Regeln für Gefahrstoffe, Risikobezogenes Maßnahmenkonzept für Tätigkeiten mit krebserzeugenden Gefahrstoffen, Bundesanstalt für Arbeitsschutz und Arbeitsmedizin, Ausschuss für Gefahrstoffe. 2015. Available online: <http://www.baua.de/de/Themen-von-A-Z/Gefahrstoffe/TRGS/TRGS-910.html> (accessed on 31 December 2016).
8. Reimann, P.; Schütze, A. Fire detection in coal mines based on semiconductor gas sensors. *Sens. Rev.* **2012**, *32*, 47–58. [[CrossRef](#)]
9. Pearce, T.C.; Schiffman, S.S.; Nagle, H.T.; Gardner, J.W. *Handbook of Machine Olfaction: Electronic Nose Technology*; Wiley: Weinheim, Germany, 2006.
10. European Collaborative Action Indoor Air Quality & Its Impact on Man: Sampling Strategies for Volatile Organic Compounds (VOCs) in Indoor Air. Available online: <http://www.buildingeconomy.com/iaq/useful-publications/european-collaborative-action-on-urban-air-indoor-environment-and-human-exposure-reports-1/> (accessed on 31 December 2016).
11. ISO 16000-3:2011, Indoor Air—Part 3: Determination of Formaldehyde and Other Carbonyl Compounds in Indoor Air and Test Chamber Air—Active Sampling Method (2011). Available online: http://www.iso.org/iso/catalogue_detail.htm?csnumber=51812 (accessed on 31 December 2016).
12. Watson, N.; Davies, S.; Wevill, D. Air Monitoring: New Advances in Sampling and Detection. *Sci. World J.* **2011**, *11*, 2582–2598. [[CrossRef](#)] [[PubMed](#)]
13. Morrison, S.R. Semiconductor Gas Sensors. *Sens. Act.* **1982**, *2*, 329–341. [[CrossRef](#)]
14. Leidinger, M.; Sauerwald, T.; Reimringer, W.; Ventura, G.; Schütze, A. Selective detection of hazardous VOCs for indoor air quality applications using a virtual gas sensor array. *J. Sens. Sens. Syst.* **2014**, *3*, 253–263. [[CrossRef](#)]
15. Bastuck, M.; Bur, C.; Sauerwald, T.; Schütze, A. Quantification of volatile organic compounds in the ppb-range using partial least squares regression. In Proceedings of the SENSOR 2015—17th International Conference on Sensors and Measurement Technology, Nuremberg, Germany, 19–21 May 2015.

16. Kohl, D.; Kelleter, J.; Petig, H. Detection of Fires by Gas Sensors. In *Sensors Update*; WILEY-VCH: Weinheim, Germany, 2001; Volume 9, pp. 161–223.
17. Bärsan, M.; Hübner, N.; Weimar, U. Conduction mechanism in semiconducting metal oxide sensing films: Impact on transduction. In *Semiconductor Gas Sensors*, 1st ed.; Jaaniso, R., Tan, O.K., Eds.; Woodhead Publishing: Cambridge, UK, 2013; pp. 35–63.
18. Comini, E. Metal oxide nano-crystals for gas sensing. *Anal. Chim. Acta* **2006**, *568*, 28–40. [\[CrossRef\]](#) [\[PubMed\]](#)
19. Ramgir, N.; Datta, N.; Kaur, M.; Kailasaganapathi, S.; Debnath, A.K.; Aswal, D.K.; Gupta, S.K. Metal oxide nanowires for chemiresistive gas sensors: Issues, challenges and prospects. *Colloids Surf. A* **2013**, *439*, 101–116. [\[CrossRef\]](#)
20. Llobet, E. Gas sensors using carbon nanomaterials: A review. *Sens. Actuators B Chem.* **2013**, *179*, 32–45. [\[CrossRef\]](#)
21. Wang, Y.; Yeow, J.T. W. A Review of Carbon Nanotubes-Based Gas Sensors. *J. Sens.* **2009**. [\[CrossRef\]](#)
22. Wulan Septiani, N.L.; Yuliarto, B. Review—The Development of Gas Sensor Based on Carbon Nanotubes. *J. Electrochem. Soc.* **2016**, *163*. [\[CrossRef\]](#)
23. Huotari, J.; Kekkonen, V.; Haapalainen, T.; Leidinger, M.; Sauerwald, T.; Puustinen, J.; Liimatainen, J.; Lappalainen, J. Pulsed laser deposition of metal oxide nanostructures for highly sensitive gas sensor applications. *Sens. Actuators B Chem.* **2016**, *236*, 978–987. [\[CrossRef\]](#)
24. Leidinger, M.; Huotari, J.; Sauerwald, T.; Lappalainen, J.; Schütze, A. Selective detection of naphthalene with nanostructured WO_3 gas sensors prepared by pulsed laser deposition. *J. Sens. Sens. Syst.* **2016**, *5*, 147–156. [\[CrossRef\]](#)
25. Baur, T.; Schütze, A.; Sauerwald, T. Optimierung des temperaturzyklischen Betriebs von Halbleitergassensoren. *Technisches. Messen.* **2015**, *82*, 187–195. [\[CrossRef\]](#)
26. Sauerwald, T. Model based improvement of temperature cycled operation of tin oxide gas sensors. In Proceedings of the IX International Workshop on Semiconductor Gas Sensors, Zakopane, Poland, 13–16 December 2015.
27. Zhang, S.P.; Lei, T.; Li, D.; Zhang, G.Z.; Xie, C. UV light activation of TiO_2 for sensing formaldehyde: How to be sensitive, recovering fast, and humidity less sensitive. *Sens. Actuators B Chem.* **2014**, *202*, 964–970. [\[CrossRef\]](#)
28. Jin, H.; Haick, H. UV regulation of non-equilibrated electrochemical reaction for detecting aromatic volatile organic compounds. *Sens. Actuators B Chem.* **2016**, *237*, 30–40. [\[CrossRef\]](#)
29. Reimann, P.; Schütze, A. Sensor arrays, virtual multisensors, data fusion, and gas sensor data evaluation. In *Gas. Sensing Fundamentals*; Kohl, C.-D., Wagner, T., Eds.; Springer Series on Chemical Sensors and Biosensors, Volume 15; Springer: Berlin Heidelberg, Germany, 2014; pp. 67–107.
30. Clifford, P.K.; Tuma, D.T. Characteristics of semiconductor gas sensors II. transient response to temperature change. *Sens. Actuators* **1983**, *3*, 255–281. [\[CrossRef\]](#)
31. Lee, A.P.; Reedy, B.J. Temperature modulation in semiconductor gas sensing. *Sens. Actuators B Chem.* **1999**, *60*, 35–42. [\[CrossRef\]](#)
32. Gramm, A.; Schütze, A. High performance solvent vapor identification with a two sensor array using temperature cycling and pattern classification. *Sens. Actuators B Chem.* **2003**, *95*, 58–65. [\[CrossRef\]](#)
33. Bur, C.; Reimann, P.; Andersson, M.; Schütze, A.; Spetz, A.L. Increasing the Selectivity of Pt-Gate SiC Field Effect Gas Sensors by Dynamic Temperature Modulation. *IEEE Sens. J.* **2011**, *12*, 1906–1913. [\[CrossRef\]](#)
34. Fricke, T.; Sauerwald, T.; Schütze, A. Study of Pulsed Operating Mode of a Microstructured Pellistor to Optimize Sensitivity and Poisoning Resistance. In Proceedings of the IEEE Sensors Conference 2014, Valencia, Spain, 2–5 November 2014.
35. Ankara, Z.; Schütze, A. Low Power Virtual Sensor System based on a Micromachined Gas Sensor for Security Applications and Warning Systems. In Proceedings of the Eurosensors XXII Conference 2008, Dresden, Germany, 7–10 September 2008.
36. Schüler, M.; Sauerwald, T.; Schütze, A. A novel approach for detecting HMDSO poisoning of metal oxide gas sensors and improving their stability by temperature cycled operation. *J. Sens. Sens. Syst.* **2015**, *4*, 305–311. [\[CrossRef\]](#)
37. Bur, C.; Andersson, M.; Lloyd Spetz, A.; Schütze, A. Detecting Volatile Organic Compounds in the ppb Range with Gas Sensitive Platinum gate SiC-Field Effect Transistors. *IEEE Sens. J.* **2014**, *14*, 3221–3228. [\[CrossRef\]](#)

38. Weimar, U.; Göpel, W.A.C. Measurements on tin oxide sensors to improve selectivities and sensitivities. *Sens. Actuators B Chem.* **1995**, *26*–27, 13–18. [\[CrossRef\]](#)

39. Bastuck, M.; Bur, C.; Lloyd Spetz, A.; Andersson, M.; Schütze, A. Gas identification based on bias induced hysteresis of a gas-sensitive SiC field effect transistor. *J. Sens. Sens. Syst.* **2014**, *3*, 1–11. [\[CrossRef\]](#)

40. Reimann, P.; Dausend, A.; Darsch, S.; Schüler, M.; Schütze, A. Improving MOS Virtual Multisensor Systems by Combining Temperature Cycled Operation with Impedance Spectroscopy. In Proceedings of the ISOEN 2011, International Symposium on Olfaction and Electronic Nose, New York, NY, USA, 2–5 May 2011.

41. Bur, C.; Bastuck, M.; Lloyd Spetz, A.; Andersson, M.; Schütze, A. Selectivity enhancement of SiC-FET gas sensors by combining temperature and gate bias cycled operation using multivariate statistics. *Sens. Actuators B Chem.* **2014**, *193*, 931–940. [\[CrossRef\]](#)

42. Kammerer, T.; Ankara, Z.; Schütze, A. GaSTON—A versatile platform for intelligent gas detection systems and its application for fast discrimination of fuel vapors. In Proceedings of the Eurosensors XVII Conference 2003, Guimarães, Portugal, 22–24 September 2003.

43. Conrad, T.; Hiray, P.; Schütze, A. PuMaH—A temperature control and resistance read-out system for microstructured gas sensors based on PWM signals. In Proceedings of the IEEE Sensors Conference 2005, Irvine, CA, USA, 31 October–3 November 2005.

44. Conrad, T.; Fricke, T.; Reimann, P.; Schütze, A. A versatile platform for the efficient development of gas detection systems based on automatic device adaptation. In Proceedings of the Eurosensors XX Conference 2006, Göteborg, Sweden, 17–20 September 2006.

45. 3S-Toolbox. Available online: <http://www.3s-ing.de/3s-technology/3s-toolbox/?L=1> (accessed on 30 December 2016).

46. Reimringer, W.; Rachel, T.; Conrad, T.; Schütze, A. Outdoor odor nuisance monitoring by combining advanced sensor systems and a citizens network. In Proceedings of the ISOEN 2015, 16th International Symposium on Olfaction and Electronic Noses, Dijon, France, 28 June–1 July 2015.

47. Stahl-Offergeld, M.; Hohe, H.P.; Jung, R.; Leidinger, M.; Schütze, A.; Sauerwald, T. Highly integrated sensor system for the detection of trace gases. In Proceedings of the IMCS’16–16th International Meeting on Chemical Sensors, Jeju Island, Korea, 10–14 July 2016.

48. Schüler, M.; Sauerwald, T.; Schütze, A. Metal oxide semiconductor gas sensor self-test using Fourier-based impedance spectroscopy. *J. Sens. Sens. Syst.* **2014**, *3*, 213–221. [\[CrossRef\]](#)

49. Sauerwald, T.; Schüler, M.; Schütze, A. *Erforschung einer Strategie und Entwicklung einer Messplattform zur Selbstüberwachung von Gasmesssystemen auf Basis von Halbleitergassensoren*; Bundesministerium für Wirtschaft und Energie: Berlin, Germany, 2015.

50. Leonardos, G.; Kendall, D.; Barnard, N. Odor Threshold Determinations of 53 Odorant Chemicals. *J. Air Pollut. Control. Assoc.* **1969**, *19*, 91–95. [\[CrossRef\]](#)

51. Akbar, M.; Restaino, M.; Agah, M. Chip-scale gas chromatography: From injection through detection. *Microsyst. Nanoeng.* **2015**, *1*, 15039. [\[CrossRef\]](#)

52. Zampolli, S.; Elmi, I.; Stürmann, J.; Nicoletti, S.; Dori, L.; Cardinali, G.C. Selectivity enhancement of metal oxide gas sensors using a micromachined gas chromatographic column. *Sens. Actuators B Chem.* **2005**, *105*, 400–406. [\[CrossRef\]](#)

53. Leidinger, M.; Rieger, M.; Sauerwald, T.; Nägele, M.; Hürttlen, J.; Schütze, A. Trace gas VOC detection using metal-organic frameworks micro pre-concentrators and semiconductor gas sensors. *Procedia Eng.* **2015**, *120*, 1042–1045. [\[CrossRef\]](#)

54. Leidinger, M.; Rieger, M.; Sauerwald, T.; Alépée, C.; Schütze, A. Integrated pre-concentrator gas sensor microsystem for ppb level benzene detection. *Sens. Actuators B Chem.* **2016**, *236*, 988–996. [\[CrossRef\]](#)

55. SENSIndoor clip. Available online: <http://sensindoor.eu/film> (accessed on 30 December 2016).

56. Helwig, N.; Schüler, M.; Bur, C.; Schütze, A.; Sauerwald, T. Gas mixing apparatus for automated gas sensor characterization. *Meas. Sci. Technol.* **2014**, *25*, 055903. [\[CrossRef\]](#)

57. OSS Foundation: Atmospheric Composition. Available online: ossfoundation.us/projects/environment/global-warming/atmospheric-composition (accessed on 30 December 2016).

58. Deutscher Wetterdienst (DWD): Composition of the Atmosphere–Trace Gases–Carbon Monoxide. Available online: www.dwd.de/EN/research/observing_atmosphere/composition_atmosphere/trace_gases/cont_nav/co_node.html (accessed on 30 December 2016).

59. Schultealbert, C.; Baur, T.; Schütze, A.; Böttcher, S.; Sauerwald, T. A novel approach towards calibrated measurement of trace gases using metal oxide semiconductor sensors. *Sens. Actuators B Chem.* **2017**, *239*, 390–396. [[CrossRef](#)]
60. Nanotechnology-Based Intelligent Multi-SENsor System with Selective Pre-Concentration for Indoor Air Quality Control, Website of the SENsIndoor Project. Available online: www.sensindoor.eu/ (accessed on 30 December 2016).
61. Lappalainen, J.; Huotari, J.; Leidinger, M.; Baur, T.; Alépée, C.; Komulainen, S.; Puustinen, J.; Schütze, A. Tailored Metal Oxide Nanoparticles, Agglomerates, and Nanotrees for Gas Sensor Applications. In Proceedings of the IX International Workshop on Semiconductor Gas Sensors, Zakopane, Poland, 13–16 December 2015.
62. Kekkonen, V.; Alépée, C.; Liimatainen, J.; Leidinger, M.; Schütze, A. Gas sensing characteristics of nanostructured metal oxide coatings produced by ultrashort pulsed laser deposition. In Proceedings of the Eurosensors XXIX Conference 2015, Freiburg, Germany, 6–9 September 2015.
63. Puglisi, D.; Eriksson, J.; Andersson, M.; Huotari, J.; Bastuck, M.; Bur, C.; Lappalainen, J.; Schütze, A.; Lloyd Spetz, A. Exploring the Gas Sensing Performance of Catalytic Metal/Metal Oxide 4H-SiC Field Effect Transistors. *Mater. Sci. Forum* **2016**, *858*, 997–1000. [[CrossRef](#)]
64. Puglisi, D.; Eriksson, J.; Bur, C.; Schütze, A.; Lloyd Spetz, A.; Andersson, M. Catalytic metal-gate field effect transistors based on SiC for indoor air quality control. *J. Sens. Sens. Syst.* **2015**, *4*, 1–8. [[CrossRef](#)]
65. Metrology for VOC Indicators in Air Pollution and Climate Change, Website of the KEY-VOCs Project. Available online: www.key-vocs.eu (accessed on 30 December 2016).
66. Spinelle, L.; Gerboles, M.; Kok, G.; Sauerwald, T. Sensitivity of VOC Sensors for Air Quality Monitoring within the EURAMET Key-VOC project. In Proceedings of the Fourth EuNetAir Scientific Meeting, Linköping, Sweden, 3–5 June 2015.
67. Reimringer, W.; Howes, J.; Conrad, T. Implementation of Complex Gas Sensor Systems: Ideas for a Structural Model. In Proceedings of the Sixth EuNetAir Scientific Meeting, Prague, Czech Republic, 5–7 October 2016.



© 2017 by the authors. Licensee MDPI, Basel, Switzerland. This article is an open access article distributed under the terms and conditions of the Creative Commons Attribution (CC BY) license (<http://creativecommons.org/licenses/by/4.0/>).

4.3.3 Paper 5 – Highly Sensitive Benzene Detection with Metal Oxide Semiconductor Gas Sensors - an Inter-laboratory Comparison

T. Sauerwald¹, T. Baur¹, M. Leidinger¹, W. Reimringer², L. Spinelle³, M. Gerboles³, G. Kok⁴, A. Schütze¹

¹Saarland University, Lab for Measurement Technology, Saarbrücken, Germany

²3S GmbH—Sensors, Signal Processing, Systems, Saarbrücken, Germany

³European Commission—Joint Research Centre, Directorate for Energy, Transport and Climate, Ispra, Italy

⁴VSL, Thijsseweg 11, Delft, the Netherlands

J. Sens. Sens. Syst. (2018), 7, 235-243

The original paper and supplementary data can be found, in the online version, at

<https://doi.org/10.5194/jsss-7-235-2018>.

© 2018 by the authors. This article is an open access article distributed under the terms and conditions of the Creative Commons Attribution (CC BY) license (<http://creativecommons.org/licenses/by/4.0/>).



Highly sensitive benzene detection with metal oxide semiconductor gas sensors – an inter-laboratory comparison

Tilman Sauerwald¹, Tobias Baur¹, Martin Leidinger¹, Wolfhard Reimringer², Laurent Spinelle³, Michel Gerboles³, Gertjan Kok⁴, and Andreas Schütze¹

¹Laboratory for Measurement Technology, Saarland University, Saarbrücken, 66123, Germany

²3S GmbH, Saarbrücken, 66121, Germany

³European Commission—Joint Research Centre, Directorate for Energy,
Transport and Climate, 21027 Ispra, Italy

⁴VSL, Tijsseweg 11, 2629 JA Delft, the Netherlands

Correspondence: Tilman Sauerwald (t.sauerwald@lmt.uni-saarland.de)

Received: 29 September 2017 – Revised: 5 February 2018 – Accepted: 11 February 2018 – Published: 5 April 2018

Abstract. For detection of benzene, a gas sensor system with metal oxide semiconductor (MOS) gas sensors using temperature-cycled operation (TCO) is presented. The system has been tested in two different laboratories at the concentration range from 0.5 up to 10 ppb. The system is equipped with three gas sensors and advanced temperature control and read-out electronics for the extraction of features from the TCO signals. A sensor model is used to describe the sensor response in dependence on the gas concentration. It is based on a linear differential surface reduction (DSR) at a low temperature phase, which is linked to an exponential growth of the sensor conductance. To compensate for cross interference to other gases, the DSR is measured at three different temperatures (200, 250, 300 °C) and the calculated features are put into a multilinear regression (partial least square regression – PLSR) for the quantification of benzene at both laboratories. In the tests with the first set-up, benzene was supplied in defined gas profiles in a continuous gas flow with variation of humidity and various interferents, e.g. toluene and carbon monoxide (CO). Depending on the gas background and interferents, the quantification accuracy is between ± 0.2 and ± 2 ppb. The second gas mixing system is based on a circulation of the carrier gas stream in a closed-loop control for the benzene concentration and other test gases based on continuously available reference measurements for benzene and other organic and inorganic compounds. In this system, a similar accuracy was achieved for low background contaminations and constant humidity; the benzene level could be quantified with an error of less than 0.5 ppb. The transfer of regression models for one laboratory to the other has been tested successfully.

1 Introduction

Air quality is an important pre-requisite for public health. The pollution of the air with gaseous compounds contributes relevantly to the burden of disease in industrial and developing countries (Bernstein et al., 2008). One of the most important pollutants is benzene (WHO Regional Office for Europe, 2010). Due to its toxicity and its carcinogenicity, very low concentrations of benzene should be detected and monitored; threshold limits are in the ppb range, e.g. the European Air

Quality Directive set the limit value at $5 \mu\text{g m}^{-3}$ or 1.6 ppb as the long-term environmental limit (European Parliament and Union, 2008). The benzene detection is also an important topic for indoor air quality and workplace safety, where several national regulations have been put in force, e.g. the Bundesanstalt für Arbeitsschutz und Arbeitsmedizin (2014). For environmental monitoring, analytic techniques, e.g. gas chromatography (GC), are used. In Europe, monitoring of benzene in ambient air is mandatory. The European Air Quality Directive states that the reference method for the mea-

surement of benzene must consist of active or online sampling followed by desorption and gas chromatography (BSI, 2015). Due to the high price and maintenance costs of these methods, the number of points in the measurement network is very limited, but the necessity for a higher spatial resolution of pollution control has been reported (Batterman et al., 1994; Heimann et al., 2015). Within the EMRP project KEY-VOCs, therefore, the use of sensor systems as an indicative method for the measurement of benzene has been tested in order to assess whether the demand for a low-cost measurement device for benzene can be met. A review (Spinelle et al., 2017b) of the existing sensor technology and its commercially available systems has revealed that only very few manufacturers are targeting this concentration range and that it is doubtful whether one of these systems can meet the criteria of detection limit, selectivity and stability (Spinelle et al., 2017a). Therefore, micro analytical systems and prototype sensor systems have been included in the tests. The result of one prototype using metal oxide semiconductor (MOS) gas sensors with temperature cycle operation (TCO) is reported in this paper. This approach has previously been studied for the selective detection of volatile organic compounds (VOCs), e.g. benzene in indoor air (Leidinger et al., 2014; Schütze et al., 2017). MOS gas sensors are very robust and sensitive devices (Morrison, 1981; Sasahara et al., 2004) sensitive to a broad variety of reducing gases. The resistance of the sensor (Eq. 1) is dominated by ionized oxygen at the surface which causes an energy barrier E_B and the height of the barrier depends in a quadratic function on the density of the ionized oxygen N_S .

$$G = G_0 \cdot e^{-\frac{E_B}{k_B T}} \quad \text{with} \quad E_B \propto N_S^2 \quad (1)$$

The reaction of the reducing gas with the reactive surface oxygen reduces the energy barrier and increases the conductance strongly. For constant temperature and gas concentration the change of surface charge can be described by a mass action law of chemisorbed species leading to a power law for the dependence of conductance and gas concentration (Barsan and Weimar, 2001; Madou and Morrison, 1989). While in a few cases the selectivity of the sensors can be increased by special preparation methods for example described in Hennemann et al. (2012), Kemmler et al. (2012), and Leidinger et al. (2016b), typically multi-signal methods like TCO are used. TCO is a well-known method for the improvement of selectivity reported in a multitude of papers, e.g. Eicker (1977), Gramm and Schütze (2003), and Lee and Reedy (1999). It is dynamic operation (Nakata et al., 1998a, b) and in this sense it enables sensor properties that cannot be found in a sensor at any constant temperature. Following this line, some of us could prove in the last few years that an optimized TCO can increase the sensitivity (Baur et al., 2015) and the stability (Schultealbert et al., 2017) of the sensor signal as well. The model-based optimization uses a set of rate equations for the trapping and release in surface states pro-

posed by Ding et al. (2001). For the quantification of VOC concentrations at the ppb level, a technique based on the relaxation of the conductance at a low temperature phase has been demonstrated (Baur et al., 2015). The technique utilizes the fact that the equilibrium surface coverage with ionized oxygen depends on the sensor temperature. At high temperature (e.g. at 450 °C) the surface coverage and thereby the barrier height are higher than at low temperature (e.g. 200 °C) (Schultealbert et al., 2017). For a fast temperature reduction, an excess of surface coverage can be obtained (Baur et al., 2015). At this stage, the reaction at the sensor surface is far from equilibrium as the ionosorption of oxygen is very unlikely. The sensor surface is then predominantly reduced by gases, e.g. benzene, causing a strong increase in sensor response compared to isothermal operation. This increase can be several orders of magnitude in terms of relative conductance. The reduction of the surface is linear to the applied gas dosage or gas concentration given that the concentration is constant over one surface reduction (Baur, 2017). The change in the logarithmic sensor conductance $\ln G_{\text{init}}$ at the beginning of a low temperature plateau (beginning at $t_0 = 0$) is linear to the gas concentration c_{gas} .

$$\frac{d \ln G_{\text{init}}(t)}{dt} \sim \text{const} \sim k_{\text{gas}} \cdot c_{\text{gas}} + k_0 \quad (2)$$

Please note that Eq. (2) is only valid if the surface charge is still high above equilibrium; otherwise, the ionosorption of new surface charge is not negligible anymore. A detailed discussion can be found in Schultealbert et al. (2017).

Following this line, we could show that the benzene concentration in the range from 500 ppt to 10 ppb air can be quantified very accurately in a purified air background, whereby compensation of the ubiquitous gas background and interfering gas reduces the accuracy of detection (Leidinger et al., 2017).

2 Experimental

2.1 Sensor system

The sensor system is equipped with three different commercial MEMS gas sensor elements. Two sensor elements are integrated in a dual-sensor package (MiCS 4510 from SGX, Switzerland) and the third sensor is a single-sensor device (AS-MLV from ams Sensor Solutions, Germany). All sensors are operated in TCO with independent control and readout. A block diagram of the sensor system can be found in the Supplement (Fig. S1). Rapid temperature changes from a high temperature of 450 °C to lower temperatures (200/250/300 °C) are used. The duration of the high temperature plateau is 10 s each, for the 200 and 250 °C plateau the duration is 35 s, and for the 300 °C plateau it is 20 s. The TCO control and the read-out are done using a modified sensor system (SensorToolbox, 3S GmbH, Germany)

that can support up to four sensor modules (ToolboxModule). The sensor signal S_{\log} for each sensor is measured using a logarithmic amplifier comparing the sensor current I_{sens} with a reference current $I_{\text{ref}} = 1 \text{ mA}$. The sensor is operated at a constant voltage of 0.25 V ; hence, the sensor current $I_{\text{sens}} = 0.25 \text{ V} \cdot G_{\text{sens}}$ is directly linear to the sensor conductance. The output of the logarithmic amplifier is divided by a subsequent voltage divider to match with the voltage range of the analogue-digital converter of the ToolboxModule (Eq. 1). Corresponding to this, a virtual reference conductance G_{ref} can be calculated. The output of the logarithmic amplifier of $U_{\text{LogAmp}} = 0.5 \text{ V}$ per decade is divided by a subsequent voltage divider to match with the voltage range of the analogue-digital converter of the ToolboxModule, yielding a voltage U_{\log} of 0.25 V per decade.

This output voltage (Eq. 3) is defined as sensor signal S_{\log} which is linear to the logarithm of the conductance G_{sens} of the gas sensing layers.

$$\begin{aligned} S_{\log} &= 0.25 \text{ V} \cdot \log_{10} \left(\frac{I_{\text{ref}}}{I_{\text{sens}}} \right) \\ &= 0.25 \text{ V} \cdot \log_{10} \left(\frac{I_{\text{ref}}}{G_{\text{sens}} \cdot 0.25 \text{ V}} \right) \end{aligned} \quad (3)$$

This measuring method allows us to cover a large signal range, as MOS gas sensor resistances can vary within several orders of magnitude during rapid temperature changes (Baur et al., 2015). Please note that this sensor signal is different from the commonly used sensor response, which is defined as G/G_0 . A change in the sensor signal $\Delta S_{\log} = S_{\log} - S_{\log 0}$ can be easily transformed to a sensor response by $S = 10^{\Delta S_{\log}/0.25 \text{ V}}$. However, the definition of S_{\log} allows a facile calculation of the change surface charge as the time-derived sensor signal S_{\log} is proportional to the rate constant k of surface reduction (Eq. 2), which is itself linear depending on the gas (benzene) concentration (Eq. 4).

$$\begin{aligned} \frac{dS(t)}{dt} &\sim \frac{d \ln G_{\text{init}}(t)}{dt} \sim -k \sim -c \cdot k_{\text{gas}} - k_0 \\ \text{for small } (t - t_0) \end{aligned} \quad (4)$$

2.2 Data processing

We used our DAV³E toolbox (Bastuck et al., 2016) for the data processing. The data processing was performed in three steps: feature extraction, feature selection and quantification. The feature extraction reduces the dimensionality of the classification problem.

A set of features of each temperature cycle was extracted from the signals, which describes the shape of the signal (mean values and slopes). The slopes correspond in first approximation to the rate constant (derivative of the sensor signal Eq. (4)). These features were calculated from several segments of the cyclic sensor signal, covering all set temperatures. The ranges of the features have been varied to find the

best selection by the feature selection. Feature selection was performed using a recursive feature elimination support vector machine (RFESVM) (Schüler et al., 2017) to choose the best features for classification.

Using these feature sets and the known benzene concentrations, a PLSR model (partial least squares regression) (Bastuck et al., 2015b; Wold et al., 2001) is calculated, which generates a linear combination of the features to allow an estimation of the benzene concentration.

2.3 Gas tests at the Lab for Measurement Technology (LMT)

In the first laboratory (LMT – Lab for Measurement Technology, Saarbrücken, Germany) the sensor system has been tested using a gas mixing apparatus (GMA) operating by the principle of dynamic dilution. The set-up of this system has been reported in detail previously (Helwig et al., 2014). A two-stage dilution system is used to produce the benzene test gas, starting from a gas cylinder containing 50 ppm benzene in synthetic air. The benzene is diluted with zero air, generated from a cascade of two gas purifiers. The first purifier includes a coarse filter to remove particles and oil. Subsequently, humidity and CO_2 are removed by two alternating molar sieves (pressure swing) and hydrocarbons ($>\text{C}_3$) are removed by an active charcoal filter. The second purifier has an additional pre-filter and pressure swing followed by a catalytic combustion of hydrogen, carbon monoxide and short chain hydrocarbons ($<\text{C}_4$). The catalytic converter is furthermore equipped with a nitrogen oxide scrubber. The pure air is split into eight gas lines, of which five have been used in this investigation. In the first line, pure air saturated with humidity is generated at a dew point of 20°C using an isothermal blubber with HPLC grade water (low organic carbon). The second line is used for dry air. The third line is a two-step dilution using a dry stream of purified air and diluted benzene test gas from a cylinder in the first dilution step. The second dilution step is the combination with the humid and dry main gas stream from the first two lines. In the fourth line, toluene is added to the test gas; it uses the same set-up as the benzene line. The fifth line uses a two-step dilution to generate a background of 500 ppb hydrogen, 150 ppb carbon monoxide and 1820 ppb methane from a gas cylinder with a dilution of these gases in air. These three gases are the main reducing compounds in pure environmental air (Ehhalt and Rohrer, 2009; Gilge et al., 2010). This gas background has a strong impact on the sensor response as well as on the detection limit of the sensor (Leidinger et al., 2017). A mixture of pure zero air with this background will be defined as standard air. The sensors have been tested directly in gas flow of 200 sccm in a stainless steel sensor housing.

2.4 Gas tests at JRC

For the second laboratory campaign, the evaluation was carried out using the JRC (Joint Research Center) exposure chamber. This chamber allows the control of numerous gaseous mixtures including benzene and a set of selected interfering compounds (toluene, m,p-xylene, ethane, propane, n-butane and n-pentane) plus temperature, relative humidity and wind velocity. The exposure chamber is an “O”-shaped ring-tube system, covered with dark insulation material. The full system has already been described elsewhere (Spinelle et al., 2014). All gaseous compounds are added to pure zero air. The micro-sensors in the stainless steel housing described above were directly placed inside the ring tube. High concentration cylinders were used to generate specific levels of pollutants based on the dynamic dilution principle. A specific LabView software using multiple proportional-integral-derivative (*PID*) feedback loops ensured the stability of the concentration. The reference value for the feedback loop was measured using a PTR-MS (proton-transfer-reaction mass spectrometer) and the reference values were measured by a gas chromatograph with a photo ionization detector (GC-PID 955 from Syntech). The direct input of reference measurements of gaseous compounds, temperature, humidity and wind speed is used to auto-correct the gas mixture, temperature controlling cryostat and wind velocity by means of an internal fan. In particular, this set-up allows one to set independent criteria for the stability of each parameter and for a defined period of time.

3 Measurement results and data analysis

3.1 Benzene quantification capabilities

The sensor system has been tested in the LMT system in pure zero air towards benzene at six gas concentrations from 0.5 to 10 ppb and three relative humidities (10, 25, 40 %RH) to test the quantification and humidity compensation. Due to the high purity of the zero air, the conductance of the sensors at the beginning of the low temperature phases is very low. The sensor response shows a high noise. The derivative of the sensor response is obviously an even worse signal. Thus, a feature selection tool as described above has been used instead of using the model-based feature directly. The feature selection selected only signals from the less noisy parts of the response curve. To test the quantification of benzene a PLSR has been calculated using the measurement of 0.5, 3 and 10 ppb benzene at 10 and 40 %RH (Fig. 1a). The PLSR is in general a regression of the measured values (e.g. sensor system output) with the “true” values (or a proper estimate, e.g. from a reference measurement). Please note that the value of the concentration set point (x -axis) also adds an additional uncertainty to the regression. As the LMT gas mixing system does not provide continuous reference measurements of the benzene concentration, an estimate of the real value is de-

rived from the mixing ratio of the gas flows and the certified concentration of the gas cylinders. The gas flows are continuously measured and recorded by the gas mixing system. The proper function of the gas mixing system was confirmed as the error of the recorded flow rates is within the error margin. As estimates for the true concentration, the set points of the gas mixing system were used. Figure 1 shows that the PLSR is very accurate. The sensor system output is obviously a linear function for benzene concentration and the compensation of humidity cross-sensitivity is very good. The error of the predicted response is below 0.2 ppb for all trained concentrations. The PLSR model was applied to untrained concentrations of benzene (1, 2 and 5 ppb) at 10 and 40 %RH and to the six concentrations of benzene tested at 25 %RH. This test of the model prediction is shown in Fig. 1b. The full circles denote the trained data points and open circles denote the untrained “test” data point. The test data points do not show any decisive deviation from the trained data points. The interpolation of the benzene concentration and a compensation of an untrained humidity background are demonstrated by this result. However, the quantification of benzene in ambient air at the sub-ppb level cannot be derived from this result since even clean air contains significant inorganic reducing gas components as described in Sect. 2. A similar test therefore has been made under standard air (cf. Sect. 2.2) instead of zero air. The quantification properties have been tested in detail under standard air and other interfering gases in a previous work (Leidinger et al., 2017) showing the strong impact of gas background on the accuracy of the detection. Measurements were made with the dynamic dilution set-up at LMT. In the first case (Fig. 2a), two sweeps of the benzene concentration are included, one in pure zero air without interferences and one with a 2 ppb toluene background, at a constant gas humidity of 25 %RH. The benzene concentrations predicted by the PLSR model still show a very small error of below 200 ppt with respect to the concentration set point. The introduction of standard air has a strong impact on the quantification of benzene. In Fig. 2a the PLSR is shown in standard air, including a variation of the CO concentration between 150 ppb (ubiquitous) and 500 ppb (lightly polluted air). Still, the PLSR shows a linearity between the sensor system output and the set-point concentration, but the error of the prediction is between 1 and 2 ppb depending on the benzene concentration. The addition of interferences like toluene between 2 and 20 ppb (Fig. 2c) seems to reduce the accuracy of the benzene quantification further. However, the strongest impact comes from the standard air conditions. The quantification error can be reduced if the data from 10 %RH are removed from the data set corresponding to a reduction of interfering complexity. Figure 2d contains only two gas humidities; the signals recorded at the lowest value are not taken into account. For this condition the quality of quantification of benzene was improved; compared to the scenarios in Fig. 2b and c, the groups are more compact and error for

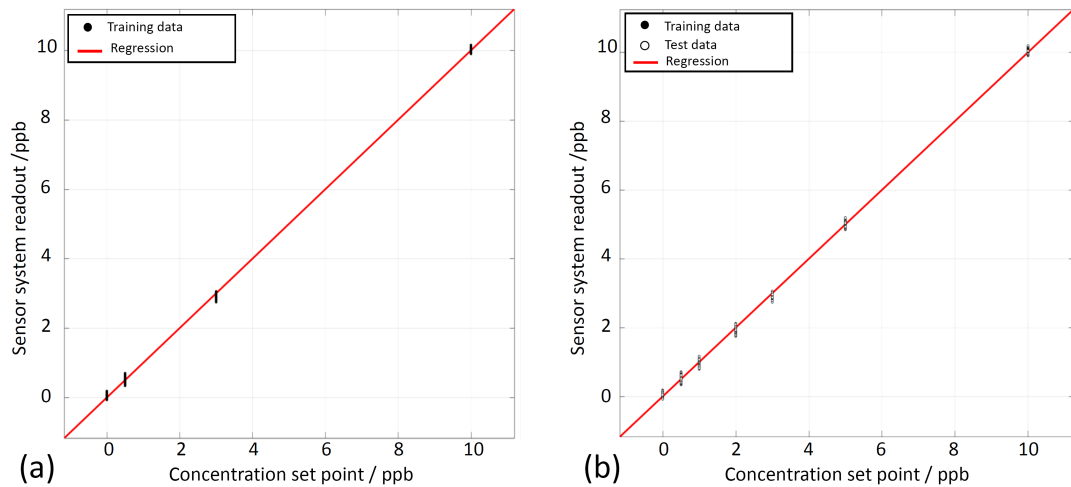


Figure 1. Quantification of benzene in zero air using feature extraction and PLSR. (a) Only training data. (b) Training and test data.

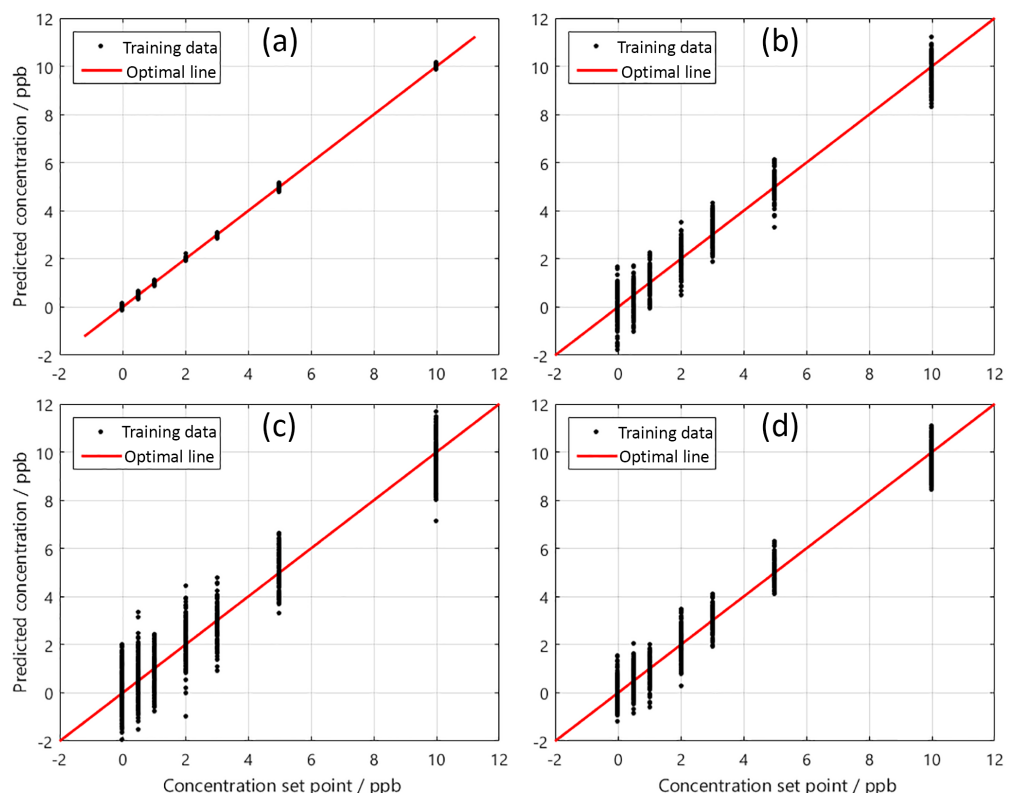


Figure 2. PLSR benzene quantification results for four different background and interferent configurations (Leidinger et al., 2017): (a) benzene in pure zero air and with 2 ppb of toluene added, at 25 %RH. (b) Benzene in standard air and variation of CO background, 10, 25 and 40 %RH. (c) Benzene in standard air and variation of toluene, 10, 25 and 40 %RH. (d) Benzene in standard air and variation of toluene and CO, 25 and 40 %RH.

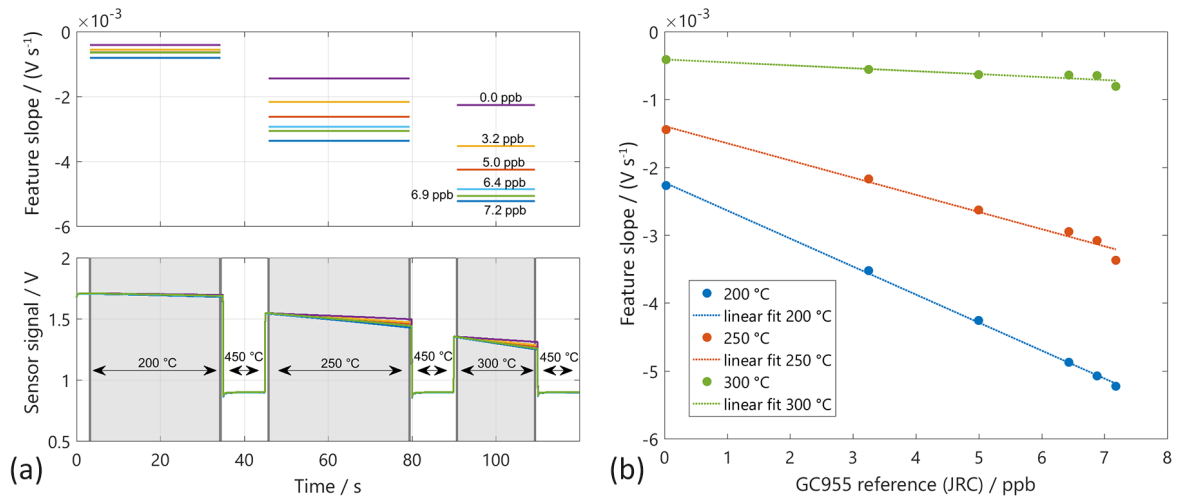


Figure 3. (a) Sensor signals in temperature-cycled operation (temperature ranges: blue arrows). The relaxation constants (slope feature) are calculated from the grey marked domains. (b) Feature slope over benzene concentration according to the GC955 reference measurement.

the benzene concentration is below 1.8 ppb over the whole concentration range.

3.2 Lab intercomparison

After the initial calibration at LMT, the system was transferred to the JRC. During this transfer, the interface of the read-out electronic of the dual sensor (MiCS4514) was damaged. For the lab intercomparison the remaining sensor (AS-MLV) has been used and the signal processing has been re-trained. Only tests with zero air background at various humidity and interferent levels have been compared, as in the JRC set-up no addition of the inorganic background was foreseen. The features have been calculated according to Eq. (4) directly, without selection of the feature ranges using RFESVM. However, a short time span at the beginning of the low temperature has been left out manually to reduce the noise (cf. Fig. 3; the sections for feature extraction are marked in grey). The sensor signal S_{\log} in the low temperature plateaus has a good linearity over the full temperature plateau in good agreement with Eq. (4) for all temperature plateaus at all tested benzene concentrations (Fig. 3). Obviously, the strongest response of the sensor to benzene can be found at 300 °C (Fig. 3). Using these features a PLSR model has been trained from the data of the JRC measurement and tested with the data from the LMT measurements. Please note that only three features can be calculated from the single sensor and that the impact of the feature at 200 °C is very small, leading to an incomplete compensation compared to the three-sensor system described in Sect. 3.1. Therefore, only measurement results with pure benzene have been evaluated. For the training of the PLSR, the data of the reference measurement from the GC-PID 955 were used as estimates of the true values. We compared the transfer of a PLSR model

obtained by training data of one test system to test data obtained by the other test system (Fig. 4). The transfer of the model trained with JRC test data to LMT test data is shown on the left side in Fig. 4. The black circles denote the trained data points from the JRC lab and the red circles denote the untrained data points from the LMT lab. The benzene concentrations predicted by the PLSR model for the JRC data at 60 %RH still show a very small error of below 200 ppt with respect to the concentration measured by the GC-PID 955. We see two different trend lines of the predicted data points from the LMT lab. Each trend line shows a specific humidity at 10 %RH and 25 %RH. Both trend lines show a good linearity and the same slope, but also an offset to the optimal line. The transfer from the model obtained with LMT data is shown in Fig. 4 on the right. The training was performed with only a single humidity (25 %RH), as obviously the humidity compensation of the single sensor system is not sufficient. The test data from the JRC as well as the test data from the LMT show a good linearity, but also an offset to the training data. The offset is probably due to the humidity as the data with 60 %RH exhibit a negative offset, while the data with 10 %RH exhibit a positive offset.

4 Discussion and conclusion

The presented MOS gas sensor system shows very good performance for benzene quantification, especially in pure air even with low levels of interfering toluene, including the interpolation of unknown benzene concentrations over the full humidity range tested. However, at standard air and a realistic background level of interferents, especially CO, the error of quantification is in the range of 1–2 ppb. For the environmental monitoring, especially in rural areas, even lower

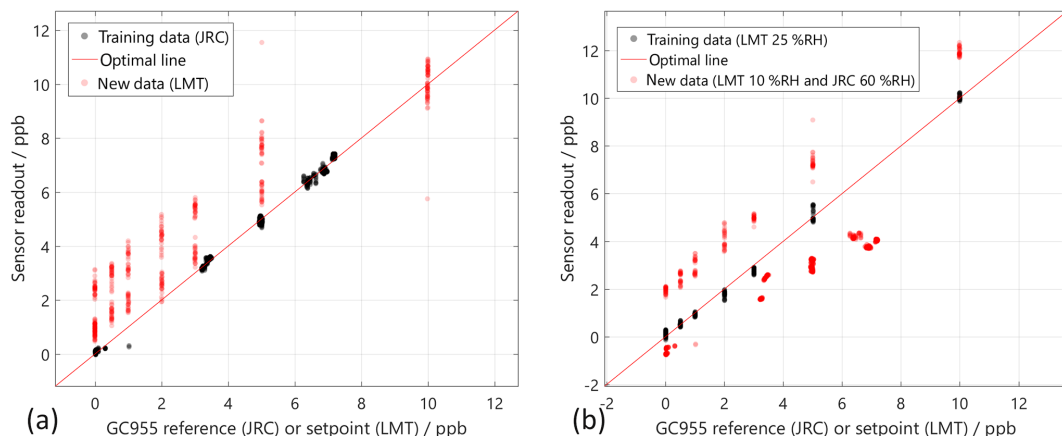


Figure 4. Transfer of the PLSR model from training data of one gas mixing system to test data from another gas mixing system. **(a)** Training using the JRC measurement (60 %RH black solid circles) and test data from the LMT measurement (10 and 25 %RH open red circles). **(b)** Training using LMT measurements (25 %RH black circle) and test using the JRC data (60 %RH) and the LMT data (10 %RH). Both test data are shown in open red circles.

detection limits are needed to monitor the benzene concentration (Schneidemesser et al., 2010). A possible strategy for the further reduction of the detection limit are sensor/pre-concentrator micro systems (Leidinger et al., 2016a) and a further optimization of the sensor system electronics to reduce the noise of the signal (Baur and Schütze, 2017). For the quantification of benzene, a combination of the DSR model for feature extraction and a multilinear regression for the compensation of interferences has been tested successfully. Within the measured sensor signals all tested benzene concentrations were in good agreement with the prediction of the DSR model. The multilinear regression yields very good compensation of humidity and even toluene interference. The regression for all conditions shows a good linearity without further pre-processing of the signal; this is an advantage of the system over other TCO modes, which usually does not yield a linear signal with concentration requiring a special pre-processing before PLSR (Bastuck et al., 2015a). The system can be successfully calibrated at different labs and testing conditions, indicating that the very different methods of generating benzene yield similar levels of test gas. The transfer of a regression model from the JRC test data to the LMT test data shows good linearity of the measured benzene concentration but an offset of the response curve on the order of 2 ppb. The observed offset is probably due to the different humidity as the humidity compensation of the single-sensor system is not as good as in the three-sensor system. Moreover, a residual contamination of the GMA with VOC can contribute. Test of the VOC background of the LMT system showed that it is typically in the range of a few $\mu\text{g m}^{-3}$ (Helwig et al., 2014), which is in the same range as the benzene concentration tested. The result demonstrates the need for the definition of common test standards for trace gas sensor systems and the high potential of those systems for the quantita-

tive detection even of small levels of pollutants like benzene. This is an important step for the development of monitoring grids with high resolution using indicative sensor systems to increase the number of nodes strongly.

Data availability. The underlying measurement data are not publicly available and can be requested from the authors if required.

Supplement. The supplement related to this article is available online at: <https://doi.org/10.5194/jsss-7-235-2018-supplement>.

Competing interests. The authors declare that they have no conflict of interest.

Special issue statement. This article is part of the special issue “Sensor/IRS2 2017”. It is a result of the AMA Conferences, Nuremberg, Germany, 30 May–1 June 2017.

Acknowledgements. The work has been funded by EMRP Joint Research Project ENV56 KEY-VOCs. The EMRP is jointly funded by the EMRP participating countries within EURAMET and the European Union. Some foundations, especially the set-up of the sensor system, were laid within the SENSIndoor project (funding by the European Union’s Seventh Framework Programme for research, technological development and demonstration under grant agreement no. 604311 is acknowledged).

Edited by: Jens Zosel

Reviewed by: two anonymous referees

References

Barsan, N. and Weimar, U.: Conduction Model of Metal Oxide Gas Sensors, *J. Electroceram.*, 7, 143–167, <https://doi.org/10.1023/A:1014405811371>, 2001.

Bastuck, M., Leidinger, M., Sauerwald, T., and Schütze, A.: Improved quantification of naphthalene using non-linear Partial Least Squares Regression, in: 16th International Symposium on Olfaction and Electronic Nose, Dijon, France, 28 June–1 July 2015, 1–2, available at: <http://arxiv.org/abs/1507.05834> (last access: 2 February 2018), 2015a.

Bastuck, M., Bur, C., Sauerwald, T., Spetz, A. L., Andersson, M., and Schütze, A.: Quantification of Volatile Organic Compounds in the ppb-range using Partial Least Squares Regression, Proceedings SENSOR 2015, 19–21 May 2015, Nuremberg, Germany, 584–589, <https://doi.org/10.5162/sensor2015/D5.1>, 2015b.

Bastuck, M., Baur, T., Schütze, A., and Sauerwald, T.: DAV³E: Data Analysis and Verification/Visualization/Validation Environment für die Multisensor-Datenfusion, 18. GMA/ITG-Fachtagung Sensoren und Messsyst. 2016, 10–11 May 2016, Nuremberg, Germany, 729–734, <https://doi.org/10.5162/sensoren2016/P7.3>, 2016.

Batterman, S., Chambliss, S., and Isakov, V.: NIH Public Access, *Atmos. Environ.*, 94, 518–528, 1994.

Baur, T. and Schütze, A. T. S.: Detection of short trace gas pulses, *Proc. Sens.* 2017, 87–91, available at: <https://www.ama-science.org/proceedings/details/2497> (last access: 2 February 2018), 2017.

Baur, T., Schütze, A., and Sauerwald, T.: Optimierung des temperaturzyklischen Betriebs von Halbleitergassensoren, *Tech. Mess.*, 82, 187–195, <https://doi.org/10.1515/teme-2014-0007>, 2015.

Bernstein, J. A., Alexis, N., Bacchus, H., Bernstein, I. L., Fritz, P., Horner, E., Li, N., Mason, S., Nel, A., Oullette, J., Reijula, K., Reponen, T., Seltzer, J., Smith, A., and Tarlo, S. M.: The health effects of nonindustrial indoor air pollution, *J. Allergy Clin. Immun.*, 121, 585–591, <https://doi.org/10.1016/j.jaci.2007.10.045>, 2008.

BSI: BS EN 14662-3:2015: Ambient air – Standard method for the measurement of benzene concentrations. Automated pumped sampling with in situ gas chromatography, BSI, London, UK, 2015.

Bundesanstalt für Arbeitsschutz und Arbeitsmedizin: TRGS 910: Risikobezogenes Maßnahmenkonzept für Tätigkeiten mit krebserzeugenden Gefahrstoffen, GmbH (64), 1313, 2014.

Ding, J., McAvoy, T. J., Cavicchi, R. E., and Semancik, S.: Surface state trapping models for SnO₂-based micro-hotplate sensors, *Sensor. Actuat. B-Chem.*, 77, 597–613, [https://doi.org/10.1016/S0925-4005\(01\)00765-1](https://doi.org/10.1016/S0925-4005(01)00765-1), 2001.

Ehhalt, D. H. and Rohrer, F.: The tropospheric cycle of H₂: A critical review, *Tellus*, 61, 500–535, <https://doi.org/10.1111/j.1600-0889.2009.00416.x>, 2009.

Eicker, H.: Method and apparatus for determining the concentration of one gaseous component in a mixture of gases, US Patent 4012692A, 1977.

European Parliament and Council of the European Union: Directive 2008/50/EC of the European Parliament and of the Council of 21 May 2008 on ambient airquality and cleaner air for Europe, available at: <http://eur-lex.europa.eu/legal-content/EN/TXT/?uri=OJ:L:2008:152:TOC> (last access: 2 February 2018), 2008.

Gilge, S., Plass-Duelmer, C., Fricke, W., Kaiser, A., Ries, L., Buchmann, B., and Steinbacher, M.: Ozone, carbon monoxide and nitrogen oxides time series at four alpine GAW mountain stations in central Europe, *Atmos. Chem. Phys.*, 10, 12295–12316, <https://doi.org/10.5194/acp-10-12295-2010>, 2010.

Gramm, A. and Schütze, A.: High performance solvent vapor identification with a two sensor array using temperature cycling and pattern classification, *Sensor. Actuat. B-Chem.*, 95, 58–65, [https://doi.org/10.1016/S0925-4005\(03\)00404-0](https://doi.org/10.1016/S0925-4005(03)00404-0), 2003.

Heimann, I., Bright, V. B., McLeod, M. W., Mead, M. I., Popoola, O. A. M., Stewart, G. B., and Jones, R. L.: Source attribution of air pollution by spatial scale separation using high spatial density networks of low cost air quality sensors, *Atmos. Environ.*, 113, 10–19, <https://doi.org/10.1016/j.atmosenv.2015.04.057>, 2015.

Helwig, N., Schüler, M., Bur, C., Schütze, A., and Sauerwald, T.: Gas mixing apparatus for automated gas sensor characterization, *Meas. Sci. Technol.*, 25, 55903, <https://doi.org/10.1088/0957-0233/25/5/055903>, 2014.

Hennemann, J., Sauerwald, T., Kohl, C. D., Wagner, T., Bognitzki, M., and Greiner, A.: Electrospun copper oxide nanofibers for H₂S dosimetry, *Phys. Status Solidi A*, 209, 911–916, <https://doi.org/10.1002/pssa.201100588>, 2012.

Kemmler, J. A., Pokhrel, S., Birkenstock, J., Schowalter, M., Rosenauer, A., Bärsan, N., Weimar, U., and Mädler, L.: Quenched, nanocrystalline In₄Sn₃O₁₂ high temperature phase for gas sensing applications, *Sensor. Actuat. B-Chem.*, 161, 740–747, <https://doi.org/10.1016/j.snb.2011.11.026>, 2012.

Lee, A. P. and Reedy, B. J.: Temperature modulation in semiconductor gas sensing, *Sensor. Actuat. B-Chem.*, 60, 35–42, [https://doi.org/10.1016/S0925-4005\(99\)00241-5](https://doi.org/10.1016/S0925-4005(99)00241-5), 1999.

Leidinger, M., Sauerwald, T., Reimringer, W., Ventura, G., and Schütze, A.: Selective detection of hazardous VOCs for indoor air quality applications using a virtual gas sensor array, *J. Sens. Sens. Syst.*, 3, 253–263, <https://doi.org/10.5194/jsss-3-253-2014>, 2014.

Leidinger, M., Rieger, M., Sauerwald, T., Alépée, C., and Schütze, A.: Integrated pre-concentrator gas sensor microsystem for ppb level benzene detection, *Sensor. Actuat. B-Chem.*, 236, 988–996, <https://doi.org/10.1016/j.snb.2016.04.064>, 2016a.

Leidinger, M., Huotari, J., Sauerwald, T., Lappalainen, J., and Schütze, A.: Selective detection of naphthalene with nanostructured WO₃ gas sensors prepared by pulsed laser deposition, *J. Sens. Sens. Syst.*, 5, 147–156, <https://doi.org/10.5194/jsss-5-147-2016>, 2016b.

Leidinger, M., Baur, T., Sauerwald, T., Schütze, A., Reimringer, W., Spinelle, L., and Gerboles, M.: Highly sensitive benzene detection with MOS gas sensors, Proc. AMA Conf. 2017, Nuremberg, Germany, 31 May–1 June 2017, 92–97, 2017.

Madou, M. J. and Morrison, S. R.: Chemical Sensing with Solid State Devices, Academic Press, San Diego, USA, 1989.

Morrison, S. R.: Semiconductor gas sensors, *Sensor. Actuator.*, 2, 329–341, [https://doi.org/10.1016/0250-6874\(81\)80054-6](https://doi.org/10.1016/0250-6874(81)80054-6), 1981.

Nakata, S., Nakasuiji, M., Ojima, N., and Kitara, M.: Characteristic nonlinear responses for gas species on the surface of different semiconductor gas sensors, *Appl. Surf. Sci.*, 135, 285–292, [https://doi.org/10.1016/S0169-4332\(98\)00290-6](https://doi.org/10.1016/S0169-4332(98)00290-6), 1998a.

T. Sauerwald et al.: Highly sensitive benzene detection

Nakata, S., Ozaki, E., and Ojima, N.: Gas sensing based on the dynamic nonlinear responses of a semiconductor gas sensor: Dependence on the range and frequency of a cyclic temperature change, *Anal. Chim. Acta*, 361, 93–100, [https://doi.org/10.1016/S0003-2670\(98\)00013-0](https://doi.org/10.1016/S0003-2670(98)00013-0), 1998b.

Sasahara, T., Kido, A., Sunayama, T., Uematsu, S., and Egashira, M.: Identification and quantification of alcohol by a micro gas sensor based on adsorption and combustion, *Sensor. Actuat. B-Chem.*, 99, 532–538, <https://doi.org/10.1016/j.snb.2004.01.002>, 2004.

Schneidemesser, E. Von, Monks, P. S., and Plass-Duelmer, C.: Global comparison of VOC and CO observations in urban areas, *Atmos. Environ.*, 44, 5053–5064, <https://doi.org/10.1016/j.atmosenv.2010.09.010>, 2010.

Schüler, M., Schneider, T., Sauerwald, T., and Schütze, A.: Impedance based detection of HMDSO poisoning in metal oxide gas sensors, *Tech. Mess.*, 84, 697–705, <https://doi.org/10.1515/teme-2017-0002>, 2017.

Schultealbert, C., Baur, T., Schütze, A., Böttcher, S., and Sauerwald, T.: A novel approach towards calibrated measurement of trace gases using metal oxide semiconductor sensors, *Sensor. Actuat. B-Chem.*, 239, 390–396, <https://doi.org/10.1016/j.snb.2016.08.002>, 2017.

Schütze, A., Baur, T., Leidinger, M., Reimringer, W., Jung, R., Conrad, T., and Sauerwald, T.: Highly Sensitive and Selective VOC Sensor Systems Based on Semiconductor Gas Sensors: How to?, *Environments*, 4, 20, <https://doi.org/10.3390/environments4010020>, 2017.

Spinelle, L., Michel, G., and Aleixandre, M.: Report of laboratory and in-situ in situ validation of micro-sensor sensor for monitoring ambient air pollution, ambient air pollution, Publication Office of the European Union, Luxembourg, <https://doi.org/10.2788/4277>, 2014.

Spinelle, L., Gerboles, M., Kok, G., Persijn, S., and Sauerwald, T.: Performance Evaluation of Low-Cost BTEX Sensors and Devices within the EURAMET Key-VOCS (Lv), MDPI Proceedings 2017, 1, 425, EUROSENSORS 2017, 3–6 September 2017 Paris, France, 30–33, <https://doi.org/10.3390/proceedings1040425>, 2017a.

Spinelle, L., Gerboles, M., Kok, G., Persijn, S., and Sauerwald, T.: Review of portable and low-cost sensors for the ambient air monitoring of benzene and other volatile organic compounds, *Sensors*, 17, 1520, <https://doi.org/10.3390/s17071520>, 2017b.

WHO Regional Office for Europe: WHO guidelines for indoor air quality: selected pollutants, Copenhagen, Denmark, 2010.

Wold, S., Sjöström, M., and Eriksson, L.: PLS-regression: A basic tool of chemometrics, *Chemometr. Intell. Lab.*, 58, 109–130, [https://doi.org/10.1016/S0169-7439\(01\)00155-1](https://doi.org/10.1016/S0169-7439(01)00155-1), 2001.



Supplement of

Highly sensitive benzene detection with metal oxide semiconductor gas sensors – an inter-laboratory comparison

Tilman Sauerwald et al.

Correspondence to: Tilman Sauerwald (t.sauerwald@lmt-uni-saarland.de)

The copyright of individual parts of the supplement might differ from the CC BY 4.0 License.

Supplementary material:

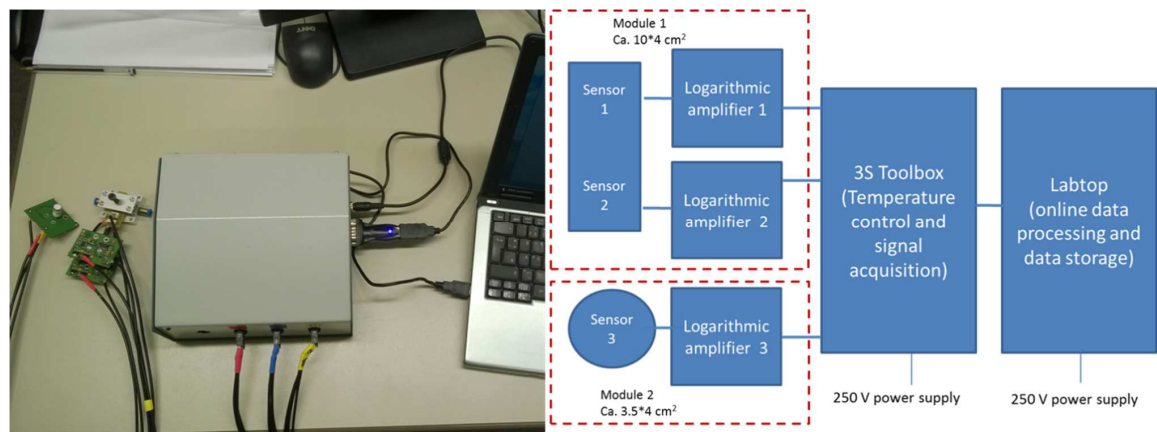


Figure S1: Picture (left) and block diagram (right) of the sensor system.

5

1

4.3.4 Paper E – Comparison of ppb-level Gas Measurements with a Metal-oxide Semiconductor Gas Sensor in two independent Laboratories

M. Bastuck^{1,2}, T. Baur¹, M. Richter³, B. Mull^{3,4}, A. Schütze¹, T. Sauerwald¹

¹*Saarland University, Lab for Measurement Technology, Saarbrücken, Germany*

²*Linköping University, Div. of Applied Sensor Science, Linköping, Sweden*

³*Bundesanstalt für Materialforschung und -prüfung (BAM), Berlin, Germany*

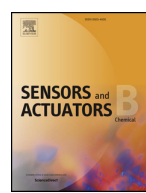
⁴*Present address: Fraunhofer Wilhelm-Klauditz-Institut, D-38108, Braunschweig, Germany.*

Sensors and Actuators B: Chemical. (2018), 273, 1037-1046

The original paper and supplementary data can be found, in the online version, at

<https://doi.org/10.1016/j.snb.2018.06.097>.

© Used with permission of Elsevier Science & Technology Journals, from *Comparison of ppb-level gas measurements with a metal-oxide semiconductor gas sensor in two independent laboratories*, Sauerwald, T.; Schütze, A.; Mull, B.; Richter, M.; Baur, T.; Bastuck, M., 273, 2022; permission conveyed through Copyright Clearance Center, Inc.



Comparison of ppb-level gas measurements with a metal-oxide semiconductor gas sensor in two independent laboratories

M. Bastuck^{a,b,*}, T. Baur^a, M. Richter^c, B. Mull^{c,1}, A. Schütze^a, T. Sauerwald^a

^a Lab for Measurement Technology, Saarland University, D-66123, Saarbrücken, Germany

^b Div. of Applied Sensor Science, Linköping University, SE-58183, Linköping, Sweden

^c Bundesanstalt für Materialforschung und -prüfung (BAM), D-12205, Berlin, Germany

ARTICLE INFO

Keywords:

Indoor air quality
Volatile organic compounds
Calibration transfer
Selective quantification
Inter-lab comparison

ABSTRACT

In this work, we use a gas sensor system consisting of a commercially available gas sensor in temperature cycled operation. It is trained with an extensive gas profile for detection and quantification of hazardous volatile organic compounds (VOC) in the ppb range independent of a varying background of other, less harmful VOCs and inorganic interfering gases like humidity or hydrogen. This training was then validated using a different gas mixture generation apparatus at an independent lab providing analytical methods as reference. While the varying background impedes selective detection of benzene and naphthalene at the low concentrations supplied, both formaldehyde and total VOC can well be quantified, after calibration transfer, by models trained with data from one system and evaluated with data from the other system. The lowest achievable root mean squared errors of prediction were 49 ppb for formaldehyde (in a concentration range of 20–200 ppb) and 150 µg/m³ (in a concentration range of 25–450 µg/m³) for total VOC. The latter uncertainty improves to 13 µg/m³ with a more confined model range of 220–320 µg/m³. The data from the second lab indicate an interfering gas which cannot be detected analytically but strongly influences the sensor signal. This demonstrates the need to take into account all sensor relevant gases, like, e.g., hydrogen and carbon monoxide, in analytical reference measurements.

1. Introduction

Continuous air quality monitoring, and indoor air quality (IAQ) monitoring in particular, has become more and more important in recent years due to the ever-increasing concern for air pollution [1–3]. Besides compounds like carbon monoxide (CO) and nitrogen oxides (NO_x) which mainly originate from the incoming air, most efforts concentrate on identification and quantification of volatile organic compounds (VOCs) with electronic noses [4–9]. Certain VOCs like benzene and formaldehyde can have a strong negative impact on human health already in very low concentrations in the lower parts per billion (ppb) range [1,10], whereas others like ethanol are tolerated in much higher concentrations without any impact. Therefore, being able to selectively quantify hazardous VOCs in a constantly varying background comprised of many non-hazardous compounds is an important step towards improved indoor air quality.

Electronic noses usually consist of an array of gas sensors, all of which react differently when exposed to a certain mixture of gases [11,12]. These different reactions arise either from careful selection of different sensor types, or simply from variations in the manufacturing

process. The generated patterns are used to train pattern recognition algorithms like linear discriminant analysis (LDA) or partial least squares regression (PLSR) [12,13]. However, the training can never comprise all possible compounds and variations the system will encounter in the field, i.e. the initially well-working model will degrade over time (through sensor drift) and at new locations. Together with a third issue, transferring a model from one master system to several slave systems, this class of problems is known as calibration transfer [4,13–16].

Additionally, there is the question of validity of the initial calibration. Especially for the required ppb concentrations, carryover or drift in the calibration equipment can lead to inconsistencies in the results. It is therefore important to monitor the test gas generation by use of alternative techniques, e.g. chromatography. Furthermore, the test gas concentration should be chosen in a range around the average values that can be expected indoors in reality.

In this work, we present the performance of a newly developed sensor systems, based on a commercial gas sensor in temperature cycled operation (TCO) [17], especially considering the transfer between two calibration systems. An exhaustive training data set was acquired at the

* Corresponding author.

E-mail address: m.bastuck@lmt.uni-saarland.de (M. Bastuck).

¹ Present address: Fraunhofer Wilhelm-Klauditz-Institut, D-38108, Braunschweig, Germany.

LMT lab (Saarbrücken, Germany), and the resulting models are subsequently tested with a data set generated at the BAM lab (Berlin, Germany) with the same sensor systems.

2. Experimental setup and methods

2.1. Transducer and operating mode

A commercial metal-oxide semiconductor (MOS) gas sensor, the AS-MLV² (ams Sensor Solutions Germany GmbH), was used in this work. It consists of a semiconducting, sensitive tin oxide layer on a micro-mechanical heater. The surface of the tin oxide is covered with ionosorbed oxygen increasing its resistivity. To promote this effect, these sensors typically have a grainy structure. Reducing or oxidizing gases change the oxygen surface coverage and, thus, change the device's resistance [18,19].

Both the chemical reactions on the surface as well as the material's electrical properties depend strongly on the device temperature. This insight has led to the development of virtual multisensors [17,20–23], a technique that simulates a sensor array by operating one physical sensor at many different temperatures (temperature cycled operation, TCO). Like a sensor array, TCO improves the selectivity of the sensor significantly [5,22–25]. Moreover, TCO is a dynamic operation method, which means that it can lead to states that cannot be obtained with isothermal operation. This is due to the fact that the equilibrium of the surface states is temperature-dependent and that the time constant for the relaxation to equilibrium can by far exceed the time constant for temperature modulation [26,27]. Based on this concept some of us have shown in an earlier work that a TCO with strongly increased sensitivity can be developed [28,29]. It relies on a very sensitive mode due to high negative surface state coverage right after a temperature drop to a lower sensing temperature, which is very reactive to reducing gases. Variation of the temperature step size provides improved selectivity for the discrimination of gases. In this work, a temperature cycle with a total duration of two minutes and four sensing temperatures (150, 200, 250, 300 °C) was employed (Fig. 1a).

2.2. Electrical and mechanical setup

We tested six very different sensor systems at the same time. Of these six systems, only two systems are presented in this paper. From the other four systems, one system did not run due to a technical failure, two other systems were not sensitive enough, and the remaining system was not selective enough to detect or quantify gases in the highly variable conditions of the training data. These systems were experimental, and a detailed description is out of the scope of this paper.

The presented systems both use an AS-MLV sensor with logarithmic amplifier and PID temperature control. A detailed description of the electronics can be found in [30]. The only difference between the two systems is the type of logarithmic amplifier (LOG114 and LOG112, Texas Instruments) and variations in sensor chamber geometry. As both systems are conceptually very similar, only the most promising one is presented in detail. Results of the other system, especially the calibration transfer, are shown in the supplementary figures (Figs. S1, S2) for comparison.

Chaining all these systems in series could have led to crosstalk where systems upstream influence systems downstream by consuming gas or injecting reaction products into the gas stream. Therefore, a parallel setup with six branches was designed using flow restrictions. To ensure equal flow rates in each branch, the flow resistance of the restrictions was chosen much higher than that of the various employed measurement chambers, making their different resistances negligible. To this end, 10 cm of 1/16" tubing was installed in each branch.

² Outdated, its successor is the AS-MLV-P2.

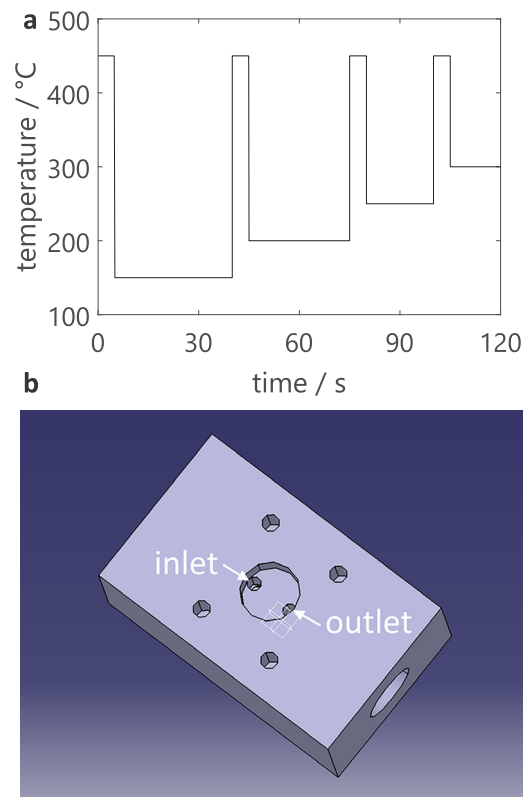


Fig. 1. (a) Temperature cycle and (b) measurement chamber of the sensor system.

The electrical resistances encountered in the described operating mode of the sensor varies over a large range [28] and can be up to the magnitude of several gigohms [31,32]. To measure these resistances quickly (2 kHz) and reliably, the sensor signal was converted close to the sensor with a logarithmic amplifier (LOG114, Texas Instruments).

The measurement chamber of the presented system (Fig. 1b) was designed from stainless steel such that the gas flow is vectored directly at the sensor instead of relying on slow diffusion. Additionally, the sensor's cap was removed for an even quicker response. Signal noise through flow variations and, thus, changes in sensor temperature, can be compensated with a PID temperature control [30].

The other, conceptually similar system works with the slower LOG112 and a larger, diffusion-based measurement chamber.

2.3. Gas mixture generation at LMT

An extensive calibration measurement including variations in target and background gas concentration as well as relative humidity was performed at LMT with the system described in [33]. Air from a zero-air generator (VICI DBS GT Ultra-Zero Air Generator) with catalytic combustion to remove VOCs, CO and H₂ was used as carrier gas. After humidification (see below), this gas was enriched with controlled amounts of usual environmental concentrations of methane (CH₄, 1840 ppb), carbon monoxide (CO, 150 ppb), and hydrogen (H₂, 500 ppb) to generate a more realistic baseline. These gases are, except for CO at higher concentrations, not relevant for human health or air quality, however, both CO and H₂ have strong influence on the signal of a MOS sensor. A background of VOCs was produced with two permeation ovens containing several permeation tubes with pure substances each, resulting in VOC mixture 1 (acetaldehyde, acetone, n-decane, hexanal, toluene) and VOC mixture 2 (d-limonene, α -pinene) which can be independently controlled. A third permeation oven

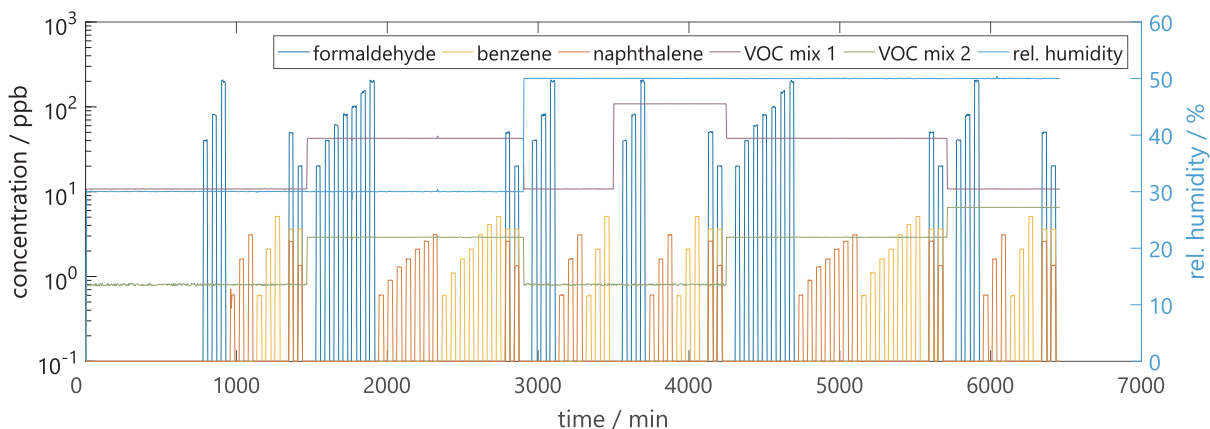


Fig. 2. Training gas profile at LMT lab.

contained a naphthalene tube, while the other two target gases, benzene and formaldehyde, were taken from gas cylinders and diluted to reach low ppb concentrations of both gases in the final mixture. Carrier gas with 100% relative humidity was generated in a bubbler flask and mixed with the dry carrier to achieve the desired relative humidity in the final mixture. The total flow was held at 400 ml/min, i.e. 67 ml/min per sensor system. The precision of the applied concentrations, i.e. the noise, is 5% of the target value in the worst case. Typical values are 5% for the background mixture, 0.4% (30% RH) and 0.8% (50% RH) for humidity, 0.3% for formaldehyde, and a range between 0.2% for the largest and 4% for the lowest concentrations of all other compounds (see also section A in supplementary materials). The measurement gas profile is summarized in Fig. 2 and Table 1 (L1-L75) and contains data of 2159 sensor temperature cycles, i.e. observations. These observations will later be referred to as LMT data.

2.4. Gas mixture generation at BAM

The VOC gas mixture for the comparison measurement at BAM was generated as described by Richter et al. [34]. It is based on the controlled evaporation of the pure liquid substances of the individual components filled into stainless steel bottles that are individually kept at a certain temperature. The substance gas developed in the bottle's gas space is taken up by an inert carrier gas (nitrogen), which is introduced into the substance bottle. The carrier gas is then removed through a stainless-steel capillary and led to a gas mixing chamber fed with purified and humidified air (50% RH) and equipped with a ventilator to ensure a homogeneous gas distribution. The air is cleaned with an activated charcoal filter which, however, does not remove all inorganic gases, e.g. environmental hydrogen.

To be able to adjust different concentration levels of the target compounds (formaldehyde, benzene, naphthalene) while maintaining the concentration levels of the background VOCs (toluene, hexanal, n-decane, limonene, α -pinene, n-dodecane), two mixing chambers were operated, one for the target compounds (MC1) and the other one for the background VOC mixture (MC2). Finally, both gas mixtures are united in a third chamber (MC3) providing the test gas for the sensor test. From the target substances, formaldehyde was provided from the same gas cylinder that was used in the LMT measurement. The different concentration levels of the target compounds were obtained by variation of the gas flow from MC1 into MC3 by means of a valve. "Zero" concentration of target compounds was obtained by disconnecting the respective supply capillary.

Prior to each sensor measurement, the test gas concentrations were controlled by duplicate air sampling. For the determination of the formaldehyde concentration 30 l of the gas mixture in MC3 was sampled on DNPH cartridges and analyzed with HPLC-DAD (High Performance

Liquid Chromatography with a Diode Array Detector) according to ISO 16000-3:2011 [35]. For the other compounds 3 and 51 of the gas mixture in MC3 were sampled on Tenax® TA and analyzed with GC-MSD (Gas Chromatography with Mass Selective Detector) according to ISO 16000-6:2011 [36]. The detection limit of both analytical procedures is, depending on the components, 1 $\mu\text{g}/\text{m}^3$ or below. The precision was estimated by repeating every analytical measurement, where the resulting difference was typically below 1 $\mu\text{g}/\text{m}^3$ and never exceeded 5 $\mu\text{g}/\text{m}^3$ (see also section A in supplementary materials).

The total flow was held at 240 ml/min, i.e. 40 ml/min per sensor. Due to the large volumes and mixing times, random concentration uncertainties are negligible. The measurement is summarized in Fig. 3 and Table 1 (B1-B5) and consists of 58 cycles, i.e. observations. The data is later referred to as BAM data. Note that these are analytically determined values, whereas only set values can be given for the LMT measurement.

The BAM test data were generated approximately one month before the LMT training data, and several other measurements were performed with the presented sensor systems in-between, so that, additionally to a simulated relocation, also drift over time of the sensor systems is considered in the data.

2.5. Data evaluation

2.5.1. Feature extraction

In principle, all data points of one cycle could be regarded as individual features. However, there are two main reasons to favor a more sophisticated approach in this work. First, there are 12,000 data points in a cycle, whereas only about 2000 observations are available. A number of 2000 samples from a feature space with 12,000 dimensions can only represent a very limited subset of said space which leads to a poor model – an effect known as curse of dimensionality [12]. Second, most of these data points are highly correlated, especially those in close proximity, so that each point contributes very little new information. The aim of feature extraction is to concentrate this information into as few, ideally independent, features as possible. This can be achieved by applying prior knowledge to the data, in this case stemming from the theoretical model presented in section 2.1 and [28]. The model suggests that the slope of the logarithmic resistance ("signal") after a temperature step is proportional to the reaction rate of a gas on the sensor surface. As this rate is, in general, different for each gas, the signal slope in these cycle ranges can be a highly sensitive and selective feature. The selectivity is further increased by choosing four different sensing temperatures. After some time, when the surface charge approaches thermodynamic equilibrium, the signal reaches a plateau, where, obviously, no more information about gases and concentrations can be gained from the signal slope. However, the appearance of this plateau depends

Table 1
Summary of all gas exposures evaluated in this work. L1-L75 refer to LMT data, B1-5 to BAM data (analytically determined values). For clarity, zero concentrations are left blank.

Exposure	target VOCs		background VOCs						background								
	#	CAS-No.	Formaldehyde	Benzene	Naphthalene	Acetaldehyde	n-Decane	Hexanal	Toluene	limonene	α-Pinene	n-Dodecane	RH	Background (CH ₄ /H ₂ /CO)	TVOC		
conv. factor / $\mu\text{g m}^{-3}$ / ppb	unit	ppb	ppb	ppb	ppb	ppb	ppb	ppb	ppb	ppb	ppb	ppb	ppb	ppm	$\mu\text{g/m}^3$		
L1	40	50-00-0	1.23	3.19	91-20-3	5.24	71-43-2	0.51	75-07-0	0.39	67-64-1	5.82	124-18-5	4.09	108-88-3	3.76	
L2	80														5.57		
L3	200			0.5													
L4				1.5													
L5				3	0.5												
L6					0.5												
L7					2												
L8						5											
L9						2.5	3.5	3.5	1.25	1.55	5	0.675	1.5	1.9	0.425	0.275	
L10						60	62	62	20	2.7	6	0.675	1.5	1.9	0.425	0.275	
L11						80	62	62	20	2.7	6	0.675	1.5	1.9	0.425	0.275	
L12						100	62	62	20	2.7	6	0.675	1.5	1.9	0.425	0.275	
L13						150	62	62	20	2.7	6	0.675	1.5	1.9	0.425	0.275	
L14						40	62	62	20	2.7	6	0.675	1.5	1.9	0.425	0.275	
L15						60	62	62	20	2.7	6	0.675	1.5	1.9	0.425	0.275	
L16						80	62	62	20	2.7	6	0.675	1.5	1.9	0.425	0.275	
L17						150	62	62	20	2.7	6	0.675	1.5	1.9	0.425	0.275	
L18						200	62	62	20	2.7	6	0.675	1.5	1.9	0.425	0.275	
L19						0.5	62	62	20	2.7	6	0.675	1.5	1.9	0.425	0.275	
L20						0.8	62	62	20	2.7	6	0.675	1.5	1.9	0.425	0.275	
L21						1.2	62	62	20	2.7	6	0.675	1.5	1.9	0.425	0.275	
L22						1.5	62	62	20	2.7	6	0.675	1.5	1.9	0.425	0.275	
L23						2	62	62	20	2.7	6	0.675	1.5	1.9	0.425	0.275	
L24						2.5	62	62	20	2.7	6	0.675	1.5	1.9	0.425	0.275	
L25						3	62	62	20	2.7	6	0.675	1.5	1.9	0.425	0.275	
L26						0.5	62	62	20	2.7	6	0.675	1.5	1.9	0.425	0.275	
L27						1	62	62	20	2.7	6	0.675	1.5	1.9	0.425	0.275	
L28						1.5	62	62	20	2.7	6	0.675	1.5	1.9	0.425	0.275	
L29						2	62	62	20	2.7	6	0.675	1.5	1.9	0.425	0.275	
L30						3	62	62	20	2.7	6	0.675	1.5	1.9	0.425	0.275	
L31						4	62	62	20	2.7	6	0.675	1.5	1.9	0.425	0.275	
L32						5	62	62	20	2.7	6	0.675	1.5	1.9	0.425	0.275	
L33						2.5	62	62	20	2.7	6	0.675	1.5	1.9	0.425	0.275	
L34						3.5	62	62	20	2.7	6	0.675	1.5	1.9	0.425	0.275	
L35						40	5	1.55	0.675	1.5	0.675	1.5	1.9	0.425	0.275	0.275	
L36						80	1.55	5	0.675	1.5	0.675	1.5	1.9	0.425	0.275	0.275	
L37						200	1.55	5	0.675	1.5	0.675	1.5	1.9	0.425	0.275	0.275	
L38						0.5	1.55	5	0.675	1.5	0.675	1.5	1.9	0.425	0.275	0.275	
L39						1.5	1.55	5	0.675	1.5	0.675	1.5	1.9	0.425	0.275	0.275	
L40						40	15.81	51	6.885	15.3	6.885	15.3	19.4	0.425	0.275	0.275	
L41						80	15.81	51	6.885	15.3	6.885	15.3	19.4	0.425	0.275	0.275	
L42						2	15.81	51	6.885	15.3	6.885	15.3	19.4	0.425	0.275	0.275	
L43						5	15.81	51	6.885	15.3	6.885	15.3	19.4	0.425	0.275	0.275	
L44						40	15.81	51	6.885	15.3	6.885	15.3	19.4	0.425	0.275	0.275	
L45						80	15.81	51	6.885	15.3	6.885	15.3	19.4	0.425	0.275	0.275	
L46						200	0.5	15.81	51	6.885	15.3	6.885	15.3	19.4	0.425	0.275	0.275
L47						20	1.5	15.81	51	6.885	15.3	6.885	15.3	19.4	0.425	0.275	0.275
L48						3	1.5	15.81	51	6.885	15.3	6.885	15.3	19.4	0.425	0.275	0.275
L49						149	15.81	51	6.885	15.3	6.885	15.3	19.4	0.425	0.275	0.275	

(continued on next page)

Table 1 (continued)

Exposure	target VOCs						background VOCs						background		
	#	CAS-No.	Benzene	Naphthalene	Acetaldehyde	Acetone	n-Decane	Hexanal	Toluene	limonene	α-Pinene	n-Dodecane	Background (CH ₄ /H ₂ /CO)	TVOC	
50-00-0	71-43-2	91-20-3	0.51	0.39	67-64-1	124-18-5	66-25-1	108-88-3	138-86-3	80-56-8	5.57	6.97	—	—	
1.23	3.19	5.24	ppb	ppb	ppb	ppb	ppb	ppb	ppb	ppb	ppb	ppb	ppm	μg/m ³	
1.50		0.5	15.81	51	6.885	15.3	19.4	0.425	0.275	50	1.84/0.50/0.15	210.06			
1.51		2	15.81	51	6.885	15.3	19.4	0.425	0.275	50	1.84/0.50/0.15	217.92			
1.52		5	15.81	51	6.885	15.3	19.4	0.425	0.275	50	1.84/0.50/0.15	233.64			
1.53	50	2.5	3.5	15.81	51	6.885	15.3	19.4	0.425	0.275	50	1.84/0.50/0.15	295.26		
1.54	20	1.25	3.5	15.81	51	6.885	15.3	19.4	0.425	0.275	50	1.84/0.50/0.15	254.37		
1.55	20	6.2	20	2.7	6	7.6	1.7	1.1	1.1	1.1	1.1	1.1	50	1.84/0.50/0.15	119.99
1.56	40	6.2	20	2.7	6	7.6	1.7	1.1	1.1	1.1	1.1	1.1	50	1.84/0.50/0.15	144.59
1.57	60	6.2	20	2.7	6	7.6	1.7	1.1	1.1	1.1	1.1	1.1	50	1.84/0.50/0.15	169.19
1.58	80	6.2	20	2.7	6	7.6	1.7	1.1	1.1	1.1	1.1	1.1	50	1.84/0.50/0.15	193.79
1.59	100	6.2	20	2.7	6	7.6	1.7	1.1	1.1	1.1	1.1	1.1	50	1.84/0.50/0.15	218.39
1.60	150	6.2	20	2.7	6	7.6	1.7	1.1	1.1	1.1	1.1	1.1	50	1.84/0.50/0.15	279.89
1.61	200	6.2	20	2.7	6	7.6	1.7	1.1	1.1	1.1	1.1	1.1	50	1.84/0.50/0.15	341.39
1.62	0.5	6.2	20	2.7	6	7.6	1.7	1.1	1.1	1.1	1.1	1.1	50	1.84/0.50/0.15	96.98
1.63	0.8	6.2	20	2.7	6	7.6	1.7	1.1	1.1	1.1	1.1	1.1	50	1.84/0.50/0.15	97.94
1.64	1.2	6.2	20	2.7	6	7.6	1.7	1.1	1.1	1.1	1.1	1.1	50	1.84/0.50/0.15	99.22
1.65	1.5	6.2	20	2.7	6	7.6	1.7	1.1	1.1	1.1	1.1	1.1	50	1.84/0.50/0.15	100.17
1.66	2	6.2	20	2.7	6	7.6	1.7	1.1	1.1	1.1	1.1	1.1	50	1.84/0.50/0.15	101.77
1.67	2.5	6.2	20	2.7	6	7.6	1.7	1.1	1.1	1.1	1.1	1.1	50	1.84/0.50/0.15	103.36
1.68	3	6.2	20	2.7	6	7.6	1.7	1.1	1.1	1.1	1.1	1.1	50	1.84/0.50/0.15	104.96
1.69	0.5	6.2	20	2.7	6	7.6	1.7	1.1	1.1	1.1	1.1	1.1	50	1.84/0.50/0.15	98.01
1.70	1	6.2	20	2.7	6	7.6	1.7	1.1	1.1	1.1	1.1	1.1	50	1.84/0.50/0.15	100.63
1.71	1.5	6.2	20	2.7	6	7.6	1.7	1.1	1.1	1.1	1.1	1.1	50	1.84/0.50/0.15	103.25
1.72	2	6.2	20	2.7	6	7.6	1.7	1.1	1.1	1.1	1.1	1.1	50	1.84/0.50/0.15	105.87
1.73	3	6.2	20	2.7	6	7.6	1.7	1.1	1.1	1.1	1.1	1.1	50	1.84/0.50/0.15	111.11
1.74	4	6.2	20	2.7	6	7.6	1.7	1.1	1.1	1.1	1.1	1.1	50	1.84/0.50/0.15	116.35
1.75	5	6.2	20	2.7	6	7.6	1.7	1.1	1.1	1.1	1.1	1.1	50	1.84/0.50/0.15	121.59
B1	50	2.5	3.4	4.5	15	1.7	0.5	9.9	6.7	—	—	—	50	285.85	
B2	19	1.3	3.6	4.5	15	1.7	0.5	9.5	7	—	—	—	50	244.80	
B3	78	3.6	3.6	4.5	15	1.7	0.7	11	6.9	—	—	—	50	322.00	
B4	3.4	3.6	4.5	15	1.7	0.5	11	6.9	50	235.79					
B5	3.4	3.4	4.5	15	1.7	0.7	10	7.1	50	220.83					

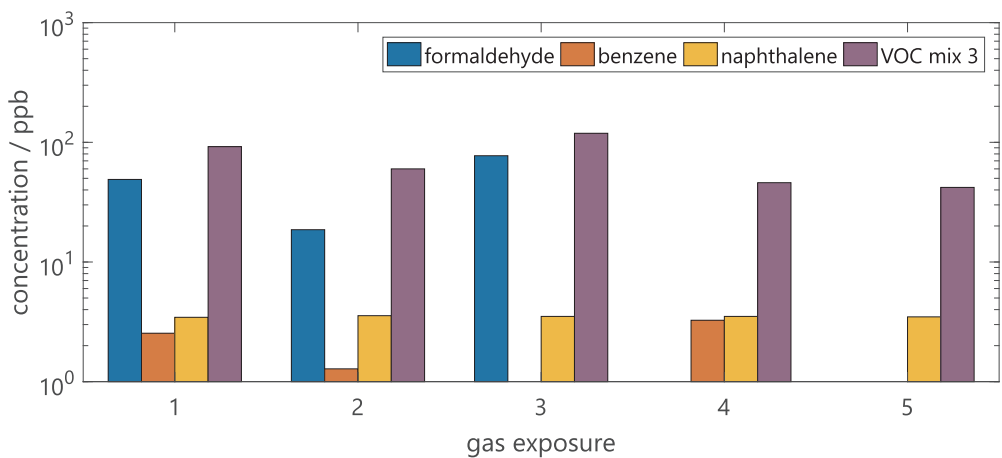


Fig. 3. Evaluated gas exposures from the BAM lab.

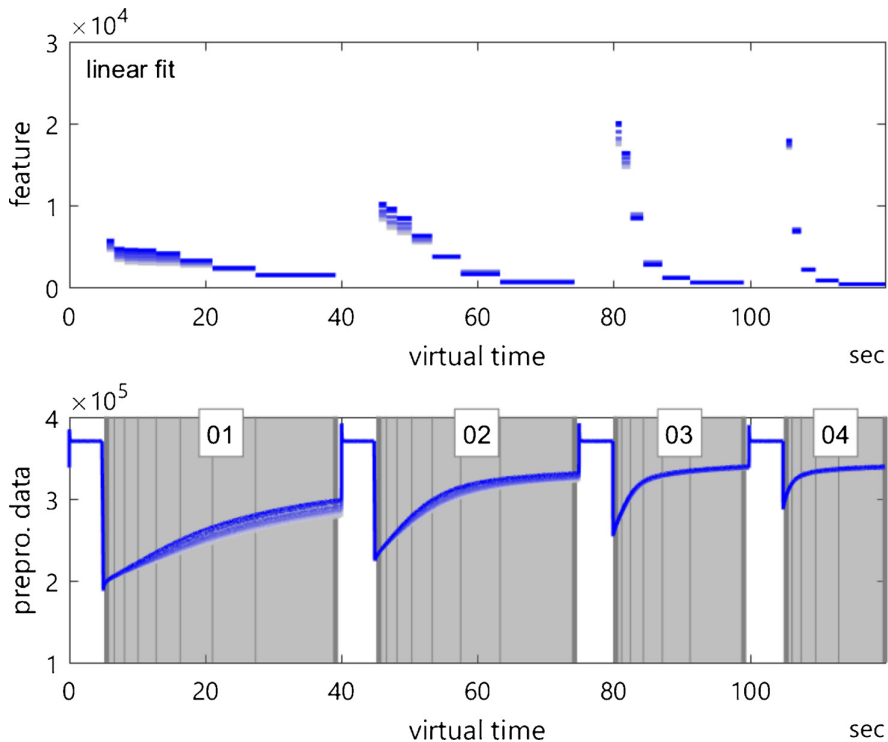


Fig. 4. The sensor signal resulting from the temperature cycle (lower graph) with feature ranges indicated. The slope in these ranges is determined for all cycles and plotted in the top graph. The color coding indicates small (light blue) and high (dark blue) formaldehyde concentrations independent of other, interfering gases (For interpretation of the references to color in this figure, the reader is referred to the web version of this article).

on sensing temperature and gas concentrations. As the latter can, usually, not be determined beforehand, we chose to extract several slopes from each of the four sensing plateaus to ensure that the slope will be represented in some of the features. As the strongest signal change is seen early after the temperature step, we start here with the shortest feature range. Their length then increases logarithmically until the end of the sensing plateau. This results in the 26 features shown in the upper graph of Fig. 4, extracted from the cycle regions depicted in the lower graph.

2.5.2. Statistical models

The previous step results in 26 features describing each cycle. Now, a model shall be found that takes the features as an input and calculates a concentration of, e.g., formaldehyde. A tool often used for this task in chemometrics and related areas of research is partial least squares (PLS) regression (PLSR) [37]. It has one model parameter, the number of PLS

components, or latent variables (LV), that the data is projected on. Choosing this parameter incorrectly can lead to poor model performance: too few LVs produce an underfitted model which omits key aspects of the relation between input and output, and too many LVs lead to overfitting where the model does not generalize well to new data. To determine the optimal number of LVs, we proceed as follows. First, we compute the root mean squared error of calibration (RMSEC) and the RMSE of cross-validation (RMSECV) for all possible numbers of LVs, 1–26, i.e. the number of features. The RMSE is generally computed as

$$\text{RMSE} = \sqrt{\frac{\sum_{i=1}^n (y_i - \hat{y}_i)^2}{n}},$$

where n is the number of observations, y_i the i th observed value, and \hat{y}_i the corresponding predicted value. The RMSEC is computed from the residuals of the training data. Cross-validation is done with a modified

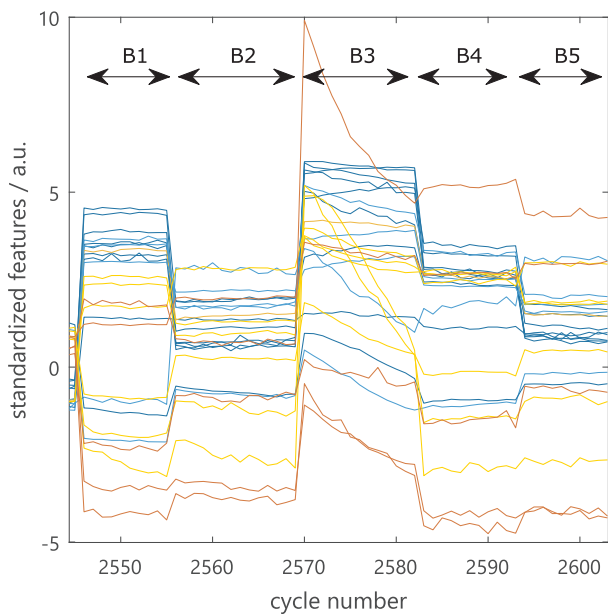


Fig. 5. The 26 slope features over the course of the BAM measurement (pauses between exposures not shown). The indices B1–5 refer to Table 1.

10-fold cross-validation algorithm, which divides the training dataset into ten parts, nine of which are then used to train a model which predicts the tenth part. While the usual algorithm assigns individual observations to these parts at random, our modified version works with groups of observations. A group contains all observations recorded at identical experimental conditions, i.e. concentrations of gases. This procedure ensures that all the highly correlated observations from a group are in one set. If individual observations would be chosen at random, each set would most likely contain points from all exposures, which, due to their correlation, would lead to overoptimistic validation results. There are 79 groups in the LMT dataset (75 gas exposures and 4 different background conditions) and 5 groups in the BAM data. There are 11 observations in each gas exposure group (or 10–14 in case of the BAM data), and 100–200 observations in the background groups.

The cross-validation performs ten (or, in general, k) iterations, and each iteration uses a different of the ten parts as “unknown” data. The RMSE computed from all predicted data is called RMSECV. We compute the standard error of the mean, SE, for the RMSECV as

$$SE = \frac{1}{\sqrt{k}} \sqrt{\frac{\sum_{i=1}^k (\text{RMSECV}_i - \overline{\text{RMSECV}})^2}{k-1}},$$

where RMSECV_i is the RMSE from the i th fold, and $\overline{\text{RMSECV}}$ is the mean of all RMSECV_i .

A high RMSEC usually appears for few latent variables and hints to an underfitted model, i.e. the model is “too simple” to capture the actual relations between features and target value. In reality, this often means that the sensor’s cross-sensitivity to other gases cannot be compensated well. On the other hand, a model can become overfitted with too many latent variables, which becomes apparent through a small RMSEC in concurrence with a large RMSECV. Hence, a good model is one with as few latent variables as possible, a small RMSEC, and a small difference between RMSEC and RMSECV. Several strategies exist to choose the optimal number of LVs. In this work, we adapt the criterion proposed in [37] by adding all up to the last LV that fulfills the stopping criterion

$$\frac{\text{RMSECV}_a}{\text{RMSECV}_{a-1}} < 0.95 \quad (1)$$

where a is the stopping LV’s index. In [37], a limit “around 0.9” is proposed, and [38] mentions values between 0.95 and 1.0 as good practical values. With the present data, the criterion selects reasonable numbers of LVs where either the change in RMSECV becomes very small or RMSEC and RMSECV start to drift apart.

The LMT data are used as training data and, with modified 10-fold cross-validation, as validation data to determine the optimal number of latent variables. An independent test set is then required to determine the model’s actual performance. This test set consists of the BAM data, so that a model trained with data from one lab is used to predict similar data generated in a different lab. The resulting metric is the RMSE of prediction (RMSEP), which should be close to RMSEC and RMSECV for the model to be good.

The evaluation was done in MATLAB using our toolbox for cyclic data evaluation, DAV³E [39]. It uses, where possible, the MATLAB implementation of algorithms like PLSR, but provides also custom-made algorithms like the described modified cross-validation.

3. Results and discussion

3.1. Quantification in highly variable background

Formaldehyde is one of the main target gases in indoor air quality monitoring. Its exposure limit lies at 80 ppb over 30 min [40], which makes it a considerably easier target than the other hazardous target gases (naphthalene, 2 ppb, and benzene, < 1 ppb [40]). Especially with the large variations in interfering gases in the training data set, formaldehyde is the only of the three gases for which a statistical model with good correlation to the actual formaldehyde concentration could be found. The model for naphthalene shows poor correlation and widespread groups, and benzene cannot be detected at all within this environment, so that further evaluation of these models cannot lead to meaningful results. Indeed, the stopping criterion (Eq. (1)) does not even select one LV for both models. Selective detection of such low concentrations in a highly variable background is a challenge in itself, whereas this paper wants to focus on the issue of the comparability of two datasets generated with the same sensor system in two different laboratories. Hence, we will in the following sections only evaluate models with good correlation, in this case selective formaldehyde concentration as well as the TVOC value. It should be kept in mind that there is a distinct, unexplained signal drift in the exposure B3 (Fig. 5). The best explanation for this is an additional gaseous component that was neither actively controlled nor seen in the analytical measurements and which then could have influenced the other exposures in the BAM measurements as well. A likely candidate is hydrogen, H_2 . As other permanent gases, H_2 is not removed with the activated carbon filter at the BAM lab as it does not interfere with analytical systems for VOC detection. Unfortunately, hydrogen is consequently not covered by the available reference measurement methods. In general, it is very hard to detect H_2 reliably in low concentrations, a reducing compound photometer being one of few possibilities [41,42]. As H_2 is not of any concern to human health or hazardous in any other way at naturally occurring concentrations, its detection is actually not necessary for indoor air quality, but the problem is reversed: many gas sensor types, including the AS-MLV, are sensitive to H_2 [43]. Moreover, the H_2 concentration in a room can vary quite a bit with human presence due to excretion of hydrogen [44,45]. Hence, it must be calibrated into the sensor model as a background gas. Since analytical equipment for H_2 quantification at such low levels is rarely available, we claim that the easiest way to achieve this goal is to first remove H_2 from the test and carrier gas, e.g. through catalytical combustion, and then again add concentrations of 500 ppb hydrogen, reflecting a clean air background [41].

3.2. Quantification of formaldehyde

Fig. 6a shows the training data from LMT (black), and test data from

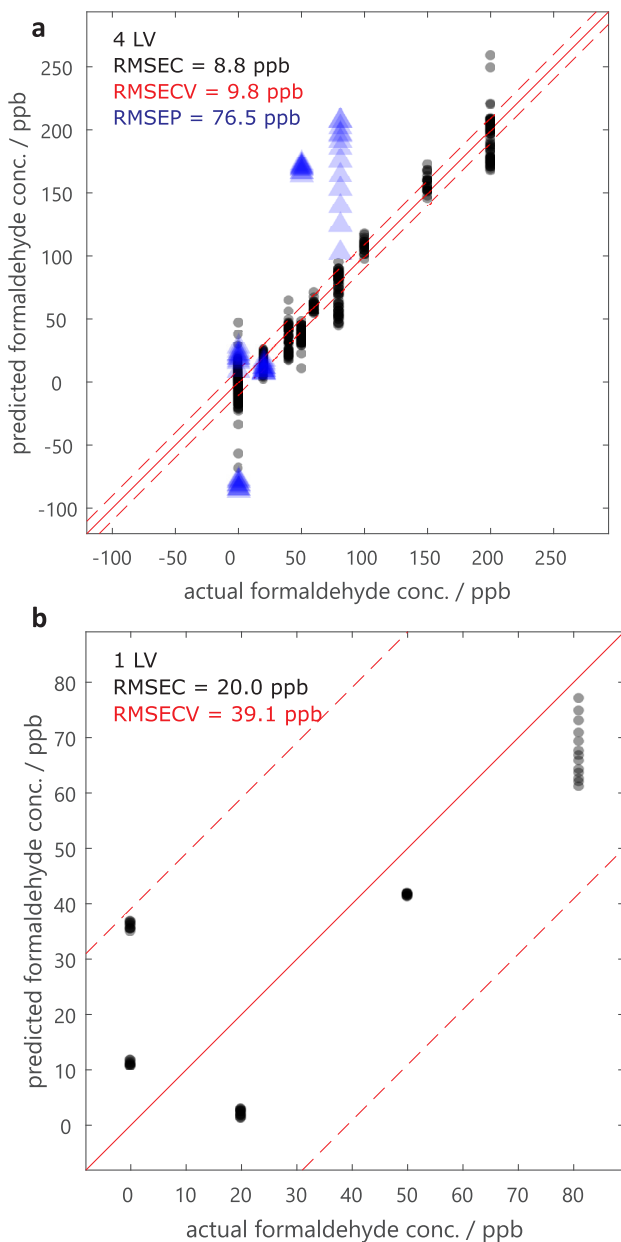


Fig. 6. (a) A PLSR model trained with LMT data (black) showing similar RMSEC and RMSECV (red, dashed). The RMSEP is considerably higher, but predictions are in the same range as the training data despite background variations which were not included in the training. (b) The variations in the BAM data vanish when they are used as training data (For interpretation of the references to color in this figure legend, the reader is referred to the web version of this article).

BAM (blue) predicted with the trained model. The RMSECV (red, dashed) is 8.8 ppb, while the RMSEP, computed from the blue colored data points, lies eight times higher, at 76 ppb. This difference arises, obviously, from the comparatively large deviations of the predicted data from their true values. Five compact groups can be identified, which correspond to the five gas exposures in the BAM data (cf. section 2.4). Especially the split of the “0” group into two parts (there are two gas exposures without formaldehyde in the BAM data) and the apparent drift of the group with the largest concentration, 80 ppb, suggests that the model is cross-sensitive to a component, potentially H₂, which is not

controlled in the BAM setup. This assumption is supported by the fact that a model trained with the BAM data can predict the same data with an RMSECV of only 39 ppb (Fig. 6b). This value was determined with a modified 5-fold CV which, in this case, is the same as a leave-one-out CV and is slightly pessimistic because extrapolation is necessary in one out of five CV iterations. Thus, the model has learned, even with few training data, to ignore the varying background of the BAM measurement to some extent, just as all other varying background gases are ignored in the model trained with LMT data (Fig. 6a).

We tried updating the LMT model by training it again with a subset of the BAM data included in the training. B3, B4 and B5, ca. 35 observations, were additionally included in the measurement, representing lowest and highest formaldehyde concentration as well as some of the unknown drift in the BAM measurement. This led to a better RMSEP of 49 ppb, while simply ignoring those groups does not significantly change the RMSEP of 76 ppb of the original model. However, this result should be validated with more data points in the future.

3.3. Quantification of TVOC

Although there is no standardized TVOC measurement method that can easily be applied for sensor systems [46], the total amount of VOCs (TVOC) is currently used in many consumer systems as an indicator for air quality. In order to determine the TVOC for IAQ monitoring, different measurement methods need to be used because of the different physicochemical properties of the broad range of compound classes appearing in real rooms. The most important ones are described in the ISO standards 16000-3 (sampling on DNPH cartridges followed by HPLC measurement) [35] and 16000-6 (sampling on Tenax TA® followed by GC measurement) [36]. Depending on the volatility of the VOC, also different adsorbents and/or chromatography columns need to be used. Hence, if a system can perform selective quantification of specific target VOCs and, at the same time, give a reading for the TVOC value, this can increase trust in the system and lead to quicker implementation and acceptance.

The approach to find a suitable model is as before. First, a model is trained with LMT data (Fig. 7a). With 4 significant LVs, despite an RMSEC of 31 µg/m³ and no overfitting, its prediction performance is very poor (RMSEP: 1017 µg/m³). The predicted baseline seems to be much higher, which could be caused by the unknown gas component or the known, but previously not seen n-dodecane in the background of the BAM measurement. One possible interpretation of this result is that a model must be sensitive to many non-specific compounds to predict TVOC, so that unknown or unexpectedly varying components will lead to much larger errors compared to more specific models, e.g. as for formaldehyde concentration.

However, a model trained with BAM data (13 LV) which predicts LMT data in the same range reaches an RMSEP of 13 µg/m³ and an RMSECV of 16 µg/m³ which must be compared with an RMSEC around 1 µg/m³. We believe that the model is, despite those values, not overfitted, and that the relatively large RMSECV arises from the fact that two out of five CV iterations must extrapolate data. Indeed, any addition of LMT data for prediction outside the trained range lets the RMSEP quickly deteriorate. Moreover, it is unlikely that an overfitted model would show such a good performance on new data. It should be noted that, while the model was trained only on 50% RH, it was able to predict observations in both 30 and 50% RH.

With this observation, it seems likely that the large offset in prediction when predicting BAM data with LMT model is caused by fluctuations of permanent gas components like H₂. These components are present in both systems, but in the LMT system the permanent gases H₂ and CO are kept constant, whereas in the BAM system these components will probably have fluctuations from the incoming zero air as described above. If the shift were due to the n-dodecane only present in the BAM measurement, a similar offset in the other direction should

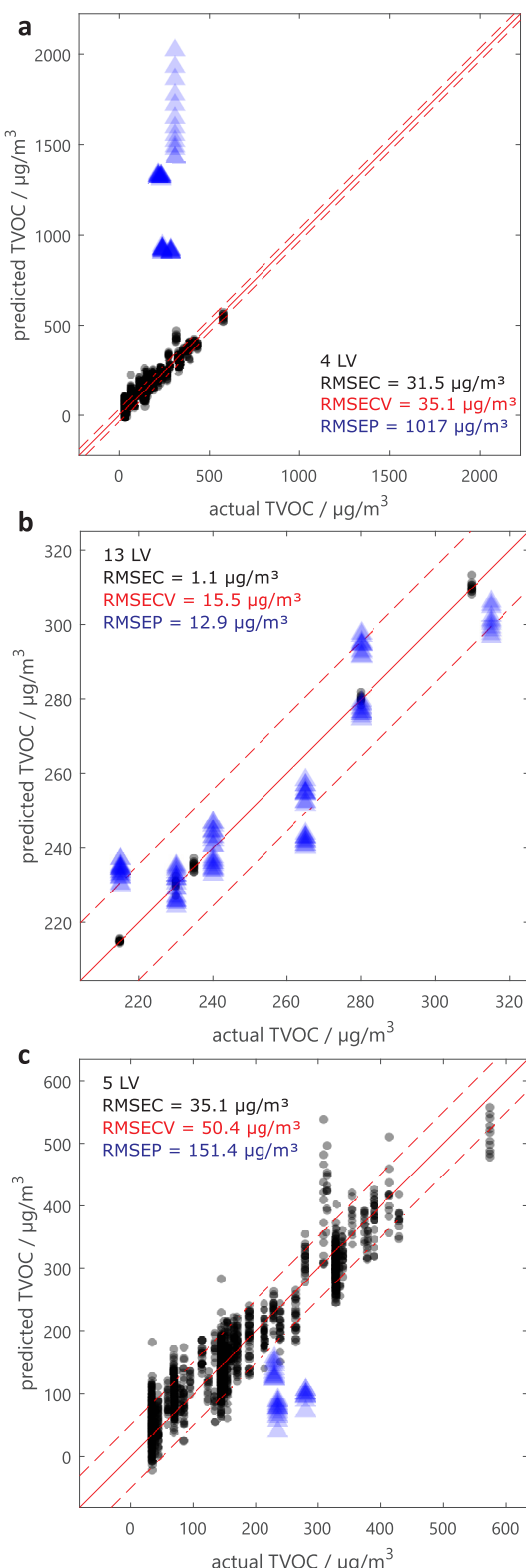


Fig. 7. (a) The LMT model for TVOC quantification initially shows very poor prediction ability for the BAM data, although (b) a model trained with BAM can predict the LMT data well. (c) Inclusion of the highest and lowest TVOC concentrations from the BAM measurement mostly corrects the predicted baseline.

be observable when predicting LMT data with the BAM model. Instead, the BAM model was trained to ignore this fluctuating component, while the LMT model only saw a constant concentration – assuming that this component is actually H₂. Adding any of the five BAM exposures in the training of the LMT model reduces the RMSEP to at least half its previous value, and an RMSEP of 150 µg/m³ can be reached with addition of the highest and lowest TVOC concentration in the BAM measurement (B3 and B5).

4. Conclusions

In this work, we used two different gas mixture generation strategies in two independent laboratories to simulate relocation of a gas sensor system after calibration. PLS regression models for the quantification of formaldehyde and TVOC were trained with over 2000 observations from 79 different experimental conditions with background variations from one system, which were then used to predict data generated in the second system with a previously unseen gas background. Formaldehyde prediction was, without changes to the model, possible with an RMSEP of 76 ppb, which is eight times as high as the model's RMSECV and very close to the recommended exposure limit of 80 ppb and, thus, does not allow reliable detection of said limit. Including three of five states from the evaluation system in the training improved the uncertainty to 49 ppb. The TVOC model requires calibration transfer strategies to reach a reasonable prediction accuracy of 150 µg/m³ and otherwise shows a strong baseline offset. However, a model trained with data from the evaluation system performs well when predicting data from the training system. This and other phenomena in the data hint to an uncontrolled gaseous compound present during the measurements. A likely candidate is an inorganic gas, potentially hydrogen, which is not removed in the BAM gas generation system. Hydrogen cannot be detected with standard analytical methods. While it is not relevant to human health, it has a strong influence on the response of semiconductor gas sensors and must, therefore, not be neglected in the design of gas mixing systems for sensor calibration.

Acknowledgements

This project has received funding from the European Union's Seventh Framework Programme for research, technological development and demonstration under grant agreement No. 604311.

Appendix A. Supplementary data

Supplementary material related to this article can be found, in the online version, at doi:<https://doi.org/10.1016/j.snb.2018.06.097>.

References

- [1] L. Mølhave, Volatile organic compounds, indoor air quality and health, *Indoor Air* 1 (1991) 357–376, <http://dx.doi.org/10.1111/j.1600-0668.1991.00001.x>.
- [2] M.J. Jantunen, O. Hanninen, K. Katsouyanni, H. Knopfel, N. Kuenzli, E. Lebret, et al., Air pollution exposure in European cities: the “EXPOLIS” study, *J. Expo. Anal. Environ. Epidemiol.* 8 (1998) 495–518.
- [3] P. Kumar, C. Martani, L. Morawska, L. Norford, R. Choudhary, M. Bell, et al., Indoor air quality and energy management through real-time sensing in commercial buildings, *Energy Build.* 111 (2015) 145–153, <http://dx.doi.org/10.1016/j.enbuild.2015.11.037>.
- [4] E.J. Wolfrum, R.M. Meglen, D. Peterson, J. Sluiter, Calibration transfer among sensor arrays designed for monitoring volatile organic compounds in indoor air quality, *IEEE Sens. J.* 6 (2006) 1638–1643, <http://dx.doi.org/10.1109/JSEN.2006.884558>.
- [5] M. Leidinger, T. Sauerwald, W. Reimringer, G. Ventura, A. Schütze, Selective detection of hazardous VOCs for indoor air quality applications using a virtual gas sensor array, *J. Sensors Sens. Syst.* 3 (2014) 253–263, <http://dx.doi.org/10.5194/jsss-3-253-2014>.
- [6] D.L.A. Fernandes, M.T.S.R. Gomes, Development of an electronic nose to identify and quantify volatile hazardous compounds, *Talanta* 77 (2008) 77–83, <http://dx.doi.org/10.1016/j.talanta.2008.05.042>.
- [7] S. Zampolli, I. Elmí, F. Ahmed, M. Passini, G.C. Cardinali, S. Nicoletti, et al., An electronic nose based on solid state sensor arrays for low-cost indoor air quality

monitoring applications, *Sens. Actuators B Chem.* 101 (2004) 39–46, <http://dx.doi.org/10.1016/j.snb.2004.02.024>.

[8] F.C. Tian, C. Kadri, L. Zhang, J.W. Feng, L.H. Juan, P.L. Na, A novel cost-effective portable electronic nose for indoor/in-car air quality monitoring, *Proc. - 2012 Int. Conf. Comput. Distrib. Control Intell. Environ. Monit. CDCIEM 2012* (2012) 4–8, <http://dx.doi.org/10.1109/CDCIEM.2012.9>.

[9] L. Zhang, F. Tian, H. Nie, L. Dang, G. Li, Q. Ye, et al., Classification of multiple indoor air contaminants by an electronic nose and a hybrid support vector machine, *Sens. Actuators B Chem.* 174 (2012) 114–125, <http://dx.doi.org/10.1016/j.snb.2012.07.021>.

[10] L. Mølhave, B. Bach, O.F. Pedersen, Human reactions to low concentrations of volatile organic compounds, *Environ. Int.* 12 (1986) 167–175, [http://dx.doi.org/10.1016/0160-4120\(86\)90027-9](http://dx.doi.org/10.1016/0160-4120(86)90027-9).

[11] T.C. Pearce, S.S. Schiffman, H.T. Nagle, J.W. Gardner (Eds.), *Handbook of Machine Olfaction*, Wiley-VCH Verlag GmbH & Co. KGaA, Weinheim, FRG, 2002, <http://dx.doi.org/10.1002/3527601597>.

[12] R. Gutierrez-Osuna, Pattern analysis for machine olfaction: a review, *IEEE Sens. J.* 2 (2002) 189–202, <http://dx.doi.org/10.1109/JSEN.2002.800688>.

[13] S. Marco, A. Gutierrez-Galvez, Signal and data processing for machine olfaction and chemical sensing: a review, *IEEE Sens. J.* 12 (2012) 3189–3214, <http://dx.doi.org/10.1109/JSEN.2012.2192920>.

[14] R. Feudale, N. Woody, H. Tan, A. Myles, S. Brown, J. Ferre, Transfer of multivariate calibration models: a review, *Chemom. Intell. Lab. Syst.* 64 (2002) 181–182, [http://dx.doi.org/10.1016/S0169-7439\(02\)00085-0](http://dx.doi.org/10.1016/S0169-7439(02)00085-0).

[15] L. Zhang, F. Tian, C. Kadri, B. Xiao, H. Li, L. Pan, et al., On-line sensor calibration transfer among electronic nose instruments for monitoring volatile organic chemicals in indoor air quality, *Sens. Actuators, B Chem.* 160 (2011) 899–909, <http://dx.doi.org/10.1016/j.snb.2011.08.079>.

[16] J. Fonollosa, L. Fernández, A. Gutiérrez-Gálvez, R. Huerta, S. Marco, Calibration transfer and drift counteraction in chemical sensor arrays using direct standardization, *Sens. Actuators B Chem.* 236 (2016) 1044–1053, <http://dx.doi.org/10.1016/j.snb.2016.05.089>.

[17] P. Reimann, A. Schütze, *Sensor Arrays, Virtual Multisensors, Data Fusion, and Gas Sensor Data Evaluation*, in: C.-D. Kohl, T. Wagner (Eds.), *Gas Sens. Fundam.* Springer Berlin Heidelberg, Berlin, Heidelberg, 2014, pp. 67–107, <http://dx.doi.org/10.1007/978-3-642-54519-1>.

[18] P.T. Moseley, B.C. Tofield, Semiconductor gas sensors, *Mater. Sci. Technol.* 1 (1985) 505–509, <http://dx.doi.org/10.1179/026708385790124486>.

[19] G. Sberveglieri, Recent developments in semiconducting thin-film gas sensors, *Sens. Actuators B. Chem.* 23 (1995) 103–109, [http://dx.doi.org/10.1016/0925-4005\(94\)01278-P](http://dx.doi.org/10.1016/0925-4005(94)01278-P).

[20] H. Eicker, Method and apparatus for determining the concentration of one gaseous component in a mixture of gases, US Pat. 4,012,692, 1977.

[21] A. Schütze, A. Gramm, T. Rühl, Identification of organic solvents by a virtual multisensor system with hierarchical classification, *IEEE Sens. J.* 4 (2004) 857–863, <http://dx.doi.org/10.1109/JSEN.2004.833514>.

[22] S. Nakata, S. Akabane, M. Nakasuji, K. Yoshikawa, Gas sensing based on a nonlinear response: discrimination between hydrocarbons and quantification of individual components in a gas mixture, *Anal. Chem.* 68 (1996) 2067–2072, <http://dx.doi.org/10.1021/ac9510954>.

[23] A.P. Lee, B.J. Reedy, Temperature modulation in semiconductor gas sensing, *Sensors Actuators, B Chem.* 60 (1999) 35–42, [http://dx.doi.org/10.1016/S0925-4005\(99\)00241-5](http://dx.doi.org/10.1016/S0925-4005(99)00241-5).

[24] A. Gramm, A. Schütze, High performance solvent vapor identification with a two sensor array using temperature cycling and pattern classification, *Sens. Actuators B Chem.* 95 (2003) 58–65, [http://dx.doi.org/10.1016/S0925-4005\(03\)00404-0](http://dx.doi.org/10.1016/S0925-4005(03)00404-0).

[25] D. Kohl, J. Kelleter, H. Petig, Detection of fires by gas sensors, *Sensors Updat.* 9 (2001) 161–223, [http://dx.doi.org/10.1002/1616-8984\(20010509:1<161::AID-SEUP161>3.0.CO;2-A](http://dx.doi.org/10.1002/1616-8984(20010509:1<161::AID-SEUP161>3.0.CO;2-A).

[26] S. Nakata, M. Nakasuji, N. Ojima, M. Kitara, Characteristic nonlinear responses for gas species on the surface of different semiconductor gas sensors, *Appl. Surf. Sci.* 135 (1998) 285–292, [http://dx.doi.org/10.1016/S0169-4332\(98\)00290-6](http://dx.doi.org/10.1016/S0169-4332(98)00290-6).

[27] J. Ding, T.J. McAvoy, R.E. Cavicchi, S. Semancik, Surface state trapping models for SnO₂-based microhotplate sensors, *Sens. Actuators B Chem.* 77 (2001) 597–613, [http://dx.doi.org/10.1016/S0925-4005\(01\)00765-1](http://dx.doi.org/10.1016/S0925-4005(01)00765-1).

[28] T. Baur, A. Schütze, T. Sauerwald, Optimierung des temperaturzyklischen Betriebs von Halbleitergassensoren, *Tm - Tech. Mess.* 82 (2015) 187–195, <http://dx.doi.org/10.1515/teme-2014-0007>.

[29] C. Schultealbert, T. Baur, A. Schütze, S. Böttcher, T. Sauerwald, A novel approach towards calibrated measurement of trace gases using metal oxide semiconductor sensors, *Sens. Actuators B Chem.* 239 (2017) 390–396, <http://dx.doi.org/10.1016/j.snb.2016.08.002>.

[30] T. Baur, C. Schultealbert, A. Schütze, T. Sauerwald, Device for the detection of short trace gas pulses, *Tm - Tech. Mess.* (2018).

[31] T. Baur, A. Schütze, T. Sauerwald, Detection of short gas pulses for trace gas analysis, *Tech. Mess.* 84 (2017), <http://dx.doi.org/10.1515/teme-2017-0035>.

[32] T. Baur, C. Schultealbert, A. Schütze, T. Sauerwald, Novel method for the detection of short trace gas pulses with metal oxide semiconductor gas sensors, *J. Sens. Sens. Syst.* 7 (2018) 411–419, <http://dx.doi.org/10.5194/jsss-7-411-2018>.

[33] N. Helwig, M. Schüler, C. Bur, A. Schütze, T. Sauerwald, Gas mixing apparatus for automated gas sensor characterization, *Meas. Sci. Technol.* 25 (2014) 055903, <http://dx.doi.org/10.1088/0957-0233/25/5/055903>.

[34] M. Richter, O. Jann, W. Horn, L. Pyza, O. Wilke, System to generate stable long-term VOC gas mixtures of concentrations in the ppb range for test and calibration purposes, *Gefahrstoffe Reinhaltung Der Luft* 73 (2013) 103–106.

[35] International Organization for Standardization, Indoor Air - Part 3: Determination of formaldehyde and other carbonyl compounds - Active sampling method (ISO 16000-3.2011), ISO 16000-3, 2011.

[36] International Organization for Standardization, Indoor Air - Part 6: Determination of volatile organic compounds in indoor and test chamber air by active sampling Tenax TA(R) sorbent, thermal desorption and gas chromatography using MS/FID (ISO 16000-6.2011), ISO 16000-6, 2011.

[37] S. Wold, M. Sjöström, L. Eriksson, PLS-regression: a basic tool of chemometrics, *Chemom. Intell. Lab. Syst.* 58 (2001) 109–130, [http://dx.doi.org/10.1016/S0169-7439\(01\)00155-1](http://dx.doi.org/10.1016/S0169-7439(01)00155-1).

[38] H. Abdi, Partial least squares regression and projection on latent structure regression, *Wiley Interdiscip. Rev. Comput.* 2 (2010) 97–106, <http://dx.doi.org/10.1002/wics.051>.

[39] M. Bastuck, T. Baur, T. Schneider, A. Schütze, DAV³E – a comprehensive toolbox for multisensor data fusion not only for gas sensors, *Sixth Sci. Meet. EuNetAir* (2016) 50–53, <http://dx.doi.org/10.5162/EuNetAir2016/13>.

[40] WHO Regional Office for Europe, WHO Guidelines for Indoor Air Quality, WHO, Geneva, 2010, <http://dx.doi.org/10.1186/2041-1480-2-S2-11>.

[41] A. Jordan, B. Steinberg, Calibration of atmospheric hydrogen measurements, *Atmos. Meas. Tech.* 4 (2011) 509–521, <http://dx.doi.org/10.5194/amt-4-509-2011>.

[42] M. Steinbacher, A. Fischer, M.K. Vollmer, B. Buchmann, S. Reimann, C. Hueglin, Perennial observations of molecular hydrogen (H₂) at a suburban site in Switzerland, *Atmos. Environ.* 41 (2007) 2111–2124, <http://dx.doi.org/10.1016/j.atmosenv.2006.10.075>.

[43] C. Schultealbert, T. Baur, A. Schütze, T. Sauerwald, Facile Quantification and Identification Techniques for Reducing Gases Over a Wide Concentration Range Using a MOS Sensor in Temperature-Cycled Operation, *MDPI Sensors*. accepted, 2018.

[44] K. Tadesse, D. Smith, M.A. Eastwod, Breath hydrogen (H₂) and methane (CH₄) excretion patterns in Normal Man and in clinical practice, *Q. J. Exp. Physiol. Cogn. Med. Sci.* 65 (1980) 85–97, <http://dx.doi.org/10.1113/expphysiol.1980.sp002502>.

[45] D. Marthinsen, S.E. Fleming, Excretion of breath and flatus gases by humans consuming high-fiber diets, *J. Nutr.* 112 (1982) 1133–1143.

[46] L. Mølhave, G.D. Nielsen, Interpretation and limitations of the concept “Total volatile organic compounds”(TVOC) as an indicator of human responses to exposures of volatile organic compounds (VOC) in indoor air, *Indoor Air* 2 (1992) 65–77.

Manuel Bastuck studied Microtechnology and Nanostructures at Saarland University, Germany, and received his Master's degree in 2014. He is currently a joint Ph.D. student at both the Lab for Measurement Technology (Saarland University) and the Applied Sensor Science group at Linköping University, Sweden. His research interests are multivariate data evaluation approaches, especially for cyclically operated gas sensors, as well as new operating modes and materials for gas-sensitive field-effect transistors.

Matthias Richter, PhD in Environmental Engineering. Working at BAM since 2007 in the field of emissions of organic and inorganic pollutants from materials into indoor air. Special research interests are generation of complex VOC reference gas standards as well as development of reference materials for testing and QA/QC purposes. He is member of related national and European standardization working groups.

Birte Mull studied chemistry at the Freie Universität Berlin, Germany, and received her Master's degree in 2009. In 2013 she received her doctor's degree from the Technische Universität Berlin, Germany. From 2009–2017 she worked as a research assistant at the Bundesanstalt für Materialforschung und -prüfung, Germany, in the field of the analysis of (semi) volatile organic compounds ((S)VOC) in test chamber and indoor air. Since 2017 she works at the Fraunhofer Wilhelm-Klauditz-Institut, Germany. Her research interests are the analysis of SVOC in indoor air and the influence of textiles on the dermal SVOC uptake.

Tobias Baur studied microtechnology and nanostructures at Saarland University and received his master's degree in 2016. He is currently a Ph.D. student at the Lab for Measurement Technology at Saarland University and focusses on the modeling and optimization of the operating mode of semiconductor gas sensors. He is also working on the combination of analytics and micro gas sensors.

Andreas Schütze studied Physics at RWTH Aachen and received his doctorate in Applied Physics from Justus-Liebig-Universität in Gießen in 1994 with a thesis on micro gas sensor systems. After some years in industry, he joined the University of Applied Sciences in Krefeld, Germany, as professor for Microsystems Technology from 1998 to 2000. Since 2000 he is a full professor for measurement science and technology in the Department of Mechatronics at Saarland University, Saarbrücken, Germany. His research interests include microsensors and microsystems, especially advanced chemical sensor systems, both for gas and liquid phase, for environmental monitoring, security and control applications.

Tilman Sauerwald received his PhD in 2007 at the University of Giessen working on the influence of surface reactions to the multi-signal generation of metal oxide sensors. Subsequently he has worked in the field of nanostructured sensor material and bio-inspired sensor systems. Since 2011 he is working at the Lab of Measurement Technology at the Saarland University. His current focus is the detection of trace gases and the automated monitoring of the sensor integrity by developing of model based techniques for multi-signal generation.

Supplementary Materials

A. Uncertainty estimates

The LMT system provides three different types of gas generation which all feed into the 400 ml/min gas flow used to test the sensor systems.

- direct: the mixture from the gas cylinder is fed into the gas stream via an MFC
- pre-dilution: the mixture from the gas cylinder is diluted using two MFCs, and the resulting mixture is fed into the gas stream via a third MFC
- permeation: a permeation oven is constantly flushed with 200 ml/min air, and the resulting mixture is fed into the gas stream via an MFC

The MFCs in use are “MF-1” manufactured by MKS. They have a repetition error (precision) of 0.2 % F.S. (full scale) and a control range of 2 to 100 % F.S. In the system, they are usually not opened below 5 % F.S. to provide a safety margin. We use 500 ml/min F.S. for high flows like carrier gas, humidity, and dilution, and 20 ml/min F.S. for gas dosage.

Especially the precision, i.e. the “noise”, of the measurement is of interest. Gas concentration is proportional to gas flow, so that the precision can be computed as:

$$\text{precision} = \frac{0.2\% \cdot \text{F.S.}}{\text{current flow}}$$

This leads to precision values of 4 % to the lowest possible flow (and concentration), and 0.2 % for the highest possible flow (and concentration). For most gases, the whole flow range had been used, with the exception being the background mix of CH₄, CO, and H₂, for which the MFC was opened slightly below 5 %, resulting in a precision of also 5 %.

For pre-dilution lines, the mixing stage introduces additional uncertainty in terms of target gas concentration c , generated from the bottle concentration c_0 , which can be quantified as:

$$\frac{c}{c_0} = \frac{\dot{q}_1}{\dot{q}_1 + \dot{q}_2}$$
$$\text{precision} = \left| \frac{\partial c}{\partial \dot{q}_1} \Delta \dot{q}_1 \right| + \left| \frac{\partial c}{\partial \dot{q}_2} \Delta \dot{q}_2 \right| = \left| \frac{\dot{q}_2}{(\dot{q}_1 + \dot{q}_2)^2} \Delta \dot{q}_1 \right| + \left| \frac{\dot{q}_1}{(\dot{q}_1 + \dot{q}_2)^2} \Delta \dot{q}_2 \right|$$

Here, \dot{q}_1 is the flow through the 20 ml/min target gas MFC, and \dot{q}_2 is the flow through the 500 ml/min dilution MFC. With these values, the maximum concentration error is about 0.08 % and, thus, mostly negligible.

The precision for permeation gas lines is similar to direct gas lines. It should be noted that the accuracy for permeation tubes is rather poor with an uncertainty given by the manufacturer of up to 50 %. This difference is, however, constant over the whole measurement and adds only an (in this case insignificant) systematic error and no random noise.

The BAM system uses larger gas volumes and mixing times compared to the LMT system, so that random errors are mostly cancelled out over time. To estimate the error in the analytical measurements, the concentration of each substance was determined twice at each exposure. The difference between the two measurements is typically below 1 $\mu\text{g}/\text{m}^3$ and never exceeds 5 $\mu\text{g}/\text{m}^3$. The differences are given in Tab. S2.

In both systems, additional systematic and random errors of around 1 % for RH can arise from ambient temperature fluctuations ($22^\circ\text{C} \pm 1^\circ\text{C}$).

Tab. S2. Differences between the results of two repeated analytical measurements for each substance and exposure at BAM.

Exposure	#	Supplied VOC concentration / $\mu\text{g}/\text{m}^3$								
		Formaldehyde	Benzene	Naphthalene	Toluene	Hexanal	n-Decane	Limonene	α -Pinene	n-Dodecane
	CAS-No.	50-00-0	71-43-2	91-20-3	108-88-3	66-25-1	124-18-5	138-86-3	80-56-8	112-40-3
B1		61 \pm 2.5	8 \pm 0.8	18 \pm 0.8	8 \pm 0.5	61 \pm 5.0	17 \pm 0.0	3 \pm 0.2	55 \pm 2.5	47 \pm 1.7
B2		23 \pm 3.0	4 \pm 0.3	19 \pm 0.2	8 \pm 0.1	61 \pm 1.4	17 \pm 0.4	3 \pm 0.0	53 \pm 2.3	49 \pm 1.2
B3		96 \pm 0.5	0	19 \pm 0.2	8 \pm 0.2	61 \pm 0.8	17 \pm 0.3	4 \pm 0.3	60 \pm 0.7	48 \pm 2.3
B4		0	11 \pm 0.2	19 \pm 0.2	8 \pm 0.0	63 \pm 1.3	17 \pm 0.3	3 \pm 0.2	62 \pm 0.3	48 \pm 0.7
B5		0	0	18 \pm 0.3	8 \pm 0.5	62 \pm 1.0	17 \pm 0.2	4 \pm 0.5	58 \pm 0.7	50 \pm 1.0

B. Results with similar sensor system

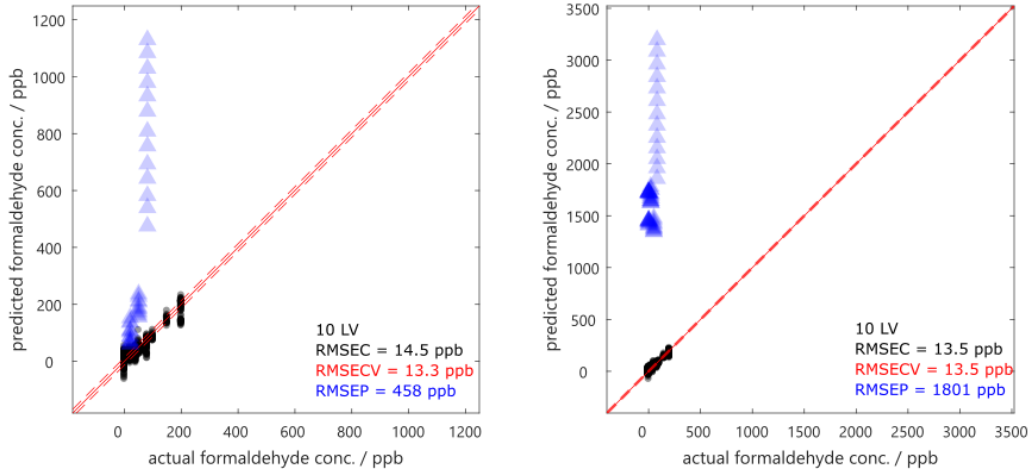


Fig. S8. (a) Poor prediction of the test data with the LMT model (formaldehyde quantification) for the sensor system with diffusion-based measurement chamber and LOG112. (b) Including B4 and B5 cannot eliminate the drift during the B3 exposure, but leads, otherwise, to a significantly improved model with an RMSEP of 458 ppb (111 ppb without B3). We chose more components than suggested by the stopping criterion (3) because the RMSECV was consistently lowered by including more components.

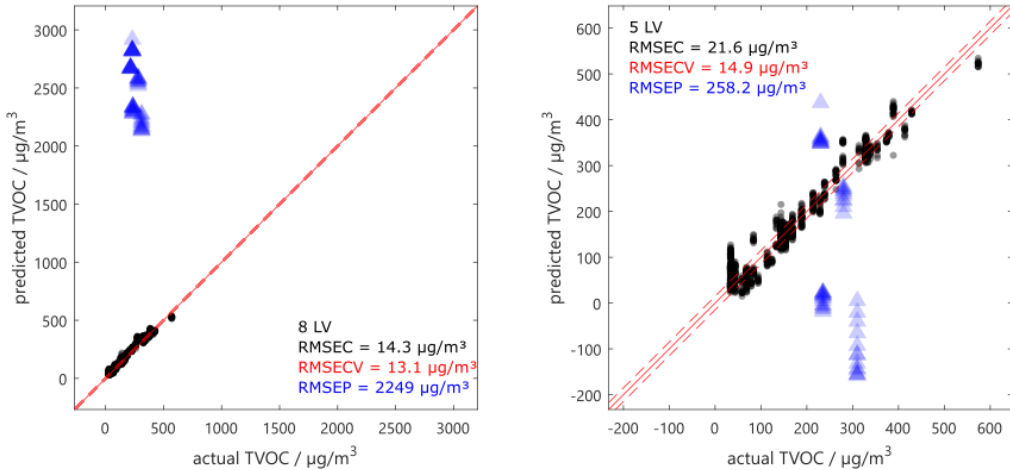


Fig. S9. (a) Poor prediction of the test data with the LMT model (TVOC) for the sensor system with diffusion-based measurement chamber and LOG112. (b) Including B5 leads to a much better model with an RMSEP of 258 $\mu\text{g}/\text{m}^3$. We chose more components than suggested by the stopping criterion (3) because the RMSECV was consistently lowered by including more components.

4.3.5 Paper 6 – Field Study of Metal Oxide Semiconductor Gas Sensors in Temperature Cycled Operation for Selective VOC Monitoring in Indoor Air

T. Baur, J. Amann, C. Schultealbert, A. Schütze

Saarland University, Lab for Measurement Technology, Saarbrücken, Germany

Atmosphere (2021), 12(5), 647

The original paper can be found, in the online version, at

<https://doi.org/10.3390/atmos12050647>.

© 2021 by the authors. This article is an open access article distributed under the terms and conditions of the Creative Commons Attribution (CC BY) license (<http://creativecommons.org/licenses/by/4.0/>).



Article

Field Study of Metal Oxide Semiconductor Gas Sensors in Temperature Cycled Operation for Selective VOC Monitoring in Indoor Air

Tobias Baur * , Johannes Amann, Caroline Schultealbert and Andreas Schütze

Lab for Measurement Technology, Saarland University, Campus A5 1, 66123 Saarbrücken, Germany; j.amann@lmt.uni-saarland.de (J.A.); c.schultealbert@lmt.uni-saarland.de (C.S.); schuetze@lmt.uni-saarland.de (A.S.)

* Correspondence: t.baur@lmt.uni-saarland.de

Abstract: More and more metal oxide semiconductor (MOS) gas sensors with digital interfaces are entering the market for indoor air quality (IAQ) monitoring. These sensors are intended to measure volatile organic compounds (VOCs) in indoor air, an important air quality factor. However, their standard operating mode often does not make full use of their true capabilities. More sophisticated operation modes, extensive calibration and advanced data evaluation can significantly improve VOC measurements and, furthermore, achieve selective measurements of single gases or at least types of VOCs. This study provides an overview of the potential and limits of MOS gas sensors for IAQ monitoring using temperature cycled operation (TCO), calibration with randomized exposure and data-based models trained with advanced machine learning. After lab calibration, a commercial digital gas sensor with four different gas-sensitive layers was tested in the field over several weeks. In addition to monitoring normal ambient air, release tests were performed with compounds that were included in the lab calibration, but also with additional VOCs. The tests were accompanied by different analytical systems (GC-MS with Tenax sampling, mobile GC-PID and GC-RCP). The results show quantitative agreement between analytical systems and the MOS gas sensor system. The study shows that MOS sensors are highly suitable for determining the overall VOC concentrations with high temporal resolution and, with some restrictions, also for selective measurements of individual components.



Citation: Baur, T.; Amann, J.; Schultealbert, C.; Schütze, A. Field Study of Metal Oxide Semiconductor Gas Sensors in Temperature Cycled Operation for Selective VOC Monitoring in Indoor Air. *Atmosphere* **2021**, *12*, 647. <https://doi.org/10.3390/atmos12050647>

Academic Editors: Kostas Karatzas and Nuria Castell

Received: 5 April 2021

Accepted: 13 May 2021

Published: 19 May 2021

Publisher's Note: MDPI stays neutral with regard to jurisdictional claims in published maps and institutional affiliations.



Copyright: © 2021 by the authors. Licensee MDPI, Basel, Switzerland. This article is an open access article distributed under the terms and conditions of the Creative Commons Attribution (CC BY) license (<https://creativecommons.org/licenses/by/4.0/>).

1. Introduction

Air pollution is one of the main environmental concerns in Europe and worldwide with outside and indoor air contributing similarly to the overall burden of disease according to the EU project Healthvent [1]. In recent years, indoor air quality has gained increasing relevance and awareness of its importance is rising [2]. Quality in this context includes many parameters, from temperature to particles to volatile organic compounds (VOCs) and others [3]. With technology becoming cheaper and Internet of Things (IoT) devices being available to a broader public, measurement systems for every parameter are in demand.

For indoor air quality assessment carbon dioxide (CO_2) is the de facto standard because it provides reliable results due to the physical measurement principle. As humans emit a cocktail of VOCs [4–6], and this is mainly responsible for poor air quality in indoor situations, a CO_2 measurement is often referred to as indirect VOC measurement based on the studies of Pettenkofer [7]. However, this approach neglects other VOC sources such as furniture and building materials as well as those coming from human activities like cleaning or cooking [8]. Furthermore, these sensors are relatively large, power-hungry, and expensive compared to metal oxide semiconductor (MOS) gas sensors, especially

in the context of IoT. MOS sensors provide excellent sensitivity and a broad response spectrum covering almost all kinds of VOCs [9,10]. Due to their broad sensitivity spectrum, most commercially available sensors provide a sum signal often designated as total VOC (TVOC) concentration [11]. However, permanent gases like hydrogen (H_2) or carbon monoxide (CO) could also contribute to this sum signal as MOS sensors often show high sensitivity towards these gases [12]. Moreover, chemical sensors can change their chemical properties during operation due to irreversible reactions, so drift is often reported [13]. The latest sensor models offered by different manufacturers are typically smaller than $3 \times 3 \times 1 \text{ mm}^3$, require less than 10 mW of power and include integrated electronics offering a direct digital interface allowing simple integration in various (IoT) devices. Some of these sensors [11,14] use multiple gas-sensitive layers to provide an even wider response spectrum and allow multisensor evaluation. With more sophisticated data treatment and more complex operation modes, like temperature cycled operation (TCO), it is possible to improve the selectivity of these sensors [15–17]. This was often shown in lab measurements and first studies on inter-laboratory comparisons are available [18], but proof concerning the feasibility of such an approach and its stability in the field is missing. Before a broader public can use the sensors and benefit from their results, the performance needs to be ensured in field studies with comparisons to analytical instrumentation.

We present a study on selective VOC measurements with MOS sensors and their stability in a real-world scenario. A multilayer sensor combined with TCO is used to achieve good selectivity. The capabilities of this low-cost approach for determining the overall VOC concentration independent of interference by ambient humidity, CO and H_2 and also selective quantification of single gases are evaluated. After calibration in the lab, the sensors were installed in an office where several release tests of different substances were conducted to prove the ability to selectively detect and quantify certain VOCs; a method that could also be used as a simple functionality test for the general public. The lab calibration was repeated twice after several weeks of operation each to evaluate the drift of the sensor elements and stability of the model prediction.

2. Materials and Methods

2.1. Experimental Setup

All measurements in this study were performed with sensor hardware designed in-house. The sensor hardware is based on a microcontroller board (Teensy 4.0, PJRC.com LLC, Sherwood, Oregon, USA), which communicates with an SGP30 sensor (Sensirion AG, Stäfa, Switzerland) via I²C interface. The SGP30 multilayer MOS sensor contains four gas-sensitive layers on a common MEMS micro hotplate [11]. It is possible to digitally program the sensor to set the temperature from 100 °C to 425 °C in 25 °C steps and to synchronously read out the resistance of the four different layers. The commands for temperature control and resistance readout are not described in the sensor datasheet and were provided by Sensirion under a non-disclosure agreement. Our sensor hardware allows us to operate the sensor in TCO mode and readout of the layers' resistances and transfer the data to a PC with a sample rate of 20 Hz. The selected temperature cycle (TC) comprises 10 temperature jumps from high to low temperature [19,20]. Figure 1 shows the TC with 10 steps at 400 °C with a duration of 5 s each are followed by different low-temperature steps, which are set to 100, 125, 150, 175, 200, 225, 300, 325, 350 and 375 °C with a duration of 7 s each resulting in a total duration of the TC of 120 s. The SGP30 sensors were installed in sensor chambers (alumina and polytetrafluoroethylene). The sensor systems including electronics were mounted on a trolley with PC and monitor allowing us to move them from the laboratory to the field test room and back. The trolley carries a flow-regulated micro pump drawing room air through the sensor chambers for the field tests, to ensure similar flow conditions over the sensor in the field as during calibration in the laboratory.

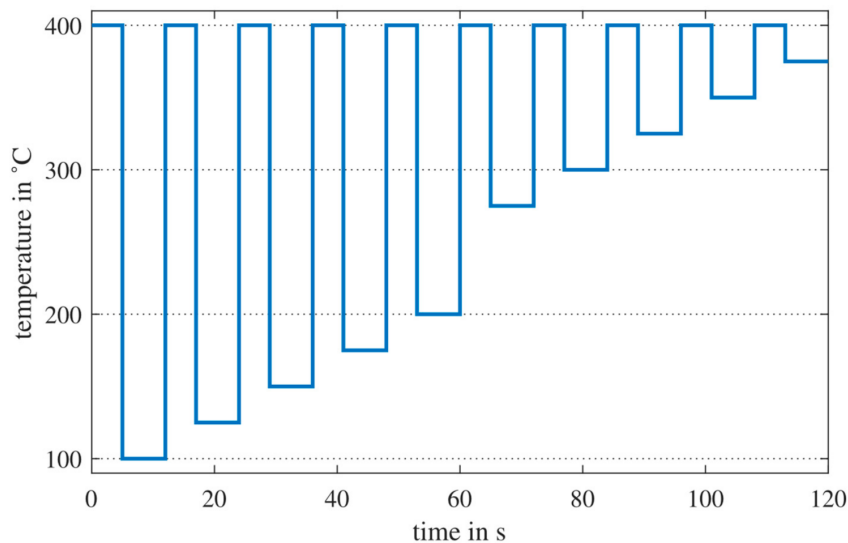


Figure 1. Temperature cycle of the SGP30.

The calibration measurements were done with our custom-built gas mixing apparatus (GMA), which is described in detail in [21]. Figure 2 shows a schematic overview of the GMA and the connection to the sensor hardware. The GMA is based on the principle of dynamic mass flow injection of different test gases into a carrier gas flow. The carrier line consists of two 500 mL/min mass flow controllers (MFC), one for dry and one for humidified zero air, for a dynamic humidity setting. Zero air is generated by a GT PLUS 15000 ULTRA-ZERO Air Generator (Schmidlin Labor + Service GmbH & Co. KG, Dettingen, Germany) with different filter steps to remove water vapor, carbon mon-/dioxide, VOCs, nitrogen oxide (NO_x), sulfur oxide (SO_x) and ozone. For humidification, dry zero air is passed through a wash bottle filled with HPLC-grade water followed by a filter to remove particles and droplets. Both the wash bottle and filter are kept at 20 °C (thermostat) to keep the humidity level constant. To achieve reliable low concentrations of the test gases, we use test gas cylinders with concentrations of at least 100 ppm of the target gas in synthetic air with a purity of >99.999% and, if required to achieve low concentrations below 1 ppm, add a predilution step before injection into the carrier gas. For the predilution, the test gas flow from the gas cylinder is diluted once with zero air by two MFCs with 10 or 20 mL/min for the test gas and 500 mL/min for zero air. The test gas from the gas cylinder or the diluted test gas is injected into the carrier gas with another MFC (10/20 mL/min). The GMA includes one test gas line for direct injection and five test gas lines with integrated predilution. The total flow entering the sensor chambers is always kept constant. Therefore, we can dynamically mix six different test gases and humidity in one measurement. In addition to the SGP30 described here, further sensor systems were included in the measurement campaign. To avoid crosstalk between the sensors due to reactions on the sensor elements, the total volume flow of 300 mL/min was divided into four parallel flows using restrictions (1/16", 20 cm), resulting in 75 mL/min per line. The total flow after the sensor chambers is measured with a mass flow meter (MFM) to ensure the tightness of the system.

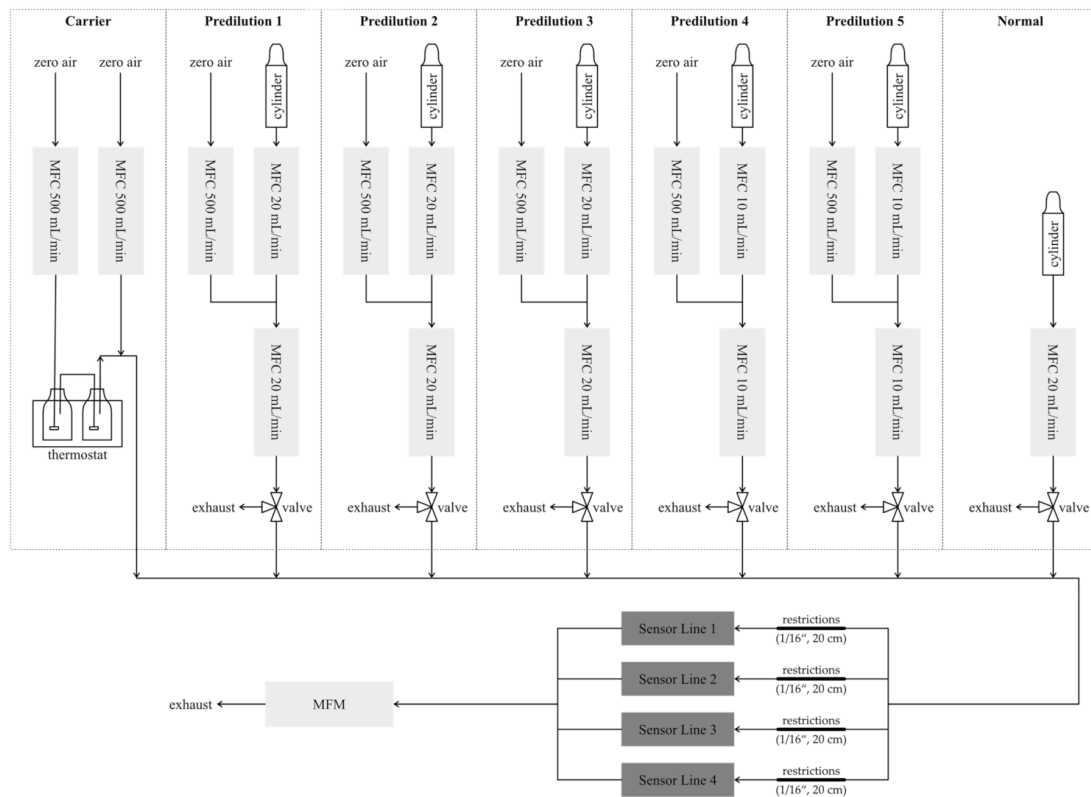


Figure 2. Schematic overview of the calibration setup with the gas mixing apparatus and the sensor systems.

The field tests are accompanied by three different analytical methods. All three systems are based on gas chromatographic separation with different detectors.

1. Thermo desorption gas chromatography-mass spectrometry (TD-GC-MS, Markes International Ltd, Llantrisant, Wales, UK, Thermo Fisher Scientific Inc., Waltham, MA, USA), similar to ISO 16000-6. TENAX® tubes were sampled with room air for 10 min at 50 mL/min. This system was used to quantify toluene during the release tests. The TD-GC-MS was calibrated in the same way with known concentrations from the GMA (7 tubes with 50–500 ppb toluene). The calibration was done 3 days before the specific release test. LOQ is smaller than 50 ppb, and the uncertainty is estimated to be 20%, based on the gas cylinder and the sampling method;
2. Peak Performer 1 (Peak Laboratories LLC, Mountain View, CA, USA), a gas chromatograph with a reducing compound photometer as detector (GC-RCP), allows selective quantification of hydrogen with a LOD of 10 ppb and a resolution of 10% of reading or LOD (whichever is higher). The Peak Performer 1 requires nitrogen or another inert carrier gas from a pressure cylinder and provides a time resolution of 3.6 min;
3. Dräger X-pid 9500 (Dräger Safety AG & Co KGaA, Lübeck, Germany), a portable GC-PID offering a broad range of measured gases including acetone (LOQ: 500 ppb, LOD: 170 ppb), toluene (LOQ: 1000 ppb, LOD: 330 ppb), isopropyl alcohol (LOQ: 3000 ppb, LOD: 1000 ppb), and xylene (LOQ: 3000 ppb, LOD: 1000 ppb). The X-pid 9500 requires a daily function test with a test gas cylinder (10 ppm isobutene and 10 ppm toluene). Depending on the selected gases, a single measurement requires 2–3 min.

2.2. Calibration and Recalibration in the GMA

The aim of the calibration is to achieve a reliable mathematical model for the prediction of different VOC, interfering gases, and sum signals, e.g., the sum of all VOCs in indoor air, in our field tests from the multi-dimensional gas sensor data. Analytic studies of VOCs in indoor air show that more than 400 different VOCs representing more than 14 chemical classes can be found in indoor air [22,23]. Studies on other substances besides VOC in indoor air are less diverse. From previous studies, we learned that hydrogen and carbon monoxide, which have a strong influence on MOS sensors, both show large variations in indoor air [24,25]. It is obviously not feasible to include all VOCs or interfering substances in the calibration, therefore a reduced substance list for the calibration strategy is needed. For the calibration, we are restricted to six different gases due to the used GMA. The following criteria were defined to select a reduced list of substances:

1. Divide the list of VOCs found in studies in indoor environments into the most common chemical classes (also named substance types or groups): alcohols, aldehydes, alkanes, alkenes, aromatics, esters, glycols and glycol ethers, halocarbons, ketones, siloxanes, terpenes and organic acids;
2. Sort the chemical classes according to their total concentrations;
3. For each chemical class, select the substance with the highest concentration.

The idea behind this approach is the assumption that most substances of a certain chemical class react similarly on the sensor surface, therefore one single gas could represent each class. However, it is difficult to verify this assumption based on reaction similarity because this would have to be assessed for each sensor model and hundreds of gases. On the other hand, if the assumption is true, it would mean that compounds are difficult to quantify selectively. In addition, the substance occurring with the highest concentration may not be the most reactive on the sensor. This means that substances with lower concentrations can still generate a higher sensor response. The behavior still needs to be investigated in more detail. Table 1 shows the 90th and 95th percentile concentration values determined from the analytical studies for the eight chemical classes with the highest sum concentration.

Table 1. 90th (P90) and 95th (P95) percentile sum concentration in $\mu\text{g}/\text{m}^3$ and ppb (calculated from the individual substances dominating for each chemical class) for the eight chemical classes with the highest sum concentrations as determined from analytical studies [22,23] in alphabetical order. The substance in parentheses is the representative with the highest concentration for this chemical class.

Chemical Class (Representative)	P90 in $\mu\text{g}/\text{m}^3$ (ppb)	P95 in $\mu\text{g}/\text{m}^3$ (ppb)
Alcohols (Ethanol)	320 (~170)	520 (~790)
Aldehydes (Formaldehyde)	340 (~270)	480 (~390)
Alkanes (n-Hexane, n-Heptane)	180 (~50)	350 (~90)
Aromatics (Toluene)	190 (~50)	370 (~90)
Esters (Ethyl acetate)	140 (~30)	280 (~70)
Ketones (Acetone)	250 (~100)	420 (~170)
Terpenes (Limonene, α -Pinene)	170 (~30)	330 (~60)
Organic acid (Acetic acid)	150 (~60)	240 (~100)

The chemical classes with the highest sum concentrations are alcohols, aldehydes, and ketones, followed by alkanes, aromatics, terpenes, and organic acid in similar magnitude. We selected ethanol (alcohols), formaldehyde (aldehyde), acetone (ketones) and toluene (aromatics) as the four VOC representatives for calibration. In addition, we included hydrogen and carbon monoxide as interfering gases for the calibrations.

The calibration strategy is based on randomized gas mixing as described in [26]. The aim of the strategy is to calibrate the sensor with a more realistic measurement including masking effects and other gas interactions. Therefore, statistically distributed gas profiles with unique randomized gas mixtures are measured, and not only single gases with ascending concentrations compared to classical sequential calibration. For the calibration, a randomized gas mixture profile was generated. The distribution is based on Latin Hypercube sampling [27] for each target substance, with the aim to achieve low correlation coefficients between the various target substances. The gas mixture profile was run in the GMA and each gas mixture was kept constant for 20 min or 10 sensor T-cycles at a total flow of 300 mL/min.

We defined concentration ranges based on the analytical studies describing VOC concentrations in empty rooms (background) as well as literature values [28,29] for the interfering gases, cf. Table 2.

Table 2. Background concentration ranges for different substances in the initial calibration and the resulting range for VOC_{sum} calculated from the single VOCs (Acetone, Toluene, Formaldehyde and Ethanol).

Substance	Min.	Max.
Carbon Monoxide	150 ppb	2000 ppb
Hydrogen	400 ppb	2000 ppb
Humidity	25 %RH	70 %RH
Acetone	14 ppb	300 ppb
Toluene	4 ppb	300 ppb
Formaldehyde	1 ppb	400 ppb
Ethanol	4 ppb	300 ppb
VOC_{sum}	300 ppb	1200 ppb

Note that the analytical studies are based on average measurements (sampling time >1 h) according to ISO16000-6 in empty rooms. This results in considerable differences between analytical reference measurements according to the ISO standard and actual real-time measurements with MOS sensors in occupied rooms. Therefore, the concentration ranges are likely to be underestimated because emissions from people in the room as well as during, e.g., cooking and cleaning, are not considered. For the field tests, we performed different release tests to verify the quantification performance and to compare the MOS sensor system with analytical instruments. To cover the higher concentration range during these tests, additional calibration with a larger concentration range for a single gas was added to the calibration scheme, while the range for the remaining gases was kept to the background concentration. The extended calibration schemes for single gases included acetone (14–1000 ppb), toluene (4–1000 ppb), ethanol (4–1000 ppb) and hydrogen (400–4000 ppb) as these four gases were to be used in the release tests.

To test our assumption that a single compound could represent all VOCs of its chemical class we performed additional measurements substituting some gases; in the first test we replaced formaldehyde with acetaldehyde and, in a second, we additionally replaced toluene with benzene for a limited number of gas exposures. At the end of the measurement campaign, we also tested m/p-xylene as another representative for aromatic compounds and limonene as an example of a chemical class (terpenes) not previously included in the calibration. Table 3 gives an overview of the entire measurement campaign with pre-tests, initial calibration, recalibrations, and field test periods.

Table 3. Overview of all performed measurements in the laboratory.

		Measurement Description	Unique Gas Mixtures
Pre-tests		background with acetaldehyde instead of formaldehyde	60
		background with acetaldehyde instead of formaldehyde and benzene instead of toluene	15
		background only	100
Initial calibration		background with modified acetone range: 14–1000 ppb	100
		background with modified toluene range: 4–1000 ppb	100
		background with modified ethanol range: 4–1000 ppb	100
		background with modified hydrogen range: 400–4000 ppb	100
1st Recalibration		1st field test period (4 weeks)	
		background only	100
		background with modified acetone range: 14–1000 ppb	100
		background with modified toluene range: 4–1000 ppb	100
		background with modified ethanol range: 4–1000 ppb	100
2nd Recalibration		background with modified hydrogen range: 400–4000 ppb	100
		2nd field test period (3 weeks)	
		background only without toluene *	100
2nd Recalibration		background only with m/p-xylene instead of toluene	50
		background only with limonene instead of toluene	50

* The measurement was performed without toluene due to the delayed delivery of a test gas cylinder.

2.3. Field and Release Tests

The field tests were performed in a regular office in our building (Figure 3). The office has a floor area of $3.5\text{ m} \times 6.3\text{ m}$ and a height of 2.8 m, thus a total volume of 61.8 m^3 (Room 2.30 in [30]). The room contains one door to a long corridor and, on the opposite side, one window. The furnishing includes one wall cabinet, three desks, three office chairs and two shelves. The flooring is carpet and the walls are wallpapered and painted. Due to the age of the furnishing, flooring and wall coverings of over 20 years, we did not expect high VOC emissions in this office. After the field tests, VOC analysis according to ISO 16000-6 and very volatile organic compound (VVOC) analyses, evaluated by a certified laboratory, obtained a TVOC concentration of $130\text{ }\mu\text{g/m}^3$ in the room. The substances with the highest concentrations were n-hexadecane ($25\text{ }\mu\text{g/m}^3$) and acetic acid ($9\text{ }\mu\text{g/m}^3$). Two VVOCs were reported at the highest concentrations: 2-propanol with $66\text{ }\mu\text{g/m}^3$ and ethanol with $21\text{ }\mu\text{g/m}^3$. Probably due to the current COVID-19 pandemic, an increased use of disinfectants based on 2-propanol and ethanol contributed to this result. Figure 3 shows a schematic top view of the room indicating the locations of the measurement trolley, the location for the release tests and a fan to ensure continuous air circulation in the room.

VOC release tests were performed via evaporation of a certain volume of the target compound liquid at the location marked in Figure 3. The expected increase in concentration during the evaporation can be estimated with Equation (1):

$$\Delta C_{\text{target}} = V_{\text{target,gas}} / V_{\text{room}} \quad (1)$$

V_{room} is the volume of the room and $V_{\text{target,gas}}$ is the volume of the VOC after evaporation. $V_{\text{target,gas}}$ can be calculated with Equation (2), where n is the amount of substance, R the gas constant, T the room temperature, p the pressure, M the molar mass, m the released VOC mass, ρ the density and $V_{\text{target,liquid}}$ the volume of the VOC in liquid form:

$$V_{\text{target,gas}} = n \cdot R \cdot T \cdot p^{-1} \text{ with } n = m/M \text{ and } m = \rho / V_{\text{target,liquid}} \quad (2)$$

Note that the increase of the concentration according to Equation (1) is a theoretical value assuming homogeneous distribution in a sealed room without air exchange. The release tests have an estimated uncertainty of 10%, due to the accuracy of the pipette and the handling of the liquid (e.g., evaporation during the process).

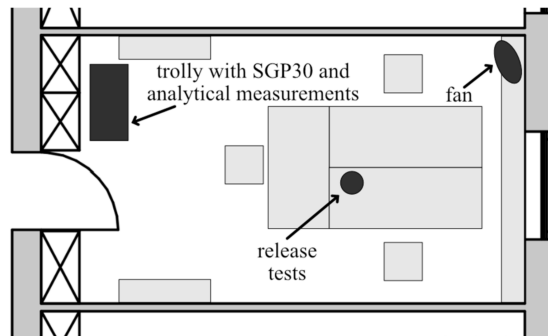


Figure 3. Schematic top view of the field test room, a standard office in our building. The locations of the trolley containing sensor systems and analytical measurements, release test and a fan are indicated (modified from [30]).

Furthermore, hydrogen was released at the same location from a pressure cylinder with a concentration of 2000 ppm in the air at a constant rate of 500 mL/min controlled by a mass flow controller for different durations. The estimated uncertainty is 4%, due to the dominating accuracy of the used gas cylinder compared to the accuracy of the MFC and time measurement. To be more comparable to the analytical studies, the field tests were performed without human presence as much as possible. However, the room had to be entered briefly for ventilation after release tests as well as to allow operation of the analytical systems or to collect samples. Analytical measurements were performed at the same location as the sensor measurements, cf. Figure 3.

2.4. Data Evaluation

Data evaluation of the gas sensor data is performed with the open-source software DAV³E [31]. Figure 4 shows the flowchart of the data evaluation. The data evaluation is divided into two parts. The first part (left) is the calculation of the initial regression model (IRM) with feature selection and hyperparameter optimization. The second part (right) is the calculation of a drift compensated regression model (DCRM) with an additional recalibration dataset.

Both parts of data evaluation start with data preprocessing and feature extraction. We excluded the first four and the last temperature cycle in each gas exposure in the datasets to ensure stable gas mixtures, thus each tested gas mixture yields five patterns for data evaluation. The raw signal of the SGP30 is the sensor resistance of each layer. Based on our model concept for MOX gas sensors in TCO [19,20], the optimal signal for data evaluation is the logarithmic sensor conductance. Therefore, the preprocessed data is the common logarithm of the reciprocal sensor resistance. In the feature extraction, we divide each cycle into 120 equidistant segments. For each segment, mean and slope is calculated resulting in 240 features for each gas-sensitive layer of the SGP30 and a total of 960 for the sensor with 4 layers. Since, in some cases, the measurement range of the SGP30 is exceeded at low temperatures the features of those segments are excluded.

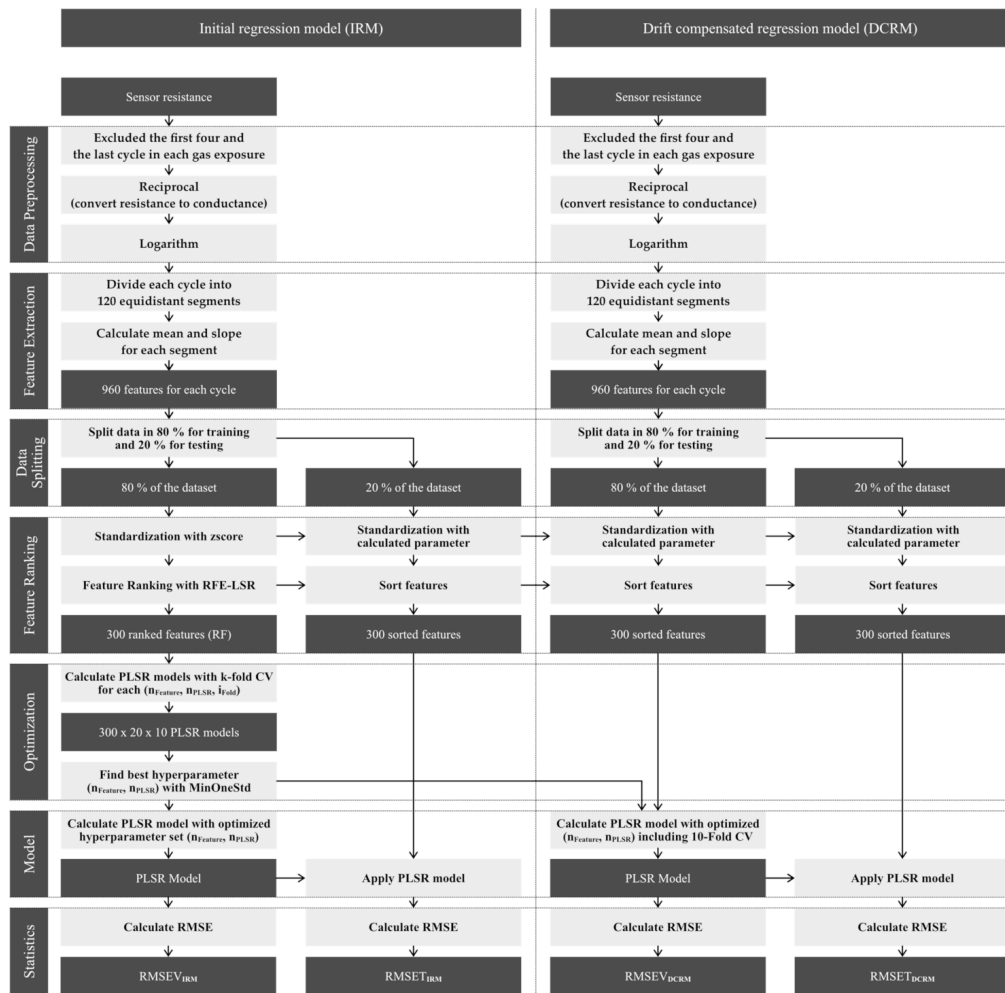


Figure 4. Flowchart of the data evaluation for an initial and drift-compensated regression model.

For the initial calibration, the dataset is split into trainings (80%) and testing (20%). Dimensionality reduction is performed by feature selection. In the feature selection, the 300 highest ranked features are selected with feature ranking. Feature ranking is done by (ordinary) least squares regression (LSR) with recursive feature elimination (RFE) to determine the relative weights or the importance of all features. The features are sorted according to their linear coefficients. A flowchart of the feature ranking can be found in the Appendix A (Figure A1). In the next step, we use partial least square regression (PLSR) as a learning algorithm for the regression model. For hyperparameter optimization (number of PLSR components n_{PLSR} and number of the features $n_{feature}$), 10-fold group-based cross-validation [32] is performed, where the folds are determined based on gas exposures and not on individual temperature cycles. This ensures that complete gas exposures are used as validation data, i.e., the validation does not only check for overfitting but also for the ability of the model to correctly interpolate between various gas mixtures. A flowchart of the learning algorithm with k-fold cross-validation and hyperparameter optimization can also be found in the Appendix A (Figure A1). Iteratively, for each combination of (n_{PLSR} , $n_{feature}$, i_{fold}) a PLSR model is calculated with 1 to 20 PLSR components, 1 to 300 features and 10 folds. The root mean square error of validation for the initial regression model ($RMSEV_{IRM}$) is calculated as the mean over all folds for each

combination (n_{PLSR} , $n_{feature}$). The optimal combination of PLSR components and features is determined from the resulting $RMSEV_{IRM}$ matrix with a dimension of 20×300 (number of PLSR components \times selected features). Therefore, we defined a criterion to find a stable and good model with a small number of dimensions: MinOneStd [26]. MinOneStd searches the absolute minimum of the matrix and adds the standard deviation as the threshold. The combination with the minimum product of number of features, times PLSR components, where the $RMSEV_{IRM}$ is smaller than this threshold, is selected as the optimal combination. With this optimal combination, 20% holdout of the dataset is tested to determine the root-mean-square error of testing ($RMSET_{IRM}$).

To compensate for the drift of the sensor, a regression model is calculated with the additional recalibration dataset (initial calibration and only background of 1st recalibration), but without new feature ranking and hyperparameter optimization. The data preprocessing and feature extraction are the same as for the initial calibration. The data is also split in the training (80%) and testing dataset (20%) for statistics. Features are sorted with the trained feature ranking from the initial calibration. The PLSR model is trained with an optimized hyperparameter from the initial calibration and the resulting $RMSEV_{DCRM}$ is calculated. With the new regression model, 20% holdout of the dataset is tested to determine the $RMSET_{DCRM}$.

3. Results

Results for hydrogen calibration and field tests including a comparison to the analytical instrument were recently published [25]; in this contribution, we focus primarily on selective VOC quantification and the overall VOC concentration, VOC_{sum} .

3.1. Calibration and Recalibration

For the generation of the prediction models for different targets, we used the dataset of the initial calibration and first recalibration (background only, i.e., without higher concentration exposures). One sensitive layer of the SGP30 gas sensor shows a small drift of the raw signal (logarithmic resistance) over time. Therefore, to compensate for this, but also other drift effects which are not as obvious, a part of the first recalibration after four weeks was included in the calibration data to optimize the model for drift stability as previously reported [33]. Figure 5 shows different prediction models for VOC_{sum} proving this approach using extended calibration to compensate drift: (a) and (b) trained with the initial calibration dataset only and (c) trained with extended calibration set (initial calibration combined with background only of the 1st recalibration). Figure 5a shows a stable and linear VOC_{sum} prediction model for training data and test data, i.e., 20 % holdout of the calibration dataset. Prediction of the 1st recalibration dataset reveals good linear correlation, but with an offset of approx. 200 ppb and a somewhat larger $RMSET$, Figure 5b. By extending the training dataset with the first part of the 1st recalibration (background only, i.e., only low concentrations) the model in Figure 5c is obtained. It yields comparable prediction results as the initial calibration, Figure 5a, also for the additional gas exposure with higher concentrations from the 1st recalibration and for the 2nd recalibration. Compared to Figure 5b, the offset between the training and testing data is eliminated, only the $RMSET$ is approx. doubled. Thus, the extended calibration provides a stable model for the VOC_{sum} prediction for the total duration of this study, i.e., at least 11 weeks. The prediction models of the other target gases reveal similar results. Figure 6 provides an overview of the RMSE of all prediction models for the 10-fold validation and 20% holdout testing for the initial and the drift compensated PLSR model. The smallest RMSE values are achieved for acetone with approx. 10 ppb followed by formaldehyde, ethanol, and toluene with 20–35 ppb for validation and testing in the initial calibration. The RMSEs for the models of hydrogen and VOC_{sum} are in the range of 30–40 ppb. The worst prediction is obtained for carbon monoxide with an RMSE of approximately 80 ppb, because no sensitive layer of the SGP30 shows a high sensitivity to carbon monoxide. The drift compensated model compared to the initial PLSR model shows similar RMSE values for acetone, toluene,

hydrogen, and VOC_{sum} . Ethanol, formaldehyde, and carbon monoxide show slightly higher RMSE values. For formaldehyde, it can be probably be explained with the gas cylinder change between the initial and the 1st re-calibration. The formaldehyde cylinders have a large systematic uncertainty of nearly 20% and in previous investigations [34] we saw the same behavior. Compared to the tested target ranges for the single VOCs we achieved a dynamic range [26] between 10 to 20 even for the low background level with 300–400 ppb; the highest dynamic range (>100) is achieved for hydrogen with an RMSET of approx. 35 ppb for concentrations up to 4000 ppb. In Table 4 the $\text{RMSET}_{\text{DCRM}}$ and the estimated accuracy and precision of the GMA are shown. The accuracy and precision depend on the MFC opening settings during the measurement. Therefore, the ranges—in percent of the set concentration and in parts per billion (ppb)—are shown. The GMA accuracy is dominated by the gas pressure cylinders. The $\text{RMSE}_{\text{DCRM}}$ is larger compared to the expected precision of the GMA. This indicates that the uncertainty of the models is due to cross-sensitivity to the other gases or other sensor effects, but not from the GMA.

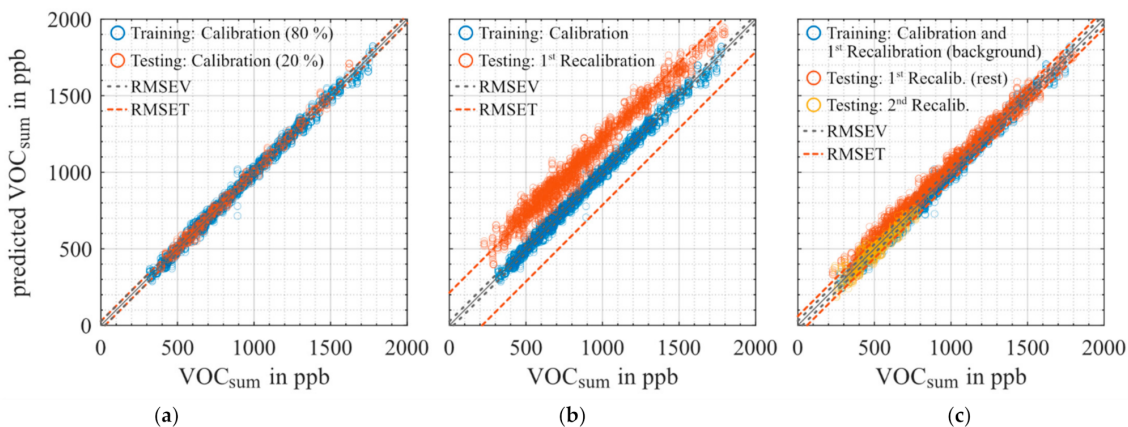


Figure 5. PLSR model for quantification of VOC_{sum} for (a) training and testing with data from the initial calibration (initial regression model), (b) training with initial calibration, testing with 1st recalibration, (c) the drift compensated regression model (training with initial calibration plus background only of the 1st recalibration), testing with extended range data from 1st recalibration as well as 2nd recalibration. Dashed lines indicate the root-mean-square-error of validation (RMSEV) based on the training data set and of testing (RMSET), respectively.

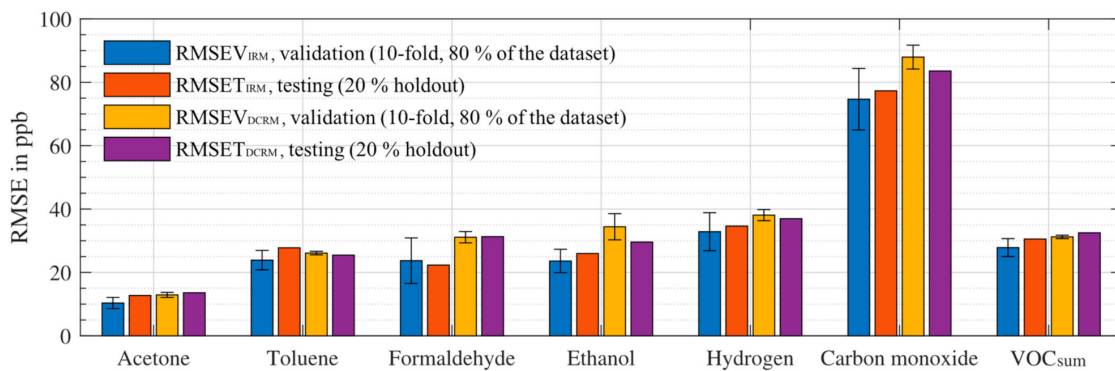


Figure 6. RMSE of the models for different target VOCs for the initial ($\text{RMSEV}_{\text{IRM}}$, $\text{RMSET}_{\text{IRM}}$) and the drift compensated regression model ($\text{RMSEV}_{\text{DCRM}}$, $\text{RMSET}_{\text{DCRM}}$). For each model RMSEV for 10-fold validation during training (error bars indicate the standard deviation of the RMSEV for the different folds) and testing (20% holdout).

Table 4. RMSE_{DCRM} for different prediction models and the accuracy and precision of the calibration measurements. The accuracy and precision depend on the MFC settings during the measurement. The accuracy is dominated by the used gas pressure cylinders, which have an accuracy of between 3 and 20%.

Substance	RMSE _{DCRM} in ppb	GMA Accuracy ¹ in % (ppb)	GMA Precision ¹ in % (ppb)
Acetone	13.6	5.0–6.5 (1–50)	0.7–4.1 (1–6)
Toluene	25.5	2.1–2.8 (0.1–23)	0.5–1.8 (0.1–10)
Formaldehyde	31.3	20.0–20.3 (0.3–82)	0.6–3.5 (0.1–10)
Ethanol	29.6	3.1–4.7 (0.2–35)	0.6–3.5 (0.2–17)
VOC _{sum}	32.5	1.8–15 (8–93)	0.6–1.8 (2–19)
Carbon Monoxide	83.6	2.2–4.2 (6–49)	0.9–3.7 (6–20)
Hydrogen	37.0	2.1–3.9 (16–85)	0.5–3.3 (14–23)

¹ Accuracy and precision are calculated by the propagation of uncertainty from the accuracy and precision of the MFCs and gas cylinder used for the calibration measurements.

3.2. Field Tests

During the time in the field, we performed 17 release tests, mostly by evaporation of VOCs, but also using test gas bottles and MFCs as well as burning a tea candle. Table 5 provides an overview of all release tests giving the start time, substance, type of release and the idealized concentration increase in the room calculated using Equation (1). A complete list of all events, including persons entering the room, ventilation etc. is given in Table A1.

Table 5. Overview of calibration, recalibration, and all release tests. The complete list of all events is given in Table A1.

Release	Event	Time	Substance (Type of Release)	Released Amount of Substance (Approx. Increase in Room Conc.)
Pre-tests and Initial calibration				
1	11	06 October, 17:42	Hydrogen (MFC, gas cylinder)	2000 ppm @ 500 mL/min for 62 min (~1 ppm ± 4%)
2	12	07 October, 16:01	Hydrogen (MFC, gas cylinder)	2000 ppm @ 500 mL/min for 124 min (~2 ppm ± 4%)
3	16	13 October, 15:00	Toluene (MFC, gas cylinder)	100 ppm @ 500 mL/min for 497 min (~300 ppb ± 10%)
5	22	16 October, 14:50	Acetone (evaporation) Toluene (evaporation)	0.114 mL (~600 ppb ± 10%) 0.164 mL (~600 ppb ± 10%)
6	23	16 October, 18:00	Acetone (evaporation) Toluene (evaporation)	0.114 mL (~600 ppb ± 10%) 0.164 mL (~600 ppb ± 10%)
1st Recalibration				
7	28	02 November, 16:50	Toluene (evaporation)	0.164 mL (~600 ppb ± 10%)
9	32	04 November, 16:22	Acetone (evaporation)	0.114 mL (~600 ppb ± 10%)
10	34	05 November, 15:10	Acetone (evaporation) Toluene (evaporation)	0.114 mL (~600 ppb ± 10%) 0.164 mL (~600 ppb ± 10%)
11	36	06 November, 10:03	Limone (evaporation)	0.251 mL (~600 ppb ± 10%)
12	39	09 November, 18:00	Ethanol (evaporation)	0.1 mL (~664 ± 10%)
13	41	10 November, 14:30	Isopropyl alcohol (evaporation)	0.12 mL (~600 ppb ± 10%)
14	43	11 November, 15:49	m/p-Xylene (evaporation)	0.189 mL (~600 ppb ± 10%)
15	45	12 November, 15:08	Toluene (evaporation) m/p-Xylene (evaporation)	0.164 mL (~600 ppb ± 10%) 0.189 mL (~600 ppb ± 10%)

Table 5. Cont.

Release	Event	Time	Substance (Type of Release)	Released Amount of Substance (Approx. Increase in Room Conc.)
16	47	13 November, 14:30	Acetone (evaporation)	0.114 mL (~600 ppb \pm 10%)
			Toluene (evaporation)	0.164 mL (~600 ppb \pm 10%)
			Ethanol (evaporation)	0.1 mL (~664 ppb \pm 10%)
17	50	16 November, 17:06	Hydrogen (MFC, gas cylinder)	2000 ppm @ 500 mL/min for 134 min (~2 ppm \pm 4%)
18	52	17 November, 18:24	Ethanol (evaporation)	0.1 mL (~664 ppb \pm 10%)
19	54	19 November, 12:02	Carbon monoxide etc. (tea candle)	4 h burn time
2nd Recalibration				

The presented signals are based on the drift compensated PLSR model (DCRM). Note, that with this model, we are using the future to predict the past for the first field tests (release #1–#6). The release tests in the second field test (release #7–#19) were all conducted after the 1st recalibration.

Figure 7 shows results recorded during release tests for toluene (release test #7), acetone (#9), ethanol (#10), and the simultaneous release of all three (#16). In a sealed room with homogeneous distribution, the release of 0.164 mL toluene should lead to an increase of the toluene concentration of approx. 600 ppb \pm 10 %. Since the amount released and the homogeneous distribution in the room may vary, there may be deviations in the level of the expected concentration. With the start of the toluene release, the MOS sensor model for toluene indicates a quick increase from nearly zero to 620 ppb. After full evaporation of the toluene, the model prediction slowly decreases again over several hours. The X-pid 9500 shows a similar course of the toluene signal as the MOS sensor model, but \sim 150 ppb higher; the increase vs. the base level before release is approx. 700 ppb. Note that the manufacturer gives a limit of quantification (LOQ) for toluene of 1000 ppb. The model predictions for the other target gases show only small changes with the onset of the evaporation and nearly constant results afterward. Only the VOC_{sum} model indicates an increase of approximately 600 ppb, thus a consistent prediction. Note that calculating the sum of the four individual VOC model predictions (dashed line) yields a similar increase with a small offset of approx. 50 ppb. No statement can be made about the true absolute concentration since these releases were not accompanied by any analytical reference for this concentration range. However, the MOS sensor model and X-pid 9500 show similar signals in the same order of magnitude of the expected concentration for the release tests.

Similarly, the release of acetone and ethanol show an increase in the corresponding prediction models. The acetone model with a higher base level of approximately 120 ppb indicates an increase of 350 ppb to a peak value of 570 ppb. The same increase can be observed in the VOC_{sum} model as well as the calculated sum of the individual VOC signals. Again, the other model does not show a reaction and remains nearly constant, except for carbon monoxide and hydrogen. Carbon monoxide shows an increase of nearly 150 ppb after the start of evaporation and hydrogen increases during the acetone signal decrease. Note that, during the field tests, the hydrogen signal shows more variations than all other models [25]. Similar to toluene, the acetone signal of the X-pid 9500 shows a higher increase of the concentration but confirms the course vs. time.

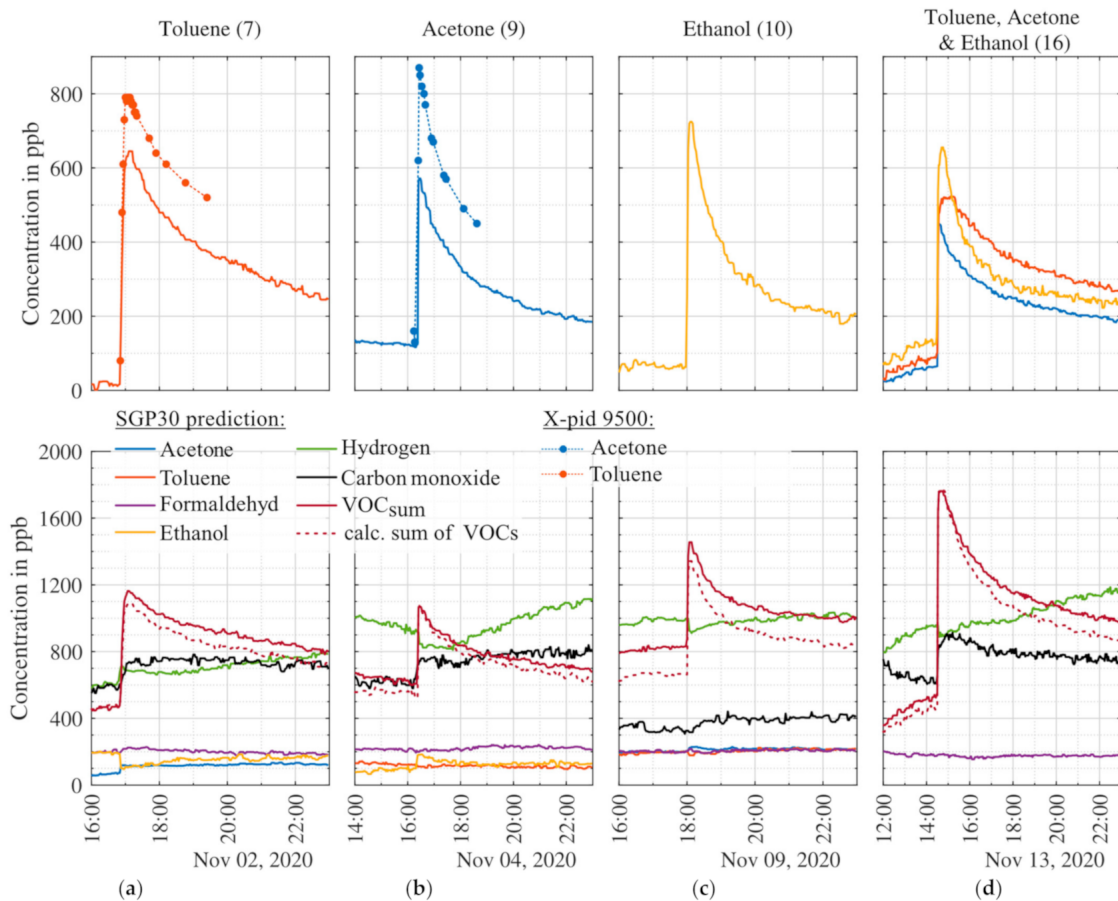


Figure 7. Results recorded during four release tests with toluene (a), acetone (b), ethanol (c), and the simultaneous release of toluene, acetone, and ethanol (d). The upper graphs show the PLSR prediction of the MOS sensor model for the released gases and, if available, reference data (dots); all other signals are shown in the lower graphs. The signals are smoothed over five points (10 min). Numbers in parenthesis behind the released substances refer to the release tests, cf. Table 4.

The ethanol release test shows an increase of 660 ppb (expected $664 \text{ ppb} \pm 10\%$). At the start of the evaporation, the hydrogen signal decreases by nearly 100 ppb, while all other single target signals remain constant. The VOC_{sum} signal increases from 830 ppb to 1455 ppb, corresponding to an increase of 625 ppb, again very similar to the ethanol signal itself. The sum of the four single VOC signals is lower with an offset of approx. 180 ppb.

In release test #16 we tested the simultaneous evaporation of all three substances: toluene ($\sim 600 \text{ ppb} \pm 10\%$), acetone ($\sim 600 \text{ ppb} \pm 10\%$) and ethanol ($\sim 664 \text{ ppb} \pm 10\%$). The toluene model shows an increase of 380 ppb, acetone of 430 ppb, and ethanol of 530 ppb. All three VOC models yield consistently lower concentrations compared to the individual release tests. This might be because during calibration only one gas at a time had higher concentrations and, thus, the models have to extrapolate the prediction beyond the calibrated range. The VOC_{sum} model prediction as well as the sum of the four single VOC models shows similar increases.

In Figure 8 two release tests with hydrogen and two with acetone and toluene are shown. The hydrogen releases were designed to yield an increase of approx. 2 ppm in the room. Because the hydrogen molecule is very small and has a high diffusion constant, we expect a somewhat faster diffusion out of the room and, thus, a smaller peak. The first hydrogen release (2) yields an increase of the model prediction of 1440 ppb, the second (17) of 1500 ppb. The second release was also monitored with the hydrogen measurement

system (GC-RCP). A high correlation between analytical and MOS sensor model prediction can be observed. Compared to the MOS model prediction the GC-RCP indicates a nearly identical increase of 1490 ppb, but with a constant offset of 150 ppb. Other signals show minimal changes except for Carbon monoxide wherein both releases a small change can be observed. The ethanol model shows an inverse effect during the second release, but no reaction during the first release.

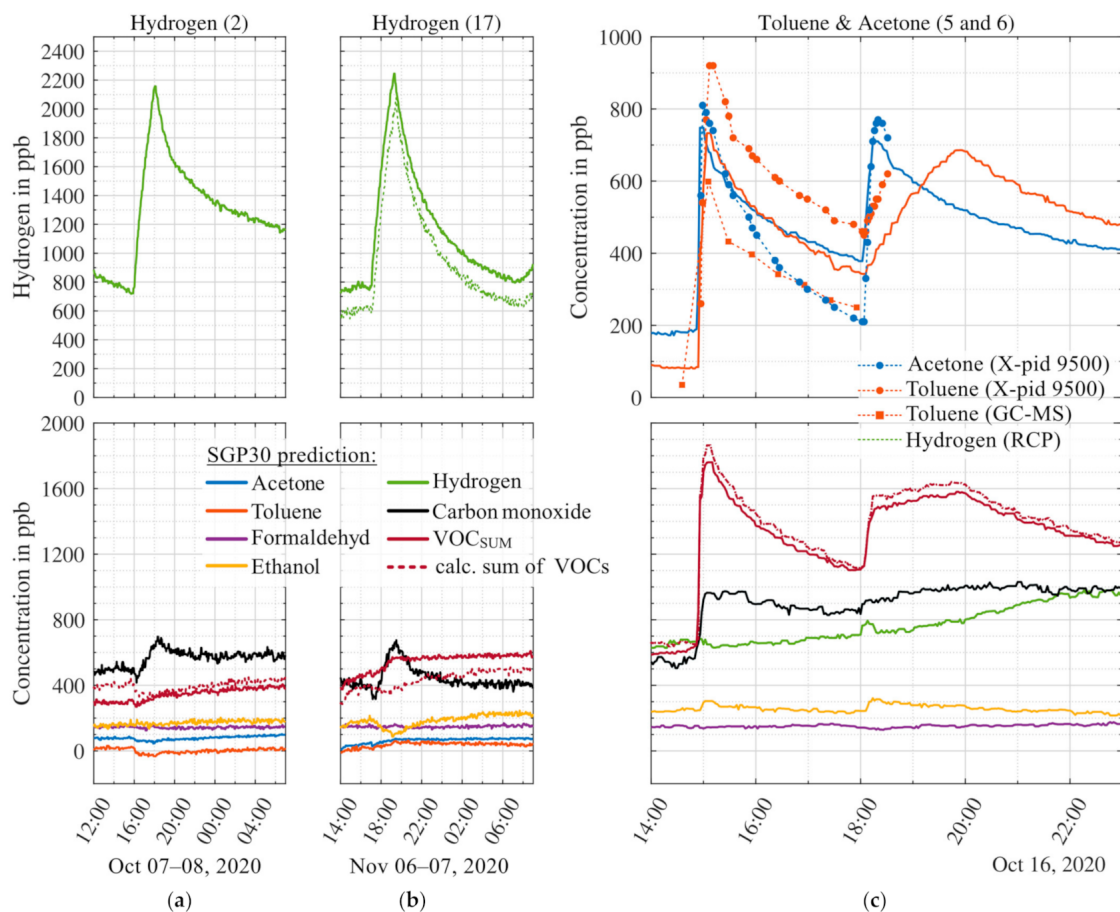


Figure 8. Results recorded during three release tests with hydrogen (a,b) and the simultaneous release of toluene and acetone (c). The upper graphs show the PLSR prediction of the MOS sensor model for the released gases and, if available, reference data (dots indicate distinct sampling times); all other signals are shown in the lower graphs. The signals are smoothed over five points (10 min). Numbers in parenthesis behind the released substances refer to the release tests, cf. Table 4.

Figure 8c shows two release tests with acetone (~ 600 ppb $\pm 10\%$) and toluene (~ 600 ppb $\pm 10\%$). The first toluene peak shows an increase of 600 ppb above the baseline level, similar to the result shown in Figure 7 for the same amount of substance released. During the first release in Figure 8c samples were taken with Tenax sampling tubes for analysis by GC-MS in addition to the X-pid 9500 measurements. The X-pid 9500 indicates an increase of 920 ppb, thus slightly higher compared to release #7, cf. Figure 7. The GC-MS analysis, on the other hand, yields an increase of 560 ppb. Thus, comparing the MOS sensor with X-pid 9500 and GC-MS, the toluene concentration predicted by the model is much closer to the GC-MS. Note that the GC-MS and the MOS sensor are calibrated with gas

mixtures from the GMA with the same gas cylinders, and therefore, the accuracy of the gas cylinder (which brings along the highest uncertainty) has no influence on the comparison.

All three signals show the same time temporal development. The first acetone release in Figure 8c yields an increase of 570 ppb, again comparable to release #9 in Figure 7. The X-pid 9500 again yields a higher absolute acetone signal. The second release shows the same trends as before, only the toluene evaporation is slower in comparison to the first release. The reason for the different evaporation and diffusion speed can be a lower ambient temperature, because of the experiment being performed later in the day. The increase of both signals is nearly the same as during the first release. The VOC_{sum} model prediction also indicates an increase due to the release of acetone and toluene and corresponds to the sum of the four single VOC signals. Other than as observed during the release of the triple mixture (toluene, acetone, and ethanol), cf. Figure 7, the model signals during the release of the double mixture (toluene and acetone) are higher and comparable to the release tests with single gases.

3.3. Uncalibrated Substances

In Section 2.2 we described the general idea of the calibration scheme based on the selection of representatives for different chemical classes to simplify the VOC composition. One assumption is that the substances of a certain class react similarly on MOS sensor surfaces yielding a similar response patterns in the TCO and thus all VOCs of a type can be represented by one specific compound. In order to test this assumption, additional substances of chemical classes previously included and also not included in the calibration were tested. Figure 9 shows release tests with two substances not included in the calibration: m/p-xylene (aromatic) and isopropyl alcohol. The chemical class aromatics was represented in the calibration by toluene. Indeed, the m/p-xylene release, Figure 9b, results in an increase of the toluene signal, i.e., the MOS sensor model trained for toluene. The corresponding toluene signal indicates an increase of only 460 ppb, compared to 630 ppb for the same amount of toluene #7. In addition, the carbon monoxide signal shows a slight increase and the same trend as the toluene signal. Thus, for m/p-xylene and toluene as two aromatic compounds our assumption is confirmed, but with different response factors and an additional interference with the carbon monoxide signal. Note that this approach is similar to quantifying unknown substances with the response factor of toluene in GC-MS analysis (ISO16000-6). The simultaneous release of toluene and m/p-xylene (#15) results in an increase of the MOS sensor model of 910 ppb.

For the chemical class alcohol, only ethanol was contained in the calibration. A release test with isopropyl alcohol was performed to check the reaction of the various model to this second alcohol. While the X-pid 9500 confirms the release, Figure 9d, the MOS sensor models for ethanol and all other targets stay constant, although we observe a reaction to isopropyl alcohol in the raw sensor data. This means that the sensor does react to isopropyl alcohol but that the models, especially the model for ethanol, compensates for this reaction. Thus, the assumption of similar reaction patterns is not valid in this case and ethanol is not suitable to represent the chemical class of alcohol, at least not alone.

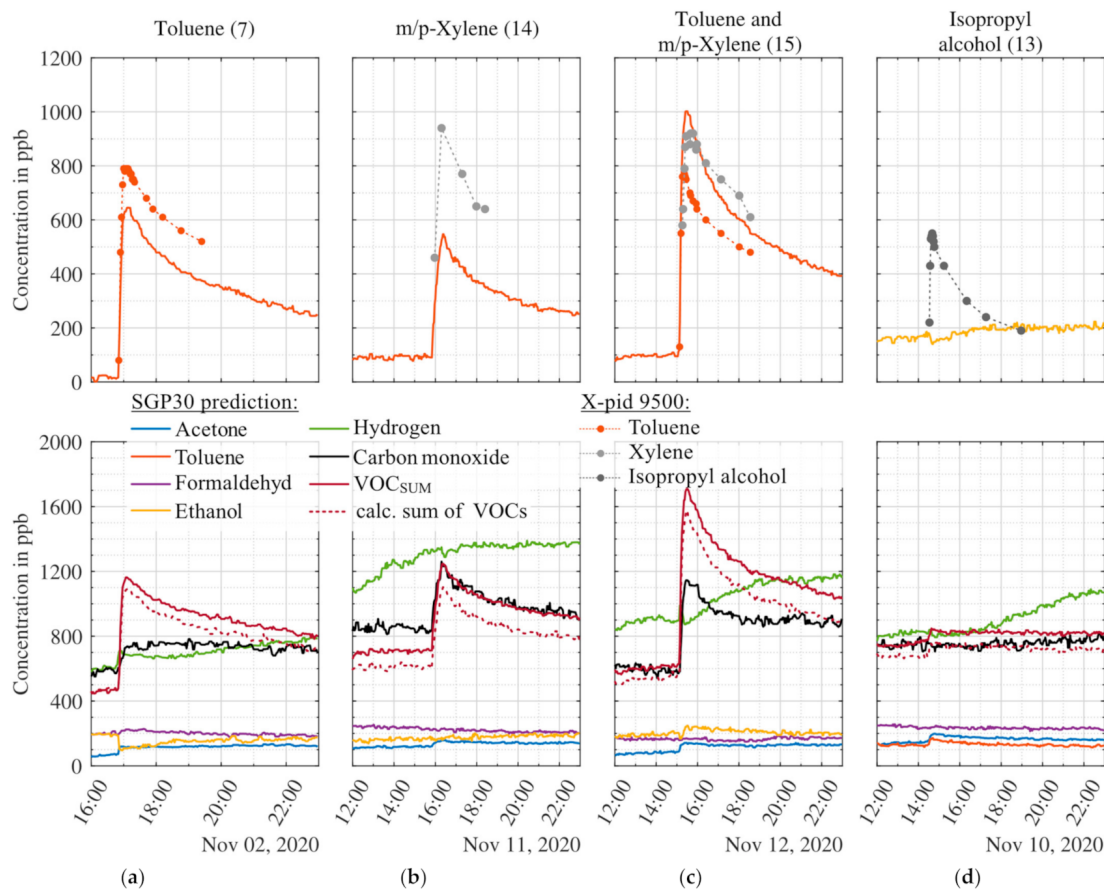


Figure 9. Results recorded during four release tests with toluene (a), m/p-xylene (b), simultaneous release of toluene and m/p-xylene (c), and isopropyl alcohol (d). The upper graphs show the PLSR prediction of the MOS sensor model for the same types of VOC and, if available, reference data (dots); all other signals are shown in the lower graphs. The signals are smoothed over five points (10 min). Numbers in parenthesis behind the released substances refer to the release tests, cf. Table 4.

4. Discussion

In this study, a SGP30 sensor in TCO was successfully calibrated for VOC quantification, both for the overall sum and selective signals, using a randomized calibration scheme in the laboratory. The randomized calibration scheme was based on our previous study [26] with an improved randomized gas mixture generation based on Latin Hypercube sampling. The calculated models yield low RMSE values for different VOC targets based on the lab measurements. The performance of the models is similar to those achieved previously with other MOS sensor types (AS-MLV and AS-MLV-P2, ScioSense B.V., Eindhoven, The Netherlands) [26]. Both studies are not completely identical due to some different gases being used but the results indicate that the SGP30 achieves lower RMSE values for all gases except carbon monoxide. This can be attributed to the higher information obtained from the four different gas-sensitive layers of the SGP30, all of which show only low sensitivity to carbon monoxide. For VOC measurements in indoor air, this might be beneficial, because large variations of the carbon monoxide concentration are possible in room air. Sensor drift, which was especially obvious for one layer off the SGP30, could be effectively eliminated from the models by extended calibration based on two GMA measurements spread over a period of several weeks.

The field tests show quantitative and repeatable results for VOC release tests which were performed by the evaporation of different substances. This method has proven to also be a reliable option for simple verification of the sensor performance. Release tests with substances included in the calibration (toluene, acetone, ethanol, and hydrogen) show concentration increases close to theoretically expected values. Analytical measurements with GC-MS, GC-PID and GC-RCP show the same temporal course during the release tests. Absolute concentrations obtained from the MOS sensor model prediction and the analytical systems are similar but reveal some offsets, also between the different analytical systems. However, these offsets are not higher than normally expected for trace gas measurements even using high-cost lab analysis. Compared to GC-MS, the X-pid 9500 provides better temporal resolution but has a high LOQ, higher than the concentrations tested here. For an exact time-resolved quantification, further analytical measurements with optimized sampling methods for the GC-MS or other analytical measurement systems, like PTR-MS, are required. The difference between the MOS sensor toluene model and the GC-MS, which is the gold standard in VOC analysis, is small (<100 ppb) and similar to the RMSE value determined during calibration. One reason can be that the GC-MS and the MOS sensor are calibrated with gas mixtures from the GMA and the same gas cylinders. Therefore, the accuracy of the gas cylinder (with the highest uncertainty) has no influence on the comparison.

During the release test of hydrogen, the GC-RCP consistently indicated approx. 150 ppb lower concentrations than the hydrogen model of the SGP30. In fact, during ventilation of the room, the GC-RCP indicated a concentration of less than 500 ppb, i.e., below the atmospheric background, indicating that the GC-RCP is underestimating the actual hydrogen concentration. The difference of the two systems is within the error range of the two systems; the RCP has an accuracy of 10% and the MOS sensor system at least 3–5% (uncertainty of the gas mixtures for calibration; model, stability and drift of the system are not considered).

We tested the assumption that substances of the same chemical class react similarly on the sensor surface and can therefore be represented by one single compound. Release tests with m/p-xylene and a laboratory test with benzene indeed showed a reaction of the toluene sensor model, indicating that this model does indeed represent all aromatic compounds, although with different response factors. On the other hand, this means that selectively measuring individual aromatics independent of each other needs further investigation and will at least require more comprehensive calibration. The second chemical class-tested was alcohols where calibration was based on ethanol and a release test was performed with isopropyl alcohol. However, other than for the three aromatics, the ethanol model does not respond to isopropyl alcohol. In the raw sensor signals, a reaction towards isopropyl alcohol was observed but the gases obviously have different reaction processes leading to different sensor response patterns. The approach with a single representative is not valid for this type of VOC, which means that at least two alcohols will be needed for a valid calibration.

5. Conclusions

In this study, we have demonstrated that using MOS gas sensor systems can provide quantitative and selective results not only in the laboratory but also in field measurements as demonstrated by release tests accompanied by analytical measurements. TCO dynamic operation, randomized calibration, and optimized model training are suggested as necessary and practical tools for achieving this performance with commercially available sensor elements. We were able to successfully demonstrate that the sensor can measure calibrated substances in real-time selectively and quantitatively while being released in a room. Also, further investigations about the metrological accuracy or precision and long-term stability of the sensor system are required. Two contrary behaviors concerning the approach of detecting VOC by type were observed, so further work on this approach is required to simplify calibration for complex environments. Even more important for industrial appli-

cation of the demonstrated elaborate calibration, as presented in this manuscript, is the optimization of the model stability without the need for a 2nd calibration after some time in the field. While the approach using extended calibration yields excellent results, this is a very inefficient approach, at least for the calibration of high volumes. Therefore, a study and optimization of long-term stable features and models is necessary. Also, the transfer of the feature selection and of full evaluation models between sensors of the same type should be investigated.

Author Contributions: Conceptualization, T.B., C.S. and A.S.; methodology, T.B., C.S. and J.A.; software, T.B. and J.A.; validation, T.B., C.S. and J.A.; formal analysis, J.A. and T.B.; investigation, J.A.; resources, A.S.; data curation, J.A.; writing—original draft preparation, T.B.; writing—review and editing, T.B., C.S., J.A. and A.S.; visualization, T.B. and J.A.; supervision, T.B., C.S. and A.S.; project administration, A.S. All authors have read and agreed to the published version of the manuscript.

Funding: Part of this research was performed within the project “SE-ProEng” funded by the European Regional Development Fund (ERDF). We acknowledge support by the Deutsche Forschungsgemeinschaft (DFG, German Research Foundation) and Saarland University within the funding program Open Access Publishing.

Institutional Review Board Statement: Not applicable.

Informed Consent Statement: Not applicable.

Data Availability Statement: The underlying data is available on Zenodo and was published with our first publication about the field tests: DOI:10.5281/zenodo.4593853. Title: Measuring Hydrogen in Indoor Air with a Selective Metal Oxide Semiconductor Sensor: Dataset. Authors: Johannes Amann, Tobias Baur, Caroline Schultealbert, <https://zenodo.org/record/4593853> (accessed on 17 May 2021).

Acknowledgments: We thank Rainer Lammertz Pure Gas Products for providing the Peak Performer 1 reference instrument and the Dräger Safety AG & Co KGaA for providing the X-pid 9500 for this study.

Conflicts of Interest: The authors declare no conflict of interest.

Appendix A

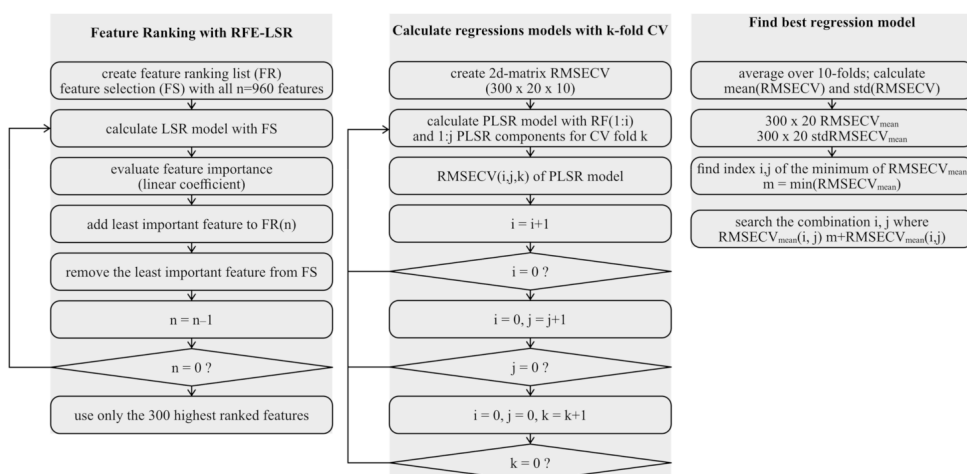


Figure A1. Flowchart of different data evaluation steps. Indices i: number of features, j: number of PLSR components and k: current fold during 10-fold cross validation.

Table A1. Overview of all release tests and events during the field tests.

Number	Time	Type of Event
1	29 September, 09:35–09:48	Door opened
2	30 September, 09:24–09:58	Window opened
3	01 October, 09:10–09:30	Window opened
4	01 October, 11:47–12:05	Door and window opened
5	01 October, 18:30–02 October, 06:30	No specifiable event
6	2 October, 09:00–09:30	Door and window opened
7	02 October, 14:00–05 October, 10:00	Days without events and human presence
8	05 October, 10:10–10:30	Door and window opened
9	05 October and 05 October	Several short periods of human presence
10	06 October, 13:08–16:51	Door and window opened
11	06 October, 17:42–18:44	Release test: 1 ppm H ₂
12	07 October, 16:01–18:05	Release test: 2 ppm H ₂
13	08 October, 10:46–11:00	Door and window opened
14	08 October to 13 October	Days without events and human presence
15	13 October, 09:25–14:00	Door and window opened, human presence
16	13 October, 15:00	Release test: toluene
17	14 October, 09:30–10:05	Door and window opened
18	08 October to 13 October	Sporadic human presence, no specifiable events
19	15 October, 09:00–09:30	Door and window opened
20	15 October, 15:00	Release test: acetone
21	16 October, 09:40–10:10	Door and window opened
22	16 October, 14:50	Release test: acetone and toluene
23	16 October, 18:00	Release test: acetone and toluene
24	17 October to 19 October	Days without events and human presence
25	29 October, 12:55–13:10	Door and window opened
26	29 October to 02 November	Days without events and human presence
27	02 November, 12:40–12:55	Door and window opened
28	02 November, 16:50	Release test: toluene
29	03 November, 10:55–11:10	Door and window opened
30	03 November, 15:30	Release test: acetone followed by defect of the pump, human presence during fixing
31	04 November, 09:00–09:15	Door and window opened
32	04 November, 16:22	Release test: acetone
33	05 November, 09:26–09:41	Door and window opened
34	05 November, 15:10	Release test: acetone and toluene. Unidentified event due to construction inside the building
35	05 November, 18:30–18:50	Door and window opened
36	06 November, 10:03	Release test: limonene
37	06 November to 09 November	Days without events and human presence
38	09 November, 12:21–13:01	Door and window opened

Table A1. Cont.

Number	Time	Type of Event
39	09 November, 18:00	Release test: ethanol
40	10 November, 09:10–09:25	Door and window opened
41	10 November, 14:30	Release test: isopropyl alcohol
42	11 November, 09:28–09:48	Door and window opened
43	11 November, 15:49	Release test: m/p-xylene
44	12 November, 09:15–09:30	Door and window opened
45	12 November, 15:08	Release test: toluene and m/p-xylene
46	13 November, 09:28–11:06	Door and window opened
47	13 November, 14:30	Release test: acetone, toluene, and ethanol
48	13 November–16 November	Days without events and human presence
49	16 November, 11:55–12:20	Door and window opened
50	16 November, 17:06–19:20	Release test: 2 ppm H ₂
51	17 November, 09:54–10:24	Door and window opened
52	17 November, 18:24	Release test: ethanol
53	18 November, 09:36–09:56	Door and window opened
54	19 November, 12:02–16:00	Release test: carbon monoxide (tea candle)

References

- Asikainen, A.; Carrer, P.; Kephalopoulos, S.; Fernandes, E.D.O.; Wargocki, P.; Hänninen, O. Reducing burden of disease from residential indoor air exposures in Europe (HEALTHVENT project). *Environ. Health* **2016**, *15*, S35. [\[CrossRef\]](#) [\[PubMed\]](#)
- Settimo, G.; Manigrasso, M.; Avino, P. Indoor Air Quality: A Focus on the European Legislation and State-of-the-Art Research in Italy. *Atmosphere* **2020**, *11*, 370. [\[CrossRef\]](#)
- Spaul, W.A. Building-related factors to consider in indoor air quality evaluations. *J. Allergy Clin. Immunol.* **1994**, *94*, 385–389. [\[CrossRef\]](#) [\[PubMed\]](#)
- Herberger, S.; Herold, M.; Ulmer, H.; Burdack-Freitag, A.; Mayer, F. Detection of human effluents by a MOS gas sensor in correlation to VOC quantification by GC/MS. *Build. Environ.* **2010**, *45*, 2430–2439. [\[CrossRef\]](#)
- Buszewski, B.; Kesy, M.; Ligor, T.; Amann, A. Human exhaled air analytics: Biomarkers of diseases. *Biomed. Chromatogr.* **2007**, *21*, 553–566. [\[CrossRef\]](#)
- Veres, P.R.; Faber, P.; Drewnick, F.; Lelieveld, J.; Williams, J. Anthropogenic sources of VOC in a football stadium: Assessing human emissions in the atmosphere. *Atmos. Env.* **2013**, *77*, 1052–1059. [\[CrossRef\]](#)
- Pettenkofer, M. Über den Luftwechsel in Wohngebäuden; Literarisch-Artistische Anstalt der J.G. Cotta'schen Buchhandlung. 1858. Available online: <https://opacplus.bsb-muenchen.de/title/BV013009721> (accessed on 17 May 2021).
- Liu, Y.; Misztal, P.K.; Xiong, J.; Tian, Y.; Arata, C.; Weber, R.J.; Nazaroff, W.W.; Goldstein, A.H. Characterizing sources and emissions of volatile organic compounds in a northern California residence using space- and time-resolved measurements. *Indoor Air* **2019**, *29*, 630–644. [\[CrossRef\]](#)
- Madou, M.J.; Morrison, S.R. *Chemical Sensing with Solid State Devices*; Academic Press, Inc.: San Diego, CA, USA, 1989; ISBN 978-0-12-464965-1.
- Bârsan, N.; Weimar, U. Understanding the fundamental principles of metal oxide based gas sensors; the example of CO sensing with SnO₂ sensors in the presence of humidity. *J. Phys. Condens. Matter* **2003**, *15*, 813–839. [\[CrossRef\]](#)
- Rüffer, D.; Hoehne, F.; Bühler, J. New digital metal-oxide (MOx) sensor platform. *Sensors* **2018**, *18*, 1052. [\[CrossRef\]](#)
- Schultealbert, C.; Baur, T.; Schütze, A.; Sauerwald, T. Facile Quantification and Identification Techniques for Reducing Gases over a Wide Concentration Range Using a MOS Sensor in Temperature-Cycled Operation. *Sensors* **2018**, *18*, 744. [\[CrossRef\]](#)
- Korotcenkov, G.; Cho, B.K. Instability of metal oxide-based conductometric gas sensors and approaches to stability improvement (short survey). *Sens. Actuators B* **2011**, *156*, 527–538. [\[CrossRef\]](#)
- ScioSense ENS160 Datasheet. Available online: <https://www.sciosense.com/wp-content/uploads/documents/SC-001224-DS-1-ENS160-Datasheet-Rev-0.95.pdf> (accessed on 4 April 2021).
- Schütze, A.; Baur, T.; Leidinger, M.; Reimringer, W.; Jung, R.; Conrad, T.; Sauerwald, T. Highly Sensitive and Selective VOC Sensor Systems Based on Semiconductor Gas Sensors: How to? *Environments* **2017**, *4*, 20. [\[CrossRef\]](#)
- Kohl, D.; Kelleter, J.; Petig, H. Detection of Fires by Gas Sensors. *Sens. Updat.* **2001**, *9*, 161–223. [\[CrossRef\]](#)

17. Leidinger, M.; Sauerwald, T.; Reimringer, W.; Ventura, G.; Schütze, A. Selective detection of hazardous VOCs for indoor air quality applications using a virtual gas sensor array. *J. Sens. Sens. Syst.* **2014**, *3*, 253–263. [CrossRef]

18. Bastuck, M.; Baur, T.; Richter, M.; Mull, B.; Schütze, A.; Sauerwald, T. Comparison of ppb-level gas measurements with a metal-oxide semiconductor gas sensor in two independent laboratories. *Sens. Actuators B* **2018**, *273*, 1037–1046. [CrossRef]

19. Baur, T.; Schütze, A.; Sauerwald, T. Optimierung des temperaturzyklischen Betriebs von Halbleitergassensoren. *Tech. Mess.* **2015**, *82*, 187–195. [CrossRef]

20. Schultealbert, C.; Baur, T.; Schütze, A.; Böttcher, S.; Sauerwald, T. A novel approach towards calibrated measurement of trace gases using metal oxide semiconductor sensors. *Sens. Actuators B* **2017**, *239*, 390–396. [CrossRef]

21. Leidinger, M.; Schultealbert, C.; Neu, J.; Schütze, A.; Sauerwald, T. Characterization and calibration of gas sensor systems at ppb level—a versatile test gas generation system. *Meas. Sci. Technol.* **2018**, *29*, 015901. [CrossRef]

22. Baur, T.; Bastuck, M.; Schultealbert, C.; Sauerwald, T.; Schütze, A. Random gas mixtures for efficient gas sensor calibration. *J. Sens. Sens. Syst.* **2020**, *9*, 411–424. [CrossRef]

23. Hofmann, H.; Plieninger, P. Bereitstellung einer Datenbank zum Vorkommen von flüchtigen organischen Verbindungen in der Raumluft. *WaBoLu Hefte* **2008**, *5*, 161.

24. Hofmann, H.; Erdmann, G.; Müller, A. Zielkonflikt energieeffiziente Bauweise und gute Raumluftqualität—Datenerhebung für flüchtige organische Verbindungen in der Innenraumluft von Wohn- und Bürogebäuden (Lösungswege); 2014. Available online: <https://www.agoef.de/forschung/fue-ll-voc-datenerhebung/abschlussbericht.html> (accessed on 17 May 2021).

25. Traynor, G.W.; Apte, M.G.; Carruthers, A.R.; Dillworth, J.F.; Grimsrud, D.T.; Gundel, L.A. Indoor air pollution due to emissions from wood-burning stoves. *Environ. Sci. Technol.* **1987**, *21*, 691–697. [CrossRef] [PubMed]

26. Schultealbert, C.; Amann, J.; Baur, T.; Schütze, A. Measuring Hydrogen in Indoor Air with a Selective Metal Oxide Semiconductor Sensor. *Atmosphere* **2021**, *12*, 366. [CrossRef]

27. WHO. WHO Regional Office for Europe WHO Guidelines for Indoor Air Quality: Selected Pollutants; World Health Organization. Regional Office for Europe: Copenhagen, Denmark, 2010; Volume 9, ISBN 978-92-890-0213-4.

28. Schultealbert, C.; Baur, T.; Schütze, A.; Sauerwald, T. Investigating the role of hydrogen in the calibration of MOS gas sensors for indoor air quality monitoring. In Proceedings of the Indoor Air, Philadelphia, PA, USA, 22–27 July 2018.

29. Loh, W.-L. On Latin Hypercube Sampling. *Ann. Stat.* **1996**, *24*, 2058–2080. [CrossRef]

30. Floor Plan of Building A5 1 at Saarland University. Available online: https://www.uni-saarland.de/fileadmin/upload/footer/grundriss/SBC-13_00-002.pdf (accessed on 4 April 2021).

31. Bastuck, M.; Baur, T.; Schütze, A. DAV³E—a MATLAB toolbox for multivariate sensor data evaluation. *J. Sens. Sens. Syst.* **2018**, *7*, 489–506. [CrossRef]

32. Youssef, S.; Zimmer, C.; Szielasko, K.; Schütze, A. Automatic feature extraction of periodic time signals using 3MA-X8 method. *Tm Tech. Mess.* **2019**, *86*, 267–277. [CrossRef]

33. Bur, C.; Engel, M.; Horras, S.; Schütze, A. Drift compensation of virtual multisensor systems based on extended calibration, IMCS 2014—the 15th International Meeting on Chemical Sensors. In Proceedings of the IMCS 2014—The 15th International Meeting on Chemical Sensors, Buenos Aires, Argentina, 16–19 March 2014.

34. Robin, Y.; Goodarzi, P.; Baur, T.; Schultealbert, C.; Schütze, A.; Schneider, T. Machine Learning based calibration time reduction for Gas Sensors in Temperature Cycled Operation. In Proceedings of the IEEE International Instrumentation and Measurement Technology Conference (I2MTC), Glasgow, Scotland, 17–20 May 2021.

4.3.6 Paper F – Measuring Hydrogen in Indoor Air with a Selective Metal Oxide Semiconductor Sensor

C. Schultealbert, J. Amann, T. Baur, A. Schütze
Saarland University, Lab for Measurement Technology, Saarbrücken, Germany

Atmosphere. (2021), 12(3), 366

The original paper can be found, in the online version, at
<https://doi.org/10.3390/atmos12030366>.

© 2021 by the authors. This article is an open access article distributed under the terms and conditions of the Creative Commons Attribution (CC BY) license (<http://creativecommons.org/licenses/by/4.0/>).



Article

Measuring Hydrogen in Indoor Air with a Selective Metal Oxide Semiconductor Sensor

Caroline Schultealbert Johannes Amann, Tobias Baur and Andreas Schütze

Lab for Measurement Technology, Saarland University, Campus A5 1, 66123 Saarbruecken, Germany;
amann.johannes@web.de (J.A.); t.baur@lmt.uni-saarland.de (T.B.); schuetze@lmt.uni-saarland.de (A.S.)

* Correspondence: c.schultealbert@lmt.uni-saarland.de

Abstract: Hydrogen is a ubiquitous but often neglected gas. In analytical measurements hydrogen—as a harmless gas—often is not considered so no studies on hydrogen in indoor air can be found. For metal oxide semiconductor (MOS) gas sensors that are increasingly pushed into the application as TVOC (total volatile organic compounds) sensors, hydrogen is a severe disturbance. On the other hand, hydrogen can be an intentional choice as indicator for human presence similar to carbon dioxide. We present a field-study on hydrogen in indoor air using selective MOS sensors accompanied by an analytical reference device for hydrogen with an accuracy of 10 ppb. Selectivity is achieved by siloxane treatment combined with temperature cycled operation and training with a complex lab calibration using randomized gas mixtures, yielding an uncertainty of 40–60 ppb. The feasibility is demonstrated by release tests with several gases inside a room and by comparison to the reference device. The results show that selective MOS sensors can function as cheap and available hydrogen detectors. Fluctuations in hydrogen concentration without human presence are measured over several days to gain insight in this highly relevant parameter for indoor air quality. The results indicate that the topic needs further attention and that the usage of hydrogen as indicator for human presence might be precluded by other sources and fluctuations.



Citation: Schultealbert, C.; Amann, J.; Baur, T.; Schütze, A. Measuring Hydrogen in Indoor Air with a Selective Metal Oxide Semiconductor Sensor. *Atmosphere* **2021**, *12*, 366. <https://doi.org/10.3390/atmos12030366>

Academic Editor: Elisabete Carolina

Received: 6 February 2021

Accepted: 5 March 2021

Published: 11 March 2021

Publisher's Note: MDPI stays neutral with regard to jurisdictional claims in published maps and institutional affiliations.



Copyright: © 2021 by the authors. Licensee MDPI, Basel, Switzerland. This article is an open access article distributed under the terms and conditions of the Creative Commons Attribution (CC BY) license (<https://creativecommons.org/licenses/by/4.0/>).

1. Introduction

Indoor air quality (IAQ) is a general term comprising a multitude of parameters like temperature, humidity, air flow or the concentration of many trace gases [1]. The term is known since 1970 and of increasing interest during the last decades [2]. Among these trace gases are specific harmful pollutants like nitrogen dioxide (NO_2); formaldehyde or benzene [3,4]; carbon dioxide (CO_2), which is often used as indicator for human presence [5,6]; many organic compounds, often simply referred to as VOCs (volatile organic compounds) [7]; and others. Despite this high complexity inexpensive sensors are wanted for the purpose of IAQ monitoring. Nondispersive infrared sensors (NDIR) for CO_2 monitoring are state of the art for demand-controlled ventilation if concentrations are above 1000 ppm, although this level is not harmful: Pettenkofer, who introduced this guideline value, already stated in 1858 that CO_2 is only an indicator for other harmful and smelly organic substances emitted by human beings [5] and recent results from aerospace research support this assessment [8]. In today's world VOCs are not only emitted by humans but also from other sources like furniture, personal care products or cleaning agents, so this approach of indirect VOC measurement might be erroneous [9].

Up-and-coming for real-time and direct VOC measurements are metal oxide semiconductor (MOS) gas sensors, which can already be found in many available IAQ monitors. These sensors show high sensitivity towards a wide range of reducing gases. Their selectivity—e.g., to a group of gases like VOCs—can be optimized by cyclically changing the temperature of the sensing layer (TCO, temperature cycled operation) [10,11]. This type

of operation has been known for a long time [12], but is still often only used in research. Commercially available devices are typically operated at constant temperature yielding a simple sum signal for reducing gases.

Another trace gas that is not directly linked to IAQ, because it does not have a specific health effect, is hydrogen (H_2), which can be found in the atmosphere at a concentration of 500 ppb [13]. MOS sensors are very sensitive to this gas especially at higher operating temperatures, where the sensors are generally operated. Since H_2 in this concentration range (500 ppb and above) is not covered by typical analytical measurement techniques in gas measurement science (gas chromatography, sorption tubes, mass spectrometry, infrared spectrometry, photoionization detectors, etc.) little is known on the presence and dynamic of this gas in indoor air. For outdoor and atmospheric concentrations some studies can be found, indicating that H_2 is a product of chemical industry and emitted from cars and other traffic [14], but also from the photochemical oxidation of methane (CH_4) and VOCs [15,16]. An annual cycle with an amplitude of approximately 40 ppb and a diurnal cycle with an amplitude of approximately 3 ppb can be observed [14,15]. Therefore, even in outdoor air significant variations of the H_2 concentration are expected in industrial and residential areas [17] and therefore also some variations are likely in indoor air. Therefore, when using MOS sensors as VOC or TVOC (total volatile organic compounds) monitors H_2 needs to be considered as interferent gas because MOS sensors are normally very sensitive to this gas.

Additionally, human beings emit significant amounts of H_2 as a product of digestion via breath and flatus [18–22] and other sources might exist (photochemical reactions, metabolism of plants and microorganisms [23,24]). Assuming that humans are the dominant source, H_2 could be used as an indicator for human presence similar to CO_2 , including the same drawback of other VOC sources than humans. Sensirion AG claims to measure a CO_2 -equivalent with their SGP30 MOS sensor by measuring H_2 as a substitute [25]. A proof for this correlation is missing. Moreover, the correlation between emitted (harmful and smelly) VOCs and both H_2 and CO_2 excretion is of high relevance to assess the best IAQ indicator for indoor air quality. Due to the mentioned lack of reference data for H_2 no such studies can be found so far.

Since MOS sensors are excellent detectors for H_2 they can help closing this gap in knowledge. In 2018, we presented a first and short field test on the role of H_2 in indoor air and found a concentration increase of up to 2.5 ppm H_2 inside a meeting room with 13 persons over 1 h [26]. In this manuscript we present an extended field-study over two months inside an office at the university with a focus on H_2 to get a better overall idea on the topic of H_2 in indoor air—as interferent and as target gas. Two approaches for achieving selective H_2 quantification were combined: TCO followed by pattern analysis with machine learning (ML) algorithms [10,11] and a pre-treatment of the sensitive layer with siloxane, which in other circumstances is called poisoning since it deteriorates all sensitivities except for H_2 [27–31]. The performance of the sensor signals is validated by release tests and a GC with reducing compound photometer (RCP) detector (Peak Performer 1, Peak Laboratories Inc., Mountain View, CA, USA), which to our knowledge is the only analytical device for online measurement of hydrogen with ppb-level resolution.

2. Experiments

SGP30 multilayer MOS sensors (four sensitive layers on one hotplate, Sensirion AG, Stäfa, Switzerland) were used for this study. One sensor device was installed as delivered and another one was pre-treated with Octamethylcyclotetrasiloxane at 2 ppm over 18 h yielding a H_2 selective sensor (compare [26,28]). The temperature cycle is specifically designed to achieve high sensitivity and selectivity by using the differential surface reduction (DSR) method, which is described in detail in previous publications [32–34]. For this purpose, the temperature cycle of the untreated sensor consists of several steps from high to low temperature, always starting for 5 s at 400 °C followed by 7 s each at 100, 125, . . . , 325 °C resulting in a total cycle duration of 120 s. For the pre-treated sensor, this cycle was adjusted as the sensor reaction is slower after siloxane treatment. Longer temperature

plateaus and increased temperatures are required to compensate this effect: 10 s at 400 °C are here followed by 20 s each at 275, 300, 325, and 350 °C again resulting in a total duration of 120 s. Temperature control and sensor read-out are done using the SGP30's integrated ASIC. Via a tiny 4.0 microcontroller board the temperatures from the TCO are controlled and the data is transferred to a computer. The sampling rate is 25 Hz.

The machine learning is performed with our open source toolbox DAV³E [35]. The sensor cycles are divided into 120 sections of 1 s duration and in each of these sections the linear slope of the logarithm of the sensor conductance is computed. Due to the four layers in each sensor 480 features are obtained from every individual sensor. For each sensor, feature selection is performed by recursive feature elimination and PLSR (partial least squares regression) models predicting the concentration of H₂ are trained [36]. Each model is validated by 10-fold cross-validation to define an appropriate number of PLSR components yielding the root mean squared error for validation (RMSE_V) [37]. During hold-out all cycles of one random gas mixture are always left out from the training to avoid vulnerability to over-fitting [37]. Moreover, 20% of the data is held out during the ML optimization process and applied as test data in the end yielding RMSE_T as a final step to guarantee proper model functionality [37].

In a first step, the sensors were lab-calibrated inside a gas mixing system [38,39] using randomized gas mixtures [40], which means that all gases connected to the system, in this case six, are applied at once and their concentrations are randomly chosen from defined ranges (acetone 17–1000 ppb, carbon monoxide 150–2000 ppb, ethanol 4–1000 ppb, formaldehyde 1–400 ppb, hydrogen 400–4000 ppb, and toluene 4–1000 ppb). For the generation of this randomized mixtures Latin hypercube sampling is performed to ensure proper scanning of the full measurement range and the obtained concentration values are stored for training of the sensor models [41]. This method yields perfectly suited data for the training of machine learning algorithms as described before [40]. Each gas exposure has a duration of 20 min, 400 independent mixtures were measured during the calibration.

The sensors were then brought to the field—a normal office—where they were installed for two months interrupted by an additional lab measurement after four weeks. This measurement has the identical structure as the initial calibration and is used to identify and compensate drift in the sensor signals. For this purpose, both measurements—initial and repeated lab-calibration—were used to determine the ML models and evaluate the data presented in this manuscript.

During this time in the field several release tests were conducted inside the room: acetone, ethanol, isopropanol, limonene, and toluene were released by evaporating liquid in the middle of the room (the full amount of liquid of 0.1 to 0.16 mL—depending on the substance—inside a petri dish that was placed on a desk). Carbon monoxide was released by burning a tea candle. Hydrogen was released from a pressure cylinder with a concentration of 2000 ppm in air at a rate of 500 mL/min using a mass flow controller. During several days, a gas chromatograph with a reducing compound photometer as detector (Peak Performer 1, PeakLaboratories Inc., Mountain View, California, USA, detection limit and accuracy 10 ppb H₂) was installed in the room in parallel to the sensor systems as reference for the H₂ concentration. The instrument was provided on free loan and in that short period of time we were not be able to perform a proper recalibration which would have been needed according to the manual.

A plan of the field test room is shown in Figure 1. The area is 21.91 m², the total volume of the room is 61.35 m³. The releases were performed close to the centre of the room and a fan from the corner was installed to produce some air flow and improve the (ideally uniform) distribution of released substances. From a CO₂ release and the decay curve measured by NDIR CO₂ sensors (SCD40, Sensirion AG, Stäfa, Switzerland) the air exchange rate with closed window and door is approximately 0.17 h⁻¹.

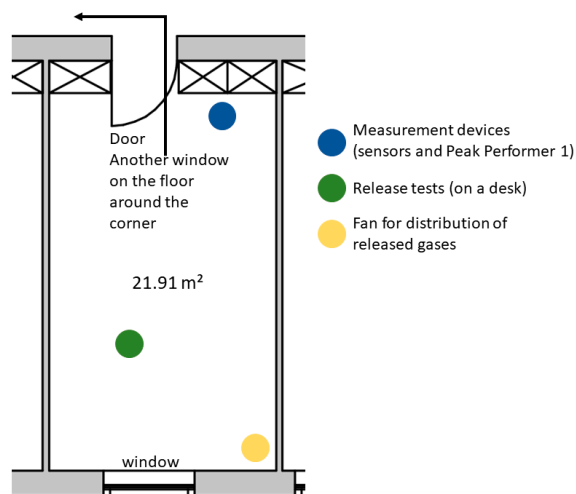


Figure 1. Field test room and positions of the measurement devices, release tests, and a fan for improved distribution of the evaporated substances inside the room.

3. Results

3.1. Lab Calibration

From the lab calibration the PLSR models shown in Figure 2 were obtained for both sensors. Each data point represents one cycle. The obtained values from the calibration are $\text{RMSE}_V = 44.8 \text{ ppb}$ and $\text{RMSE}_T = 40.5 \text{ ppb}$ for the untreated sensor and $\text{RMSE}_V = 56.0 \text{ ppb}$ and $\text{RMSE}_T = 60.0 \text{ ppb}$ for the pre-treated sensor. Since the pre-treatment enhances selectivity by reducing the sensitivity towards other gases more than towards H_2 , it is not surprising that quantification is somewhat worse for the pre-treated sensor. On the other hand, this sensor is chemically selective, whereas the untreated sensor might fail if gas compounds occur which were not part of the calibration dataset. Therefore, in the following we will always show both sensors, to check for synchronicity.

3.2. Validation in the Field

To check the functionality of the calibrated PLSR models directly in the field, we performed several H_2 release tests. During the first two release tests no reference was available. Two consecutive releases were performed, the first one with a calculated concentration increase of 1 ppm inside the room and the second one with a calculated concentration increase of 2 ppm. These concentrations would be obtained if the gas released from the cylinder is evenly distributed inside the room and if there is no loss through ventilation, adsorption, or reaction; on average, somewhat lower values due to unavoidable losses are expected.

Figure 3a,b show the recorded concentration predictions based on the PLSR model during the first (1 ppm) and second release test (2 ppm), respectively; the start and end points of the releases are marked. The untreated sensor shows slightly (100–200 ppb) lower absolute values than the pre-treated sensor over the whole course. The H_2 concentration increase during the first release is 900 ppb for the untreated sensor and 890 ppb for the pre-treated sensor. During the second H_2 release the predicted increases are 1430 ppb and 1240 ppb for the untreated and pre-treated sensor, respectively.

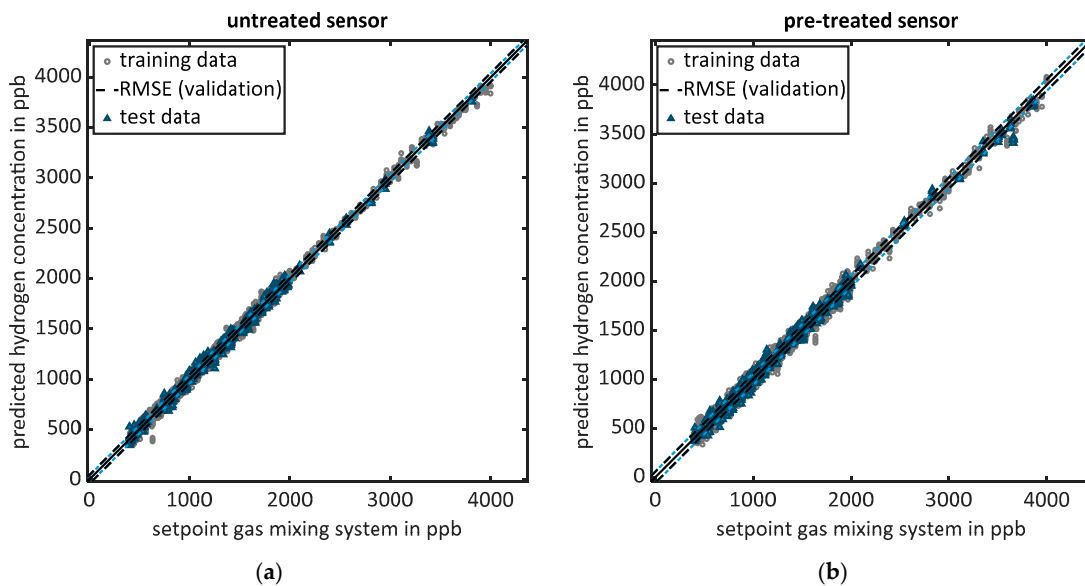


Figure 2. Partial least squares regression (PLSR) models for the prediction of H_2 concentration based on the calibration inside the lab: (a) untreated sensor: root mean squared error for validation (RMSE_V) = 44.8 ppb and RMSE_T = 40.5 ppb; (b) sensor pre-treated with siloxane: RMSE_V = 56.0 ppb and RMSE_T = 60.0 ppb. Grey circles are part of the training, blue triangles part of the independent test data (20% of the data); both PLSR models show no indication of overfitting.

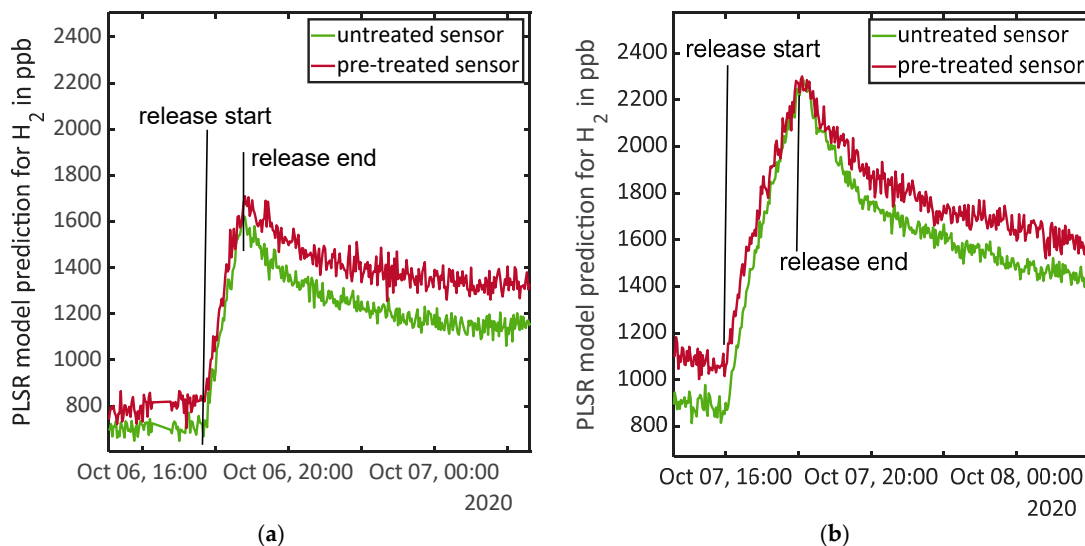


Figure 3. PLSR model predictions for H_2 for both sensors (untreated and pre-treated) during two release tests of H_2 supplied from a pressure cylinder with constant rate provided by a mass flow controller: (a) first release with calculated increase of 1 ppm; (b) second release with calculated increase of 2 ppm.

During two periods a reference instrument (Peak Performer 1) was available. Figure 4a shows the first of these periods, where data from the reference instrument was recorded in parallel with both sensors over one weekend. While only minimal concentration changes were observed during that period, good correlation between all three signals is nevertheless evident. The untreated sensor shows an offset of approximately 200 ppb and only slightly

higher noise than the analytical reference instrument. The pre-treated sensor shows an even higher offset of 500 ppb and, in accordance with the calibration results, a significantly higher noise level with almost double amplitude.

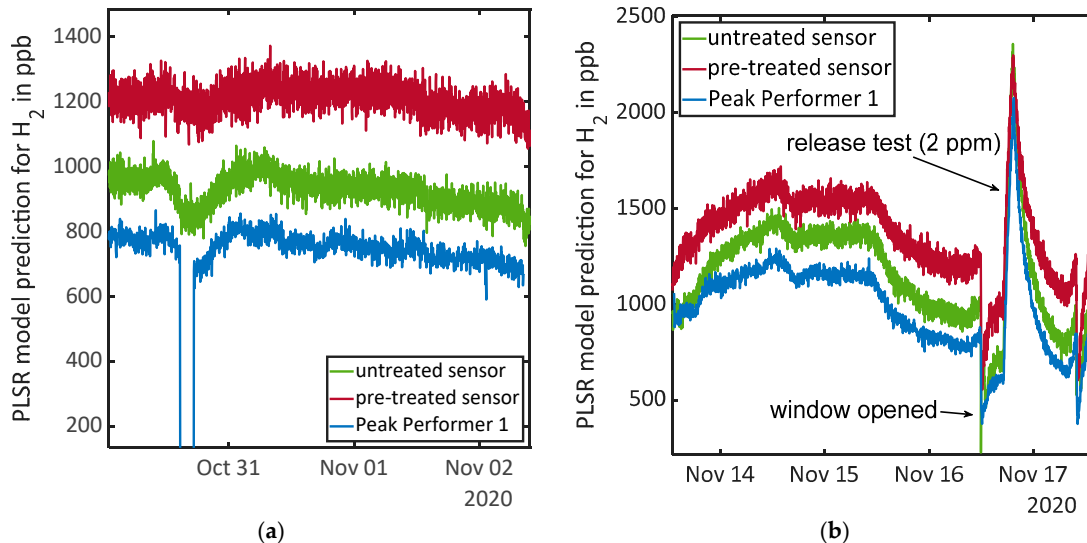


Figure 4. PLSR model predictions for H_2 for both sensors (untreated and pre-treated) compared to an analytical reference instrument (Peak Performer 1): (a) a weekend without additional events, the reference instrument was not connected to the pump for a short period of time and indicates 0 ppb during that period; (b) during a weekend followed by a release test with a calculated concentration increase of 2 ppm H_2 .

The second test period including the reference instrument is shown in Figure 4b. Again, we measured over one weekend, but this time some significant changes in H_2 concentration were observed. Both sensor signals show a very good correlation to the reference device. On the final day a release test with a calculated concentration of 2 ppm H_2 was performed. The room was thoroughly ventilated through open window and door before this release test. The reference instrument indicated a concentration increase during the release of 1465 ppb. The two sensors indicate an increase of 1650 ppb (untreated sensor) and 1365 ppb (pre-treated sensor). Despite the higher offset, the relative PLSR signal of the chemically selective MOS sensor correlates better with the analytical measurement (7% deviation vs. 13% deviation in the observed concentration increase).

A correlation analysis over the whole period when the reference device was measuring in parallel was performed. Due to the different sampling rates (2 min for the sensors and 3.6 min for the Peak Performer 1) the data were resampled to obtain data points every minute using linear interpolation, Figure 5. From the 9560 data points per device (covering 160 h) Pearson correlation coefficients between the Peak Performer 1 and the PLSR model predictions from the untreated sensor and the pre-treated sensor were obtained of 0.97 and 0.95, respectively.

In field measurements it is impossible to gain uncertainty levels from noise calculation that are free of doubt because one cannot distinguish between changes in concentration and pure signal noise. However, we chose a 2 h window on 1 November with tolerably constant concentration level. A Lilliefors test was applied to the data points of all devices indicating they are normally distributed (5% significance level for rejection of the null hypothesis) so the assumption of constant concentration is reasonable [42]. The standard deviation of the Peak Performer 1 on that time scale is 15.9 ppb, which is close to the given accuracy of the instrument of 10 ppb. The untreated sensor shows a standard deviation of 29.8 ppb and the pre-treated sensor 36.1 ppb.

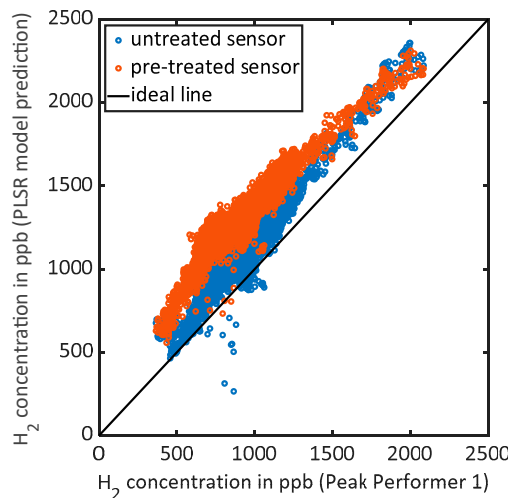


Figure 5. Concentrations obtained from the PLSR model predictions of both sensors vs. concentration indicated by the Peak Performer 1.

To judge the absolute accuracy of all three devices the ventilation event before the release test can be used. The atmosphere contains 500 ppb of H_2 so lower levels are unrealistic—higher levels might be possible due to sources nearby (traffic or industry) [13,14]. The Peak Performer 1 shows a minimum concentration of 380 ppb during this ventilation, the untreated sensor 465 ppb and the pre-treated sensor 560 ppb. Thus, in this case the offset for the analytical reference device is at least -120 ppb and for the untreated sensor at least -35 ppb, the absolute accuracy of the pre-treated sensor cannot be determined.

3.3. Results during Field Tests

The first 25 days of the field test before the interim calibration is shown in Figure 6, the second part after that calibration spanning 22 days in Figure 7. Indicated H_2 concentrations are between 450 ppb and 2300 ppb. During most of the time, the indicated concentration inside the room is around 1000 ppb, which is high compared to the atmospheric background level of 500 ppb. Numbers along the line mark events or periods, a detailed description of these is given in Appendix A, Table A1. All events labelled below the traces of the PLSR model predictions indicate ventilation events, i.e., the window and/or door of the room were opened, and the room thoroughly ventilated to achieve a clean baseline before and after the conducted release tests.

Events 11 and 12 indicate the H_2 release tests shown in Figure 3a,b, #25 indicates the weekend with the data of the reference instrument recorded in parallel (cf. Figure 4a), and #47–49 the weekend and H_2 release test with the second recording of the reference instrument in parallel (cf. Figure 4b).

Weekends are indicated by #7, 14, 23, 25, 36, and 47. During these days no one entered the room, and no release tests were conducted. Nevertheless, ascending as well as descending concentrations are observed, especially at #14, where oscillating values indicate a diurnal cycle. The maxima of these cycles are typically reached in the morning around 6–8 a.m., the corresponding minima in the evening around 6–8 p.m. During other weekends, this clear correlation with time is less obvious, but in general descending values are more likely in the afternoon.

During the field tests, release tests were also performed with different VOCs. The amount of evaporated liquid was always chosen to theoretically reach 600 ppb inside the room assuming ideal uniform distribution and no ventilation, corresponding to 0.1 to 0.16 mL. Here, an increase of the H_2 concentration 2–6 h after the VOC release is observed.

This increase often starts around 6 p.m., which is the same time at which the minimum in the diurnal cycle is observed. Looking at those days with release tests, during which a higher H₂ concentration is observed than on the day before (#16, 20, 22, 27, 29, 31, 40, 42, and 46) a correlation to the substances acetone, isopropanol, toluene and xylene is found. Release of limonene (#35) results in an immediate increase of the PLSR output of the chemically selective pre-treated sensor, while the signal of the untreated sensor shows a less pronounced increase after 5–6 h.

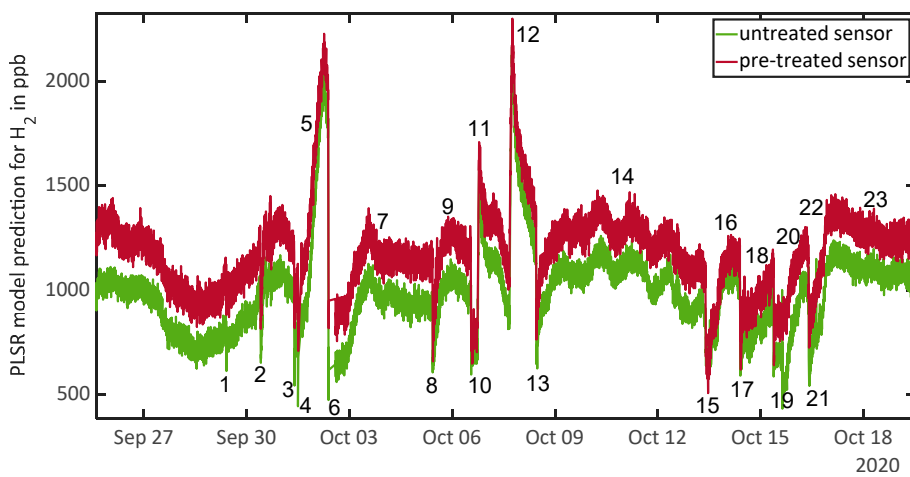


Figure 6. PLSR model predictions for H₂ from both sensors (untreated and pre-treated) over several days. Descriptions of the labelled events and periods can be found in Appendix A, Table A1.

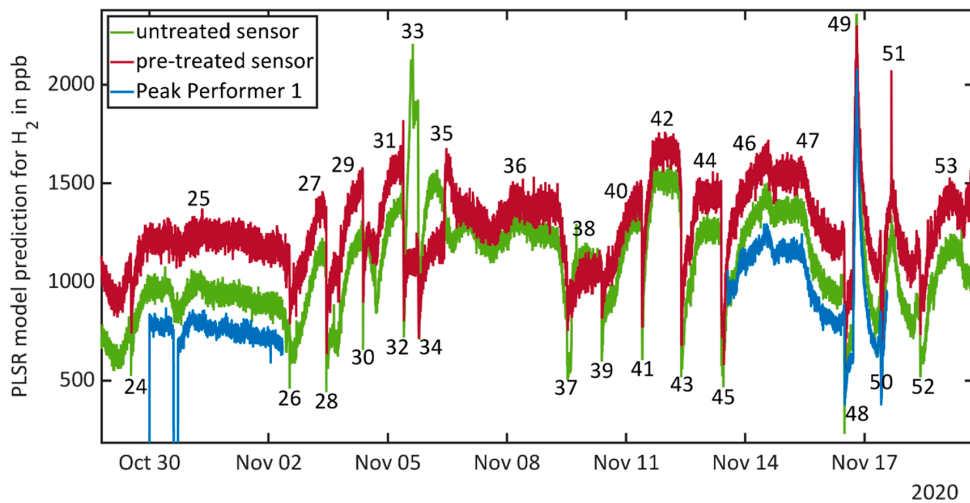


Figure 7. PLSR model predictions for H₂ from both sensors (untreated and pre-treated) over several days. Descriptions of the labelled events and periods can be found in Appendix A, Table A1.

Event 5 shows a strong increase in H₂ concentration overnight after a day without any identified events or tests during that day. Event 33 shows a very strong increase of the H₂ concentration prediction only from the untreated sensor while the signal obtained from the pre-treated sensor stays nearly constant. After ventilation (34) on the next day again a milder increase is observed with the same pattern. We were able to attribute these events

to construction work inside the building using a binding agent, which was done on the same floor as the field test room on the first day and on the floor below on the second day.

Due to the Covid-19 pandemic no systematic investigation of the effect of human presence was possible. Only on some days (#9, 15, 29, and 45) individual persons sporadically entered the room and for every release test one person entered the room. However, in none of these cases could the human presence be observed from the H₂ signal.

4. Discussion

Two questions arising from the results need to be discussed in more detail: (1) can MOS sensors function as reliable H₂ detectors also in further research, and (2) what do we learn from the results concerning H₂ in indoor environments?

Especially Figure 4—the PLSR predictions obtained from the MOS sensors recorded in parallel with an analytical reference instrument—strongly suggests, that the calibrated sensors can correctly measure relative fluctuations. For absolute measurements, an in-field one-point calibration might be sufficient to eliminate the observed but constant offset between the three devices. Similar to low-cost CO₂ sensors, this could be realized with an automatic baseline correction, i.e., setting the lowest value over a longer period to the atmospheric background concentration. It is remarkable, that applying this approach during a ventilation event yields, that the analytical reference shows the highest offset from the baseline level of 500 ppb. Keeping in mind that the analytical device is three orders of magnitude more expensive than MOS sensors the performance of the sensors is very good with approximately doubled noise level compared to the analytical device and correlation coefficients of 0.95 and 0.97, respectively.

As the sensors are running parallel in almost all situations and given the very different methods of achieving the selective H₂ signal, this also strongly implies the capability of MOS sensors to reliably measure H₂ at least at ppm and sub-ppm concentrations. There are two events where significant deviations between both models occur: #33, where an emission during construction work was classified as H₂ by the untreated sensor. In this situation, the chemically selective pre-treated sensor proves to be more reliable when untrained and unusual gases occur. During the release tests of limonene (#35), the opposite effect is observed: the model of the pre-treated sensor indicates an increase of H₂, while the model of the untreated sensor remains at a constant value during the release and only indicates increasing values several hours after the release test. Since in contrast to all the other released gases we do not see any sensor reaction in the raw sensor data, we assume that the sealing membrane on the sensor prevents the large limonene molecules reaching the sensor surface. For the pre-treatment this membrane was removed, thus limonene can reach the hot sensor surface of the pre-treated sensor. We assume that limonene reacts on the hot surface releasing H₂ (cf. [43]), resulting in a sensor response and an increase of the PLSR model prediction. Reapplying the sealing membrane would help to resolve this issue. Thus, in terms of selectivity the pre-treated sensor would be more reliable. In return a lower signal to noise ratio needs to be accepted. In contrast to a pre-treated sensor at constant temperature, which can be found in literature and suffers from low response times [30,44], the DSR mode overcomes this issue.

From the field tests we observe that releasing VOCs like toluene and acetone is followed by an increase in H₂ concentration hours later. This might be due to decomposition processes such as photochemical oxidation [15]. However, this effect is also overlaid by the observed diurnal cycle with minimum H₂ concentrations in the evening. This diurnal cycle is not fully correlated with the time of day, because we do not observe it every day. Probably also incident solar radiation, which is higher in the afternoon because the window is directed westwards, or temperature play a role. Therefore, high VOC levels probably also cause high H₂ levels. During the field tests Tenax samples were drawn and analyzed by GC-MS, but no unusually high concentrations of any substance were found. Thus, the observed H₂ base level inside the room, which was confirmed by the reference instrument to be significantly higher than atmospheric level, cannot be explained

and is not fully understood. It seems that an unknown H₂ source is inside the room as only lower concentrations were found in neighboring rooms and outside using the same sensors. Perhaps this high base level is caused by some unknown VOC source [16], e.g., from building materials or furniture, or by microorganisms, which can emit H₂ from their metabolism (in fact, they are the cause for human H₂ emissions).

Unfortunately, the observed changes of the H₂ concentration overshadow all moments with human presence, which were short and only included one person. Thus, it was not possible to detect any effect of human presence against this background. In former experiments we found an increase of 2500 ppb over a span of 1 h in a room of similar size while 13 people were inside (same building, same floor). This correlates to an increase of approximately 200 ppb per person and hour. In a normal indoor air environment this can represent a valid indicator for human presence, but effects of VOC release, i.e., from cleaning agents would have to be considered. In any case, further experiments to determine H₂ concentrations and fluctuations in different rooms under normal use (e.g., cooking, cleaning etc.) are required.

5. Conclusions

Two important conclusions can be drawn from the presented field test results: first, MOS sensors can reliably detect and quantify H₂ in indoor environments; second, H₂ is a dynamic parameter that needs more attention. More research is required on many open questions: Does H₂ emitted by humans dominate in normal rooms so that it can be used as indicator for human presence? Does H₂ represent a good indicator for other relevant and potentially harmful situations, e.g., high VOC values or microbial issues such as mold? Do many TVOC monitors based on MOS sensors, especially when driven at constant temperature, mainly measure H₂?

Author Contributions: Conceptualization, C.S., T.B. and A.S.; methodology, C.S., T.B. and J.A.; software, T.B. and J.A.; validation, C.S., T.B. and J.A.; formal analysis, J.A.; investigation, J.A.; resources, A.S.; data curation, J.A.; writing—original draft preparation, C.S.; writing—review and editing, C.S., T.B. and A.S.; visualization, C.S. and J.A.; supervision, C.S., T.B. and A.S.; project administration, A.S. All authors have read and agreed to the published version of the manuscript.

Funding: This research received no external funding.

Institutional Review Board Statement: Not applicable.

Informed Consent Statement: Not applicable.

Data Availability Statement: The underlying data is available on Zenodo. DOI: 10.5281/zenodo.4593853. Title: Measuring Hydrogen in Indoor Air with a Selective Metal Oxide Semiconductor Sensor: Dataset. Authors: Johannes Amann, Tobias Baur, Caroline Schultealbert, <https://zenodo.org/record/4593853>. (accessed on 10 March 2021).

Acknowledgments: We thank Rainer Lammertz Pure Gas Products for providing the Peak Performer 1 reference instrument for this study.

Conflicts of Interest: The authors declare no conflict of interest.

Appendix A

Table A1. List of all events (release tests, ventilation and other) during the field tests and the observed sensor behavior during that time.

Number	Time	Type of event	Observation
1	29 September, 09:35–09:48	Door opened	Lower H ₂ concentration due to ventilation effect
2	30 September, 09:24–09:58	Window opened	Lower H ₂ concentration due to ventilation effect
3	1 October, 09:10–09:30	Window opened	Lower H ₂ concentration due to ventilation effect
4	1 October, 11:47–12:05	Door and window opened	Lower H ₂ concentration due to ventilation effect
5	1 October, 18:30–2 October, 06:30	No specifiable event	Strong increase of H ₂ concentration over night
6	2 October, 09:00–09:30	Door and window opened	Lower H ₂ concentration due to ventilation effect

Table A1. Cont.

Number	Time	Type of event	Observation
7	2 October, 14:00–5 October, 10:00	Days without events and human presence	Maximum of H ₂ concentration at 3 October, 13:00
8	5 October, 10:10–10:30	Door and window opened	Lower H ₂ concentration due to ventilation effect
9	5 October and 6 October	Several short periods of human presence	No increasing H ₂ concentration for short presence of one person
10	6 October, 13:08–16:51	Door and window opened	Lower H ₂ concentration due to ventilation effect
11	6 October, 17:42–18:44	Release test: 1 ppm H ₂	Compare Figure 3a
12	7 October, 16:01–18:05	Release test: 2 ppm H ₂	Compare Figure 3b
13	8 October, 10:46–11:00	Door and window opened	Lower H ₂ concentration due to ventilation effect
14	8 October to 13 October	Days without events and human presence	Oscillating H ₂ concentration with maximums typically around 06:00–08:00 and minimums typically around 18:00–20:00
15	13 October, 09:25–14:00	Door and window opened, human presence	Lower H ₂ concentration due to ventilation effect
16	13 October, 15:00	Release test: toluene	Increase of H ₂ concentration 3 h after release (18:00)
17	14 October, 09:30–10:05	Door and window opened	Lower H ₂ concentration due to ventilation effect
18	8 October to 13 October	Sporadic human presence, no specifiable events	Slow increase of H ₂ concentration over day and night
19	15 October, 09:00–09:30	Door and window opened	Lower H ₂ concentration due to ventilation effect
20	15 October, 15:00	Release test: acetone	Untreated sensor reacts to acetone release with a short peak and displays lower concentration afterwards.
21	16 October, 09:40–10:10	Door and window opened	Three hours after release both sensors indicate increasing H ₂ concentration
22	16 October, 14:50 and 18:00	Release test: acetone and toluene	Lower H ₂ concentration due to ventilation effect
23	17 October to 19 October	Days without events and human presence	Untreated sensor reacts to release with a short peak and displays lower concentration afterwards. Five hours after first release both sensors indicate increasing H ₂ concentration
24	29 October, 12:55–13:10	Door and window opened	Almost constant H ₂ concentration
25	29 October to 2 November	Days without events and human presence	Lower H ₂ concentration due to ventilation effect
26	2 November, 12:40–12:55	Door and window opened	Almost constant H ₂ concentration
27	2 November, 16:50	Release test: toluene	Lower H ₂ concentration due to ventilation effect
28	3 November, 10:55–11:10	Door and window opened	Short reaction of untreated sensor upon release, constant increase of H ₂ concentration over day and night
29	3 November, 15:30	Release test: acetone followed by defect of the pump, human presence during fixing	Lower H ₂ concentration due to ventilation effect
30	4 November, 09:00–09:15	Door and window opened	Three hours after release test increase of H ₂ concentration (coincides with present person for pump fixing)
31	4 November, 16:22	Release test: acetone	Lower H ₂ concentration due to ventilation effect
32	5 November, 09:26–09:41	Door and window opened	Untreated sensor signal drops again upon release, increase of H ₂ concentration 2 h after release
33	5 November, 15:10	Release test: acetone and toluene. Unidentified event due to construction inside the building	Lower H ₂ concentration due to ventilation effect
34	5 November, 18:30–18:50	Door and window opened	Very strong increase in signal of the untreated sensor long before the release tests. Release then again causes a drop in the untreated sensor's signal, and 2.5 h after release also the pre-treated sensor signal increases slightly.
35	6 November, 10:03	Release test: limonene	Lower H ₂ concentration due to ventilation effect
36	6 November to 9 November	Days without events and human presence	Pre-treated sensor detects limonene release immediately, untreated sensor shows increasing H ₂ concentration after 5–6 h, after 10 h signals go parallel again
37	9 November, 12:21–13:01	Door and window opened	Almost constant H ₂ concentration, slight oscillation with maximum at 06:30 and minimums at 15:00 and 16:30
38	9 November, 18:00	Release test: ethanol	Lower H ₂ concentration due to ventilation effect
39	10 November, 09:10–09:25	Door and window opened	One outlier towards higher concentration for untreated sensor upon release, almost constant H ₂ concentration
40	10 November, 14:30	Release test: isopopanol	Lower H ₂ concentration due to ventilation effect
41	11 November, 09:28–09:48	Door and window opened	Four hours after first release both sensors indicate increasing H ₂ concentration
42	11 November, 15:49	Release test: xylene	Lower H ₂ concentration due to ventilation effect
43	12 November, 09:15–09:30	Door and window opened	Increase of H ₂ concentration until release test, constant concentration afterwards
44	12 November, 15:08	Release test: toluene and xylene	Lower H ₂ concentration due to ventilation effect
45	13 November, 09:28–11:06	Door and window opened	Increase of the H ₂ concentration over the day (independent from release) and constant value after 19:00
46	13 November, 14:30	Release test: acetone and ethanol	Lower H ₂ concentration due to ventilation effect
			Small drop in sensor signal for untreated sensor, ascending H ₂ concentration over day and night

Table A1. Cont.

Number	Time	Type of event	Observation
47	13 November–16 November	Days without events and human presence	Decreasing H ₂ concentration between 13:30 and 17:00 on first day and after 11:30 over the whole night on second day
48	16 November, 11:55–12:20	Door and window opened	Lower H ₂ concentration due to ventilation effect
49	16 November, 17:06–19:20	Release test: 2 ppm H ₂	Compare Figure 4b
50	17 November, 09:54–10:24	Door and window opened	Lower H ₂ concentration due to ventilation effect
51	17 November, 18:24	Release test: ethanol	Maximum in H ₂ concentration at 16:30, outlier in pre-treated signal due to pump switching, no signal change upon release, increasing H ₂ concentration after 06:30
52	18 November, 09:36–09:56	Door and window opened	Lower H ₂ concentration due to ventilation effect
53	19 November, 12:02–16:02	Release test: carbon monoxide (tea candle)	Pre-treated sensor signal shows slight increase of H ₂ concentration during burning candle

References

- Spaul, W.A. Building-related factors to consider in indoor air quality evaluations. *J. Allergy Clin. Immunol.* **1994**, *94*, 385–389. [\[CrossRef\]](#)
- Settimi, G.; Manigrasso, M.; Avino, P. Indoor Air Quality: A Focus on the European Legislation and State-of-the-Art Research in Italy. *Atmosphere* **2020**, *11*, 370. [\[CrossRef\]](#)
- World Health Organization. *WHO Air Quality Guidelines for Particulate Matter, Ozone, Nitrogen Dioxide and Sulfur Dioxide: Global Update 2005: Summary of Risk Assessment*; World Health Organization: Geneva, Switzerland, 2006.
- Krzyzanowski, M.; Cohen, A. Update of WHO air quality guidelines. *Air Qual. Atmos. Health* **2008**, *1*, 7–13. [\[CrossRef\]](#)
- Pettenkofer, M. *Besprechung Allgemeiner auf die Ventilation bezüglicher Fragen*; J.G. Cottaische Buchhandlung: München, Germany, 1858.
- Szczurek, A.; Maciejewska, M.; Pietrucha, T. CO₂ and Volatile Organic Compounds as indicators of IAQ. In Proceedings of the 36th AIVC Conference—Effective Ventilation in High Performance Buildings, Madrid, Spain, 23–24 September 2015; pp. 118–127.
- Rovelli, S.; Cattaneo, A.; Fazio, A.; Spinazzè, A.; Borghi, F.; Campagnolo, D.; Dossi, C.; Cavallo, D. VOCs Measurements in Residential Buildings: Quantification via Thermal Desorption and Assessment of Indoor Concentrations in a Case-Study. *Atmosphere* **2019**, *10*, 57. [\[CrossRef\]](#)
- Scully, R.R.; Basner, M.; Nasrini, J.; Lam, C.; Hermosillo, E.; Gur, R.C.; Moore, T.; Alexander, D.J.; Satish, U.; Ryder, V.E. Effects of acute exposures to carbon dioxide on decision making and cognition in astronaut-like subjects. *NPJ Microgravity* **2019**, *5*, 17. [\[CrossRef\]](#)
- Liu, Y.; Misztal, P.K.; Xiong, J.; Tian, Y.; Arata, C.; Weber, R.J.; Nazaroff, W.W.; Goldstein, A.H. Characterizing sources and emissions of volatile organic compounds in a northern California residence using space- and time-resolved measurements. *Indoor Air* **2019**, *29*, 630–644. [\[CrossRef\]](#)
- Leidinger, M.; Sauerwald, T.; Reimringer, W.; Ventura, G.; Schütze, A. Selective detection of hazardous VOCs for indoor air quality applications using a virtual gas sensor array. *J. Sens. Sens. Syst.* **2014**, *3*, 253–263. [\[CrossRef\]](#)
- Schütze, A.; Baur, T.; Leidinger, M.; Reimringer, W.; Jung, R.; Conrad, T.; Sauerwald, T. Highly Sensitive and Selective VOC Sensor Systems Based on Semiconductor Gas Sensors: How to? *Environments* **2017**, *4*, 20. [\[CrossRef\]](#)
- Lee, A.P.; Reedy, B.J. Temperature modulation in semiconductor gas sensing. *Sens. Actuators B Chem.* **1999**, *60*, 35–42. [\[CrossRef\]](#)
- Schleyer, R.; Bieber, E.; Wallasch, M. *Das Luftmessnetz des Umweltbundesamtes*; Umweltbundesamt: Dessau-Roßlau, Germany, 2013.
- Barnes, D.H.; Wofsy, S.C.; Fehlau, B.P.; Gottlieb, E.W.; Elkins, J.W.; Dutton, G.S.; Novelli, P.C. Hydrogen in the atmosphere: Observations above a forest canopy in a polluted environment. *J. Geophys. Res. Space Phys.* **2003**, *108*, 4197. [\[CrossRef\]](#)
- Ehhalt, D.H.; Rohrer, F. The tropospheric cycle of H₂: A critical review. *Tellus B Chem. Phys. Meteorol.* **2009**, *61*, 500–535. [\[CrossRef\]](#)
- Grant, A.; Archibald, A.T.; Cooke, M.C.; Nickless, G.; Shallcross, D.E. Modelling the oxidation of 15 VOCs to track yields of hydrogen. *Atmos. Sci. Lett.* **2010**, *11*, 265–269. [\[CrossRef\]](#)
- Forster, G.L.; Sturges, W.T.; Fleming, Z.L.; Bandy, B.J.; Emeis, S. A year of H₂ measurements at Weybourne Atmospheric Observatory, UK. *Tellus B Chem. Phys. Meteorol.* **2012**, *64*, 17771. [\[CrossRef\]](#)
- Marthinsen, D.; Fleming, S.E. Excretion of Breath and Flatus Gases by Humans Consuming High-Fiber Diets. *J. Nutr.* **1982**, *112*, 1133–1143. [\[CrossRef\]](#)
- Tomlin, J.; Lowis, C.; Read, N.W. Investigation of normal flatus production in healthy volunteers. *Gut* **1991**, *32*, 665–669. [\[CrossRef\]](#)
- Tadesse, K.; Smith, D.; Eastwood, M.A. Breath Hydrogen and Methane Excretion Patterns in Normal man and in Clinical Practices. *J. Experimental Physiol.* **1980**, *65*, 85–97. [\[CrossRef\]](#)
- Levitt, M.D. Production and excretion of hydrogen gas in man. *N. Engl. J. Med.* **1969**, *281*, 122–127. [\[CrossRef\]](#)
- Sone, Y.; Tanida, S.; Matsubara, K.; Kojima, Y.; Kato, N.; Takasu, N.; Tokura, H. Everyday Breath Hydrogen Excretion Profile in Japanese Young Female Students. *J. Physiol. Anthr. Appl. Hum. Sci.* **2000**, *19*, 229–237. [\[CrossRef\]](#)
- Appel, J.; Schulz, R. Hydrogen metabolism in organisms with oxygenic photosynthesis: Hydrogenases as important regulatory devices for a proper redox poisoning? *J. Photochem. Photobiol. B Biol.* **1998**, *47*, 1–11. [\[CrossRef\]](#)
- Nandi, R.; Sengupta, S. Microbial Production of Hydrogen: An Overview. *Crit. Rev. Microbiol.* **1998**, *24*, 61–84. [\[CrossRef\]](#)
- Rüffer, D.; Hoehne, F.; Bühler, J. New digital metal-oxide (MOx) sensor platform. *Sensors* **2018**, *18*, 1052. [\[CrossRef\]](#)

26. Schultealbert, C.; Baur, T.; Schütze, A.; Sauerwald, T. Investigating the role of hydrogen in the calibration of MOS gas sensors for indoor air quality monitoring. In Proceedings of the Indoor Air Conference, Philadelphia, PA, USA, 22–27 July 2018.

27. Meng, X.; Zhang, Q.; Zhang, S.; He, Z. The Enhanced H₂ Selectivity of SnO₂ Gas Sensors with the Deposited SiO₂ Filters on Surface of the Sensors. *Sensors* **2019**, *19*, 2478. [\[CrossRef\]](#) [\[PubMed\]](#)

28. Schultealbert, C.; Uzun, I.; Baur, T.; Sauerwald, T.; Schütze, A. Siloxane treatment of metal oxide semiconductor gas sensors in temperature-cycled operation—Sensitivity and selectivity. *J. Sens. Sens. Syst.* **2020**, *9*, 283–292. [\[CrossRef\]](#)

29. Hyodo, T.; Baba, Y.; Wada, K.; Shimizu, Y.; Egashira, M. Hydrogen sensing properties of SnO₂ varistors loaded with SiO₂ by surface chemical modification with diethoxydimethylsilane. *Sens. Actuators B Chem.* **2000**, *64*, 175–181. [\[CrossRef\]](#)

30. Tournier, G.; Pijolat, C. Selective filter for SnO₂-based gas sensor: Application to hydrogen trace detection. *Sens. Actuators B Chem.* **2005**, *106*, 553–562. [\[CrossRef\]](#)

31. Katsuki, A.; Fukui, K. H₂ selective gas sensor based on SnO₂. *Sens. Actuators B Chem.* **1998**, *52*, 30–37. [\[CrossRef\]](#)

32. Schultealbert, C.; Baur, T.; Schütze, A.; Böttcher, S.; Sauerwald, T. A novel approach towards calibrated measurement of trace gases using metal oxide semiconductor sensors. *Sens. Actuators B Chem.* **2017**, *239*, 390–396. [\[CrossRef\]](#)

33. Schultealbert, C.; Baur, T.; Schütze, A.; Sauerwald, T. Facile Quantification and Identification Techniques for Reducing Gases over a Wide Concentration Range Using a MOS Sensor in Temperature-Cycled Operation. *Sensors* **2018**, *18*, 744. [\[CrossRef\]](#)

34. Baur, T.; Schultealbert, C.; Schütze, A.; Sauerwald, T. Novel method for the detection of short trace gas pulses with metal oxide semiconductor gas sensors. *J. Sens. Sens. Syst.* **2018**, *7*, 411–419. [\[CrossRef\]](#)

35. Bastuck, M.; Baur, T.; Schütze, A. DAV³E—A MATLAB toolbox for multivariate sensor data evaluation. *J. Sens. Sens. Syst.* **2018**, *7*, 489–506. [\[CrossRef\]](#)

36. Amann, J. Möglichkeiten und Grenzen des Einsatzes von Halbleitergassensoren im temperaturzyklischen Betrieb für die Messung der Innenraumluftqualität—Kalibrierung, Feldtest, Validierung. Master’s Thesis, Universität des Saarlandes, Saarbrücken, Germany, 2021.

37. Bastuck, M. *Improving the Performance of Gas Sensor Systems with Advanced Data Evaluation, Operation, and Calibration Methods*; Shaker Verlag GmbH: Düren, Germany, 2019; ISBN 978-3-8440-7075-0.

38. Leidinger, M.; Schultealbert, C.; Neu, J.; Schütze, A.; Sauerwald, T. Characterization and calibration of gas sensor systems at ppb level—a versatile test gas generation system. *Meas. Sci. Technol.* **2018**, *29*, 015901. [\[CrossRef\]](#)

39. Helwig, N.; Schüller, M.; Bur, C.; Schütze, A.; Sauerwald, T. Gas mixing apparatus for automated gas sensor characterization. *Meas. Sci. Technol.* **2014**, *25*, 055903. [\[CrossRef\]](#)

40. Baur, T.; Bastuck, M.; Schultealbert, C.; Sauerwald, T.; Schütze, A. Random gas mixtures for efficient gas sensor calibration. *J. Sens. Sens. Syst.* **2020**, *9*, 411–424. [\[CrossRef\]](#)

41. Loh, W.-L. On Latin Hypercube Sampling. *Ann. Stat.* **1996**, *24*, 2058–2080. [\[CrossRef\]](#)

42. Lilliefors, H.W. On the Kolmogorov-Smirnov Test for Normality with Mean and Variance Unknown. *J. Am. Stat. Assoc.* **1967**, *62*, 399–402. [\[CrossRef\]](#)

43. Martin-Luengo, M.A.; Yates, M.; Rojo, E.S.; Huerta Arribas, D.; Aguilar, D.; Ruiz Hitzky, E. Sustainable p-cymene and hydrogen from limonene. *Appl. Catal. A Gen.* **2010**, *387*, 141–146. [\[CrossRef\]](#)

44. Fleischer, M.; Kornely, S.; Weh, T.; Frank, J.; Meixner, H. Selective gas detection with high-temperature operated metal oxides using catalytic filters. *Sens. Actuators B Chem.* **2000**, *69*, 205–210. [\[CrossRef\]](#)

5 Discussion

The presented thesis describes the evaluation of commercial MOS gas sensors with model-based and statistical methods. This chapter does not provide a basic summary and discussion of each paper because each individual paper contains its own discussion. Instead, individual important topics are discussed across all papers.

5.1 Model for MOS Gas Sensor in TCO

Different models for MOS gas sensors are presented in several publications [72; 81; 84]. They usually use self-fabricated, non-commercial sensors in static operation. Ding et al. [94] introduce a model of micro-hotplate MOS gas sensors in TCO. The model assumes the main contribution to be grain-grain boundaries in the polycrystalline layer, as in the previous models. Therefore, the logarithmic sensor conductance is proportional to the energy barrier between the grain-grain boundaries divided by the sensor temperature.

In this thesis, the sensor response in TCO with fast temperature changes between high and low temperature steps on micro-hotplates is described. The description of the conductance shortly after a temperature change is specifically considered. The sensitivity in this phase is up to 800 higher than in static operation. The model is based on the publication of Ding et al. [94] and provides an extension for the phase after a fast temperature change. The simple model for a commercial MOS gas sensor, the AS-MLV, in TCO has been successfully demonstrated. Some simplifying assumptions are made for the model to be applicable:

- One oxygen species dominates on the surface of the semiconductor and is involved in the reaction.
- The temperature change is so fast that the coverage of the previous equilibrium is maintained and can be taken as the initial state after the jump.
- A one-step reaction with the surrounding reducing gas takes place, and there are no other reactions taking place that affect the sensor signal.
- The concentration of the reducing gas is small.

Seconds to minutes after the temperature step the logarithmic sensor conductance can be approximated linearly. The duration of this linear phase depends on the surrounding atmosphere and the sensor temperature. During this phase the surface is strongly occupied with oxygen due to the previous high temperature phase. As a result, the energy barrier is high. To achieve equilibrium at low temperature, the excess oxygen must be removed, decreasing the energy barrier. The change of the energy barrier can be described by a differential equation with a first term for the adsorption of oxygen and a second term for the desorption of oxygen due to the reaction with reducing gases. The term for adsorption of new oxygen is negligible due to the high oxygen coverage. Only the term for the reaction with the surrounding reducing gas leads to a change of the energy barrier. The solution of the reduced differential equation can be simplified to the linear term using a Taylor expansion. The resulting slope of the energy barrier change is proportional to the rate constant of the reaction with the reducing gases.

The rate constant is dependent on temperature, substance and concentration and, therefore, a good parameter for the discrimination of gases. This is demonstrated for

benzene and ethanol from 1 to 1000 ppb in Paper A (Section 4.1). The rate constant corresponds in the form of a linear or power function to the concentration, as shown in Paper B, 1 and C (Section 4.1). Gases can also be discriminated with the time constant of relaxation for higher concentrations and over a wide concentration range. It is demonstrated in Paper C (Section 4.1) that this parameter also follows a linear or power law with concentration. Paper 1 (Section 4.1) shows a dose effect of the rate constant. That is, the logarithmic conductance signal after a temperature change is proportional to the integrated rate constant. An important property is the superposition of the rate constants (for low concentrations), which makes the background compensation in Paper B (Section 4.1) possible.

The appropriateness of the model-based evaluation can not only be demonstrated for a micro-heater sensor, but also for the sensor GGS 1530T from UST Umweltsensortechnik GmbH with a ceramic heater [266]. The quantification of acetone from 100 to 5000 ppb for breath analysis was demonstrated. This indicates that the model is not only applicable to the AS-MLV, but also to other SnO₂-based sensors. Further commercial sensors were successfully investigated [263]. This thesis shows that the evaluation of model-based parameters works for many of the commercially available sensors. However, overlaid effects, e.g. multi-step reactions or faster intrinsic effects can be observed for some of them. Other limiting effects of the model are described in Paper 1 and C (Section 4.1). The linear dosing effect is limited and applies only to a maximum dose, for example <1000 ppb s ethanol in Paper 1 (Section 4.1). Above, the correlation signal curve no longer follows a linear but power function. The same can be seen when calculating the slope for gas exposures with constant concentration. For higher concentrations, the time frame where the linear approximation is suitable is reduced. Automatic parameter determination can be helpful. Different automatic methods for slope calculations are shown in [263].

The limitations of the model, as well as the optimization of sensor layers for TCO, need further investigation, preferably together with sensor manufacturers. The model should be further developed. Schultealbert describes the behavior of the sensor at high temperature and the readsorption of oxygen as a measure of surface reactivity [263]. This can be used to compensate poisoning effects due to siloxane exposure on the sensor [263].

5.2 Model-based Data Evaluation

In Paper B (Section 4.1), a novel approach towards calibrated measurement of trace gases using MOS gas sensors with model-based data evaluation is presented. Evaluating the linear rate constant allows to measure toluene at least from 10 ppb to 10 ppm. With the rate constant and its superposition property, the compensation of background and therefore also quantitative measurements in pure and ambient air are possible. The quantitative compensation of different backgrounds in Paper B (Section 4.1) is only possible through the model. The results illustrate that the rate constant is less affected by short- or long-term sensor drifts than the sensor conductance. As a result, a quantitative measurement can be performed with the first cycle after a gas change and is independent of run-in effects.

Schultealbert et al. [267] demonstrate for example the selective quantification of hydrogen sulfide between 50 and 400 ppb in a varied background of hydrogen and

methane with the model-based evaluation of the rate constant at 150 °C. The rate constant is linear to the hydrogen sulfide concentration and independent of hydrogen and methane concentration. The evaluation of the conductance at 150 °C, on the other hand, provides an unstable, non-linear signal. With model-based data evaluation, Joppich et al. [268] show for example the interpolation between models for different gases to create a new model for mixtures of these gases, which is made possible by superposition of the rate constants.

Schultealbert et al. [263; 269] investigate the change of model-based features due to siloxane exposure on the sensor. An irreversible decrease (poisoning) in the rate constant with increasing siloxane exposure is observed. With a second model-based feature, the time constant of the readsorption of oxygen at high temperature, a successful detection and compensation of poisoning effects are achievable.

A second important model-based evaluation is the detection of short trace gas pulses in Paper 1 (Section 4.1). For the measurement of short gas pulses, a sufficient duration is necessary where the linear approximation is applicable. For this, the low temperature is reduced to 100 °C. As a result, a linear approximation with a duration of more than 10 min is achieved. At the very low temperature of 100 °C the sensor shows high reactivity to ethanol. The detection of benzene and toluene gas pulses is also tested [270]. The sensor signal is found to be lower by a factor of 10 for benzene and toluene. Experimental results show for ethanol (Paper B, Section 4.1), benzene and toluene [270] a linear behavior between the integrated rate constant and the dose over 3 orders of magnitude. The baseline-return of the sensor signal after the gas pulse takes longer for benzene and toluene compared to ethanol. Less reactive reducing gases, like toluene or benzene, a higher sensor temperature might be required (Paper A, Section 4.1), which also reduces the duration of the linear phase. This is likely to produce higher sensor signals as well as faster baseline-return due to the faster desorption of the products after full reaction.

Reproducible and fast measurements of short trace gas pulses require that the gas peak has to reach the sensor without peak broadening. The reduction of the dead volume in the sensor chamber enables to measure these short gas pulses. The sensor consumption is estimated (FEM simulation) to be 1.6 % of the injected gas quantity. If the reaction would be optimized to 100 % efficiency, the theoretical detection limit is 47 fg for ethanol. There is still a dead volume due to the round area of the sensor mount with a diameter of approx. 8 mm compared to the sensor chip size of approx. 2 x 2 mm. For gas exposures that are not exposed as peak, the dead volume also has a major impact on the time needed to reach a stable signal and should be generally considered [271].

Small and inexpensive detectors for GC systems can be realized with this method which shows a dose effect and is linear to the dose in a certain range. The combination of MOS gas sensor with GC is used for example in [30; 272; 273]. In all these publications, the sensor is operated with constant temperature and the signal follows the eluting concentration, so that an additional integration is needed. With the model-based evaluation, the result is obtained directly and a lower limit of detection can be achieved due to the improved sensitivity in this operation mode. However, the method is limited to a maximum dose that the sensor can detect linearly. Beyond that, the signal would have to be compensated, or a second sensor would have to be used alternately. The demand for mobile gas analysis systems for selective detection of trace gases, for example outdoor [10; 112; 274], indoor [275; 276] or medical diagnostics [4], has increased over the past

few years. The miniaturization of GC and its components [277–280] are investigated. A MOS gas sensor is easier and less expensive to miniaturize compared to a flame ionization detector (FID), mass spectrometer (MS) or photoionization detector (PID). Other applications also require the detection of gas pulses. For example, the combination of a MOS gas sensor with a preconcentrator is presented [31; 281]. The preconcentrator at room temperature is a sorbent material like TENAX or MOF. The preconcentrator on a micro-heater can be heated up quickly, releasing the accumulated gas as a gas pulse. With the model-based data evaluation, these gas pulses can be quantified [282]. Another example is leak detection of supposedly gas-tight parts in industrial environments. A test part is filled with forming gas (containing 5 % hydrogen and 95 % nitrogen) and placed in a measurement chamber. The measurement chamber is gas-tight and during a first accumulation phase the hydrogen flows out of the leakage. During this time, a gas sensor is operated at high temperature and in clean air. After the accumulation phase the sensor temperature jumps to a low temperature and the atmosphere in the measurement chamber is flushed to the sensor. This gas pulse can be measured with the presented method for the detection of gas pulses which is included in a Patent i.

5.3 Calibration and Field Testing

Calibration and field testing are necessary for successful development of gas sensor systems for specific applications. The model-based evaluation works for quantifying individual gases, such as the detection of gas pulses after a separation in GC or in leakage detection. For other applications with more complex gas compositions, more sophisticated methods and calibration procedures are needed to achieve reliable target value output. For example, cost-effective VOC measurements in indoor or outdoor air, odor monitoring or disease analysis are among such applications. Two thematically different but strongly linked areas have to be considered during calibration: design of experiment with data generation and data evaluation.

5.3.1 *Design of Experiment*

Design of Experiment (DoE) is an important point in data generation. For a successful DoE, the application must be fully defined. Target gases, interfering gases, concentration ranges and other influencing factors must be known. In the interlaboratory tests with the JRC (Paper 5, Section 4.3), for example, calibration is performed in different humidity ranges at LMT compared to JRC. In the interlaboratory tests with BAM, hydrogen and carbon monoxide which are present in the BAM lab's background air are not included in the calibration at LMT because it is removed during carrier gas processing. DoE also includes the sequence of a calibration measurement. The DoE in Paper A or 1 (Section 4.1) consists of single gases which does not reveal any masking effects or other gas interactions altering the sensor response for complex applications. Calibration in Paper 5 and E (Section 4.3) is done with the classical sequential DoE, like in other publications [39; 48; 51; 52; 55–59]. These studies define between three and five fixed concentration levels for each gas. Restriction to a few fixed points can lead to the fact that the correct operating point is not covered properly, for example the wrong humidity in Paper 5 (Section 4.3). A second problem is the influence on the data evaluation. Too few levels for the quantization of a continuous quantity or classification of different

substances easily lead to overfitting, which is illustrated for regression models with artificial neural networks (ANN) and partial least squares regression (PLSR) in [55] or for classification in [60]. For successful calibration of complex applications, a more realistic design of experiments is necessary. Therefore, a DoE based on random excitation [283] is demonstrated in Paper 3 (Section 4.2). This calibration is based on randomized gas mixtures which scans the parameter space much more efficiently than permutations of a few fixed gas concentrations. Comparing sequential and randomized calibration, the sequential measurement can be predicted with randomized calibration, but not vice versa. The calibration is successfully tested in the field tests in Paper 6 and F (Section 4.3).

However, there are still some points that need to be examined in more detail. Paper 3 (Section 4.2) uses for the creation of the gas mixture composition a complex scheme with several uniform distributions for atmospheric background (carbon monoxide, hydrogen and relative humidity) and selected VOCs. Paper 6 (Section 4.3) relies on a gas mixture composition based on Latin hypercube sampling (LHS) [284]. It has to be investigated which distribution for the composition of gas mixtures is most successful and how reality can be represented best. However, data evaluation must also be considered to ensure that the distribution results in an optimal model.

The number of gas exposures and the reduction of measurement points per gas exposure needs to be studied to save calibration time. Bastuck [124] was able to demonstrate during the analysis of the data from Paper 3 (Section 4.2) that the number of gas exposures can be reduced to fewer than 40 while maintaining good results. However, this is only tested with laboratory measurements and the same should be investigated based on the field tests from Paper 6 (Section 4.3). Robin et al. [285] show machine-learning-based calibration time reduction for the dataset from Paper 3 (Section 4.2).

Field tests should also be included in the DoE. Field testing can assist in obtaining more stable and better models. In addition, it can also reveal limits. In this context, the presented release tests are a simple type of connecting lab to field measurements. Background fluctuations and undefined events, such as the hydrogen fluctuations and the event due to construction, would be better revealed by continuous all-encompassing analytical monitoring – which is almost impossible to achieve. For hydrogen, it was possible to have a reference device monitoring in parallel for several days (Paper F, Section 4.3). For VOCs a PTR-MS would be a possibility for continuous monitoring [247]. Only in combination with analytical systems are annotated and traceable field testing possible. For outdoor air, calibration in real environments is possible. Several parameters are measured on site with reference measurement systems today, which was for example presented for benzene [111] or ozone [113]. However, it must be kept in mind that different gases can occur in combination and have correlations. For example, carbon monoxide and hydrogen have such a correlation [286] or nitrogen dioxide and ozone [287]. This means that the measurement data are not statistically independent. The resulting models might fully or partially rely on the correlation. Therefore, field tests should always be combined with statistically independent laboratory tests. Additional aspects must be considered when moving from the laboratory to the field. For example, VOC emissions from the housing or PCB are possible. The sensor in the gas flow is shielded from housing or PCB in the lab but not in the real application. Hence, the emissions can increase the VOC concentrations and influence the measurement results [288].

5.3.2 Data Evaluation

Calibration always requires data evaluation. Machine learning algorithms and artificial neural networks usually play an important role in this process. Paper 3 (Section 4.2) presents a data evaluation chain with two-stage dimensionality reduction and a PLSR for regression. The first dimensionality reduction is done by the calculation of mean and slope of 120 equidistant ranges in each cycle. The second dimensionality reduction is done by calculating the first 20 PCA components based on the features. The models reached good results for all gases and groups. Amann [289] studied different feature selection methods on this dataset and achieved the lowest errors for all targets with RFE-LSR. He used the same data evaluation chain but replaced the second dimensional reduction with a feature selection, which is called feature extraction selection regression (FESR). This chain is used to evaluate the field tests in Paper 6 and F (Section 4.3) and produced impressive results. Robin et al. in Paper v [290] present an advanced data evaluation on these field tests with 10-layer deep convolutional neural network (TCOCNN). The net uses the raw data as input without any feature extraction. With the same validation and testing data, the TCOCNN outperformed FESR data evaluation with a 10 to 51 % lower error for the different models. Higher accuracy and lower noise can be achieved at the same temporal resolution, especially in real application environments. The TCOCNN was originally developed for formaldehyde prediction which explains that the error for this gas improves the most and halves in relation to the previous result. Further advancements for other gases could result from specific optimizations of similar kind. However, the higher computational effort for the training of the TCOCNN has to be considered. Also, the FESR model was optimized for highest dimension reduction and minimal error. If the minimum error is weighted higher in the optimization, the RMSE could probably be improved.

This illustrates that further data evaluation methods and combinations need to be investigated and further improvements are always possible. In particular, the data generated from random gas mixtures can leverage the strengths of neural networks for gas sensing. Due to the statistically independent data, the risk of overfitting is reduced and even deep neural networks are applicable. An advantage of gas sensor technology is the fast, flexible and parallel generation of measurement data. This can create a huge database with almost infinite variations. For example, each calibration in Paper 3 (Section 4.2) and Paper 6 and F (Section 4.3) contains more than 1,000 different annotated groups (gas mixtures) and over 10,000 testing points (temperature cycles).

However, some points are still unresolved. Drift compensation performed, for example in Paper 6 (Section 4.3), must be taken into consideration. Transfer of the models to other sensors or re-calibration of the sensors (i.e. expanding the model with preferably little new training data) needs to be investigated [54; 291]. Neural networks with the concept of transfer learning offer good conditions for this [292–294]. Robin et al. [295] demonstrated that transfer learning reduces the calibration time to 30 % of the initial calibration. It was possible to transfer a model for xylene (RMSE of approx. 13 ppb) calibrated with 500 unique gas mixtures from one sensor to two others (RMSE of approx. 16.5) with only minor adaptations.

Long-term stability needs to be investigated further. The system in Paper 6 (Section 4.3) shows reasonable results for more than one year [296]. The statistical

evaluation and determination of properties, for example the limit of detection, has to be defined and studied [297; 298]. Above all, data evaluation must be considered as part of the calibration process and thus also in the design of experiment.

5.4 Measurement of VOCs

“VOC measurement” has no clear definition. This starts with the fact that there is no clear definition of VOC, as presented in Subsection 3.3.2. For a few VOCs there are guideline, guide or limit values as shown in Table 3. For example, the carcinogenic gases benzene and formaldehyde have such limits. But is formaldehyde a VOC? Not according to the definition of analytics in ISO16000-6, where formaldehyde belongs to the VVOCs. Assessment values for total VOC (TVOC) are also oriented along this definition which accordingly means that formaldehyde is not part of this. All substances eluting between n-hexane and n-hexadecane after GC separation are VOCs and included in the TVOC value. However, this does not mean that the organic substances released before or after have less influence on humans. But there is no standardized analytical method for these. This also leads to the fact that the sum of VVOCs, VOCs and SVOCs according to ISO16000-6 does not correspond to the sum of all VOCs. Salthammer described the VVOC as an understudied class of indoor air pollutants and criticizes that there is no clear definition for it [239].

This lack of knowledge is not caused by the lack of interest for broader VOC measurements, but the lack of fully comprehensive analytical methods. This is also obvious in the available studies where only VOCs according to the standardized analytical procedure are measured. In the case of VVOCs, if at all, only a small selection is measured, usually aldehydes. Alcohols, for example, are seldom considered [21; 198; 256]. The health effects of many VOCs on humans are also unclear [23]. In most studies, humans are exposed to only a few VOCs and the effects are examined [26]. Assessing the human exposure to organic pollutants is complicated due to the variety of substances, the evaluation on humans and measurement methodology [27]. Therefore, the assessment values for TVOCs are derived from statistical analytical VOC analysis and such health studies [200; 299]. However, the TVOC concept is viewed critically [23; 300] and concepts to focus on the biologic relevance of organic compounds in indoor air are proposed [301].

As described in Section 3.3.2, the personal exposure is higher than typical indoor air concentration in standardized measurements, which are in turn greater than outdoor concentrations [255]. That means that personal activities like cooking, cleaning or smoking account for a large part of the total exposure. Such short time events and human influence are normally not considered in most analytical measurements, which, however, would be necessary for a comprehensive analysis of indoor air quality and its influence on human health. Only a few studies are done in single homes with PTR-MS for a short time in real life [247] or with scripted experiments (e.g. cooking, cleaning) [246]. Both studies find, e.g. high concentrations of ethanol, acetic acid, methanol and formic acid during cooking or high siloxane emissions from personal care products. COVID-19 has also greatly changed the VOC composition in the interior due to intensive use of disinfectant sprays and emissions of ethanol, monoterpenes and monoterpenoids, but also nano-sized particles [250]. PTR-MS or other currently available analytical methods are

not feasible for large-scale cohort studies as they are expensive. Low-cost VOC sensors can support such studies with continuous monitoring [28]. However, it is essential that these sensor systems are stable and comparable to obtain a proper data basis for analysis. Low-cost sensors like MOS gas sensors, however, detect more than the VOCs in the analytical definition. They also detect VVOCs and other interferent gases such as hydrogen or carbon monoxide. Therefore, a common test standard must be created for the multitude of sensors so that comparability and traceability is ensured. Moreover, a clear definition for VOCs, adapted for low-cost sensors, is needed. The comparison with analytics still must be possible. For this purpose, a draft standard VDI/VDE 3518 Blatt 4 is currently being prepared in the technical committee VDI/VDE-GMA FA 2.62 [302]. The draft is accompanied by the research project VOC4IAQ at LMT [303]. Through a comparable measurement of VOCs and further studies on the effects of VOCs on humans, these VOC monitors can be used in future for optimal ventilation control and improved air quality.

One difficulty in calibrating and testing of sensor-based VOC monitors is the variety of different VOCs. It is not feasible to test the sensors for all possible indoor VOCs. One assumption reducing the test space is that sensors react similarly to similar VOCs or substance groups. This hypothesis was tested during the mentioned field tests in Paper 6 (Section 4.3) for a few substances with mixed results for gases not included in the calibration. Benzene and m/p-xylene cause a response on the calibrated toluene and VOC_{sum} signal. This shows that the gases tested that belong to the aromatics react very similar for the specific sensor type (SGP30) and calibration with toluene produces an aromatic signal. Isopropanol, on the other hand, caused no response in the calibrated ethanol signal, although the release was detectable in the raw sensor data. Hence, the similarity in the reactions of the three aromatics is not easily transferable to other substance groups. The investigation of further substances and substance groups, their reaction patterns and optimal calibration are part of VOC4IAQ [303] and other future projects. A few improvements should be considered for upcoming calibration and release tests. The VOC_{sum} and also single VOC baselines in the room could not be validated because no analytical reference measurement was performed. A PTR-MS could be a suitable reference instrument for continuous and time-resolved monitoring of release tests [247]. The sorption measurement over >10 min and the analysis in the laboratory is not feasible on a continuous basis. Additional substances should be investigated and included in the calibration. A new GMA with more lines is available now at LMT for this purpose [123]. Also enhanced DoE, data evaluation, long term tests and so on, as discussed in Subsections 5.3.1 and 5.3.2, should be considered.

In the following, two VOCs, benzene and formaldehyde, will be discussed more deeply. These two VOCs are relevant target gases for interlaboratory tests in this thesis due to their carcinogenicity.

The aim of the first interlaboratory test is the selective measurement of benzene. Benzene is a carcinogenic gas [24] and the limit values are therefore very low. The preliminary guideline value of the UBA is 4.5 $\mu\text{g}/\text{m}^3$ or 1.4 ppb [223] and the limit value in the European Union is 5 $\mu\text{g}/\text{m}^3$ or 1.5 ppb in mean over one year [210; 218].

The interlaboratory test in Paper 5 (Section 4.3) was performed at JRC. The tested system achieves an error in the range of 1 to 2 ppb after calibration with the LMT-GMA. In the GMA at JRC an offset of nearly 2-3 ppb due to different humidity conditions is

observed. During additional tests at JRC [10] the sensor system (marked as MOS+TCO) was tested for different interfering gases (toluene, xylene, ethane, propane, butane and pentane). Compared with other low-cost benzene sensors or sensor systems, our sensor system together with a mini-GC shows a good sensitivity to benzene and the lowest confounding effects¹⁰ [10]. All other sensors like PID, other MOS, electrochemical or silicon carbide field effect transistor gas sensors exhibit strong cross-sensitivity to interferents [10]. With an increasing amount of interfering gases, a higher error is to be expected. For environmental monitoring even lower detection limits (<1 ppb) and resolutions are necessary to be able to monitor the benzene concentration [304]. One study shows a level below 4 $\mu\text{g}/\text{m}^3$ in 95 % of the investigated German buildings (3647) [198]. A decrease is seen in all percentiles between 2002 and 2012. For example, the P95 value decreased from 7 $\mu\text{g}/\text{m}^3$ in 2002 to 3 $\mu\text{g}/\text{m}^3$ in 2021 [198]. However, these are spot measurements and not annual averages. The Kinder-Umwelt-Survey of the UBA [256] in 2003 found in more than 10 % (P90 = 5.7 $\mu\text{g}/\text{m}^3$) of the investigated rooms an annual average of benzene above the limit value. Significantly higher concentrations of benzene were found in households where smokers lived [256].

An improvement can be the combination of a preconcentrator with a MOS gas sensor. Leidinger et al. [305] show for a preconcentrator based on MOFs a preconcentration factor of almost 10. The preconcentration effect also applies to toluene [305], which could lead to problems due to the higher indoor concentration of toluene compared to benzene [21]. One possibility for mitigation of the toluene reaction would be different adsorption and desorption temperatures or a temperature ramp to implement thermal desorption. Winter et al. [306] describe a thermal desorption with temperature ramp for a nanoporous silica preconcentrator. The relation between the temperature at the desorption peak and the boiling point of the compound is linear. A separation similar to a GC can be achieved. Another possibility is the filtering of interfering gases. Weber et al. [307] present the combination of a MOS gas sensor with a catalytic filter made from WO_3 . Heated to 240 °C, the filter removes gases like xylene, toluene, acetone, ethanol and others. The relatively poor reported detection limit of only 12 ppb could be improved through a preconcentrator or TCO. A non-low-cost solution is a miniaturized GC which provides reliable separation of BTEX and very low limits of detection. Zampolli et al. [30] show the combination of a preconcentration column, a separation column and a MOS gas sensor array as detector. With this setup they can achieve measurements in the sup-ppb range. They studied the detection of each compound of BTEX down to 100 ppt.

The aim of the second interlaboratory test in Paper E (Section 4.3) was, among other things, the selective measurement of formaldehyde. Formaldehyde is classified as carcinogenic [25]. The guide value I of the UBA [224] and the guideline value of the WHO [217] is 0.1 mg/m^3 or 80 ppb at 20 °C. In German buildings formaldehyde is ubiquitous and can be measured in almost every investigated building (446 [21], 2035 [198]) above the limit of quantification (LOQ). In more than 5 % of the buildings the levels are above 80 ppb.

In the laboratory comparison test, no satisfactory result is achieved for the detection of formaldehyde with the tested system. With calibration at LMT a validation error of 10 ppb is observed, but the prediction of the BAM measurement results in an error of

¹⁰ This paper only shows correlation of signals to the measurand. Thus, it only shows whether the sensor can be calibrated. A quantitative study was not carried out.

77 ppb. However, as discussed in Paper E (Section 4.3), this can be explained by the parameter space not being fully covered. Good results can be achieved with the SGP30 and randomized gas exposures of VOC gas mixtures and other interferents in different GMA measurements in Paper 3 (Section 4.2) and Paper 6 (Section 4.3). With this complex calibration, an RMSE of 30 ppb is achieved with the FESR model in Paper 6 (Section 4.3) and even reduced to 15 ppb with the enhanced TCOCNN model in Paper v [290]. However, we were unable to validate the model in the field. Due to the carcinogenic properties, no release tests were performed and there was no reference instrument available. Therefore, further investigations need to be conducted.

The ideas discussed for improving benzene measurement cannot simply be applied to formaldehyde. It is not possible to use a preconcentrator due to the high volatility of formaldehyde. Therefore, more selective sensors or other sensor principles need to be used. A review over different sensor principles for formaldehyde is given in [308]. Van den Broek [32] shows the measurement of formaldehyde with a MOS gas sensor (PD-doped SnO_2) in combinations with a compact packed bed column of nanoporous polymer sorbent (TENAX) for separation. Also, some commercial formaldehyde electrochemical cells from Sensirion AG [309] or EC Sense GmbH [310] are today available on the market and should be tested.

5.5 Interfering Gases

Interfering gases are the main challenge in many applications. Their concentrations are often in the order of magnitude of the target gas concentration or even much higher. For example, hydrogen and carbon monoxide are ubiquitous background gases. The atmosphere median background of hydrogen is 500 ppb [223] and of carbon monoxide between 100 and 300 ppb [219]. However, in most applications, hydrogen and carbon monoxide are not constant and can be emitted by anthropogenic sources. Carbon monoxide can vary by up to several ppm due to various combustion events indoor and outdoor [217]. There is no literature for hydrogen variation in indoor air.

We see large fluctuations indoors due to human activities [311]. Levitt [312] and Tomlin et al. [313] study the emission of hydrogen by humans. Paper F (Section 4.3) shows hydrogen variations over several ppm measured with two MOS gas sensors and a reference system in field tests that are not due to the presence of humans. Two effects can be observed. First, an increase of hydrogen is observed after the release of some VOCs such as toluene and acetone. This is probably due to decomposition processes such as photochemical oxidation [314]. Second, there is a diurnal hydrogen concentration cycle with its lowest point in the evening (6–8 pm) and highest in the morning (6–8 am).

Barnes et al. [315] study hydrogen in the atmosphere and took one measurement every 24 minutes for three years in a Harvard Forest. They observe a diurnal cycle with the highest concentrations in the afternoon (2–8 pm) and lowest in the morning (6–7 pm). The diurnal cycle is inversely in time compared to the results in Paper F (Section 4.3). However, they measured only a small variation of less than 10 ppb. A main cause for the variation is the removal of hydrogen due to the uptake by forest soils and oxidation by hydroxyl group [315; 316]. They mention additional factors contributing to the hydrogen variation. Sources are for example fossil fuel combustion from motor traffic, oxidation of methane and VOCs and other urban or industrial emissions of hydrogen [315].

Schmidt and Seiler [317] recorded in the 1970s hydrogen concentrations ranging from 400 to 1300 ppb close to a road outside of Mainz. Grant et al. [318], at the Weybourne atmospheric observatory (UK), observe during atmospheric hydrogen monitoring some events where the hydrogen level increases by 1000 ppb. They attribute these events to unusual wind directions from the Benelux countries, where many hydrogen-emitting (petrochemical) companies operate. Patterson et al. [319] describe the increase of hydrogen concentration in the atmosphere during the last 150 years in 2021. A 70 % increase between 1852 and 2003 was reconstructed based on atmospheric air taken from firn¹¹. In the mid to late 19th century, the atmospheric value was nearly constant at 300 ppb and increased to 550 ppb during the 20th century. They explain the large increase by increased methane oxidation and more anthropogenic sources.

This illustrates that there is a large variation of hydrogen in the atmosphere and probably even stronger indoors. Hydrogen fluctuations and the relationship between VOCs and hydrogen need further study, not only in the atmosphere but also indoors. The example of hydrogen shows how difficult it is to obtain reliable studies on some background gases.

Table 5 lists some ubiquitous background gases in the atmosphere. Methane and nitrous oxide create negligible sensor response compared to hydrogen and carbon monoxide for the used MOS gas sensors. Ozone and nitric oxide are oxidizing gases and are expected to create measurable sensor responses. The concentration of ozone and nitric oxide indoors correlates with the outdoor concentrations. Main source is the motor traffic [320]. Therefore, the influence of these and other background gases and their variation in the indoor environment needs to be investigated further. Not all interferent gases have to be calibrated if their influence is negligible. But this needs to be checked first for every possible interferent.

5.6 Gas Mixing Apparatus

Gas mixing apparatuses are necessary for reproducible characterization of gas sensor systems. Reproducible gas mixtures are a prerequisite for testing, validation and comparing different systems. This is especially important when measuring trace gases in a complex atmosphere, such as VOCs indoors. When setting low concentrations in the ppb range, the construction of such systems plays an essential role. Therefore, the GMA at LMT works with two-stage dilutions of gas from pressurized gas cylinders. This is necessary because of the contamination in pressurized gas cylinders, even when produced with synthetic air 5.0 or 6.0. Such synthetic air contains for example up to 1 ppm carbon monoxide and up to 50 ppb hydrocarbons [321]. Therefore, a high concentration of the target gas inside the bottle is diluted with the background gas of the measurement. As a result, the contamination in the bottle plays less of a role and can almost be neglected. With the use of various filters, the background residual concentration can be reduced as far as possible, e.g. with a zero air generator for carrier gas. All experiments presented in this thesis are measuring offset concentrations on a (very low) unknown background concentration.

¹¹ A type of snow that has been left over from past seasons, which is the intermediate stage between snow and glacial ice

The use of different carrier gases in the interlaboratory tests shows problems that can occur when contamination exist that only occur in one GMA. The carrier gas at BAM is active-charcoal-purified compressed air. The carrier gas at LMT is produced by a zero air generator with catalytic purification, which also removes for example hydrogen and carbon monoxide.

The atmospheric hydrogen level is 500 ppb [223] and shows a sensor response in TCO of one order of magnitude. Hence, with MOS gas sensors, gases can become important that do not play a role in classic VOC analysis, such as hydrogen or carbon monoxide as discussed in Section 5.5.

Additionally, contamination with VOCs must be taken into consideration. Tests in a GMA at LMT typically have contamination of a few $\mu\text{g}/\text{m}^3$ [42], which is in the same order of magnitude as targeted benzene concentrations. The components of a GMA must be carefully selected according to their material and shape. Leidinger et al. [43] studied different materials for tubing and observed that the glass, stainless-steel tubing with and without silica coating suffer less from sticking effects of VOC compared to aluminum or PFA (perfluoroalkoxy alkane). If additional gases, such as ozone or nitrogen dioxide, are to be analyzed in the future, the material selection of the GMA must be revisited. Inert materials such as glass or vitrified stainless steel can be tested, as in the GMA at the JRC [125; 126]. Analytical measurements of the gas stream might be necessary, due to interaction of different gases [117; 125; 126].

The GMAs used for the studies in this thesis can provide a maximum of six gases plus humidity as a gas mixture. If more background gases and VOCs are to be considered, this number is not sufficient. A GMA with more than six gases could be used, such as the latest GMA at the LMT [123] which allows a total of 18 gases to be combined independently. Another possibility is the use of gas mixtures in pressurized gas cylinders or the calibration with fewer gases and change of a pressurized gas cylinder during the measurement. All possibilities are currently being investigated in VOC4IAQ [303].

5.7 Electronics

For the use of semiconductor gas sensors in TCO, an electronic platform for analog and digital MOS gas sensors – the Sensor Control – was developed in the scope of this dissertation presented in Paper 2 and Paper vii which was used for the measurements in Paper 3, 6 and F.

Currently, there are no such universal electronics commercially available for MOS gas sensors in TCO. For analog sensors and early papers included in this thesis, the Toolbox of 3S GmbH as mentioned in Paper D was used. Due to the limitation of the measurement range, this was improved with a logarithmic read-out circuit based on the logarithmic amplifier LOG112 (Texas Instruments) at LMT. By the using the LOG114 from Texas Instruments, a faster measurement can be achieved (Paper D, Figure 3). Through the direct connection of the Log-Board (Paper 2 and Paper vii with the sensor boards and due to the optimization of the circuit design a low-noise and faster measurement of the sensor resistance is achieved by Sensor Control (Paper 2, Figure 5).

Compared to the MOXstick [322] and the GIGAstick [323] (JLM Innovation GmbH) which have a measurement range of 3.5 decades up to $10 \text{ M}\Omega$ and $1 \text{ T}\Omega$, respectively, the Sensor Control includes a much higher range of 8 decades. With both sticks, temperature

cycling is principally possible but only over voltage control and no resistance closed-loop control is included.

For the measurement of higher resistances in the $T\Omega$ range, there is new electronics available that could be tested which is able to measure even lower currents down to fA [324]. Especially when used for the detection of short gas pulses, for example in GC, such electronics can improve the performance.

The combination of sensor elements with the electronics in a sensor with integrated ASIC that are nowadays available enables new possibilities [6; 8; 9; 76]. Advantages of miniaturizing and integrating the electronics include energy-efficiency, possibility of fast temperature changes in TCO and facile integration into systems. There is no commercial hardware on the market yet to run full TCO with these sensors. The electronics Sensor Control Digital presented in Paper vii enables TCO in analogy to the analog sensors, through extended access to the communication protocol and interface. In addition, other digital sensors can easily be integrated for sensor fusion.

However, the disadvantage is that electronics and sensor layer cannot be examined independently in this case. This means that no statements can be made about the accuracy, linearity and noise behavior of the electronics. In addition, most ASICs are limited in terms of measurement range, temperature setting and flexibility, which can lead to limitations, especially in research. Through collaboration with manufacturers and closer collaboration between universities with different focuses (sensor manufacturing, electronics design and sensor fusion) the development of enhanced sensors and sensor operation modes can be promoted.

5.8 Interlaboratory Tests

Interlaboratory tests or round-robin tests are a standard procedure in chemical analysis and necessary for standardized measurements [325]. The tests can involve multiple scientists or laboratories with the same method but different equipment or a variety of equipment and methods. Such tests are also necessary for ensuring reproducibility and reliable comparison of MOS gas sensor systems. Two things need to be distinguished here: Is the GMA or the sensor system being compared or tested? In the field of MOS gas sensors, virtually no interlaboratory tests can be found in literature. Buttner et al. [326] did some interlaboratory tests with three hydrogen safety sensor types (thermal conductivity sensor, combustible gas sensor and a palladium thin-film sensor) at JRC and the U.S. Department of Energy, National Renewable Energy Laboratory (NREL).

Two interlaboratory tests were performed during this thesis. The aim of both interlaboratory tests was to compare a sensor system in different laboratories.

The interlaboratory test with the JRC in Ispra showed good results and comparable sensor signals in Paper 5 (Section 4.3). The GMA concepts at both sites are entirely different. However, in both cases the target gas benzene at ppb level was diluted with the carrier gas zero air and the only additional background was humidity. The humidity range was not coordinated, as described in Paper 5 (Section 4.3). This difference had the greatest impact on the outcome. Nevertheless, the linearity of the model could be maintained, and the calibration had a pure offset.

In the second interlaboratory test at BAM in Paper E (Section 4.3), the sensor system should also be compared. The setting for this one was more complex and in addition to

benzene, formaldehyde concentrations were to be quantified. In addition to humidity, a low-level VOC background was varied. However, the VOC background had different compositions at BAM and LMT. The GMAs were also structured quite differently. However, the most considerable difference was the used carrier gas. Hydrogen and carbon monoxide that were not filtered at BAM (Section 5.6) thus probably made the most considerable difference. The results were difficult to compare due to the different carrier gas and background VOC mixtures. Finally, the main outcome was the comparison of two GMAs.

Therefore, it must be distinguished whether an interlaboratory test is performed for sensor systems or GMAs. The system with material, purity, carrier gas, accuracy, etc. must be clearly defined beforehand. In the same way, the measurement task, which is very multifaceted in the case of VOC measurement, must be defined. This is the first challenge for comparability. Bringing MOS gas sensors out of the lab to the field and application requires successful interlaboratory tests. More interlaboratory tests are planned in context of VOC4IAQ [303].

6 Conclusion and Outlook

In this thesis, challenges for successful integration of MOS gas sensors in an application-specific gas measurement system were illustrated and solutions were proposed and tested. The importance of a physical and chemical understanding of a semiconductor gas sensor in TCO for the optimized development of operation modes and data evaluation was presented. This does not require a full physical and chemical description of every single aspect of the sensor's behavior, but rather the relevant information required for targeted development activities. With the model-based description, the generation of more stable signals, the tailored detection of short gas pulses or leakage detection are possible. Besides this, it was shown that the system consists of more than just the sensor. When developing a sensor system, several points must be considered, e.g. the sensor itself, the mode of operation, the electronics and the calibration. The application and measurement target must be clearly defined and the most important influencing factors must be known. Optimized operation, calibration and data evaluation of semiconductor gas sensors enable the exploitation of new applications in gas sensing technology. For the measurement of VOCs, the feasibility, the possibilities and the challenges were outlined. Interlaboratory tests with two independent laboratories were conducted successfully, revealing the importance and challenges of gas mixture generation. The calibration of different VOCs in the laboratory was successfully demonstrated in the laboratory and field using the proposed techniques of model-based feature extraction, randomized DoE and data evaluation with machine learning methods. The calibrated models were able to successfully predict different release tests in the field. Compared to the analytical methods used, the MOS gas sensor system achieved comparable results, which is unique in current research.

In future research, different aspects of the complete sensor system can and should be further improved. The model and the model-based data evaluation can be extended and improved, especially concerning harsh environments. An extension concerning the description of the high-temperature stage and the influence of siloxane on the model-based parameters given in [263] is only a first step. The extension to other sensors or even sensing materials and the integration of the method for detecting short gas pulses as detector for a GC can be tested. The TCO optimization should be improved further, for example by automated evaluation, which can speed up the application development. Due to the superposition property, it might be even feasible to build up a database covering the sensor response to a huge number of different gases to obtain a first guess for an application-specific operation mode without doing a single measurement.

The design of experiment still offers enormous potential for optimization. For the successful commercial application of the randomized method, the calibration time must be shortened. The gas exposures must be optimally exploited so that more measuring points are used for evaluation. First approaches with automatic detection of outliers by applying novelty detection were already presented [285]. Optimized gas mixing in multi-stage dilution systems, short gas exchange times and realistic fluidic sensor connections with low dead volume play important roles in optimizing calibration duration. The use of even more gases for more complex applications and more realistic calibration is made possible by new GMAs [123]. The concentration composition of the randomized gas mixtures in DoE was demonstrated with two different distributions. The concentration

distribution in the gas mixture composition among each other plays an essential role for successful calibration. It needs to be investigated further and improved. Should this distribution preferably represent the application as much as possible, or is it better to tune the model's accuracy in distinct directions?

The data evaluation can be improved with new or combined methods. First promising approaches with deep learning, neural networks and transfer learning are already ongoing and first results were published [290; 295]. There are many other methods in the field of feature extraction and selection, regression or hyperparameter optimization that can be tested and used. The training of global models over several sensors, the transfer of models to other sensors or the recalibration of sensors must be considered. These methods could significantly reduce calibration time and be used efficiently for high-volume applications which cannot be addressed by systems that need to be individually calibrated over days.

In the case of VOC measurement, some key facts are still unknown or have not yet been investigated. Even the sum of VOC is not clearly defined. The test standard draft, the accompanying research project VOC4IAQ [303] and other projects will make a difference and clarify aspects. Studies on the impact of VOCs on humans needs further attention especially beyond the analytical definition of VOCs. This allows new and clear measurands to be identified. The influence of oxidizing gases such as ozone or nitrogen dioxide or other interfering gases on the sensor response and on the calibrated model must be studied. For selective measurement of VOC, a combination of MOS gas sensors with other technologies as described in the discussion can be used to enhance such sensor systems and make them more similar to analytical instruments. The use of a MOS gas sensor with preconcentrator, different sensitive materials, filter or with a micro column are several ideas.

Interlaboratory tests and field tests, especially for VOC measurements, should be considered as indispensable methods for successful and reproducible sensor systems. This will help those systems to gain importance also in studies and applications, where the importance of traceable measurement is high such as health studies.

The model, methods, tools and ideas for efficient and realistic MOS gas sensor calibration and testing in this thesis enable the realization of advanced sensor systems development. The methods can also be applied to other applications such as outdoor air quality, breath analysis or odor monitoring to make significant progress in measurement quality. The highlighted challenges and developed methods can be applied to many other gas sensor-based systems. The randomized calibration and data evaluation methods can be applied to all sensor systems with multiple raw signals. The combination of several sensor principles or sensors in dynamic mode of operation such as electrochemical cells (EC) with cyclic voltammetry are examples of an application of these methods. The shown challenges for interlaboratory tests and for the application of VOC measurements do not only concern MOS gas sensors but also apply to other gas sensors like PID or EC sensors. Because all these methods and tools can be connected and interfaces were developed, a very fast workflow from identification of an application to detection algorithm has been successfully established.

7 References

- [1] J. Kelleter: *Künstliche Nase für gasförmige Emissionen aus unvollständiger Verbrennung (Dissertation)*. Shaker Verlag, 1997. ISBN: 978-3-8265-2072-3.
- [2] D. Kohl, J. Kelleter, and H. Petig: *Detection of Fires by Gas Sensors*, Sensors Update, 9:1 (161–223), 2001, DOI: 10.1002/1616-8984(200105)9:1<161::aid-seup161>3.0.co;2-a.
- [3] GTE Industrielektronik GmbH: *GSME*. <https://www.adicos.de/public/gsme/> (accessed May 22, 2021).
- [4] A. Bajtarevic, C. Ager, M. Pienz, M. Klieber, K. Schwarz, M. Ligor, T. Ligor, W. Filipiak, H. Denz, M. Fiegl, W. Hilbe, W. Weiss, P. Lukas, H. Jamnig, M. Hackl, A. Haidenberger, B. Buszewski, W. Miekisch, J. Schubert, and A. Amann: *Noninvasive detection of lung cancer by analysis of exhaled breath*, BMC Cancer, 9:1 (348), 2009, DOI: 10.1186/1471-2407-9-348.
- [5] C. Lourenço and C. Turner: *Breath Analysis in Disease Diagnosis: Methodological Considerations and Applications*, Metabolites, 4:2 (465–498), 2014, DOI: 10.3390/metabo4020465.
- [6] D. Rüffer, F. Hoehne, and J. Bühler: *New digital metal-oxide (MOx) sensor platform*, Sensors, 18:4 (1052), 2018, DOI: 10.3390/s18041052.
- [7] Bosch Sensortec GmbH: *Products - Environmental Sensors - Gas Sensors - BME680*. <https://www.bosch-sensortec.com/products/environmental-sensors/gas-sensors/bme680/> (accessed May 22, 2021).
- [8] Renesas Electronics Corporation: *Products - Sensor Products - Environmental Sensors - Digital Gas Sensors - ZMOD4410*. <https://www.renesas.com/us/en/products/sensor-products/environmental-sensors/digital-gas-sensors/zmod4410-indoor-air-quality-sensor-platform> (accessed May 22, 2021).
- [9] Sciosense B.V.: *Products - Environmental Sensors - Digital Multi Gas Sensor*. <https://www.sciosense.com/products/environmental-sensors/digital-multi-gas-sensor/> (accessed May 22, 2021).
- [10] L. Spinelle, M. Gerboles, G. Kok, S. Persijn, and T. Sauerwald: *Performance Evaluation of Low-Cost BTEX Sensors and Devices within the EURAMET Key-VOCS Project*, Proceedings, 1:4 (425), 2017, DOI: 10.3390/proceedings1040425.
- [11] A. L. Clements, W. G. Griswold, R. S. Abhijit, J. E. Johnston, M. M. Herting, J. Thorson, A. Collier-Oxandale, and M. Hannigan: *Low-cost air quality monitoring tools: From research to practice (A workshop summary)*, Sensors (Switzerland), 17:11, 2017, DOI: 10.3390/s17112478.
- [12] L. Fang, D. P. Wyon, G. Clausen, and P. O. Fanger: *Impact of indoor air temperature and humidity in an office on perceived air quality, SBS symptoms and performance*, Indoor Air, 14:s7 (74–81), 2004, DOI: 10.1111/j.1600-0668.2004.00276.x.
- [13] A. Cincinelli and T. Martellini: *Indoor Air Quality and Health*, International Journal of Environmental Research and Public Health, 14:11 (1286), 2017, DOI: 10.3390/ijerph14111286.
- [14] P. Wolkoff: *Indoor air humidity, air quality, and health – An overview*, International Journal of Hygiene and Environmental Health, 221:3 (376–390), 2018, DOI: 10.1016/j.ijehh.2018.01.015.
- [15] J. M. Samet, M. C. Marbury, and J. D. Spengler: *Health effects and sources of indoor air pollution. Part I*, American Review of Respiratory Disease, 136:6 (1486–1508), 1987, DOI: 10.1164/ajrccm/136.6.1486.

[16] T. Salthammer: *Luftverunreinigende organische Substanzen in Innenräumen*, Chemie in unserer Zeit, 28:6 (280–290), 1994, DOI: 10.1002/ciuz.19940280603.

[17] A. P. Jones: *Indoor air quality and health*, Atmospheric Environment, 33:28 (4535–4564), 1999, DOI: 10.1016/s1352-2310(99)00272-1.

[18] Bekanntmachung des Umweltbundesamtes: *Ermittlung und Beurteilung chemischer Verunreinigungen der Luft von Innenraumarbeitsplätzen (ohne Tätigkeit mit Gefahrstoffen)*, Bundesgesundheitsblatt - Gesundheitsforschung - Gesundheitsschutz, 57:8 (1002–1018), 2014, DOI: 10.1007/s00103-014-2004-6.

[19] M. Pettenkofer: *Über den Luftwechsel in Wohngebäuden*. Literarisch-Artistische Anstalt der J.G. Cotta'schen Buchhandlung, 1858. Accessed: Jan. 16, 2022. Available: <https://www.digitale-sammlungen.de/de/view/bsb10767804?page=5>

[20] *Gesundheitliche Bewertung von Kohlendioxid in der Innenraumluft*, Bundesgesundheitsblatt - Gesundheitsforschung - Gesundheitsschutz, 51:11 (1358–1369), 2008, DOI: 10.1007/s00103-008-0707-2.

[21] H. Hofmann and P. Plieninger: *Bereitstellung einer Datenbank zum Vorkommen von flüchtigen organischen Verbindungen in der Raumluft*, WaBoLu-Hefte, 5 (1–161), 2008, Accessed: Jan. 16, 2022. Available: <https://www.umweltbundesamt.de/publikationen/bereitstellung-einer-datenbank-vorkommen-von>

[22] H. Hofmann, G. Erdmann, and A. Müller: *Zielkonflikt energieeffiziente Bauweise und gute Raumluftqualität – Datenerhebung für flüchtige organische Verbindungen in der Innenraumluft von Wohn- und Bürogebäuden (Lösungswege) - Anhang*, 2014. Accessed: Jun. 11, 2022. Available: https://www.agoef.de/fileadmin/user_upload/dokumente/forschung/A GOEF-Abschlussbericht_VOCDB_II_Anhang-nicht-barrierefrei.pdf

[23] P. Wolkoff and G. D. Nielsen: *Organic compounds in indoor air—their relevance for perceived indoor air quality?*, Atmospheric Environment, 35:26 (4407–4417), 2001, DOI: 10.1016/s1352-2310(01)00244-8.

[24] M. T. Smith: *Advances in Understanding Benzene Health Effects and Susceptibility*, Annual Review of Public Health, 31 (133–148), 2010, DOI: 10.1146/annurev.publhealth.012809.103646.

[25] J. A. Swenberg, B. C. Moeller, K. Lu, J. E. Rager, R. C. Fry, and T. B. Starr: *Formaldehyde Carcinogenicity Research: 30 Years and Counting for Mode of Action, Epidemiology, and Cancer Risk Assessment*, Toxicologic Pathology, 41:2 (181–189), 2013, DOI: 10.1177/0192623312466459.

[26] L. Mølhave: *Volatile Organic Compounds, Indoor Air Quality and Health*, Indoor Air, 1:4 (357–376), 1991, DOI: 10.1111/j.1600-0668.1991.00001.x.

[27] T. Salthammer, Y. Zhang, J. Mo, H. M. Koch, and C. J. Weschler: *Assessing Human Exposure to Organic Pollutants in the Indoor Environment*, Angewandte Chemie - International Edition, 57:38 (12228–12263), 2018, DOI: 10.1002/anie.201711023.

[28] A. M. Collier-Oxandale, J. Thorson, H. Halliday, J. Milford, and M. Hannigan: *Understanding the ability of low-cost MOx sensors to quantify ambient VOCs*, Atmospheric Measurement Techniques, 12:3 (1441–1460), 2019, DOI: 10.5194/amt-12-1441-2019.

[29] I. Elmi, S. Zampolli, E. Cozzani, F. Mancarella, and G. C. Cardinali: *Development of ultra-low-power consumption MOX sensors with ppb-level VOC detection capabilities for emerging applications*, Sensors and Actuators, B: Chemical, 135:1 (342–351), 2008, DOI: 10.1016/j.snb.2008.09.002.

[30] S. Zampolli, I. Elmi, F. Mancarella, P. Betti, E. Dalcanale, G. C. Cardinali, and M.

Severi: *Real-time monitoring of sub-ppb concentrations of aromatic volatiles with a MEMS-enabled miniaturized gas-chromatograph*, Sensors and Actuators B: Chemical, 141:1 (322–328), 2009, DOI: 10.1016/j.snb.2009.06.021.

[31] M. Leidinger, T. Sauerwald, W. Reimringer, G. Ventura, and A. Schütze: *Selective detection of hazardous VOCs for indoor air quality applications using a virtual gas sensor array*, Journal of Sensors and Sensor Systems, 3:2 (253–263), 2014, DOI: 10.5194/jsss-3-253-2014.

[32] J. van den Broek, D. Klein Cerrejon, S. E. Pratsinis, and A. T. Güntner: *Selective formaldehyde detection at ppb in indoor air with a portable sensor*, Journal of Hazardous Materials, 399 (123052), 2020, DOI: 10.1016/j.jhazmat.2020.123052.

[33] D. Degler, U. Weimar, and N. Barsan: *Current Understanding of the Fundamental Mechanisms of Doped and Loaded Semiconducting Metal-Oxide-Based Gas Sensing Materials*, ACS Sensors, 4:9 (2228–2249), 2019, DOI: 10.1021/acssensors.9b00975.

[34] K. Großmann, S. Wicker, U. Weimar, and N. Bârsan: *Impact of Pt additives on the surface reactions between SnO₂, water vapour, CO and H₂; an operando investigation*, Physical chemistry chemical physics : PCCP, 15:44 (19151–19158), 2013, DOI: 10.1039/c3cp52782d.

[35] G. Tournier and C. Pijolat: *Selective filter for SnO₂-based gas sensor: application to hydrogen trace detection*, Sensors and Actuators B: Chemical, 106:2 (553–562), 2005, DOI: 10.1016/j.snb.2004.06.037.

[36] J. Fonollosa, A. Solórzano, J. M. Jiménez-Soto, S. Oller-Moreno, and S. Marco: *Gas sensor array for reliable fire detection*, Procedia Engineering, 168 (444–447), 2016.

[37] O. Kiesewetter, N. Kiesewetter, A. Kraußer, C. Loos, and M. May: *E6.1 - Technology platform for customized ceramic sensors for gases, temperatures and flows - Innovative gas sensors for selected applications in safety and medical engineering*, in *Proceedings SENSOR 2013*, 2013, (642–647). DOI: 10.5162/sensor2013/e6.1.

[38] R. E. Cavigchi, J. S. Suehle, K. G. Kreider, M. Gaitan, and P. Chaparala: *Optimized temperature-pulse sequences for the enhancement of chemically specific response patterns from micro-hotplate gas sensors*, Sensors and Actuators B: Chemical, 33:1–3 (142–146), 1996, DOI: 10.1016/0925-4005(96)01821-7.

[39] A. Heilig, N. Bârsan, U. Weimar, M. Schweizer-Berberich, J. W. Gardner, and W. Gopel: *Gas identification by modulating temperatures of SnO₂-based thick film sensors*, Sensors and Actuators B: Chemical, 43:1–3 (45–51), 1997, DOI: 10.1016/s0925-4005(97)00096-8.

[40] A. Gramm and A. Schütze: *High performance solvent vapor identification with a two sensor array using temperature cycling and pattern classification*, Sensors and Actuators B: Chemical, 95:1–3 (58–65), 2003, DOI: 10.1016/s0925-4005(03)00404-0.

[41] A. Schütze and T. Sauerwald: *Chapter Twelve - Dynamic operation of semiconductor sensors*, in *Semiconductor Gas Sensors*, 2nd ed., (385–412), R. Jaaniso and O. K. Tan, Eds. Woodhead Publishing Series in Electronic and Optical Materials, 2019. DOI: 10.1016/b978-0-08-102559-8.00012-4.

[42] N. Helwig, M. Schüler, C. Bur, A. Schütze, and T. Sauerwald: *Gas mixing apparatus for automated gas sensor characterization*, Measurement Science and Technology, 25:5 (055903), 2014, DOI: 10.1088/0957-0233/25/5/055903.

[43] M. Leidinger, C. Schultealbert, J. Neu, A. Schütze, and T. Sauerwald: *Characterization and calibration of gas sensor systems at ppb level – a versatile*

test gas generation system, Measurement Science and Technology, 29:1 (015901), 2018, DOI: 10.1088/1361-6501/aa91da.

[44] G. Heiland: *Homogeneous semiconducting gas sensors*, Sensors and Actuators, 2 (343–361), 1981, DOI: 10.1016/0250-6874(81)80055-8.

[45] N. Bârsan and A. Tomescu: *The temperature dependence of the response of SnO_2 -based gas sensing layers to O_2 , CH_4 and CO* , Sensors and Actuators B: Chemical, 26:1–3 (45–48), 1995, DOI: 10.1016/0925-4005(94)01553-t.

[46] M. Bastuck and T. Fricke: *Temperature-modulated gas sensor signal (1.0.0) [Data set]*, Zenodo, 2018, DOI: 10.5281/zenodo.1411209.

[47] M. C. Horrillo, J. Getino, J. Gutiérrez, L. Arés, J. I. Robla, C. García, and I. Sayago: *Measurements of VOCs in soils through a tin oxide multisensor system*, Sensors and Actuators B: Chemical, 43:1–3 (193–199), 1997, DOI: 10.1016/s0925-4005(97)00153-6.

[48] J. Getino, M. C. Horrillo, J. Gutiérrez, L. Arés, J. I. Robla, C. García, and I. Sayago: *Analysis of VOCs with a tin oxide sensor array*, Sensors and Actuators B: Chemical, 43 (200–205), 1997, DOI: 10.1016/s0925-4005(97)00152-4.

[49] M. Hausner, J. Zacheja, and J. Binder: *Multi-electrode substrate for selectivity enhancement in air monitoring*, Sensors and Actuators B: Chemical, 43 (11–17), 1997, DOI: 10.1016/s0925-4005(97)00140-8.

[50] J. Santos, P. Serrini, B. O’Beirn, and L. Manes: *A thin film SnO_2 gas sensor selective to ultra-low NO_2 concentrations in air*, Sensors and Actuators B: Chemical, 43:1–3 (154–160), 1997, DOI: 10.1016/s0925-4005(97)00115-9.

[51] J. Fonollosa and R. Huerta: *Gas sensor array under dynamic gas mixtures [Data set]*, UCI Machine Learning Repository, 2015, Accessed: Mar. 31, 2020. Available: <https://archive.ics.uci.edu/ml/datasets/Gas+sensor+array+under+dynamical+gas+mixtures>

[52] J. Fonollosa, S. Sheik, R. Huerta, and S. Marco: *Reservoir computing compensates slow response of chemosensor arrays exposed to fast varying gas concentrations in continuous monitoring*, Sensors and Actuators B: Chemical, 215 (618–629), 2015, DOI: 10.1016/j.snb.2015.03.028.

[53] J. Fonollosa: *Twin gas sensor arrays [Data set]*, UCI Machine Learning Repository, 2016, Accessed: Mar. 31, 2020. Available: <https://archive.ics.uci.edu/ml/datasets/Twin+gas+sensor+arrays>

[54] J. Fonollosa, L. Fernández, A. Gutiérrez-Gálvez, R. Huerta, and S. Marco: *Calibration transfer and drift counteraction in chemical sensor arrays using Direct Standardization*, Sensors and Actuators B: Chemical, 236 (1044–1053), 2016, DOI: 10.1016/j.snb.2016.05.089.

[55] H. Sundgren, F. Winquist, I. Lukkari, and I. Lundstrom: *Artificial neural networks and gas sensor arrays: quantification of individual components in a gas mixture*, Measurement Science and Technology, 2:5 (464), 1991, DOI: 10.1088/0957-0233/2/5/008.

[56] E. Magori, G. Reinhardt, M. Fleischer, R. Mayer, and H. Meixner: *Thick film device for the detection of NO and oxygen in exhaust gases*, Sensors and Actuators, B: Chemical, 95:1–3 (162–169), 2003, DOI: 10.1016/s0925-4005(03)00406-4.

[57] C. Cantalini, L. Valentini, I. Armentano, L. Lozzi, J. M. Kenny, and S. Santucci: *Sensitivity to NO_2 and cross-sensitivity analysis to NH_3 , ethanol and humidity of carbon nanotubes thin film prepared by PECVD*, Sensors and Actuators B: Chemical, 95:1–3 (195–202), 2003, DOI: 10.1016/s0925-4005(03)00418-0.

[58] E. J. Wolfrum, R. M. Meglen, D. Peterson, and J. Sluiter: *Calibration Transfer Among Sensor Arrays Designed for Monitoring Volatile Organic Compounds in*

Indoor Air Quality, IEEE Sensors Journal, 6:6 (1638–1643), 2006, DOI: 10.1109/jsen.2006.884558.

[59] L. Zhang, F. Tian, S. Liu, J. Guo, B. Hu, Q. Ye, L. Dang, X. Peng, C. Kadri, and J. Feng: *Chaos based neural network optimization for concentration estimation of indoor air contaminants by an electronic nose*, Sensors and Actuators, A: Physical, 189 (161–167), 2013, DOI: 10.1016/j.sna.2012.10.023.

[60] N. Dennler, S. Rastogi, J. Fonollosa, A. van Schaik, and M. Schmuker: *Drift in a Popular Metal Oxide Sensor Dataset Reveals Limitations for Gas Classification Benchmarks*, Sensors and Actuators B: Chemical, 361 (131668), 2021, DOI: 10.1016/j.snb.2022.131668.

[61] D. E. Williams: *Semiconducting oxides as gas-sensitive resistors*, Sensors and Actuators B: Chemical, 57:1–3 (1–16), 1999, DOI: 10.1016/s0925-4005(99)00133-1.

[62] B. Kamp, R. Merkle, and J. Maier: *Chemical diffusion of oxygen in tin dioxide*, Sensors and Actuators B: Chemical, 77:1–2 (534–542), 2001, DOI: 10.1016/s0925-4005(01)00694-3.

[63] B. Kamp, R. Merkle, R. Lauck, and J. Maier: *Chemical diffusion of oxygen in tin dioxide: Effects of dopants and oxygen partial pressure*, Journal of Solid State Chemistry, 178:10 (3027–3039), 2005, DOI: 10.1016/j.jssc.2005.07.019.

[64] P. Andersson, R. Pavelko, and A. Rotzetter: *Gas sensor with filter*, US11204346B2, Sep. 21, 2016 Accessed: Jan. 28, 2022. Available: <https://patents.google.com/patent/US11204346B2/en?oq=US11204346B2>

[65] C. Bur, M. Engel, S. Horras, and A. Schütze: *Drift compensation of virtual multisensor systems based on extended calibration*, IMCS 2014 - the 15th International Meeting on Chemical Sensors, in IMCS 2014 - the 15th International Meeting on Chemical Sensors, 2014.

[66] W. H. Brattain and J. Bardeen: *Surface Properties of Germanium*, The Bell System Technical Journal, 32:1 (1–41), 1953, DOI: 10.1002/j.1538-7305.1953.tb01420.x.

[67] G. Heiland: *Zum Einfluß von adsorbiertem Sauerstoff auf die elektrische Leitfähigkeit von Zinkoxydkristallen*, Zeitschrift für Physik, 138:3 (459–464), 1954, DOI: 10.1007/bf01340692.

[68] T. Seiyama, A. Kato, K. Fujiishi, and M. Nagatani: *A New Detector for Gaseous Components Using Semiconductive Thin Films*, Analytical Chemistry, 34:11 (1502–1503), 1962, DOI: 10.1021/ac60191a001.

[69] N. Taguchi: *Gas-detecting device*, US3631436A, 1970 Accessed: May 22, 2021. Available: <https://patents.google.com/patent/US3631436A/en>

[70] Figaro Engineering Inc.: *Company - Outline*. <https://www.figaro.co.jp/en/company/outline.html> (accessed May 16, 2021).

[71] I. Simon, N. Bârsan, M. Bauer, and U. Weimar: *Micromachined metal oxide gas sensors: Opportunities to improve sensor performance*, Sensors and Actuators B: Chemical, 73:1 (1–26), 2001, DOI: 10.1016/s0925-4005(00)00639-0.

[72] N. Barsan and U. Weimar: *Conduction Model of Metal Oxide Gas Sensors*, Journal of Electroceramics, 7:3 (143–167), 2001, DOI: 10.1023/a:1014405811371.

[73] G. Wieglob: *Gasmesstechnik in Theorie und Praxis*, 1st ed. Springer Vieweg, Wiesbaden, 2016. DOI: 10.1007/978-3-658-10687-4.

[74] H. D. Le Vine: *Method and apparatus for operating a gas sensor*, US3906473A, 1975 Accessed: May 22, 2021. Available: <https://patents.google.com/patent/US3906473A/en>

[75] H. Eicker: *Method and apparatus for determining the concentration of one gaseous*

component in a mixture of gases, US4012692A, 1974 Accessed: May 22, 2021. Available: <https://patents.google.com/patent/US4012692A/en>

[76] Bosch Sensortec GmbH: *Products - Environmental Sensors - Gas Sensors - BME688*. <https://www.bosch-sensortec.com/products/environmental-sensors/gas-sensors/bme688/> (accessed May 22, 2021).

[77] Sciosense B.V.: *Products - Environmental Sensors - ACM family*. <https://www.sciosense.com/products/environmental-sensors/acm-family/> (accessed May 22, 2021).

[78] UST Umweltsensorstechnik GmbH: *Gas Sensors - UST Triplesensor®*. <https://www.umweltsensorstechnik.de/en/gas-sensors/ust-triplesensorR.html> (accessed May 22, 2021).

[79] C. Pijolat, C. Pupier, M. Sauvan, G. Tournier, and R. Lalauze: *Gas detection for automotive pollution control*, Sensors and Actuators B: Chemical, 59:2–3 (195–202), 1999, DOI: 10.1016/s0925-4005(99)00220-8.

[80] J. Robertson: *Defect levels of SnO_2* , Physical Review B, 30:6 (3520–3522), 1984, DOI: 10.1103/physrevb.30.3520.

[81] D. Kohl: *Surface processes in the detection of reducing gases with SnO_2 -based devices*, Sensors and Actuators, 18:1 (71–113), 1989, DOI: 10.1016/0250-6874(89)87026-x.

[82] Ç. Kılıç and A. Zunger: *Origins of coexistence of conductivity and transparency in SnO_2* , Physical Review Letters, 88:9 (955011–955014), 2002, DOI: 10.1103/physrevlett.88.095501.

[83] Y. Porte, R. Maller, H. Faber, H. N. AlShareef, T. D. Anthopoulos, and M. A. McLachlan: *Exploring and controlling intrinsic defect formation in SnO_2 thin films*, Journal of Materials Chemistry C, 4 (758–765), 2015, DOI: 10.1039/c5tc03520a.

[84] M. J. Madou and S. R. Morrison: *Chemical Sensing with Solid State Devices*. San Diego: Academic Press, Inc., 1989. DOI: 10.1016/c2009-0-22258-6.

[85] T. S. Rantala, V. Lantto, and T. T. Rantala: *Rate equation simulation of the height of Schottky barriers at the surface of oxidic semiconductors*, Sensors and Actuators B: Chemical, 13:1–3 (234–237), 1993, DOI: 10.1016/0925-4005(93)85369-1.

[86] S. Samson and C. G. Fonstad: *Defect structure and electronic donor levels in stannic oxide crystals*, Journal of Applied Physics, 44:10 (4618–4621), 1973, DOI: 10.1063/1.1662011.

[87] T. S. Rantala, V. Lantto, and T. T. Rantala: *Effects of mobile donors on potential distribution in grain contacts of sintered ceramic semiconductors*, Journal of Applied Physics, 79:12 (9206–9212), 1996, DOI: 10.1063/1.362593.

[88] A. Gurlo: *Interplay between O_2 and SnO_2 : Oxygen Ionosorption and Spectroscopic Evidence for Adsorbed Oxygen*., ChemPhysChem, 7:10 (2041–52), 2006, DOI: 10.1002/cphc.200600292.

[89] K. V. Sopiha, O. I. Malyi, C. Persson, and P. Wu: *Chemistry of Oxygen Ionosorption on SnO_2 Surfaces*, ACS Applied Materials and Interfaces, 13:28 (33664–33676), 2021, DOI: 10.1021/acsami.1c08236.

[90] K. Hauffe: *Anwendung der Halbleiter-Theorie auf Probleme der heterogenen Katalyse*, Angewandte Chemie, 67:7 (189–207), 1955, DOI: 10.1002/ange.19550670702.

[91] S. R. Morrison: *The Chemical Physics of Surfaces*, 1st ed. Springer Boston, 1977. DOI: 10.1007/978-1-4615-8007-2.

[92] S. R. Morrison: *Semiconductor gas sensors*, Sensors and Actuators, 2 (329–341), 1981, DOI: 10.1016/0250-6874(81)80054-6.

[93] A. Gurlo and R. Riedel: *In Situ and Operando Spectroscopy for Assessing Mechanisms of Gas Sensing*, Angewandte Chemie International Edition, 46:21 (3826–3848), 2007, DOI: 10.1002/anie.200602597.

[94] J. Ding, T. J. McAvoy, R. E. Cavicchi, and S. Semancik: *Surface state trapping models for SnO_2 -based microhotplate sensors*, Sensors and Actuators B: Chemical, 77:3 (597–613), 2001, DOI: 10.1016/s0925-4005(01)00765-1.

[95] C. Blackman: *Do We Need “ionosorbed” Oxygen Species? (Or, “a Surface Conductivity Model of Gas Sensitivity in Metal Oxides Based on Variable Surface Oxygen Vacancy Concentration”)*, ACS Sensors, 6:10 (3509–3516), 2021, DOI: 10.1021/acssensors.1c01727.

[96] Y. Zhang, A. Kolmakov, Y. Lilach, and M. Moskovits: *Electronic Control of Chemistry and Catalysis at the Surface of an Individual Tin Oxide Nanowire*, The Journal of Physical Chemistry B, 109:5 (1923–1929), 2005, DOI: 10.1021/jp045509l.

[97] U. Pulkkinen, T. T. Rantala, T. S. Rantala, and V. Lantto: *Kinetic Monte Carlo simulation of oxygen exchange of SnO_2 surface*, Journal of Molecular Catalysis A: Chemical, 166:1 (15–21), 2001, DOI: 10.1016/s1381-1169(00)00466-0.

[98] L. Armelao, D. Barreca, E. Bontempi, C. Canevali, L. E. Depero, C. M. Mari, R. Ruffo, R. Scotti, E. Tondello, and F. Morazzoni: *Can electron paramagnetic resonance measurements predict the electrical sensitivity of SnO_2 -based film?*, Applied Magnetic Resonance, 22:1 (89–100), 2002, DOI: 10.1007/bf03170525.

[99] S. Morandi, G. Ghiotti, A. Chiorino, and E. Comini: *FT-IR and UV-Vis-NIR characterisation of pure and mixed MoO_3 and WO_3 thin films*, Thin Solid Films, 490:1 (74–80), 2005, DOI: 10.1016/j.tsf.2005.04.020.

[100] S. Lenaerts, J. Roggen, and G. Maes: *FT-IR characterization of tin dioxide gas sensor materials under working conditions*, Spectrochimica Acta Part A: Molecular and Biomolecular Spectroscopy, 51:5 (883–894), 1995, DOI: 10.1016/0584-8539(94)01216-4.

[101] R. Pohle, M. Fleischer, and H. Meixner: *Infrared emission spectroscopic study of the adsorption of oxygen on gas sensors based on polycrystalline metal oxide films*, Sensors and Actuators B: Chemical, 78:1–3 (133–137), 2001, DOI: 10.1016/s0925-4005(01)00803-6.

[102] A. K. Elger and C. Hess: *Elucidating the Mechanism of Working SnO_2 Gas Sensors Using Combined Operando UV/Vis, Raman, and IR Spectroscopy*, Angewandte Chemie - International Edition, 58:42 (15057–15061), 2019, DOI: 10.1002/anie.201908871.

[103] K.-D. Schierbaum and W. Göpel: *Chemische Sensoren: Grundlagen und Anwendungen in Arrays*, in *Multisensorikpraxis*, (61–100), H. Ahlers, Ed. Springer, Berlin, Heidelberg, 1997. DOI: 10.1007/978-3-642-60348-8_3.

[104] V. A. Myamlin and Y. V. Pleskov: *Electrochemistry of Semiconductors*, 1st ed. Springer Boston, 1967. DOI: 10.1007/978-1-4612-6533-2.

[105] S. Marco and A. Gutierrez-Galvez: *Signal and Data Processing for Machine Olfaction and Chemical Sensing: A Review*, IEEE Sensors Journal, 12:11 (3189–3214), 2012, DOI: 10.1109/jsen.2012.2192920.

[106] C. Osborne: *Statistical Calibration: A Review*, International Statistical Review / Revue Internationale de Statistique, 59:3 (309–336), 1991, DOI: 10.2307/1403690.

[107] P. J. Brown: *Measurement, regression, and calibration*. Oxford Science Publications, 1993. ISBN: 978-0-19-852245-4.

[108] G. Upton and I. Cook: *A Dictionary of Statistics*, 3ed ed. Oxford University Press,

2008. DOI: 10.1093/acref/9780199679188.001.0001.

[109] Bureau Internatioal des Poids et Measures (BIPM): *International Vocabulary of Metrology – Basic and General Concepts and Associated Terms (VIM)*, 2012. Accessed: Nov. 01, 2021. Available: https://www.bipm.org/documents/20126/2071204/JCGM_200_2012.pdf/f0e1ad45-d337-bbeb-53a6-15fe649d0ff1

[110] S. De Vito, M. Piga, L. Martinotto, and G. Di Francia: *CO, NO₂ and NO_x urban pollution monitoring with on-field calibrated electronic nose by automatic bayesian regularization*, Sensors and Actuators, B: Chemical, 143:1 (182–191), 2009, DOI: 10.1016/j.snb.2009.08.041.

[111] S. De Vito, E. Massera, M. Piga, L. Martinotto, and G. Di Francia: *On field calibration of an electronic nose for benzene estimation in an urban pollution monitoring scenario*, Sensors and Actuators B: Chemical, 129:2 (750–757), 2008, DOI: 10.1016/j.snb.2007.09.060.

[112] L. Spinelle, M. Gerboles, M. G. Villani, M. Aleixandre, and F. Bonavitacola: *Field calibration of a cluster of low-cost available sensors for air quality monitoring. Part A: Ozone and nitrogen dioxide*, Sensors and Actuators B: Chemical, 215 (249–257), 2015, DOI: 10.1016/j.snb.2015.03.031.

[113] J. Gordon Casey and M. P. Hannigan: *Testing the performance of field calibration techniques for low-cost gas sensors in new deployment locations: Across a county line and across Colorado*, Atmospheric Measurement Techniques, 11:11 (6351–6378), 2018, DOI: 10.5194/amt-11-6351-2018.

[114] J. Namieśnik: *Generation of standard gaseous mixtures*, Journal of Chromatography A, 300 (79–108), 1984, DOI: 10.1016/s0021-9673(01)87581-6.

[115] *Gasanalyse - Herstellung von Kalibriergasgemischen mit Hilfe von dynamischen Verfahren - Teil 1: Allgemeine Aspekte*, EN ISO 6145-1:2019, 2020

[116] R. S. Barratt: *The preparation of standard gas mixtures. A review*, Analyst, 106:1265 (817–849), 1981, DOI: 10.1039/an9810600817.

[117] M. Richter: *Entwicklung, Validierung und Anwendung eines Verfahrens zur Erzeugung langzeitstabiler VOC-Gasgemische*. BAM Bundesanstalt für Materialforschung und -prüfung, 2010. Accessed: Aug. 28, 2021. Available: <https://d-nb.info/1122741049/34>

[118] S. Sari, R. Timo, H. Jussi, and H. Panu: *Dynamic calibration method for reactive gases*, Measurement Science and Technology, 31:3 (034001), 2019, DOI: 10.1088/1361-6501/ab4d68.

[119] L. D. Caracciolo and W. J. Masschelein: *Ozone generator and method of producing ozone*, US6193852B1, Dec. 14, 1997 Accessed: Nov. 20, 2021. Available: <https://patents.google.com/patent/US6193852B1/en>

[120] M. A. Malik: *Nitric Oxide Production by High Voltage Electrical Discharges for Medical Uses: A Review*, Plasma Chemistry and Plasma Processing, 36:3 (737–766), 2016, DOI: 10.1007/s11090-016-9698-1.

[121] S. Shiva Kumar and V. Himabindu: *Hydrogen production by PEM water electrolysis –A review*, Materials Science for Energy Technologies, 2:3 (442–454), 2019, DOI: 10.1016/j.mset.2019.03.002.

[122] R. Maric and H. Yu: *Proton Exchange Membrane Water Electrolysis as a Promising Technology for Hydrogen Production and Energy Storage*, Nanostructures in Energy Generation, Transmission and Storage, 2018, DOI: 10.5772/intechopen.78339.

[123] D. Arendes, T. Baur, H. Lensch, J. Amann, and A. Schütze: *P13.1 - Modular design of a gas mixing apparatus for complex trace gas mixtures*, in 15. Dresdner

Sensor-Symposium 2021-12-06 - 2021-12-08 Online, 2021, (326–331).
 DOI: 10.5162/15dss2021/p13.1.

[124] M. Bastuck: *Improving the Performance of Gas Sensor Systems with Advanced Data Evaluation, Operation, and Calibration Methods (Dissertation)*. Linköping University Electronic Press, Linköping, 2019. DOI: 10.3384/diss.diva-159106.

[125] L. Spinelle: *Report of laboratory and in-situ validation of micro-sensor for monitoring ambient air sensor, EUR 30476 EN*. Publications Office of the European Union, 2013. DOI: 10.2788/4277.

[126] T. Sauerwald, T. Baur, M. Leidinger, W. Reimringer, L. Spinelle, M. Gerboles, G. Kok, and A. Schütze: *Highly sensitive benzene detection with metal oxide semiconductor gas sensors – an inter-laboratory comparison*, *Journal of Sensors and Sensor Systems*, 7:1 (235–243), 2018, DOI: 10.5194/jsss-7-235-2018.

[127] C. Borrego, A. M. Costa, J. Ginja, M. Amorim, M. Coutinho, K. Karatzas, T. Sioumis, N. Katsifarakis, K. Konstantinidis, S. De Vito, E. Esposito, P. Smith, N. André, P. Gérard, L. A. Francis, N. Castell, P. Schneider, M. Viana, M. C. Minguillón, W. Reimringer, R. P. Otjes, O. von Sicard, R. Pohle, B. Elen, D. Suriano, V. Pfister, M. Prato, S. Dipinto, and M. Penza: *Assessment of air quality microsensors versus reference methods: The EuNetAir joint exercise*, *Atmospheric Environment*, 147 (246–263), 2016, DOI: 10.1016/j.atmosenv.2016.09.050.

[128] N. Castell, F. R. Dauge, P. Schneider, M. Vogt, U. Lerner, B. Fishbain, D. Broday, and A. Bartonova: *Can commercial low-cost sensor platforms contribute to air quality monitoring and exposure estimates?*, *Environment International*, 99 (293–302), 2017, DOI: 10.1016/j.envint.2016.12.007.

[129] A. A. Tomchenko, G. P. Harmer, and B. T. Marquis: *Detection of chemical warfare agents using nanostructured metal oxide sensors*, *Sensors and Actuators B: Chemical*, 108:1–2 (41–55), 2005, DOI: 10.1016/j.snb.2004.11.059.

[130] C. Yu, Q. Hao, S. Saha, L. Shi, X. Kong, and Z. L. Wang: *Integration of metal oxide nanobelts with microsystems for nerve agent detection*, *Applied Physics Letters*, 86:6 (1–3), 2005, DOI: 10.1063/1.1861133.

[131] M. Bastuck, T. Baur, and A. Schütze: *DAV³E – a MATLAB toolbox for multivariate sensor data evaluation*, *Journal of Sensors and Sensor Systems*, 7:2 (489–506), 2018, DOI: 10.5194/jsss-7-489-2018.

[132] G. James, D. Witten, T. Hastie, and R. Tibshirani: *An introduction to Statistical Learning*, *Current medicinal chemistry*, 7:10 (995–1039), 2000, DOI: 10.1007/978-1-4614-7138-7.

[133] W. K. Härdle and L. Simar: *Applied multivariate statistical analysis*, *Applied Multivariate Statistical Analysis*, (1–516), 2013, DOI: 10.1007/978-3-642-17229-8.

[134] I. H. Witten, E. Frank, M. A. Hall, and C. J. Pal: *Data Mining: Practical Machine Learning Tools and Techniques*, *Data Mining: Practical Machine Learning Tools and Techniques*, (1–621), 2016, DOI: 10.1016/c2009-0-19715-5.

[135] B. D. Ripley: *Pattern Recognition and Neural Networks*, *Pattern Recognition and Neural Networks*, (1–403), 1996, DOI: 10.1017/cbo9780511812651.

[136] S. C. Lowe: *Stratified Validation Splits for Regression Problems*, 2016. <https://scottclowe.com/2016-03-19-stratified-regression-partitions/> (accessed Jul. 17, 2021).

[137] R. D. Snee: *Validation of Regression Models: Methods and Examples*, *Technometrics*, 19:4 (415–428), 1977, DOI: 10.1080/00401706.1977.10489581.

[138] L. Xu, O. Hu, Y. Guo, M. Zhang, D. Lu, C. B. Cai, S. Xie, M. Goodarzi, H. Y. Fu, and Y. Bin She: *Representative splitting cross validation*, *Chemometrics and*

Intelligent Laboratory Systems, 183 (29–35), 2018, DOI: 10.1016/j.chemolab.2018.10.008.

[139] B. Efron and R. J. Tibshirani: *An Introduction to the Bootstrap*. Chapman and Hall/CRC, 1994. DOI: 10.1201/9780429246593.

[140] R. Kohavi: *A Study of Cross-Validation and Bootstrap for Accuracy Estimation and Model Selection*, International Joint Conference of Artificial Intelligence, (1137–1143), 1995, Accessed: Jul. 17, 2021. Available: <https://citeseerx.ist.psu.edu/viewdoc/summary?doi=10.1.1.48.529>

[141] J. H. Kim: *Estimating classification error rate: Repeated cross-validation, repeated hold-out and bootstrap*, Computational Statistics and Data Analysis, 53:11 (3735–3745), 2009, DOI: 10.1016/j.csda.2009.04.009.

[142] C. Beleites, R. Baumgartner, C. Bowman, R. Somorjai, G. Steiner, R. Salzer, and M. G. Sowa: *Variance reduction in estimating classification error using sparse datasets*, Chemometrics and Intelligent Laboratory Systems, 79:1–2 (91–100), 2005, DOI: 10.1016/j.chemolab.2005.04.008.

[143] M. Stone: *Cross-Validatory Choice and Assessment of Statistical Predictions*, Journal of the Royal Statistical Society: Series B (Methodological), 36:2 (111–133), 1974, DOI: 10.1111/j.2517-6161.1974.tb00994.x.

[144] S. Varma and R. Simon: *Bias in error estimation when using cross-validation for model selection*, BMC Bioinformatics, 7:1 (1–8), 2006, DOI: 10.1186/1471-2105-7-91.

[145] S. Parvandeh, G. A. Poland, R. B. Kennedy, and B. A. McKinney: *Multi-Level Model to Predict Antibody Response to Influenza Vaccine Using Gene Expression Interaction Network Feature Selection*, Microorganisms, 7:3 (79), 2019, DOI: 10.3390/microorganisms7030079.

[146] G. C. Cawley and N. L. C. Talbot: *On Over-fitting in Model Selection and Subsequent Selection Bias in Performance Evaluation*, Journal of Machine Learning Research, 11:70 (2079–2107), 2010, Accessed: Jul. 17, 2021. Available: <http://jmlr.org/papers/v11/cawley10a.html>

[147] I. Tsamardinos, A. Rakhshani, and V. Lagani: *Performance-Estimation Properties of Cross-Validation-Based Protocols with Simultaneous Hyper-Parameter Optimization*, in *Artificial Intelligence: Methods and Applications. SETN 2014. Lecture Notes in Computer Science*, 2014, 8445 (1–14). DOI: 10.1007/978-3-319-07064-3_1.

[148] P. Laird and R. Saul: *Automated feature extraction for supervised learning*, in *Proceedings of the First IEEE Conference on Evolutionary Computation. IEEE World Congress on Computational Intelligence*, 1994, 2 (674–679). DOI: 10.1109/icec.1994.349977.

[149] T. Schneider, N. Helwig, and A. Schütze: *Automatic feature extraction and selection for classification of cyclical time series data*, in *XXX. Messtechnisches Symposium*, Sep. 2016, (61–68). DOI: 10.1515/9783110494297-009.

[150] S. Youssef, C. Zimmer, K. Szielasko, and A. Schütze: *Automatic feature extraction of periodic time signals using 3MA-X8 method*, Technisches Messen, 86:5 (267–277), 2019, DOI: 10.1515/teme-2018-0074.

[151] T. Schneider, N. Helwig, and A. Schütze: *Automatic feature extraction and selection for condition monitoring and related datasets*, 2018 IEEE International Instrumentation and Measurement Technology Conference (I2MTC), (1–6), 2018, DOI: 10.1109/i2mtc.2018.8409763.

[152] M. Bastuck, M. Leidinger, T. Sauerwald, and A. Schütze: *Improved quantification of naphthalene using non-linear Partial Least Squares Regression*, in *16th*

International Symposium on Olfaction and Electronic Nose, Dijon, France, 2015, (1–2). DOI: 10.48550/arxiv.1507.05834.

[153] A. S. Medishetty, N. S. Muthavarapu, S. G. Goli, B. Sirisha, and B. Sandhya: *Health Monitoring of Hydraulic System Using Feature-based Multivariate Time-series Classification Model*, Lecture Notes in Electrical Engineering, 744 LNEE (81–92), 2021, DOI: 10.1007/978-981-33-6781-4_7.

[154] L. Carmel, S. Levy, D. Lancet, and D. Harel: *A feature extraction method for chemical sensors in electronic noses*, Sensors and Actuators B: Chemical, 93:1–3 (67–76), 2003, DOI: 10.1016/s0925-4005(03)00247-8.

[155] R. A. Fisher: *The Use of Multiple Measurements in Taxonomic Problems*, Annals of Human Genetics, 7:2 (179–188), 1936, DOI: 10.1111/j.1469-1809.1936.tb02137.x.

[156] K. Backhaus, B. Erichson, W. Plinke, and R. Weiber: *Multivariate Analysemethoden*, 14th ed. Springer Berlin Heidelberg, 2016. DOI: 10.1007/978-3-662-46076-4.

[157] Y. Saeys, I. Inza, and P. Larrañaga: *A review of feature selection techniques in bioinformatics*, Bioinformatics, 23:19 (2507–2517), 2007, DOI: 10.1093/bioinformatics/btm344.

[158] R. Tibshirani: *Regression Shrinkage and Selection Via the Lasso*, Journal of the Royal Statistical Society: Series B (Methodological), 58:1 (267–288), 1996, DOI: 10.1111/j.2517-6161.1996.tb02080.x.

[159] H. Deng and G. Rungger: *Feature selection via regularized trees*, Proceedings of the International Joint Conference on Neural Networks, 2012, DOI: 10.1109/ijcnn.2012.6252640.

[160] R. Kohavi and G. H. John: *Wrappers for feature subset selection*, Artificial Intelligence, 97:1–2 (273–324), 1997, DOI: 10.1016/s0004-3702(97)00043-x.

[161] K. Kira and L. Rendell: *The Feature Selection Problem: Traditional Methods and a New Algorithm*, in *AAAI-92 Proceedings*, 1992, (129–134). Accessed: Jul. 18, 2021. Available: <https://www.aaai.org/Papers/AAAI/1992/AAAI92-020.pdf>

[162] I. Kononenko, E. Šimec, and M. Robnik-Šikonja: *Overcoming the Myopia of Inductive Learning Algorithms with RELIEFF*, Applied Intelligence, 7:1 (39–55), 1997, DOI: 10.1023/a:1008280620621.

[163] M. Robnik-Šikonja and I. Kononenko: *Theoretical and Empirical Analysis of ReliefF and RReliefF*, Machine Learning, 53:1–2 (23–69), 2003, DOI: 10.1023/a:1025667309714.

[164] M. Robnik-Šikonja and I. Kononenko: *An adaptation of Relief for attribute estimation in regression*, in *ICML '97: Proceedings of the Fourteenth International Conference on Machine Learning*, 1997, (296–304). ISBN: 978-1-55860-486-5.

[165] J. Goldberger, S. Roweis, G. Hinton, and R. Salakhutdinov: *Neighbourhood Components Analysis*, in *Advances in Neural Information Processing Systems 17*, 2014. Accessed: Nov. 01, 2021. Available: <https://proceedings.neurips.cc/paper/2004/file/42fe880812925e520249e808937738d2-Paper.pdf>

[166] W. Yang, K. Wang, and W. Zuo: *Neighborhood component feature selection for high-dimensional data*, Journal of Computers, 7:1 (162–168), 2012, DOI: 10.4304/jcp.7.1.161-168.

[167] MathWorks Deutschland: *Neighborhood Component Analysis (NCA) Feature Selection - MATLAB & Simulink*. <https://de.mathworks.com/help/stats/neighborhood-component->

analysis.html#bvf818 (accessed Jul. 18, 2021).

[168] S. Wold, E. Johansson, and M. Cocchi: *PLS: Partial Least Squares Projections to Latent Structures*, in *3D QSAR in Drug Design: Theory, Methods and Applications.*, (523–550), H. Kubinyi, Ed. 1993. ISBN: 9789072199140.

[169] L. Eriksson, T. Byrne, J. E., J. Trygg, and C. Vikström: *Multi- and Megavariate Data Analysis Basic Principles and Applications*, First. Umetrics Academy, 2013. ISBN: 9789197373050.

[170] T. Mehmood, S. Sæbø, and K. H. Liland: *Comparison of variable selection methods in partial least squares regression*, *Journal of Chemometrics*, 34:6 (e3226), 2020, DOI: 10.1002/cem.3226.

[171] G. H. John, R. Kohavi, and K. Pfleger: *Irrelevant Features and the Subset Selection Problem*, *Machine Learning Proceedings 1994*, (121–129), 1994, DOI: 10.1016/b978-1-55860-335-6.50023-4.

[172] S. Theodoridis and K. Koutroumbas: *Pattern recognition*. Academic Press, 2009. ISBN: 978-1597492720.

[173] P. Pudil, J. Novovičová, and J. Kittler: *Floating search methods in feature selection*, *Pattern Recognition Letters*, 15:11 (1119–1125), 1994, DOI: 10.1016/0167-8655(94)90127-9.

[174] I. Guyon, J. Weston, S. Barnhill, and V. Vapnik: *Gene Selection for Cancer Classification using Support Vector Machines*, *Machine Learning*, 46:1 (389–422), 2002, DOI: 10.1023/a:1012487302797.

[175] E. B. Huerta, R. M. Caporal, M. A. Arjona, and J. C. H. Hernández: *Recursive Feature Elimination Based on Linear Discriminant Analysis for Molecular Selection and Classification of Diseases*, in *Intelligent Computing Theories and Technology. ICIC 2013. Lecture Notes in Computer Science*, 2013, 7996 (244–251). DOI: 10.1007/978-3-642-39482-9_28.

[176] F. Soares and M. J. Anzanello: *Support vector regression coupled with wavelength selection as a robust analytical method*, *Chemometrics and Intelligent Laboratory Systems*, 172 (167–173), 2018, DOI: 10.1016/j.chemolab.2017.12.007.

[177] W. You, Z. Yang, and G. Ji: *PLS-based recursive feature elimination for high-dimensional small sample*, *Knowledge-Based Systems*, 55 (15–28), 2014, DOI: 10.1016/j.knosys.2013.10.004.

[178] T. C. Pearce, S. S. Schiffman, H. T. Nagle, and J. W. Gardner: *Handbook of Machine Olfaction*. Wiley, 2002. DOI: 10.1002/3527601597.

[179] S. Wold, M. Sjöström, and L. Eriksson: *PLS-regression: A basic tool of chemometrics*, *Chemometrics and Intelligent Laboratory Systems*, 58:2 (109–130), 2001, DOI: 10.1016/s0169-7439(01)00155-1.

[180] S. de Jong: *SIMPLS: An alternative approach to partial least squares regression*, *Chemometrics and Intelligent Laboratory Systems*, 18:3 (251–263), 1993, DOI: 10.1016/0169-7439(93)85002-x.

[181] P. Geladi and B. R. Kowalski: *Partial least-squares regression: a tutorial*, *Analytica Chimica Acta*, 185:C (1–17), 1986, DOI: 10.1016/0003-2670(86)80028-9.

[182] V. N. Vapnik: *The Nature of Statistical Learning Theory*, 1st ed. Springer New York, 2000. DOI: 10.1007/978-1-4757-3264-1.

[183] X. Wu, V. Kumar, Q. J. Ross, J. Ghosh, Q. Yang, H. Motoda, G. J. McLachlan, A. Ng, B. Liu, P. S. Yu, Z. H. Zhou, M. Steinbach, D. J. Hand, and D. Steinberg: *Top 10 algorithms in data mining*, *Knowledge and Information Systems*, 14:1 (1–37), 2007, DOI: 10.1007/s10115-007-0114-2.

[184] C. Rasmussen: *Gaussian process for machine learning*. London England: The MIT

Press, 2006. Accessed: Nov. 21, 2021. Available: <https://lccn.loc.gov/2018023826> <https://mitpress.mit.edu/books/gaussian-processes-machine-learning>

[185] D. F. Specht: *A General Regression Neural Network*, IEEE Transactions on Neural Networks, 2:6 (568–576), 1991, DOI: 10.1109/72.97934.

[186] C. J. Willmott: *Some comments on the evaluation of model performance*, Bulletin - American Meteorological Society, 63:11 (1309–1313), 1982, DOI: 10.1175/1520-0477(1982)063<1309:scoteo>2.0.co;2.

[187] N. E. Klepeis, W. C. Nelson, W. R. Ott, J. P. Robinson, A. M. Tsang, P. Switzer, J. V. Behar, S. C. Hern, and W. H. Engelmann: *The National Human Activity Pattern Survey (NHAPS) A Resource for Assessing Exposure to Environmental Pollutants*, Journal of Exposure Science & Environmental Epidemiology, 11:3 (231–252), 2001, DOI: 10.1038/sj.jea.7500165.

[188] World Health Organization. Regional Office for Europe: *Combined or multiple exposure to health stressors in indoor built environments: an evidence-based review prepared for the WHO training workshop “Multiple environmental exposures and risks”*: 16–18 October 2013, Bonn, Germany, WHO Regional Office for Europe, Copenhagen, 2014. Accessed: Jan. 16, 2021. Available: <https://apps.who.int/iris/handle/10665/350495>

[189] VELUX Deutschland GmbH: *Press Release: Gesundheitsrisiken für heutige “Indoor Generation.”* <https://presse.velux.de/gesundheitsrisiken-fur-heutige-indoor-generation/?consent=preferences,statistics,marketing&ref-original=> (accessed Mar. 31, 2021).

[190] VELUX Deutschland GmbH: *Die Indoor-Generation - Die Auwirkungen des modernen Lebens auf Gesundheit, Wohlleben und Produktivität*. <https://presse.velux.de/download/1120832/velux-tig-yougov-report-180515.pdf> (accessed Jan. 16, 2022).

[191] F. B. Benson, J. J. Henderson, and D. E. Caldwell: *Indoor-Outdoor Air Pollution Relationship: A Literature Review*, 1972. Accessed: Jan. 16, 2022. Available: <https://nepis.epa.gov/Exe/ZyPURL.cgi?Dockey=9100EERY.txt>

[192] J. J. Henderson, F. B. Benson, and D. E. Caldwell: *Indoor-Outdoor Air Pollution Relationship: Volume II, An Annotated Bibliography*, 1973. Available: <https://nepis.epa.gov/Exe/ZyPURL.cgi?Dockey=9100EEU7.txt>

[193] J. M. Samet, M. C. Marbury, and J. D. Spengler: *Health Effects and Sources of Indoor Air Pollution. Part II*, American Review of Respiratory Disease, 137:1 (221–242), 1988, DOI: 10.1164/ajrccm/137.1.221.

[194] P. S. Burge: *Sick building syndrome*, Occupational and Environmental Medicine, 61:2 (185–190), 2004, DOI: 10.1136/oem.2003.008813.

[195] H.-P. Hutter, H. Mooshammer, P. Wallner, P. Tappler, F. Twrdik, E. Ganglberger, S. Geissler, and A. Wenisch: *Auswirkungen energiesparender Maßnahmen im Wohnbau auf die Innenraumluftqualität und Gesundheit*, 2005. Accessed: Mar. 31, 2021. Available: http://www.innenraumanalytik.at/pdfs/innenraumluft_u_gesundheit.pdf

[196] A. Asikainen, P. Carrer, S. Kephalopoulos, E. D. O. Fernandes, P. Wargocki, and O. Hänninen: *Reducing burden of disease from residential indoor air exposures in Europe (HEALTHVENT project)*, Environmental Health, 15:1 (S35), 2016, DOI: 10.1186/s12940-016-0101-8.

[197] *Innenraumluftverunreinigungen - Teil 1: Allgemeine Aspekte der Probenahmestrategie*, DIN EN ISO 16000-1:2006-06, 2006

DOI: 10.31030/9719532.

- [198] H. Hofmann, G. Erdmann, and A. Müller: *Zielkonflikt energieeffiziente Bauweise und gute Raumluftqualität – Datenerhebung für flüchtige organische Verbindungen in der Innenraumluft von Wohn- und Bürogebäuden (Lösungswege)* - Abschlussbericht, 2014. Accessed: Jun. 11, 2022. Available: https://www.agoef.de/fileadmin/user_upload/dokumente/forschung/A GOEF-Abschlussbericht_VOC_DB_II-barrierefrei.pdf
- [199] Umweltbundesamt: *Beurteilung von Innenraumluftkontaminationen Mittels Referenz- und Richtwerten: Handreichung der Ad-hoc-Arbeitsgruppe der Innenraumluftthygiene- Kommission des Umweltbundesamtes und der Obersten Landesgesundheitsbehörden*, Bundesgesundheitsblatt - Gesundheitsforschung - Gesundheitsschutz, 50:7 (990–1005), 2007, DOI: 10.1007/s00103-007-0290-y.
- [200] B. Seifert: *Richtwerte für die Innenraumluft*, in *Bundesgesundheitsblatt Gesundheitsforschung Gesundheitsschutz*, 42:3 (270–278), Springer, Berlin, Heidelberg, 1999. DOI: 10.1007/978-3-662-38283-7_45.
- [201] *Innenraumluftverunreinigungen - Teil 6: Bestimmung von VOC in der Innenraumluft und in Prüfkammern, Probenahme auf Tenax TA®, thermische Desorption und Gaschromatographie mit MS oder MS-FID*, DIN ISO 16000-6:2012-11, 2012 DOI: 10.31030/1912225.
- [202] *Raumlufttechnik, Raumluftqualität - Beurteilung der Raumluftqualität*, VDI 6022 Blatt 3:2011-07, 2011 ISBN: 2557798001200.
- [203] W. Birmili, M. Kolossa-Gehring, K. Valtanen, M. Dębiak, and T. Salthammer: *Indoor air pollution—current fields of action*, Bundesgesundheitsblatt - Gesundheitsforschung - Gesundheitsschutz, 61:6 (656–666), 2018, DOI: 10.1007/s00103-018-2737-8.
- [204] RAL gGmbH: *Blauer Engel - Das Umweltzeichen*. <https://www.blauer-engel.de/de> (accessed May 30, 2021).
- [205] Danish Technological Institute: *Danish Indoor Climate Labelling*. <https://indeklimamaerket.dk/in-english/> (accessed May 30, 2021).
- [206] Rakennustietosäätiö: *Rakennustieto*. <https://cer.rts.fi/> (accessed Jan. 16, 2022).
- [207] Ministère de la Transition écologique: *Étiquetage des produits de construction*. <https://www.ecologie.gouv.fr/etiquetage-des-produits-construction> (accessed May 30, 2021).
- [208] eco-INSTITUT Germany GmbH: *eco-INSTITUT-Label*. <https://www.eco-institut-label.de/de/> (accessed May 30, 2021).
- [209] Internationaler Verein für zukunftsfähiges Bauen und Wohnen - natureplus e.V.: *natureplus Umweltzeichen*. <https://www.natureplus.org/> (accessed May 30, 2021).
- [210] *Directive 2008/50/EC of the European Parliament and of the Council of 21 May 2008 on ambient air quality and cleaner air for Europe*, Official Journal of the European Union, L 152:51 (1–44), 2008, Accessed: Jan. 16, 2022. Available: <https://eur-lex.europa.eu/legal-content/EN/TXT/PDF/?uri=OJ:L:2008:152:FULL&from=EN>
- [211] International WELL Building Institute: *WELL Certified*. <https://www.wellcertified.com/> (accessed May 30, 2021).
- [212] International WELL Building Institute: *WELL v2 pilot, Q4 2021, Feature A08 - Air Quality Monitoring and Awareness*. <https://v2.wellcertified.com/v/en/air/feature/8> (accessed May 30, 2021).
- [213] W. J. Fisk and A. T. De Almeida: *Sensor-based demand-controlled ventilation: A review*, Energy and Buildings, 29:1 (35–45), 1998, DOI: 10.1016/s0378-7788(98)00029-2.

[214] M. Mysen, J. P. Rydock, and P. O. Tjelflaat: *Demand controlled ventilation for office cubicles—can it be profitable?*, Energy and Buildings, 35:7 (657–662), 2003, DOI: 10.1016/s0378-7788(02)00212-8.

[215] S. Haddad, A. Synnefa, M. Ángel Padilla Marcos, R. Paolini, S. Delrue, D. Prasad, and M. Santamouris: *On the potential of demand-controlled ventilation system to enhance indoor air quality and thermal condition in Australian school classrooms*, Energy and Buildings, 238 (110838), 2021, DOI: 10.1016/j.enbuild.2021.110838.

[216] M. Mysen, S. Berntsen, P. Nafstad, and P. G. Schild: *Occupancy density and benefits of demand-controlled ventilation in Norwegian primary schools*, Energy and Buildings, 37:12 (1234–1240), 2005, DOI: 10.1016/j.enbuild.2005.01.003.

[217] World Health Organization. Regional Office for Europe: *WHO guidelines for indoor air quality: selected pollutants*, 9. Copenhagen: World Health Organization. Regional Office for Europe, 2010. Accessed: Jan. 16, 2022. Available: <https://apps.who.int/iris/handle/10665/260127>

[218] *Neununddreißigste Verordnung zur Durchführung des Bundes-Immissionsschutzgesetzes (Verordnung über Luftqualitätsstandards und Emissionshöchstmengen – 39. BImSchV)*, 2010 Accessed: May 30, 2021. Available: https://www.gesetze-im-internet.de/bimschv_39/

[219] *Gesundheitliche Bedeutung von Feinstaub in der Innenraumluft*, Bundesgesundheitsblatt - Gesundheitsforschung - Gesundheitsschutz, 51:11 (1370–1378), 2008, DOI: 10.1007/s00103-008-0708-1.

[220] World Health Organization. Occupational and Environmental Health Team: *WHO Air quality guidelines for particulate matter, ozone, nitrogen dioxide and sulfur dioxide: global update 2005: summary of risk assessment*, (1–20). World Health Organization, 2006. Accessed: Jan. 16, 2022. Available: <https://apps.who.int/iris/handle/10665/69477>

[221] *Ausschuss für Innenraumrichtwerte / Umweltbundesamt*. <https://www.umweltbundesamt.de/themen/gesundheit/kommissionen-arbeitsgruppen/ausschuss-fuer-innenraumrichtwerte#undefined> (accessed May 01, 2022).

[222] *Richtwerte für Toluol und gesundheitliche Bewertung von C₇-C₈-Alkylbenzolen in der Innenraumluft*, Bundesgesundheitsblatt, Gesundheitsforschung, Gesundheitsschutz, 59:11 (1522–1539), 2016, DOI: 10.1007/s00103-016-2444-2.

[223] *Vorläufiger Leitwert für Benzol in der Innenraumluft*, Bundesgesundheitsblatt, Gesundheitsforschung, Gesundheitsschutz, 63:3 (361–367), 2020, DOI: 10.1007/s00103-019-03089-4.

[224] *Richtwert für Formaldehyd in der Innenraumluft*, Bundesgesundheitsblatt - Gesundheitsforschung - Gesundheitsschutz, 59:8 (1040–1044), 2016, DOI: 10.1007/s00103-016-2389-5.

[225] *Richtwerte für monocyclische Monoterpen (Leitsubstanz d-Limonen) in der Innenraumluft. Mitteilung der Ad-hoc-Arbeitsgruppe Innenraumrichtwerte der Innenraumlufthygiene-Kommission des Umweltbundesamtes und der Obersten Landesgesundheitsbehörden*, Bundesgesundheitsblatt - Gesundheitsforschung - Gesundheitsschutz, 53:11 (1206–1215), 2010, DOI: 10.1007/s00103-010-1155-3.

[226] *Directive 2001/81/EC of the European Parliament and of the Council of 23 October 2001 on national emission ceilings for certain atmospheric pollutants*, Official Journal of the European Communities, L 309:44 (22–30), 2001, Accessed: Jun. 05, 2021. Available: <https://eur-lex.europa.eu/legal-content/EN/TXT/PDF/?uri=OJ:L:2001:309:FULL&from=EN>

[227] *31. Verordnung zur Durchführung des Bundes-Immissionsschutzgesetzes*

(Verordnung zur Begrenzung der Emissionen flüchtiger organischer Verbindungen bei der Verwendung organischer Lösemittel in bestimmten Anlagen) (31. BImSchV), 2001 Accessed: Jun. 05, 2021. Available: https://www.gesetze-im-internet.de/bimschv_31/_2.html

[228] J. Williams, R. Koppmann, S. Reimann, A. C. Lewis, A. H. Steiner, and A. L. Goldstein: *Volatile Organic Compounds in the Atmosphere: An Overview*, in *Volatile Organic Compounds in the Atmosphere*, (1–32), R. Koppmann, Ed. Blackwell Publishing Ltd, 2007. DOI: <https://doi.org/10.1002/9780470988657.ch1>.

[229] K. Sindelarova, C. Granier, I. Bouarar, A. Guenther, S. Tilmes, T. Stavrakou, J. F. Müller, U. Kuhn, P. Stefani, and W. Knorr: *Global data set of biogenic VOC emissions calculated by the MEGAN model over the last 30 years*, *Atmospheric Chemistry and Physics*, 14:17 (9317–9341), 2014, DOI: 10.5194/acp-14-9317-2014.

[230] M. Steinbacher, A. Fischer, M. K. Vollmer, B. Buchmann, S. Reimann, and C. Hueglin: *Perennial observations of molecular hydrogen (H₂) at a suburban site in Switzerland*, *Atmospheric Environment*, 41:10 (2111–2124), 2007, DOI: 10.1016/j.atmosenv.2006.10.075.

[231] L. A. Wallace, E. Pellizzari, B. Leaderer, H. Zelon, and L. Sheldon: *Emissions of volatile organic compounds from building materials and consumer products*, *Atmospheric Environment* (1967), 21:2 (385–393), 1987, DOI: 10.1016/0004-6981(87)90017-5.

[232] R. D. Edwards, C. Schweizer, V. Llacqua, H. K. Lai, M. Jantunen, L. Bayer-Oglesby, and N. Künzli: *Time-activity relationships to VOC personal exposure factors*, *Atmospheric Environment*, 40:29 (5685–5700), 2006, DOI: 10.1016/j.atmosenv.2006.04.057.

[233] A. M. Yeoman, M. Shaw, N. Carslaw, T. Murrells, N. Passant, and A. C. Lewis: *Simplified speciation and atmospheric volatile organic compound emission rates from non-aerosol personal care products*, *Indoor Air*, 30:3 (459–472), 2020, DOI: 10.1111/ina.12652.

[234] M. M. Coggon, B. C. McDonald, A. Vlasenko, P. R. Veres, F. Bernard, A. R. Koss, B. Yuan, J. B. Gilman, J. Peischl, K. C. Aikin, J. Durant, C. Warneke, S. M. Li, and J. A. De Gouw: *Diurnal Variability and Emission Pattern of Decamethylcyclopentasiloxane (D₅) from the Application of Personal Care Products in Two North American Cities*, *Environmental Science and Technology*, 52:10 (5610–5618), 2018, DOI: 10.1021/acs.est.8b00506.

[235] L. Mølhav: *Indoor air pollution due to organic gases and vapours of solvents in building materials*, *Environment International*, 8:1 (117–127), 1982, DOI: 10.1016/0160-4120(82)90019-8.

[236] J. J. Schauer, M. J. Kleeman, G. R. Cass, and B. R. T. Simoneit: *Measurement of emissions from air pollution sources. 1. C₁ through C₂₉ organic compounds from meat charbroiling*, *Environmental Science and Technology*, 33:10 (1566–1577), 1999, DOI: 10.1021/es980076j.

[237] J. J. Schauer, M. J. Kleeman, G. R. Cass, and B. R. T. Simoneit: *Measurement of emissions from air pollution sources. 3. C₁–C₂₉ organic compounds from fireplace combustion of wood*, *Environmental Science and Technology*, 35:9 (1716–1728), 2001, DOI: 10.1021/es001331e.

[238] J. J. Schauer, M. J. Kleeman, G. R. Cass, and B. R. T. Simoneit: *Measurement of Emissions from Air Pollution Sources. 4. C₁–C₂₇ Organic Compounds from Cooking with Seed Oils*, *Environmental Science and Technology*, 36:4 (567–575),

2002, DOI: 10.1021/es002053m.

[239] T. Salthammer: *Very volatile organic compounds: an understudied class of indoor air pollutants*, Special Issue: Keynote: Indoor Air 2014, 26:1 (25–38), 2016, DOI: 10.1111/ina.12173.

[240] J. M. Wallace and P. V. Hobbs: *Atmospheric Science: An Introductory Survey*, 2nd ed. Academic Press, 2006. DOI: 10.1016/c2009-0-00034-8.

[241] Deutscher Wetterdienst: *Klimagase (CO₂, CH₄, N₂O)*. https://www.dwd.de/DE/forschung/atmosphaerenbeob/zusammensetzung_atmosphaere/spurengase/inh_nav/klimagase_node.html (accessed Mar. 31, 2021).

[242] R. Schleyer, E. Bieber, and M. Wallasch: *Das Luftnetz des Umweltbundesamt*, 2013. Accessed: Jan. 16, 2022. Available: https://www.umweltbundesamt.de/sites/default/files/medien/378/publicationen/das_luftmessnetz_des_umweltbundesamtes_bf_0.pdf

[243] D. Möller: *Luft: Chemie, Physik, Biologie, Reinhaltung, Recht*. De Gruyter, 2011. DOI: 10.1515/9783110200225.

[244] Deutscher Wetterdienst: *Kohlenmonoxid (CO)*. https://www.dwd.de/DE/forschung/atmosphaerenbeob/zusammensetzung_atmosphaere/spurengase/inh_nav/co_node.html (accessed Mar. 31, 2021).

[245] Deutscher Wetterdienst: *Bodennahes Ozon (O₃)*. https://www.dwd.de/DE/forschung/atmosphaerenbeob/zusammensetzung_atmosphaere/spurengase/inh_nav/o3_node.html (accessed Mar. 31, 2021).

[246] C. Arata, P. K. Misztal, Y. Tian, D. M. Lunderberg, K. Kristensen, A. Novoselac, M. E. Vance, D. K. Farmer, W. W. Nazaroff, and A. H. Goldstein: *Volatile organic compound emissions during HOMEChem*, Indoor Air, 31:6 (2099–2117), 2021, DOI: 10.1111/ina.12906.

[247] Y. Liu, P. K. Misztal, J. Xiong, Y. Tian, C. Arata, R. J. Weber, W. W. Nazaroff, and A. H. Goldstein: *Characterizing sources and emissions of volatile organic compounds in a northern California residence using space- and time-resolved measurements*, Indoor Air, 29:4 (630–644), 2019, DOI: 10.1111/ina.12562.

[248] A. Steinemann: *Volatile emissions from common consumer products*, Air Quality, Atmosphere and Health, 8:3 (273–281), 2015, DOI: 10.1007/s11869-015-0327-6.

[249] M. A. Bari, W. B. Kindzierski, A. J. Wheeler, M. È. Héroux, and L. A. Wallace: *Source apportionment of indoor and outdoor volatile organic compounds at homes in Edmonton, Canada*, Building and Environment, 90 (114–124), 2015, DOI: 10.1016/j.buildenv.2015.03.023.

[250] J. Jiang, X. Ding, K. P. Isaacson, A. Tasoglou, H. Huber, A. D. Shah, N. Jung, and B. E. Boor: *Ethanol-based disinfectant sprays drive rapid changes in the chemical composition of indoor air in residential buildings*, Journal of Hazardous Materials Letters, 2 (100042), 2021, DOI: 10.1016/j.hazl.2021.100042.

[251] A. Blondel and H. Plaisance: *Screening of formaldehyde indoor sources and quantification of their emission using a passive sampler*, Building and Environment, 46:6 (1284–1291), 2011, DOI: 10.1016/j.buildenv.2010.12.011.

[252] D. Campagnolo, D. E. Saraga, A. Cattaneo, A. Spinazzè, C. Mandin, R. Mabilia, E. Perreca, I. Sakellaris, N. Canha, V. G. Mihucz, T. Szigeti, G. Ventura, J. Madureira, E. de Oliveira Fernandes, Y. de Kluizenaar, E. Cornelissen, O. Hänninen, P. Carrer, P. Wolkoff, D. M. Cavallo, and J. G. Bartzis: *VOCs and aldehydes source identification in European office buildings - The OFFICAIR study*, Building and Environment, 115 (18–24), 2017, DOI: 10.1016/j.buildenv.2017.01.009.

[253] T. M. Sack, D. H. Steele, K. Hammerstrom, and J. Remmers: *A survey of household*

products for volatile organic compounds, Atmospheric Environment. Part A. General Topics, 26:6 (1063–1070), 1992, DOI: 10.1016/0960-1686(92)90038-m.

[254] S. H. Smedemark, M. Ryhl-Svendsen, and A. Schieweck: *Quantification of formic acid and acetic acid emissions from heritage collections under indoor room conditions. Part I: laboratory and field measurements*, Heritage Science, 8:1 (58), 2020, DOI: 10.1186/s40494-020-00404-0.

[255] L. A. Wallace: *Personal exposure to 25 volatile organic compounds. EPA's 1987 team study in Los Angeles, California*, Toxicology and Industrial Health, 7:5–6 (203–208), 1991, DOI: 10.1177/074823379100700523.

[256] C. Schulz, D. Ulrich, H. Pick-Fuß, M. Seiwert, A. Conrad, K.-R. Brenske, A. Hünken, A. Lehmann, and M. Kolossa-Gehring: *Kinder-Umwelt-Survey (KUS) 2003/06: Innenraumluft – Flüchtige organische Verbindungen in der Innenraumluft in Haushalten mit Kindern in Deutschland*, WaBoLu-Hefte, 3 (1–239), 2010, Accessed: Nov. 21, 2021. Available: <http://www.uba.de/uba-infomediens/4011.html>

[257] K. Vellingiri, J. E. Szulejko, P. Kumar, E. E. Kwon, K. H. Kim, A. Deep, D. W. Boukhvalov, and R. J. C. Brown: *Metal organic frameworks as sorption media for volatile and semi-volatile organic compounds at ambient conditions*, Scientific Reports, 6:1 (27813), 2016, DOI: 10.1038/srep27813.

[258] M. S. Claflin, D. Pagonis, Z. Finewax, A. V. Handschy, D. A. Day, W. L. Brown, J. T. Jayne, D. R. Worsnop, J. L. Jimenez, P. J. Ziemann, J. De Gouw, and B. M. Lerner: *An in situ gas chromatograph with automatic detector switching between PTR- and EI-TOF-MS: isomer-resolved measurements of indoor air*, Atmospheric Measurement Techniques, 14:1 (133–152), 2021, DOI: 10.5194/amt-14-133-2021.

[259] A. Hansel, A. Jordan, R. Holzinger, P. Prazeller, W. Vogel, and W. Lindinger: *Proton transfer reaction mass spectrometry: on-line trace gas analysis at the ppb level*, International Journal of Mass Spectrometry and Ion Processes, 149–150 (609–619), 1995, DOI: 10.1016/0168-1176(95)04294-u.

[260] A. Jordan, S. Haidacher, G. Hanel, E. Hartungen, J. Herbig, L. Märk, R. Schottkowsky, H. Seehauser, P. Sulzer, T. D. Märk, A. Jordan, S. Haidacher, G. Hanel, E. Hartungen, J. Herbig, L. Märk, R. Schottkowsky, H. Seehauser, P. Sulzer, and T. D. Märk: *An online ultra-high sensitivity Proton-transfer-reaction mass-spectrometer combined with switchable reagent ion capability (PTR + SRI - MS)*, International Journal of Mass Spectrometry, 286:1 (32–38), 2009, DOI: 10.1016/j.ijms.2009.06.006.

[261] M. Graus, M. Müller, and A. Hansel: *High Resolution PTR-TOF: Quantification and Formula Confirmation of VOC in Real Time*, Journal of the American Society for Mass Spectrometry, 21:6 (1037–1044), 2010, DOI: 10.1016/j.jasms.2010.02.006.

[262] T. Schripp, S. Etienne, C. Fauck, F. Fuhrmann, L. Märk, and T. Salthammer: *Application of proton-transfer-reaction-mass-spectrometry for Indoor Air Quality research*, Indoor Air, 24:2 (178–189), 2014, DOI: 10.1111/ina.12061.

[263] C. Schultealbert: *Siloxanvergiftung von Metallocid-Gassensoren im temperaturzyklischen Betrieb – Effekte, Erkennung, Optimierung*, Dissertation, Universität des Saarlandes, 2021.

[264] C. Fuchs, T. Baur, O. Brieger, H. Lensch, and A. Schütze: *P9.6 - Versatile platform for metal oxide semiconductor gas sensors for application specific optimization of temperature cycled operation*, in *15. Dresden Sensor-Symposium 2021-12-06 - 2021-12-08 Online*, 2021. DOI: 10.5162/15dss2021/p9.6.

[265] C. Schultealbert, R. Diener, J. Amann, T. Baur, A. Schütze, and T. Sauerwald: *Differential scanning calorimetry on micro hotplates for temperature calibration and mass quantification*, tm - Technisches Messen, 87:3 (153–163), 2020, DOI: 10.1515/teme-2019-0142.

[266] T. Baur, C. Schultealbert, A. Schütze, and T. Sauerwald: *Quantifizierung von Aceton mit MOS Sensoren für die Atemgasanalyse*, in *Sensoren und Messsysteme - 19. ITG/GMA-Fachtagung*, Jun. 2018, (4). Accessed: Jan. 02, 2022. Available: <https://www.vde-verlag.de/proceedings-de/454683135.html>

[267] C. Schultealbert, A. Schütze, and T. Sauerwald: *Selektive Quantifizierung von Schwefelverbindungen mit MOS-Sensoren*, in *Sensoren und Messsysteme - 19. ITG/GMA-Fachtagung 26.06.2018 - 27.06.2018 in Nürnberg, Deutschland*, 2018, (1–4). Accessed: Jan. 14, 2022. Available: <https://www.vde-verlag.de/proceedings-de/454683021.html>

[268] J. Joppich, M. Bastuck, A. Schütze, and T. Sauerwald: *D5.1 An Approach for Feature Interpolation Between Classes to Simplify Calibration of Sensor Systems for Odour Monitoring*, in *SMSI 2020 - Measurement Science*, Jun. 2020, (293–294). DOI: 10.5162/smsi2020/d5.1.

[269] C. Schultealbert, T. Baur, T. Sauerwald, and A. Schütze: *Erkennung und Kompensation von Vergiftung durch Siloxane auf Halbleitergassensoren im temperaturzyklischen Betrieb*, tm - Technisches Messen, 87:s1 (s120–s125), 2020, DOI: 10.1515/teme-2020-0041.

[270] T. Baur, A. Schütze, and T. Sauerwald: *Detektion von kurzen Gaspulsen für die Spurengasanalytik*, tm - Technisches Messen, 84:s1 (s88–s92), 2017, DOI: 10.1515/teme-2017-0035.

[271] L. Lopez, V. Copa, T. Hayasaka, M. A. Faustino-Lopez, Y. Wu, H. Liu, Y. Liu, E. Estacio, A. Somintac, L. Lin, and A. Salvador: *Influence of chamber design on the gas sensing performance of graphene field-effect-transistor*, SN Applied Sciences, 2:7 (1185), 2020, DOI: 10.1007/s42452-020-2676-5.

[272] N. Bârsan and R. Ionescu: *SnO₂-based gas sensors as chromatographic detectors*, Sensors and Actuators B: Chemical, 19:1–3 (470–473), 1994, DOI: 10.1016/0925-4005(93)01042-3.

[273] A. Eberheim: *Qualifizierung von Halbleiter-Gassensoren für die Detektion spezifischer organischer Rauchgaskomponenten*, Dissertation, Universität Gießen, 2003. Accessed: May 16, 2021. Available: <http://geb.uni-giessen.de/geb/volltexte/2003/1223/pdf/EberheimAndreas-2003-07-17.pdf>

[274] M. I. Mead, O. A. M. Popoola, G. B. Stewart, P. Landshoff, M. Calleja, M. Hayes, J. J. Baldovi, M. W. McLeod, T. F. Hodgson, J. Dicks, A. Lewis, J. Cohen, R. Baron, J. R. Saffell, and R. L. Jones: *The use of electrochemical sensors for monitoring urban air quality in low-cost, high-density networks*, Atmospheric Environment, 70 (186–203), 2013, DOI: 10.1016/j.atmosenv.2012.11.060.

[275] K. Koistinen, D. Kotzias, S. Kephalopoulos, C. Schlitt, P. Carrer, M. Jantunen, S. Kirchner, J. McLaughlin, L. Mølhav, E. O. Fernandes, and B. Seifert: *The INDEX project: Executive summary of a European Union project on indoor air pollutants*, Allergy: European Journal of Allergy and Clinical Immunology, 63:7 (810–819), 2008, DOI: 10.1111/j.1398-9995.2008.01740.x.

[276] O. Geiss, G. Giannopoulos, S. Tirendi, J. Barrero-Moreno, B. R. Larsen, and D. Kotzias: *The AIRMEX study - VOC measurements in public buildings and schools/kindergartens in eleven European cities: Statistical analysis of the data*, Atmospheric Environment, 45:22 (3676–3684), 2011, DOI: 10.1016/j.atmosenv.2011.04.037.

[277] J. B. Sanchez, A. Schmitt, F. Berger, and C. Mavon: *Silicon-Micromachined Gas Chromatographic Columns for the Development of Portable Detection Device*, Journal of Sensors, 2010 (409687), 2010, DOI: 10.1155/2010/409687.

[278] S. Zampolli, I. Elmi, J. Stürmann, S. Nicoletti, L. Dori, and G. C. Cardinali: *Selectivity enhancement of metal oxide gas sensors using a micromachined gas chromatographic column*, Sensors and Actuators B: Chemical, 105:2 (400–406), 2005, DOI: 10.1016/j.snb.2004.06.036.

[279] S. Zampolli, P. Betti, I. Elmi, and E. Dalcanale: *A supramolecular approach to sub-ppb aromatic VOC detection in air*, Chemical Communications, 27 (2790–2792), 2007, DOI: 10.1039/b703747c.

[280] J. W. Trzciński, R. Pinalli, N. Riboni, A. Pedrini, F. Bianchi, S. Zampolli, I. Elmi, C. Massera, F. Ugozzoli, and E. Dalcanale: *In Search of the Ultimate Benzene Sensor: The EtQxBox Solution*, ACS Sensors, 2:4 (590–598), 2017, DOI: 10.1021/acssensors.7b00110.

[281] I. Wilhelm, M. Rieger, J. Hürtten, M. Wittek, C. Alépée, M. Leidinger, and T. Sauerwald: *Novel Low-Cost Selective Pre-Concentrators Based on Metal Organic Frameworks*, Procedia Engineering, 168 (151–154), 2016, DOI: 10.1016/j.proeng.2016.11.186.

[282] T. Sauerwald, A. Schütze, C. Schultealbert, O. Brieger, R. Diener, M. Leidinger, T. Conrad, and W. Reimringer: *Verfahren und Vorrichtung zum Kalibrieren eines Fluiddetektors mit Präkonzentrator*, EP3588081A1, Jun. 22, 2018 Accessed: Jan. 03, 2022. Available: <https://patentimages.storage.googleapis.com/35/05/7c/84bf90cfffc5f/EP3588081A1.pdf>

[283] G. W. Oehlert: *A First Course in Design and Analysis of Experiments*, 57:1. University of Minnesota, 2000. DOI: 10.1198/tas.2003.s210.

[284] W.-L. Loh: *On Latin hypercube sampling*, The Annals of Statistics, 24:5 (2058–2080), 1996, DOI: 10.1214/aos/1069362310.

[285] Y. Robin, P. Goodarzi, T. Baur, C. Schultealbert, A. Schütze, and T. Schneider: *Machine Learning based calibration time reduction for Gas Sensors in Temperature Cycled Operation*, in *2021 IEEE International Instrumentation and Measurement Technology Conference (I2MTC)*, 2021, (1–6). DOI: 10.1109/i2mtc50364.2021.9459919.

[286] T. Aalto, M. Lallo, J. Hatakka, and T. Laurila: *Atmospheric hydrogen variations and traffic emissions at an urban site in Finland*, Atmospheric Chemistry and Physics, 9:19 (7387–7396), 2009, DOI: 10.5194/acp-9-7387-2009.

[287] R. Kurtenbach, J. Kleffmann, A. Niedojadlo, and P. Wiesen: *Primary NO₂ emissions and their impact on air quality in traffic environments in Germany*, Environmental Sciences Europe, 24:1 (21), 2012, DOI: 10.1186/2190-4715-24-21.

[288] M. Leidinger, T. Sauerwald, T. Conrad, W. Reimringer, G. Ventura, and A. Schütze: *Selective Detection of Hazardous Indoor VOCs Using Metal Oxide Gas Sensors*, Procedia Engineering, 87 (1449–1452), 2014, DOI: 10.1016/j.proeng.2014.11.722.

[289] J. F. Amann: *Möglichkeiten und Grenzen des Einsatzes von Halbleitergassensoren im temperaturzyklischen Betrieb für die Messung der Innenraumluftqualität – Kalibrierung, Feldtest, Validierung*, Masterarbeit, Universität des Saarlandes, 2021.

[290] Y. Robin, J. Amann, T. Baur, P. Goodarzi, C. Schultealbert, T. Schneider, and A. Schütze: *High-Performance VOC Quantification for IAQ Monitoring Using Advanced Sensor Systems and Deep Learning*, Atmosphere 2021, Vol. 12, Page

1487, 12:11 (1487), 2021, DOI: 10.3390/atmos12111487.

[291] A. Miquel-Ibarz, J. Burgués, and S. Marco: *Global calibration models for temperature-modulated metal oxide gas sensors: A strategy to reduce calibration costs*, Sensors and Actuators B: Chemical, 350 (130769), 2022, DOI: 10.1016/j.snb.2021.130769.

[292] S. Bozinovski: *Reminder of the First Paper on Transfer Learning in Neural Networks, 1976*, *Informatica*, 44:3, 2020, DOI: 10.31449/inf.v44i3.2828.

[293] F. Zhuang, Z. Qi, K. Duan, D. Xi, Y. Zhu, H. Zhu, H. Xiong, and Q. He: *A Comprehensive Survey on Transfer Learning*, *Proceedings of the IEEE*, 109:1 (43–76), 2021, DOI: 10.1109/jproc.2020.3004555.

[294] Y. C. Cheng, T. I. Chou, S. W. Chiu, and K. T. Tang: *A Concentration-Based Drift Calibration Transfer Learning Method for Gas Sensor Array Data*, *IEEE Sensors Letters*, 4:10, 2020, DOI: 10.1109/lsens.2020.3027959.

[295] Y. Robin: *Transfer Learning to Significantly Reduce the Calibration Time of MOS Gas Sensors*, (6–8).

[296] J. Amann: *Private Communications - Longterm stability*, 2022.

[297] J. Burgués and S. Marco: *Multivariate estimation of the limit of detection by orthogonal partial least squares in temperature-modulated MOX sensors*, *Analytica Chimica Acta*, 1019 (49–64), 2018, DOI: 10.1016/j.aca.2018.03.005.

[298] J. Burgués, J. M. Jiménez-Soto, and S. Marco: *Estimation of the limit of detection in semiconductor gas sensors through linearized calibration models*, *Analytica Chimica Acta*, 1013 (13–25), 2018, DOI: 10.1016/j.aca.2018.01.062.

[299] D. Breuer, H. Sagunski, M. Ball, R. Hebisch, N. Von Hahn, T. Lahrz, G. Nitz, K. H. Pannwitz, W. Rosenberger, and R. Schwabe: *Empfehlungen zur Ermittlung und Beurteilung chemischer Verunreinigungen der Luft von Innenraumarbeitsplätzen*, *Gefahrstoffe - Reinhal tung der Luft*, 74:9 (354–360), 2014.

[300] G. A. Ayoko and H. Wang: *Volatile Organic Compounds in Indoor Environments*, in *Indoor Air Pollution. Handbook of Environmental Chemistry*, 64 (69–107), P. Pluschke and H. Schleibinger, Eds. Springer, Berlin, Heidelberg, 2014. DOI: 10.1007/698_2014_259.

[301] P. Wolkoff: *Trends in Europe to reduce the indoor air pollution of VOCs*, *Indoor air*, 13:6 (5–11), 2003, DOI: 10.1034/j.1600-0668.13.s.6.1.x.

[302] *Multigassensoren - Standardisierte Prüfanweisung und Prüfgase für VOC-Detektoren zur Innenraumluftgütemessung*, VDI/VDE 3518 Blatt 4 Accessed: Jan. 07, 2022. Available: <https://www.vdi.de/richtlinien/details/vdivde-3518-blatt-4-multigassensoren-standardisierte-pruefanweisung-und-pruefgase-fuer-voc-detektoren-zur-innenraumluftguetemessung>

[303] Universität des Saarlandes - Lehrstuhl für Messtechnik: *Projects - VOC4IAQ*. <https://www.lmt.uni-saarland.de/index.php/de/forschung/49-portrait-projekte>

[304] E. von Schneidemesser, P. S. Monks, and C. Plass-Duelmer: *Global comparison of VOC and CO observations in urban areas*, *Atmospheric Environment*, 44:39 (5053–5064), 2010, DOI: 10.1016/j.atmosenv.2010.09.010.

[305] M. Leidinger, M. Rieger, T. Sauerwald, C. Alépée, and A. Schütze: *Integrated pre-concentrator gas sensor microsystem for ppb level benzene detection*, *Sensors and Actuators B: Chemical*, 236 (988–996), 2016, DOI: 10.1016/j.snb.2016.04.064.

[306] W. Winter, C. Day, J. Prestage, and T. Hutter: *Temporally resolved thermal desorption of volatile organics from nanoporous silica preconcentrator*, *Analyst*, 146:1 (109–117), 2021, DOI: 10.1039/d0an01822h.

[307] I. C. Weber, P. Rüedi, P. Šot, A. T. Güntner, and S. E. Pratsinis: *Handheld Device for Selective Benzene Sensing over Toluene and Xylene*, *Advanced Science*,

(2103853), 2021, DOI: 10.1002/advs.202103853.

[308] P. R. Chung, C. T. Tzeng, M. T. Ke, and C. Y. Lee: *Formaldehyde Gas Sensors: A Review*, Sensors, 13:4 (4468–4484), 2013, DOI: 10.3390/s130404468.

[309] Sensirion AG: *Umweltsensoren - SFA30 Formaldehyde-Sensormodul*. <https://www.sensirion.com/de/umweltsensoren/formaldehydsensor-sfa30/> (accessed Jan. 07, 2022).

[310] EC Sense GmbH: *Gas Sensor - HCHO Formaldehyde - ES1-HCHO-5*. <https://ecsense.com/product/es1-hcho-5-formaldehyde-sensor/> (accessed Jan. 07, 2022).

[311] C. Schultealbert, T. Baur, A. Schütze, and T. Sauerwald: *Investigating the role of hydrogen in the calibration of MOS gas sensors for indoor air quality monitoring*, in *Indoor Air 2018*, 2018.

[312] M. D. Levitt: *Production and excretion of hydrogen gas in man*, The New England journal of medicine, 281:3 (122–127), 1969, DOI: 10.1056/nejm196907172810303.

[313] J. Tomlin, C. Lowis, and N. W. Read: *Investigation of normal flatus production in healthy volunteers*, Gut, 32:6 (665–669), 1991, DOI: 10.1136/gut.32.6.665.

[314] D. H. Ehhalt and F. Rohrer: *The tropospheric cycle of H₂: a critical review*, Tellus, Series B: Chemical and Physical Meteorology, 61:3 (500–535), 2009, DOI: 10.1111/j.1600-0889.2009.00416.x.

[315] D. H. Barnes, S. C. Wofsy, B. P. Fehlau, E. W. Gottlieb, J. W. Elkins, G. S. Dutton, P. C. Novelli, C. Barnes, S. C. Wofsy, B. P. Fehlau, E. W. Gottlieb, J. W. Elkins, G. S. Dutton, and P. C. Novelli: *Hydrogen in the atmosphere: Observations above a forest canopy in a polluted environment*, Journal of Geophysical Research: Atmospheres, 108:D6 (4197), 2003, DOI: 10.1029/2001jd001199.

[316] P. C. Novelli, P. M. Lang, K. A. Masarie, D. F. Hurst, R. Myers, and J. W. Elkins: *Molecular hydrogen in the troposphere: Global distribution and budget*, Journal of Geophysical Research: Atmospheres, 104:D23 (30427–30444), 1999, DOI: 10.1029/1999jd900788.

[317] U. Schmidt and W. Seiler: *A new method for recording molecular hydrogen in atmospheric air*, Journal of Geophysical Research, 75:9 (1713–1716), 1970, DOI: 10.1029/jc075i009p01713.

[318] G. L. Forster, W. T. Sturges, Z. L. Fleming, B. J. Bandy, and S. Emeis: *A year of H₂ measurements at Weybourne Atmospheric Observatory, UK*, Chemical and Physical Meteorology, 64:1 (17771), 2012, DOI: 10.3402/tellusb.v64i0.17771.

[319] J. D. Patterson, M. Aydin, A. M. Crotwell, G. Pétron, J. P. Severinghaus, P. B. Krummel, R. L. Langenfelds, and E. S. Saltzman: *H₂ in Antarctic firn air: Atmospheric reconstructions and implications for anthropogenic emissions*, Proceedings of the National Academy of Sciences of the United States of America, 118:36 (1–8), 2021, DOI: 10.1073/pnas.2103335118.

[320] H. Salonen, T. Salthammer, and L. Morawska: *Human exposure to NO₂ in school and office indoor environments*, Environment International, 130 (104887), 2019, DOI: 10.1016/j.envint.2019.05.081.

[321] Linde GmbH: *EURO 6/EPA Synthetische Luft KW-frei*. https://produkte.linde-gase.de/gasgemische/Synthetische_Luft_EURO6_EPA.html (accessed Jan. 05, 2022).

[322] JLM Innovation: *MOXstick*. <https://www.jlm-innovation.de/products/moxstick> (accessed Jun. 12, 2022).

[323] JLM Innovation: *GIGAstick*. <https://www.jlm-innovation.de/products/gigastick> (accessed Jun. 12, 2022).

- [324] C. Wendt, A. Bohnhorst, S. Zimmermann, and A. Kirk: *Ultra-Low Noise Current Meter for Measuring Quickly Changing Currents from Attoampere to Nanoampere Manuscript*, tm - Technisches Messen, 2022.
- [325] R. H. Pierson and E. A. Fay: *Guidelines for Interlaboratory Testing Programs*, Analytical Chemistry, 31:12 (25A-49A), 2012, DOI: 10.1021/ac60156a708.
- [326] W. J. Buttner, R. Burgess, C. Rivkin, M. B. Post, L. Boon-Brett, G. Black, F. Harskamp, and P. Moretto: *Inter-laboratory assessment of hydrogen safety sensors performance under anaerobic conditions*, International Journal of Hydrogen Energy, 37:22 (17540–17548), 2012, DOI: 10.1016/j.ijhydene.2012.03.165.
- [327] G. E. P. Box: *Robustness in the Strategy of Scientific Model Building*, Robustness in Statistics, (201–236), 1979, DOI: 10.1016/b978-0-12-438150-6.50018-2.
- [328] B. S. Everitt: *The Cambridge Dictionary of Statistics*, Journal of the American Statistical Association, 94:446 (657), 1999, DOI: 10.2307/2670205.
- [329] German Committee on Indoor Air Guide Values / Umweltbundesamt. <https://www.umweltbundesamt.de/en/topics/health/commissions-working-groups/german-committee-on-indoor-air-guide-values#german-committee-on-indoor-air-guide-values-air> (accessed May 01, 2022).